



**HAL**  
open science

# Progenitor cell mechanisms contributing to cortical malformations: studying the role of the heterotopia gene *Eml1/EML1* in radial glia

Ana Uzquiano López

## ► To cite this version:

Ana Uzquiano López. Progenitor cell mechanisms contributing to cortical malformations: studying the role of the heterotopia gene *Eml1/EML1* in radial glia. Human genetics. Sorbonne Université, 2019. English. NNT: 2019SORUS392 . tel-03241793

**HAL Id: tel-03241793**

**<https://theses.hal.science/tel-03241793>**

Submitted on 29 May 2021

**HAL** is a multi-disciplinary open access archive for the deposit and dissemination of scientific research documents, whether they are published or not. The documents may come from teaching and research institutions in France or abroad, or from public or private research centers.

L'archive ouverte pluridisciplinaire **HAL**, est destinée au dépôt et à la diffusion de documents scientifiques de niveau recherche, publiés ou non, émanant des établissements d'enseignement et de recherche français ou étrangers, des laboratoires publics ou privés.

# Sorbonne Université

Ecole Doctorale 'Complexité du Vivant' ED515

*Institut du Fer à Moulin / Cortical Development and Pathology*

## **Progenitor cell mechanisms contributing to cortical malformations:**

*studying the role of the heterotopia gene Eml1/EML1 in radial glia.*

Ana UZQUIANO LÓPEZ

Thèse de doctorat de Génétique et Neurodéveloppement

Dirigée par Fiona FRANCIS

Présentée et soutenue publiquement le 27 Mai 2019

Devant un jury composé de :

- **SPASSKY, Nathalie**, Research Director, Institut de Biologie de l'Ecole Normale Superior, UMR 8197, Paris, France (Président).
- **HUTTNER, Wieland**, Professor, Max Planck Institute of Molecular Cell Biology and Genetics, Dresden, Germany (Rapporteur).
- **REPRESA, Alfonso**, Research Director, Institut de Neurobiologie de la Méditerranée, Marseille, France (Rapporteur).
- **MARTHIENS, Véronique**, Researcher, Institut Curie, UMR 144, Paris, France (Examineur).
- **BORRELL, Victor**, Principal Investigator, Instituto de Neurociencias de Alicante, San Juan de Alicante, Spain (Examineur).
- **FRANCIS, Fiona**, Research Director, Institut du Fer à Moulin, UMR-S 1270, Paris, France (Directeur de thèse).



*A mis padres, Trini y Juanjo*

## **Acknowledgements**

I thank my PhD director, Fiona. Thank you for welcoming me in your lab. Thank you for your trust, your support and for always encouraging me to go one step further. Thank you for your help in the difficult moments but also for the great discussions and input throughout all these years. I have learnt a lot with you and from you.

Thank you Sara, Delfina and Melissa. Sara, it was a real pleasure to 'share' project with you. Delfina, with our ups and downs, I feel lucky I got to live this experience with you by my side. We have learnt many things together, and we have also laughed about many things together. Melissa, thank you for having always been there. For being always available to discuss anything: from confocal imaging to Golgi cisternae and trafficking. But most of all, thank you for always boosting me; for not always telling me what I wanted to hear, but always with the best of your intentions and the purest honesty. Thank you.

Marika, working with you makes the lab a brighter place. Thank you for your help with scientific discussions and French corrections, but moreover, thank you for sharing and caring. I also thank all other members of the team: Laurence, Marta, Giorgia, Maxime, Richard Gael and Anne for all the discussions and the good time spent together. Special thanks to Anne, for her great involvement in my project.

Thanks to my good friends in the IFM who were always there to share this experience: Ferran, Jimmy, Maria and Melanie. You have all in your way helped me throughout these years: from sharing the first experiments, to leaving notes all over my desk to encourage me through my thesis writing. Jimmy, thank you for the many hugs and for being the chosen family while in Paris.

I thank Victor Borrell and his lab for welcoming me in Alicante. Cristina, gracias por las risas, las discusiones y los infinitos audios.

I thank the rest of my good 'Parisian' friends; Sebastian and Estefani, thank you for sharing frustrations over drinks and nice dinners. Elise and Robin, thank you for your generosity: spending time with you is a bit like being home.

Gracias a todos mis amigos de fuera que me han apoyado desde fuera, siempre interesados por mi día a día, por mi proyecto presente pero también por los futuros. Gracias por las visitas y por poquito a poquito hacer de la distancia algo relativo. María, Paloma A., Donais, Robert, Sofía, Laura, Silvia, Mario, Gonzalo, Mónica, Álvaro G. y Álvaro B., gracias. Un gracias inmenso a Sundry y Paloma. Sundry, hemos compartido esto de principio a fin, y has sido una

compañera de camino espectacular. Gracias por escuchar y aconsejarme sobre el más mínimo problema, y gracias por recordarme que a veces es bueno parar y descansar. Gracias por vivir mis alegrías de una forma tan cercana. Paloma, gracias por el apoyo, por ir entendiendo mi rutina poco a poco, por estar tan cerca estando a muchos kilómetros, por la disponibilidad absoluta cada vez que volvía a casa.

Gracias a Iñigo Azcoitia, mi profesor de Desarrollo y Plasticidad del Sistema Nervioso durante mi carrera. Gracias por guiarme en mis primeros pasos y no dejar que tirara la toalla nunca.

Gracias a mi familia, especialmente a mis tíos Pili y Jorge, y a mis primos Javi, Lola, Jorge y Julia. También a las pequeñas Silvia y Alicia. Gracias por los reencuentros y por el cariño, por el interés y por aprovechar de las ocasiones que tenemos para estar juntos. Pasar tiempo con vosotros ha sido siempre coger energía y llenarme de luz.

Papá y mamá, sin vosotros hacer una tesis no hubiera sido posible. Primero, gracias por educarme como ‘una mujer del siglo XXI’, no ponerme nunca frenos y confiar en que haría aquello que me propusiera. Gracias por dejarme volar, por adaptaros a mi ritmo (a veces frenético) y disfrutar conmigo de mis aventuras, ya sean en Madrid, Londres, Paris, o ahora Boston. Gracias por ayudarme con mudanzas, médicos, comidas y demás cosas ‘simples’ del día a día a pesar de la distancia. Gracias por los innumerables viajes. Vuestra ayuda siempre hace el camino más ligero. Gracias por seguir mi trabajo, mis viajes a conferencias, mis presentaciones, y por alegraros de cada una de mis pequeñas victorias como si fueran vuestras. Gracias por ser el soporte más estable y seguro.

Finalmente, gracias Pietro. Creo que una tesis la hace contigo quien esta día tras día, incluyendo noches de pesadillas, días muy largos de trabajo, fines de semanas delante del ordenador y muchos viajes fuera de casa. Tú has estado siempre. Gracias por compartir estos años conmigo, por escuchar mis presentaciones hasta la saciedad, ayudarme con tests estadísticos y preocuparte por la polaridad de mis progenitores tanto como yo. Gracias por ser casa, y por ser calma y tranquilidad.

## Table of contents

Aknowledgments.....	II
Table of contents.....	IV
List of figures .....	VII
<b>Introduction</b> .....	<b>1</b>
Preamble .....	2
1. From neuroectoderm to dorsal telencephalon: early events of central nervous sytem development .....	3
2. The cerebral cortex .....	6
2.1 The cortical lobes and areas .....	6
2.2 Evolutionary considerations: neocortex and allocortex.....	8
2.3 Cellular diversity in the neocortex.....	8
2.3.1 Glia .....	8
2.3.2 Projection neurons and interneurons .....	9
3. Cortical development: neural progenitor diversity and neuronal production .....	12
3.1 Progenitor cell types (adapted from Uzquiano et al., 2018) .....	13
3.1.1 Apical progenitor: neuroepithelial cells (NEs) and apical radial glial cells (aRGs).....	13
3.1.2 Basal progenitors (BPs): intermediate progenitors (IPs) and basal radial glial-like cells (bRGs) and their implication in cortical expansion.....	16
3.2 Apical radial glial cells: key features mediating their behavior (adapted from Uzquiano et al., 2018) .....	22
3.2.1 Cell cycle length considerations....	23
3.2.2 Polarity complex and cell adhesion molecules.....	24
3.2.3 Mitotic spindle and cleavage plane.....	25
3.2.4 Apical and/or basal process and radial glia cell identity .....	28
3.2.5 Membrane-bound organelles: mitochondria, endoplasmic reticulum, Golgi apparatus.....	30
3.2.6 Microtubule-based organelles: the centrosome and midbody .....	31
3.2.7 The primary cilium.....	33
3.3 Multipotency of neuronal progenitors (adapted from Uzquiano et al., 2018) .....	38
3.3.1 Subpopulations of apical radial? .....	38
3.3.2 Basal progenitors and neuronal output .....	40
3.4 From the Radial Unit Hypothesis to the Supragranular Layer Expansion Hypothesis.....	41
3.5 Cortical arealization .....	44
3.5.1 Telencephalic signaling centers, transcription factors and the progenitor compartment.....	44
3.5.2 The post-mitotic comparment .....	45
3.6 Neuronal migration.....	46

4.	Cortical malformations.....	49
4.1	Brain size: microcephaly versus macrocephaly .....	50
4.2	Cortical folding: lissencephaly type I, polymicrogyria, lissencephaly type II or cobblestone .....	51
4.3	Heterotopia: periventricular and subcortical band heterotopia.....	53
4.4	Primary cilium related pathologies: ciliopathies and impact on the neocortex ...	55
4.4.1	Classical ciliopathies .....	55
4.4.2	The primary cilium and cortical malformations .....	55
5.	<i>Eml1/EML1</i> : a heterotopia gene mutated in mouse and human .....	56
5.1	Structure of EMAP proteins .....	57
5.2	Expression in the nervous system and subcellular location and function of EMAP members .....	59
5.3	Human patients: mutations and phenotype .....	62
5.4	Rodent models of heterotopia: the <i>HeCo</i> mouse.....	64
	<b>Results</b> .....	69
	Preamble .....	70
1.	Introduction to Bizzotto, Uzquiano et al. (2017) ‘Eml1 loss impairs apical progenitor spindle length and soma shape in the developing cerebral cortex’ .....	71
1.1	Summary .....	71
1.2	Contribution.....	72
	Article .....	73
2.	Introduction to Uzquiano et al. ‘Mutations in the heterotopia gene <i>Eml1/EML1</i> severely disrupt the formation of primary cilia’ .....	74
2.1	Summary .....	74
2.2	Contribution.....	75
	Manuscript .....	77
2.3	Extra supplementary results related to Uzquiano et al.....	149
2.4	Supplementary methods .....	153
3.	Introduction to Collins, Uzquiano et al. ‘The neuroanatomy of Eml1 knockout mice, a model of subcortical heterotopia’ .....	155
3.1	Summary .....	155
3.2	Contribution.....	156
	Manuscript .....	157
3.3	Extra supplementary results related to Collins, Uzquiano et al. ....	191
2.4	Supplementary methods .....	191
	<b>Discussion</b> .....	193
1.	<i>Eml1/EML1</i> mutations lead to subcortical heterotopia in mouse and human .....	194
1.1	Cortical phenotype in <i>Eml1</i> -mutant conditions.....	194
1.2	Mouse versus human phenotype .....	196
1.3	Basal radial glia versus ectopic progenitors.....	199
1.4	A role for Eml1 in basal radial glia?.....	200
1.5	Recent models to address human specific features of cortical development ...	202
2.	Eml1 function in apical radial glia cells .....	204
2.1	Eml1 may have different roles throughout cell cycle .....	204
2.2	An unexpected role for Eml1 in primary cilium formation.....	206
2.3	EML1 interacts with the ciliary protein RPGRIP1L.....	208



2.4	The Golgi apparatus in <i>Eml1</i> -mutant conditions.....	210
2.4.1	The Golgi apparatus and cortical malformations.....	211
2.4.2	Golgi apparatus-related proteins and Eml1 .....	212
2.4.3	Golgi apparatus-derived trafficking is impaired in <i>HeCo</i> neuronal progenitors... ..	214
2.5	The adherens junction (AJ)-actin belt in <i>Eml1</i> -mutant conditions.....	215
3.	The ventricular zone in <i>Eml1</i> -mutant conditions.....	218
3.1	All radial glial cells do not seem equally affected.....	218
3.2	Space constraints in the <i>HeCo</i> ventricular zone .....	219
4.	Signaling pathways involved in the ectopic progenitor phenotype .....	222
3.1	No obvious changes in mTOR signaling although Eml1 interacts with Raptor....	222
3.2	The Hippo pathway as a convergent signaling cascade in mouse models of subcortical heterotopia .....	223
3.3	The Shh pathway is not severely perturbed in the <i>HeCo</i> developing cortex .....	226
	<b>Conclusions</b> .....	227
	Annexe I: Uzquiano et al. (2018) ‘Cortical progenitor biology: key features mediating proliferation versus differentiation’ .....	228
	Annexe II: Uzquiano and Francis (2019). ‘Rotatin the phenotypes’ .....	229
	<b>Bibliography</b> .....	230

## List of figures

<b>Figure 1.</b> Neurulation of chick embryos.....	3
<b>Figure 2.</b> The anterior neural tube is subdivided in different vesicles that will eventually become the different parts of the brain in adulthood.....	4
<b>Figure 3.</b> The neural tube is patterned along anterior-posterior and dorso-ventral axes .....	5
<b>Figure 4.</b> Patterning of the telencephalon.....	5
<b>Figure 5.</b> Schematic representation of cortical lobes and areas. ....	7
<b>Figure 6.</b> Cajal’s drawings of astrocytes.....	8
<b>Figure 7.</b> Drawings of neocortical layers from Ramon y Cajal, 1911 .....	9
<b>Figure 8.</b> Cortical interneuron origin and diversity.....	10
<b>Figure 9.</b> Classification of projection neurons based on their target. ....	11
<b>Figure 10.</b> Schematic representation of cortical development .....	14
<b>Figure 11.</b> Schematic representation of apical radial glia undergoing interkinetic nuclear migration .....	14
<b>Figure 12.</b> Mouse versus human cortical development: basal radial glial cells are characteristic of primate-human brains .....	17
<b>Figure 13.</b> Basal radial glial cells have a long basal process reaching the basement membrane and are Pax6, nestin and pVimentin positive. ....	18
<b>Figure 14.</b> Schematic representation of the different basal radial glia morphologies described in the primate SVZ.....	18
<b>Figure 15.</b> Schematic representation of apical radial glia spindle orientations .....	19
<b>Figure 16.</b> Forced basal radial glia production in the murine developing cortex can result in the appearance of fold-like structures .....	21
<b>Figure 17.</b> Schematic representation of cortical phenotype upon alteration of adherens junctions or polarity complex components .....	25
<b>Figure 18.</b> Schematic representation of mitotic spindle anchoring to the cell cortex in apical radial glia cells .....	26
<b>Figure 19.</b> Schematic representation of apical domain inheritance upon apical radial glia division .....	28
<b>Figure 20.</b> Mitochondria morphology differs between apical radial glia cells, intermediate progenitors and newborn neurons .....	30
<b>Figure 21.</b> The Golgi apparatus localizes in the apical process of radial glia cells.....	31
<b>Figure 22.</b> Centrosome localization in apical radial glia cells. ....	32
<b>Figure 23.</b> Primary cilium structure .....	33
<b>Figure 24.</b> Basal body structure .....	34
<b>Figure 25.</b> Schematic representations of ciliary trafficking .....	36
<b>Figure 26.</b> Ciliary remnants associate with the mother centriole during mitosis .....	36
<b>Figure 27.</b> Schematic representation of cortical development based on the Radial Unit Hypothesis.....	41
<b>Figure 28.</b> Schematic representation of the Supragranular Layer Expansion Hypothesis. ....	43
<b>Figure 29.</b> Arealization of the dorsal telencephalon.....	45
<b>Figure 30.</b> Schema representing the process of neuronal migration from the ventricular zone to the cortical plate .....	47
<b>Figure 31.</b> Electron micrograph showing a young migrating neuron along a radial glial fiber	47
<b>Figure 32.</b> Radially-migrating neurons in the ferret neocortex.....	48
<b>Figure 33.</b> Schemas of cortical malformations .....	49
<b>Figure 34.</b> The ciliopathy spectrum.....	55

<b>Figure 35.</b> Recombinant EML1 has a cell cycle dependent localization in neuronal progenitors .....	57
<b>Figure 36.</b> Schematic representation of mammalian EML protein structures .....	58
<b>Figure 37.</b> Schematic representation of EML1 structure.....	58
<b>Figure 38.</b> Schema illustrating EML1 trimerization and association with microtubules .....	59
<b>Figure 39.</b> Embryonic sagittal expression of Emls shown by <i>in situ</i> hybridization .....	60
<b>Figure 40.</b> EML3 and 4 co-localize with the mitotic spindle .....	61
<b>Figure 41.</b> MRIs of <i>EML1</i> mutation patients .....	62
<b>Figure 42.</b> Schematic representation of the <i>EML1</i> gene indicating the position of the mutations .....	63
<b>Figure 43.</b> Mutant EML1 shows less co-localization with the microtubule network in Vero cells .....	63
<b>Figure 44.</b> <i>HeCo</i> mice show bilateral subcortical heterotopia.....	65
<b>Figure 45.</b> The heterotopia in <i>HeCo</i> mice is mainly composed of upper layer neurons .....	66
<b>Figure 46.</b> Accumulation of neurons in the <i>HeCo</i> mouse brain.....	67
<b>Figure 47.</b> <i>HeCo</i> mice show ectopically localized proliferating Pax6+ neuronal progenitors outside the normal proliferative VZ.....	68
<b>Figure 48.</b> EML1 interacts with RAPTOR. Representative Western blot of co-immunoprecipitation experiment.....	149
<b>Figure 49.</b> Mild alterations in the Gli3A:Gli3R ratio in the <i>HeCo</i> dorsal telencephalon .....	151
<b>Figure 50.</b> <i>HeCo</i> aRGs show increased YAP levels.....	153
<b>Figure 51.</b> Primary cilia are severely disrupted in the ventricular zone of <i>Eml1</i> KO mice.....	192
<b>Figure 52.</b> <i>Eml1</i> expression level in cortical cell types.....	195
<b>Figure 53.</b> <i>Eml1</i> differential expression in three main cortical neuron subtypes during cortical development from E15.5 to P1 .....	195
<b>Figure 54.</b> The folded human neocortex presents a higher diversity of neuronal progenitors absent in the smooth mouse neocortex .....	197
<b>Figure 55.</b> Analysis of radial glia processes using Dil .....	199
<b>Figure 56.</b> <i>BAF155</i> cKOs present bRG-like cells at E16.5. ....	201
<b>Figure 57.</b> Characterization of dorsal cortical organoids.....	203
<b>Figure 58.</b> The number of detached ventricular particles does not differ between WT and <i>HeCo</i> mice at E13.5 .....	206
<b>Figure 59.</b> The mother centriole is characterized by the presence of distal and subdistal appendages. ....	207
<b>Figure 60.</b> Schematic representation of <i>RPGRIP1L</i> mutations associated with Joubert and Meckel syndromes .....	208
<b>Figure 61.</b> Joubert syndrome patient fibroblasts show longer primary cilia than control lines .....	209
<b>Figure 62.</b> Primary cilia are absent or very short in neuroepithelial cells of <i>Rpgrip1l</i> KO mice. ....	209
<b>Figure 63.</b> Knockdown of <i>Vcip135</i> leads to Golgi fragmentation in HeLa cells .....	212
<b>Figure 64.</b> Knockdown of <i>Kif7</i> in RPE1 cells leads to Golgi fragmentation .....	213
<b>Figure 65.</b> Schematic representation of the RUSH system.....	214
<b>Figure 66.</b> No differences between cis and trans Golgi vesicles in WT and <i>HeCo</i> aRGs at E13.5. ....	215
<b>Figure 67.</b> Adherens junctions are disrupted in <i>Llg1</i> cKO mouse brain.....	216
<b>Figure 68.</b> Actin depolymerization promotes ciliogenesis.....	217

<b>Figure 69.</b> Laser ablation experiments performed on the apical surface of embryonic cerebral walls of mouse and ferret .....	220
<b>Figure 70.</b> Schematic representation of progenitor overcrowding and delamination upon <i>TAG-1</i> knockdown .....	221
<b>Figure 71.</b> Schematic representation of the Hippo pathway.....	223
<b>Figure 72.</b> Cortical cell distribution abnormalities caused by <i>Fat4/Dcsh1</i> knockdown in the mouse neuroepithelium were rescued by knocking-down concomitantly YAP .....	224
<b>Figure 73.</b> <i>Par3</i> conditional knockout mice are a model of subcortical heterotopia and show increased YAP levels in the ventricular zone at early-mid corticogenesis (E13.5) .....	225
<b>Figure 74.</b> Schematic representation of the Shh signaling pathway .....	226

# **INTRODUCTION**

## **Introduction**

### **Preamble**

In the introduction of my thesis I first provide a brief description of central nervous system development, the cerebral cortex and the different cell types it contains. I then focus more specifically on aspects directly associated with the central work of my thesis. I provide an extended introduction to apical radial glial cells and features mediating their behavior. I expand on the primary cilium, an organelle which has been a focus of study in my thesis.

In this work I have studied the *HeCo* mouse model for subcortical heterotopia, in which ectopic Pax6+ proliferating progenitors were found outside the ventricular zone from early stages of mouse cortical development. These cells resemble basal radial glia-like cells, although most probably a 'pathological' version. Hence I also focused on introducing basal radial glial cells and discussing neocortical expansion, which are hot topics currently in the field.

Concerning other related aspects of cortical development, I briefly describe cortical arealization, neuronal migration and I introduce cortical malformations in more detail. I finalize by discussing the EMAP family of proteins, particularly Eml1/EML1, mutated in the *HeCo* mouse model, as well as in three families presenting severe atypical heterotopia. In this last section, I also describe the *HeCo* mouse model and the cortical phenotype described in these mice concluding with the main question of my thesis project.

## 1. From neuroectoderm to dorsal telencephalon: early events of central nervous system development

Embryonic development starts after fertilization, when the newly formed zygote undergoes a series of steps namely blastulation, gastrulation and neurulation. The nervous system develops from the outer-most germ layer in the gastrula state: the ectoderm. The epidermis and the external surface of the eyes, teeth, mouth, rectum and pineal and pituitary glands also derive from the ectoderm.

Neurulation refers to the process by which the ectoderm acquires a neural identity and eventually becomes the neural tube (Colas and Schoenwolf, 2001). Through a series of steps involving re-shaping, bending, folding and closure, the neural plate eventually becomes the neural tube, a hollow cavity surrounded by a pseudostratified neuroepithelium responsible for the development of the central nervous system (CNS) (Colas and Schoenwolf, 2001, recently reviewed by Nikolopoulo et al., 2017, Figure 1).

The anterior-most region of the neural tube undergoes drastic changes during neurulation. Three primary vesicles are formed: the forebrain (prosencephalon), which will rise to the diencephalon, hypothalamus, eyes and telencephalon, the midbrain (mesencephalon), which results in the tectum and brain peduncles, and the hindbrain (rhombencephalon, further subdivided in the metencephalon and myelencephalon), which forms the cerebellum, the pons, and the medulla oblongata. Upon closure, the posterior neural tube becomes the spinal cord (Darnell and Gilbert, 2016, Figure 2).

Changes in shape and morphology of the neural tube are accompanied by patterning mechanisms, relying on a series of signaling centers which form at the boundaries between different prospective brain regions. These signaling centers secrete morphogens which are molecules that act on a concentration-dependent manner and induce a specific cell fate. At the rostral part of the neural tube is found the anterior neural ridge (ANR),

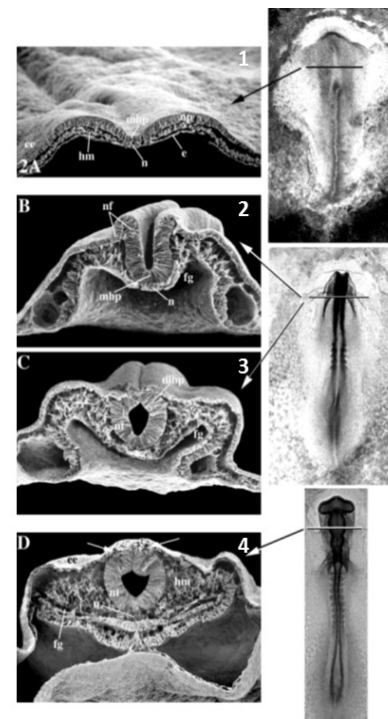


**Figure 1. Neurulation of chick embryos.** Whole mount and transverse sections viewed with scanning electron microscopy. From top to bottom image: 1) flat neural plate stage, shaping and early bending. 2) Neural groove stage 3) Incipient neural tube stage. Neural folds are in contact but not fused. 4) Final neural tube stage. From Colas and Schoenwolf, 2001.

secreting Fibroblast growth factors (Fgf), mostly Fgf8. In the mid-diencephalon is found the zona limitans intrathalamica (ZLI), secreting Sonic hedgehog (Shh). Finally, in the midbrain-hindbrain boundary is localized the isthmus organizer (ISO), secreting Fgf8 and Wingless 1 (Wnt1) (reviewed by Vieira et al., 2010, Figure 3 A).

Along the rostroventral axis, the neural tube is also patterned through the activity of different

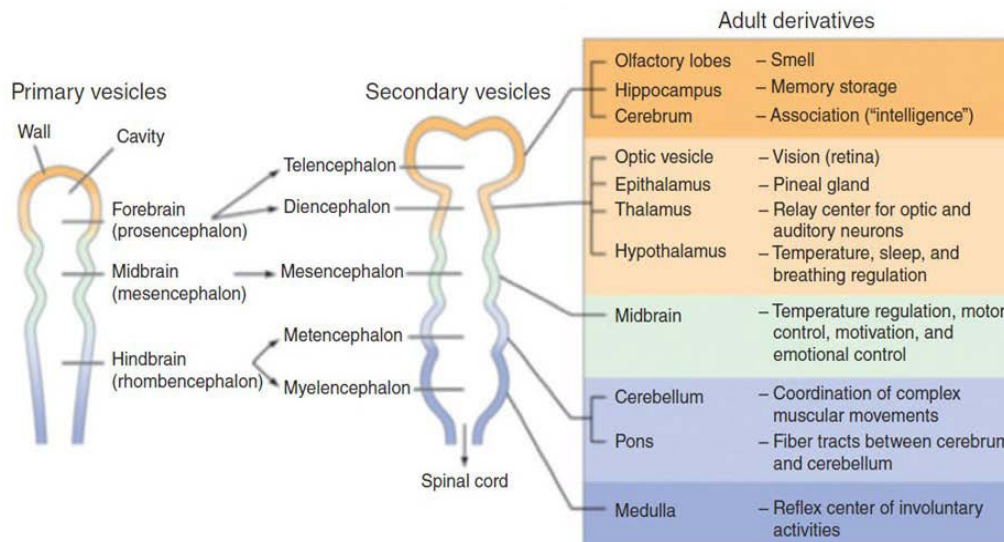


**Figure 2. The anterior neural tube is subdivided in different vesicles that will eventually become the different parts of the brain in adulthood.** From Darnell and Gilbert, 2016.

signaling centers. There are broadly two main organizing centers, which are conserved across the brain. Briefly, in the ventral region is localized the floor plate, whose secretion of Shh is induced by the notochord, lying below. In the dorsal part is positioned the roof plate, responsible for the production of Bone morphogenetic proteins (Bmp) and Wnt molecules. Other signals such as retinoic acid (RA) derived from adjacent structures (i.e. somites) are also important for patterning (Ulloa and Marti, 2010, Figure 3 B). The combination of these morphogens triggers expression of specific genes, coding for transcription factors (TFs) and proteins involved in signaling pathways which are key to inducing a particular cellular identity. As mentioned above, the telencephalon develops from the dorso-anterior forebrain. It can be subdivided into the pallium and the subpallium, located dorsally and ventrally, respectively, and separated by the pallio-subpallial boundary.



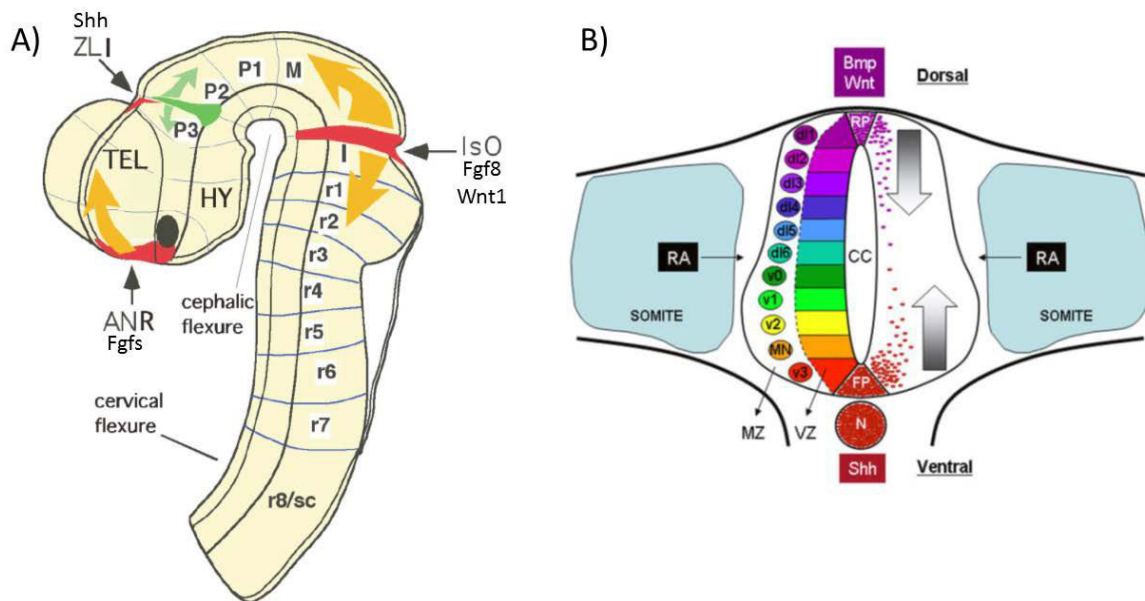


**Figure 3. The neural tube is patterned along anterior-posterior and dorso-ventral axes.** A) Schematic representation of the different signaling centers localized in between prospective brain regions which secrete morphogens responsible for neural tube patterning. The ANR, ZLI and IsO secrete Fgfs, Shh and Fgf8 and Wnt1, respectively. B) Schematic representation of the dorsoventral patterning mechanism of the neural tube. The schema represents specifically the spinal cord. The roof plate secretes Bmps and Wnts and the floor plate Shh. ANR: anterior neural ridge, ZLI: zona limitans intrathalamica, IsO: isthmus organizer, TEL: telencephalon, HY: hypothalamus, RA: retinoic acid, RP: roof plate, FP: floor plate, N: notochord. Adapted from Vieira et al., 2010 and Ulloa and Marti, 2010.

The pallium is subdivided in different regions: the medial pallium, giving rise to the hippocampus, the dorsal pallium, giving rise to the neocortex and the lateral and ventral pallium, giving rise to the olfactory bulb, amygdala and other structures. The subpallium is subdivided into the lateral, medial and caudal ganglionic eminences. These structures are responsible for the formation of the striatum, the globus pallidus, and GABAergic cortical interneurons (see section 2.3).

Patterning of the telencephalon is highly controlled by the ANR (or anterior forebrain, AF), secreting Fgf8 and thus triggering expression of FoxG1, critical for proliferation of neuroepithelial cells (Shimamura and Rubenstein, 1997, Xuan et al., 1995, Figure 4). Ventral patterning is mainly controlled by Shh secretion from the vicinity of the ANR (Rallu et al., 2002, Hebert and Fishell, 2008, Vieira et al., 2010, Figure 4).

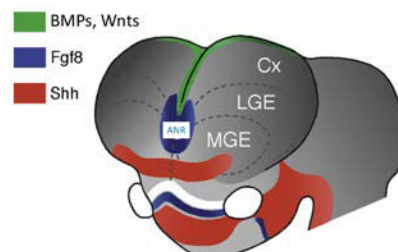


**Figure 4. Patterning of the telencephalon.** Fgf8 is secreted by the ANR, Shh is secreted ventrally and Wnts and BMPs are secreted in the dorsal midline. ANR: anterior neural ridge, Cx: cortex, LGE: lateral ganglionic eminence, MGE: medial ganglionic eminence. Adapted from Hoch et al., 2009.

In the developing telencephalon, the dorsal midline (roof plate and cortical hem) also acts as a signaling center. It is responsible for patterning of the medial and dorsal pallium through the secretion of Wnts and BMPs (Hebert and Fishell, 2008, Figure 4). As it happens for overall neural tube patterning, combinations of these morphogens trigger gene expression eventually controlling cell proliferation and fate.

## **2. The cerebral cortex**

My thesis project has focused on the development of the cerebral cortex, structure derived from the telencephalon. The cortex is responsible for higher cognitive functions and processing of the diverse sensory modalities. The cortex is an extremely complex structure, whose development depends on finely regulated events, including progenitor proliferation, neuronal migration, synaptogenesis, wiring and network establishment. It is composed of a huge diversity of cell types. The extent to which cortical cells are different from one another and across different areas and the programs underlying identity acquisition are topics of great interest in the field. When one of the steps crucial for corticogenesis is altered, severe developmental disorders arise (cortical malformations, neuropsychiatric diseases). Therefore, understanding how this structure is assembled, as well as the mechanisms required to attain such a large cell diversity and complex pattern of wiring may shed light into the etiology of these pathological conditions.

In this section I will describe the different areas of the cortex (2.1), followed by evolutionary considerations (2.2). Then I will describe the different cell types present in this structure, focusing on projection neurons (2.3).

### **2.1 Cortical lobes and areas**

The cerebral cortex is subdivided in four main lobes: the **frontal lobe**, separated by the central sulcus from the **parietal lobe** and by the lateral sulcus from the **temporal lobe**, and finally the **occipital lobe** in the caudal region of the brain and separated from the parietal lobe by the parieto-occipital sulcus (Figure 5).

In 1865, Paul Broca was the first to correlate a specific function with a particular cortical area, by demonstrating that speech was located in a region of the frontal lobe. The fact that the cerebral cortex was subdivided in regions responsible for different functions was suspected by neuroscientists since the XIX century (Lodato and Arlota, 2015). Nowadays it is well described that the cortex is divided in functional areas responsible for the processing of sensory modalities (Figure 5):

- The area responsible for processing visual information is located in the rostro-caudal regions of the cortex (the occipital lobe). This region receives inputs from the thalamus, which is the primary relay for sensory information from many sensory modalities. The visual cortex connects with visual association areas for further information processing.
- Auditory information is processed in the temporal lobe, which also receives inputs from one of the sensory nuclei of the thalamus. Auditory information is then further processed in auditory association areas as well as in Wernicke's area. Although the latter was historically thought to be the area where language comprehension occurs (Bogen and Bogen, 1976), it seems that is mainly involved in speech production (reviewed by Binder, 2015).
- The primary motor cortex is located in a specific region in the frontal lobe: the precentral gyrus, anterior to the central sulcus. It also receives inputs from the thalamus, as well as from other sensory cortical areas. It works in association with the premotor cortex and the supplementary motor area. The primary motor cortex is the main source of cortico-spinal and cortico-bulbar projections, controlling movement of the limbs and the trunk, as well as motor cranial nerves, respectively.
- The primary somatosensory cortex is located in the postcentral gyrus, posterior to the central sulcus. It receives inputs in a somatotopic fashion from the thalamus. It associates with the secondary somatosensory cortex and with the somatosensory association cortex, both located in the parietal cortex.

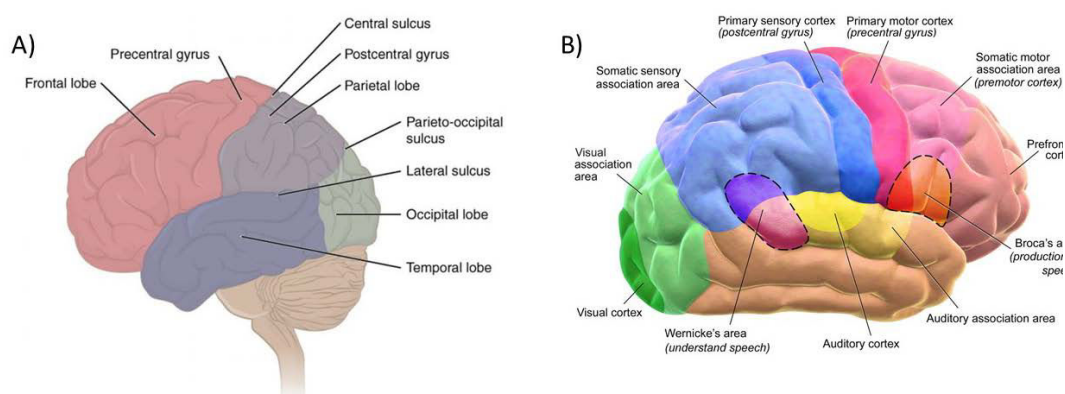


**Figure 5. Schematic representation of cortical lobes and areas.** A) The cortex is subdivided in the frontal, temporal, parietal and occipital lobes B) Primary sensory and motor areas of the cortex. Adapted from <http://library.open.oregonstate.edu/aandp/chapter/14-3-the-brain-and-spinal-cord/> and blausen.com

## 2.2 Evolutionary considerations: neocortex and allocortex

Most of the mammalian cerebral cortex is composed of the neocortex, also known as the isocortex. The neocortex is a six layered structure and encompasses the above-mentioned functional areas. The human neocortex has greatly expanded throughout evolution through mechanisms which are still not fully understood (see sections 3.1.2, 3.4). The cerebral cortex is also composed of the allocortex, a region that is phylogenetically older.

The allocortex is characterized by having only a three or four layered organization and is subdivided into the paleocortex, the archicortex and the peri-allocortex:

- Paleocortex: thin primitive cortical tissue composed of three cellular layers. Includes areas such as the olfactory bulb, olfactory tubercle and piriform cortex.
- Archicortex: this contains four layers and is represented by the hippocampus.
- Peri-allocortex: this is a transition zone between the neocortex and the allocortex. It includes regions such as the anterior insular cortex, the entorhinal cortex, the presubicular cortex, and the retrosplenial, supracallosal and subgenual areas.

My thesis work addressed aspects related to the development of the neocortex. From this section onwards I will thus focus on this region in particular.

## 2.3 Cellular diversity in the neocortex

The cerebral cortex is composed of a great variety of cellular types. In the early 20<sup>th</sup> century Ramon y Cajal depicted in detail these morphologically diverse cells. Broadly, across the neocortex these are divided into three main types: projection or pyramidal neurons (PN), interneurons, and glia.

### 2.3.1 Glia

In 1846 Virchow defined glial cells as ‘the glue of the brain’, attributing them a connective function, a view which remained for many years. However, already in the late XIX century Ramon y Cajal had foreseen the importance of these cells for a plethora of brain functions (Ramon y Cajal, 1909, reviewed by Garcia-Marin et al., 2007). Glial cells are subdivided into macroglia (i.e. astrocytes and oligodendrocytes) and microglia. Macroglial cells derive from neuroepithelial cells and thus from the same progenitors

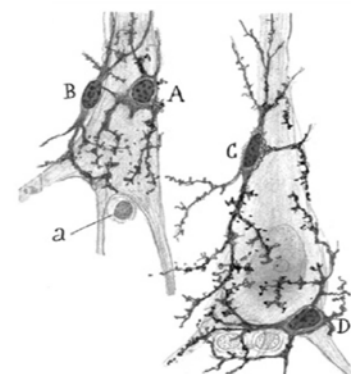


**Figure 6.** Cajal's drawings of astrocytes. A, B, C, D indicate astrocytes surrounding the soma of neurons in the pyramidal cell layer of the hippocampus. Adapted from Garcia-Marin et al., 2007.

responsible for neuron production. Astrocytes are star-shaped cells key for controlling synapse formation and pruning, synaptic communication and plasticity, ion homeostasis and neuronal metabolism (Figure 6). Oligodendrocytes generate myelin sheaths wrapping neuronal axons, which speed up conduction and also provide metabolic support (reviewed by Allen and Lyons, 2018).

Finally, microglia are known as the ‘brain resident macrophages’. They arise from the yolk sac and colonize the CNS from early stages of development. Microglia interact with most of the CNS components both during embryonic and postnatal development, and they are tightly regulated by the CNS environment. They are responsible for elimination of dead cells, synapses and antigens endangering the CNS. Additionally, they regulate neuroinflammatory responses (reviewed by Colonna and Butovsky, 2017 Li and Barres, 2017).

### 2.3.2 Projection neurons and interneurons

The neocortex is a six layered structure formed in an inside-out pattern: projection neurons born first occupy the deeper layers of the cortex, whilst upper layer neurons are born at later stages of corticogenesis. Each layer is characterized by the presence of specific projection neurons and interneurons with a characteristic identity and projection pattern. The thickness and architecture of these layers varies depending the cortical areas (Figure 7).

#### *Interneurons*

Interneurons represent 20-30% of the cortical neurons. They make local connections spanning across multiple layers and influencing neuronal circuits (Lodato and Arlotta, 2015). Interneurons are very heterogeneous and it is estimated that up to 50 different subtypes may be present in the cerebral cortex (Lim et al., 2018). They have classically been characterized by a combination of features: morphology, connectivity and biochemical properties. More recent studies have added another classification system by considering their transcriptional

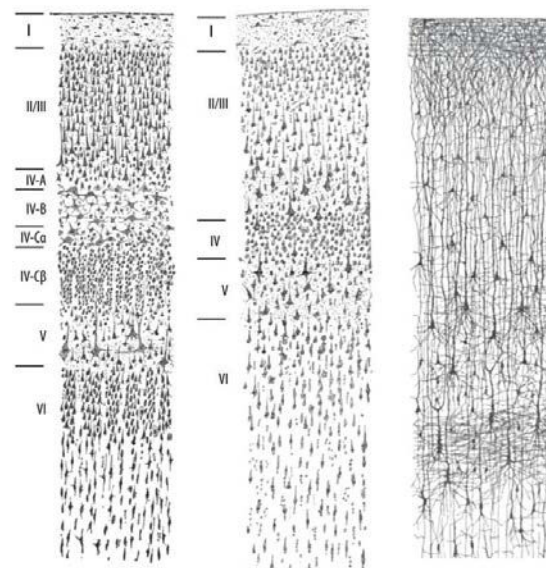


**Figure 7. Drawings of neocortical layers from Ramon y Cajal, 1911.** Left: Nissl staining of the human adult visual cortex. Middle: Nissl staining of the human adult motor cortex. Right: Golgi staining of an infant (one month and a half) human neocortex.

programs (Lim et al., 2018). Broadly, cortical interneurons can be divided in three different ‘classes’, which then can also be subdivided in ‘subclasses’.

**Parvalbumin (PV)+ fast-spiking cells** are the largest class of interneurons in the cortex. They are mostly found in deep layers (chandelier cells, basket cells and translaminar cells), although some subtypes are also found in more superficial layers (chandelier and basket cells).

**Somatostatin (SST)+ interneurons** are subdivided in Martinotti and non-Martinotti cells. Martinotti cells are localized both in upper and lower layers of the cortex, but their most characteristic features is their ascending axon which is highly branched in layer 1. Non-Martinotti cells come in two flavors: one subtype is found across all the cortical layers, and the other subtype is mainly found in deep layers and is characterized by the presence of long projecting axons connecting with other neocortical regions. Finally, the third class is constituted by **interneurons expressing the serotonin receptors 5HT3a**. The most abundant amongst the latter are those expressing vasoactive intestinal peptide (VIP), and are mostly localized in upper layers (reviewed by Lim et al., 2018, Figure 8 right panel).

In the mouse, it has been shown that interneurons derive from the ganglionic eminences (GE) localized in the subpallium, and they migrate long distances to integrate into the developing cortex (reviewed by Marin, 2013, Laclef and Metin, 2018, Lim et al 2018, Figure 8 left panel). However, the origin of primate human interneurons has been controversial: some studies support that in primates interneurons are also generated in the dorsal telencephalic germinal zones (Letinic et al., 2002, Rakic and Zecevic, 2003, Jakovcevski et al., 2011, Al-Jaberi et al., 2015), whilst others support that primate interneuron production occurs predominantly in the GE, as it happens in the mouse brain (Hansen et al., 2013, Ma et al., 2013).

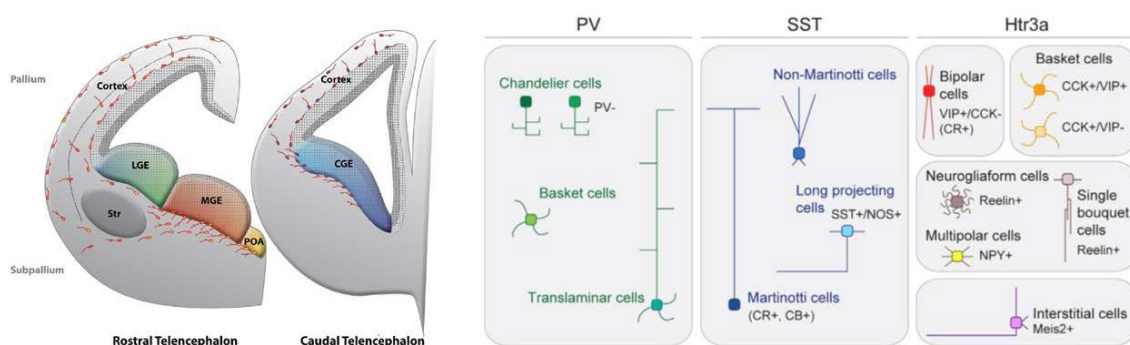


**Figure 8. Cortical interneuron origin and diversity.** On the left: schematic representation of murine coronal brain sections at rostral and caudal regions. Interneurons derive from the ganglionic eminences found in the ventral region of the telencephalon, the subpallium. On the right: schema of cortical interneuron classification. Broadly, interneurons are divided in PV, SST and HTR3A classes. These groups are further subdivided based on location, target and/or gene expression. Adapted from Laclef and Metin, 2018, Lim et al., 2018.

### Projection neurons

PN glutamatergic neurons constitute around 80% of the cells present in the cortex. They are generated by neuronal progenitors localized in the proliferative zones of the dorsal telencephalon (see section 3). Deep layer neurons (layers V-VI) are produced during early corticogenesis (E11.5-E14.5 in the mouse), whilst upper layers neurons (layers II-IV) are produced at later stages (E14.5-E17.5). The latter migrate past the former to reach their final location. Although it is a highly broad and simplistic categorization, PNs are classified by their axonal target (Figure 9). They are broadly classified as intracortical or corticofugal neurons.

Intracortical neurons project to other parts of the cortex and are mainly located in upper layers (Lodato et al., 2015). Intracortical neurons that project their axons to the same hemisphere and/or area are called associative PN. PN whose axons target the opposite hemisphere are called commissural PN (Lodato and Arlotta, 2015).

Corticofugal neurons are mostly found in deep layers and send projections outside of the cortex. Corticothalamic PN project to different nuclei of the thalamus to regulate sensory input. Subcerebral PN send their axons to distinct targets below the brain such as the pons and other nuclei of the brainstem. They also target the superior colliculus and the spinal cord. This simplified classification is far from covering the enormous PN variety in the neocortex. For instance, the presence of PN with multiple targets was identified by Cederquist and colleagues (2013), and further confirmed by Han and co-workers (2018) in a recent study analyzing the molecular

profile of approximately 600 visual neurons at a single cell resolution.

In the last five years big progress has been achieved regarding molecular profiling of PN types. An antibody-based cell isolation approach followed by transcriptome analyses (Molyneux et al., 2015)

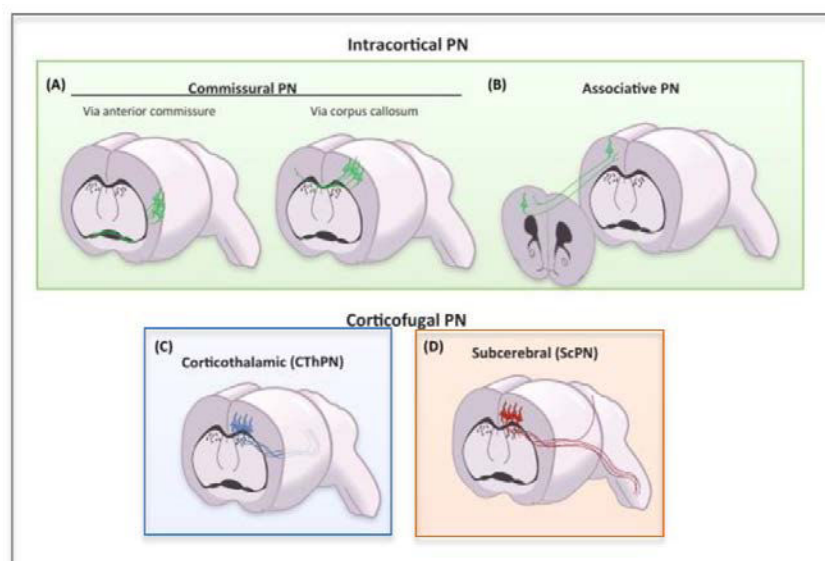


**Figure 9. Classification of projection neurons based on their target.** PN: projection neuron, CThPN: corticothalamic projection neuron, ScPN: subcerebral projection neuron. Adapted from Lodato et al., 2015.

already determined molecular profiles characteristic of distinct sets of cortical neurons. This study highlighted how specific types of neurons are characterized by a subset of specific genes, providing a fingerprint for the neuronal population (Molyneaux et al., 2015, reviewed by Mancinelli and Lodato, 2018). Recently, single cell RNA-sequencing technology has revolutionized the field, providing a whole new spectrum of possible 'cell-grouping or clustering' according to the molecular profile. Ziesel and colleagues (2015) performed the first unbiased sampling of the murine somatosensory cortex, distinguishing specific interneuron and PN subtypes in fitting with previous molecular classification. Afterwards, Tasic and co-workers performed single cell RNA-sequencing of distinct layers of the visual cortex. They performed the same approach in the anterior lateral motor cortex, which allowed them to compare population differences across two distinct cortical areas (Tasic et al., 2016 Tasic et al., 2018). Amongst the cell types described, novel, not previously identified molecular neuron subclasses were found. Nearly all the interneuron cell types were present in both cortical areas, whereas most types of projections neurons were exclusively found in one of the two areas (Tasic et al., 2016, Tasic et al., 2018, reviewed by Mancinelli and Lodato, 2018).

The mechanisms governing neuronal specification and identity are still being massively studied. Some studies suggest the existence of neuronal progenitor subpopulations responsible for the production of specific neuronal subtypes (see section 3.3). However, other mechanisms instructing cell identity occur outside of the proliferative zones. A complex network of TFs interacting with one another at early stages of post-mitotic development instructs neurons to adopt a determined fate. For instance, *Satb2* is critical for specification of upper layer PN, more precisely commissural callosal PN, whereas *Tbr1* and *Fezf2* instruct corticothalamic and corticospinal identities, respectively (reviewed by Lodato and Arlotta, 2015). The above-described recent advanced methods for molecular and transcriptional profiling will certainly contribute to elucidate the combination of factors acting as fingerprints at early stages of post-mitotic development which are crucial for establishment and maintenance of a precise neuronal identity.

### **3. Cortical development: neural progenitor diversity and neuronal production**

Cortical development depends on diverse types of progenitor cells, which produce post-mitotic neurons that migrate across the developing cortical wall to find their appropriate position in the cortical plate (CP). Rodents have been extensively used as models to unravel key features of corticogenesis. However, they are lissencephalic species and lack the complex



progenitor cell diversity found in gyrencephalic species (ferret, primate). My PhD work has been focused on studying a mouse model for a severe human cortical malformation. It is thus pertinent to describe neuronal progenitor cell behavior in lissencephalic and gyrencephalic cortices to better understand how pathological mechanisms in neuronal progenitors could contribute to both rodent and human heterotopia phenotypes.

In this section, I will focus on several aspects of embryonic development and I will discuss: 1) the different progenitor cell types in the developing cortex and their contribution to neocortical expansion; 2) specific features of apical radial glial cells; 3) the multipotency of the different progenitor types 4) the radial unit hypothesis; 5) aspects related to cortical area specification; and 6) mechanisms of neuronal migration.

### **3.1 Progenitor cell types (adapted from Uzquiano et al., 2018)**

#### **3.1.1 Apical progenitor cells: neuroepithelial cells (NEs) and apical radial glial cells (aRGs)**

The walls of the neural tube are populated by **neuroepithelial cells (NEs)** that possess an apico-basal polarity with attachment of their basal processes to the basement membrane (BM) and junctional coupling at the apical side. These NEs undergo the distinctive process of interkinetic nuclear migration (INM) during the cell cycle: their nuclei move apico-basally within the neuroepithelium, entering M-phase at the apical surface (Bertipaglia et al., 2017). NEs are characterized by the presence of occludin-positive (+) tight junctions (Aaku-Saraste et al., 1996), as well as gap junctions for inter-cellular connections and the flux of small molecules, thus enabling cellular communication (Elias and Kriegstein, 2008). They have a prominin+ apical domain that accommodates a primary cilium protruding into the ventricles (Taverna et al., 2014), which senses signals from the cerebrospinal fluid (CSF) that will influence NE behavior (Lehtinen and Walsh, 2011, Arbeille et al., 2015).

NEs divide in a symmetric proliferative fashion, amplifying their numbers and hence the neural progenitor pool (Figure 10). Upon the onset of neurogenesis from embryonic day (E)10 to 12 of murine development, NEs transit from a purely proliferative to a neurogenic state (Gotz and Huttner, 2005, Matsuzaki and Shitamukai, 2015), while their tight junctions are gradually annexed by an adherens junction (AJ) belt that is characterized by the presence of proteins such as N-cadherin and zona occludens (ZO)-1 (Aaku Saraste et al., 1996). Consequently, NEs become **apical radial glial cells (aRGs)** that comprise the predominant neuronal progenitor cell type within the developing neocortex (Malatesta et al., 2000, Noctor et al., 2001, Noctor et al., 2004, Figure 10).

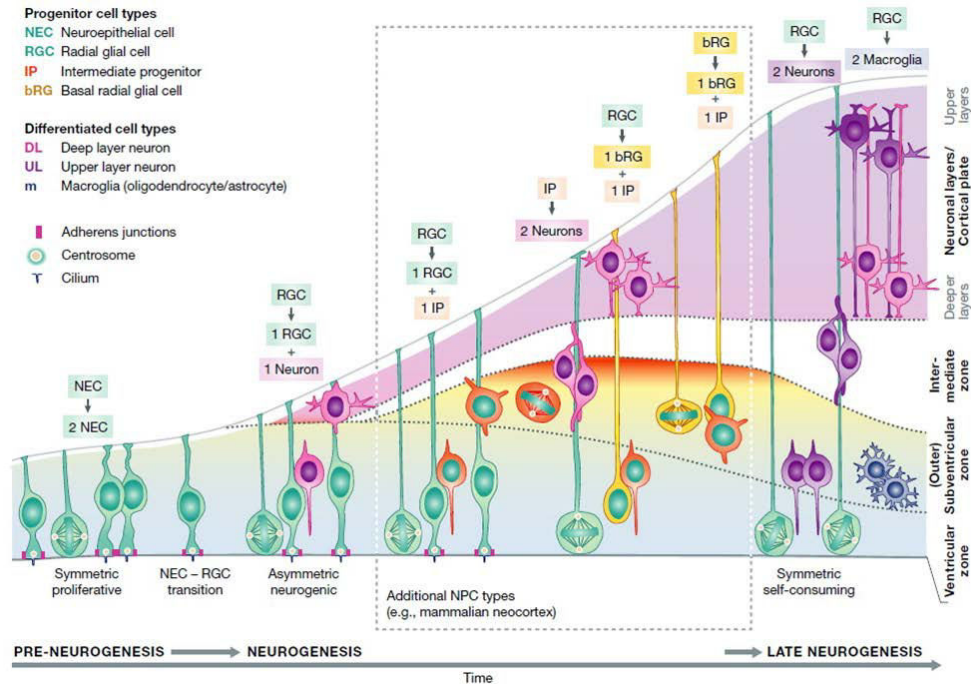


**Figure 10. Schematic representation of cortical development.** The dashed line box contains the different progenitor cell types typically found in the mammalian neocortex, although not all the possible daughter cell outcomes are shown. From Paridaen and Huttner, 2014.

aRGs are also highly polarized cells, exhibiting basal processes attached to the BM, and apical processes linked by AJs and forming a transition region (termed here the 'ventricular surface (VS)') with CSF in the ventricles (Figure 11). As for NEs, aRG apical domains are prominin+ and

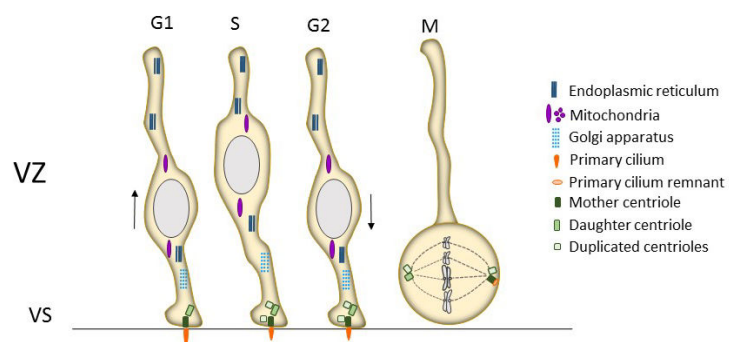


**Figure 11. Schematic representation of apical radial glia undergoing interkinetic nuclear migration.** The nuclei oscillates from the basal to the apical part of the VZ through the different stages to cell cycle. aRGs possess a long basal process reaching the basal membrane. In interphase, they have an apical process reaching the ventricular surface. VZ: ventricular zone, VS: ventricular surface. Adapted from Uzquiano et al., 2018.

also contain a primary cilium (Taverna et al., 2014). Their basal process has been extensively described to be a scaffold for migrating neurons to reach their positions in the CP (Borrell and Gotz, 2014). aRGs also undergo INM, although the nuclear oscillation is restricted to the ventricular zone (VZ), where their somata reside (Gotz and Huttner, 2005). Due to these highly dynamic nuclear movements during the cell cycle, the VZ is often described as a pseudostratified neuroepithelium. How aRGs limit their INM range (i.e. to the thickness of VZ) remains vastly unexplored. Watanabe and colleagues (2018) have however, recently shown

how differentiating cells act as a fence for aRGs thus delimiting the VZ and the INM basally-directed movement. Breaking this 'differentiated cells-barrier' causes an aRG aberrant behavior: their nuclei over-migrate basally and cell cycle progression is impaired (Watanabe et al., 2018).

The transition of NEs to aRGs is critical for determining the size of the initial pool of progenitors available to generate neurons, thereby determining the final neuronal output and brain size (Fernandez et al., 2016). Several factors involved in this transition, e.g. fibroblast growth factors (FGFs), are also key for maintaining aRG identity. Notably, FGF10 triggers expression of aRG markers in NEs (Sahara and O'Leary, 2009) and also supports an aRG fate by inhibiting their transition towards a more committed neuronal progenitor (Kang et al., 2009). The Notch signaling pathway has also been described to be important for the transition from NEs to aRGs (Gaiano et al., 2000, Hatakeyama et al., 2004, Martynoga et al., 2012). Whilst they lose tight junctions and develop the AJ belt, aRGs acquire astroglial features (Florio and Huttner, 2014, Gotz et al., 2015) and become positive for a set of astroglial markers, such as the astrocyte-specific glutamate transporter and others. They also express key neurogenic TFs, such as Pax6 (Gotz et al., 1998).

aRGs are more restricted in their proliferative potential than NEs. They mainly undergo asymmetric proliferative divisions in the rodent, self-renewing while producing post-mitotic neurons or neurogenic progenitors (Figure 10). Direct neurogenesis involves the process by which neurons are produced directly from aRGs. On the other hand, indirect neurogenesis refers to the process by which aRGs produce other intermediary types of progenitor cell that will subsequently produce neurons, thereby increasing the net neuronal output.

Another apical progenitor cell type that co-exists with, and is related to, aRGs in the VZ are the **short neural progenitors** (SNP), also known as apical intermediate progenitors (AIPS). SNPs have an apical process as aRGs, however their basal process remains constrained within the VZ and hence does not span the entire cortical wall. SNPs located in the dorsal telencephalon are mainly neurogenic progenitors, producing neurons upon symmetric division (Gal et al., 2006, Stancik et al., 2010). Although they are localized and divide in the VZ, SNPs are positive for the intermediate progenitor marker Tbr2 (Stancik et al., 2010, Hevner, 2019, see next section). Of note, SNPs found in the VZ of the GE are capable of self-renewing, as well as producing other types of progenitors (Pilz et al., 2013).

### 3.1.2 Basal progenitors (BPs): intermediate progenitors (IPs) and basal radial glia-like cells (bRGs), and their implication in cortical expansion.

As corticogenesis progresses, aRGs produce basal progenitors, mainly **intermediate progenitors** (IPs) in the rodent, which are multipolar transit-amplifying progenitors. IPs are Tbr2<sup>+</sup> (Englund et al., 2005) and they divide in a basally located germinal zone: the subventricular zone (SVZ). Several signaling pathways mediate the transition from aRG to IP fate. IPs produced from aRGs leave the VZ using a Robo2-dependent signaling mechanism in order to reach the SVZ (Borrell et al., 2012). The Notch signaling pathway is also an important regulator of IP production since its activity inhibits the production of IPs from aRGs (Mizutani et al., 2007, Martynoga et al., 2012). Another pathway modulating the switch between self-renewal and neurogenic commitment is the Wnt signaling pathway. In early corticogenesis it promotes aRG proliferation (Woohead et al., 2006), while in later stages it is crucial for IP and even neuronal production (Hirabayashi et al., 2004, Munji et al., 2011).

In the mouse, IPs are mainly neurogenic, dividing symmetrically to produce two neurons (Haubensak et al., 2004, Miyata et al., 2004, Noctor et al., 2004, Figure 10). Diverse mechanisms have been described to control this process (Borrell et al., 2012, Laguesse et al., 2015, Haushalter et al., 2017). Although most of the murine IPs mainly undergo terminal divisions to produce neurons, a recent study showed how a small Tbr2<sup>+</sup> population proliferated longer eventually producing up to 12 neurons (Mihalas and Hevner, 2018). In the primate (human) brain IPs have a higher proliferative potential, being capable of self-renewing several times before their terminal division (Ostrem et al., 2017).

The initial pool of aRGs is larger in gyrencephalic than in lissencephalic species and these cells mostly promote indirect neurogenesis by giving rise to a diversity of basally located progenitors. This results in high neuronal production, which will have an effect on cortical size and folding (Fernandez et al., 2016).

Whilst the murine progenitor population comprises predominantly aRGs and IPs, another type of progenitor can be found in very small numbers within the SVZ: the **basal radial glial cells** (bRGs, also known as outer radial glial cells, oRGs), present at less than 1% of the cortical progenitors in mouse (Shitamukai et al., 2011, Wang et al., 2011, Wong et al., 2015). These cells however, represent a large proportion of basal progenitors in gyrencephalic species (Figure 12). Murine bRGs show a different gene expression pattern compared to gyrencephalic species-bRGs, being transcriptionally closer to IPs (Florio et al., 2015). These studies cited

above identified and characterized bRGs in the mouse lateral cortex. However, Vaid and colleagues have recently identified a bRG-like population in the mouse medial cortex, which shows a human-bRG like gene signature (Vaid et al., 2018). These medial cortex bRGs are positive for the human bRG marker Hopx. Additionally, knockdown or overexpression of Hopx led to a decrease or increase of medial cortex bRGs, respectively (Vaid et al., 2018). The authors discussed how the presence of this abundant bRG population in the mouse medial neocortex could support the idea of a common gyrencephalic species from which all mammals evolved (O’Leary et al., 2013, Lewitus et al., 2014). The medial cortex is an evolutionary older region than the lateral cortex. In the context of the above-described hypothesis, it would be expected that there is a ‘gyrencephaly relict’ in medial rather than lateral regions of the cortex (Vaid et al., 2018).

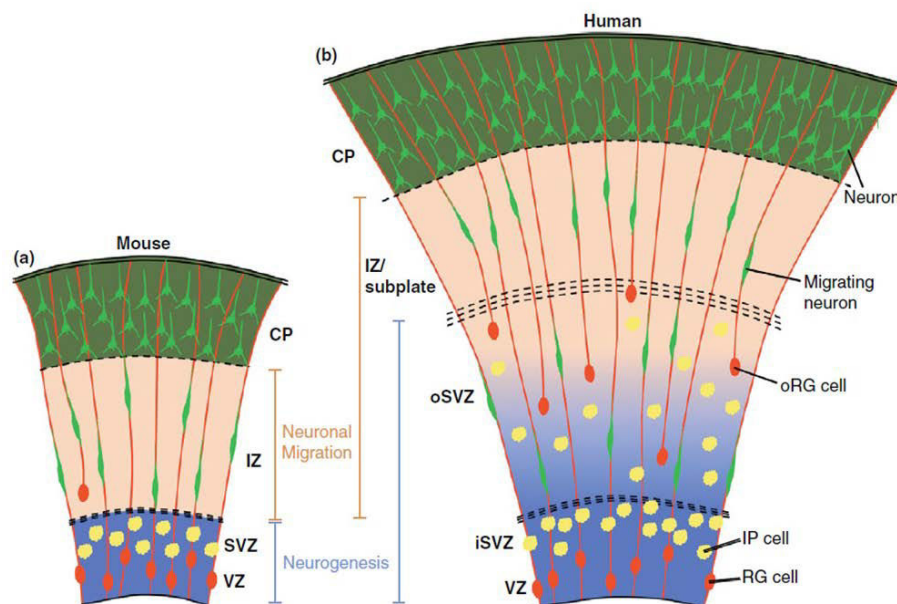


**Figure 12. Mouse versus human cortical development: basal radial glial cells are characteristic of primate-human brains.** VZ: ventricular zone, SVZ: subventricular zone, iSVZ: inner subventricular zone, oSVZ: outer subventricular zone, IZ: intermediate zone, CP: cortical plate, RG: radial glia, IP: intermediate progenitor. From LaMonica et al., 2012.

As shown in the ferret, bRGs are produced from aRGs within a specific time-window early during corticogenesis (LaMonica et al., 2013, Gertz et al., 2014, Martinez-Martinez et al., 2016), and share similar features, as well as a wide range of characteristic markers with aRGs, such as Pax6, nestin and vimentin (Figure 12, Fietz et al., 2010, Ostrem et al., 2017). bRGs are considered essential for neocortical expansion and gyrification, and have been studied in human, ferret and macaque brains (Fernandez et al., 2016, Ostrem et al., 2017). In these species, bRGs are localized in the most basal region of the SVZ, which is bisected by axons into an inner SVZ (iSVZ) and an outer SVZ (oSVZ). The oSVZ is the most proliferative germinal zone

in the developing primate and human neocortex.

bRGs are generally attached to the BM by a basal process, although they often lack the apical process characteristic of aRGs (Fietz et al., 2010, Hansen et al., 2010, Reillo et al., 2011, Wang et al., 2011, Figure 13). Although this is the classical morphological description of bRGs, it has been shown that they can present different combinations of progenitor markers and diverse shapes, and up to five different morphologies have been described in the primate SVZ (Betizeau et al., 2013, Figure 14). Upon cell division and prior to cytokinesis, their soma moves towards the developing CP in a process known as mitotic somal translocation (MST). In the mouse, they mainly divide in an exhaustive symmetric fashion to produce two neurons (Wang et al., 2011). However, in the ferret, and primate (including human) brains, bRGs are capable of self-renewing whilst producing IPs and neurons (Hansen et al., 2010, Betizeau et al., 2013, Gertz et al., 2014, Martinez-Martinez, 2016). This phenomenon results in a greater number of progenitor cells, which in turn increases the final number of neurons produced. Activation of the Notch signaling pathway has been reported to be important for human bRG proliferation (Hansen et al., 2010). aRGs mode of division has been previously associated with daughter cell fate. Briefly, aRGs can divide in a vertical fashion, when the cleavage plane is perpendicular to the VS, or in a horizontal or oblique fashion, when the cleavage plane is parallel or oblique to the VS, respectively (Figure 15, see also section 3.2.3). bRGs have been shown to be produced by aRG horizontal cell divisions (LaMonica et al., 2013, Gertz et al.,

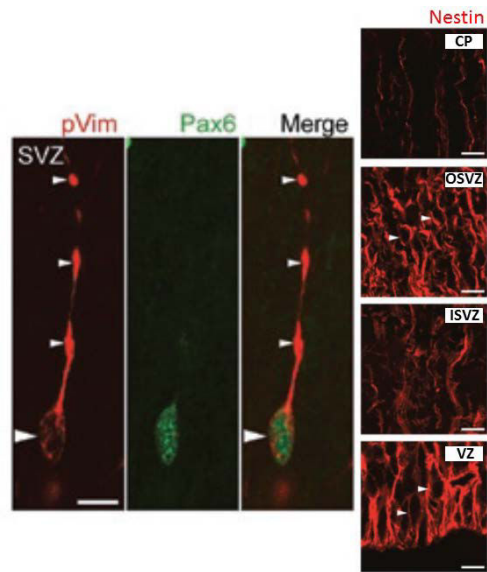


**Figure 13.** Basal radial glial cells have a long basal process reaching the basement membrane and are Pax6, nestin and pVimentin positive. Adapted from Fietz et al., 2010.

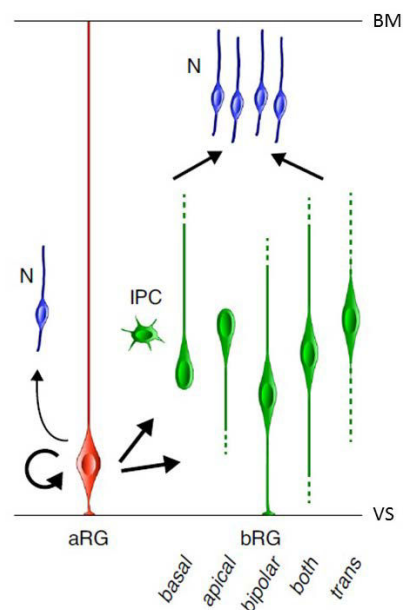


**Figure 14.** Schematic representation of the different basal radial glia morphologies described in the primate SVZ. N: neuron, aRG: apical radial glia, IPC: intermediate progenitor cell, bRG: basal radial glia, VS: ventricular surface, BM: basement membrane. Adapted from Borrell and Gotz, 2014.

shown to be produced by aRG horizontal cell divisions (LaMonica et al., 2013, Gertz et al.,

2014, Martinez-Martinez et al., 2016), although direct delamination of aRGs can also result in bRG production (Gertz et al., 2014, Tavano et al., 2018). In the mouse dorsal telencephalon most aRG divisions are vertical, but in primate-

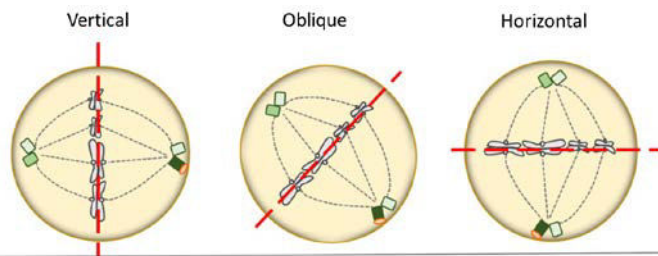


**Figure 15. Schematic representation of apical radial glia spindle orientations.** For simplicity, the basal process has not been represented. Adapted from Uzquiano et al., 2018.

human brains there is a shift towards horizontal divisions, which may be important for bRG production and oSVZ expansion (LaMonica et al., 2013). It is worth noting that the murine GE is the telencephalic region with the biggest diversity of progenitor types and a major production of BPs. GE-AP vertical divisions are less abundant, and proliferative SNPs divide mainly in a horizontal/oblique fashion (Pilz et al., 2013, Falk et al., 2017).

Two molecules were initially described to play a key role in temporally-regulated bRG production and oSVZ seeding in the ferret: *Cdh1* and *Trnp1*. Downregulation of *Cdh1* and *Trnp1* levels promotes horizontal aRG divisions and delamination from the VZ, resulting in bRG production. On the other hand, upregulation of these proteins decreases bRG production, preventing the seeding of the oSVZ (Martinez-Martinez et al., 2016). Knockdown of *Trnp1* in mouse aRGs had been previously correlated with a switch towards horizontal divisions and the production of bRG-like cells, even resulting in the appearance of folds in the otherwise smooth mouse neocortex (Stahl et al., 2013). Other pioneer studies revealed certain genes only present in human aRGs that seem to be crucial for basal progenitor production. This is the case for the growth factor PDGFD. Although the latter is expressed in murine GE-aRGs it is exclusively expressed in dorsally located aRGs in human. Expression of PDGFD or ectopic expression of its receptor PDGFR $\beta$  in the mouse dorsal neuroepithelium induces production of bRG-like cells (Lui et al., 2014). Similarly, Florio and colleagues (2015) found the gene *ARHGAP11B* to be preferentially expressed in human aRGs, and when overexpressed in the mouse neuroepithelium, it led to the generation of BPs (both IPs and bRG-like cells) (Florio et al., 2015). A recent study further reinforced the role of *ARHGAP11B* in bRG production and neocortical expansion (Kalebic et al., 2018). Overexpression of *ARHGAP11B* in the ferret neuroepithelium led to an increased production of proliferative bRGs. Additionally, the neurogenic period was extended and an increase in upper layer neurons was observed (Kalebic et al., 2018).

Related to these studies, other molecules and signaling pathways have since been shown to induce bRG production in the mouse developing cortex. For example, activation of Shh signaling in mouse aRGs during early corticogenesis leads to the expansion of both IP and bRG-like cell populations, resulting as well in the presence of folds in the mouse neocortex (Wang et al., 2016). Forced expression of Pax6 in mouse aRGs and their progeny also induces the generation of primate-like bRGs (Wong et al., 2015). Additionally, forced expression of the zinc finger TF Insm in the mouse neuroepithelium also led to aRG delamination resulting in bRG-like cells production (Tavano et al., 2018). Recently, Emx1-Cre conditional knockout mice for the chromatin remodeling BAF complex subunit BAF155 also showed an increase in bRG-like progenitors (Narayanan et al., 2018). Studies in the ferret have also contributed to shedding light on genes that could be responsible for bRG production. Johnson and colleagues identified the microcephaly gene *Aspm* (see section 5.1) to be important for bRG-like cell production. Knockout ferrets for *Aspm* showed displaced Pax6+ progenitors in the SVZ resembling bRGs. Concomitantly an increased cell death in basal cortical regions was observed, which combined with the premature depletion of the aRG pool at the expense of the bRG-like cell production likely explains the microcephaly phenotype (Johnson et al., 2018). In line with the above mentioned studies, Ju and colleagues (2016) revealed a novel function for *TBC1D3*, a great-ape specific gene which has undergone segmental duplications during evolution, in brain development and bRG production. Expression of *TBC1D3* in the mouse VZ led to the production of primate-like bRGs, indicating the potential role of this gene in neocortical evolution (Ju et al., 2016). Liu and colleagues (2017) identified the primate-specific gene *TMEM14B* as a marker for bRGs. Expression of this gene by *in utero* electroporation in the mouse VZ promoted neuronal progenitor production and expansion of the SVZ. In addition, Nestin-Cre-mediated knock-in mice for *TMEM14B* exhibited cortical folding (Liu et al., 2017). Recently, the human-specific *NOTCH2NL* gene has been shown to be critical for maintaining aRG identity and thus for controlling the final neuronal output (Fiddes et al., 2018, Suzuki et al., 2018). Concomitantly another study showed how overexpression of *NOTCH2NL* promotes IP production (Florio et al., 2018). Although *NOTCH2NL* is a hominid-specific gene, it does not seem to be directly involved in bRG production although it appears to be crucial for neuronal production and possibly neocortex expansion (Fiddes et al., 2018, Florio et al., 2018, Suzuki et al., 2018).



Taken together, these studies open the gate to the discovery of more primate and/or human-specific RG genes that could mediate the switch from aRGs towards basal progenitor production, particularly bRGs, as well as shedding light on the cellular and molecular mechanisms that promote bRG-like identity (Heide et al., 2017). Lastly, it would be of high interest to unravel why in the mouse developing cortex Pax6+ progenitors located outside the VZ sometimes lead to cortical anomalies (Cappello et al., 2012, Insolera et al., 2014, Kielar et al., 2014), while other times they behave as bRG-like cells leading to expansion of the SVZ, an increased number of upper layer neurons and/or cortical area, and ultimately the appearance of fold-like structures on the surface of the brain (Stahl et al., 2013, Florio et al., 2015, Wong et al., 2015, Ju et al., 2016, Liu et al., 2017, Figure 16).

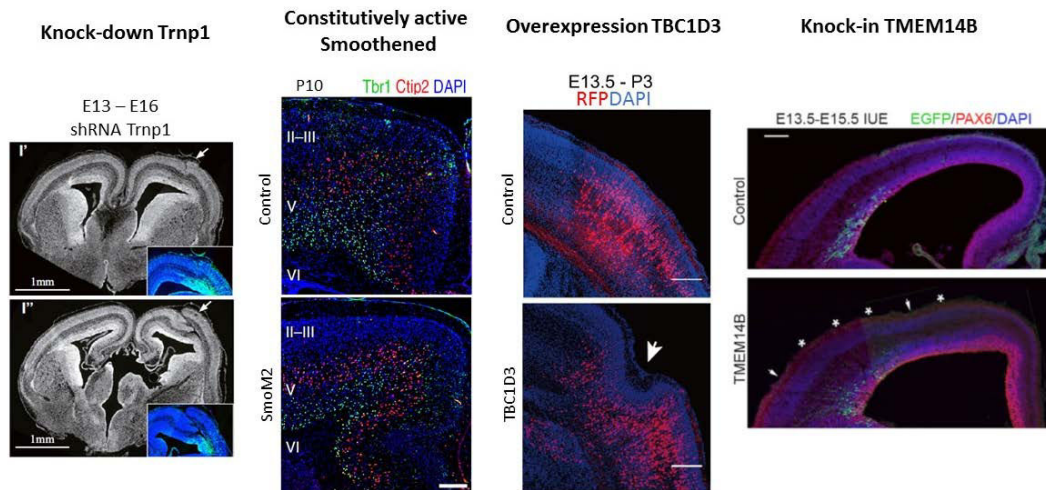


**Figure 16. Forced basal radial glia production in the murine developing cortex can result in the appearance of fold-like structures.** Adapted from Stahl et al., 2013, Wang et al., 2016, Ju et al., 2016, Liu et al., 2017.

The VZ contains aRGs, which move apico-basally through different stages of cell cycle by INM, with mitosis occurring at the VS. It is believed that INM occurs in order to create space in the VZ so more aRGs can undergo M-phase at the VS (Miyata et al., 2014). It has been hypothesized that aRGs that eventually become bRGs may leave the VZ to escape this space constraint, moving basally to the oSVZ while maintaining several aRG traits (Florio and Huttner, 2014). Although they lack apical anchoring, bRGs maintain their basal processes which are likely to be important for their self-renewal potential. For instance, integrin signaling through basal contact has been shown to be important for bRG proliferation and amplification. When integrin signaling was blocked in ferret brain organotypic slices, the pool of cycling progenitors both in the VZ and SVZ was decreased, the effect being more prominent in the SVZ (Fietz et al., 2010). The basal process of bRGs is also important for MST, and the

length, frequency and directionality of MST have been proposed to be associated with brain evolution. In human fetal brain, MST appears to be more frequent than in other species, and the distance travelled by the nuclei seems to be greater, following a straighter pattern of movement towards the pial surface (Ostrem et al., 2017).

Other features related to bRGs are likely to be important for neocortical expansion (i.e. basal fibers contributing to tangential expansion of the neocortex, see section 3.4). Additionally, this cell type is likely to be targeted in neurodevelopmental disorders, which would explain why rodent models often fail to recapitulate patient phenotypes.

### **3.2 Apical radial glial cells: key features mediating their behavior (adapted from Uzquiano et al., 2018).**

In section 3.1 I provided an overview of the different progenitor cell types composing the developing cortex. I have emphasized on the contribution of bRGs to neocortical expansion and gyrification (see also 3.1.2). In the context of my PhD project, I have focused on characterizing specific subcellular features of aRGs, which could be important for their behavior. In this section I will thus discuss aspects of aRG dynamics and subcellular components described to be critical for correct proliferation, differentiation and ultimately overall cortical development.

aRGs continuously proliferate and thus progress through the cell cycle. The latter can be broadly subdivided in two main phases: mitosis (M-phase) at the VS i.e. when replicated chromosomes are separated into the daughter cells; and interphase (G1, S and G2 phases) i.e. the rest of the cell cycle (see Figure 11). Several aspects related to cell cycle overall, or to one specific phase of the cycle can compromise aRG dynamics. Of note, the microtubule cytoskeleton plays a key role in aRGs dynamics. For instance, spindle and astral microtubules ensure correct cell division and spindle orientation. Microtubules are also responsible for the nuclear movement through INM as well as for apically and basally directed trafficking (reviewed by Mora-Bermudez and Huttner, 2015).

In the following subsections I will discuss specific features of aRGs, such as cell cycle length, AJs, mitotic spindle orientation, membrane-bound organelles and microtubule-based organelles. This is a simplified description of aRG dynamics as many subcellular structures and proteins described to be important for one specific aRG feature are also likely to be involved in other processes.

### 3.2.1 Cell cycle length considerations

Cell cycle length in progenitors is associated with aRG neurogenic potential. Early studies suggested that progenitors located in diverse brain regions had different cell cycle lengths, and that the cell cycle lengthened as development proceeds, while switching towards a more neurogenic state (Borrell and Calegari, 2014). Later studies confirmed this initial discovery (Calegari et al., 2005, Lukaszewicz et al., 2005, Arai et al., 2011), pinpointing G1 as the phase responsible for these changes in cell cycle duration (Calegari and Huttner, 2003, Lange et al., 2009, Pilaz et al., 2009, Salomoni and Calegari, 2010). In relative terms, aRG proliferative divisions were found to have a shorter cell cycle length when compared to neurogenic output (Calegari et al., 2005, Arai et al., 2011).

The direct implication of cell cycle length in neural progenitor commitment was shown by pharmacologically inhibiting or knocking-down G1-specific Cdk/Cyclins in mouse embryos. This leads to longer cell cycle and precocious neurogenesis (Calegari and Huttner, 2003, Lange et al., 2009). Accordingly, Pilaz and colleagues (2016) showed recently that mitotic delay promotes neuronal production from aRGs in the *Magoh +/-* mouse mutant. Additionally, the authors used a pharmacological approach to induce mitotic delay, reproducing the phenotype observed in *Magoh +/-* mice (Pilaz et al., 2016).

In agreement, shortening aRG cell cycle bolsters their proliferative capacity. Overexpression of *Cdk4* and/or cyclins leads to shorter cell cycles, accompanied by a higher proliferation rate and an increase of the progenitor pool (Lange et al., 2009, Pilaz et al., 2009, Nonaka-Kinoshita, et al., 2013). Thus, all these studies support the idea that cell cycle length is a parameter regulating progression of neurogenesis and progenitor fate.

Most of the studies mentioned previously were performed in the mouse neuroepithelium, in which G1 clearly appears to be critical in controlling cell cycle duration. However, a recent study performed in ferret, indicates that cell cycle duration of progenitors in this species is mainly mediated by changes in S-phase, since little variation was observed in G1 when comparing different progenitor types (Turrero-Garcia et al., 2016). Of note, regulation of S-phase seems to be important for cell cycle of bRGs (Turrero-Garcia et al., 2016, Wong et al., 2015).

There are hence multiple studies supporting a correlation between cell cycle length in progenitors with their neurodifferentiation potential. Nevertheless, a recent study showed that upon cell cycle arrest of undifferentiated aRGs, these cells still turn on a transcriptional

program associated with the neuronal output they are meant to produce (Okamoto et al., 2016). In this study, single-cell transcriptomics revealed a set of genes whose expression changes over time in undifferentiated aRGs at different developmental stages. In order to address if these transcriptional changes could be altered by defects in cell cycle progression, the authors induced cell cycle arrest of aRGs whilst maintaining them undifferentiated, and performed the same type of single-cell transcriptomics analysis. Strikingly, the pattern of expression of the genes previously identified was not altered (Okamoto et al., 2016), implying that unrelated to cell cycle progression, aRGs at different stages can produce particular neuronal cell types (McConnell and Kaznowski, 1991, Kawaguchi and Matsuzaki, 2016). As it will be discussed in section 3.3.1, it is still under debate how and why aRGs produce the appropriate neuronal cell type and if there are aRG subtypes which produce neurons destined for a specific cortical layer.

### **3.2.2 Polarity complex and cell adhesion molecules**

AJs are localized in a basolateral position in the apical endfeet of aRGs. They are linked to an F-actin belt, and the combination of the two are responsible for the anchoring of aRGs to each other to form the VS. These intercellular complexes are made up of cadherins and its downstream actors (e.g.  $\beta$ -catenin), junctional adhesion molecules (JAMs) and nectins (Aakusaraste et al., 1996, Manabe et al., 2002, Junghans et al., 2005, Kadowaki et al 2007, Singh and Solecki, 2015). The adhesion molecules making up the AJs are linked to the cytoskeleton and they coordinate different signaling pathways triggered in neighboring cells (Singh and Solecki, 2015). Multiple studies have shown that AJ components are critical for aRG proliferation and proper cortical development, highlighting the essential role of AJs and actin in maintaining aRG morphology, polarity and localization. In addition, deregulation of these proteins severely impacts aRG proliferative potential, as well as proper neuronal production and position (Figure 16).

In close vicinity to the AJ belt are localized another set of molecules critical for aRG polarity. When NEs become aRGs and the AJ belt is assembled, the polarity protein Par3 dissociates from the tight junctions characteristic of NEs and associates with the newly formed AJs. This triggers the recruitment of other polarity proteins such as  $\alpha$ PKC and Par6 to the proximity of AJs (Manabe et al., 2002). Polarity proteins are not only essential for maintaining aRG morphology, but they can also act as fate determinants upon cell division (Costa et al., 2008).

Although the Par polarity complex,  $\alpha$ PKC, Cdc42, and the Crumbs complex (Singh and Solecki, 2015) are often referred to as the ‘polarity complex’, other proteins such as RhoA, Pals1, Shootin1 and Llg1 are also important for aRG polarity, morphology and behavior (Beattie et al., 2017, Cappello et al., 2012, Jossin et al., 2017, Sapir et al., 2017) .

The outcome of deregulating aRG apical complex proteins often converges in the disruption of the aRG apical domain, which in most cases results in a decrease of the aRG pool and altered distribution of both cycling progenitors and post-mitotic neurons (Figure 17).

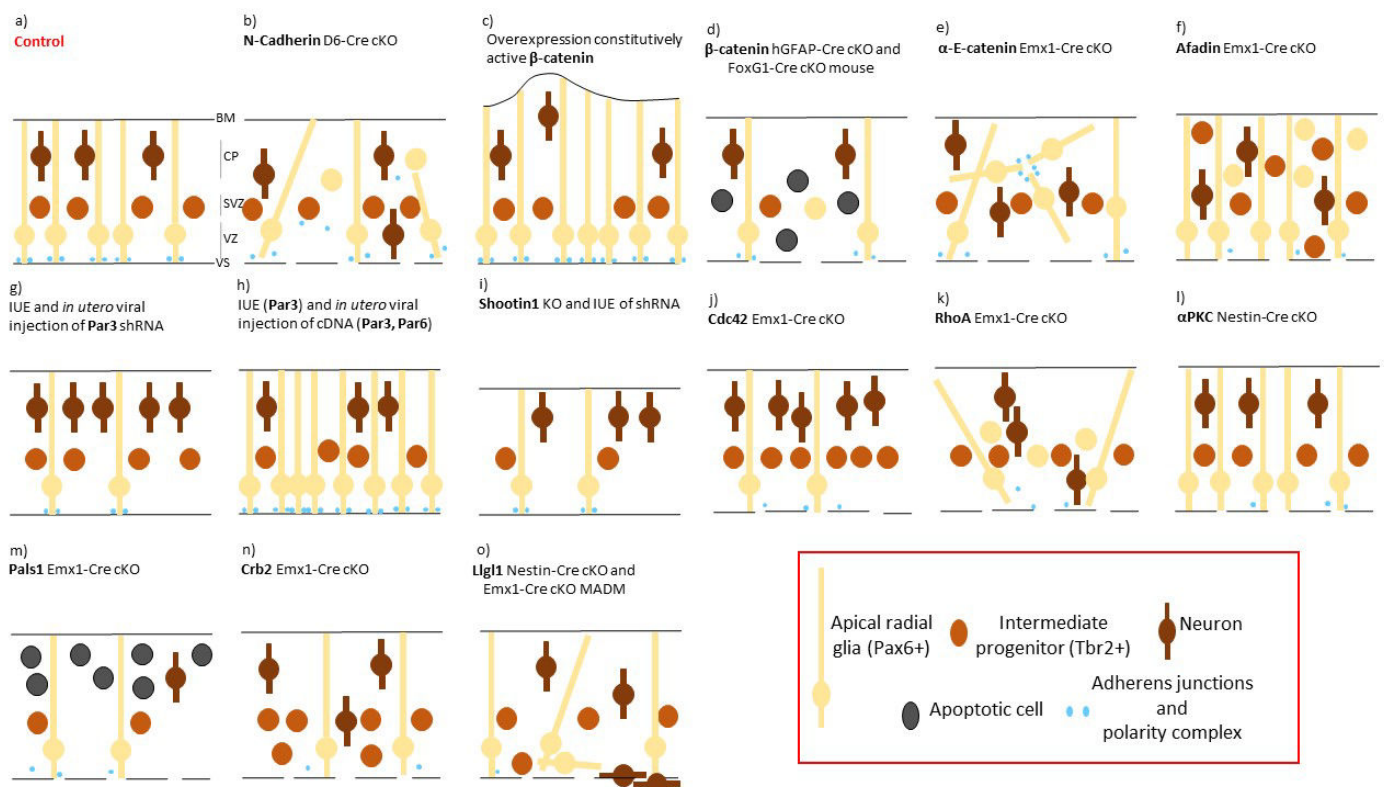


**Figure 17. Schematic representation of cortical phenotype upon alteration of adherens junctions or polarity complex components.** BM: basement membrane, CP: cortical plate, SVZ: subventricular zone, VZ: ventricular zone, VS: ventricular surface. Adapted from Uzquiano et al., 2018. Kadowaki et al., 2007 (b), Chenn and Walsh, 2002 (c), Junghans et al., 2005, Gan et al., 2014 (d), Schmid et al., 2014 (e), Gil-Sanz et al., 2010 (f), Costa et al., 2008, Bultje et al., 2009 (g), Costa et al., 2008, Bultje et al., 2009 (h), Sapir et al., (2017). (i), Cappello et al., 2006 (j), Cappello et al., 2012 (k), Imai et al., 2006 (l), Kim et al., 2010 (m), Dudok et al., 2016 (n), Beattie et al., 2017, Jossin et al., 2017 (o).

### 3.2.3 Mitotic spindle and cleavage plane

Invertebrate models have been used extensively to study the relationship between aRG spindle orientation and daughter cell fate (reviewed by di Pietro et al., 2016). In these models, cell fate determinants are asymmetrically positioned within the cell prior to mitosis. When the mitotic spindle is oriented parallel to the apico-basal gradient of fate determinants, the cleavage furrow gives rise to an uneven repartition of these factors between the daughter cells, leading to an asymmetric cell division. On the contrary, when the mitotic spindle is

positioned perpendicular to this gradient, the cleavage furrow will be oriented in the same direction of the gradient, leading to an even distribution of fate determinants: the progeny generated will acquire the same identity.

Initially it was thought that a similar situation occurs in mammalian aRGs. More precisely, symmetric divisions would be achieved by insertion of the cleavage furrow perpendicular to the VS (vertical divisions), whilst a parallel or oblique insertion of the latter (horizontal or oblique divisions, respectively) would lead to an asymmetric cell division producing two daughter cells with different fate (spindle orientations depicted in Figure 15) (Chenn and McConnell, 1995). However, association between orientation of the cleavage plane and aRG daughter cell fate is not as straightforward, and this will be discussed further here and in section 3.2.4.

Mitotic spindle assembly and attachment to the cell cortex is a tightly controlled process which can influence distribution of cell fate determinants and retention of epithelial features (i.e. apical and basal processes) upon mitosis (see section 3.2.4). Centrosomes, which are localized in the apical processes of aRGs during interphase, move a short distance basally before undergoing duplication and forming the spindle poles (Hu et al., 2013). The latter nucleate microtubules constituting the mitotic spindle. They are also associated with astral microtubules, which link the mitotic spindle to the cell cortex. Mitotic spindle orientation is regulated by a complex of proteins involved in this attachment of the mitotic spindle to the cell cortex by astral microtubules (Figure 18). This complex involves the GoLoco domain-containing protein LGN, NuMA and the dynein-dynactin complex (reviewed by di Pietro et al., 2016). Several studies have shown the impact of altering the level of these proteins on spindle orientation and aRG self-renewal potential and progeny fate after cell division. LGN is crucial for maintaining vertical cell divisions, when knocked-down it leads to randomization of the mitotic spindle resulting in the presence of aberrantly positioned cycling progenitors (Morin et al., 2007, Konno et al., 2008). The LGN-

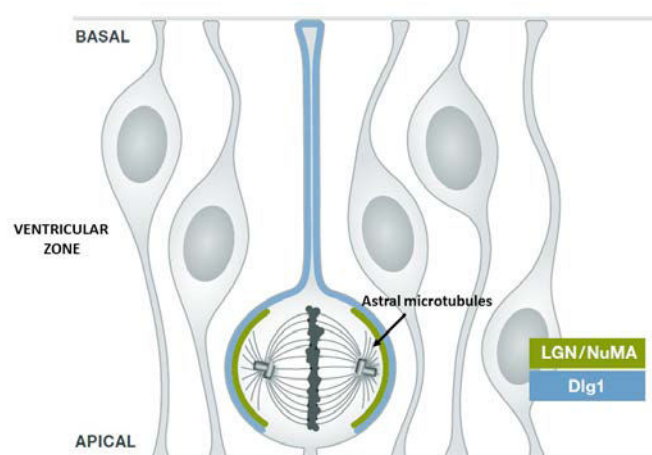


**Figure 18. Schematic representation of mitotic spindle anchoring to the cell cortex in apical radial glia cells.** Adapted from di Pietro et al., 2016

interacting protein Dlg1 also controls vertical divisions (Saadaoui et al., 2014). Mitotic spindle orientation defects have often been associated with cortical malformations (Bizzotto and Francis, 2015). Mutations in the dynein regulators Lis1 and Nde1 lead to spindle orientation defects, resulting in apical progenitor depletion, and thus affecting neuronal production (Feng and Walsh, 2004, Yingling et al., 2008). Tctex-1 (*Dynlt1*), the light chain component of the dynein motor complex, and the guanine nucleotide exchange factor Lfc (*Arhgef2*) also regulate spindle orientation in a convergent fashion, determining the balance between aRG proliferation and neuronal differentiation (Gauthier-Fisher et al., 2009).

Many genes involved in centrosome-related functions are associated with microcephaly (see section 5.1) and have been reported to influence spindle orientation. For instance, decreased levels of *Aspm* and *Cdk5rap2* perturb spindle orientation, resulting in a reduced aRG pool and eventually a decreased neuronal output (Fish et al., 2006, Lizarraga et al., 2010). Related to other cortical malformations, mutations in *Eml1*, associated with subcortical heterotopia (see sections 5.3 and 6), also lead to an increase in oblique divisions, as well as to increased mitotic spindle length (Kielar et al., 2014; Bizzotto et al., 2017). Although these disease-associated proteins have been associated with spindle orientation defects, it still remains to be elucidated if this is a main and primary phenotype observed upon their deregulation. Other microtubule associated processes, such as ciliogenesis, centrosome biogenesis and correct mitotic spindle assembly could also be altered (Ding et al., 2019, Lizarraga et al., 2010, Insolera et al., 2014, Garcez et al., 2015, Gabriel et al., 2016, Jayaraman et al., 2016, Bizzotto et al., 2017, see sections 3.2.6, 3.2.7, 5.4). Thus, further work is required to question if abnormal spindle orientation represents the direct cause and/or the consequence of other defects potentially responsible for cortical anomalies. Unrelated to spindle orientation, Delaunay and co-workers (2014) showed that the mitotic spindle *per se* could determine daughter cell fate upon aRG division: cells that become neurons preferentially arise from the daughter cell (often apical) receiving the pole with the larger-spindle volume (Delaunay et al., 2014).

Although still controversial, spindle orientation has been suggested to regulate NE and aRG progeny fate, and to ensure that the aRG pool expands enough to produce the appropriate number of neurons. Spindle orientation changes towards a horizontal/oblique aRG division have been associated with the generation of daughter cells which differentiate prematurely (Fish et al., 2006, Gai et al., 2016). In addition, as described in the previous section, bolstering horizontal and oblique divisions in the mouse neuroepithelium in early-mid corticogenesis has

been associated with the production of bRGs (Shitamukai et al., 2011, Stahl et al., 2013, Wong et al., 2015), as well as in ferret and human corticogenesis, (LaMonica et al., 2013, Martinez-Martinez et al., 2016). Thus, tilting the mitotic spindle resulting in an horizontal/oblique division can lead to depletion of the aRG pool and a decreased number of neurons (Feng and Walsh, 2004, Fish et al., 2006, Yingling et al., 2008, Gauthier-Fisher et al., 2009, Gai et al., 2016), to the presence of aberrantly positioned cycling progenitors (Konno et al., 2008, Insolera et al., 2014), as well as being related to the production of IPs and bRGs (Fish et al., 2006, Shitamukai et al., 2011, LaMonica et al., 2013, Stahl et al., 2013, Wong et al., 2015, , Gai et al., 2016, Martinez-Martinez et al., 2016). In addition, recently it has been reported that randomization of the mitotic spindle can also alter the ratios of different apical progenitor populations, decreasing aRG numbers whilst increasing the amount of SNPs (Falk et al., 2017). Therefore, the direct outcome of changes in spindle orientation still needs to be defined and could differ in each mutant situation. The above-mentioned studies could suggest that alternative mechanisms are responsible of spindle orientation defects and hence of upstream of events such as cell delamination and daughter cell fate determination.

### 3.2.4 Apical and/or basal process and radial glia cell identity

The apical and/or basal processes have often been associated with aRG cell fate and progenitor proliferative potential. For instance, it has been proposed that upon aRG division, the daughter cell inheriting the apical domain, would retain aRG identity, while the cell deprived of this apical structure would be committed to a different fate (Kosodo et al., 2004, Marthiens and ffrench-Constant, 2009, Figure 18), e.g. by being more restricted to the neuronal lineage (but see below for opposing views). Since asymmetric inheritance of the apical structure may lead to differentiative divisions, a slight tilt in spindle orientation, enough for the cleavage plane to bypass the apical domain, would thus trigger an asymmetric cell division (Kosodo et al., 2004, Marthiens and ffrench-Constant, 2009, Figure 19). Studies performing

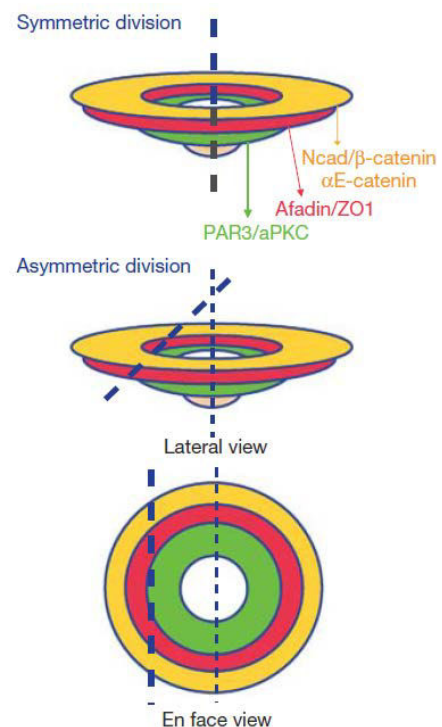


**Figure 19. Schematic representation of apical domain inheritance upon apical radial glia division.** Adapted from Marthiens and ffrench-Constant, 2009.



live-imaging instead of analyses in fixed immunostained tissue, showed that only in a relatively low proportion of cell divisions during the neurogenic period of corticogenesis, the apical domain was uniquely inherited by one of the daughter cells (Konno et al., 2008, Asami et al., 2011, Shitamukai et al., 2011). Accordingly, these observations suggest that factor(s) other than apical domain inheritance determine cell fate, and this is in agreement with the fact that during mouse neurogenesis there is a majority of vertical divisions (Matsuzaki and Shitamukai, 2015) not all of them being proliferative and symmetric. Thus, although classically the inheritance of the apical epithelial structure, dependent on cleavage furrow insertion, was believed to be key to acquiring proliferating aRG identity, this vision is currently changing, indicating that other features are crucial to determine daughter cell identity and to provide an aRG identity and self-renewal potential.

In the last decade, the aRG basal process has emerged as a key feature to determine cell fate determination and proliferative potential (Konno et al., 2008, Fietz et al., 2010, Tsunekawa et al., 2012). For instance, basal process-dependent integrin signaling appears to be important for maintaining aRG and bRG proliferative potential (Fietz et al., 2010). In addition, Tsunekawa and co-workers (2012) described how the mRNA of cyclin D2, responsible for G1 progression, is mainly present in aRG basal processes. This implies that upon aRG cell division, only the daughter cell inheriting the basal process will progress through G1 while retaining proliferative potential. Emphasizing the importance of epithelial structure inheritance, in zebrafish it was described how upon aRG division, aRG-fated daughter cells often lose their apical endfoot, which then regrows allowing maintenance of the whole epithelial structure (i.e. apical and basal processes) (Alexandre et al., 2010). Therefore, inheritance, re-growth and maintenance of epithelial features (apical and basal processes) seem to be a key factor promoting aRG fate (Matsuzaki and Shitamukai, 2015).

Although in this section I have focused on the importance of apical and basal processes for progenitor cell proliferation and fate acquisition, these structures are home to many other features key for aRG behavior. For instance, the apical process terminates by an endfoot possessing a modified centrosome, the basal body, docking a primary cilium. The importance of these other structures for maintaining aRG morphology, polarity and regulating multiple signaling pathways will hence be discussed in sections 3.2.7 and 5.4. Within the apical endfoot is localized as well the AJ-actin belt, previously discussed in section 3.2.2.

### 3.2.5 Membrane-bound organelles: mitochondria, endoplasmic reticulum, Golgi apparatus

Although membrane-bound organelles are crucial for a variety of functions such as cellular metabolism and protein processing, their role in aRGs is vastly unexplored.

Related to **mitochondria**, loss of their function in aRGs leads to defects in proliferation, disruption of cell cycle exit, and inability of cells to differentiate into neurons, resulting in cortical thinning (Khacho et al., 2017). Additionally, the acute loss or gain-of-function of Prdm16, a TF that regulates mitochondria reactive oxygen species (ROS) levels, leads to defects in aRG proliferation, whereupon differentiating cells show aberrant morphologies and locations in the cortical wall (Inoue et al., 2017). Interestingly, mitochondria morphology has been reported to differ between aRGs, IPs and neurons (Khacho et al., 2016). While mitochondria morphology is elongated both in aRGs and neurons, it has a fragmented appearance in IPs (Khacho et al., 2016, Figure 20).

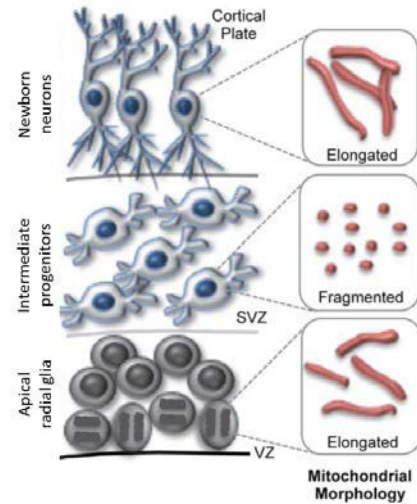


**Figure 20. Mitochondria morphology differs between apical radial glia cells, intermediate progenitors and newborn neurons.** Adapted from Khacho et al., 2017.

The **endoplasmic reticulum** (ER) has been further explored in aRGs, in particular the role of ER stress and the Unfolded Protein Response (UPR). The UPR seems to regulate the transition from direct neurogenesis to indirect neurogenesis. Particularly, the gradual suppression of basal UPR activity promotes the transition from direct to indirect neurogenesis in aRGs as corticogenesis proceeds (reviewed by Laguesse et al., 2015). The role of the UPR in aRG mode of division is supported by studies in genetic and infective mouse models whereupon ER stress induction and UPR upregulation in aRGs prolonged direct neurogenesis, resulting in reduced IP production (Laguesse et al., 2015, Gladwyn et al., 2018). The final neuronal output was hence compromised and mice from both studies displayed severe microcephaly (Laguesse et al., 2015, Gladwyn et al., 2018).

Taverna and colleagues (2016) described recently **Golgi apparatus** behavior and distribution in aRGs. The Golgi localizes in the apical process of aRGs and is organized in a series of separated stacks, not associated with the centrosome (Figure 21). When an aRG commits to an IP fate, the Golgi translocates towards a more basal position, bypassing the nucleus and locating itself in a basally located process (Taverna et al., 2016). Another role ascribed to Golgi

is in symmetric vs asymmetric divisions, since a pool of the pericentriolar fate determinant Mindbomb1 (Mib1) is stored in this organelle (Tozer et al., 2017).

In asymmetric divisions in the chick spinal cord neuroepithelium Mib1 is inherited by the daughter cell that differentiates into a neuron (Tozer et

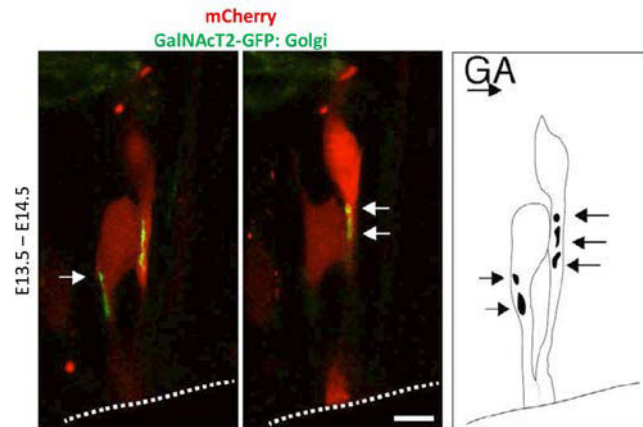


Figure 21. The Golgi apparatus localizes in the apical process of radial glia cells. Adapted from Taverna et al., 2016.

al., 2017). When a progenitor undergoes symmetric division, Mib1 is released from the Golgi to ensure its equal repartition amongst the progeny (Tozer et al. 2017, see section 3.2.6). Finally, the periventricular heterotopia protein Big2 (*Arfgef2*) is involved in Golgi-derived protein trafficking. Inhibition of Big2 impairs delivery of key AJ proteins to the plasma membrane (Sheen et al., 2004). Trafficking from the Golgi apparatus to the apical plasma membrane (i.e. AJs and primary cilium) could thus be critical for correct aRG morphology, polarity and attachment.

### 3.2.6 Microtubule-based organelles: the centrosome and the midbody

The centrosome is a microtubule-based organelle composed of a pair of barrel-shaped centrioles surrounded by pericentriolar material. It has multiple roles throughout the cell cycle: in mitosis it localizes to the spindle poles, which are crucial for mitotic spindle assembly and chromosome alignment and separation at end stages of M-phase (Figure 22). Spindle pole anchoring to the cell cortex and position within the cell are crucial for spindle orientation and accurate cell division (see section 3.2.3). In interphase, the centrosome becomes the basal body, localized in the apical endfoot at the VS (Figure 22). The basal body docks a primary cilium, a microtubule-based organelle also critical for diverse aspects of aRG function (see section 3.2.7). Centrosomal proteins are often associated with primary microcephaly (see also 3.2.3 and 5.1). These proteins can impact spindle orientation as previously described in section 3.2.3, however there are also other processes related to centrosomes that can be abnormal, leading to aRG abnormalities. For instance, progressive loss of centrosomes, centrosome amplification and impaired centriole duplication frequently result in increased cell death, depletion of the aRG pool and thus decreased neuronal production, leading to a microcephaly phenotype (Buchman et al., 2010, Insolera et al., 2014, Jayaraman et al., 2016, Lizarraga et al.,

2010, Marthiens et al., 2013). Therefore, correct function of centrosomal proteins is crucial for aRG cell cycle progression and survival.

In addition, Wang and colleagues (2009) elegantly showed that in mouse aRGs, upon asymmetric division, the daughter cell that inherits the oldest centriole, namely the “old mother” centriole, acquires the self-renewal aRG fate remaining in the VZ, while the cell inheriting the “new mother” centriole is committed to differentiate (Wang et al., 2009). Recently, it was discovered that Mib1, known for its role in the Notch signaling pathway, and mentioned above in association with the Golgi apparatus, also acts as a fate determinant by associating with centriolar satellites (Tozer et al., 2017). Inheritance of pericentriolar material components may hence be important for determining cell fate, potentially regulating signaling pathways such as Notch.

Of note, a very recent study described a new centrosomal protein, AKNA, which localizes to the mother centriole in interphase (Camargo-Ortega et al., 2019). AKNA is highly expressed in differentiating apical progenitors (Pax6+Tbr2+) at mid-stages of corticogenesis (E14) when the SVZ is expanding. Interestingly, the authors found a role for AKNA in interphase-delamination of differentiating basal progenitors; overexpression of AKNA promoted this delamination resulting in an increase of Pax6-Tbr2+ basal progenitors in the SVZ, whilst knockdown of this protein led to an increase of ventricular Pax6+Tbr2- cells (Camargo-Ortega et al., 2019). Thus AKNA is an important centrosomal protein mediating delamination from the VZ, and SVZ formation (Camargo-Ortega et al., 2019).

Related to cell division, at the end stages of mitosis, the cleavage furrow grows towards the apical membrane and microtubules of the central spindle are compacted and give rise to the **midbody**, emerging at the bridge between cells during cytokinesis. Although the role of this structure is relatively little explored in aRGs, Kif20b mouse mutants showed aberrant midbody morphology and alignment with the aRG apical plasma membrane, triggering apoptosis and

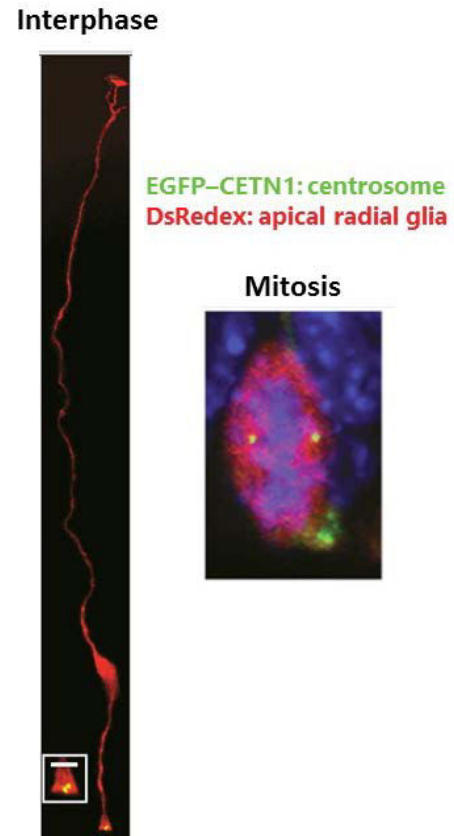


**Figure 22. Centrosome localization in apical radial glia cells.** In interphase the centrosome localizes to the apical endfoot. In mitosis, it localizes to the spindle pole. Adapted from Wang et al., 2009

thus resulting in a depletion of the aRG pool (Janisch et al., 2013). Hence correct function of this structure, known for its role in mediating the final steps of cell division, seems to be important for aRG proliferation and maintenance.

It has been recently proposed that midbody remnants are required for primary cilium assembly in epithelial cells (Bernabé-Rubio et al., 2016). Additionally, shedding and excision of midbody and primary cilium-derived particles have been described in the chick neuroepithelium (Dubreuil et al., 2007). It would thus be interesting to study the relationship between these two structures in aRGs and thus to further elucidate additional possible midbody function(s).

### 3.2.7 The primary cilium

My PhD project has focused on studying primary cilia in aRGs at early stages of corticogenesis. I will thus further describe this organelle, emphasizing its structure, formation and the signaling pathways in which it is involved.

#### Structure

The primary cilium is an antenna-like microtubule-based organelle that in aRGs protrudes towards the ventricle to sense signals from the CSF (Willaredt et al., 2013). It is composed of a specialized membrane supported by a specific microtubule network, the axoneme, which

has a '9+0' microtubule doublets structure. Localized at the base of the primary cilium it is positioned the basal body, important for primary cilia docking and nucleation (Figure 23). This structure is a modified centrosome, broadly composed of the mother centriole and pericentriolar proteins described to mediate several functions related to microtubule nucleation, primary cilium formation and disassembly (Wang and

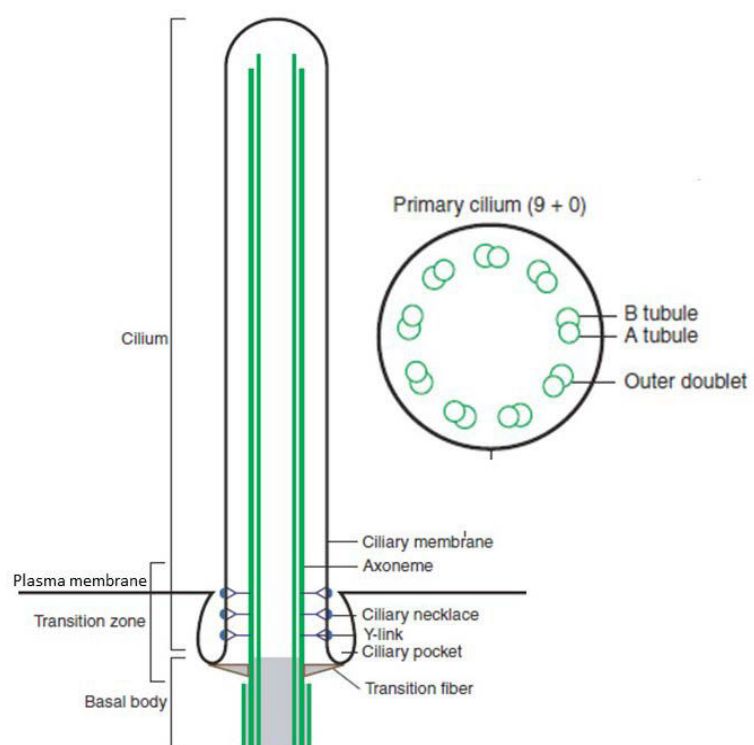


**Figure 23. Primary cilium structure.** The schema on the right represents a transverse section of the primary cilium axoneme. Adapted from Ishikawa and Marshall, 2017.

Dynlacht, 2018). The daughter centriole is positioned in close vicinity and perpendicular to the mother centriole.

The transition zone between the base of the primary cilium and the basal body is a complex encompassing structures key for primary cilium formation and function (Reiter et al., 2012). This region is characterized by Y-shaped links associating the microtubules of the axoneme to the ciliary plasma membrane. Between the transition zone and the plasma membrane, there is often an invagination called the ciliary pocket (Figure 23). This structure mediates endocytosis of ciliary components. The transition zone makes the primary cilium a 'true' cell compartment, controlling import and export of ciliary components and acting as a barrier (Garcia-Gonzalo et al., 2011, Madhivanan and Aguilar, 2014, Reiter et al., 2012). Proteins present in the transition zone include CEP290 and members of the Meckel Gruber syndrome (MKS) and Nephronophthisis (NPHP) families (Garcia-Gonzalo et al., 2011, Reiter et al., 2012, Takao et al., 2017). Mutations in these proteins have been frequently associated with ciliopathies (see section 5.4).

In distal regions of the basal body are also found the subdistal and distal appendages (Figure 24), the latter converting into transition fibers and connecting the basal body to the plasma membrane. These structures mediate centriole cohesion and vesicle reception amongst other functions (Reiter et al., 2012). Transition fibers also constitute a barrier, since the space in between the fibers is very small, limiting vesicle entry (Reiter et al., 2012). At the proximal part, the basal body sometimes presents a rootlet. This is a fibrous appendage-like structure associated with the actin cytoskeleton (Yang et al., 2005, Figure 24).

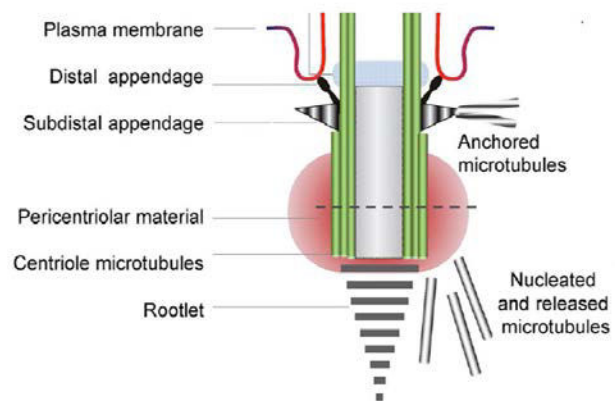


**Figure 24. Basal body structure.** Adapted from Loncarek and Bettencourt-Dias. 2018.

#### *Assembly and disassembly*

Primary cilium formation occurs after mitosis when the cell goes into interphase. At this point, the centrosome is transported towards the apical surface and becomes the basal body. In aRGs, the mother centriole associates with *de novo* synthesized membrane or ciliary remnants (Paridaen et al., 2013, see below), which are often carried in vesicle-like structures and that will then become the primary cilium. Once this complex reaches the apical plasma membrane,

the basal body is docked and the primary cilium is assembled. However, trafficking of proteins from the Golgi apparatus is still required for correct primary cilium assembly and growth (Lu and Madugala, 2018, Madhivanan and Aguilar, 2014, Figure 25).

The Golgi apparatus is broadly subdivided into cis and trans-Golgi. The cis-Golgi is in the vicinity of the ER and these two organelles continuously undergo anterograde and retrograde vesicle transport. Vesicles are also carried from the cis-Golgi to the trans-Golgi, and from the latter they are then sorted and delivered to the plasma membrane and thus to the primary cilium (Figure 25). Although ciliary cargoes have mostly been described to be trafficked through the trans-Golgi, some proteins such as polycystin-2 bypass this path and are delivered directly from the cis network (Hoffmeister et al., 2011). Another example is the intraflagellar transport protein 20 (IFT20), which localizes both to the basal body and to the Golgi apparatus and ensures correct sorting of ciliary cargoes (Follit et al., 2006, Follit et al., 2008).

Related to trans-Golgi trafficking, the Rab family of proteins has been extensively characterized in transport towards the primary cilium, especially Rab8 and Rab11, although a role for Rab10 and Rab23 in this process has been reported as well (Bernabé Rubio and Alonso, 2017). Rab6 has also been suggested to be involved in ciliary cargo sorting from the trans-Golgi network (Ward et al., 2011). ADP ribosylation factor (ARF) proteins are known to be involved in Golgi trafficking, and specifically Arf4 has been extensively described to mediate cargo delivery to primary cilia (Follit et al., 2014, Mazelova et al., 2009, Wang et al., 2017, Ward et al., 2011). Additionally, some ciliary proteins such as Tulp3, Ocr1 and Inpp5e have also been described to mediate primary cilium directed trafficking (Hua and Ferland, 2008), and other proteins previously described to be critical for mitosis seem also to be involved in the Golgi-to-primary cilium axis, for instance the kinesin KifC1 (Lee et al., 2018). Once vesicles arrive at the primary cilium base, they are sorted in the transition zone before entering the cilium axoneme. Protein transport along the axoneme relies on intraflagellar transport (IFT) (Figure 25), mediated by IFT molecules (e.g. Ift144, Ift88) and kinesin-2 (anterograde) and cytoplasmic dynein-2 (retrograde) (Lechtreck, 2015). The BBSome proteins are also important for intraciliary trafficking (reviewed by Lechtreck, 2015), and for recognizing ciliary targeting signals of proteins arriving at the base of the cilium (Reiter et al., 2012). Mutations in BBS proteins are associated with the Bardet-Biedl syndrome ciliopathy (Habbig and Liebau, 2015).

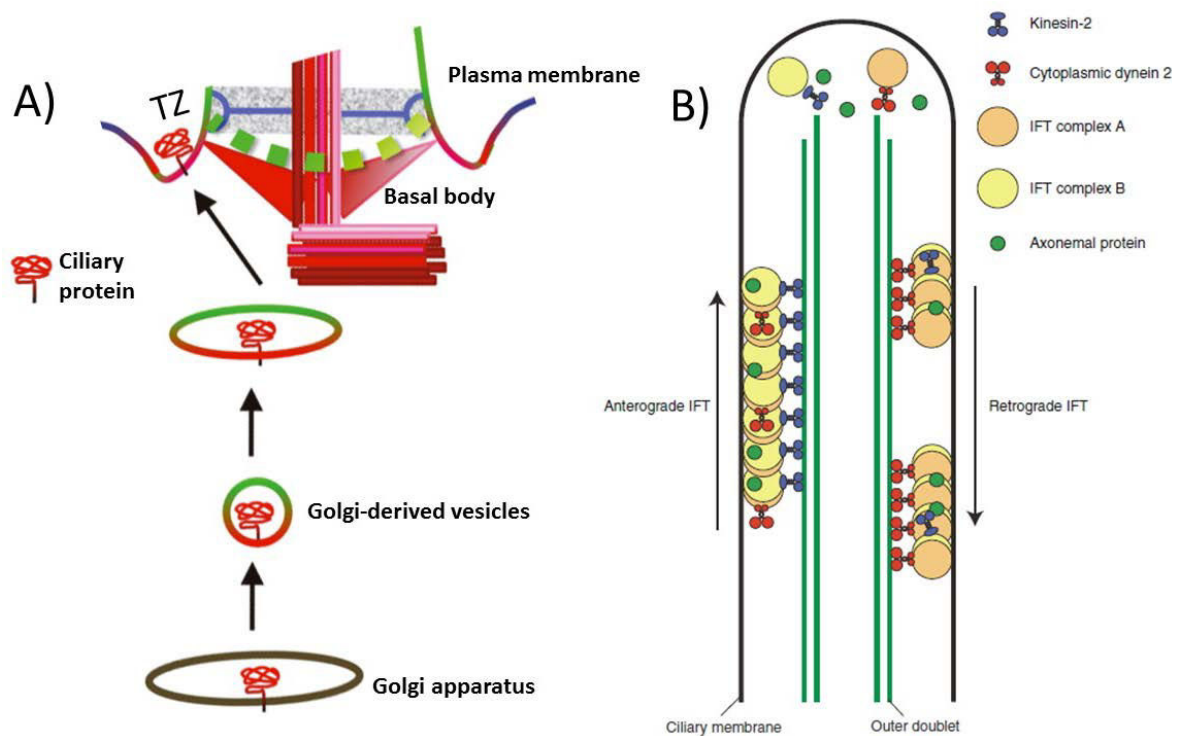


**Figure 25. Schematic representations of ciliary trafficking.** A) Vesicles derived from the Golgi apparatus carrying ciliary proteins reach the ciliary transition zone where they are recognized and thus the proteins can be integrated in the ciliary complex. B) The primary cilium depends on IFT transport for anterograde and retrograde trafficking of cargoes along the axoneme. Adapted from Madhivanan and Claudio Aguilar, 2014, Ishikawa and Marshall, 2017.

When the cell enters M-phase the primary cilium disassembles, although in aRGs the presence of ciliary remnants has been described (Paridaen et al., 2013, Figure 26). Ciliary remnants associate with the mother centriole during mitosis and are inherited by the daughter cell that acquires an aRG fate (Paridaen et al., 2013). The cell inheriting both the old mother centriole and the ciliary remnant docks a primary cilium apically before its sister cell, thus being exposed to CSF signals first (Piotrowska-Nitsche and Casparly, 2012).

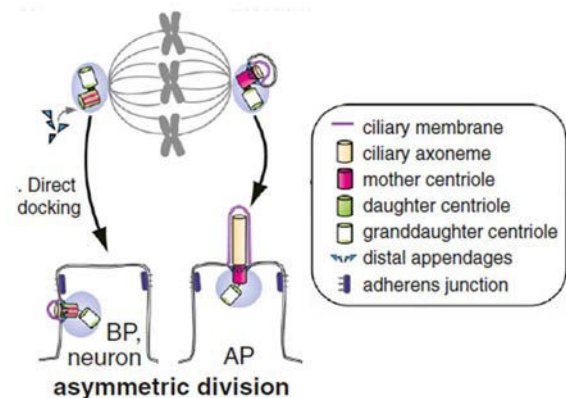


**Figure 26. Ciliary remnants associate with the mother centriole during mitosis.** The mother centriole carrying the ciliary remnants is inherited by the daughter cell acquiring an apical radial glial fate. BP: basal progenitor, AP: apical progenitor. Adapted from Paridaen et al., 2013

Phosphorylation of histone deacetylase 6 (HDAC6) by Aurora A has been described to promote deacetylation of microtubules composing the axoneme resulting in cilia disassembly (Plotnikova et al., 2012). Two depolymerizing kinesins of the Kinesin 13 family are also important for this process (Sanchez and Dynlacht, 2016). Phosphorylation by the kinases Plk1



and Nek2 of Kif2a and Kif24, respectively, promotes cilium disassembly and triggers proliferative signals (Kim et al., 2015, Miyamoto et al., 2015). Nek2 and Plk1 are expressed in S/G2 and G2/M respectively, further linking cell cycle progression with primary cilium dynamics (Sanchez and Dynlacht, 2016). Of note, other proteins such as the scaffolding protein HEF1, trichoplein and Pitchfork have also been implicated in primary cilium disassembly activity (Kinzel et al., 2010, Plotnikova et al., 2012).

Several proteins described to regulate aRG behavior and additionally to be involved in cortical malformations have ciliary functions. Nde1 and Tctex-1 have been described to localize to the transition zone and to mediate primary cilium disassembly (Kim et al., 2011, Li et al., 2011). Additionally, Gabriel and colleagues (2016) reported a new role for Cenpj in promoting cilium disassembly through an Ofd1-Nde1-AuroraA-dependent mechanism. Neuronal progenitors in organoids derived from Cenpj-mutant human induced pluripotent stem cells (hiPSCs) also showed impaired cell cycle re-entry, accompanied by premature neuronal differentiation (Gabriel et al., 2016). A very recent study analyzing a Cenpj conditional mouse model also reported cilia disassembly impairment in aRGs and severe cortical defects resulting in a small brain (Ding et al., 2019). Additionally, the authors showed that this mechanism was mediated through Kif2a (Ding et al., 2019), which had been previously shown to regulate primary cilium disassembly in neuronal progenitors as well as to be important for correct cortical development (Broix et al., 2018). Indeed, perturbing Kif2a function not only affects neuronal progenitor proliferation, it also disturbs neuronal positioning in the developing cortex (Broix et al., 2018, Ding et al., 2019).

Of note, extra-ciliary roles of proteins involved in primary cilium disassembly have also been ascribed during mitosis. For instance, Plk1 and Aurora A localize to the spindle pole during mitosis and are important for mitotic spindle assembly (reviewed by Joukov and De Nicolo, 2018).

#### *Signaling pathways mediated by the primary cilium*

Many signaling pathways triggered and/or modulated by the primary cilium have been described to be critical for corticogenesis and are often associated with impaired cortical development. The role of **Wnt** signaling in aRGs has been previously mentioned in section 3.1.1. The **Hippo** pathway, regulating cell size, shape and overall tissue morphogenesis, is emerging as a key pathway critical in aRG behavior and overall corticogenesis (Cappello et al., 2013, Liu et al., 2018, O'Neill et al., 2018a, Park et al., 2016). Another pathway related to the

primary cilium is the **mTOR** pathway, previously described to regulate aRG apical domain size (Foerster et al., 2017) and associated with a broad range of cortical malformations such as focal cortical dysplasia, ventriculomegaly and periventricular heterotopia (see section 5).

The signaling pathway most frequently associated with the primary cilium is the **Shh** pathway. Indeed, within the primary cilium are found many proteins with crucial roles in Shh signaling. Ciliopathies often comprise alterations of Shh downstream effectors i.e. the Gli TFs, impacting thus gene transcription. Increased Shh signaling has been described to promote IP and bRG production from aRGs in the mouse neocortex, leading to the presence of cortical fold-like structures (Wang et al., 2016). On the other hand, a reduction of Shh signaling impairs aRG proliferation, survival and their ability to generate basal progenitors (IPs and bRGs) and neurons (Komada et al., 2008, Komada et al., 2013, Wang et al., 2016). These studies suggest a role for Shh signaling in basal progenitor generation: both IPs and bRGs. Accordingly, Shh signaling is stronger in the developing cortex of gyrencephalic species (de Juan Romero et al., 2015, Wang et al., 2016).

### **3.3 Multipotency of neuronal progenitors (adapted from Uzquiano et al., 2018)**

#### **3.3.1 Subpopulations of apical radial glia?**

During corticogenesis, neurons populating the different layers are sequentially produced. Deep layer neurons (layers V-VI) are produced during early corticogenesis (E11.5-E14.5 in the mouse), whilst upper layers neurons (layers II-IV) are produced at later stages (E14.5-E17.5). The latter migrate past the former to reach their final location (glutamatergic neuron classification is detailed in section 2.3). However, it is still under debate concerning the multipotency of aRGs as corticogenesis proceeds, as well as the possible existence of aRG subtypes coexisting in the VZ and responsible for the production of a determined neuronal identity.

Pioneer heterochronic transplantation studies in the 90s showed that as development proceeds, ferret neuronal progenitors become more restricted in their fate potential (i.e. identity of neuronal output) (McConnell and Kaznowski, 1991, Frantz and McConnell, 1996, Desai and McConnell 2000). When transplanting early progenitors into later brains (already generating upper cortical neurons), these cells were capable of generating upper layer neurons. However, the opposite experiment showed that progenitors from later stages of corticogenesis failed to generate early neuronal fates (McConnell and Kaznowski, 1991, Frantz and McConnell, 1996, Desai and McConnell 2000). Of note, in these experiments radiolabeled

thymidine incorporation during S-phase was used as a means to identify neuronal progenitors. The latter is incorporated in cycling progenitors across the VZ and SVZ (Angevine and Sidman, 1961). Therefore, the progenitors transplanted in the ferret were likely to be a mixed population of aRGs and IPs.

Other studies supported a role for aRG fate restriction as corticogenesis proceeds by performing fate-mapping studies: retroviral-mediated labelling of individual progenitors showed that early cells could generate neurons belonging to all layers of the cortex (Luskin et al., 1988, Walsh and Cepko 1993). Recent work has taken advantage of new fate-mapping techniques, notably the Mosaic Analysis with Double Markers (MADM) approach, showing that aRG behavior and progeny can be followed accurately at the single cell level. These data studying individual cells also supported that aRG multipotency decreases as corticogenesis proceeds (Gao et al., 2014, Kaplan et al., 2017).

A very recent study deposited in BioRxiv by Oberst and colleagues (2018) potentially challenges this hypothesis and hence merits being mentioned here. The authors performed heterochronic transplantation experiments in the mouse neuroepithelium of E15 FlashTag labelled aRGs into E12 donors. The transplanted cells not only gave rise to deep layer neurons, they also showed specific features related to the 'reconversion' to E12 aRG progenitors (i.e. mode of division and membrane potential) (Oberst et al., 2018, BioRxiv). Thus, although several pieces of evidence support the hypothesis that VZ progenitors become more restricted over time to generate selective layer-specific neurons as neurogenesis progresses (Gao et al., 2014, Kaplan et al., 2017, Luskin et al., 1998, Walsh and Cepko, 1993), recent work also supports the idea that aRGs can be multipotent and plastic throughout development, retaining the ability to produce neurons of all layers (Oberst et al., 2018, BioRxiv).

Additionally, it has been questioned if different subpopulations of aRGs may be committed to produce a specific neuronal fate. This topic is still controversial, and no solid conclusions have been established. Franco and colleagues (2012) showed that aRGs expressing the TF Cux2 mainly produce upper layers neurons. A knock-in mouse (Cux2-CreERT2) was used to fate-map Cux2-positive aRGs and their progeny from early stages of neurogenesis. This approach showed that aRGs expressing Cux2 are present in the VZ from as early as E10.5. At early stages of corticogenesis, when deep layer neurons are being produced, they remain in a proliferative state in the VZ. At later stages, when upper layer neurons are generated, they switch their mode of division contributing to neuronal production. In addition, when forced to

differentiate in an early environment, Cux2-positive aRGs still produced upper layer neurons (Franco et al., 2012). Following this study, work from a different group failed to obtain the same results, using the same Cux2-CreERT2 line, as well as a Fezf2-CreERT2 BAC line (Guo et al., 2013, Eckler et al., 2015). The fact that these studies were performed in mice with different genetic backgrounds provided a potential explanation for different outcomes (Eckler et al., 2015, Gil-Sanz et al., 2015). Two very recent BioRxv studies further follow this debate and hence I also mention these here. Cadwell and colleagues (2019) used a tamoxifen inducible Cre-lox Nestin driven strategy to sparsely label E10.5 aRGs clones. As expected, the latter were composed of cells from all cortical layers, with no clone composed exclusively of deep or superficial layers neurons (Cadwell et al., 2019, BioRxv). On the other hand, Llorca et al. (2018) followed a multi-approach strategy including retroviral tracing, the MADM technique and a tamoxifen inducible Cre-lox Emx1 driven strategy to label E12.5 aRG clones and then analyze their composition. Although 80% of the clones contained neurons from deep and superficial layers, 10% were exclusively deep-layer restricted and the remaining 10% superficial-layer restricted (Llorca et al., 2018, BioRxv). Additionally, of that 80% of clones, a high proportion of them lack neurons in one or more specific layers, with pyramidal lineages adopting every possible configuration of laminar distribution in the neocortex (Llorca et al., 2018, BioRxv). To further understand if this was due to a stochastic behavior of aRGs or to the existence of different aRG populations a mathematical model was generated, which suggested that at least two subsets of aRGs would be required to generate the diversity of clones observed (Llorca et al., 2018, BioRxv). The strategy used, as well as the developmental time point selected to analyze aRG-derived pyramidal clones may influence the results obtained. It will be interesting to see the final publications of these BioRxv papers contributing to this important subject. Possibly transcriptional profiling of aRGs in the VZ throughout corticogenesis will also shed further light on this topic in the future.

### **3.3.2 Basal progenitors and neuronal output**

As previously mentioned, as neurogenesis proceeds aRGs produce IPs, which will generate a large proportion of the neurons forming the cortex. The neuronal subtype produced by IPs has also been a controversial topic: while some studies support that IPs mainly generate upper layer neurons (Tarabykin et al., 2001, Zimmer et al., 2004), other more recent studies indicate that they produce neurons belonging to all cortical layers (Vasistha et al., 2015). Mihalas et al (2016) showed that whilst early generated IPs mainly produce deep layer neurons, later

neuronal-fates are produced from IPs generated throughout corticogenesis (Mihalas et al., 2016). A recent study combining knock-in Tbr2-CreERT2 mice with the MADM fate mapping approach allowed a more specific clonal analysis of IP-derived progeny (Mihalas and Hevner, 2018). This study further showed that possibly all IPs are multipotent producing neurons with different layer identities (Mihalas and Hevner, 2018).

Finally, it is worth noting that RG progenitor cells characteristic of the primate-human brain, namely bRGs located in the oSVZ, are thought to be directly involved in the production of neurons belonging to layers II-III, which are increased in size and complexity in primates (Ostrem et al., 2017, see also section 3.1.2). These cells are hence likely to produce neurons at later stages (Martinez-Martinez et al., 2016, Nowakowski et al., 2016).

### 3.4 From the Radial Unit Hypothesis to the Supragranular Layer Expansion Hypothesis

In section 3.1.2, I briefly discussed neocortical expansion and the importance of recently-characterized bRGs in this phenomenon. However, the mechanisms and genetics underlying neocortical expansion and amplification have been a hot topic of study for many years.

Already in the 90s, Rakic proposed the first model to explain the increase in cortical surface, namely proposing the **Radial Unit Hypothesis**. This model proposed that the evolutionary increases in cortical size were dependent on the amount of founder VZ neuronal progenitors. This hypothesis postulated that post-mitotic neurons derived from the same region of the VZ are radially organized in what is termed an ontogenetic cortical column. Hence, a larger amount of founder VZ progenitors leads to an increased number of cortical columns that would result in the expansion of the cortical primordium (Rakic, 1995, Figure 27). Indeed, in primates the gestational time is longer than in rodents and apical progenitors remain in a proliferative

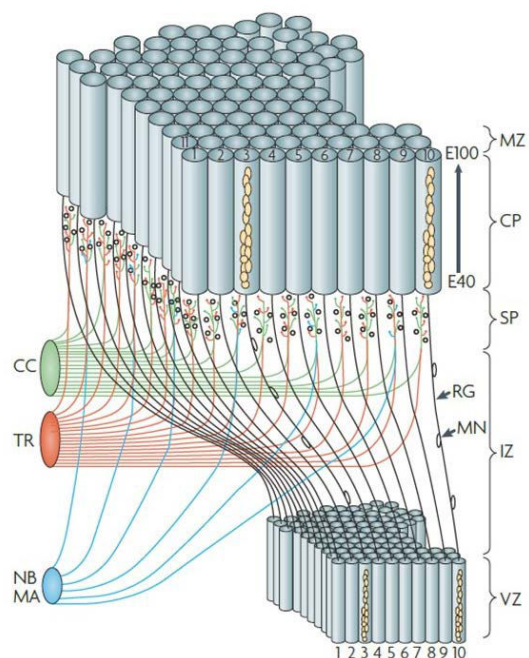


**Figure 27. Schematic representation of cortical development based on the Radial Unit Hypothesis.** MZ: marginal zone, CP: cortical plate, SP: subplate, IZ: intermediate zone, VZ: ventricular zone, RG: radial glia, MN: migrating neuron, CC: cortico-cortical connections, TR: thalamic radiation, NB: nucleus basalis, MA: monoamine subcortical centers. From Rakic, 2009.

symmetric division state for longer, which directly impacts the number of cortical columns and the final neuronal input.

Despite the importance of emphasizing radial column organization, the radial unit hypothesis was unable to take into account complex neuronal progenitor cell diversity, to provide an explanation for the presence of folds and sulci in the primate-human brain and the increased expansion of upper cortical layers in primates. Experimental approaches testing this hypothesis often led to folding of the VZ, an event that does not occur in gyrencephalic species (Chenn and Walsh, 2002, Haydar et al., 1999, Kingsbury et al., 2003, Lien et al., 2006, Siegenthaler et al., 2009).

Other hypotheses were then elaborated to explain neocortical expansion and gyrification. As described in section 3.1.2, an additional germinal layer is present in the developing neocortex: the SVZ, split into the iSVZ and oSVZ in gyrencephalic species. IPs, found in the SVZ, are indeed a major source of neurons and are also more abundant in primates than in rodents. This led to the **Intermediate Progenitor Hypothesis**, postulating that IPs determine the increase neuronal output and thus cortical expansion and folding. The relative abundance of IPs would determine the prospective folds and fissures (Kriegstein et al., 2006, Borrell and Gotz, 2014). Experimental approaches have confirmed the key role of IPs in neuronal production but fail to firmly link this type of neuronal progenitor with the appearance of folds and sulci (Cappello et al., 2006, Nonaka-Kinoshita et al., 2013, reviewed by Borrell and Gotz, 2014).

As described extensively in the previous section, bRGs appear to be critical for neocortical expansion and gyrification, supporting what is termed the **Epithelial Progenitor Hypothesis**. The latter proposes that maintenance of epithelial features by basal progenitors is critical for neocortical expansion. As well as the importance of generating a large quantity of progenitors to increase the neuronal output, bRGs also contribute to the **Tangential Divergence Hypothesis**: they provide more basal fibers, without always having corresponding apical attachments, which contribute as scaffolds for migrating neurons to reach their final position. These morphological characteristics allow a 'fan-like' pattern of neuronal migration promoting the tangential expansion of the neocortex (Florio and Huttner, 2014, Borrell and Gotz, 2014). Further supporting a role for bRGs in gyrification, observations both in the ferret and in human fetal tissue correlate the abundance of bRGs with prospective gyri or sulci: these progenitors are more abundant in future folds than in fissures (Nowakowski et al., 2016, Reillo et al., 2011).

As mentioned in section 3.3, bRGs are also thought to be important for upper layer neuron production (Ostrem et al., 2017). Recently, a study by Nowakowski and colleagues further supports this observation and highlights the contribution of bRGs to upper layer expansion (Nowakowski et al., 2016). Already previous, even early, studies suggested that aRGs in primates possessed a different morphology at late stages of corticogenesis (deAzevedo et al., 2003, Sidman and Rakic, 1973). Work in human fetal tissue at early and late stages of embryonic development showed a dramatic change in the aRG scaffold: whilst during early corticogenesis aRGs have both apical and basal process reaching the ventricular and pial surfaces, respectively, from mid-gestation they adopt a truncated morphology. The aRG basal process can terminate in the oSVZ, often reaching capillaries and endothelial cells (Nowakowski et al., 2016). The authors also report that at this same developmental time point, ventricular mitoses decrease and bRGs populating the oSVZ are the main source of neuronal production, as previously described (Lukaszenicz et al., 2005, Martinez-Cerdeno et al., 2012, Nowakowski et al., 2016). Neurons produced from this time point were mainly upper layer neurons, which due to the truncated aRG morphology, depend on bRG basal processes as scaffolds for their migration to the appropriate position in the CP (Nowakowski et al., 2016). The authors thus propose the **Supragranular Layer Expansion Hypothesis** (Figure 28), building up from the Epithelial Progenitor Hypothesis and the Tangential Divergence Hypothesis. During upper layer neurogenesis in humans, the amount of bRG fibers directly predicts the expansion of these superficial layers. They suggest that whilst bRG neurogenic divisions

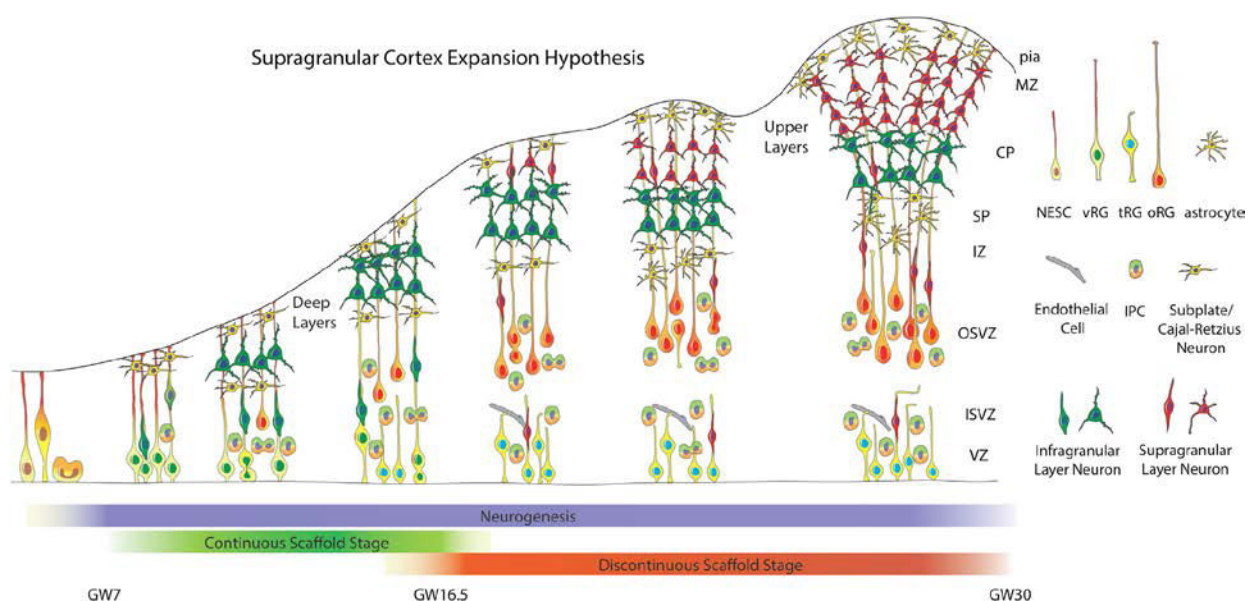


**Figure 28. Schematic representation of the Supragranular Layer Expansion Hypothesis.** From Nowakowski et al., 2016.

expand upper layers radially, proliferative bRG divisions are responsible for the consequent tangential expansion (Nowakowski et al., 2016).

I have discussed the main progenitor based hypotheses responsible for neocortical expansion and gyrification. However, particular patterns of neuronal migration are also likely to be necessary for the presence of folds and fissures, as also suggested in a recent study (section 3.6, del Toro et al., 2017). Additionally, it is worth mentioning that in parallel particular biomechanical forces are required for the complex patterns of cortical folding for which models are continuously being elaborated (reviewed by Kroenke and Bayly, 2018, Llinares-Benadero and Borrell, 2019).

### **3.5 Cortical arealization**

As described in section 2.1, the neocortex is specified in areas or territories in its tangential extension, each with particular cyto-architectures, connectivity and functions including motor and sensory processing. From early stages of corticogenesis, neuronal progenitors receive information in order to help generate these territorial distinctions.

#### **3.5.1 Telencephalic signaling centers, transcription factors and the progenitor compartment**

Once the telencephalon acquires its identity, neuronal progenitors receive information in order to shape these territories in a process known as **arealization**. Telencephalic patterning centers release morphogens which act in a dose-dependent manner influencing progenitor behavior and driving neocortical territory establishment (Alfano and Studer, 2013, Molyneaux et al., 2007). There are four principal telencephalic signaling centers driving neocortical arealization (reviewed by Alfano and Studer, 2013, Arai and Pierani, 2014, Figure 29):

- The pallial septum, which is the most anterior signaling center and releases Fgfs (Fgf8, 15 and 17) (Assimacopoulos et al., 2012, Crossley and Martin, 1995).
- The cortical hem, located adjacent to the dorsal midline in the medial cortical wall and expressing Bmps and Wnts (Groove et al., 1998, Furuta et al., 1997).
- The antihem, or pallial-subpallial boundary (PSB), located in the boundary between the dorsal and the ventral telencephalon. It expresses molecules such as Egfs (neuregulin 1 and 3), Tfg $\alpha$ , Fgf7 and the Wnt antagonist Sfrp2 (Assimacopoulos et al., 2003, Lopez-Bendito et al., 2006, Subramanian et al., 2009).
- The ventral organizer, mainly secreting Shh and driving ventral telencephalon patterning (Grove et al., 1998, Ohkubo et al., 2002).



The pallial septum, cortical hem and anti-hem are responsible for arealization in the neocortex. The morphogens secreted from these signaling centers set up a graded expression of TFs controlling dorso-ventral and rostro-caudal patterning and eventually leading to the specification of neocortical domains (Alfano and Studer, 2013). These TFs are Pax6, Emx2, Coup-Tf1 and Sp8 (reviewed by Alfano and Studer, 2013 Arai and Pierani, 2014, Figure 29). Pax6 and Sp8 are highly expressed in the frontal cortex promoting growth and specification of frontal areas. On the other hand, Emx2 and Coup-Tf1, whose expression increases gradually from rostral to caudal regions, promote growth of caudal areas (Alfano and Studer, 2013). Accordingly, loss of Pax6 and Sp8 causes an increase of caudal territories (visual processing V1 area) concomitant with a decrease of anterior regions (Bishop et al., 2002, Zembrzycki et al., 2007, O’Leary et al., 2007), and loss of Emx2 and Coup-Tf1 results in expanded anterior areas (motor and/or somatosensory cortex) and decreased caudal territories (Bishop et al., 2000, Mallamaci et al., 2000, Armentano et al., 2007).

Two other TFs are critical for neocortical domain identity. Lhx2 and Foxg1, which together repress dorsal midline fates. In the absence of Lhx2, a dramatic expansion of dorsal medial structures takes places (Bulchand et al., 2001, Monuki et al., 2001, Vyas et al., 2003).

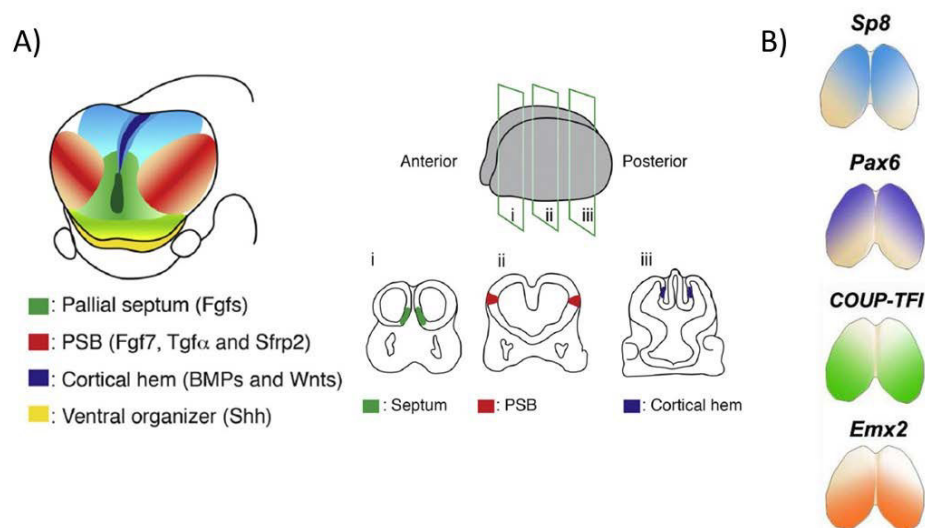


**Figure 29. Arealization of the dorsal telencephalon.** Telencephalic patterning centers (A) release morphogens acting on progenitor cells in a dose-dependent manner. This triggers the expression of specific transcription factors key for providing areal information. PSB: pallium-subpallium boundary. Adapted from Arai and Pierani, 2014, Alfano and Studer, 2013.

### 3.5.2 The post-mitotic compartment

In addition to signaling centers, post-mitotic mechanisms also influence cortical area patterning. For instance, **Cajal Retzius (CR) cells** are amongst the first born neurons and influence cortical patterning (Arai and Pierani, 2014). They arise from the pallial septum, the

PSB and the cortical hem. During early stages, CR cells migrate tangentially underneath the pial surface covering the whole cortical primordium. Depending on their origin they populate specific regions and express characteristic markers (Bielle et al., 2005; Yoshida et al., 2006). Specific deletion of a CR cell population derived from the pallial septum (E10.5-E11.5) results in overall CR cell reorganization (Griveau et al., 2010). This CR cell redistribution leads to changes in the expression of Pax6 and Sp8, altering medial and dorsal VZ progenitor proliferation. This affects early cortical regionalization subsequently leading to shifts in the positioning of cortical areas in postnatal stages (Griveau et al., 2010). Transcriptome analyses of this specific CR population uncovered the expression of many morphogens likely to influence arealization. CR cells were thus proposed to act as ‘mobile signaling units’ contributing to long range patterning in large structures (Arai and Pierani, 2014).

Related to postnatal development, thalamocortical afferent projections (TCA) and environmental factors have been shown to further refine cortical areas (Anton-Bolanos and Lopez-Bendito, 2018, Arai and Pierani, 2014, Campi and Krubitzer, 2010, Campi et al., 2011, Chou et al., 2013, Vue et al., 2013, Pouchelon et al., 2014). Additionally, there are diverse TFs known to be important for post-mitotic establishment and maintenance of areal identity. For instance, Bhlhb5 and Lmo4 regulate area-specific differentiation of cortical motor neurons (Cederquist et al., 2013, Joshi et al., 2008), whereas Ctip1 represses motor identity and activates sensory programs of gene expression, controlling sensory area development (Greig et al., 2016)

In summary, neuronal progenitors and their progeny are tightly regulated to form ‘radial columns’ of post-mitotic neurons whilst processing information about territorial specification along the tangential axis. Newborn post-mitotic neurons also depend on external factors as well as fingerprints of TFs to acquire not only a layer-specific identity, but also specific features related to the neocortical area they belong to. In the following section I will briefly describe how newly produced post-mitotic neurons reach their final position in the CP, a process dependent of structural aspects of aRGs and often target of human cortical malformations.

### **3.6 Neuronal migration**

The work of my thesis has addressed features related to aRG cell biology and progenitor behavior. Neuronal migration and maturation are also pivotal aspects of cortical development and can be disrupted leading to cortical malformations and neuropsychiatric disorders. In this

section I will briefly discuss key aspects of neuronal migration focusing on projection neurons (reviewed by Kawaguchi, 2015).

As previously described, glutamatergic projection neurons are produced in proliferative zones of the dorsal telencephalon and migrate radially through the cortical wall (i.e. intermediate zone (IZ) and developing CP) to

reach their correct positions. Deep layer neurons (layers V-VI) are produced during E11.5-E14.5 in the mouse, while upper layers neurons (layers II-IV) are produced at E14.5-E17.5. The latter migrate past the former to reach their final location.

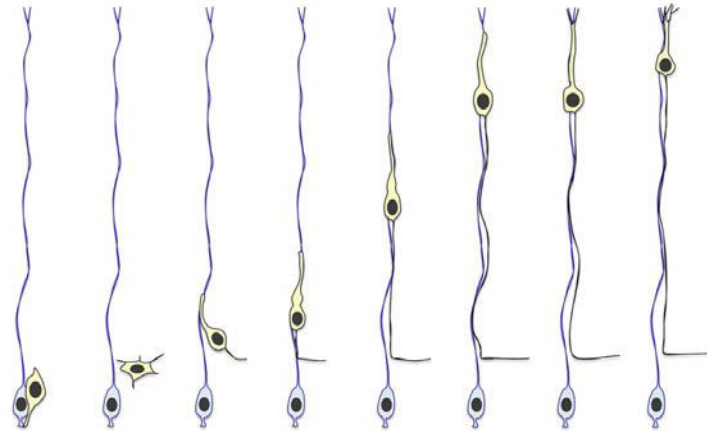


**Figure 30. Schema representing the process of neuronal migration from the ventricular zone to the cortical plate.** Blue: radial glial cell, yellow: migrating neuron. Adapted from Kawaguchi, 2015.

Neuronal migration consists of several steps. At early stages of corticogenesis (E11.5-E12.5 in the mouse cortex), newly produced neurons reach the superficial marginal zone by somal translocation. However, when the developing cortex becomes thicker, newborn neurons take on a multipolar morphology (Figure 30). At the beginning of the IZ, multipolar neurons undergo what is known as the ‘multipolar-to-bipolar transition’, becoming locomotor neurons and adopting a leading process and a trailing axon simultaneously (Kawaguchi, 2015).

Once neurons have adopted the locomotion mode, they carry out a long journey to reach their appropriate position in the CP (Figure 29). Already in the 70s, Rakic described the interaction between migrating neurons and the basal process of aRGs in the IZ of the monkey developing cortex (Figure 31). Indeed, locomotion also depends on the basal processes of radial glial cells (from both aRGs and bRGs, see sections 3.1 and 3.4), which act as a scaffold for migrating neurons (Kawaguchi et al., 2015, Buchsbaum and Cappello, 2019). This process also involves morphological changes: the leading process extends forward and forms a cytoplasmic

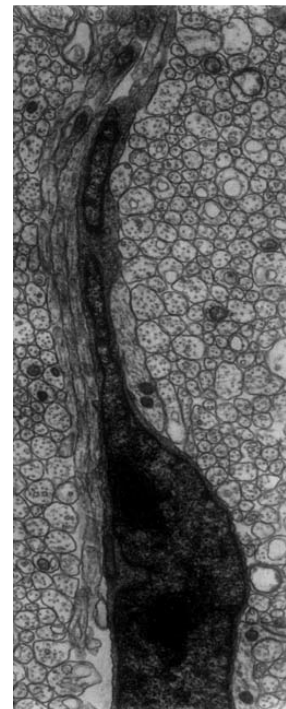


**Figure 31. Electron micrograph showing a young migrating neuron along a radial glial fiber.** Adapted from Rakic, 2002.

dilation ('swelling') close to the soma. The nucleus then elongates to enter the dilated leading process (reviewed by Kawaguchi, 2015). Once the leading process reaches the marginal zone the migrating neuron undergoes a terminal translocation independent of radial glial fibers, to reach its final destination (Figure 30).

Disruption of any of these steps can cause abnormal neuronal migration, often associated with human cortical malformations (reviewed by Stouffer et al., 2016, Buchsmaum and Cappello, 2019, see section 5). However, multiple genes involved in this process also have important functions in neuronal progenitors. Therefore, discerning between abnormal progenitor behavior and disrupted neuronal migration in the context of cortical malformations can be challenging. Indeed, both components can contribute to the etiology of severe cortical disorders.

Specific patterns of neuronal migration are emerging as features possibly contributing to neocortical expansion and folding. Deletion of the adhesion molecules Flrt1 and Flrt3 in the mouse leads to the appearance of fold- and sulci-like structures in the otherwise smooth neocortex (Del Toro et al., 2017). This effect was not due to progenitor amplification, but rather to a change in the pattern of neuronal migration, including increased migration (del Toro et al., 2017). In addition, very recently, Martinez-Martinez et al reported frequent branching of the leading process of radially migrating neurons (Martinez-Martinez et al., 2019). This work shows how the pattern of leading process branching is more complex and elaborated in ferret than in mouse. This branching did not impair migration speed, on the contrary, ferret neurons migrate faster than mouse, even if they possess a larger number of branching points (Figure 32). This differential dynamics and increased branching of the ferret neuronal leading process

may indeed contribute to the long and tortuous neuronal migration journey in gyrencephalic brains as well as to the tangential dispersion of neurons (Martinez-Martinez et al., 2019).

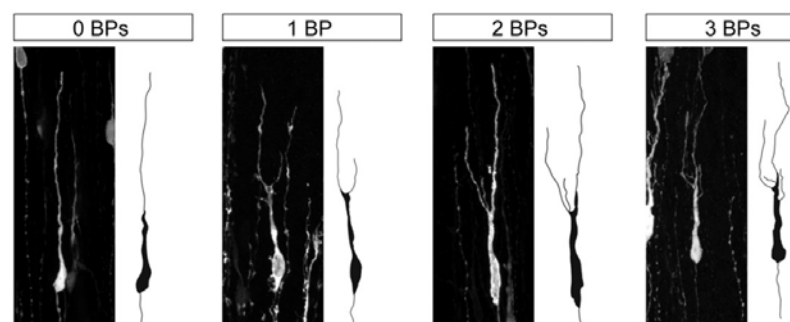


**Figure 32. Radially-migrating neurons in the ferret neocortex.** In the ferret, these neurons can exhibit up to three branch points (BPs) in their leading process (right panel). From Martinez-Martinez et al., 2019.

In addition to these two recent studies, genes known to be critical for neuronal migration (e.g. LIS1, DCX) are responsible for malformations perturbing cortical folding (Pilz et al., 1998, Pilz et al., 1999, Gleeson et al., 1999, Francis et al., 1999, Reiner and Sapir, 2013). Hence, neuronal migration and more specific features of this process in the context of gyrencephalic cortical development may actively contribute to cortical folding.

**4. Cortical malformations**

In the previous sections I have discussed the different progenitor cell types, emphasizing the critical role of aRGs as the founder neuronal progenitor, responsible for the production of other progenitor cell types, the final neuronal output and patterns of neuronal migration. I have addressed developmental mechanisms of cortical organization with radial, tangential and areal considerations. Furthermore, topical aspects of neocortical expansion and gyrification have been discussed. The combination of these sections provides an insight into the complexity of cortical development. Indeed, as previously anticipated, disruption of one of these tightly regulated events can severely impact corticogenesis, resulting in cortical malformations.

Cortical malformations can arise due to environmental insults, for instance viral infections during pregnancy (e.g. Zika virus), however the many of them are known to have a genetic basis (Buchsbaum and Cappello, 2019). Human cortical malformations are rare disorders, however their combined incidence is more than 1% in the human population. They are often associated with intractable epilepsy and intellectual disability. 14% of epileptic patients are believed to present a neuronal migration disorder. This percentage raises to 40% when just considering those patients with intractable epilepsy (Farrell et al., 1992, Meencke and Veigh, 1992, Guerrini, 2005).

Cortical malformations can broadly be subdivided in three classes, depending on the aspect affected, i.e. brain size, cortical folding or abnormal neuronal position, known as heterotopia

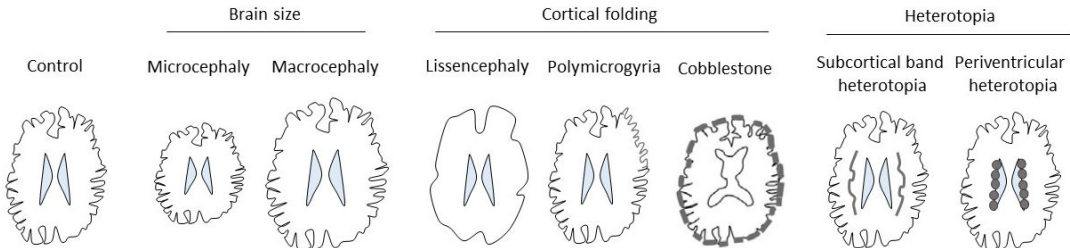


**Figure 33. Schemas of cortical malformations.** Adapted from Romero et al., 2018, Uzquiano and Francis 2019.

(Fernandez et al., 2016, Figure 33). Although each of these categories will be discussed individually, it is important to note that cortical malformations often occur as a spectrum rather than as an isolated phenotype.

#### **4.1 Brain size: microcephaly versus macrocephaly**

As discussed in sections 3.1 and 3.4, the pool of aRGs is critical for determining cortical size. Abnormal aRG cell division, proliferation and/or survival can thus severely impact brain size leading to microcephaly (small brain) or macrocephaly (enlarged brain). **Microcephaly** in humans refers to a disorder in which the size of the brain is significantly smaller than control brains (Bizzotto and Francis, 2015). Although the brain is smaller, the overall architecture of the cortex can remain not dramatically perturbed (Bizzotto and Francis, 2015). For these forms of microcephaly, mutant genes have often been found to code for centrosomal proteins (i.e. PLK4, STIL, MCPH1, ASPM, WDR62, CEP135, CDK5RAP2, CENPJ) (Bilgüvar et al., 2010, Bond et al., 2005, Darvish et al., 2010, Jackson et al., 1998, Kumar et al., 2002, Kumar et al., 2009, Martin et al., 2014, Nicholas et al., 2010, Hussain et al., 2012, Shen et al., 2005, Yu et al., 2010), regulating functions in aRGs such as centrosome duplication, centrosome cohesion, correct mitotic spindle assembly, chromosomal alignment, DNA damage response and also spindle orientation (reviewed by Megraw et al., 2011, see also sections 3.2.3 and 3.2.6). Impairment of one of the latter (e.g. centrosomal amplification, shift in spindle orientation) can prompt cell death or precocious depletion of the aRG pool, subsequently resulting in a decreased number of neurons. On the other hand, **macrocephaly** can arise due to excessive neuronal progenitor proliferation and consequently neuronal production (Fernandez et al., 2016), amongst other causes. The broad and complex diversity of progenitors found in the human cortex may also contribute to the etiology of macrocephaly, although this is yet to be shown (Bizzotto and Francis, 2015). In addition, other features such as the dendritic arborization pattern and fiber outgrowth could also contribute to the increase in cortical size (Bizzotto and Francis, 2015). Lately, the PI3K/Akt/mTOR pathway is emerging as a target at the basis of certain forms of this brain disorder (Alcantara et al., 2017, Handoko et al., 2018, Negishi et al., 2017, Yeung et al., 2017). Mutations in the DNA binding protein CHD8 are associated with autism spectrum disorder often accompanied by macrocephaly (Bernier et al., 2014, O’Roak et al., 2012). Chd8 is a DNA helicase controlling chromatin remodeling and gene transcription. Several studies have addressed its role in neuronal progenitor cells (Cotney et al., 2015, Sugathan et al., 2014, Durak et al., 2016). Knockdown of Chd8 in hiPSCs-derived neuronal

progenitors followed by RNA-sequencing led to down-regulation of genes involved in cell-adhesion and neuron differentiation amongst other categories (Sugathan et al., 2014). More recently, Durak et al. (2016) identified perturbed neuronal progenitor proliferation upon *Chd8* knockdown in the mouse neuroepithelium. They also performed RNA-sequencing experiments after *Chd8* knockdown, obtaining some overlap with the previous study; for instance, neuron differentiation also appeared as a deregulated category (Durak et al., 2016). Additionally, cell cycle genes appeared as the most down-regulated category in fitting with cell biology experiments and further pointing to an important role for *Chd8* in progenitors' proliferation (Durak et al., 2016), which could be important for the macrocephaly phenotype observed in some patients.

#### **4.2 Cortical folding: lissencephaly type I, polymicrogyria, lissencephaly type II or cobblestone**

**Lissencephaly type I** refers to a series of neuronal migration disorders, which includes a disorganized cortex either without gyri (agyria), with abnormal and simplified gyri (pachygyria), or featuring abnormally positioned ectopic neurons within the white matter resulting in a 'double cortex' or subcortical band heterotopia phenotype (Romero et al., 2017, see following subsection). It can be caused by mutations in genes coding for microtubule associated proteins such as *LIS1*, *DCX*, *TUBA1A*, *TUBB2A* and *TUBG1* (Bahi-Buisson et al., 2008, Cushion et al., 2013, Des Portes et al., 1998, Des Portes et al., 1998, Fallet-Bianco, et al., 2008, Friocourt et al., 2011, Gleeson et al., 1998, Jaglin et al., 2009, Keays et al., 2007, Morris-Rosendahl et al., 2008, Poirier et al., 2007, 2013, Reiner et al., 1993). Mutations in proteins contributing to the actin cytoskeleton compartment can also lead to lissencephaly type I-like phenotypes. Indeed, mutations in *ACTB* and *ACTG1* can result in pachygyria or lissencephaly (Verloes et al., 2015). Of note also, mutations in the extracellular glycoprotein *RELN*, also cause lissencephaly and this protein has been shown to be essential for neuronal migration and cortical lamination in rodent, as well as human (D'Arcangelo et al., 1995, Dulabon et al., 2000, Hong et al., 2000, Rice and Curran, 2001).

These anomalies disrupting cortical folding have been classically associated with neuronal migration defects (Fernandez et al., 2016). However, impairment of certain genes associated with this pathology can also impact aRGs, possibly contributing to the phenotype (e.g. *LIS1*, which can also give rise to microcephaly) (Iefremova et al., 2017, Reiner and Sapir, 2013, Yingling et al., 2008). The extensive characterization of neuronal progenitor diversity and the development of 'human-like' approaches to study physiological and pathological cortical

development suggest both aRG and bRG defects as novel components contributing to this disorder (Bershteyn et al., 2017, Iefremova et al., 2017). Recently, two different studies used brain organoids to study the mechanisms leading to Miller-Dieker syndrome (MDS) (Bershteyn et al., 2017, Iefremova et al., 2017), a contiguous gene deletion leading to a severe form of lissencephaly. While defects in aRG divisions could be detected (Bershteyn et al., 2017, Iefremova et al., 2017), potentially recapitulating what had already been found by using mouse models (Yingling et al., 2008), a defect in bRG division was also observed (Bershteyn et al., 2017). These studies highlight the importance of further developing human-like approaches to study the mechanisms underlying cortical malformations, since human-specific features are likely to contribute to the latter.

**Polymicrogyria** is associated with the development of too many folds usually too small. Although it is characterized as an isolated malformation, there can be overlapping features with lissencephaly type II (Bahi-Buisson et al., 2010, see below). Impairment of the end stages of neuronal migration most likely due to abnormal attachment of aRGs at the pial surface are the main mechanisms proposed as responsible for the etiology of polymicrogyria (Bizzotto and Francis, 2015). In agreement, mutations in *GPR56*, coding for a G-protein coupled receptor mediating cell adhesion, lead to aberrant anchoring of the aRG basal processes to the basement membrane, causing breakages in the latter through which some neurons over-migrate (Bae et al., 2014). The causative genes for human polymicrogyria as an individual entity are rare, probably due to its frequent association with other malformations (Fernandez et al., 2016). However, mutations in tubulin and mTOR pathway genes have been associated to this malformation. Mutations in *TUBB2B* were shown in cases of bilateral asymmetrical polymicrogyria (Jaglin et al., 2009). *In utero* electroporation in the mouse neuroepithelium of a shRNA or mutant form of *Tubb2b* confirmed the importance of this gene for correct neuronal migration (Jaglin et al., 2009). Mutations in the mTOR signaling component *PIK3R2* have been associated to bilateral perisylvian polymicrogyria, the most common form of regional polymicrogyria (Mirzaa et al., 2015).

**Lissencephaly type II or cobblestone** is caused by over-migration of neurons, giving rise to a disorganized cerebral cortex with multiple coarse gyri and agyric regions (Bizzotto and Francis, 2015). The basal processes of aRGs, and presumably bRGs, are a critical structure at the basis of this malformation. Breaks in the basement membrane have been associated with basal processes not being properly attached to the extracellular matrix (ECM) (Bizzotto and Francis,



2015). Accordingly, disruption of this membrane has been associated with mutations in proteins enriched in the RG basal processes or in ECM components and/or receptors e.g. related to laminins and integrins (Radmanesh et al., 2013, Graus-Porta et al., 2001). Reduced glycosylation of alpha-dystroglycan, which is fundamental to anchor the basal process dystrophin complex to the ECM, is also associated with cobblestone lissencephaly (van Rieuwijk et al., 2005, Roscioli et al., 2012, Buysse et al., 2013).

#### **4.3 Heterotopia: periventricular and subcortical band heterotopia**

As discussed in section 3.1, cortical neuronal migration is a multi-step process and when altered it can lead to misplaced neurons (heterotopia). If abnormally positioned neurons are numerous and present in periventricular or subcortical regions, this often leads to epilepsy. Although it has been classically described as a neuronal migration malformation, aRG morphology, polarity, location and behavior can also contribute to this disorder (Beattie et al., 2017, Bizzotto et al., 2017, Bizzotto and Francis, 2015, Cappello et al., 2012, Jossin et al., 2017, Kielar et al., 2014, Liu et al., 2018, O'Neill et al., 2018a, O'Neill et al., 2018b, Zhang et al., 2019).

**Subcortical band heterotopia (SBH) or 'double-cortex'** is characterized by the presence of neurons within the white matter and beneath the normotopic cortex, which in turn is often thinner. Classically it has been considered a neuronal migration disorder; the neurons in the normotopic cortex migrate normally whereas those present in subcortical regions fail to reach their final position in the CP during development (Stouffer et al., 2015). It can be associated with a delay in somatic development, intellectual disability, as well as severe epilepsy (Bahi-Buisson et al., 2013). Classical forms of SBH mainly arise due to genetic mutations affecting components of the microtubule cytoskeleton (reviewed by Stouffer et al., 2015, Romero et al., 2018). Mutations in *LIS1*, *DCX* and *TUBA1A* have been associated with SBH (Reiner et al., 1993, Des Portes et al., 1998a, Des Portes et al., 1998b, Gleeson et al., 1998, Keays et al., 2007, Poirier et al., 2007, Fallet-Bianco, et al., 2008, Bahi-Buisson et al., 2008), each protein playing different roles at the microtubule cytoskeleton (Sapir et al., 1997, Francis et al., 1999). Indeed, mutations in *LIS1* and *DCX* explain a large proportion of SBH cases (around 80%; Bahi-Buisson et al., 2013). Further highlighting the contribution of the microtubule cytoskeleton, mutations in the kinesins *KIF2A* and *KIF5C* have also been associated with SBH (Di Donato et al., 2018). Although neuronal migration arrest is frequently associated with subcortical band heterotopia, mis-localization of progenitor cells at early stages of development is strongly emerging as a contributing factor to the etiology of certain forms of this pathology (Bizzotto

et al., 2017, Cappello et al., 2012, Kielar et al., 2014, Liu et al., 2018, Zhang et al., 2019, see also section 6.4)

Finally, the presence of abnormal clusters of misplaced neurons around the ventricles is termed **periventricular heterotopia**. Neurons fail to migrate radially and remain stuck close to the ventricles, even entering into them in the form of nodules. Impairment of neuronal migration is often also associated with abnormal neuronal progenitor proliferation, breakages in the AJ-actin belt between aRGs, as well as disruptions of aRG polarity and scaffolds (Beattie et al., 2017, Carabalona et al., 2012, Cappello et al., 2013, Ferland et al., 2019, Jossin et al., 2017, Kielar et al., 2014, O'Neill et al., 2018b). Mutations in *FLNA* and *ARFGEF2* are frequently associated with PVH (Guerrini and Marini, 2006, Lange et al., 2015, Parrini et al., 2016). The former acts on the actin cytoskeleton whilst the latter is important for Golgi-derived protein trafficking (Ohta et al., 1999, Lian et al., 2019, Sheen et al., 2004). However, knocking-down both in the developing murine cortex results in a very similar phenotype, suggesting they probably act through a final common downstream trafficking mechanism (Ferland et al., 2009). Mutations in other genes associated with the microtubule component of the cytoskeleton have been reported as well in cases of PVH (*TUBG1*, Poirier et al., 2013, *KIF2A*, Poirier et al., 2013, *EML1*, Kielar et al., 2014, *MAP1B*, Heinzen et al., 2018). Lately other genes with diverse subcellular functions have also been associated with this pathology. For instance, mutations in *FAT4* and *DCHS1* proteins key for aRG cell adhesion have been reported to cause PVH in human patients (Cappello et al., 2013) and mutations in the polarity protein *LLGL1* have been described in mouse models for this malformation (Beattie et al., 2017, Jossin et al., 2017). Finally, two main signaling pathways seem to be directly involved in the etiology of PVH. Firstly, mutations in *NEDDL4* and *AKT3* relate PVH to mTOR signaling (Alcantara et al., 2017, Broix et al., 2016). Secondly, mutations in proteins involved in the Hippo signaling pathway have been reported in several cases of PVH (Cappello et al., 2013, O'Neill et al., 2018a, Sarkisian et al., 2006).

Wider disrupted signaling is also expected in a different set of malformations termed ciliopathies which I discuss in the following section. These encompass a constellation of disorders including cerebral anomalies, retinal degeneration and renal disease, amongst other phenotypes.

## 4.4 Primary cilium related pathologies: ciliopathies and impact on the neocortex

### 4.4.1 Classical ciliopathies

The primary cilium is described in section 3.2.7. Mutations in proteins critical for its assembly/disassembly and/or function often lead to ciliopathies i.e. diseases caused by abnormal primary cilia (Reiter and Leroux, 2017). Ciliopathies comprise a range of conditions whose severity is correlated with the extent to which primary cilia are perturbed. These disorders often include multi-organ phenotypes such as polycystic kidneys, deafness, retinal degeneration, polydactyly, *situs inversus*, obesity and cerebral abnormalities (Reiter and Leroux, 2017, Wheway et al., 2018, Figure 34). The most severe ciliopathy is Meckel-Gruber syndrome, a lethal condition characterized by occipital encephalocele, renal cystic dysplasia and polydactyly. Another example related to CNS pathology is Joubert syndrome, where the cerebellum is severely affected and there are also eye abnormalities and kidney disease (Habbig and Libeau, 2015). Oral-facial-digital syndrome type I is another ciliopathy associated with mutations in the basal body component OFD1 (Bisschoff et al., 2012, Toriello et al., 2002). Interestingly, mutations in this protein have also been associated with subcortical heterotopia (Del Giudice et al., 2014).

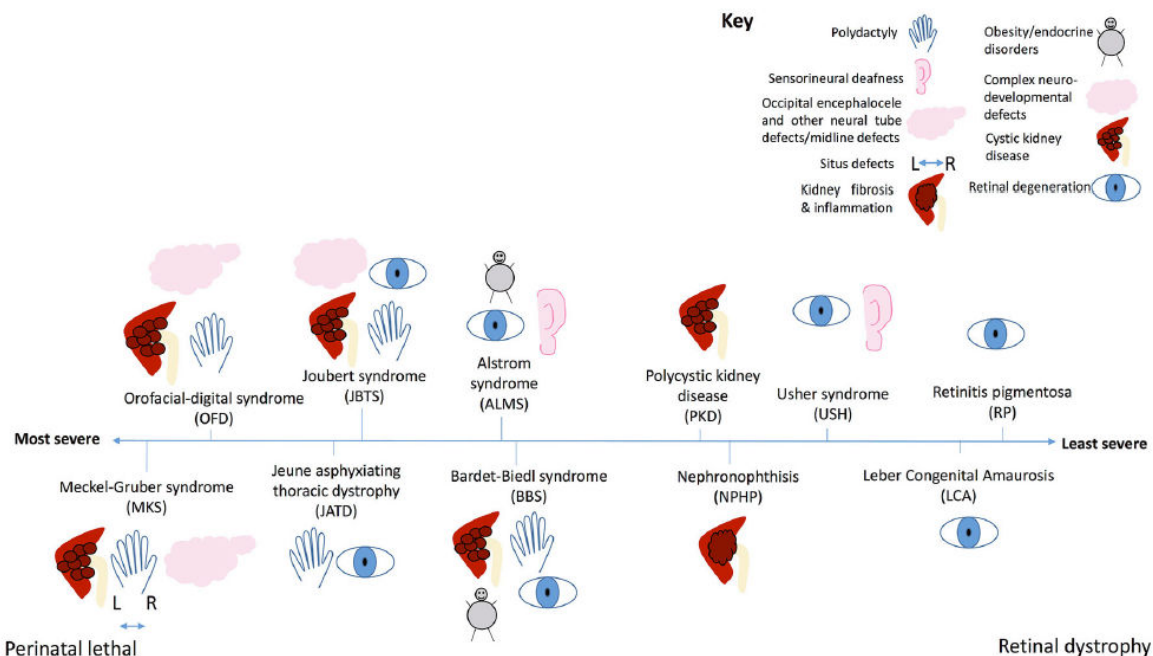


**Figure 34. The ciliopathy spectrum.** Schematic illustration of common features of classical ciliopathies, and severity of each ciliopathy along a spectrum. From Wheway et al., 2018.

### 4.4.2 The primary cilium and cortical malformations

Further related to the cortex, multiple cilia-related proteins are responsible for severe cortical anomalies. Mutations in *KIF2A* and *NDE1* lead to microcephaly and/or lissencephaly (Alkuraya

et al., 2011, Bakircioglu et al., 2011, Cavallin et al., 2017, Poirier et al., 2013). Mutations in Rotatin (RTTN), localized to the basal body, impair primary cilium formation (Kia et al., 2012) and are associated with microcephaly amongst other cortical malformations such as polymicrogyria and subcortical heterotopia (Cavallin et al., 2018, Grandone et al., 2016, Kia et al., 2012, Shamseldin et al., 2015, Wambach et al., 2018). *CENPJ* has also been associated with microcephaly (Darvish et al., 2010, Gul et al., 2006, Sajid Hussain et al., 2013).

The periventricular heterotopia gene *FLNA* has been previously reported to be involved in ciliogenesis (Adams et al., 2012). A conditional mouse mutant for the ciliary protein Kif3A shows 'rosette-like' heterotopias in the developing cortex (Wilson et al., 2012), although no patient has been identified phenocopying this model. The *HeCo* mouse model for subcortical heterotopia, the subject of this thesis, also shows a decrease in primary cilia in the VZ at early stages of corticogenesis (Bizzotto et al., 2017). Conditional knockout mice for *Ift88* and *Kif3A* also showed cortical anomalies. In these mouse models, aRGs presented an increased apical domain size, resulting in ventriculomegaly (Foerster et al., 2017). These studies point to the primary cilium as an emerging organelle disrupted in malformations other than microcephaly, especially in heterotopia.

Other studies have addressed the role of genes associated with cortical malformations in mouse models but giving rise to classical ciliopathies and not cortical malformations in human. *Arl13b* conditional knockout mice show abnormal aRG apico-basal polarity and knockdown of specific ciliopathy genes by *in utero* electroporation in the mouse neuroepithelium resulted in abnormal aRG proliferation and in the formation of 'rosette-like' structures in the VZ (Guo et al., 2015, Higginbotham et al., 2013). This work highlights the role of ciliopathy proteins in neocortical development. Finally, other proteins previously reported to cause heterotopia have been associated with the primary cilium in a non-neuronal context. This is the case of *Par3*, previously described to localize in the primary cilium of MCDK epithelial cells (Sfakianos et al., 2007). Knockdown of *Par3* in this cell line led to a reduction of primary cilia, which were also shorter (Sfakianos et al., 2007). Recent work by Liu and colleagues (2018) showed a conditional knockout mouse for *Par3* exhibiting subcortical band heterotopia (Liu et al., 2018), potentially further linking the primary cilium to this severe cortical malformation.

### **5. *Eml1/EML1*: a heterotopia gene mutated in mouse and human**

My PhD project has addressed specific aspects of cortical development at early-mid stages of corticogenesis, through the study of *Eml1* (Echinoderm microtubule-associated protein like 1),

a microtubule-associated protein showing mutations in patients presenting severe atypical heterotopia, as well as in the *Heterotopic Cortex (HeCo)* mouse model. In this section I will describe what is known about Eml1 and provide a brief description of other members of the protein family. I will then focus on human patient and *HeCo* mouse mutations and phenotypes, followed by a more detailed description of the *HeCo* cortical phenotype.

### 5.1 Structure of EMAP proteins

Eml1 belongs to the little-studied EMAP family of proteins, whose founding member was identified in the sea urchin as a 77-kDa polypeptide which co-purified with microtubules. This protein was the major non-tubulin component present in microtubule preparations from unfertilized sea urchin eggs (Suprenant et al., 1993). Afterwards, EMAP orthologues were found in other echinoderms and more distant eukaryotes such as flies, worms and vertebrates, where the term ELP or EML was adopted. Due to the lack of good antibodies, the precise location and function of these proteins have been difficult to address. However, studies using recombinant proteins have shown their association with microtubules (Eichenmuller et al., 2002, Houtman et al., 2007, Pollmann et al., 2006, Richards et al., 2015, Tegha-Dunghu et al., 2008). Additionally, several studies using peptide-specific antibodies recognizing the endogenous protein of two members of the EMAP family (EML3 and EML4) have also confirmed the microtubule association (Chen et al., 2015, Tegha-Dunghu et al., 2008). Focusing on EML1, Kielar et al. (2014) showed a cell cycle-dependent localization of the recombinant protein. At

interphase EML1 was localized in puncta form throughout the cytoplasm of neuronal progenitors. During mitosis, it localized to the mitotic spindle and to the midbody at later stages (Kielar et al., 2014, Figure 35). In

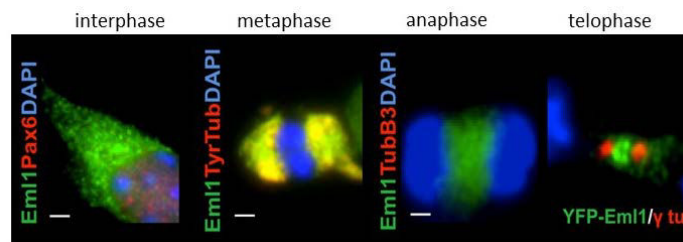


**Figure 35. Recombinant EML1 has a cell cycle dependent localization in neuronal progenitors.** E12.5-dissociated neuronal progenitors at 1 day *in vitro* (DIV). Adapted from Kielar et al., 2014. See also Figure 37.

mammals, the EMAP family comprises six EML proteins, EML1 to EML6 (Figure 36). EML1, 2, 3 and 4 contain similar protein structures. Their N-terminal domain contains approximately 175-200 residues, including a coiled-coil domain important for trimerization with other EML proteins and association with microtubules (Richards et al., 2015).

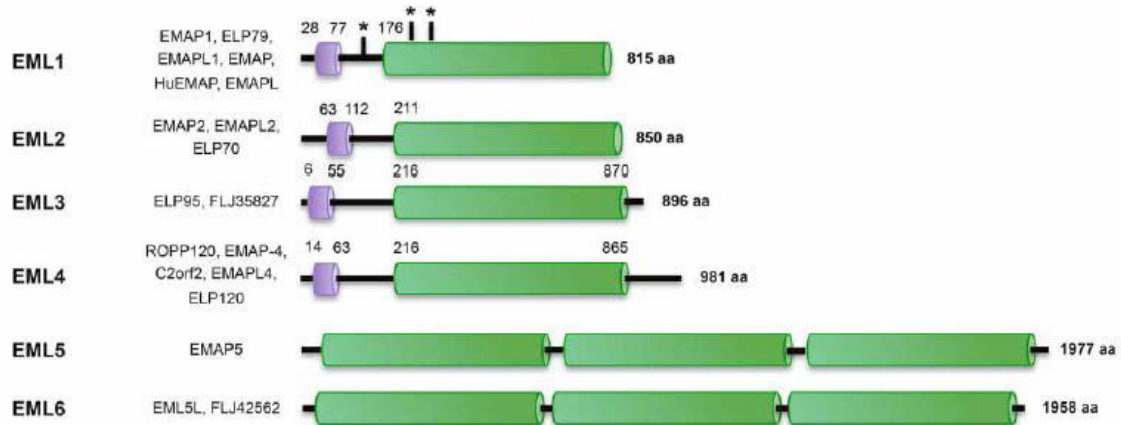


Figure 36. Schematic representation of mammalian EML protein structures. Adapted from Fry et al., 2016.

The C-terminal domain contains approximately 650 residues consisting of multiple WD (tryptophan-aspartate) repeats (Figure 34). Structural studies have determined the crystal structure of the large C-terminal domain of EML1 (residues 167-815), showing how the WD repeats form individual  $\beta$ -sheets which fold into the blades of two beta-propeller domains that are closely connected (Figure 37). The first beta-propeller (N-terminal) is formed by seven WD repeats. The second beta-propeller (C-terminal) is formed by six WD repeats and another domain consisting of separate regions of the primary sequence (Richards et al., 2014, Figure 37). EMAP proteins contain a characteristic hydrophobic EML protein (HELP) domain (Tegha-Dunghu et al., 2008, Richards et al., 2014, Richards et al., 2015). Rather than being a distinct domain, structural studies showed that it is buried at the interface of the two  $\beta$ -propellers. This particular  $\beta$ -propeller tandem configuration was termed the TAPE (tandem atypical propeller in EMLs) domain, and is a specific feature of the EMAP family (Richards et al., 2014)

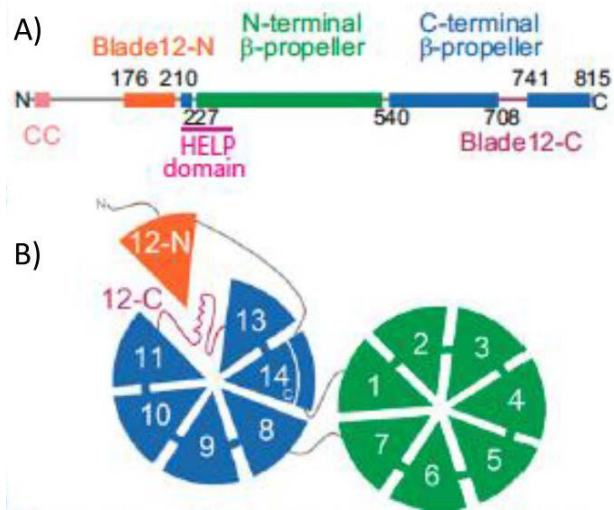


Figure 37. Schematic representation of EML1 structure.

A) Linear representation of the EML1 protein including residue numbering indicating domain boundaries. B) Cartoon representation showing the bottom face of the TAPE domain with numbered blades. Adapted from Richards et al., 2014.

The second beta-propeller (C-terminal) is formed by six WD repeats and another domain consisting of separate regions of the primary sequence (Richards et al., 2014, Figure 37). EMAP proteins contain a characteristic hydrophobic EML protein (HELP) domain (Tegha-Dunghu et al., 2008, Richards et al., 2014, Richards et al., 2015). Rather than being a distinct domain, structural studies showed that it is buried at the interface of the two  $\beta$ -propellers. This particular  $\beta$ -propeller tandem configuration was termed the TAPE (tandem atypical propeller in EMLs) domain, and is a specific feature of the EMAP family (Richards et al., 2014)

The C-terminal domains of EML2, EML3 and EML4 are also composed of WD40 repeats in close proximity to the HELP motif, forming hence also TAPE domains (Pollmann et al., 2006, Tegha-Dunghu et al., 2008, Fry et al., 2016, Figure 36).

As previously mentioned, the N-terminal domain is crucial for the interaction with microtubules (Fry et al., 2016, Richards et al., 2015). Homo and/or hetero-trimerization as well as the coiled-coil domain region seem to be important for microtubule

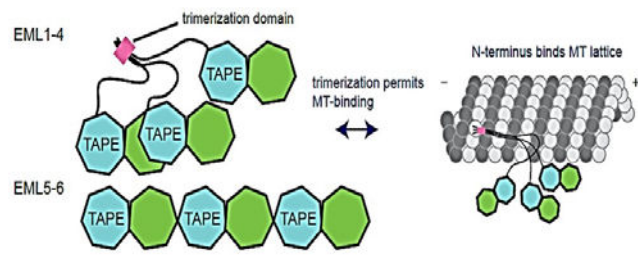


**Figure 38. Schema illustrating EML1 trimerization and association with microtubules.** Adapted from Richards et al., 2015.

association (Fry et al., 2016, Richards et al., 2015, Figure 38). The HELP domain was originally thought to be important for this association, however, the most recent studies suggest a structural function for this domain rather a microtubule-binding one (Eichenmuller et al., 2002, Pollmann et al., 2006, Richards et al., 2015, Suprenant et al., 2003). Another hypothesis suggests that the N-terminal region may mediate microtubule association through electrostatic interactions and ongoing studies may shed light in this direction (Fry et al., 2016). The C-terminal TAPE domain has been proposed to contribute to overall microtubule affinity (Eichenmuller et al., 2002), although rather than localizing to microtubules it appears to associate with soluble tubulin (Richards et al., 2014, Richards et al., 2015). It remains to be further studied if this implies a specific tubulin-binding role or if this domain also represents a second microtubule-binding site that is only effective in the context of a trimer (Fry et al., 2016).

EML5 and EML6 are the least studied members of the EMAP family. They lack the N-terminal region and have three consecutive TAPE domains. Despite of the lack of the N-terminal domain, it is hypothesized that these TAPE domains may provide a tertiary structure favoring microtubule binding (Fry et al., 2016, Figure 34). Of note, the *Drosophila* homolog ELP-1, also known as DCX-EMAP, contains a DCX-like domain within its N-terminus, which contributes to microtubule binding (Bechstedt et al., 2010). While this may suggest different mechanisms to associate to microtubules than human EMLs, it also highlights the contribution of the N-terminal domain to microtubule binding (Fry et al., 2016).

## **5.2 Expression in the nervous system and subcellular location and function of EMAP members**

Eml1-6 are expressed in the CNS in adulthood. After mutations were identified, Eml1 was further shown to be expressed in the cortex, hippocampus and thalamus (Kielar et al., 2014) and publicly available resources show it is also expressed in the olfactory bulb and the

cerebellum (Allen Brain Atlas). Eml2 shows a broader pattern of expression, with a decreased expression in the cerebellum when compared to other regions (Allen Brain Atlas). Eml3 is predominantly expressed in the hippocampus and the thalamus (Allen Brain Atlas). As Eml2, Eml4 also has a broad pattern of expression. It seems to be highly expressed throughout the cerebrum, with a lower expression in subcortical regions such as the thalamus, hypothalamus, striatum, globus pallidus and the cerebellum (Allen Brain Atlas). Eml5 is broadly expressed throughout the brain, whilst Eml6 was only detected in the cortex (Allen Brain Atlas).

Focusing on early stages of development and more precisely in the developing cortex (Figure 39), Eml1 was shown to be expressed in the VZ from early stages of cortical development (E12.5), as well as in the CP as corticogenesis progresses, evident from E14.5 (Bizzotto et al., 2017, Kielar et al., 2014). Eml4 has a very similar pattern of expression to Eml1 (GenePaint and unpublished data, Francis lab). Eml3 expressed in the VZ only (E14.5, Gene Paint) and Eml2, Eml5 and Eml6 show a faint pattern of expression in the CP (E14.5, Gene Paint).

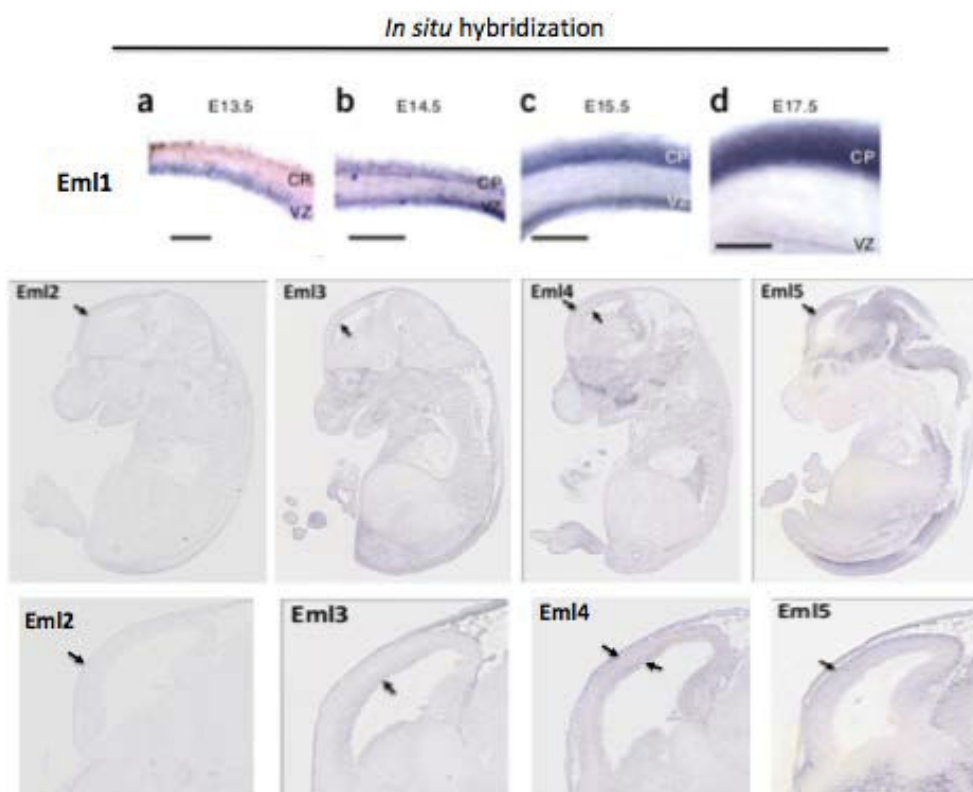


**Figure 39. Embryonic sagittal expression of Emls shown by *in situ* hybridization.** Above Eml1 in the developing cortex at different stages. Although labeling is faint, black arrows indicate ventricular zone and/or cortical plate expression. Adapted from Kielar et al., 2014. GenePaint (E14.5).

From a cellular perspective, several Eml proteins appear to have functions both in proliferating and differentiated cells. Interestingly, in neurons, the *C. elegans* EMAP homolog ELP-1 has



been previously reported to have a role in mechanotransmission: cells that lacked ELP-1 showed reduced touch sensitivity (Hueston et al., 2008). Consistently, the *Drosophila* homolog ELP-1 is expressed in ciliated neurons of the auditory organ, and when mutated it leads to mechanosensation defects (Bechstedt et al., 2010).

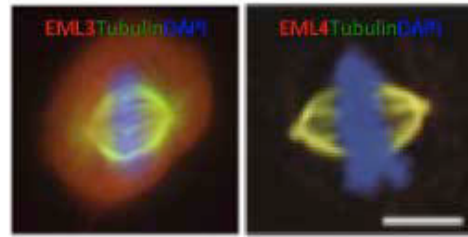


**Figure 40. EML3 and 4 co-localize with the mitotic spindle.** Adapted from Chen et al., 2015, Kielar et al., 2014, Tegha-Dunghu et al., 2008.

When focusing on proliferating cells, EML1, 3 and 4 have been reported to localize to the mitotic spindle during mitosis (Figure 35 and Figure 40), as well as to localize to the microtubule network during interphase (Eichenmuller et al., 2002, Kielar et al., 2014, Pollmann et al., 2006, Tegha-Dunghu et al., 2008). However, the relative affinity of EML proteins for microtubules in interphase and mitosis appears to differ, with potentially lower affinity during mitosis (Fry et al., 2016). Lately it has been proposed that this differential affinity for microtubules may be mediated by phosphorylation. This hypothesis is supported by studies showing hyperphosphorylation of EML4; NEK-6 dependent phosphorylation of EML3; and also phosphorylation of the sea urchin EMAP, all in mitotic cells (Brisch et al., 1996, Fry et al., 2016, Pollmann et al., 2006). In the case of EML3 its phosphorylation was shown to decrease its affinity for microtubules (Fry et al., 2016). Additionally, phosphoproteomic studies show a high concentration of phosphorylation sites in the N-terminal region of EMLs, further supporting a role for this process in mediating microtubule affinity (Fry et al., 2016).

Studies on the sea urchin EMAP suggested a role for the EMLs in microtubule dynamics (Hamill et al., 1998). However, the role of these individual proteins still remains unclear and whilst some seem to promote microtubule stabilization (e.g. EML4; Houtman et al., 2007, Pollmann et al., 2006), others appear to promote their destabilization (e.g. EML2; Eichenmuller et al., 2002). Recently, Bizzotto and colleagues (2017) analyzed microtubule plus-end growth in Eml1-mutant neuronal progenitors, describing a role for this protein favoring microtubule polymerization (Bizzotto et al., 2017).

Focusing on their mitotic spindle localization and their potential role related to this structure, EML3 has been shown to be important for metaphase chromosome alignment and a very recent study by Luo et al. showed its role in promoting microtubule nucleation to ensure proper assembly of the mitotic spindle (Luo et al., 2019, Tegha-Dunghu et al., 2008). EML4 has been reported to be important for the organization of the mitotic spindle, and more precisely,

for the correct attachment of spindle microtubules to kinetochores in metaphase (Brisch et al., 1996, Chen et al., 2015). Several mitotic-related defects have been described in Eml1-mutant conditions in neuronal progenitors, such as abnormal spindle orientation and increased spindle length (Bizzotto et al., 2017, Kielar et al., 2014, see below).

Although all these studies strongly support a microtubule-related function for the different members of the EMAP family, the exact mechanisms by which they mediate these processes still need to be unraveled. It seems likely that the EML proteins have different microtubule dynamic functions, although this may depend on their phosphorylation state, as well as the cell type. Several EMLs appear to favor correct spindle assembly and function, although potentially playing different roles in this process. Soluble tubulin binding and heterotrimerization of these proteins has not yet been taken into account for these functions.

### 5.3 Human patients: mutations and phenotype

My thesis has focused on the study of Eml1/EML1 in the context of cortical development and cortical malformations. Before going into the details of the latter, it is important to mention that EML proteins have been previously associated with different types of cancer. EML1, EML4 and EML6 form oncogenic fusion proteins involved in leukemia and lung cancer (De Keersmaecker et al., 2005, De Keersmaecker et al., 2006, Sasaki et al., 2010, Zhao et al., 2018).

Hence it is important to fully understand their functions, especially in proliferative cells.

Focusing on the nervous system, mutations in EML1 have been reported in three families presenting severe atypical heterotopia, corpus callosum agenesis and macrocrania (Kielar et al., 2014, Shaheen et al., 2017, Figure 41).

Two of these families were reported in a study performed by the Francis lab in collaboration with Dr. A. Croquelois, Switzerland, and French and Dutch clinicians (Kielar et al., 2014). The first family (P135) showed compound

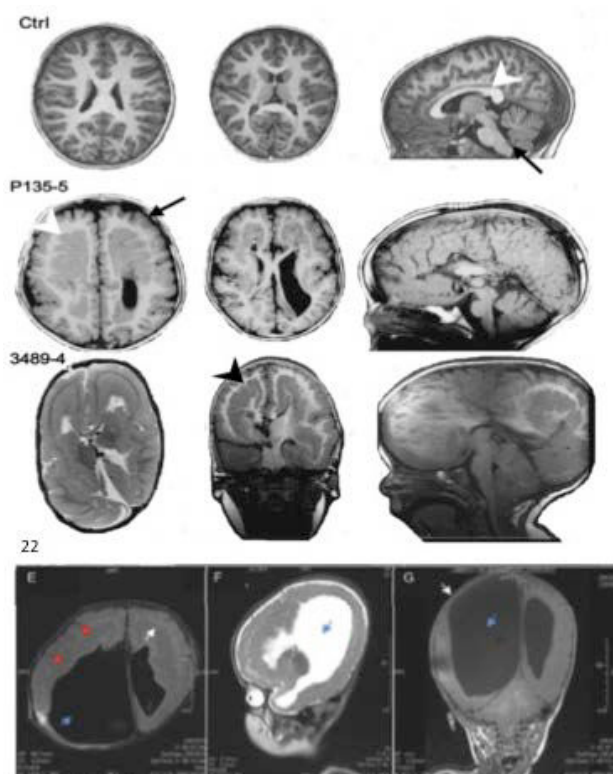
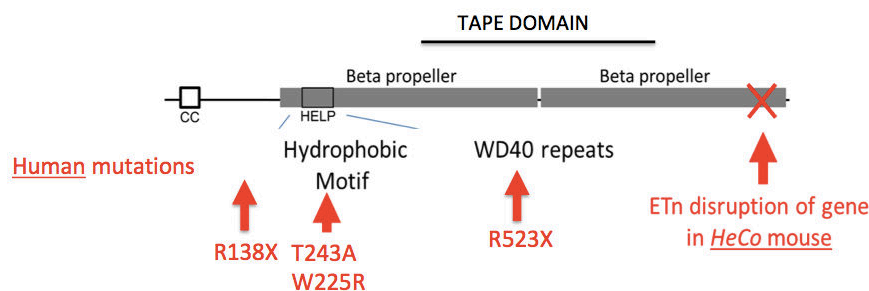


Figure 41. MRIs of *EML1* mutation patients. Adapted from Kielar et al., 2014. Shaheen et al., 2017.

heterozygous mutations in their three children. This consisted of a c.481C>T nucleotide mutation in exon 5, changing an arginine residue to a stop codon (R138X), transmitted from the mother, and a c.796A>G mutation in exon 8 changing a threonine into an alanine residue (T243A). The second family (P3489) had one child affected with a homozygous c.673T>C mutation, changing a tryptophan into an arginine residue (W225R) (Figure 42). These patients are males presenting intellectual disability and epilepsy (Kielar et al., 2014). The third family (22) was described recently, with a girl presenting a very similar phenotype to the patients described above. A c.1567>T mutation in exon 14 of EML1 was reported, changing an arginine residue to a stop codon (R523X) (Shaheen et al., 2017, Figure 42). Of note, families P3489 and 22 also presented hydrocephaly, whilst families P135 and 22 showed polymicrogyria (Kielar et al., 2014, Shaheen et al., 2017).



**Figure 42. Schematic representation of the EML1 gene indicating the position of the mutations.** The schema also shows the Eml1 mutation present in the *HeCo* mouse (see next section). Adapted from Kielar et al. 2014, Shaheen et al., 2017, Richards et al., 2015.

Further work is required in order to check EML1 RNA and protein levels and to test the effect of these mutations. Nonsense mutations are expected to lead to nonsense-mediated RNA decay. The missense mutation found in family P3489 (W225R) is predicted to severely impact the conformation of the EML1 TAPE domain, resulting in protein degradation (R. Bayliss, U.K., personal communication). Thus, the only known mutation that may still allow correct protein production and stability is the missense mutation found in family P135 (T243A). Indeed, a recombinant version of this protein appeared equivalent to wild-type on Western blots (Kielar et al., 2014). Experiments in Vero cells were performed to assess microtubule association. A reduced association with interphase microtubules was observed with the recombinant T243A protein

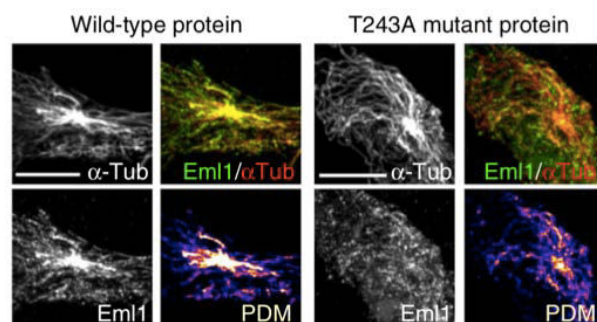


**Figure 43. Mutant EML1 shows less co-localization with the microtubule network in Vero cells.** From Kielar et al., 2014.

(Kielar et al., 2014, Figure 43), suggesting an alteration of microtubule-binding in the presence of the patient mutation.

#### **5.4 Rodent models of heterotopia: the *HeCo* mouse**

Rodent models for genes mutated in human subcortical heterotopia often fail to recapitulate the phenotype. However, some rodent models have emerged which are good resources to study the pathological mechanisms associated to this severe malformation. Knockdown of *Dcx* by *in utero* electroporation in the rat neuroepithelium causes heterotopia (Ramos et al., 2006, Lapray et al., 2010), however this phenotype is not observed in chronic genetic mutant mouse models (Corbo et al., 2002, Kappeler et al., 2006, Nosten-Bertrand et al., 2008). Following a similar experimental approach, overexpression of *Wnt3a* in the mouse neuroepithelium by *in utero* electroporation also leads to heterotopia formation, although *Wnt3a* has not been associated to human patients (Munji et al., 2011). Additionally, several rodent models have been identified in which mutations in genes lead to heterotopia formation. This is the case of the spontaneous BXD29 mouse model (Rosen et al., 2013). These mice present subcortical heterotopia composed mainly of upper layer neurons (Rosen et al., 2013, Ramos et al., 2016). Conditional knockout mice for *Rapgef2*, *RhoA*, *Ligl1* and *Par3* also present a heterotopia phenotype (Bilasy et al., 2009, Beattie et al., 2017, Cappello et al., 2012, Jossin et al., 2017, Liu et al., 2018). Interestingly, the last three mouse models mentioned above showed neuronal progenitor cell anomalies that could be responsible for the heterotopia emerging at later stages. *RhoA* conditional knockout mice show abnormal scattered *Pax6+* and *Tbr2+* progenitors throughout the cortical wall. Additionally, the aRG scaffold was disrupted (Cappello et al., 2012). aRGs in *Ligl1* conditional knockout mice showed abnormal polarity and AJ disruption (Beattie et al., 2017, Jossin et al., 2017). Finally, *Par3* conditional knockout mice show the presence of ectopic *Pax6+* progenitors outside the VZ from early stages of corticogenesis (Liu et al., 2018). The heterotopia in this case is mainly composed of upper layer neurons, as in the BXD29 model (Liu et al., 2018, Ramos et al., 2016, Rosen et al., 2013). One of the earliest rodent models described to present SH is the *tish* (telencephalic internal structural heterotopia) rat (Lee et al., 1997). As in the *Par3* conditional knockout mouse, ectopic *Pax6+* progenitors were found dividing outside the VZ and the aRG scaffold seemed to be disrupted (Fitzgerald et al., 2011). All of these chronic models are of great interest to study the etiology of severe heterotopia as well as the pathologic consequence of the aberrant

cortical phenotypes. However, the genes responsible for the murine phenotypes have not been directly correlated with patients presenting cortical malformations.

In my project I have been working with the *HeCo* (heterotopic cortex) mouse, a model for subcortical heterotopia in which the *Eml1* gene is mutated. As mentioned in section 5.3, autosomal recessive mutations in *EML1* were described in families presenting severe atypical heterotopia. Working with the *HeCo* mouse model and further dissecting *Eml1* function are hence an excellent entry point to elucidate the developmental mechanisms responsible for the etiology of severe heterotopia, both in mice and humans.

The *HeCo* mouse arose as a spontaneous mutant arising in a colony on the NOR/CD1 genetic background (Croquelois et al., 2009). The mutation in *Eml1* consists of the insertion of a retrotransposon in the last intron of the gene (see Figure 42). This leads to the absence of full length transcripts, although some shortened transcripts (containing exons 3 and 4) and trace amounts of chimeric transcripts could be detected (Kielar et al., 2014). The mode of transmission is autosomal recessive (Croquelois et al., 2009). The *HeCo* mouse presents bilateral subcortical heterotopia located in the dorso-medial part of the neocortex, constituting the 'heterotopic cortex' (Figure 44). The latter is separated from the normotopic cortex by a thick layer of white matter (Croquelois et al., 2009). Individual mice showed different degrees of severity, however the heterotopia was always conserved. Additionally, a mild ventricular enlargement was described (Croquelois et al., 2009). Other parts of the brain (i.e. hippocampus, striatum, thalamus, cerebellum and brainstem), as well as other organs were reported to have a normal microscopic appearance (Croquelois et al., 2009).

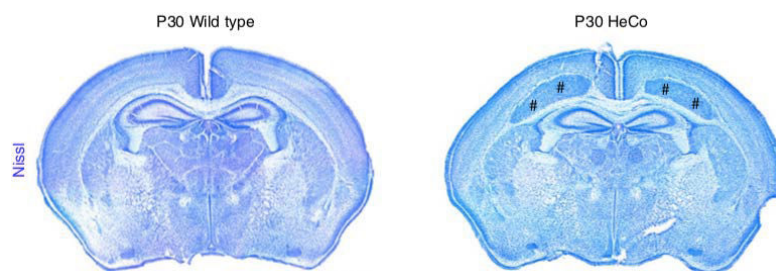


**Figure 44.** *HeCo* mice show bilateral subcortical heterotopia. (Indicated by #) From Kielar et al., 2014.

In agreement with the patient phenotypes, *HeCo* mice are susceptible to epilepsy. Young animals (4-5 weeks) present spontaneous myoclonic jerks as well as an increased tendency to develop seizures in the pilocarpine-induced model of epilepsy (Croquelois et al., 2009). These mice also present a significantly delayed somatic and locomotor maturation. Moreover, there

is a significant effect of aging on memory performance during task acquisition, while younger animals have relatively preserved memory abilities (Croquelois et al., 2009).

#### *Cortical phenotype of the HeCo mouse*

The heterotopia present in the *HeCo* mouse is mostly composed of Cux2+ ‘upper layer’ neurons (Figure 45). The presence of GABAergic interneurons was also noted. The normotopic cortex appeared thinner than in wild type mice, and the thickness and cell density of the upper layers was significantly reduced (Croquelois et al., 2009). Afferent projections were described to reach the heterotopic cortex (Croquelois et al., 2009).

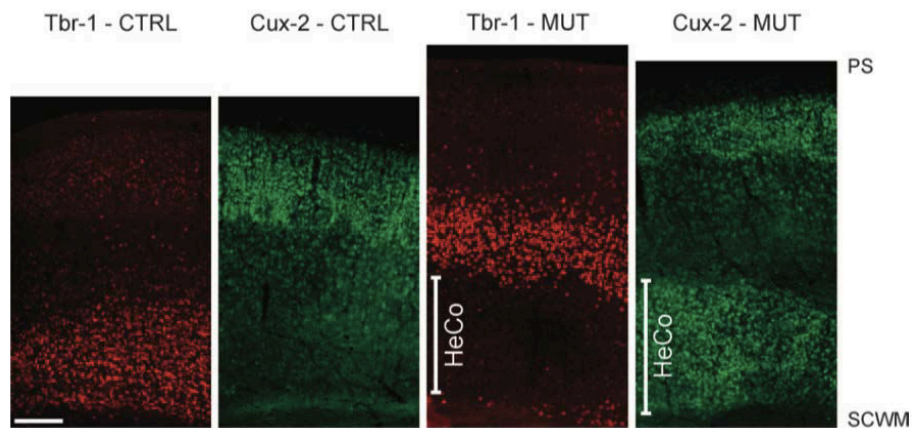


**Figure 45. The heterotopia in *HeCo* mice is mainly composed of upper layer neurons.** Cux2: upper layer marker; Tbr1: deep layer marker. PS: pial surface, SCWM: subcortical white matter. From Croquelois et al., 2009.

Different stages of cortical development were assessed to further investigate the mechanisms of heterotopia formation. Aberrantly positioned Tbr1+ (deeper layers) and Cux1+ (upper layers) neurons could be detected in the IZ at E17 in *HeCo* mice (Kielar et al, 2014). Tbr1+ neurons were abundant both in the heterotopia and in basal regions reaching the CP, whilst in wild type conditions these cells had already migrated to the CP. Analyses at P3 revealed that most of the Tbr1+ cells had reached their position in the *HeCo* CP, whilst Cux1+ failed to migrate and were still present in the heterotopia. At P7, when upper layer neuronal migration was completed in wild type mice, Cux1+ cells were still trapped in the heterotopia and columns of Cux1+ cells were observed migrating towards the CP. Therefore, the heterotopia is first populated by early-born neurons, followed by late-born neurons. Whilst the former manage to migrate to their correct positions in the CP, the latter remain trapped in the white matter (Kielar et al., 2014, Figure 46).

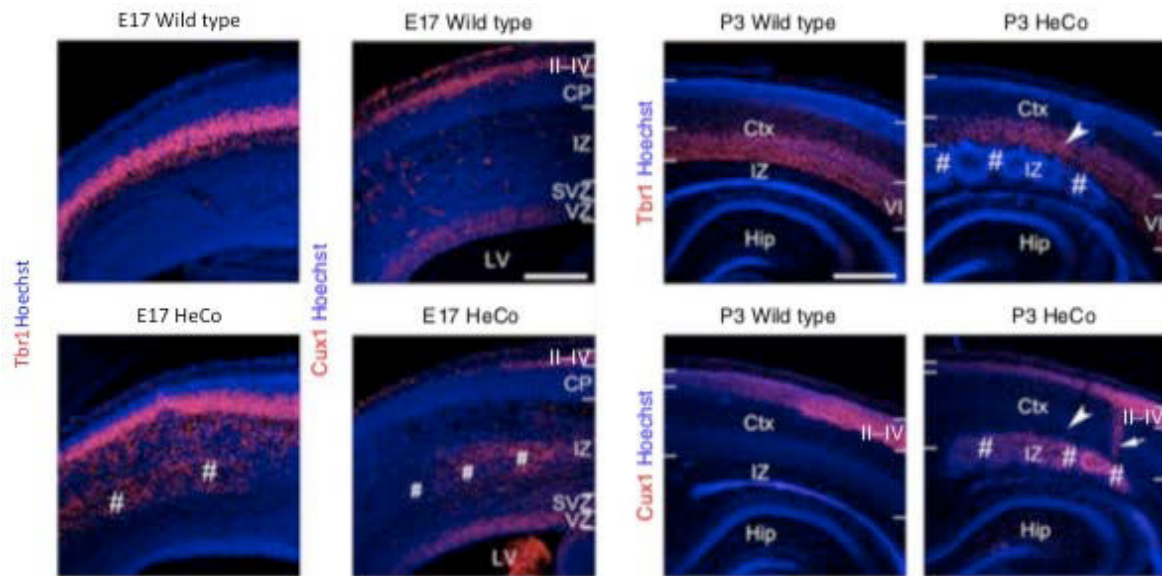


**Figure 46. Accumulation of neurons in the *HeCo* mouse brain.** CP: cortical plate, IZ: intermediate zone, SVZ: subventricular zone, VZ: ventricular zone, LV: lateral ventricle, Ctx: cortex, Hip: hippocampus. Adapted from Kielar et al., 2014.

Neuronal migration was assessed by performing *ex utero* electroporation at E15.5 and analyzing neuronal behavior at later stages. Although fewer electroporated cells reached the CP in the *HeCo* mouse, motility parameters did not differ between the genotypes (speed, pause frequency, pauses/h, pause duration, trajectory orientation). Nevertheless, some *HeCo* electroporated cells remained blocked in the IZ (Kielar et al., 2014). Additionally, transplantation studies of *HeCo* cortical cells in isochronic wild type cortices showed that in a normal environment, these neurons could migrate as wild-type. These results suggested that neuronal migration *per se* was not hampered; rather other external mechanisms were responsible for the perturbation of some migrating cells and the development of the heterotopia.

The authors then focused on earlier developmental stages, identifying cycling, Pax6<sup>+</sup> neuronal progenitors ectopically localized outside the normal proliferative VZ (Figure 47). This phenotype was observed from E13. Delamination of progenitors from the VZ has been associated with changes in spindle orientation, as well as with disruption of the AJ-actin belt. Therefore, spindle orientation was analyzed at E13 and E16 and at both time points a shift towards oblique divisions was described. However, analyses of AJ or polarity markers ( $\beta$ -catenin, Par3) at the same developmental stages did not reveal any obvious defects (Kielar et al., 2014). The aberrant progenitor cell dynamics and their accumulation in the IZ where the heterotopia develops are likely to be a primary cause leading to the heterotopia phenotype.

Although analyses of the *HeCo* VZ revealed mitotic defects (i.e. spindle orientation) (Kielar et al., 2014), the mechanisms causing neuronal progenitors to leave their proliferative zone remained unknown. This subject became the main topic of my PhD thesis.

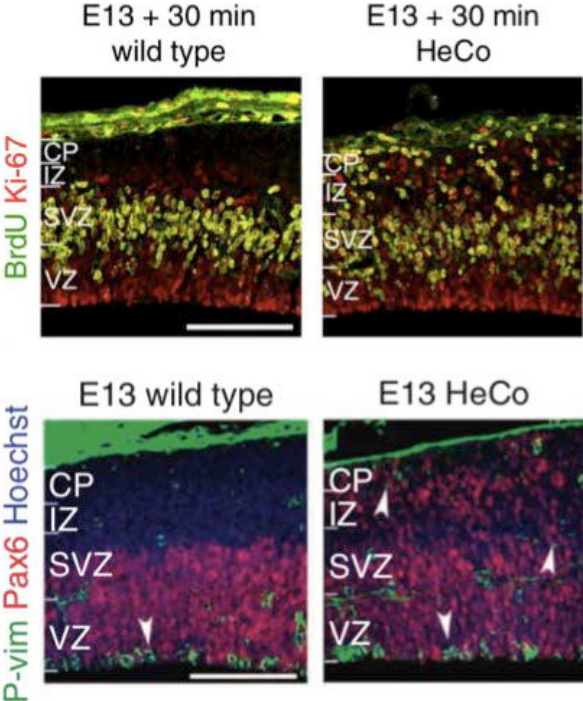


**Figure 47. *HeCo* mice show ectopically localized proliferating Pax6+ neuronal progenitors outside the normal proliferative VZ.** CP: cortical plate, IZ: intermediate zone, SVZ: subventricular zone, VZ: ventricular zone. Adapted from Kielar et al., 2014.



## **RESULTS**

## Results

### Preamble

This section is presented in the form of three manuscripts (one published, two submitted) on which I am first or co-first author. In each case I provide a brief summary, as well as specifying my contribution, before presenting the paper. When appropriate, I also describe additional data I produced relevant to the work, this data appearing after the manuscript (2 and 3).

In section 6 of the introduction I described the heterotopia phenotype exhibited by the *HeCo* mouse, as well as the microtubule-associated protein Eml1, mutated in this mouse model. From early stages of cortical development, ectopically located Pax6+ progenitors (i.e. aRGs) were found outside the VZ in the *HeCo* mouse brain. aRG delamination from the VZ may be the primary cause perturbing neuronal migration and organization, and resulting in heterotopia in adulthood. However, why some aRGs leave the VZ remains vastly unexplored and this was the focus of my thesis work.

In Articles 1 and 2, we focused on analyzing aRGs in wild type and Eml1-mutant conditions to shed light on 'pathological' mechanisms contributing to the etiology of the ectopic progenitor phenotype. Given the interaction of Eml1 with microtubules during the different stages of cell cycle, we examined microtubule-dependent processes in aRGs, including during mitosis (article 1) and during interphase (article 2). Article 3 consists of the neuroanatomical characterization of a newly generated Eml1 knockout mouse.

## **1. Introduction to Bizzotto, Uzquiano et al. (2017) 'Eml1 loss impairs apical progenitor spindle length and soma shape in the developing cerebral cortex.'**

As previously described in section 6.2 of the introduction, Eml1 has a cell cycle-dependent localization. Focusing on mitosis, recombinant Eml1 was found at the spindle poles, while at later stages it localized to the midbody (Kielar et al., 2014). In Bizzotto, Uzquiano et al, we began to assess the role of Eml1 during mitosis, and more precisely its relationship with the mitotic spindle.

### **1.1 Summary**

Given the association of Eml1 with microtubules, we first decided to investigate the growth properties of the latter. Neuronal progenitor cultures were transfected with EB3-mCherry followed by time-lapse imaging, allowing the measurement of the microtubule plus-end elongation rate. We observed that **microtubule growth speed was decreased in *HeCo* aRGs when compared to WT.**

We then analyzed aRGs in their tissue environment by performing experiments directly in brain slices. By performing immunohistochemistry followed by confocal imaging, we assessed the position of centrosomes ( $\gamma$ -tubulin) and primary cilia (Arl13b) in the VZ of WT and *HeCo* mice at early stages of cortical development (E13.5), when ectopic progenitors were first described (Kielar et al., 2014). These two organelles showed different localizations in *HeCo* brains when compared to WT. **There was a decrease in the number of centrosomes located at the VS, where they are normally positioned in interphase aRGs.** However, an increase was detected in the number of basally located centrosomes, which were not obviously associated with dividing cells. **When assessing primary cilia, these organelles were decreased in the VS** and no obvious corresponding increase was observed in basally located regions, thus leading to a decrease in the overall number of these organelles detected in the *HeCo* VZ. These results seem to suggest diverse behaviors of these two normally tightly linked organelles in mutant aRGs. Additionally, these results indicate VS anomalies, potentially linked to apical endfeet detachment.

As described in section 3.2.3 of the introduction, mitotic spindle assembly and dynamics have been previously correlated with aRG behavior, impaired corticogenesis and even bRG production. We thus focused our analysis on mitotic aRGs and more precisely mitotic spindle characteristics, notably length (pole-to-pole distance). 3D reconstructions of (pro)-metaphase aRGs were performed and  $\gamma$ -tubulin immunodetections were used to recognize the spindle

poles. **On average, spindle length was increased in *HeCo* aRGs at E13.5, supporting mitotic microtubule anomalies in *Eml1* mutant conditions.**

To further understand the phenotype observed and elucidate the molecular mechanisms that could be involved, **a mass spectrometry (MS) screen was performed searching for *Eml1*-interacting protein partners.** These experiments were carried out using an EML1 N-ter construct, the protein domain required for trimerizing with other members of the EMAP family and also interacting with microtubules. Pull down experiments were performed with purified GST-EML1 N-ter and E13.5 embryonic cortex lysates, followed by MS analyses. After data acquisition and filtering, a list of 176 potential *Eml1* interacting partners was obtained. **Gene Ontology (GO) analyses of the latter pointed to cell cycle, cell division and transport as the most represented categories.** Additionally several centrosome-related proteins were obtained (e.g. Plk1, Nde1). **In agreement with results obtained by other approaches, several proteins involved in regulation of spindle length were also present in the list** (e.g. KifC1, Kif2A, Kif22, Kif2C, Tpx2, Dync1h1).

Finally, we investigated if the change in spindle length was associated with an increase in cell size. In order to analyze cell size and shape, immunostainings were performed for N-Cadherin or F-actin combined with Hoechst, to observe cell boundaries and DNA condensation, respectively. This was followed by *en face* confocal imaging and measurements of 2D-cell areas of (pro)-metaphase aRGs at E13.5. ***HeCo* (pro)-metaphase aRG area was on average larger when compared to WT aRGs.** Strikingly, when we assessed the volume of these cells, there was not a significant difference between WT and *HeCo* aRGs cells. However, the latter differed in their height, implying that ***HeCo* cells are flatter than WT**, which could explain the increase in 2D area.


These combined results may indicate an impact of abnormal mitotic microtubule-dependent processes (increased spindle lengths) on VZ dynamics: the abnormally shaped aRGs during division could lead to increased horizontal forces, creating cell constraints and encouraging some aRGs to delaminate from the VZ and divide in more basal positions.

## **1.2 Contribution**

When I arrived in the lab I worked closely with Sara Bizzotto, a 4<sup>th</sup> year PhD student in the Francis team. I contributed to this article by performing immunohistochemistry experiments in brain slices and *en face* imaging followed by confocal microscopy. More precisely, I performed immunodetections for protein partners, *en face* imaging for F-actin combined with

Hoechst and *in situ* hybridization of Eml1 at E12.5. I performed  $\gamma$ -tubulin and Arl13b+ VZ experiments and analyses. These were crucial for the central project of my thesis (see next section, article 2). Finally, I actively contributed to manuscript writing and revisions and data interpretation.

# SCIENTIFIC REPORTS



OPEN

## Eml1 loss impairs apical progenitor spindle length and soma shape in the developing cerebral cortex

Sara Bizzotto<sup>1,2,3,10,11,12</sup>, Ana Uzquiano<sup>1,2,3</sup>, Florent Dingli<sup>4</sup>, Dmitry Ershov<sup>5</sup>, Anne Houllier<sup>1,2,3</sup>, Guillaume Arras<sup>4</sup>, Mark Richards<sup>6</sup>, Damarys Loew<sup>4</sup>, Nicolas Minc<sup>5</sup>, Alexandre Croquelois<sup>7,8</sup>, Anne Houdusse<sup>9</sup> & Fiona Francis<sup>1,2,3</sup>

The ventricular zone (VZ) of the developing cerebral cortex is a pseudostratified epithelium that contains progenitors undergoing precisely regulated divisions at its most apical side, the ventricular lining (VL). Mitotic perturbations can contribute to pathological mechanisms leading to cortical malformations. The *HeCo* mutant mouse exhibits subcortical band heterotopia (SBH), likely to be initiated by progenitor delamination from the VZ early during corticogenesis. The causes for this are however, currently unknown. Eml1, a microtubule (MT)-associated protein of the EMAP family, is impaired in these mice. We first show that MT dynamics are perturbed in mutant progenitor cells *in vitro*. These may influence interphase and mitotic MT mechanisms and indeed, centrosome and primary cilia were altered and spindles were found to be abnormally long in *HeCo* progenitors. Consistently, MT and spindle length regulators were identified in EML1 pulldowns from embryonic brain extracts. Finally, we found that mitotic cell shape is also abnormal in the mutant VZ. These previously unidentified VZ characteristics suggest altered cell constraints which may contribute to cell delamination.

The mammalian cerebral cortex develops from neural progenitors that form a specialized proliferative layer in the developing brain, the VZ. Radial glial cells (RGCs), also named apical progenitors (APs), are the most abundant cells that divide in this zone, and are able to both self-renew and to produce other cell types, being crucial for post-mitotic neuron development in the cortex. These cells have a specialized morphology with apical and basal processes that anchor them to the VL and pial surface respectively<sup>1</sup>. In interphase RGCs, centrosomes are located at the extremity of apical processes and delineate the VL. The centrosome is tightly connected with the primary cilium, which is also localized in apical end-feet of RGCs during interphase. The primary cilium is an MT-based organelle, which projects towards the ventricle in order to sense signals from the cerebrospinal fluid<sup>2</sup>. RGC nuclei move apico-basally during the cell cycle in a characteristic process known as interkinetic nuclear migration (INM). Mitosis occurs when the nuclei are in contact with the VL. Prior to mitosis, centrosomes move a short distance basally before undergoing duplication and forming the spindle poles<sup>3</sup>. Ciliary remnants keep in close contact with the mother centriole and may play a role in daughter cell fate<sup>4</sup>. The importance of correctly regulated RGC morphology and division is indicated by the numerous cortical malformation phenotypes observed in mouse mutants with a perturbed VZ<sup>5</sup>.

<sup>1</sup>INSERM UMR-S 839, 17 rue du Fer à Moulin, Paris, 75005, France. <sup>2</sup>Sorbonne Universités, Université Pierre et Marie Curie, 4 Place Jussieu, Paris, 75005, France. <sup>3</sup>Institut du Fer à Moulin, 17 rue du Fer à Moulin, Paris, 75005, France. <sup>4</sup>Institut Curie, PSL Research University, Centre de Recherche, Laboratoire de Spectrométrie de Masse Protéomique, 26 rue d'Ulm, 75248 Cedex 05, Paris, France. <sup>5</sup>Institut Jacques Monod, UMR7592 CNRS, Paris, France. <sup>6</sup>Department of Biochemistry, University of Leicester, Henry Wellcome Building, Lancaster Road, Leicester, LE1 9HN, UK. <sup>7</sup>Department of Clinical Neuroscience, Centre Hospitalier Universitaire Vaudois and University of Lausanne, 21 rue du Bugnon, 1011, Lausanne, Switzerland. <sup>8</sup>Department of Fundamental Neurosciences, University of Lausanne, 1005, Lausanne, Switzerland. <sup>9</sup>Structural Motility, Institut Curie, Centre de Recherche; CNRS, UMR144, 26 rue d'Ulm, Cedex 05, Paris, 75248, France. <sup>10</sup>Present address: Departments of Pediatrics and Neurology, Harvard Medical School, Boston, MA, USA. <sup>11</sup>Present address: Broad Institute of MIT and Harvard, Cambridge, MA, USA. <sup>12</sup>Present address: Division of Genetics and Genomics, Manton Center for Orphan Disease, and Howard Hughes Medical Institute, Boston Children's Hospital, Boston, MA, USA. Sara Bizzotto and Ana Uzquiano contributed equally to this work. Correspondence and requests for materials should be addressed to F.F. (email: [fiona.francis@inserm.fr](mailto:fiona.francis@inserm.fr))

We focus here on the spontaneous *HeCo* mouse mutant<sup>6,7</sup>, which shows heterotopia and a proportion of abnormal RGCs dividing outside the VZ during development<sup>7</sup>. Ectopic proliferating cells expressing RGC markers are found in the intermediate zone (IZ) and cortical plate (CP) at embryonic day (E) 13.5, coincident with early-mid corticogenesis, which supports the idea that delamination of a proportion of cells from the VZ might be the primary cause of the heterotopia phenotype<sup>7</sup>. The mechanisms responsible for delamination, which occur in a number of mouse mutants and physiologically in primate and human brains<sup>8,9</sup>, are however still unclear and the focus of intense interest. Apical cell junction markers do not appear to be majorly disrupted in the *HeCo* VL<sup>7</sup> which has been shown to be a sign of RGC abnormalities in other mutants<sup>10,11</sup>.

The mutant gene in *HeCo* mice is *Eml1* (*Echinoderm microtubule-associated protein like-1*, also known as *Emapl-1*), coding for a MT-binding protein expressed in the VZ during cortical development<sup>7</sup> and whose function in APs is unknown. The mutation found in *HeCo* *Eml1* consists of the insertion of a retrotransposon in the last intron of the gene, leading to the absence of the full-length transcript and protein<sup>7</sup>. We showed previously that recombinant Eml1 binds directly to MTs *in vitro* and strongly co-localizes with the MT network during both interphase and mitosis in progenitor cells<sup>7</sup>. Several other members of the EMAP family, such as sea urchin EMAP, *Xenopus* XMAP, and mammalian EML2, EML3 and EML4, also participate in the regulation of MT dynamics, including within the mitotic spindle<sup>12–16</sup>. However, this family of proteins, and especially EML1, remains poorly studied.

Regulation of the spindle is a finely controlled process, and mutations have been found in several spindle genes which severely disrupt the formation of the cortex<sup>5</sup>. In a given cell type, the steady-state metaphase spindle is characterized by constant pole-to-pole spacing<sup>17</sup>, which is determined by the balance between intrinsic factors influencing MT dynamics and assembly, as well as cell boundary constraints<sup>17–22</sup>. The correct interplay between metaphase spindle length, cell size and shape is important for the accurate positioning of the spindle within the cell, which influences chromosome segregation and selection of the cell division plane<sup>23–25</sup>. This is known to be critical for correct cortical development. In the *HeCo* developing telencephalon, AP mitotic spindles were found to have a significantly increased percentage of oblique cleavage planes at anaphase<sup>7</sup>. The causes of this phenotype are not yet known.

Cells change their size, shape, number and position during development, which is fundamental for proper tissue morphogenesis<sup>26,27</sup>. These cell properties have up till now been little studied in the neuroepithelium of the developing cortex. Developmental changes in the VZ require APs like other epithelial cells, to respond to surrounding mechanical forces<sup>28,29</sup>. It is also well-known that intrinsic cellular characteristics, as well as space constraints can together control cell proliferation<sup>30</sup>. INM has been proposed to generate space for mitosis<sup>29</sup>, occurring as nuclei reach the VL. Factors, which are as yet little-known, must regulate spindle assembly and orientation, symmetric versus asymmetric division, as well as daughter cell attachment or detachment. It seems important then to consider features of the mitotic spindle, as well as cell size and shape to learn more about these processes.

Focusing on *HeCo* mice, showing gene mutations in the MT-binding protein Eml1, we show altered MT dynamics in mutant cells compared to wild-type (WT) *in vitro*. In E13.5 APs in brain slices, centrosomes and primary cilia are perturbed and there are abnormal prometaphase/metaphase ((pro)metaphase) spindle lengths. We also assessed cell shape and density in this region and show that (pro)metaphase cells dividing at the VL have abnormal shapes in the mutant brain. This work thus defines novel pathological VZ characteristics that may contribute to the delamination of a proportion of APs during early-mid corticogenesis.

## Results

**MT dynamics are perturbed in *HeCo* progenitors *in vitro*.** Recombinant Eml1 was initially shown to be enriched at the MT-organizing center (MTOC) and potentially associated with polymerizing MTs in non-neuronal interphase cells in culture<sup>7</sup>. A co-localization was also shown with MTs in Pax6-positive (+) progenitors *in vitro*<sup>7</sup>. Here we tested MT growth in mutant neural progenitors in culture by measuring the plus-end elongation rate by live-imaging. Primary cultures enriched for neural progenitors were prepared from embryonic WT and *HeCo* cortices dissected at E12.5, a time-point when Eml1 is already expressed in the VZ (Supplementary Fig. S1a). These were co-transfected with plasmids expressing fluorescent plus end-binding (EB)3-mCherry protein and Enhanced Green Fluorescent Protein (EGFP), the latter under the control of the brain lipid-binding protein (BLBP) promoter<sup>31</sup> which is specifically active in RGCs. Cells were then analyzed at two days *in vitro* (DIV), allowing for expression of fluorescent proteins (Fig. 1a), and at a time-point approximately equivalent to the developmental stage E13.5–E14.5 *in vivo*. Clusters of EGFP + interphase cells were live-imaged for EB3-mCherry (Supplementary Video S1), and the movies obtained analyzed to track EB3 movement (Supplementary Video S2). The growth speed of single MTs was lower in *HeCo* progenitors, compared to WT cells (Fig. 1b). We compared the frequency of stalling during MT growth and although a tendency for increased pausing was possible, the differences were not significant between WT and *HeCo* (Fig. 1c). Thus, interphase *HeCo* mutant cells in culture have perturbed MT plus-end growth dynamics compared to WT, mostly associated with a decreased polymerization rate.

We attempted to rescue the MT dynamic phenotype by reintroducing Eml1 in cultured *HeCo* progenitors through transfection of a construct expressing both Eml1 and EGFP, under the control of the BLBP promoter (pBLBP-Eml1-IRES-EGFP)<sup>7</sup>. However, consistent with an Eml1 overexpression phenotype also decreasing MT polymerization observed in Neuroblastoma-2A (N2A) cells (Supplementary Fig. S1b–d), MT growth rate was still lower in EGFP + *HeCo* progenitors after Eml1 transfection, showing no significant difference compared to mutant progenitors transfected with the control vector pBLBP-EGFP (Supplementary Fig. S1e,f). *HeCo* progenitors transfected with Eml1 also showed an increase in the frequency of stalling during the polymerization. A similar tendency was also observed upon Eml1 overexpression in N2A cells. Comparing growth rates without taking into account the pauses still showed significantly reduced growth rates in both cell types (Supplementary Fig. S1g,h). Thus, these combined results suggest that MT growth rate is altered in *HeCo* progenitors and that

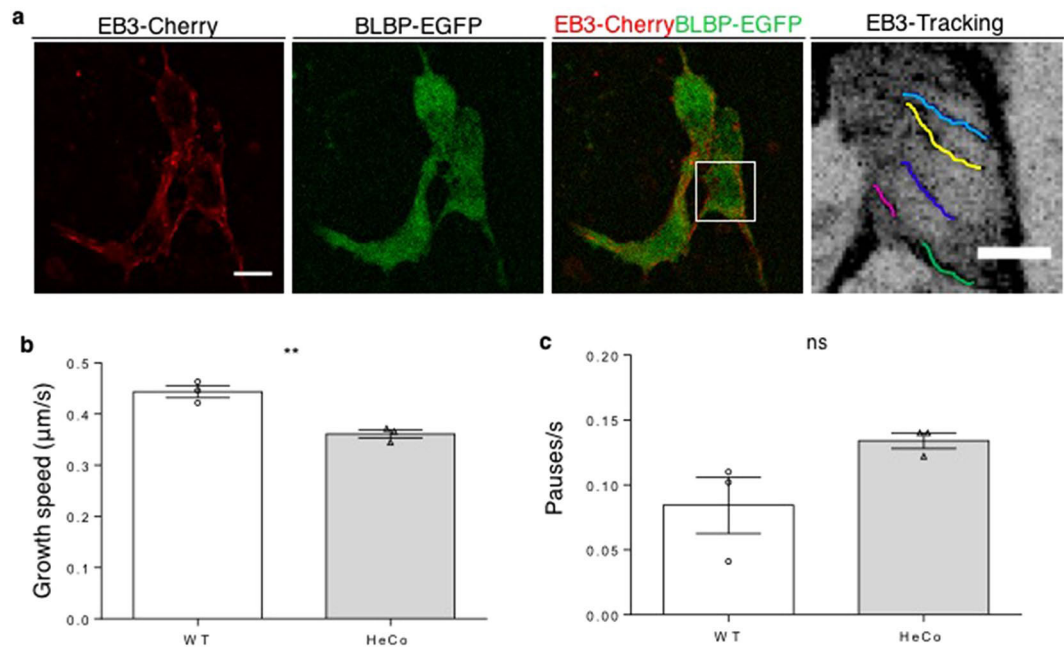


**Figure 1.** *HeCo* progenitors show perturbed MT dynamics. (a) Cultured dissociated neural progenitors from E12.5 mouse cortices transfected with EB3-mCherry (red) and BLBP-EGFP (green). Interphase BLBP+ cells were imaged to assess EB3 tracking. Each colored line in the higher magnification (right) shows one EB3 track. (b) EB3-labelled MT plus-ends advance more slowly in *HeCo* cells compared to WT. Each dot (WT) or triangle (*HeCo*) represents a different experiment. Average track speed for the two conditions is shown by bars. (c) EB3-labelled MT plus-ends do not show significantly increased pause frequencies in *HeCo* progenitors. N = 3, 198 total tracks from 23 cells measured for WT, 180 total tracks from 17 cells measured for *HeCo*. Unpaired *t*-test. \*\* $P < 0.01$ , ns = non-significant. Scale bars, 10 µm (a, lower magnification), 5 µm (a, higher magnification).

*Eml1* is crucial for MT dynamics, and either an absence or overexpression of the protein reduces MT growth rate. *Eml1* re-expression in mutant cells under these conditions was not therefore able to rescue the phenotype.

### Centrosome and primary cilia defects, as well as abnormally long (pro)metaphase spindles in the *HeCo* VZ at E13.5.

MT dynamics are critical for several aspects of the cell cycle<sup>32–35</sup>. We analyzed APs in the VZ directly in dorso-medial WT and *HeCo* developing cortex (Fig. 2a), analyzing cells in their 3D tissue environment. We performed this at E13.5, when *Eml1* is expressed in the VZ, and a proportion of ectopic progenitors are already identifiable in the mutant cortex<sup>7</sup>. In WT VZ,  $\gamma$ -tubulin staining revealed apical well-aligned centrosomes (Fig. 2b), and more basally located centrosomes associated with dividing cells. In *HeCo* brains,  $\gamma$ -tubulin revealed a more disorganized staining (Fig. 2c). We quantified the number of  $\gamma$ -tubulin + puncta at the VL (3 µm thick), and above in a three-soma height within the VZ, and found that *HeCo* VLs contained significantly less puncta compared to WT (Fig. 2d). In addition, more  $\gamma$ -tubulin + puncta were present above the VL, not obviously associated with dividing cells. Overall, the total number of centrosomes did not differ between WT and *HeCo*, suggesting a changed position of some centrosomes toward more basal positions in the mutant.

Because centrosomes are closely related to primary cilia in RGC apical processes<sup>4</sup>, we also performed a co-staining between  $\gamma$ -tubulin and ADP ribosylation factor like GTPase 13b (Arl13b), a primary cilium marker, to check their mutual localization in WT versus *HeCo* VZ (Fig. 2e–h). We quantified the number of Arl13b + puncta again at the VL and in a 3-soma height of the VZ (Fig. 2i). A reduction in the number of Arl13b-puncta was observed in the *HeCo* VL but the rest of the VZ showed similar numbers compared to WT. Overall, the total number of puncta was reduced in the mutant. Thus, as confirmed by our images, the excess of basally-localized  $\gamma$ -tubulin puncta are often not associated with Arl13b (Fig. 2h), and primary cilia numbers appear reduced at the VL of *HeCo* mice. These results show different behaviors of two highly associated organelles in APs, potentially indicating apical end-foot detachment and/or VL anomalies.

We next focused on spindle length, a parameter that is finely regulated by MT dynamics and previously unexplored in APs<sup>17</sup>. Hoechst staining, together with  $\gamma$ -tubulin, was used to identify different phases of the cell cycle. WT and mutant metaphase and pro-metaphase cells appeared indistinguishable in number and aspect, and there are no indications of delayed mitosis in *HeCo* APs<sup>7</sup>. The resolution of images, together with 3D reconstruction of confocal z-stacks corresponding to cropped single cells at the dorso-medial VL (see Materials and Methods for more details on the analysis), allowed us to distinguish the different mitotic phases (Fig. 2j), although it was not possible based on DNA shape to firmly discriminate between pro-metaphase and metaphase.  $\gamma$ -tubulin was used to identify the separated spindle poles when they were located at the opposite sides of the metaphase plate, and allowed individual pole-to-pole distances to be measured in (pro)metaphase cells, which we referred to as spindle lengths (Fig. 2k–n). These are likely to be maximal (metaphase) or near-maximal (pro-metaphase).



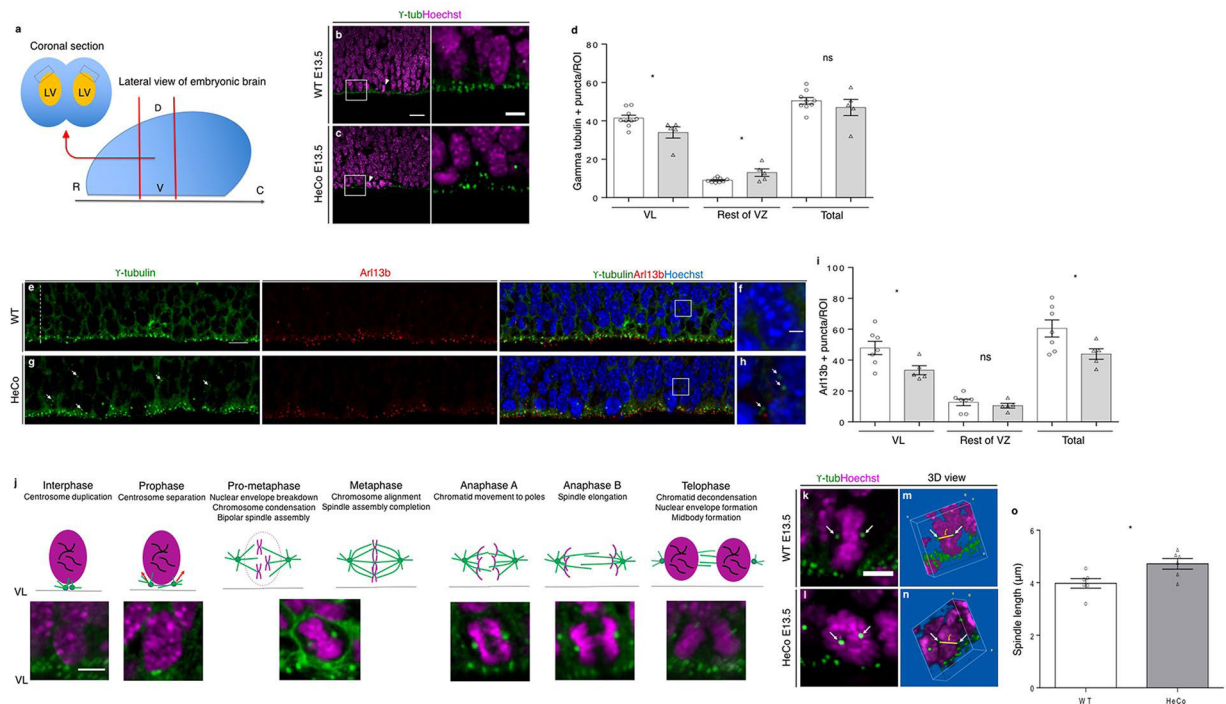


**Figure 2.** VL anomalies and abnormal (pro)metaphase spindle length in the *HeCo* VZ. **(a)** Coronal sections corresponding to the region delimited by red lines were immunostained and the VL analyzed (grey boxes top left). **(b,c)**  $\gamma$ -tubulin (green) and Hoechst (magenta) staining in WT **(b)** and *HeCo* **(c)** E13.5 brain sections. Higher magnifications show perturbed  $\gamma$ -tubulin staining in *HeCo* brains. **(d)** Less centrosomes in the *HeCo* VL and increased number in more basal positions. The total number of VZ centrosomes does not change between WT and *HeCo*. **(e–h)**  $\gamma$ -tubulin (green), Arl13b (red) and Hoechst (blue) staining in E13.5 WT and *HeCo* VZ. Small white line indicates the VL. Dashed white line indicates the rest of the VZ (3-soma height). Higher magnifications **(f,h)** show mislocalized basal centrosomes (white arrows) not associated with primary cilia in *HeCo*. **(i)** Less Arl13b + puncta in the *HeCo* VL but no change in the rest of the VZ. Overall, less primary cilia in the *HeCo* VZ compared to WT. **(j)** Mitotic phases and corresponding images from APs in brain slices. Purple, nuclei and chromosomes; green dots, centrosomes; green lines, MTs. Pro-metaphase and metaphase are not distinguishable from our images. **(k,l)** Isolated single (pro)metaphase cells. Spindle poles labelled by  $\gamma$ -tubulin (white arrows) are visible. **(m,n)** 3D reconstructions illustrating pole-to-pole distance measurements. Yellow bars indicate the pole-to-pole (white arrows) distance (l) measured. Only (pro)metaphase cells located at the VL were measured. **(o)** Spindles are longer in *HeCo* brains at E13.5 compared to WT. Circles (WT) and triangles (*HeCo*) represent single embryos. Average for each condition is represented by bars.  $\gamma$ -tubulin: WT, N = 9 embryos from 3 litters; *HeCo*, N = 5 embryos from 3 litters. Arl13b: WT, N = 7 embryos from 5 litters; *HeCo*, N = 5 embryos from 4 litters. Spindle length: N = 6 embryos from 3 litters for each condition. WT, 176 cells; *HeCo*, 160 cells. Unpaired *t*-test. \**P* < 0.05, ns = non-significant. Scale bars, 20  $\mu$ m **(b,e)**, 10  $\mu$ m **(e,g)**, 5  $\mu$ m (higher magnification in **b,j,k**) and 2  $\mu$ m (higher magnification **f**). R, rostral; C, caudal; V, ventral; D, dorsal; LV, lateral ventricle; VL, ventricular lining; VZ, ventricular zone.

Remarkably, average spindle length was found to be longer in E13.5 *HeCo* APs compared to WT (Fig. 2o). We also checked whether longer (pro)metaphase spindles were associated with oblique/horizontal cleavage planes (metaphase plate orientation with respect to the VL) shown to be increased in mutant APs<sup>7</sup>. However, we found that spindle lengths during (pro)metaphase were on average the same for vertical or non-vertical cleavage planes (Supplementary Fig. S2a), which suggests that spindle length in (pro)metaphase APs is not a predictor of spindle orientation and *vice versa*.

We also assessed whether spindle length was altered in cells dividing in more basal positions, away from the VL (non-VL). Basally positioned (pro)metaphase cells were identified in *HeCo* cortices by their location as well as DNA condensation, as previously performed for the VZ. We found that these cells had spindle lengths which were comparable to *HeCo* VL cells (Supplementary Fig. S2b). Similarly, a tendency for longer mutant spindles was also revealed when directly comparing basal (pro)metaphase WT to *HeCo* basally dividing cells (Supplementary Fig. S2c). Thus, as well as centrosome and primary cilia defects, our results show a defect in pro(metaphase) spindle pole-to-pole distance at early-mid corticogenesis in the mutant.

**Eml1 MT-related protein partners in E13.5 cortices.** To identify molecular partners of Eml1 in embryonic brain, we performed pull down experiments from mouse E13.5 cortices. Structural studies showed that the isolated EML1 N-terminal domain (N-ter, amino acids 1–174, 91% identity with mouse Eml1) contains a

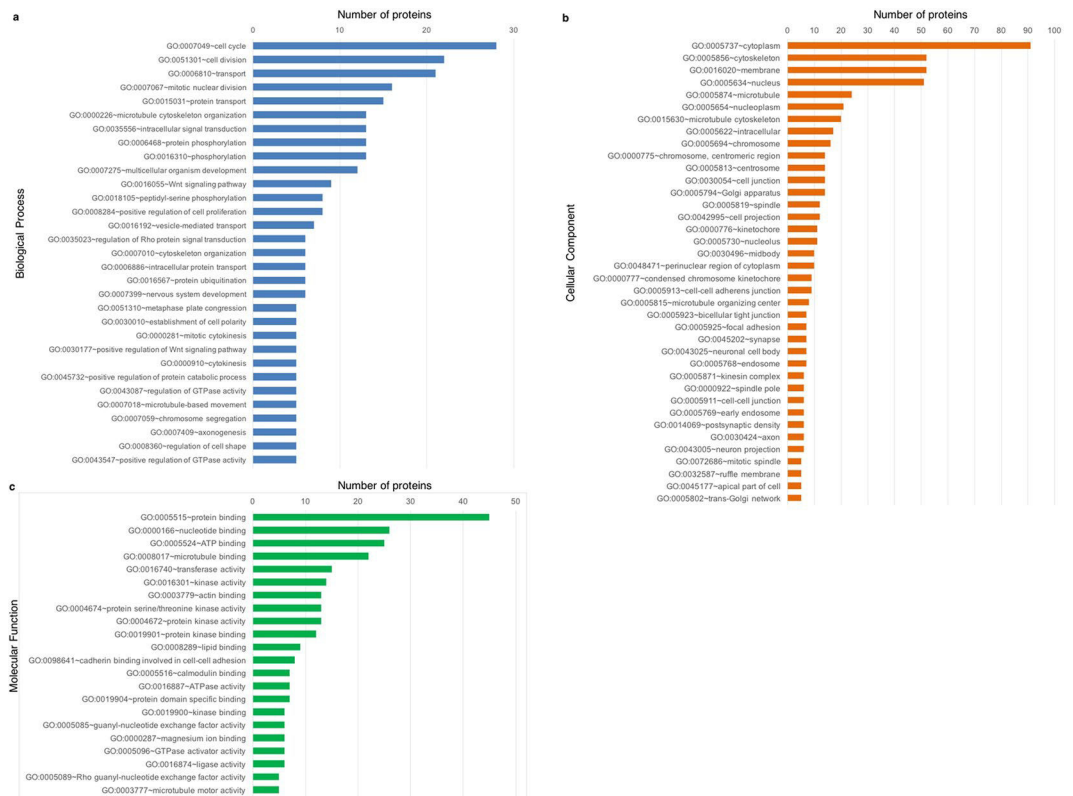


**Figure 3.** MS analyses reveal EML1 N-ter interactors. (a–c) GO analyses for the filtered 176 protein list performed with the DAVID Functional Annotation Tool. Classified proteins are specific for EML1 N-ter based label-free quantification analysis. GOs based on biological process (a), cellular component (b), and molecular function (c) were generated.

coiled-coil region, mediates homo-trimerization, and binds MTs<sup>36,37</sup>. The larger C terminal domain contains WD40 repeats making up tandem beta-propeller structures<sup>36</sup>. We searched for protein partners potentially influencing MT association, since two of the missense mutations identified in patients may directly or indirectly affect this function (R138X disrupting N-ter, and T243A, previously shown to sediment less with MTs<sup>7</sup>). Pull-down experiments were performed with purified glutathione-S-transferase (GST)-tagged EML1 N-ter and E13.5 WT embryonic cortex extracts (Supplementary Fig. S3). Samples were analyzed by mass spectrometry (MS) to identify direct and/or indirect partners of the protein. Label-free quantitative analyses based on the extracted ion chromatogram (XIC) method, comparing GST-Nter EML1 to GST control samples, revealed a list of 1059 proteins (listed in Supplementary Table S1) uniquely associated with EML1 N-ter. This list was further filtered to exclude proteins often found abundant in MS analyses and therefore less likely to be specific partners of Eml1, such as histones and RNA-processing proteins. Nuclear proteins associated with nucleic acids (e.g. transcription factors), and extracellular matrix proteins were also excluded since Eml1 is found primarily in the cytoplasmic compartment. A new list of 176 proteins was obtained after filtering (Supplementary Table S2). Gene ontology (GO) analyses were performed using the Database for Annotation, Visualization and Integrated Discovery (DAVID) Functional Annotation Tool<sup>38</sup> (<https://david.ncifcrf.gov/home.jsp>) (Fig. 3a–c, also see Supplementary Table S2). The most represented biological processes were cell cycle, cell division and transport (Fig. 3a). Concerning cellular component, proteins were classified mainly as cytoplasmic, as expected based on our exclusion criteria. Among these, many proteins were found in the cytoskeleton and membrane categories (Fig. 3b). Molecular function classification identified the majority of proteins as having protein binding activity, and nucleotide, ATP and MT binding were well represented (Fig. 3c).

The 176 list was then analyzed using the Search Tool for the Retrieval of Interacting Genes/Proteins (STRING) Functional Protein Association Network<sup>39</sup> ([string-db.org](http://string-db.org)) based on known and predicted protein-protein interactions (Fig. 4). The software was able to connect the majority of items, with only a small percentage of disconnected nodes. A large network of highly interacting nodes was revealed (grey box in Fig. 4a). This contained several proteins already known to be mutated in cortical malformations and related to neural progenitor function, such as kinesin superfamily protein (Kif) 20b, Kif2A, polo kinase 1 (Plk1), nuclear distribution E neurodevelopment protein 1 (Nde1), Nde1-like (Ndel1) and dynein heavy chain 1 (Dync1h1)<sup>40–42</sup>. Two additional smaller clusters were also obvious: one (blue box in Fig. 4a) containing mostly protein kinases and phosphatases involved in the regulation of actin and MT cytoskeletons; a smaller cluster (green box in Fig. 4a) contained proteins involved in vesicle coating and intracellular transport.

We confirmed by the STRING GO tool that a high proportion of proteins was related to the MT cytoskeleton (red items in Fig. 4a), and this was especially true for the highly interacting nodes. Eml1, Eml2 and Eml4 were

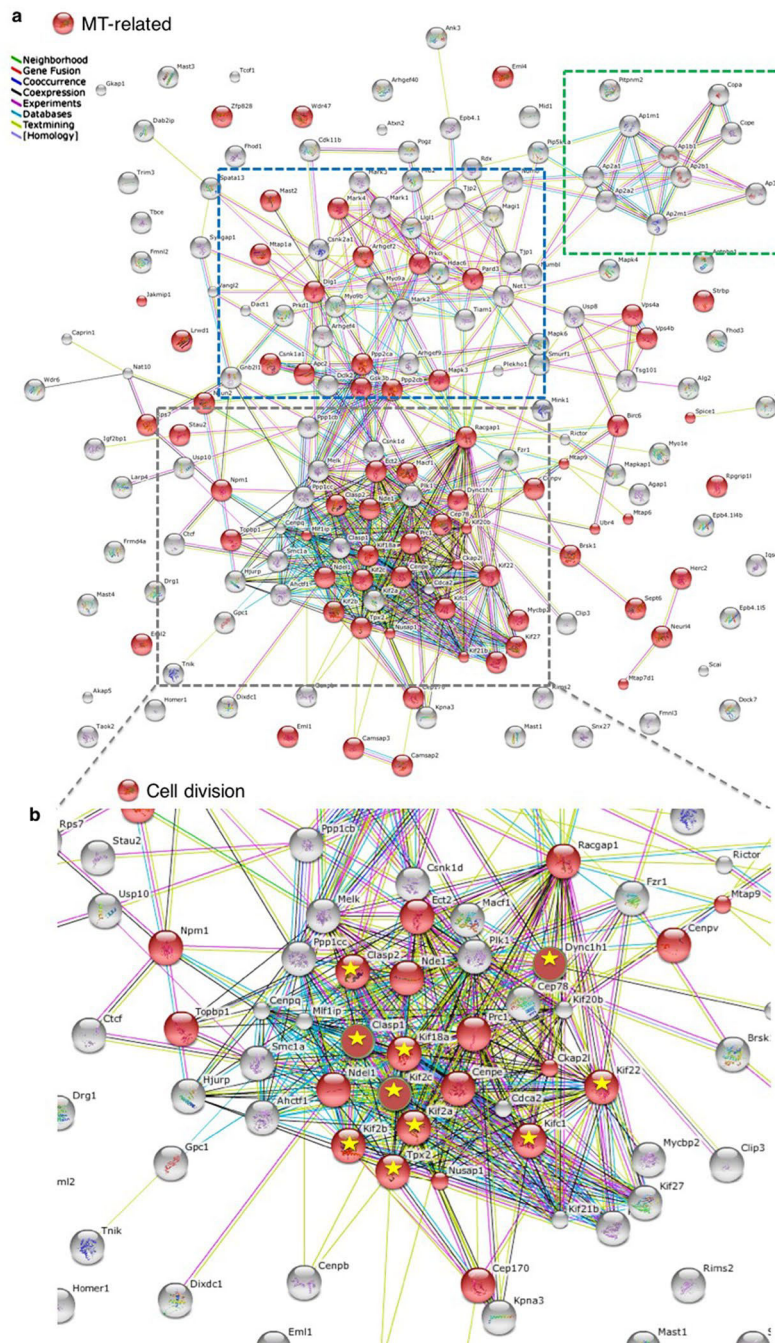


**Figure 4.** EML1 N-ter interactors are involved in cell division, MT processes and spindle length regulation. **(a)** STRING functional protein association network performed on the 176 protein list. Red items are proteins associated with the MT cytoskeleton based on STRING GO classification which contains functional categories as defined for the Clusters of Orthologous Groups (COG) database.  $P$ -value  $< 0.05$ . Grey, blue and green dotted lines indicate highly interconnected protein clusters. **(b)** The network boxed in grey in A is shown in higher magnification. Red items are proteins associated with the mitotic spindle based on STRING GO classification.  $P$ -value  $< 0.05$ . Proteins marked by yellow stars are associated with spindle length regulation based on literature searches (see also Table 1).

identified amongst these proteins revealing probable heteromerization of these Emls in brain developmental cells. In the major STRING cluster (grey box), half of the nodes were associated with cell division (Fig. 4b, red nodes) and amongst these 15 molecules had motor activity, 10 being kinesins (listed in Supplementary Table S2). Notably as well, among the interconnected mitotic spindle proteins, a number<sup>10</sup> are known already to regulate spindle length (yellow stars in Fig. 4b; see also Table 1). Using publicly available resources (<http://www.gene-paint.org>), *Kif2C* and *Tpx2* (targeting protein for *Xklp2*) *in situ* hybridization also showed strong expression in the VZ (Supplementary Fig. S4a), and *Kif1C*, *Kif2A*, *Kif22* and *Dync1h1* showed expression in both the VZ and

Protein	Action on MTs	Inactivation effect on spindle length	Expression in the VZ during corticogenesis	Reference
KifC1 (kinesin-14)	Cross-linking and bundling of parallel MTs (minus-end directed)	Shorter spindles	Yes	17,62
Kif22 (kinesin-10)	Cross-linking and bundling of parallel MTs (plus-end directed)	Shorter spindles?	Yes	17,54
Kif18A (kinesin-8)	Plus-end capping motor that halt MT growth	Longer spindles	?	63
Kif2A (kinesin-13)	MT depolymerization (minus-end)	Longer spindles	Yes	64,65
Kif2B (kinesin-13)	MT depolymerization	?	?	64,65
Kif2C (kinesin-13)	MT depolymerization (plus-end)	Longer spindles	Yes	64,65
Kif10 (Cenp-E)	MT stabilization (through binding to CLASPs)	?	?	66
Tpx2	MT bundling and nucleation	Shorter spindles	Yes	67
Clasp1	MT stabilization (plus-end)	Shorter spindles	?	68,69
Clasp2	MT stabilization (plus-end)	Shorter spindles	Yes	68,69
Dync1h1	Minus-end directed motor	Longer spindles	Yes	17
Eml4	Overexpression decreases MT growth rate	?	Yes	15
Eml1	Absence of functional Eml1 leads to slower MT plus-end growth	Longer in E13.5	Yes	This study

**Table 1.** Spindle length regulators identified by MS analysis for EML1 N-ter, and summary of their effects on MT dynamics and spindle length. Proteins are indicated that give rise to shorter or longer spindles following inactivation that give rise to shorter or longer spindles following inactivation. Known expression in the VZ during mouse cortical development is reported (see also Supplementary Figure S4a). Eml1 is also shown in the table for comparison.

CP, similar to *Eml1* at the same age<sup>7</sup> (Supplementary Fig. S4a). In addition, to assess if Eml1-interacting proteins present a different pattern of expression in *HeCo* brains compared to WT, we performed immunohistochemistry (IHC) for some selected partners: Kif22, Kif18A and Dync1h1. Notably, the MT motor protein Kif22 showed a different pattern of expression in *HeCo* cortices. Compared to WT, where Kif22 seems to be relatively concentrated at the VL, and localized to a lesser extent basally in the VZ, Kif22 staining was more obvious throughout the VZ in the mutant, with a relative reduced intensity at the apical surface (Supplementary Fig. S4b). In these preliminary IHC studies, no differences were observed for Kif18A and Dync1h1 (Supplementary Fig. S4c,d).

Thus, in fitting with the perturbed length of *HeCo* spindles, MS analyses for Eml1 partners identify a tight network of proteins, many of which are involved in MT function and spindle length regulation, as well as centrosome behavior.

### (Pro)metaphase APs show abnormal soma shape in *HeCo* brains at early-mid corticogenesis.

To further understand the impact of the defect in *HeCo* spindle size, we looked more carefully at the E13.5 VZ. Because the size of the spindle may influence cell size and *vice versa*<sup>20</sup>, (pro)metaphase cell area was first measured using N-cadherin staining and *en face* imaging (Fig. 5). N-cadherin participates in the assembly of adherens junctions between APs and can thus be used as a marker of cell boundaries<sup>43</sup>. Embryonic dorso-medial brain explants were performed from WT and *HeCo* E13.5 embryos, analyzing the same brain region previously assessed for spindle length (Fig. 5a) and in the area where the heterotopia later develops. Explants were stained for N-cadherin, together with Hoechst, and *en face* confocal imaging<sup>44</sup> was performed to obtain a clear outline of APs at the VL (Fig. 5b–e). No obvious defects were observed in N-cadherin staining in *HeCo* brains. (Pro)metaphase cells were identified using the whole z-stack based on the characteristic shape of the DNA condensed at the metaphase plate (Fig. 5c,e) and cell area was first measured in a single plane corresponding to the widest cell diameter selected by navigating the apico-basal z-stack (Fig. 5c,e,f). *HeCo* E13.5 single plane cell areas were on average significantly bigger than WT (Fig. 5g). To assess whether the increase in (pro)metaphase cell area reflected an overall increase in the 3D volume of the soma, 10 WT and 10 *HeCo* (pro)metaphase cells were segmented based on F-actin staining, delineating cell boundaries, following *en face* confocal imaging (Fig. 5h,i). Analyses of 3D-segmented mutant (pro)metaphase cells revealed volumes comparable to WT (Fig. 5j). However, the apico-basal height of *HeCo* (pro)metaphase APs was reduced compared to WT (Fig. 5k), leading to a distorted cell shape, with cells being flatter. This data fits the 2D measurements showing increased *en face* single plane areas of *HeCo* (pro)metaphase APs.

To assess the impact on overall tissue morphology of increased horizontal area occupied by (pro)metaphase cell somata, we evaluated cell density in WT and *HeCo* VLs. Indeed, when integrated in a tissue cells adapt to the presence of other cells around them that exert pushing forces proportionate to their density<sup>30</sup>. Due to INM, AP nuclei are only visible at the VL when they are in the G2-M transition, during mitosis, and during M-G1 transition. We thus counted the number of nuclei that were visible in the same *en face* z-stack where the area of (pro)metaphase cells was measured (Fig. 5b,d). The total number of cells was counted in four regions of interest (ROIs) per brain. The average number of nuclei/ROI quantified at E13.5 was found not to differ between WT and *HeCo* brains (Fig. 5l).

To further test cell adaptations within the neuroepithelium, we next checked the horizontal 2D area of (pro)metaphase cells in correlation with the density of nuclei at the VL (Fig. 5m,n). We first found that E13.5 WT (pro)metaphase cell horizontal area was inversely correlated with the total number of nuclei/ROI, with smaller areas

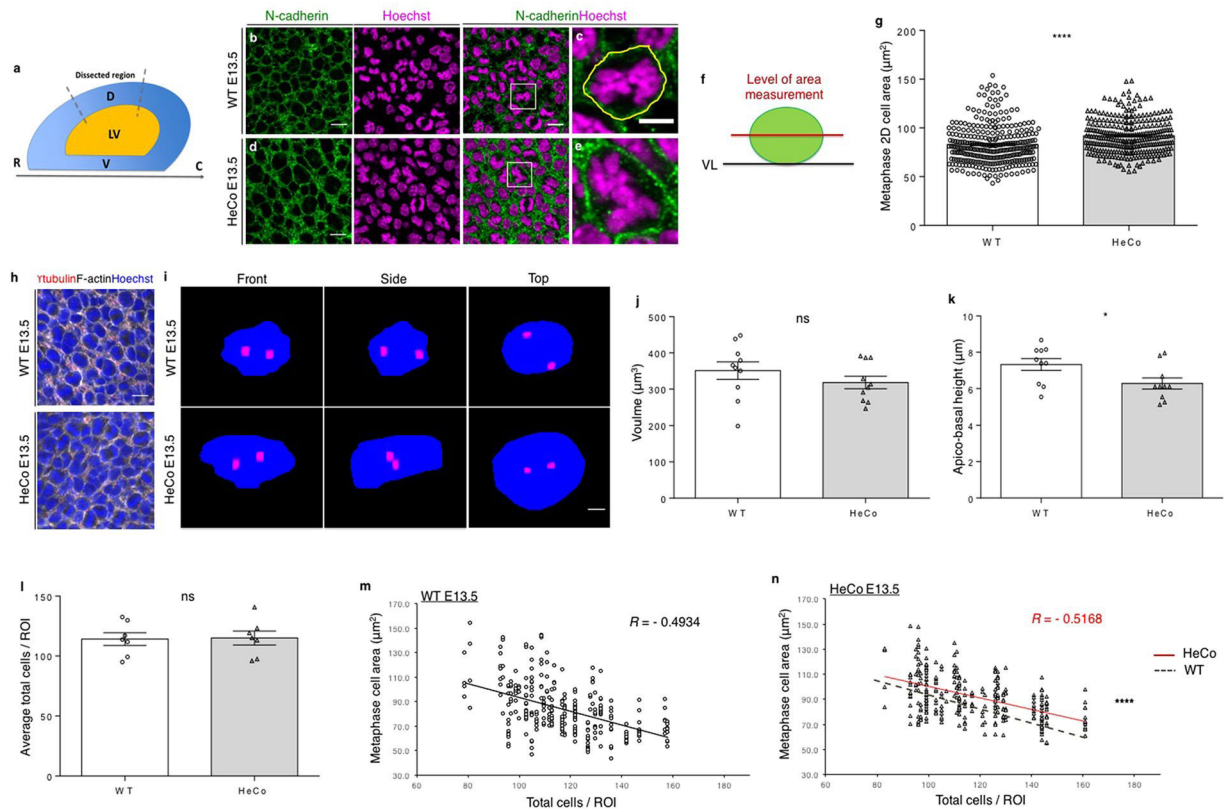


**Figure 5.** *HeCo* (pro)metaphase somata at the VL have an abnormal shape at E13.5. **(a)** Brain region dissected for *en face* immunohistochemistry (dashed lines). **(b–e)** N-cadherin (green) and Hoechst (magenta) staining for *en face* confocal imaging of WT and *HeCo* VL in E13.5 brains. Higher magnifications **(c,e)** show boxed regions revealing a single metaphase cell. An example of single plane cell area measurement is shown **(c)**, yellow line. **(f)** Lateral view of the level (red line) of the *en face* z-stack at which the cell area was measured. Green circle represents the soma of a metaphase cell at the VL (black line). **(g)** Average horizontal area of (pro) metaphase cells is bigger in *HeCo* compared to WT. Single points in the graph represent individual cells. Areas are highly variable (see also **m,n**). **(h)** WT versus *HeCo* *en face* F-actin (grey) and  $\gamma$ -tubulin (red) staining, combined with Hoechst (blue). **(i)** Representations after 3D segmentation of single (pro)metaphase RGCs. The 3D soma volume is shown in blue from three views (front, lateral, top). Centrosomes ( $\gamma$ -tubulin) are shown in red. **(j)** *HeCo* somata volumes are comparable to WT. **(k)** Somata apico-basal height is reduced in *HeCo* cells. Circles (WT) and triangles (*HeCo*) represent different cells and bars represent the average. **(l)** Cell densities do not differ between WT and *HeCo* E13.5 VLs. Single points in the graph refer to different embryos. Bars represent averages for the two conditions. **(m,n)** Correlations between (pro)metaphase cell areas and total cells/ROI in E13.5 WT **(m)** and *HeCo* **(n)** VLs. Single points in the graph represent single cells.  $N = 7$  embryos from 3 females for each condition for area measurement. WT E13.5 = 37; *HeCo* E13.5 = 34 total ROIs. WT E13.5 = 302; *HeCo* E13.5 = 294 total cell areas.  $N = 10$  cells derived from 3 embryos for each condition for volume segmentation. Unpaired *t*-test **(g,j,k,l)**. *R*, Pearson's correlation coefficients **(m,n)**. Linear regression was calculated for comparison of WT and mutant tendencies **(n)**. ns, non-significant; \* $P < 0.05$ , \*\*\* $P < 0.0001$ . LV, lateral ventricle; D, dorsal; V, ventral; R, rostral; C, caudal. Scale bars, 10  $\mu\text{m}$  **(b,d,h)**, 5  $\mu\text{m}$  **(c,e)** and 2  $\mu\text{m}$  **(i)**.

found in higher density conditions (Fig. 5m). The same was true for E13.5 *HeCo* APs, however, with increasing total nuclei/ROI, although mutant areas decreased, the elevation of the correlation line became increasingly different from WT (Fig. 5n). Thus, mutant E13.5 (pro)metaphase cells have bigger horizontal areas and whilst both WT and mutant cells appear to reduce their size according to the level of crowding of the tissue, mutant cells occupy more space than WT, this difference becoming more accentuated with increasing cell densities.

## Discussion

This work examines the structural characteristics of the mouse VZ, and especially the most apical region, the VL, where mitosis occurs. We provide new insights into the function of *Eml1* in APs and the cellular mechanisms affected by its loss in the *HeCo* developing cortex. *Eml1* mutant cells show aberrant MT polymerization, centrosomes and primary cilia, mitotic spindle length, as well as cell shape, which together will influence tissue dynamics. WT metaphase cells have relatively round somata and are adaptable, adjusting their diameters depending on cell density. In *Eml1* mutant conditions, altered cell shape and decreased adaptability may lead to reduced space, eventually causing some progenitors to delaminate. The identification of mislocalized  $\gamma$ -tubulin + puncta,

corresponding to centrosomes not associated with dividing cells, supports this hypothesis since these are likely to belong to detaching apical processes<sup>45,46</sup>.

In our previous work at the cellular level, we showed ectopic progenitors in the *HeCo* mouse, but we did not identify any intrinsic defect in post-mitotic neurons<sup>7</sup>. It is indeed possible that other post-mitotic MT factors e.g. Dcx, or other members of the EMAP family, might compensate for Eml1's role during neuronal development. Indeed, Eml2, Eml4 and Eml5 are all expressed in the mouse developing CP. Heterotopia formation in the *HeCo* model, related to abnormal neuronal migration, is thus likely to be due to extrinsic perturbations, including local cell production and clustering in the IZ, and aberrant RGC guides. Our targeted pull-down experiments reveal a number of Eml1's potential partners expressed in the VZ, with some having already known functions during the cell cycle. The tight network of partners also highlights roles in MT function and spindle length regulation. Our combined observations suggest that Eml1-dependent MT regulation may be more critical in progenitors than in post-mitotic neurons. Interphase MT growth defects in BLBP+ progenitors, as well as centrosome, primary cilia and spindle length defects in brain slices are in fitting with this. Thus, it is likely that Eml1 plays an MT-dependent role in RGCs at early corticogenesis, not compensated for by other proteins.

To further assess the pertinence of dampened MT dynamics in *HeCo* mutant progenitors *in vitro*, we attempted a rescue experiment. However, Eml1 overexpression in our experimental conditions also decreased MT growth, as shown by similar experiments in N2A cells. Further strategies are hence required to functionally rescue MT growth in mutant progenitors. Due to the difficulty in identifying and live-imaging dividing progenitors in primary cultures, we were not able to track MT growth during mitosis. However, perturbed MT growth in interphase cells, together with the association of Eml1 with mitotic spindles<sup>7</sup>, strongly suggest that MT dynamics could be affected throughout different phases of the cell cycle. This is further suggested by the finding that (pro)metaphase spindle length, strongly influenced by MT dynamics<sup>17</sup>, is abnormal in *HeCo* APs. The growth speed of MTs may indeed impact spindle size<sup>47</sup>. The slower speeds of MT growth we show in this study could have been predicted to lead to shorter MTs and thus shorter mitotic spindles<sup>48–50</sup>. However, recent studies highlight the limitation of classical models of MT growth, especially when explaining the effects of certain MAPs, and suggest that the regulation might be much more complex than initially thought<sup>51</sup>. Indeed, the mitotic spindle is a structure characterized by constant and fast MT rearrangements<sup>33,52</sup>. Thus, due to the complexity of MT dynamics regulation, as well as spindle assembly and function, the slower MT plus-end growth seen *in vitro* in interphase could also be associated with increased (pro)metaphase spindle length in *HeCo* E13.5 APs in the brain.

A large number of MAPs and MT motor proteins are involved in spindle assembly and function<sup>53</sup>, and our combined molecular and cellular data strongly suggest that Eml1 helps regulate these processes. We identified increased spindle lengths during (pro)metaphase stages where the pole-to-pole distance is likely to be near maximum. Despite longer spindles and changed cell shape, no other obvious morphological differences were observed in mutant (pro)metaphase cells. Furthermore, no labeling index or cell cycle exit defects were previously identified in *HeCo* APs in the VZ<sup>7</sup>, suggesting that cell cycle length remains unchanged. The interaction between MT regulators is tightly controlled during the cell cycle, and the removal of one of the players, in this case Eml1, is likely to change the behavior of many other proteins, including Eml1's partners. Screening WT versus mutant *HeCo* brains by IHC has already revealed Kif22 differences. This MT motor protein plays an established role in mitosis<sup>17,54</sup> and our new data, although preliminary, strongly suggest an interaction with the Eml1 pathway. Furthermore, we cannot exclude a change in trimerization stoichiometry with other members of the EMAP family, due to the absence of Eml1. Future studies will elucidate the nature of the interaction between Eml1 and candidate partners (as well as those identified in new screens with the full length protein) and clarify how Eml1 loss and/or mutation, including missense mutations identified in patients, impacts the function of these molecules.

*HeCo* E13.5 spindles in the VZ show increased pole-to-pole distance during (pro)metaphase, and we propose that this may be why these mutant cells are abnormally shaped, elongated in the medio-lateral axis but shorter in the apico-basal axis, and hence flatter than WT cells, at a stage of corticogenesis in which spindles are mostly oriented horizontal to the VL and RGCs frequently undergo self-renewal (Fig. 6a). Because of the potential role of Eml1 in the regulation of MT dynamics and its probable interaction with spindle length regulators, it seems reasonable to think that the perturbation in spindle size may change cell shape, instead of *vice versa*. Indeed, a longer spindle in *HeCo* progenitors may lead astral MTs to relax the cell poles and produce cell elongation along the spindle axis<sup>55</sup>. This is further suggested by the fact that the average difference in horizontal area of (pro)metaphase cells between WT and mutant increases in regions of the VZ where cellular nuclei are denser (Fig. 5l–n). This suggests that intrinsic properties of mutant cells may hamper the adaptation of somata to cell density in brain tissue.

Assessing (pro)metaphase spindle length at an earlier time-point might reinforce the hypothesis that (pro)metaphase cell defects contribute to ectopic progenitor localization. Indeed, Eml1 transcripts are detectable in the VZ at E12.5 (Supplementary Fig. S1a) and it is thus possible that spindle length as well as other RGC features described here may begin to show alterations already at these earlier stages of corticogenesis. In addition, providing spindle length and cell shape data for later stages of development in both WT and mutant brains would also be interesting to shed further light on progenitor behavior during corticogenesis. The cortical VZ is known to change over time, including transitions from symmetrical to asymmetrical division<sup>1</sup>, and testing tissue dynamics in this way could contribute to our overall comprehension of cortical development.

We have focused here on the mutant VZ but an important area also concerns abnormal cells in the IZ. We show in *HeCo* early-mid corticogenesis that spindle lengths of dividing IZ mutant cells appear comparable to APs dividing at the VL, which also favors the intrinsic nature of the spindle length phenotype. Ectopic progenitors are likely to provide a local source of daughter cells including post-mitotic neurons. It remains to be seen if some perturbed protein partners also contribute to progenitor cell/neuron clustering in the IZ which may be important for heterotopia formation.

Concerning the VZ phenotypes, there may be additional roles for Eml1 in other MT-related functions that influence cell shape, which in turn may explain the increase in spindle length. This prompted us to verify primary

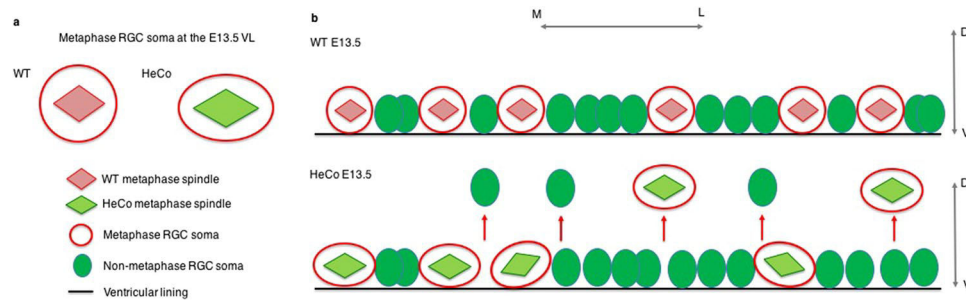


**Figure 6.** Schematic representation of spindle length and cell shape, and delamination hypothesis for *HeCo* APs. **(a)** Lateral view of spindle length and cell shape differences in WT and *HeCo* metaphase cells dividing at the VL. *HeCo* cells have a longer spindle and a flatter soma. **(b)** Delamination hypothesis for *HeCo* progenitors based on the interplay between spindle length, cell density and metaphase cell shape. At E13.5 in the WT a number of metaphase cells are present at the VL. At E13.5 in *HeCo*, spindles are longer and metaphase cells flatter, which reflects in an increase in the horizontal (with respect to the VL) space they occupy. This may cause increased mechanical stress in the VZ and especially at the VL and encourage delamination (red arrows), with some RGCs pushed outside the VZ during early-corticogenesis. For simplicity the VZ is not represented as pseudo-stratified but only cell somata at the VL are shown, without RGC apical and basal processes. M, medial; L, lateral; D, dorsal; V, ventral.

cilia in *HeCo* brains with the Arl13b ciliary marker. The reduced staining indicates less numerous and/or defective primary cilia in the VL. Together with centrosome basal displacement, the reduced primary cilia in the mutant VZ may indicate AP apical process detachment. The reduction of primary cilia suggests that these organelles may be excised and secreted into the ventricle, while the apical process of the delaminating AP retracts, carrying along with it the centrosome. Indeed, the budding and shedding of primary cilium-derived particles from APs into the ventricles has been previously described<sup>56</sup>. Apical process retraction followed by shedding of primary cilium-related particles was also described in the chick neuroepithelium for newly produced neurons leaving the VL<sup>57</sup>. In *HeCo* mice, reduced primary cilia in the VL may be a consequence of cell delamination, however in this case, it is mutant Pax6 + progenitors that escape from the VZ. Future studies are required to further understand this phenotype and it will also be important to investigate potential anomalies in signaling pathways, such as mTOR, Wnt and Shh, in which the primary cilium appears to be a critical organelle<sup>58</sup>. It is premature to conclude in the *HeCo* model that primary cilia defects are responsible for the detected cell shape and spindle length anomalies, nevertheless this warrants further analyses. Alternatively, as well as intrinsic spindle perturbations, cell membrane properties could also influence the shape of the cell and its response to mechanical stress, allowing e.g. responsiveness of the membrane on the basal side but less adaptability horizontally. It is interesting to note that in *C. elegans* it has been suggested that the Emap Elp, plays a role in mechano-transduction<sup>59</sup>. Considering the role of Eml1 in each of these functions should help clarify the mechanisms by which mutant cells show abnormal shape.

We reveal changes in spindle length and cell shape at early-mid corticogenesis that might impact RGC position and cell fate. We hypothesize that for mechanical reasons and tissue constraints, some mutant cells may begin to be pushed away from the VZ, contributing to the presence of ectopic progenitors in the IZ and CP (Fig. 6). Indeed, delamination is a known response to increased cell densities in other epithelial tissues<sup>60,61</sup>, and has also been identified in one other study in the cortical VZ<sup>28</sup>. Whether delamination is initiated during mitosis by impacting spindle lengths and orientations, or in interphase, via cell signaling leading directly to apical endfoot detachment, is currently not clear. Live-imaging experiments during the cell cycle with centrosome and chromatin markers may shed further light on primary events, as well as possibly identifying further mitotic defects. It is important to identify these cellular abnormalities since they initiate a series of detrimental steps affecting corticogenesis, with the severe consequences of heterotopia.

## Materials and Methods

**Animals.** Research was conducted according to national and international guidelines (EC directive 86/609, French MESR 00984.02) with protocols followed and approved by local ethical committees (Charles Darwin committee (Paris, France) and Office Vétérinaire Cantonal (Lausanne, Switzerland)). *HeCo* mutant mice arose spontaneously in a colony of NOR-CD1 outbred stock, and selective inbreeding including crossing of living relatives and backcrossing were used to increase the occurrence of the phenotype in offspring as described in ref.<sup>6</sup>. WT and *HeCo* mice derived by separate but regularly crossed colonies were used for developmental analyses and primary neuronal cultures. The mode of inheritance of the phenotype is autosomal recessive. Normal, full-length transcripts of *Eml1* are absent in *HeCo* brains due to the insertion of an early retrotransposon (ETn) in the last intron of the gene<sup>7</sup>, and are replaced by trace levels of shortened and chimeric *Eml1*-ETn transcripts. Timed-pregnant Swiss mice used for embryonic cortex lysate preparation were provided by Janvier Labs (<http://www.janvier-labs.com/home.html>). For staging of embryos, the day of vaginal plug was considered E0.5. Mice were housed with a standard 12 h light/dark schedule (lights on at 07:00 a.m.).

**MT plus-end tracking – video-microscopy.** Primary cultures of cortical progenitors were prepared from E12.5 embryos derived from timed-pregnant NORCD1 WT and *HeCo* mice. Cortices from both hemispheres were dissected in ice-cold Leibovitz-15 (L-15, Gibco BRL) medium. After removal of the meninges cortices were washed in 4 °C dissection-dissociation medium (HEPES 20 mM, HBSS 1X, Life Technologies). Cells were mechanically dissociated in DMEM Glucose (Life Technologies) supplemented with 10% Fetal Calf Serum (FCS, Thermo Scientific) before electroporation with BLBP-IRES-EGFP and EB3-mCherry (3 µg total DNA) using an Amaxa mouse Nucleofector kit (Lonza). Rescue experiments in *HeCo* progenitors were performed with pBLBP-Eml1-IRES-GFP<sup>7</sup>. Neuro-2A cells were transfected with either EGFP alone (pEGFP C3, Clontech) or EGFP-Eml1, in combination with EB3-mCherry (see Supplementary Information for Neuro-2A cell culture). Cells were seeded in 35 mm diameter glass bottom Ibidi dishes suitable for video-microscopy previously coated with poly-L-lysine and laminin (Sigma-Aldrich). Progenitors were cultured and maintained in B27/N2 medium (Gibco BRL), which is a mixture (1:4) of Neurobasal/B27 medium without vitamin A and DDM medium (DMEM/F12 with Glutamax, supplemented with N2, 0.1 mM nonessential amino acids, 1 mM sodium pyruvate, 500 µg/ml BSA, 0.1 mM 2-mercaptoethanol and Primocin 100 U/ml, Lonza). EGFP+ cells were filmed at 2 DIV. Video-microscopy was performed using a Spinning Disk rapid inverted confocal (Leica DMI4000) equipped with a temperature-maintaining chamber and an intensified camera, and piloted by Metamorph. A 63X objective and 591-laser were used to film EB3-labeled growing MT plus-ends during 2 min with a time-interval of 1 sec (3 z-stacks of 300 ms exposure per time-frame). Tracking was performed on stack images using the Manual Tracking plugin of the ImageJ software. Only EB3+ comets recognizable during at least 5 consecutive time points were considered for analysis.

**Immunohistochemistry on coronal sections.** Mouse embryonic brains were fixed by immersion overnight (O/N) at 4 °C in 4% w/v paraformaldehyde (PFA) in 0.1 M phosphate buffer, pH 7.4. Brains were cut in 70 µm thick coronal sections using a vibrating blade microtome (Leica VT1000 S). Blocking was performed for 1 hour at RT with blocking solution (PBS 1X with 10% Goat Serum and 0.5% Triton X-100) before incubation O/N at 4 °C with the following primary antibodies: mouse  $\gamma$ -tubulin (GTU-88, T6557, Sigma-Aldrich, 1:500), rabbit Arl13b (17711-1-AP, Proteintech, 1:500), rabbit Kif22 (13403-1-AP, Proteintech, 1:150), rabbit Kif18A (1925-1-AP, Proteintech, 1:150), rabbit Dync1h1 (R-325, sc-9115, Santa Cruz Biotechnology, 1:200). After extensive washes, sections were incubated with secondary anti-mouse Alexa 488 or anti-rabbit Alexa 568 (Life Technologies, 1:800-1:1000). Antigen retrieval was performed before the blocking step for Kif18A and Dync1h1 antibodies. For this, sections were incubated in sodium citrate 10 mM pH 6 at 95 °C for 20 minutes and cooled down before blocking. Sections were subsequently incubated with Hoechst 1:1000-1:5000 and mounted with Fluoromount G (Southern Biotechnology). Fluorescently stained sections were imaged with confocal microscopes (Olympus FV10i and TSC Leica SP5-II) equipped with 10x phase contrast objective/NA 0.4 and 60x phase contrast oil-immersion objective/NA 1.35, and 10x, 40x oil Plan-Neofluor, 63x, 100x oil Plan-Apochromat objectives. Fluorophore excitation and scanning were performed with argon lasers at 488 nm (blue excitation for GFP, Alexa 488) and 568 (red excitation for Alexa 568), and with a diode laser at 405 nm (for Hoechst staining). Confocal images were acquired with a 0.17 µm or 0.3 µm z-stack depth. Images were analyzed using Image J (Fiji) to obtain the whole z-stack data set and for  $\gamma$ -tubulin and Arl13b quantification. At least two ROIs of 120 × 35 µm were quantified per embryo. The Imaris software was used for single-cell 3D reconstruction and spindle length measurement. Single (pro)metaphase cells were recognized from DNA shape and centrosome position and cropped from whole-section images to isolate them. Z-stacks of cropped single cells were reconstructed in 3D by applying voxel depth, and pole-to-pole distance was measured.

**Pull-down.** E13.5 timed-pregnant Swiss mice (Janvier Labs, France) were sacrificed by cervical dislocation. Embryos were dissected and both brain hemispheres collected in L-15 medium, and explants immediately frozen in liquid nitrogen and ground into a powder. This was re-suspended in 10 µl/mg lysis buffer (Tris HCl 50 mM, NaCl 150 mM, EDTA 1 mM pH 8) supplemented with 1% NP-40 and protease inhibitors 1X (Protease Inhibitor Cocktail Tablets EDTA-Free, Sigma-Aldrich). The lysate was homogenized by rotation during 45 min at 4 °C, then centrifuged for pre-clearing 30 min at 15000 rcf and 4 °C. Cortex extracts (15 µg tissue) were incubated overnight with pre-washed Glutathione-Agarose resin (Sigma-Aldrich) previously coupled with either purified GST-EML1 N-ter<sup>36</sup> or GST as control (4 µg total purified protein). Extracts were centrifuged (200 rcf, 1 min) to pellet the resin, supernatants were collected as un-bound fractions, and resins (bound fractions) were extensively washed with lysis buffer to remove non-specific interactions. Resins were re-suspended in freshly-made Laemmli buffer, heated 10 min at 95 °C and centrifuged 2 min at maximum speed to dissociate the complexes from the resin and denature the proteins.

The EML1 N-ter construct, is predicted to bind MTs and not soluble tubulin<sup>36</sup>. Indirect protein partners due to MT-mediated interactions were not favored because of the sample preparation conditions (4 °C cold treatment causing depolymerization). The unlikely occurrence of soluble tubulin-mediated interactions was further confirmed by detection in Western blots of pull-down samples identifying  $\alpha$ -tubulin only in the unbound fractions (Supplementary Fig. S3).

**Mass Spectrometry.** Two independent pull-down purifications (GST and GST-EML) were simultaneously separated by SDS-PAGE and stained with colloidal blue (LabSafe Gel Blue GBiosciences). Seven gel slices were excised for each purification. After washing, proteins were reduced with 10 mM DTT prior to alkylation with 55 mM iodoacetamide. After washing and shrinking of the gel pieces with 100% acetonitrile, in-gel digestion was performed using trypsin (Gold, Promega) overnight in 25 mM ammonium bicarbonate at 30 °C. Peptides extracted from each band were analyzed by nano Liquid Chromatography (LC)-MS/MS using an Ultimate 3000



system (Dionex S.A.) coupled to an LTQ-Orbitrap XL mass spectrometer (Thermo Scientific). Data-dependent acquisition was performed in the positive ion mode. Survey MS scans were acquired in the 475–1200 m/z range for each sample, with the resolution set to a value of 60 000. Each scan was recalibrated in real time by co-injecting an internal standard from ambient air into the C-trap ('lock mass option'). The 5 most intense ions per survey scan were selected for CID fragmentation and the resulting fragments were analyzed in the linear trap (LTQ). Target ions already selected for MS/MS were dynamically excluded for 180 s. Data were acquired using the Xcalibur software and the resulting spectra analyzed via the Mascot™ Software (Thermo Scientific). All peptide/protein identification data were further processed using the Institut Curie developed software myProMS (<http://myproms.curie.fr/>)<sup>70–72</sup>, version 3.0. The mass spectrometry proteomics data were deposited to the ProteomeXchange Consortium via the PRIDE<sup>73</sup> partner repository with the dataset identifier PXD006837. Protein lists were analyzed using the DAVID Functional Annotation Tool<sup>38</sup> (<https://david.ncifcrf.gov/home.jsp>) for Gene Ontology generation, and STRING Functional Protein Association Network<sup>39</sup> ([string-db.org](http://string-db.org)) to reveal interactions between proteins. See also Supplementary Information for more details on MS data analysis.

**En face immunohistochemistry.** Following the protocol adapted from ref.<sup>44</sup>, mouse embryonic brains were fixed in 4% w/v PFA (Sigma-Aldrich, France). Cortical explants were dissected and incubated 15 min at RT in PBST 1% (PBS 1X containing 1% Triton X-100 v/v and 0.02% sodium azide). Explants were then incubated 2 h at RT in blocking solution (PBS 1X, 0.3% Triton X-100 v/v, 0.02% sodium azide, 3% w/v Bovine Serum Albumin). Primary antibody mouse monoclonal anti-N-cadherin (C70320, Transduction Laboratories, 1:2000) or  $\gamma$ -tubulin (GTU-88, T6557, Sigma-Aldrich, 1:500) were applied O/N at RT. After extensive washing in blocking solution explants were incubated O/N at RT with secondary antibody anti-mouse Alexa 488 (1:800, Thermo Fisher Scientific) together with Hoechst (1:1000–5000, Thermo Fisher Scientific). Washes in blocking solution and PBS 1X, were performed before mounting the explants with Fluoromount G positioned as flat as possible with the ventricular surface up to obtain an *en face* view of the ventricular side of the cortex. For F-actin immunofluorescence, Alexa Fluor 633 Phalloidin (1:100, Life Technologies) was incubated in PBST 1% O/N at RT. Extensive washing was performed in PBST 1% and PBS 1X before mounting the explants. Fluorescently stained sections were imaged as previously described. Confocal images were acquired with a 0.2  $\mu$ m z-stack depth for a total depth of 9–10  $\mu$ m (Olympus FV10i microscope and TCS Leica SP5-II). At least two randomly-chosen ROIs were imaged for each hemisphere. Images were analyzed using Image J (Fiji) to obtain the whole z-stack data set and the cell counter and measuring plugins for quantification. Cell counting and single metaphase cell area measurements were performed in the same ROIs (100  $\times$  100  $\mu$ m) and on the first layer of cells starting from the VL. Areas were measured on the z-stack corresponding to the largest diameter of metaphase cells. For cell volume and height measurements, individual (pro)metaphase cells were recognized from DNA shape and centrosome position, and cropped for manual segmentation. 3D-reconstruction of cropped single cells was done with the Imaris software by tracing manually cells' contours (from stained F-actin), and interpolating all contours with a surface in 3D.

**Plasmids.** The pGEX-EML1-174 and GST control constructs are as described in ref.<sup>36</sup>. The BLBP-IRES-GFP construct was obtained from the N. Heintz laboratory (Rockefeller University, New York) and modified to include Eml1<sup>7</sup>. The EB3-mCherry plasmid was a kind gift from A. Andrieux (Grenoble Institute of Neurosciences, Grenoble, France).

**Statistical analysis.** Statistical analyses were performed using StatView, BiostaTGV ([marne.u707.jussieu.fr/biostatgv/](http://marne.u707.jussieu.fr/biostatgv/)) and GraphPad Prism. Normal distribution of the data was verified before applying statistical tests. The unpaired *t*-test was applied to compare WT and *HeCo* EB3 tracking,  $\gamma$ -tubulin and Arl13b + puncta, spindle length, metaphase cell area, volume and height. *Pearson's* correlation coefficients and respective *P*-values were calculated. Linear regression tests were applied for comparison of correlations. No data points were excluded. All data were processed in a blind manner. No statistical methods were used to predetermine sample sizes, but our sample sizes are similar to those generally employed in the field<sup>7,10,58</sup>.

**Data availability.** The datasets generated during and/or analyzed during the current study are available from the corresponding author on reasonable request.

## References

1. Taverna, E., Götz, M. & Huttner, W. B. The cell biology of neurogenesis: toward an understanding of the development and evolution of the neocortex. *Annu. Rev. Cell Dev. Biol.* **30**, 465–502 (2014).
2. Willaredt, M. A., Tasouri, E. & Tucker, K. L. Primary cilia and forebrain development. *Mech. Dev.* **130**, 373–380 (2013).
3. Hu, D. J.-K. *et al.* Dynein recruitment to nuclear pores activates apical nuclear migration and mitotic entry in brain progenitor cells. *Cell*. **154**(6), 1300–1313 (2013).
4. Paridaen, J. T. M. L., Wilsch-Bräuninger, M. & Hutner, W. Asymmetric inheritance of centrosome-associated primary cilium membrane directs ciliogenesis after cell division. *Cell*. **155**, 333–344 (2013).
5. Bizzotto, S. & Francis, F. Morphological and functional aspects of progenitors perturbed in cortical malformations. *Front Cell Neurosci.* **9**, 30, <https://doi.org/10.3389/fncel.2015.00030> (2015).
6. Croqueolois, A. *et al.* Characterization of the *HeCo* mutant mouse: a new model of subcortical band heterotopia associated with seizures and behavioral deficits. *Cereb. Cortex.* **19**, 563–575 (2009).
7. Kielar, M. *et al.* Mutations in Eml1 lead to ectopic progenitors and neuronal heterotopia in mouse and human. *Nat. Neurosci.* **17**, 923–933 (2014).
8. Betizeau, M. *et al.* Precursor diversity and complexity of lineage relationships in the outer subventricular zone of the primate. *Neuron*. **80**, 442–457 (2013).
9. Hansen, D. V., Lui, J. H., Parker, P. R. L. & Kriegstein, A. R. Neurogenic radial glia in the outer subventricular zone of human neocortex. *Nature*. **464**, 554–561 (2010).
10. Cappello, S. *et al.* The Rho-GTPase cdc42 regulates neural progenitor fate at the apical surface. *Nat. Neurosci.* **9**, 1099–1107 (2006).

11. Junghans, D., Hack, I., Frotscher, M., Taylor, V. & Kemler, R. Beta-catenin- mediated cell-adhesion is vital for embryonic forebrain development. *Dev Dyn.* **233**, 528–39 (2005).
12. Hamill, D. R., Howell, B., Cassimeris, L. & Suprenant, K. A. Purification of a WD repeat protein, EMAP, that promotes microtubule dynamics through an inhibition of rescue. *J. Biol. Chem.* **273**, 9285–9291 (1998).
13. Vasquez, R. J., Gard, D. L. & Cassimeris, L. XMAP from *Xenopus* eggs promotes rapid plus end assembly of microtubules and rapid microtubule polymer turnover. *J. Cell Biol.* **127**, 985–993 (1994).
14. Eichenmuller, B., Everley, P., Palange, J., Lepley, D. & Suprenant, K. A. The human EMAP-like protein-70 (ELP70) is a microtubule destabilizer that localizes to the mitotic apparatus. *J. Biol. Chem.* **277**, 1301–1309 (2002).
15. Houtman, S. H., Rutteman, M., De Zeeuw, C. I. & French, P. J. Echinoderm microtubule-associated protein like protein 4, a member of the echinoderm microtubule-associated protein family, stabilizes microtubules. *Neuroscience.* **144**, 1373–1382 (2007).
16. Tegha-Dunghu, J. *et al.* EML3 is a nuclear microtubule-binding protein required for the correct alignment of chromosomes in metaphase. *J. Cell. Sci.* **121**, 1718–1726 (2008).
17. Goshima, G. & Scholey, J. M. Control of mitotic spindle length. *Annu. Rev. Cell Dev. Biol.* **26**, 21–57 (2010).
18. Hazel, J. *et al.* Changes in cytoplasmic volume are sufficient to drive spindle scaling. *Science.* **342**, 853–856 (2013).
19. Good, M. C., Vahey, M. D., Skandarajah, A., Fletcher, D. A. & Heald, R. Cytoplasmic volume modulates spindle size during embryogenesis. *Science.* **342**, 856–860 (2013).
20. Jiang, H. Cell size modulates oscillation, positioning and length of mitotic spindles. *Sci Rep.* **5**, 10504 (2015).
21. Crowder, M. E. *et al.* A comparative analysis of spindle morphometrics across metazoans. *Curr. Biol.* **25**, 1542–1550 (2015).
22. Novakova, L. *et al.* A balance between nuclear and cytoplasmic volumes controls spindle length. *PLoS ONE.* **11**, e0149535 (2016).
23. Stevermann, L. & Liakopoulos, D. Molecular mechanisms in spindle positioning: structures and new concepts. *Curr. Opin. Cell Biol.* **24**, 816–824 (2012).
24. McNally, F. J. Mechanisms of spindle positioning. *J. Cell Biol.* **200**, 131–140 (2013).
25. Cadart, C., Zlotek-Zlotkiewicz, E., Le Berre, M., Piel, M. & Matthews, H. K. Exploring the function of cell shape and size during mitosis. *Dev. Cell.* **29**, 159–169 (2014).
26. Heisenberg, C.-P. & Bellaïche, Y. Forces in tissue morphogenesis and patterning. *Cell.* **153**, 948–962 (2013).
27. Heller, E. & Fuchs, E. Tissue patterning and cellular mechanics. *J. Cell Biol.* **211**, 219–231 (2015).
28. Okamoto, M. *et al.* TAG-1-assisted progenitor elongation streamlines nuclear migration to optimize subapical crowding. *Nat. Neurosci.* **16**, 1556–1566 (2013).
29. Miyata, T., Okamoto, M., Shinoda, T. & Kawaguchi, A. Interkinetic nuclear migration generates and opposes ventricular-zone crowding: insight into tissue mechanics. *Front Cell Neurosci.* **8**, 473, <https://doi.org/10.3389/fncel.2014.00473> (2014).
30. Streichan, S. J., Hoerner, C. R., Schneid, T., Holzer, D. & Hufnagel, L. Spatial constraints control cell proliferation in tissues. *Proc. Natl. Acad. Sci. USA* **111**, 5586–5591 (2014).
31. Anthony, T. E., Mason, H. A., Gridley, T., Fishell, G. & Heintz, N. Brain lipid-binding protein is a direct target of Notch signaling in radial glial cells. *Genes Dev.* **19**, 1028–1033 (2005).
32. Gelfand, V. I. & Bershadsky, A. D. Microtubule dynamics: mechanism, regulation, and function. *Annual Review of Cell Biology.* **7**, 93–116 (1991).
33. Inoué, S. & Salmon, E. D. Force generation by microtubule assembly/disassembly in mitosis and related movements. *Mol Biol Cell.* **6**, 1619–1640 (1995).
34. Kwon, M. & Scholey, J. M. Spindle mechanics and dynamics during mitosis in *Drosophila*. *Trends Cell Biol.* **14**, 194–205 (2004).
35. Dumont, S. & Mitchison, T. J. Force and length in the mitotic spindle. *Curr. Biol.* **19**, R749–761 (2009).
36. Richards, M. W. *et al.* Crystal structure of EML1 reveals the basis for Hsp90 dependence of oncogenic EML4-ALK by disruption of an atypical  $\beta$ -propeller domain. *Proc. Natl. Acad. Sci. USA* **111**, 5195–5200 (2014).
37. Richards, M. W. *et al.* Microtubule association of EML proteins and the EML4-ALK variant 3 oncoprotein require an N-terminal trimerization domain. *Biochem. J.* **467**, 529–536 (2015).
38. Huang, D. W., Sherman, B. T. & Lempicki, R. A. Systematic and integrative analysis of large gene lists using DAVID Bioinformatics Resources. *Nature Protoc.* **4**(1), 44–57 (2009).
39. Szklarczyk, D. *et al.* STRINGv10: protein-protein interaction networks, integrated over the tree of life. *Nucleic Acids Res.* **43**, D447–452 (2015).
40. Janisch, K. M. *et al.* The vertebrate-specific Kinesin-6, Kif20b, is required for normal cytokinesis of polarized cortical stem cells and cerebral cortex size. *Development.* **140**, 4672–4682 (2013).
41. Pawlisz, A. S. *et al.* Lis1-Nde1-dependent neuronal fate control determines cerebral cortical size and lamination. *Hum. Mol. Genet.* **17**, 2441–2455 (2008).
42. Poirier, K. *et al.* Mutations in TUBG1, DYNC1H1, KIF5C and KIF2A cause malformations of cortical development and microcephaly. *Nat. Genet.* **45**, 639–647 (2013).
43. Marthiens, V. & French-Constant, C. Adherens junction domains are split by asymmetric division of embryonic neural stem cells. *EMBO Rep.* **10**, 515–520 (2009).
44. Rujano, M. A., Basto, R. & Marthiens, V. New insights into centrosome imaging in *Drosophila* and mouse neuroepithelial tissues. *Methods Cell Biol.* **129**, 211–227 (2015).
45. Loulier, K. *et al.*  $\beta$ 1 integrin maintains integrity of the embryonic neocortical stem cell niche. *PLoS Biology.* **7**, e1000176 (2009).
46. Wang, X., Tsai, J., LaMonica, B. & Kriegstein, A. R. A new embryonic subtype of progenitor cell in the mouse embryonic neocortex. *Nat. Neurosci.* **14**, 555–562 (2011).
47. Li, J. & Jiang, H. Geometric asymmetry induces upper limit of mitotic spindle size. *Biophys. J.* **112**, 1503–1516 (2017).
48. Mitchison, T. & Kirschner, M. Dynamic instability of microtubule growth. *Nature.* **312**, 237–242 (1984).
49. Carlier, M. F. & Pantaloni, D. Kinetic analysis of guanosine 5'-triphosphate hydrolysis associated with tubulin polymerization. *Biochemistry.* **20**(7), 1918–24 (1981).
50. Hill, T. L. & Carlier, M. F. Steady-state theory of the interference of GTP hydrolysis in the mechanism of microtubule assembly. *Proc. Natl. Acad. Sci. USA* **80**, 7234–7238 (1983).
51. Bowne-Anderson, H., Hibbel, A. & Howard, J. Regulation of microtubule growth and catastrophe: unifying theory and experiment. *Trends Cell Biol.* **25**, 769–779 (2015).
52. Gelfand, V. I. & Bershadsky, A. D. Microtubule dynamics: mechanism, regulation, and function. *Ann. Rev. Cell Biol.* **7**, 93–116 (1991).
53. Cross, R. A. & McAnish, A. Prime movers: the mechanochemistry of mitotic kinesins. *Nat. Rev. Mol. Cell Biol.* **15**, 257–271 (2014).
54. Tokai-Nishizumi, N., Ohsugi, M., Suzuki, E. & Yamamoto, T. The chromokinesin Kid is required for maintenance of proper metaphase spindle size. *Mol. Biol. Cell.* **16**, 5455–5463 (2005).
55. Ramkumar, N. & Baum, B. Coupling changes in cell shape to chromosome segregation. *Nat. Rev. Mol. Cell Biol.* **17**(8), 511–521 (2016).
56. Dubreuil, V., Marzesco, A. M., Corbeil, D., Huttner, W. B. & Wilsch-Bräuninger, M. Midbody and primary cilium of neural progenitors release extracellular membrane particles enriched in the stem cell marker prominin-1. *J. Cell Biol.* **174**, 483–495 (2007).
57. Das, R. M. & Storey, K. Apical abscission alters cell polarity and dismantles the primary cilium during neurogenesis. *Science.* **343**, 200–204 (2014).
58. Foerster, P. *et al.* mTORC1 signaling and primary cilia are required for brain ventricle morphogenesis. *Development.* **144**, 201–210 (2017).

59. Hueston, J. L. *et al.* The C. elegans EMAP-like protein, ELP-1 is required for touch sensation and associates with microtubules and adhesion complexes. *BMC Developmental Biology*. **8**, 110, <https://doi.org/10.1186/1471-213X-8-110> (2008).
60. Marinari, E. *et al.* Live-cell delamination counterbalances epithelial growth to limit tissue overcrowding. *Nature*. **484**, 542–545 (2012).
61. Levayer, R., Dupont, C. & Moreno, E. Tissue crowding induces Caspase-dependent competition for space. *Curr. Biol.* **26**, 670–677 (2016).
62. Cai, S., Weaver, L. N., Ems-McClung, S. C. & Walczak, C. E. Kinesin-14 family proteins HSET/XCTK2 control spindle length by cross-linking and sliding microtubules. *Mol. Biol. Cell.* **20**, 1348–1359 (2009).
63. Garcia, M. A., Koonrugsa, N. & Toda, T. Two kinesin-like Kin I family proteins in fission yeast regulate the establishment of metaphase and the onset of anaphase A. *Curr. Biol.* **12**, 610–621 (2002).
64. Brust-Mascher, I. & Scholey, J. M. Microtubule flux and sliding in mitotic spindles of *Drosophila* embryos. *Mol. Biol. Cell.* **13**, 3967–3975 (2002).
65. Brust-Mascher, I., Civelekoglu-Scholey, G., Kwon, M., Mogilner, A. & Scholey, J. M. Model for anaphase B: role of three mitotic motors in a switch from poleward flux to spindle elongation. *Proc. Natl. Acad. Sci. USA* **101**, 15938–15943 (2004).
66. Goshima, G., Wollman, R., Stuurman, N., Scholey, J. M. & Vale, R. D. Length control of the metaphase spindle. *Curr. Biol.* **15**, 1979–1988 (2005).
67. Fu, J. *et al.* TPX2 phosphorylation maintains metaphase spindle length by regulating microtubule flux. *J. Cell Biol.* **210**, 373–383 (2015).
68. Inoue, Y. H. *et al.* Orbit, a novel microtubule-associated protein essential for mitosis in *Drosophila melanogaster*. *J. Cell Biol.* **149**, 153–166 (2000).
69. Lemos, C. L. *et al.* Mast, a conserved microtubule-associated protein required for bipolar mitotic spindle organization. *EMBO J.* **19**, 3668–3682 (2000).
70. Pouillet, P., Carpentier, S. & Barillot, E. myProMS, a web server for management and validation of mass spectrometry-based proteomic data. *Proteomics*. **7**, 2553–2556 (2007).
71. Käll, L., Storey, J. D. & Stafford Noble, W. Non-parametric estimation of posterior error probabilities associated with peptides identified by tandem mass spectrometry. *Bioinformatics*. **24**, i42–i48 (2008).
72. Valot, B., Langella, O., Nano, E. & Zivy, M. MassChroQ: a versatile tool for mass spectrometry quantification. *Proteomics*. **11**(17), 3572–3577 (2011).
73. Vizcaino, J. A. *et al.* ProteomeXchange provides globally co-ordinated proteomics data submission and dissemination. *Nat. Biotechnol.* **32**, 223–226 (2014).

## Acknowledgements

We thank Michel Kielar, Laurence Goutebroze, Richard Belvindrah, Marika Nosten-Bertrand, Delfina Romero and Melissa Stouffer for helpful advice. We thank Richard Bayliss and Andrew Fry for the gift of the EML1-N-ter construct and for helpful discussions on Eml1 structure and function. We thank Melissa Stouffer for help with *in situ* hybridizations, Veronique Marthiens for advice on *en face* imaging, N. Heintz and A. Andrieux for supplying plasmids, and C. Metin for certain antibodies. We thank the IFM animal house and imaging facilities. We thank the Ile-de-France region for support of imaging and animal house facilities and the FRC Rotary. We thank the IFM animal house experimentation and imaging platforms and the CNRS-TAAM for *HeCo* mouse mutant housing. FF, SB and AU were associated with the BioPsy Labex project and the Ecole des Neurosciences de Paris Ile-de-France (ENP) network. We thank the French Agence Nationale de la Recherche (ANR-13-BSV4-0008-01), Inserm, CNRS, UPMC, Fondation Bettencourt Schueller, Fédération pour la Recherche sur le cerveau (FRC), the European Union (EU-HEALTH-2013, DESIRE, No 60253), the JTC 2015 Neurodevelopmental Disorders and the ANR (for NEURON8-Full-815-006 STEM-MCD) for grant support to FF, the French Ministry of Research, Fondation pour la Recherche Médicale for PhD funding to SB, the Ecole des Neurosciences de Paris for PhD funding, and the Company of Biologists for a travel grant to AU.

## Author Contributions

S.B. conceived or designed the experiments, performed the experiments, analyzed the data and wrote the manuscript. A.U. designed experiments, performed *in situ* hybridizations, immunodetections, microscopy and data analyses. D.E. analyzed the cell volume data, guided by N.M. F.D. and G.A. performed the experiments and/or analyzed the mass spectrometry data. D.L. and AHoud helped in designing these experiments. AHoud provided technical assistance for biochemistry experiments. M.R. generated constructs for recombinant protein preparation. A.C. provided mice. A.U. and D.L. contributed to paper writing. F.F. conceived the experiments, was involved in data analysis and interpretation, and wrote the manuscript.

## Additional Information

**Supplementary information** accompanies this paper at <https://doi.org/10.1038/s41598-017-15253-4>.

**Competing Interests:** The authors declare that they have no competing interests.

**Publisher's note:** Springer Nature remains neutral with regard to jurisdictional claims in published maps and institutional affiliations.



**Open Access** This article is licensed under a Creative Commons Attribution 4.0 International License, which permits use, sharing, adaptation, distribution and reproduction in any medium or format, as long as you give appropriate credit to the original author(s) and the source, provide a link to the Creative Commons license, and indicate if changes were made. The images or other third party material in this article are included in the article's Creative Commons license, unless indicated otherwise in a credit line to the material. If material is not included in the article's Creative Commons license and your intended use is not permitted by statutory regulation or exceeds the permitted use, you will need to obtain permission directly from the copyright holder. To view a copy of this license, visit <http://creativecommons.org/licenses/by/4.0/>.

© The Author(s) 2017

## **Em11 loss impairs apical progenitor spindle length and soma shape in the developing cerebral cortex**

Sara Bizzotto<sup>1-3,#,§</sup>, Ana Uzquiano<sup>1-3,#</sup>, Florent Dingli<sup>4</sup>, Dmitry Ershov<sup>5</sup>, Anne Houllier<sup>1-3</sup>, Guillaume Arras<sup>4</sup>, Mark Richards<sup>6</sup>, Damarys Loew<sup>4</sup>, Nicolas Minc<sup>5</sup>, Alexandre Croquelois<sup>7,8</sup>, Anne Houdusse<sup>9</sup>, Fiona Francis<sup>1-3,\*</sup>

<sup>1</sup> INSERM UMR-S 839, 17 rue du Fer à Moulin, Paris 75005, France.

<sup>2</sup> Sorbonne Universités, Université Pierre et Marie Curie, 4 Place Jussieu, Paris 75005, France.

<sup>3</sup> Institut du Fer à Moulin, 17 rue du Fer à Moulin, Paris 75005, France.

<sup>4</sup> Institut Curie, PSL Research University, Centre de Recherche, Laboratoire de Spectrométrie de Masse Protéomique, 26 rue d'Ulm, 75248 Cedex 05 Paris, France.

<sup>5</sup> Institut Jacques Monod, UMR7592 CNRS, Paris, France.

<sup>6</sup> Department of Biochemistry, University of Leicester, Henry Wellcome Building, Lancaster Road, Leicester, LE1 9HN, U.K.

<sup>7</sup> Department of Clinical Neuroscience, Centre Hospitalier Universitaire Vaudois and University of Lausanne, 21 rue du Bugnon, 1011 Lausanne, Switzerland.

<sup>8</sup> Department of Fundamental Neurosciences, University of Lausanne, 1005 Lausanne, Switzerland.

<sup>9</sup> Structural Motility, Institut Curie, Centre de Recherche; CNRS, UMR144, 26 rue d'Ulm, Cedex 05, Paris 75248, France.

<sup>§</sup> Current affiliation: Division of Genetics and Genomics, Manton Center for Orphan Disease, and Howard Hughes Medical Institute, Boston Children's Hospital, Boston, MA, USA. Departments of Pediatrics and Neurology, Harvard Medical School, Boston, MA, USA. Broad Institute of MIT and Harvard, Cambridge, MA, USA.

<sup>#</sup> These authors contributed equally to this work.

<sup>\*</sup> *Corresponding author*: Fiona Francis, Institut du Fer à Moulin, 17 rue du Fer à Moulin, 75005 Paris France. Tel: +33145876145 Email: [fiona.francis@inserm.fr](mailto:fiona.francis@inserm.fr)

## Supplementary information

### Supplementary Materials and Methods

***In situ* hybridization.** Mouse digoxigenin (DIG)-labeled riboprobes were generated by *in vitro* transcription of a fragment amplified from the *Eml1* 3' UTR region (chr12 nt 109776616 to 109777469, Genome Browser, <http://genome.ucsc.edu/>) and subcloned in pBluescript II KS vector (7). Frozen 20 µm thick cryostat sections were hybridized at 65°C overnight with the DIG-labeled probes diluted 1:100 in hybridization buffer (50% deionized formamide, 10% dextran sulphate, 1 mg/ml Yeast RNA, 1x Denhardt's solution). The next day, sections were sequentially washed twice (45 minutes) in 1X saline sodium citrate (SSC), 50% formamide and Tween 0.1% at 65°C. Sections were washed extensively with PBS Tween 20 (PBST) 0.1% followed by PBS 1X. For immunological detection of DIG-labeled hybrids, sections were first blocked (10% sheep serum, 0.1% Tween in PBS 1X) and then incubated overnight at 4°C in the same solution containing sheep anti-DIG-alkaline phosphatase-conjugated Fab fragments (Roche Diagnostics) diluted 1:2000. The following day, sections were washed 3 x 15 minutes in PBST 0.1% and 30 min in NTMT buffer (100 mm NaCl, 100 mm Tris-HCl, pH 9.5, 50 mm MgCl<sub>2</sub>, 0.1% Tween 20). The alkaline phosphatase chromogen reaction was performed in NTMT buffer containing 100 mg/ml nitroblue tetrazolium (Roche Diagnostics) and 50 mg/ml 5-bromo-4-chloro-3-indolyl phosphate (Roche) at room temperature for 2-4 hours and stopped with PBS 1X. Sections were mounted with Mowiol. Images were acquired with an EVOS Digital Microscope.

**N2A cell transfection and culture.** Cells were cultured in 10% fetal bovine serum (FBS)-supplemented Dulbecco Modified Eagle Medium (DMEM) (Sigma-Aldrich). N2A cells were co-transfected with either pEGFP-C3 control vector (Clontech) or pEGFP-Eml1, and EB3-mCherry (10 µg total DNA) using the Neon Transfection System (Thermo Fisher Scientific), and seeded in 35 mm diameter glass bottom Ibidi dishes suitable for video-microscopy. Video-microscopy was performed as for neural progenitors at 2 DIV.

**MS data processing and statistical analysis.** Data were acquired using the Xcalibur software and the resulting spectra were analyzed via the Mascot™ Software created with Proteome Discoverer (Thermo Scientific) using the *Mus musculus* database containing 16587 protein sequences. Carbamidomethylation of cysteines, oxidation of methionine and protein N-terminal acetylation were set as variable modifications for searches. Specificity of trypsin digestion was set and two missed cleavage sites were allowed. The mass tolerances in MS and MS/MS were

set to 2 ppm and 0.5 Da, respectively. All peptide/protein identification data were further processed using the Institut Curie developed software myProMS (<http://myproms.curie.fr/>) (62) version 3.0. The false discovery rate (FDR) for peptide identification was fixed to less than 1% at the peptide level for the whole study, and the QUALITY algorithm (63) was used. For label-free quantification, peptide XICs (Extracted Ion Chromatograms) were computed with MassChroQ v1.2.1 (73) using OBI-Warp alignment algorithm. Protein ratios were computed as the geometrical mean of related peptides. To estimate ratio significance, a two-tailed *t*-test was performed with a Benjamini–Hochberg FDR control threshold set to 0.05. Data were analyzed using the DAVID Functional Annotation Tool (38) (<https://david.ncifcrf.gov/home.jsp>) for Gene Ontology generation, and STRING Functional Protein Association Network ([string-db.org](http://string-db.org)) (39) to reveal interactions between proteins.

### **Supplementary Video legends**

Supplementary Video S1. **Example of WT EB3-mCherry live-imaging.** E12.5 mouse WT cortices were dissected and neural progenitors were dissociated and co-transfected with plasmids expressing EB3-mCherry and the RGC marker BLBP-EGFP. Cells were cultured at 37°C and 5% CO<sub>2</sub> two days before imaging. EGFP-positive cells were imaged for EB3-mCherry (red) using time-lapse confocal microscopy and Metamorph software during 2 min with frame acquisitions every 1 sec. Three confocal planes were acquired (300 ms exposure) and z-stack projections were made for each frame. Display rate: 10 frames/second. Related video still is shown in Figure 1a.

Supplementary Video S2. **EB3 tracking.** Higher magnification of one cell shown in Supplementary Video 1 and Figure 1a showing EB3 tracks. Each colored track represents a single EB3-positive MT. EB3-mCherry is shown in black on a white background. Tracks were generated manually using the Manual Track ImageJ plugin on stack images corresponding to 1 frame generated by max projection of three confocal planes. Display rate: 10 frames/second. Related video still is shown in Figure 1a (higher magnification).

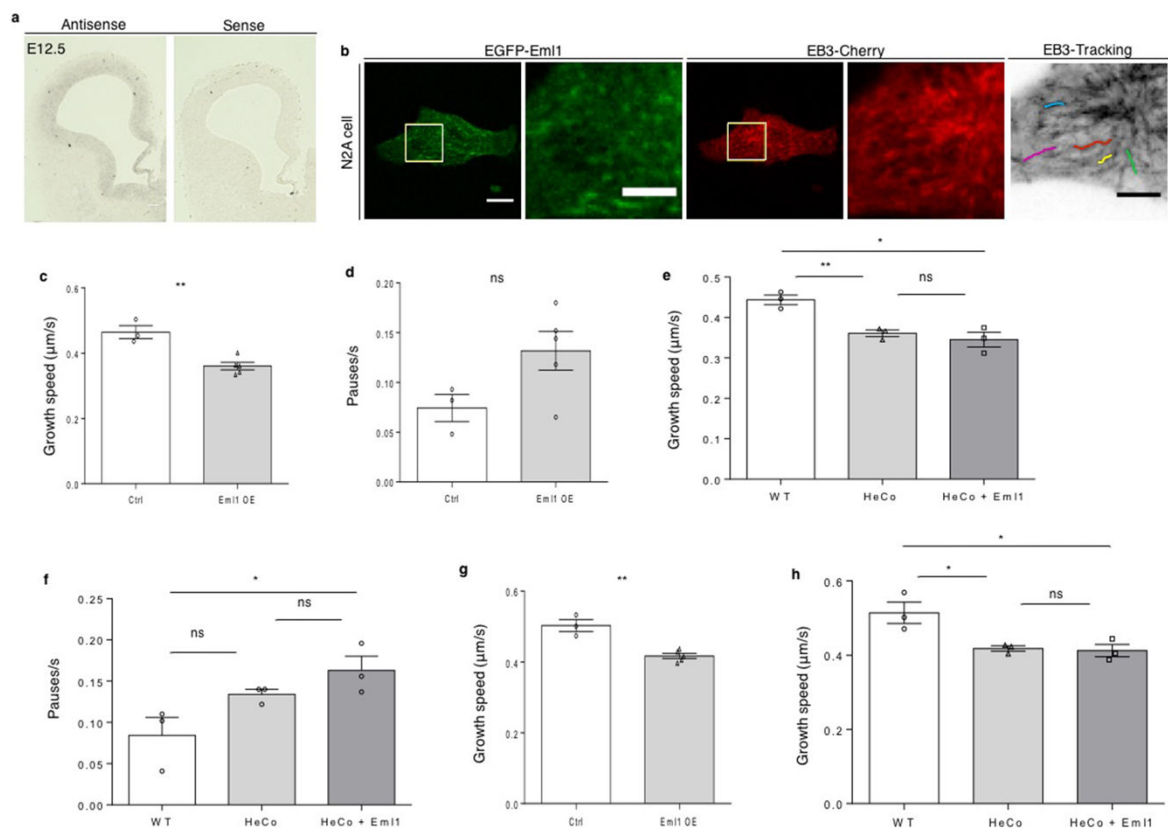
### **Supplementary Table legends**

Supplementary Table S1. **List of the 1059 proteins uniquely associated with GST-EML1 N-ter samples based on XIC quantification.** Gene ontologies based on the three categories: biological process (BP), cellular component (CC), and molecular function (MF) were generated using the DAVID functional annotation tool.

Supplementary Table S2. **List of the 176 proteins that passed filtering of the 1059 proteins uniquely associated with GST-EML1 N-ter.** Gene ontologies based on the three categories biological process (BP), cellular component (CC), and molecular function (MF) were generated using the DAVID functional annotation tool. A list of 10 kinesins is also reported.

# Supplementary Figures

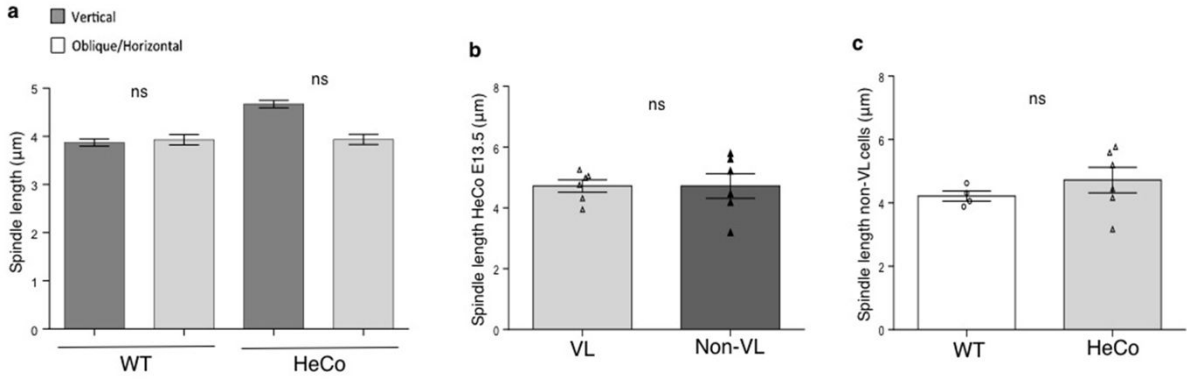
## Supplementary Figure S1





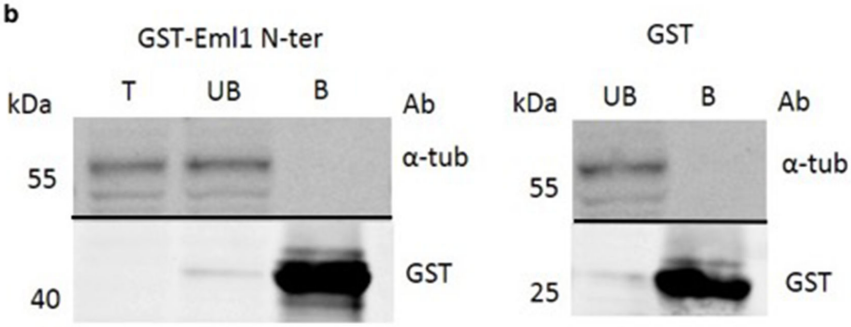
Supplementary Figure S1. **Eml1 overexpression reduces MT growth in N2A cells and does not rescue MT dynamics in *HeCo* progenitors.** (a) Eml1 transcripts are detected in the cortical VZ of WT E12.5 embryos. (b) N2A cells co-transfected with either EGFP (Ctrl) or EGFP-Eml1 and EB3-mCherry. Fluorescent EB3 was filmed with a confocal microscope equipped with a spinning disk and EB3-positive plus-ends tracked using Image J. Colored lines in the far right image show a representation of tracking. Higher magnifications of the boxed areas are shown. (c) EGFP-Eml1 overexpression (Eml1 OE) reduces MT growth rate. (d) Pause frequency during MT growth does not change significantly upon Eml1 OE although there is a tendency for increased pauses. Ctrl, N = 3; Eml1 OE, N = 4 independent experiments. Circles and triangles in the graphs represent different experiments. A total of 19 cells were analyzed for both Ctrl and Eml1 OE. Ctrl, 114; Eml1 OE, 102 total single EB3-positive MTs tracked. (e,f) EB3-MT growth in neural progenitors from dissociated cultures prepared from E12.5 embryonic cortices. First two bars shown for comparison represent the same data as shown in Figure 1b. WT and *HeCo* progenitors were transfected with either BLBP-IRES-EGFP or BLBP-Eml1-IRES-EGFP and EB3-mCherry. EB3 comet tracking was performed and quantified in EGFP+ cells. MT growth speed is still reduced upon transfection of Eml1 in *HeCo* progenitors compared to WT and does not change compared to *HeCo* (e). Eml1 overexpression in *HeCo* progenitors significantly increases the MT pause frequency compared to WT but not compared to *HeCo* (f). (g,h) Growth rate comparisons without taking into account pauses give results comparable to when pauses are included in the calculation, for both N2A cells (g) and neural progenitors (h). N= 3 independent experiments for each condition. *HeCo* +Eml1, 17 cells analyzed for a total of 156 single MTs tracks. Unpaired *t*-test, ns, non significant; \*  $P < 0.05$ ; \*\*  $P < 0.01$ . Scale bars 100  $\mu\text{m}$  (a), 10  $\mu\text{m}$  (b) and 5  $\mu\text{m}$  (high magnifications).

Supplementary Figure S2



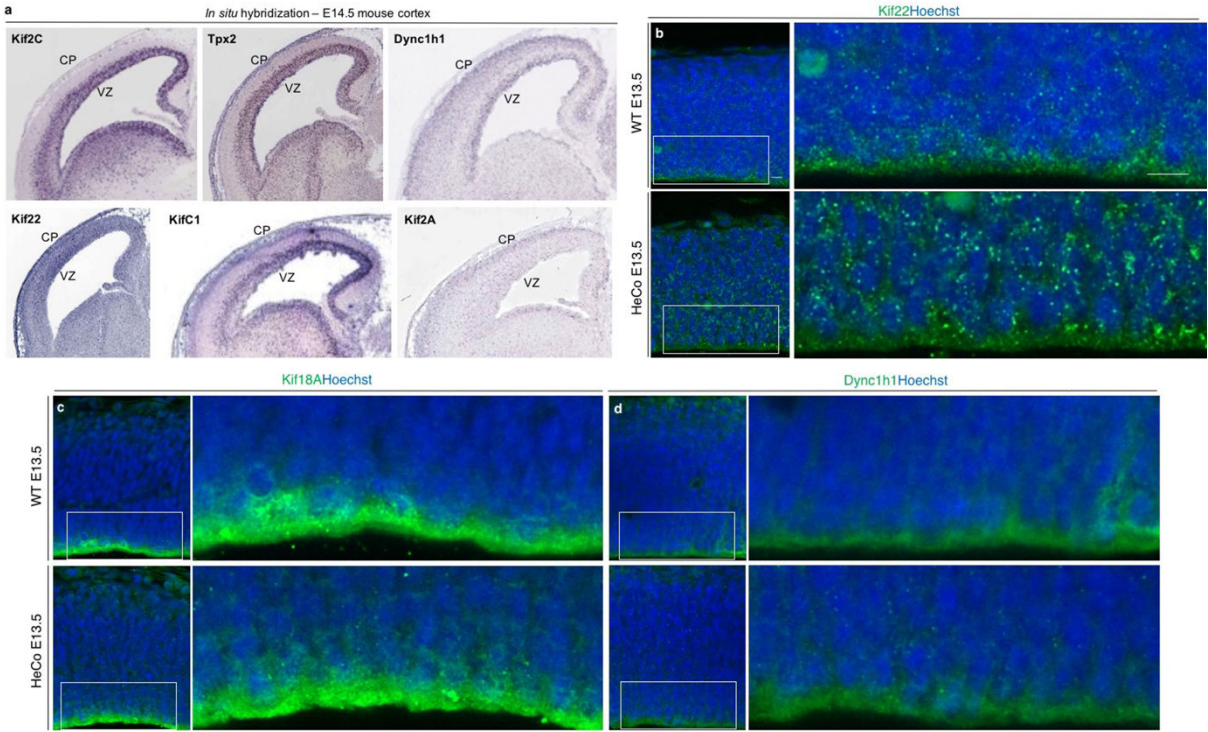
Supplementary Figure S2. **Spindle length does not change between vertical and oblique/horizontal spindle orientations and *HeCo* VL and non-VL progenitors.** (a) Spindles were classified from 3D-reconstructed single (pro)metaphase cells at the VL as having vertical or oblique/horizontal cleavage planes (DNA plate orientation with respect to the VL) and average lengths were compared for the two categories for each genotype and developmental stage. No significant differences were observed. (b,c) Spindle length was measured in WT and *HeCo* brains in cells dividing within the VZ but far from the VL as well as in cells dividing outside the VZ (WT = 19, *HeCo* = 31 total cells). No significant difference was found between VL and non-VL cells in *HeCo* brains. Spindle lengths are more variable in non-VL *HeCo* dividing cells. This variability could be due to an increased sensitivity of the latter to external forces, and/or to increased spindle length oscillations in (pro)metaphase when cells are located in this region. Variability may also be due to the fact that other types of basally located cells may be included in the analysis, as well as ectopic apical progenitors. (b) Spindle length of VL cells is not significantly different between WT and *HeCo*, however, there is a tendency for longer spindles in *HeCo* basal (pro)metaphase cells (c). Unpaired *t*-test. ns,  $P > 0.05$ .

Supplementary Figure S3



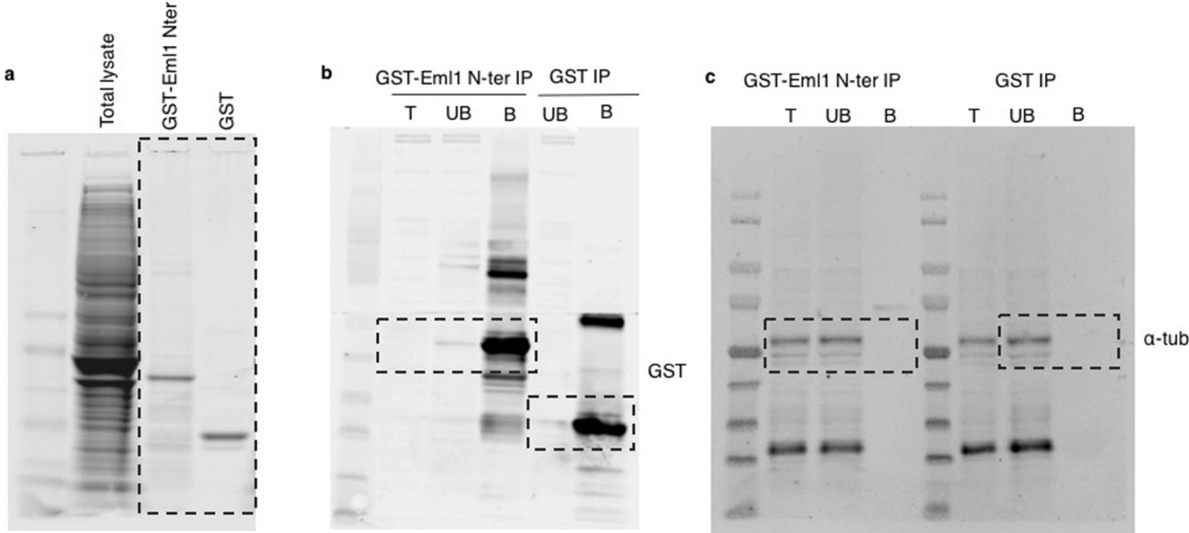
Supplementary Figure S3. **Controls for GST-EML1 Nter pull-down.** (a) Control gel with pull-down samples for GST-EML1 N-ter and GST control stained with Colloidal Blue. (b) Western Blot showing no binding of alpha-tubulin to GST-EML1 N-ter after pull-down. Black lines separate blots which were not run together, see Supplementary Figure S5 for full blots. Antibodies: mouse anti-alpha-tubulin 1:10000 (DM1A clone, Sigma-Aldrich T9026), rabbit anti-GST 1:1000 (Sigma-Aldrich, G7781) T, total fraction; UB, un-bound fraction; B, bound fraction.

Supplementary Figure S4



Supplementary Figure S4. **MS proteins involved in spindle length regulation are expressed in the mouse VZ, and the microtubule motor protein Kif22 shows a different pattern of expression in *HeCo* developing cortex.** (a) *In situ hybridization* images obtained from publicly available resources (<http://www.genepaint.org>) showing *KifC1*, *Kif2A*, *Kif22* and *Dync1h1* expression in the VZ and CP of the mouse developing cortex at E14.5, and expression of *Kif2C* and *Tpx2* in the VZ only. (b) IHC for Kif22 in WT and *HeCo* E13.5 cortices showing altered expression in *HeCo* VZ. White boxes delineate the higher magnification images. (c,d) Kif18A and *Dync1h1* IHC show similar levels of the proteins and similar expression patterns in WT versus *HeCo* E13.5 cortices. Scale bars 10  $\mu$ m.

Supplementary Figure S5





Supplementary Figure S5. **Full-length pictures of the gel and blots presented in Supplementary Fig. S3.** (a) gel in Supplementary Fig. S3a. (b,c) Original blots from which the bands shown in Supplementary Fig. S3b were cropped. The same IP samples were run twice on two different gels due to the necessity of detecting GST-Eml Nter and control GST (b) separately from alpha-tubulin (c) to avoid possible band overlap due to similar molecular weight of the proteins. Regions cropped in Supplementary Fig. S3 are indicated by boxed regions.

## 2. Introduction to Uzquiano et al. 'Mutations in the heterotopia gene *Eml1/EML1* severely disrupt the formation of primary cilia.'

Eml1 not only localizes to microtubules during mitosis, it also co-localizes with the microtubule network in interphase. In Bizzotto et al. 2017, we identified an altered distribution and numbers of centrosomes and primary cilia, respectively, in the *HeCo* VZ, indicating abnormalities of *HeCo* aRGs during interphase. These experiments formed the basis of the central work of my thesis, in which I have addressed **perturbed mechanisms in interphase in Eml1-mutant conditions**. Although most of my work has focused on analyzing *HeCo* aRGs (in tissue and *in vitro*), I also performed experiments in patient fibroblasts, and through collaborations the data was complemented by studies in human induced pluripotent stem cell (hiPSC)-derived cortical progenitors (Dr. J. Ladewig, Germany).

### 2.1 Summary

In this article, I uncovered an unexpected function for Eml1 in primary cilium formation in aRGs at early stages of corticogenesis. Combining *en face* imaging with electron microscopy (EM), we showed that **mutant primary cilia in the apical plasma membrane are either shorter, or these organelles are found in intracellular vesicle-like compartments, often showing an aberrant basal orientation**. Furthermore, immunocytochemistry and EM in *EML1* mutant patient fibroblasts and hiPSC-derived cortical progenitors, respectively, further confirmed the abnormal primary cilia phenotypes.

The intracellular pathways in which EML1 is involved have not up till now been described. **We identified the ciliary protein RPGRIP1L as an EML1 interactor**. Additionally, **we report the first subcortical heterotopia patient with mutations in RPGRIP1L**. Using biochemistry, we show that patient mutations in either EML1 or RPGRIP1L impair the interaction between these proteins, suggesting convergent molecular mechanisms responsible for the etiology of the heterotopia when these proteins are mutated.

Further querying the upstream mechanisms which may contribute to the primary cilium phenotype, **we performed mass spectrometry analyses to identify additional EML1 interacting partners**. In this screen, pull downs were performed with purified Strep-EML1 full length and embryonic cortex lysates from E13.5 embryos, followed by mass spectrometry. After data analysis and filtering, a list of 113 potential EML1 interactors was obtained. **Several cilia-related candidates appeared in the mass spectrometry data**. Notably though, **GO**

**analyses also pointed to Golgi apparatus and protein transport as enriched functional categories**, suggesting that EML1 may be involved in these mechanisms.

Trafficking of proteins from the Golgi apparatus is essential for the assembly and maintenance of the basal body-primary cilium complex. Therefore, the mass spectrometry data prompted us to **investigate the Golgi apparatus in *Eml1/EML1* mutant conditions**. Performing *in utero* electroporations in the mouse brain, as well as EM, **we identified severe alterations in Golgi apparatus distribution and structure in *HeCo* aRGs**. In addition, an *in vitro* assay (analyses of thermosensitive VSVG-GFP dynamics) in *HeCo* aRG cultures showed that Golgi-derived **trafficking is impaired** in these cells. Golgi anomalies were also revealed in patient fibroblast and iPSC-derived cortical progenitors (using immunocytochemistry and EM, respectively). Finally, we also confirmed the interaction of EML1 with the Golgi partner, VCIP135, further supporting a Golgi-related function for EML1.

The data gathered in this manuscript suggest that **the Golgi-to-primary cilium axis is perturbed in *Eml1/EML1* mutant conditions**. This is quite novel and has never previously been described for cortical malformations. We reveal novel intracellular pathways pivotal for aRG dynamics in the context of a severe neurodevelopmental disorder.

The primary cilium serves as platform to integrate signaling pathways, several of which were previously reported to influence aRG behavior (e.g. Wnt, mTOR, Shh, Hippo). It is thus important to assess these pathways in *Eml1*-mutant conditions to understand the downstream consequences of the primary cilium phenotype observed. The data included in the manuscript indicates that mTOR signaling does not appear altered in the *HeCo* cortex at early stages of corticogenesis. Further data concerning Shh and Hippo signaling is provided as extra supplementary information following the manuscript.

## **2.2 Contribution**

This manuscript represents the main work of my thesis. I designed most of the experiments with my thesis supervisor, Dr. F. Francis. I performed experiments and analyzed data, and collaborations were established for certain aspects of the manuscript. EM experiments were performed in collaboration with Dr. C. Cifuentes-Diaz, head of the EM platform at the Institute du Fer à Moulin. Identification of the *RPGRIP1L* mutations in the heterotopia patient was achieved by Dr. D. Romero, a post-doc in the Francis lab, C. Maillard (PhD student) and Dr. N. Bahi-Buisson (clinician and researcher) at the Imagine Institute, Paris, together with Anne Boland and Jean-François Deleuze at the CNRGH, Evry who performed the exome sequencing.

Biochemistry experiments and mass spectrometry sample preparation was performed with the help of A. Houllier, technician in the Francis lab. Mass spectrometry was performed in collaboration with the Institute Curie Proteomics Platform, Paris. Ferret experiments were performed by the Borrell lab, Alicante. hIPSC experiments were performed in collaboration with the team of Dr. J. Ladewig, Mannheim.

Mutations in the heterotopia gene *Eml1/EML1* severely disrupt the formation of primary cilia

Ana Uzquiano <sup>1,2,3</sup>, Carmen Cifuentes-Diaz<sup>1,2,3</sup>, Ammar Jabali <sup>4,5,6</sup>, Delfina Romero <sup>1,2,3</sup>, Anne Houllier <sup>1,2,3</sup>, Florent Dingli <sup>7</sup>, Camille Maillard <sup>8,9</sup>, Cristina Llinares-Benadero <sup>10</sup>, Anne Boland <sup>11</sup>, Jean-François Deleuze <sup>11</sup>, Damarys Loew <sup>7</sup>, Grazia M. S. Mancini <sup>12</sup>, Victor Borrell <sup>10</sup>, Nadia Bahi-Buisson <sup>8,9,13,14</sup>, Julia Ladewig <sup>4,5,6</sup>, Fiona Francis <sup>1,2,3</sup>.

1. INSERM U 1270, Paris, France

2. Sorbonne Université, UMR-S 1270, F-75005 Paris, France

3. Institut du Fer à Moulin, Paris, France

4. Central Institute of Mental Health, Medical Faculty Mannheim, Heidelberg University, Mannheim, Germany

5. HITBR Hector Institute for Translational Brain Research gGmbH, Mannheim, Germany

6. German Cancer Research Center (DKFZ), Heidelberg, Germany

7. Institut Curie, PSL Research University, Centre de Recherche, Laboratoire de Spectrométrie de Masse Protéomique, Paris, France

8. Laboratory of genetics and development of the cerebral cortex, INSERM UMR1163 Imagine Institute, Paris, France

9. Paris Descartes-Sorbonne Paris Cité University, Imagine Institute, Paris, France

10. Instituto de Neurociencias, Agencia Estatal Consejo Superior de Investigaciones Científicas and Universidad Miguel Hernández, San Juan de Alicante, Spain

11. Centre National de Recherche en Génomique Humaine (CNRGH), Institut de Biologie François Jacob, CEA, Université Paris-Saclay, F-91057, Evry, France

12. Department of Clinical Genetics, ErasmusMC University Medical Center, 3015CN, Rotterdam, The Netherlands

13. Pediatric Neurology APHP- Necker Enfants Malades University Hospital, Paris, France

14. Centre de Référence, Déficiences Intellectuelles de Causes Rares, APHP- Necker Enfants Malades University Hospital, Paris, France

\**Corresponding author and lead contact:* Fiona Francis, Institut du Fer à Moulin, 17 rue du Fer à Moulin, 75005 Paris France. Tel: +33145876145 Email: [fiona.francis@inserm.fr](mailto:fiona.francis@inserm.fr)

**Keywords:** subcortical heterotopia, cortical development, progenitor, radial glia, cortical malformation, primary cilium, Golgi apparatus, microtubule, ventricular zone.

## Summary

Apical radial glia (aRGs) are predominant progenitors during cerebral cortical development. Perturbing their function leads to cortical malformations. *EML1/Eml1* mutations cause subcortical heterotopia in patients, as well as *HeCo* mutant mice. In *HeCo* brains, aRGs are abnormally positioned away from the ventricular zone (VZ). Unraveling *EML1/Eml1* function can help clarify mechanisms maintaining aRGs in the VZ. We pinpoint a previously unknown *EML1/Eml1* function in primary cilium formation in *HeCo* aRGs, as well as patient fibroblasts and human cortical progenitors. The ciliary protein *RPGRIP1L* was identified as a new *EML1*-interactor and *RPGRIP1L* mutations were subsequently revealed in a heterotopia patient. Questioning upstream mechanisms, Golgi-related *EML1* interactors were revealed and Golgi apparatus abnormalities identified in *EML1/Eml1* mutant cells. Perturbation of the Golgi-primary cilium axis has not been previously described in heterotopia and is likely to contribute to aRG delamination. We reveal key subcellular mechanisms impacting aRG dynamics in physiological and pathological conditions.

## Introduction

The cerebral cortex is a highly organized structure whose development depends on different progenitor cell types. These give rise to post-mitotic neurons that migrate across the developing cortical wall to their final positions in the cortical plate. Apical radial glia cells (aRGs) are the main progenitor type in early corticogenesis, responsible for the production of other progenitors, hence regulating the final neuronal output (Uzquiano et al., 2018). aRGs are localized in the proliferative ventricular zone (VZ) and have a characteristic morphology, including a basal process extending to the pial surface and an apical process descending to the ventricular surface. The apical process of aRGs terminates by an endfoot characterized by the presence of a centrosome that during interphase acts as a basal body docking a primary cilium. These two structures are crucial for aRG polarity and function, and abnormal behavior of aRGs disrupts neocortical development causing severe cortical malformations (Bizzotto and Francis, 2015). Primary cilium anomalies, as well as defects in pathways dependent on this organelle are expected to severely impact different steps of corticogenesis (Ding et al., 2019, Foerster et al., 2017, Guo et al., 2015, Higginbotham et al., 2013, Yabut and Pleasure, 2018).

We identified pathogenic mutations in *Eml1/EML1* in a specific group of cortical malformations, characterized by atypical subcortical heterotopia (SH), corpus callosum agenesis and macrocrania (Kielar et al, 2014; Shaheen et al., 2017). *EML1* codes for a microtubule-associated protein. Remarkably, mutations in the mouse ortholog *Eml1* lead to a similar phenotype in the *Heterotopic cortex 'HeCo'* mouse mutant (Croquelois et al., 2009, Kielar et al., 2014). This represents a unique model to decipher the biological basis of this cortical malformation.

The *HeCo* mouse shows severe progenitor anomalies from early stages of corticogenesis thought to be responsible for the heterotopia phenotype (Bizzotto et al., 2017, Kielar et al., 2014). Some aRGs leave the normal proliferative zone and divide in aberrant basal positions (Kielar et al., 2014). However, the pathological mechanisms leading to the detachment of these cells in the *HeCo* VZ remain vastly unexplored.

The primary cilium is a microtubule-based antenna-like structure that serves as platform for signaling pathways. In apical endfeet of interphase aRGs, this organelle protrudes towards the ventricle in order to sense signals from the cerebrospinal fluid. It is formed after mitosis, when the centrosome, composed of two centrioles at the spindle pole, is trafficked towards the apical surface. During this journey the centrosome associates with *de novo* synthesized membrane or ciliary remnants, which are often carried in vesicle-like structures, and that will then become the basal body-primary cilium complex (Bernabé-Rubio and Alonso, 2017, Paridaen et al., 2013). Once this complex reaches the apical plasma membrane, the basal body is docked and the primary cilium is inserted in the apical membrane. Trafficking of proteins from the Golgi apparatus is essential for the assembly of the basal body-primary cilium complex (Bernabé-Rubio and Alonso, 2017, Madhivanan and Aguilar, 2014). Therefore, the correct formation of primary cilia depends on diverse subcellular processes and disruption of any one of them could be responsible for the appearance of cilia-related pathologies (Madhivanan and Aguilar, 2014).

Here we reveal a severe disruption of primary cilia in *Eml1/EML1* mutant conditions, not only in *HeCo* aRGs, but also in patient fibroblasts and human induced pluripotent stem cell (iPSC)-derived cortical progenitors. We also uncover a new ciliary partner of EML1, RPGRIP1L, and report the first heterotopia patient showing mutations in this protein. Searching for upstream mechanisms potentially responsible for perturbed primary cilia, converging data pointed towards abnormal Golgi apparatus function in *Eml1/EML1* mutant conditions. The function of



the Golgi apparatus in aRGs remains vastly unexplored. We show that the Golgi apparatus has a different distribution in *HeCo* aRGs when compared to WT, and shows signs of abnormal structure and/or function in *HeCo* aRGs, patient fibroblasts and human cortical progenitors. This work hence unravels Golgi-primary cilium anomalies that are likely to contribute to aRG delamination. It also uncovers novel functions for *Eml1/EML1* and highlights the importance of further studying membrane-bound organelles and their function(s) in neuronal progenitors, both in physiological and pathological conditions.

## Results

### Primary cilia formation is impaired in *Eml1* mutant conditions

Alterations in the number and distribution of  $\gamma$ -tubulin- and Arl13b-positive (+) puncta, identifying centrosomes and primary cilia respectively, were recently observed in the VZ of *HeCo* mouse brains at early stages of corticogenesis (Bizzotto et al., 2017). For a more global view of the ventricular surface, *en face* imaging was performed in combination with these two markers in WT and *HeCo* embryonic mouse brain at the same developmental time point. Using this approach, we confirmed a decrease in numbers of  $\gamma$ -tubulin+ and Arl13b+ puncta at the *HeCo* ventricular surface (Figure 1 A, B, C). We questioned if, as well as reduced numbers, other defects could be identified. Primary cilia length was measured from the Arl13b immunodetections, a parameter often studied to investigate defects in their assembly/disassembly (Gabriel et al., 2016, Kia et al., 2012). As well as the decrease in number, primary cilia were shorter at the *HeCo* ventricular surface at E13.5 (Figure 1 D). These results hence point towards ciliary-related anomalies in *Eml1* mutant conditions.

Centrosomes and primary cilia play specific roles during the different phases of the cell cycle (Hua and Ferland, 2018, Paridaen et al., 2013 and Figure 1 E). In order to further examine the *HeCo* centrosome-primary cilium phenotype, we analyzed the ultrastructure and subcellular localization of these organelles in WT and *HeCo* brains at E13.5 by electron microscopy (EM) (Figure 1 F). In WT interphase aRG endfeet, centrioles are observed in close vicinity to the apical plasma membrane, the mother centriole acting as basal body and thus docking a primary cilium protruding in the ventricle (Figure 1 F). Strikingly, a series of severe anomalies were observed in *HeCo* aRGs. In agreement with the *en face* imaging findings, primary cilia measured from EM data were found to be shorter at the *HeCo* apical membrane when compared to WT (Figure 1 F middle panel, G). In addition, although short primary cilia were observed, these structures often lacked a properly formed basal body. Instead, densely

packed microtubules were often present in the place of centrioles (Figure 1 F, middle panel, red arrow). A significant increase in the number of primary cilia within vesicle-like structures was also evident in *HeCo* aRGs compared to WT (Figure 1 F, blue asterisk in right panel and H). *HeCo* aRGs also frequently contained mis-oriented primary cilia: rather than facing the ventricle, these organelles were oriented basally (Figure 1 F, red asterisk in right panel and I). Thus, a decrease in the number and length of ventricular primary cilia, which are also often found within vesicles inside the cell, suggest defects in their formation in *HeCo* aRGs at early stages of cortical development.

### ***HeCo* mice have larger apical domains but show no change in mTOR activity**

Absent primary cilia have been associated with an increase of aRG apical domain size, mediated by a hyperactivation of the mTOR pathway (Foerster et al., 2017). Since metaphase aRGs in *HeCo* brains at E13.5 were shown to have increased cell areas compared to WT (Bizzotto et al., 2017), this prompted us to investigate interphase apical domain area in this model. *En face* imaging was performed using F-actin immunodetection to delineate cell boundaries (Marthiens et al., 2010), combined with centrosome and primary cilium markers ( $\gamma$ -tubulin and Arl13b, respectively) to further identify endfeet (Figure 2 A). F-actin confocal images were segmented (Aigouy et al., 2010) and all apical domain areas were measured (Figure 2 B) (Lamprecht et al., 2007, Foerster et al., 2017). Overall, apical domain size was significantly increased in *HeCo* brains (Figure 2 C). When identifying *HeCo* apical endfeet specifically at the ventricular surface, these also showed significantly increased areas (Figure 2 D). This increase in apical domain and endfeet area was accompanied with a decrease in the number of both of these apical structures per ROI, their density was hence not increased (Figure 2 C, D).

To further consolidate these data, and since *Em1* is expressed in the mouse VZ as early as E12.5 (Bizzotto et al., 2017), WT and *HeCo* cortices were also compared at this earlier time point. First, a 30 min BrdU pulse was performed to analyze the position of cycling progenitor cells in the E12.5 cortical wall. Immunohistochemistry for BrdU combined with the proliferation marker Ki67 confirmed the presence of a proportion of aberrant superficially localized BrdU+Ki67+ progenitor cells as previously observed at E13.5 (Figure S1 A, B). *En face* imaging showed no significant change in the number of  $\gamma$ -tubulin+ and Arl13b+ puncta at the *HeCo* ventricular surface compared to WT, although tendencies for a decrease were observed, possibly indicating an incipient phenotype (Figure S1 C-E). Primary cilia length was already

significantly reduced at E12.5, supporting at this time point the phenotype observed at later stages (Figure S1 F). Apical domain and endfeet areas were analyzed (Figure S2 A, B) revealing tendencies similar to the E13.5 data (Figure S2 C, D). A significant decrease in the number of apical endfeet per ROI was observed at E12.5 (Figure S2 D). Thus, primary cilia are abnormal and less aRG endfeet are present in *HeCo* compared to WT, as early as E12.5.

In order to shed light on the mechanisms leading to increased aRG areas, mTOR pathway activity was analyzed. Western blots were performed from cortex lysates (E12.5 and E13.5) to detect the phosphorylated form of proteins known to be key players in this pathway (mTOR itself, S6R and 4EBP1). No significant differences were observed for any of these proteins comparing WT and *HeCo* cortices (Figure 2 E, F, Figure S2 E, F), suggesting that shortened and abnormal cilia phenotypes have different consequences from a complete absence of these organelles (Foerster et al., 2017), and that other mechanisms may lead to increased area.

Analyses of numbers of centrosomes, primary cilia and aRG endfeet at E12.5 and E13.5 support the hypothesis that some *Eml1* mutant aRGs delaminate from the ventricular surface at early stages of corticogenesis. We focused on the more severely affected E13.5 stage to further understand the mechanisms involved. Although the mTOR signaling pathway does not appear to alter cell and tissue dynamics in the *HeCo* VZ, other molecular mechanisms and intracellular pathways related to primary cilia and important for tissue architecture are likely to be disturbed in mutant aRGs.

#### **Protein partners of *Eml1*: *RPGRIP1L*, a new heterotopia gene.**

*Eml1* appears to have crucial functions regulating aRG behavior (Kielar et al., 2014; Bizzotto et al., 2017, this study), although the molecular pathways in which it is involved have not yet been clearly linked to aRG phenotypes. Focusing on the primary cilium, and performing a comprehensive analysis of potential *Eml1*-interacting partners identified in a previous screen (Bizzotto et al., 2017), the ciliary protein *Rpgrip1l* was identified. This protein is known to localize to the base of the primary cilium, in the transition zone (Wiegering et al., 2018). Additionally, *RPGRIP1L* is a known ‘ciliopathy’ gene, with mutations previously identified in Joubert and Meckel syndromes (Wiegering et al., 2018). To confirm the interaction between *Eml1* and *Rpgrip1l*, Neuro2A cells were co-transfected with Flag-EML1 and c-myc-RPGRIP1L plasmids, 48 h later lysates were prepared for co-immunoprecipitation (co-IP) and Western blot experiments. Co-IP experiments confirmed the interaction between these proteins with

either anti-Flag (Figure 3 A) or anti-myc (Figure S3 C) antibodies. These results further support that Eml1 may play a role in primary cilium-related protein complexes.

Simultaneously, compound heterozygous variations in *RPGRIP1L* (NM\_015272.2) were identified in a patient (P700-5) presenting SH (Figure 3 B, C, D, Table S1). P700-5 also exhibited agenesis of the corpus callosum and cerebellar dysplasia (Figure 3 D4 and D5, Table S2). Nucleotide variations were confirmed by Sanger sequencing. A c.3706C>T pathogenic variation in exon 24 (R1236C, SIFT <https://sift.bii.a-star.edu.sg/> 0.03, damaging) was transmitted from the father. A c.3562G>A nucleotide change in exon 22 (V1188M, SIFT tolerated) was transmitted from the mother (Figure 3 C, Table S1). Autosomal recessive mutations in *RPGRIP1L* have previously been associated with Joubert and Meckel syndromes (OMIM 610937). The unusual C-terminal (C-ter) mutations identified here may lead to the different cortical phenotype observed (Figure 3 E).

Given the interaction of EML1 and RPGRIP1L, and the resemblance of the phenotypes found in patients, we postulated that the interaction between these proteins may be altered in the presence of patient mutations. Site-directed mutagenesis was performed for each of the newly identified heterotopia-*RPGRIP1L* mutations, and co-IP experiments were performed as described previously (Figure 3 F, Figure S3 A, B). Both individual mutations led to a dramatic loss of interaction with EML1, using either anti-Flag or anti-myc (Figure 3 G, Figure S3, C, D) for immunoprecipitation. The RPGRIP1L interaction was also tested using an EML1 construct expressing a patient mutation (family P135, mutation T243A, Kielar et al., 2014). Under these conditions, dramatically reduced quantities of Flag-EML1-T243A were observed in anti-myc immunoprecipitates (Figure S3 B, D). These data confirm that when either RPGRIP1L or EML1 is mutated the interaction between the proteins is compromised.

These combined data suggest convergent primary-cilia related mechanisms responsible for the heterotopia in EML1 and RPGRIP1L patients and prompted us to perform further cellular studies.

### **Primary cilia formation is impaired in *EML1* and *RPGRIP1L* patient fibroblasts**

Convergent suggestions for a role of EML1 in primary cilia led us to assess the growth dynamics of this organelle in human fibroblasts. A cell culture approach for analyzing primary cilia assembly/disassembly was adopted (Gabriel et al., 2016, Kia et al., 2012). Five different lines of human fibroblasts were cultured from two EML1-patients (P3489 and P135, Kielar et al., 2014), the above-described RPGRIP1L-heterotopia patient (P700-5), and two similarly aged

controls (control 1 and control 2). Three different conditions were analyzed to study primary cilium formation: under basal conditions (72 h after plating), or after serum starvation (SS) which was performed for 48 or 96 h (Figure 4 A, Figure S4 A, B). SS induces cells to enter quiescence (G0) and thus to grow a primary cilium (Figure S4 A).

The percentage of cells presenting a primary cilium in the three different culture conditions (72 h, 48 h SS and 96 h SS) was analyzed. Under basal conditions (Figure S4 C) and 48 h after SS (Figure 4B), each of the three patient lines showed significantly fewer cells possessing a primary cilium. At 96 h, one of the *EML1* patient lines (P3489) reached similar levels to the control lines, whilst the other patient lines continued to show a significantly decreased proportion of primary cilium-containing fibroblasts (Figure 4 D). Primary cilia length was also analyzed (Figure 4 C, E, Figure S4 D). Under basal conditions and 48 h after SS, length did not seem to be severely compromised compared to control lines (although the P135 and P700 fibroblast lines showed a tendency to have shorter primary cilia, Figure 4 C, Figure S4 D). However, when performing SS for 96h, primary cilia length was compromised: all patient lines showed a significant decrease in the length of primary cilia, compared to control conditions (Figure 4 E).

Both *EML1*- and *RPGRIP1L*-mutant fibroblasts hence show a reduced number of primary cilia, and/or reduced length after 48h or 96 h of SS. Importantly, *RPGRIP1L*-patient fibroblasts showed the same dynamics as *EML1*-patient fibroblasts, further suggesting that mechanisms underlying the heterotopia phenotype may converge. These results support a role for *EML1* and *RPGRIP1L* in regulating primary cilia number and length.

***Eml1* is expressed in proliferative zones of gyrencephalic species and heterotopia mutations in human cortical progenitors also lead to primary cilium anomalies.**

To learn more about *Eml1* expression during gyrencephalic brain development, ferret *in situ* hybridization was performed at E30 (similar to E12 in mouse), E34 (similar to E13 in mouse), until P6 (similar to E16.5 in mouse). At E30, *Eml1* expression was observed in the VZ and developing CP. At E34 the expression was stronger, and also observed in the ISVZ (Figure S5 A, B). As previously described, *Eml1* was expressed across the different proliferative zones and CP at P1 (E15 in mouse, Kielar et al., 2014), and a similar pattern of expression was observed at P6 (Figure S5 C, D). Microarray experiments (Martinez-Martinez et al., 2016) showed a significant differential expression of *Eml1* in the ferret VZ between E30 and P1, the expression

being 1.4 fold higher at E30 compared to P1. These results robustly confirm the expression of *Eml1* in VZ progenitors of gyrencephalic species, especially at early stages of corticogenesis. Given the importance of Eml1 for correct aRG behavior in mouse cortical development and its high expression in the VZ of gyrencephalic species, we decided to assess primary cilia by EM in human cortical progenitor cells (Gaspard et al., 2008, Shi et al., 2012, Figure S4 E), derived from iPSCs from two control individuals and two *EML1*-mutation patients (controls 1.1 and 2.1, P3489 and P135, Figure 4 F). These cells continuously proliferate assembling and disassembling primary cilia dynamically. Primary cilia were difficult to identify in patient cells when compared to control. Additionally, none of the primary cilia observed were properly structured. P135 cells often showed 'ciliary-like structures' with no proper microtubule arrangement. In P3489, ciliary pockets appeared distended (Figure 4 F). Thus, the centrosome-primary cilium complex appears perturbed both in mouse and human progenitors, suggesting a conserved role of Eml1/EML1 across evolution.

**Subcellular localization and EML1-interacting proteins shed light on potential pathways involved in the centrosome-primary cilia phenotype.**

EML1 has previously been shown to have a cell cycle-dependent localization in mouse neuronal progenitor cells *in vitro* (Kielar et al., 2014). Additionally, it was shown to co-localize with the microtubule network in interphase Vero cells (Kielar et al., 2014). A ciliary localization has not previously been described for EML1 or other EMAP family members (Fry et al., 2016). Its localization was hence further explored in aRGs, as well as in a ciliated human cell line (Retinal Pigmented Epithelial Cells, RPE1 cells), using exogenous expression of an EML1-tagged plasmid, since there are no known reliable antibodies to detect the endogenous protein. Transfection of pCAG-IRES-Tomato/GFP combined with either YFP-EML1 or Flag-EML1 in RPE1 cells showed recombinant EML1 throughout the cytoplasm of the cell, including in perinuclear regions, however there was no obvious association with the centrosome (Figure S5 E), nor the primary cilium (Figure S5 F). *In utero* electroporation of pCAG-IRES-Tomato (to delineate aRG morphology) and EGFP-EML1 identified recombinant EML1 in apical processes of aRGs. EGFP-EML1 appeared to be ubiquitously expressed throughout the apical process and endfoot (Figure S5 G).

To learn more about EML1's role, we further studied its interacting partners. We screened for new partners using full length EML1. Indeed, most of the mutations found in this protein fall in the C-ter  $\beta$  propeller structure (Fry et al., 2016), indicating the potential importance of

interactions with this domain. Pull down experiments were performed with purified Strep-tagged EML1 and E13.5 WT mouse embryonic cortex lysates, and a Strep-tag empty vector was used as control (Figure 5 A). Captured proteins were identified by mass spectrometry (MS, n=4 samples/condition). Label-free quantitative analyses based on the extracted ion chromatogram (XIC) method revealed a list of 240 proteins enriched in the Strep-tagged EML1 condition (Table S3). We compared this 240-protein list with the protein list obtained for the EML1-N-ter protein (Bizzotto et al., 2017). 85 out of 240 proteins commonly interacted with EML1-N-ter and full length proteins, confirming the specificity of the full-length EML1 screen (Figure 5 B). The remaining proteins are hence potentially N-ter or C-ter specific. EML4 appeared in the list of 85 'common' proteins. EML1 is expected to interact with EML4 via its N terminus (Fry et al., 2016), and both show a similar pattern of expression in the cortical wall across embryonic development (Kielar et al., 2014, Bizzotto et al., 2017; and data not shown). Co-IP experiments performed here validated the EML1-EML4 interaction (Figure S6), further confirming the specificity of the full-length screen.

To further identify cytoplasmic proteins, the new 240 protein list was further filtered to exclude nuclear proteins, such as RNA processing and nucleic acid-associated proteins (previously performed in Bizzotto et al., 2017), and a final list of 113 proteins was obtained (Table S3). The expression pattern across the murine developing cortical wall (E14.5) was examined for these proteins using publicly available resources (GenePaint, <https://gp3.mpg.de/>, data available for 71/113 proteins, Figure 5 C). 63.4 % of the 113 proteins clearly showed expression in the VZ (8.9 % showed a CP expression only, and a further 27.7 % were of unknown expression). Gene Ontology (GO) analyses for the 113 protein list were performed using the DAVID (Database for Annotation, Visualization and Integrated Discovery Functional Annotation Tool, <https://david.ncifcrf.gov/home.jsp>) and STRING (Search Tool for the Retrieval of Interacting Genes/Proteins (<https://string-db.org>) publicly available resources (Figure 5 D, Figure S6 A, Table S4, Table S5, Table S6). Cell-cell adhesion, microtubule and actin-associated proteins, and Golgi derived protein transport were identified amongst others in DAVID GO analyses (Figure 5 D, Table S4, Table S5). The N-ter protein list also showed similar GO categories (Bizzotto et al., 2017, and unpublished). STRING analyses revealed similar results including membrane-bounded organelle, cytoskeleton and cell junction amongst the most enriched 'Cellular component' GO categories (Figure S6 A, Table S6). 'Biological process' categories included metabolic processes, developmental

process, organelle organization, vesicle-mediated transport, as well as protein metabolism and modification (Figure S6 B, Table S6). Given the primary cilium phenotype observed in *Eml1/EML1* mutant conditions, we searched for cilia-related proteins in both lists (Table S5), obtaining a total of 42 potential cilia-related EML1 interactors.

The prominent apical process localization of recombinant EML1 in interphase aRGs, as well as the GO categories identified, prompted us to further focus on pathways involved in the formation of primary cilia, and specifically protein and membrane trafficking from the Golgi apparatus, localized in aRG apical processes (Taverna et al., 2016). These processes have up till now been little described in aRG pathology.

### **Novel Golgi-related protein partners of Eml1: VCIP135**

Given the importance of cargo trafficking and Golgi-derived protein transport for primary cilium formation, we searched for Golgi-related proteins in the MS lists (Table S5). VCIP135 (also known as VCPIP1) was an interesting candidate, showing high specificity for the EML1-bound condition. This protein mediates Golgi cisternae regrowth after mitosis as well as maintenance of the structure of this organelle during interphase. Knockdown of VCIP135 is known to lead to Golgi fragmentation (Uchiyama et al., 2002, Zhang et al., 2014, Zhang and Wang, 2015). The interaction of EML1 with VCIP135 was tested by performing co-IP experiments. Neuro2A cells were transfected with Strep-EML1 and Flag-VCIP135. An interaction was confirmed using either anti-Flag or Strep for co-IP (Figure 5 E-H). We next checked if EML1 mutation perturbed this interaction, performing co-IP experiments with GFP-EML1 T243A and Flag-VCIP135. Using anti-Flag and anti-GFP, a loss of the interaction between the two proteins (72% and 70% decrease, respectively) was observed (Figure 5 E-H). Therefore, mutant EML1 disrupts the interaction with VCIP135, suggesting that EML1 also plays a role associated with the Golgi apparatus.

To test if EML1 loss of interaction could be compensated for by other members of the EMAP family known to be expressed in the VZ at early stages of corticogenesis, Neuro2A cells were transfected with the YFP-EML4 and Flag-VCIP135 constructs, followed by co-IP experiments. No obvious interaction between EML4 and VCIP135 was observed when precipitating with either anti-Flag or anti-GFP (Figure S6 C-F). Therefore, it seems unlikely that EML4 could fully compensate for the lack of interaction between VCIP135 and EML1 when the latter is mutated. Since VCIP135 was found to interact with EML1, and this interaction is lost when the latter is mutated, we decided to knock-down (KD) *Vcip135* in aRGs at E13 (Figure S7 A), a time when



ectopic aRGs are found in *Eml1* mutant conditions (Kielar et al., 2014). A shmiRNA against *Vcip135*, as well as a scrambled control shmiRNA (shmiRNA control) were generated. Efficiency was tested by performing transfections of these constructs in Neuro2A cells, followed by RT-qPCR. These experiments confirmed a decrease of *Vcip135* expression by 40% in the *Vcip135* KD condition (Figure S7 B). *In utero* electroporation together with a pCAG-IRES-Tomato construct was performed at E13, and brains were analyzed 24 h later (Figure S7 A). Quantifying Tomato+ cells across 6 equally-sized bins spanning the cortical wall in both conditions, the percentage of cells in the region encompassing the VZ was assessed (bins 1-3) compared to the percentage in the SVZ, IZ and CP (bins 4-6, Figure S7 A, C). A significant shift of Tomato+ cells was observed from the VZ towards more basal positions in the *Vcip135* KD condition (Figure S7 C). This suggests that Golgi-related proteins, and more specifically the Eml1-interacting protein *Vcip135*, may be important for progenitor cell position. Thus, we link Golgi apparatus-dependent pathways with ectopic aRG progenitor phenotypes.

### **The Golgi apparatus is severely disrupted in *HeCo* neuronal progenitors**

We next set out to assess the Golgi apparatus in *HeCo* aRGs. This organelle has recently been described to be restricted to aRG apical processes, where it exists as a series of individualized stacks (Taverna et al., 2016), defined here as ‘Golgi elements’. *In utero* electroporation of a pCAG-IRES-Tomato plasmid for aRG morphology and a pCAG-Galt-EGFP plasmid targeting the Golgi apparatus was performed at E13, and WT and *HeCo* brains were analyzed at E13.5. Golgi position was assessed in WT and *HeCo* aRGs as in Taverna et al., 2016, and the number of perinuclear Golgi elements was also assessed.

Golgi apparatus distribution was strikingly different in *HeCo* aRGs when compared to WT aRGs at E13.5 (Figure 6 A-F). The number of Golgi elements was significantly reduced, as was the extension of this organelle in the apical process (Figure 6 C and D, respectively). Consistently, there were significantly less Golgi elements in perinuclear regions, and elements were significantly further away from the soma (Figure 6 E and F, respectively). These data indicate that the Golgi apparatus is subdivided in less stacks and does not span as far across the apical process of aRGs in the *HeCo* VZ (depicted in Figure 6 B).

In order to further examine the Golgi apparatus phenotype by analyzing its ultrastructure, several parameters were assessed by EM (Figure 6 G-J). Golgi cisternae width was significantly increased in *HeCo* aRGs (Figure 6 G, H), and there was a tendency of increased vesicles surrounding this organelle (Figure 6 I). We also assessed if the Golgi apparatus showed signs

of anastomosis, a process characterized by the fusion and aberrant branching of Golgi cisternae. Indeed, there was a significant increase in the percentage of Golgi presenting anastomosis in *HeCo* aRGs when compared to WT (Figure 6 G, red arrow, J). These abnormal Golgi features of *HeCo* aRGs at E13.5 point towards a severe disruption of this organelle.

The multiple Golgi apparatus phenotypes in *HeCo* cells suggest there may also be functional alterations of this organelle, critical for protein processing, cargo sorting and trafficking. An *in vitro* approach was established to assess cargo sorting and/or Golgi-derived trafficking in aRG-like cells in culture. Pax6+ progenitor-enriched cell cultures (modified protocol from Sun et al., 2011) were prepared from the dorsal telencephalon of E13.5 WT and *HeCo* embryos (Figure 7 A). These cells were transfected with the thermosensitive Vesicular Stomatitis Virus G Protein, VSVts405-G-EGFP (VSVG-EGFP). This modified protein is stored in the ER-Golgi compartment when cells are incubated at 39.5 °C. Upon incubation at 32°C, the protein starts to exit the ER-Golgi compartments and is trafficked towards the plasma membrane (Alterio et al., 2015, Bergmann et al 1989). Using this approach combined with immunocytochemistry for the Golgi marker GM130, VSVG-EGFP anterograde trafficking was analyzed 5 and 30 min after incubation at 32°C (Figure 7 B). The presence or absence of GFP+ puncta outside the Golgi apparatus was assessed at these two time points, and the number of puncta quantified. As expected, 5 min after incubation at 32°C most of the VSVG-EGFP protein was found within the Golgi both in WT and *HeCo* cells, with only some sparse GFP+ puncta found in the cytoplasm (average of 2 puncta/cell in both conditions, data not shown, Figure 7 B, C). However, analyses at 30 min showed less *HeCo* cells presenting GFP+ puncta outside of the Golgi (17% decrease) (Figure 7 B, D). This decrease was significant when considering 2 GFP+ puncta/cell as the baseline (Figure 7 E). *HeCo* cells also showed a lower number of puncta compared to WT cells (Figure 7 F). Our data hence converge to suggest that Golgi apparatus structure and its protein-derived transport are perturbed in *HeCo* cells, with a reduction in post-Golgi trafficking demonstrated in the VSVG-EGFP assay.

### ***EML1* patient fibroblasts and human cortical progenitors also show Golgi anomalies**

We queried if the Golgi apparatus was also perturbed in *EML1* patient fibroblasts. The Golgi marker TGN46 was assessed in basal conditions (72 h), quantifying the number of Golgi fragments as well as Golgi volume (Figure S7 D-F). The P135 line showed an increased number of Golgi fragments as well as an increased volume, and the P3489 line showed similar tendencies (Figure S7 D-F).

As previously performed for WT and *HeCo* aRGs, we similarly assessed the Golgi apparatus by EM in hiPSC-derived cortical progenitors (Figure 7 G). A significant increase in the percentage of cells presenting vacuolized Golgi (Figure 7 G red asterisk, 7 H), was observed in patient-derived cortical progenitors. Thus, the Golgi apparatus is also perturbed in human patient-derived *EML1* mutant progenitor cells. Primary cilia defects have been previously found associated with anomalies of Golgi apparatus-dependent processes (Hua and Ferland, 2018). *EML1* mutant Golgi defects are hence highly likely to be associated with the severe centrosome-primary cilium defects identified.

## **Discussion**

Our study unravels an unprecedented role for the heterotopia protein Eml1/EML1 in primary cilia formation. Through a plethora of approaches, we report severe anomalies in this organelle in *Eml1/EML1* mutant conditions, and have confirmed a novel EML1 ciliary protein partner, RPGRIP1L. We identified a first heterotopia patient presenting mutations in *RPGRIP1L*, gene which was previously only associated with Joubert and Meckel syndromes (Wiegering et al., 2018). We hypothesize that the heterotopia phenotype may reflect the consequence of specific compound heterozygous mutations localized within the RID domain of the protein. Importantly, heterotopia mutations alter the interaction of RPGRIP1L with EML1 suggesting a convergent role for mutations in these proteins in the subcortical heterotopia pathophysiology. Importantly, our data also pinpoint upstream defects, affecting Golgi transport as being involved in the pathogenesis.

Severe defects were first identified in the centrosome-primary cilium complex in aRGs in the *HeCo* mouse, as well as in *EML1* patient fibroblasts and cortical progenitor cells *in vitro*. These microtubule-based organelles are known to be critical for regulating aRG behavior and when altered, severe brain and/or cortical malformations can arise (reviewed in Bizzotto and Francis 2015). Centrosomal proteins are mostly associated with microcephaly (Bizzotto and Francis, 2015, Uzquiano et al., 2018), whilst defects in primary cilia have been associated with microcephaly, polymicrogyria, periventricular heterotopia (PV), focal cortical dysplasia, as well as ciliopathies (Ding et al., 2019, Gabriel et al., 2016, Kia et al., 2012, Park et al., 2018, Sheen, 2014). Of interest, certain rare mutations in OFD1, localized in the basal body and involved in primary cilium formation, have been previously associated with subcortical heterotopia (Del Giudice et al., 2014). Our study further links the primary cilium to this cortical malformation.

Additionally, this is one of the few studies linking abnormal primary cilia to epilepsy (Canning et al., 2018, Park et al., 2018), also suffered by *EML1* mutation patients.

Our data suggest that EML1 is predominantly outside the primary cilium in interphase cells, we hence investigated the molecular mechanisms which might be upstream of its insertion in the apical plasma membrane. Searching for new interactors, we identified an appealing list of candidate partners (Table S5) that may play a role in the phenotype. We focused on the Golgi apparatus, a category enriched in the MS data, since cargo sorting and trafficking are known to be critical for the correct formation of the centrosome-primary cilium complex (Bernabé-Rubio and Alonso, 2017, Madhivanan and Aguilar, 2014). As well as VCIP135, other Golgi-related proteins identified by MS have been shown to either co-localize with this organelle e.g. CK1δ; to be important for its structure, morphology and function, e.g. Scyl1, Map4, Camsap3, Clasp1/2; or to mediate cilia-targeted protein transport e.g. Arf4. It is worth noting that some MS partners also showed ciliary localization and/or functions e.g. Nup98, Neurl4, and some were even reported to be localized both in the Golgi and in the centrosome-primary cilium e.g. CK1δ, Map4, Usp9x, and to be important for their structure and/or function e.g. Stauf2, KifC1, Kif7, Macf1. Of note as well, Rpgrip1l appears also to be partially localized outside the cilia (Sang et al., 2011).

An interaction of EML1 with the Golgi protein VCIP135 was confirmed by heterologous expression in Neuro2A cells. These data suggest a Golgi-related role for EML1. Our data also point towards a cargo sorting/trafficking defect in *HeCo* aRG-like cells *in vitro*. Furthermore, the Golgi apparatus in *Eml1/EML1* mutant conditions showed an abnormal distribution and structure in mouse aRGs, in patient fibroblasts and human cortical progenitor cells. We hence have convincing cumulative evidence that this organelle normally requires Eml1/EML1 in these cell types. Correct Golgi-derived function(s) is also critical for primary cilium formation (Bernabé-Rubio and Alonso, 2017, Madhivanan and Aguilar, 2014), which leads us to suggest that these Golgi phenotypes may be upstream of the centrosome-primary cilium defect identified in *Eml1/EML1* mutant conditions.

Previous studies have tentatively associated Golgi defects with cortical malformations e.g. *ARFGEF2* mutations leading to microcephaly and PV (Sheen et al., 2004), and *DYNC1H1* mutations mainly leading to posterior pachygyria, polymicrogyria and microcephaly (Schiavo et al., 2013). However, experiments reporting Golgi apparatus anomalies in the context of mutations in these two proteins were performed *in vitro* and not directly in neuronal

progenitor cells (Fiorillo et al., 2014, Jaarsma and Hoogenraad, 2015, Sheen et al., 2004). To our knowledge, this is the first study assessing Golgi anomalies in neuronal progenitor cells (human and mouse), including in mouse aRGs *in vivo*, as well as linking for the first time Golgi anomalies to the pathogenesis of severe subcortical heterotopia.

Golgi-derived protein transport is also important for the correct establishment of other structures found in the plasma membrane e.g. those mediating cell-cell contacts (Asada et al., 2004, Lock et al., 2005, Sheen et al., 2004, Wang et al., 2005), a functional category appearing in the MS analyses. aRGs are linked to each other by an adherens junctions (AJ)-actin belt, which is crucial for their polarity and behavior (Uzquiano et al., 2018). Indeed, interfering with AJ components often leads to aberrant cortical development (Bizzotto and Francis, 2015, Uzquiano et al., 2018). It remains to be elucidated if the Golgi function(s) altered in *Eml1/EML1*-mutant conditions impacts exclusively the centrosome-primary cilium pathway. If Golgi-dependent protein transport is more widely perturbed, it could also affect delivery of key AJ components to the plasma membrane. This could loosen cell contacts between aRGs allowing their delamination, contributing hence to the ectopic progenitor phenotype.

Related to the phenotypes identified in *HeCo*, there are several signaling pathways integrated by the primary cilium (i.e. mTOR, Shh, Hippo, Wnt; Wheway et al., 2018) that could be disrupted in *Eml1/EML1* mutant conditions. Changes in the mTOR signaling pathway have been previously associated with diverse pathological cortical phenotypes (Benova and Jacques, 2018, D’Gama et al., 2017, Foerster et al., 2017, Park et al., 2018). However, no obvious anomalies in this pathway were identified at the time when ectopic progenitors are first observed (E12.5 and E13.5), suggesting that it is probably not a key player at this stage contributing to the ectopic progenitor phenotype. Assessing other pathways known to be mediated by the primary cilium could help shed light on the downstream pathological mechanisms contributing to progenitor phenotypes. This organelle is known to be crucial for Shh signaling (Wheway et al., 2018), and there is broad evidence involving the Shh pathway in neocortical development and aRG dynamics (Wang et al., 2016; Yabut and Pleasure, 2018). Thus, it would be interesting to assess this pathway in the *HeCo* developing cortex at early stages of corticogenesis, when the severe centrosome-primary cilium defects were observed and ectopic progenitors arise.

Another pathway associated with the primary cilium is the Hippo pathway (Wheway et al., 2018), although the relationship remains relatively unexplored. This pathway is known to

regulate tissue homeostasis, and hence to regulate cell growth, size and shape (Ma et al., 2018). Primary cilium defects combined with changes in apical domain/endfeet area and metaphase cell shape (Bizzotto et al., 2017, this study) make this pathway an appealing candidate underlying abnormal VZ dynamics in *Eml1* mutant conditions. Mutations in proteins involved in Hippo signaling have been previously associated with cortical malformations (Cappello et al., 2013, O'Neill et al., 2018). A recent study in the mouse also reported changes in the levels of key Hippo pathway proteins in the VZ of a model for subcortical heterotopia, largely phenocopying the *HeCo* mouse phenotype (Liu et al., 2018). Therefore, assessing this pathway in *Eml1* mutant conditions would shed further light on the molecular mechanisms downstream of the Golgi-primary cilium aRG phenotype, responsible for the generation of *Eml1*-mutant ectopic progenitors linked to subcortical heterotopia (Kielar et al., 2014, Li et al., 2018).

In this study we focused on the role of *Eml1/EML1* in interphase, however, this protein is likely to play various roles during the cell cycle (Bizzotto et al., 2017). This may be consistent with the extra-ciliary role of many proteins important for the centrosome-primary cilium (Hua and Ferland, 2018). Starting with a primary cilia phenotype, several indicators led us to study the Golgi apparatus, which uncovered quite novel data for this organelle. Indeed, the relevance of Golgi-derived trafficking has not previously been pinpointed in neuronal progenitors in the context of cortical malformations, even if this process is crucial for the correct establishment of many structures mediating aRG behavior. Further experiments are required to understand the possible downstream mechanisms related to Golgi-plasma membrane phenotypes in *Eml1/EML1* mutant conditions, as well as in other cortical malformation models.

#### Acknowledgements

We thank Dr. M. Nosten-Bertrand for advice with statistical analyses and Dr. M. Stouffer, Dr. S. Bizzotto, Dr. A. Andreu-Cervera G. Martinez Lorenzana and A. Muzerelle for experimental help. We thank Guillaume Arras from the LSMP for his assistance in MS data analysis. We thank Dr. Shihavuddin for his help with *en face* imaging data analysis. We are grateful to the following people for kindly gifting us materials and sharing protocols: Dr. C. Delevoye (TGN46 antibody), Dr. B. Goud (VSVG-GFP construct), Dr. A. Baffet (RPE1 cells, neuronal progenitor cell culture), Dr. V. Marthiens (neuronal progenitor cell culture), Dr. A. Fry (YFP-EML4 construct), Dr. Zhang (Flag-VCIP135 construct), Dr. R. Bayliss (Strep-YFP-EML1 construct), Dr.

Murakami (pCAG-Galt-EGFP construct), Dr. F. Watrin (shRNA empty vector) and Dr. S. Schneider-Maunoury (c-myc-RPGRIP1L construct and mTOR pathway antibodies). We thank the IFM animal experimentation facility and cellular and tissue imaging platforms at the Institut du Fer à Moulin, supported also by the Région Ile de France and the FRC Rotary. We thank Alexandre Croquelois for original mice and the TAAM (CDTA Orleans) for the maintenance of the *HeCo* mouse line.

For patients, sample provision and sequencing we thank Mélanie Jennesson Lyve and Jacques Motte (Reims hospital), Anne-Gaelle le Moing (Amiens hospital), the Institut Imagine Biobank, Jamel Chelly (IGBMC, Strasbourg), Robert Olaso, Jean-Baptist Petit and Vincent Meyer (CNRGH, Evry), Mara Cavallin and Karine Poirier (Institut Imagine, Paris) for their very helpful support, and all families for kindly agreeing to provide samples.

### **Funding**

AU, DR, AH and FF are associated with the BioPsy Labex project and the Ecole des Neurosciences de Paris Ile-de-France (ENP) network. Our salaries and labs were supported by Inserm, Centre national de la recherche scientifique (CNRS), Sorbonne Université, French Agence National de la Recherche (ANR-13-BSV4-0008-01; ANR-16-CE16-0011-03, to FF and NBB), Fondation Bettencourt Schueller (FF), the European Union (EU- HEALTH-2013, DESIRE, No 60253, to FF and NBB), the JTC 2015 Neurodevelopmental Disorders affiliated with the ANR (for NEURON8-Full- 815-006 STEM-MCD, to FF, NB and JL), the Fondation Maladies Rares/Phenomin (project IR4995, FF), the European Cooperation on Science and Technology (COST Action CA16118 , including GM, NBB and FF) and the Hector foundation II (to JL). AU received an ENP PhD grant, a Company of Biologists travel grant, and is currently funded by the Fondation de France (Prix Valérie Chamillard, selected by the Fondation Française pour la Recherche sur l'Epilepsie). DL was supported by "Région Ile-de-France" and Fondation pour la Recherche Médicale grants.

### **Authors contribution**

A. U. conceived, designed and performed experiments, analyzed data and wrote the manuscript. C. C. D. performed electron microscope experiments and data analyses. A. J. performed hiPSC-derived neuronal progenitor cell cultures under the supervision of J. L., D. R. contributed to identification of the mutated gene for the P700 family and performed experiments. A. H. performed biochemistry experiments. F. D. carried out the MS

experimental work and D. L. supervised MS and data analysis. A. B. and J.-F. D. performed exome-sequencing experiments, C.M. contributed to confirmation of *RPGRIP1L* gene mutations, under the supervision of N. B.-B. C. L.-B. performed experiments in ferret supervised by V.B. G. M. S. M. provided P3489 fibroblasts and contributed to cilia discussions. F. F. conceived and designed experiments, helped with data interpretation and wrote the manuscript.

### **Declaration of interest**

No conflicts of interest declared.

### **References**

- Alterio, J., Masson, J., Diaz, J., Chachlaki, K., Salman, H., Areias, J., Al Awabdh, S., Emerit, M. B., Darmon, M. (2015) Yif1B is involved in the anterograde traffic pathway and the Golgi architecture. *Traffic*, 16 (9), 978-993.
- Aigouy B, Farhadifar R, Staple DB, Sagner A, Roper JC, Julicher F, Eaton S. 2010. Cell flow reorients the axis of planar polarity in the wing epithelium of *Drosophila*. *Cell*, 142, 773-786.
- Asada, M., Irie, K., Yamada, A., Takai, Y. (2004). Afadin and  $\alpha$ -actinin-binding protein ADIP directly binds  $\beta'$ -COP, a subunit of the coatamer complex. *Biochem. and Biophys. Res. Comm*, 321, 350–354.
- Bergmann, J. E. (1989) Using temperature-sensitive mutants of VSV to study membrane protein biogenesis. *Methods Cell Biol.*, 32, 85-110.
- Bernabé, R., Alonso, M. A. (2017) Routes and machinery of primary cilium biogenesis. *Cell. Mol. Life Sci.*, 74, 4077-4095.
- Benova, B., Jacques, T. S. (2018) Genotype-phenotype correlations in focal malformations of cortical development: a pathway to integrated pathological diagnosis in epilepsy surgery. *Brain Pathol.*, doi: 10.1111/bpa.12686
- Bizzotto, S. and Francis, F. (2015) Morphological and functional aspects of progenitors perturbed in cortical malformations. *Front Cell Neurosci*, 9, 30.
- Bizzotto, S., Uzquiano, A., Dingli, F., Ershov, D., Houllier, A., Arras, G., Richards, M., Loew, D., Minc, N., Croquelois, A., Houdusse, A., Francis, F. (2017) Eml1 loss impairs apical progenitor spindle length and soma shape in the developing cortex. *Sci. Rep.* 7:17308.
- Bustin, S.A., Benes, V., Garson, J. A., Hellemans, J. Huggett, J. Kubista, M., Mueller, R., Nolan, T., Pfaffl, M. W., Shipley, G. L. Vandesompele, J. Wittwer, C. T. (2009) The MIQE guidelines:



minimum information for publication of quantitative real-time PCR experiments. *Clin. Chem.* 55 (4), 611-622.

Canning, P., Park, K., Gonçalves, J. Li, C., Howard, C. J., Sharpe, T. D., Holt, L. J., Pelletier, L., Bullock, A. N., Leroux, M. R. (2018) CDKL family kinases have evolved distinct structural features and ciliary function. *Cell Rep*, 22 (4), 885-894.

Cappello, S., Gray, M.J., Badouel, C., Lange, S., Einsiedler, M., Srour, M., Chitayat, D., Hamdan, F. F., Jenkins, Z.A., Morgan, T., et al. (2013) Mutations in genes encoding the cadherin receptor-ligand pair DCHS1 and FAT4 disrupt cerebral cortical development. *Nat. Genet.* 45, 1300–1308

Croquelois, A., Giuliani, F., Savary, C., Kielar, M., Amiot, C., Schenk, F., Welker, E. (2009) Characterization of the HeCo mutant mouse: a new model of subcortical band heterotopia associated with seizures and behavioral deficits. *Cereb Cortex* 19(3):563-575.

D’Gamma, A. M., Woodworth, M. B., Hossain, A. A., Bizzotto, S., Hatem, N. E., LaCoursiere, C.M., Naim, I., Ying, Z., Barkovich, A. J., et al. (2017) Somatic mutations activating the mTOR pathway in dorsal telencephalic progenitors cause a continuum of cortical dysplasias. *Cell Rep.*, 21 (13), 3754-3766.

Ding, W., Wu, Q., Sun, L., Pan, N.C., Wang, X. (2019) Cenpj regulates cilia disassembly and neurogenesis in the developing mouse cortex. *J. Neurosci.*, doi: 10.1523/JNEUROSCI.1849-18.2018.

Delous, M., Baala, L., Salomon, R., Laclef, C., Vierkotten, J., Tory, K., Golzio, C., Lacoste, T., Besse, L., Ozilous, C., et al. (2007) The ciliary gene RPGRIP1L is mutated in cerebello-oculo-renal syndrome (Joubert syndrome type B) and Meckel syndrome. *Nat. Genet.*, 39, 875-881.

Del Giudice, E., Macca, M., Imperati, F., D’Amico, A., Parent, P., Pasquier, L., Layet, V., Lyonnet, S., Stamboul-Darmency, V., Thauvin-Robinet, C., Franco, B. (2014). *Orphanet J. Rare Dis.*, 10, 9:74.

Fiorillo, C., Moro, F. Yi J., Weil, S. Brisca, G., Astrea, G., Severino, M., Romano, A., Battini, R., Rossi, A., Minetti, C. Bruno, C., Santorelli, F. M., Vallee, R. (2014). Novel dynein DYNC1H1 neck and motor domain mutations link distal spinal muscular atrophy and abnormal cortical development. *Hum. Mut.*, 35 (3), 298-302.

Foerster, P., Daclin, M., Asm, S., Faucourt, M., Boletta, A., Genovesio, A. and Spassky, N. (2017) mTORC1 signaling and primary cilia are required for brain ventricle morphogenesis. *Development*, 144, 201-210.

Fry, A., O'Regan, L., Montgomery, J., Adib, R., Bayliss, R. (2016) EML proteins in microtubule regulation and human disease. *Biochem. Soc. Trans.*, 44, 1281-1288.

Gabriel, E., Wason, A., Ramani, A., Gooi, L. M., Keller, P., Pozniakovsky, A., Poser, I., Noack, F., Telugu, N. N., Calegari, F., et al (2016) CPAP promotes timely cilium disassembly to maintain neural progenitor pool. *EMBO J.*, 35 (8), 803-819.

Gaspard, N., Bouchet, T., Hourez, R., Dimidschtein, J., Naeje, G., van den Aemele, J., Espuny-Camacho, I., Herpoel, A., Pssant, L., Schiffmann, S. N., Gaillard, A., Vandergaeghen, P. (2008) An intrinsic mechanism of corticogenesis from embryonic stem cells. *Nature*, 455 (7211), 351-357.

Guo, J., Higginbotham, H., Li, J., Nichols, J., Hirt, J., Ghukasuan, V., Anton, E. S. (2015) Developmental disruptions underlying brain abnormalities in ciliopathies. *Nat. Comm.*, 6:7857.

Higginbotham, H., Guo, J., Yokota, Y., Umberger, N. L., Su, C., Li, J., Verma, N., Hirt, J., Ghukasyan, V., Caspary, T., Anton E. S. (2013) Ar13b-regulated cilia activities are essential for polarized radial glial scaffold formation. *Nat. Neuro.*, 6 (8), 1000-1008.

Hua, K., Ferland, R. J. (2018). Primary cilia proteins: ciliary and extraciliary sites and functions. *Cell. Mol. Life Sci.*, 75, 1521-1540.

Iefremova, V., Manikakis, G., Krefft, O., Jabali, A., Weynans, K., Wilkens, R., Marsoner, F., Brändl, B., Müller, F. J., Koch, P., Ladewig, J. (2017) An Organoid-Based Model of Cortical Development Identifies Non-Cell-Autonomous Defects in Wnt Signaling Contributing to Miller-Dieker Syndrome. *Cell Rep.*, 19 (1), 50–59.

Jaarsma, D., Hoogenraad, C. (2015). Cytoplasmic dynein and its regulatory proteins in Golgi pathology in nervous system disorders. *Front. Neuro.*, 9, art 397.

Kia, S. K., Verbeek, E., Engelen, E., Schot, R., Poot, R. A., de Coo, I. F. M., Lequin, M. H., Poulton, C. T., Pourfarzad, F., Grosveld, F. G., et al (2012) RTTN mutations link primary cilia function to organization of the human cerebral cortex. *American J. Hum. Gen.*, 91, 533-540.

Kielar, M., Phan Dinh Tuy, F., Bizzotto, S., Lebrand, C., de Juan Romero, C., Poirier, K., Oegema, R., Mancini, G. M., et al. (2014) Mutations in Eml1 lead to ectopic progenitors and neuronal heterotopia in mouse and human. *Nat Neurosci* 17(7):923-933.

Kimura, T., Murakami, F. (2014) Evidence that dendritic mitochondria negatively regulate dendritic branching in pyramidal neurons in the neocortex. *J. Neurosci.*, 34 (20) 6938-3951.

Lamprecht MR, Sabatini DM, Carpenter AE. 2007. CellProfiler: free, versatile software for automated biological image analysis. *BioTechniques*, 42, 71-75.

Liu, W. A., Chen, S., Li, Z., Lee, C. H., Mirzaa, G., Dobyns, W. B., Ross, M. E., Zhang, J., Shi, S. H. (2018). PARD3 dysfunction in conjunction with dynamic HIPPO signaling drives cortical enlargement with massive heterotopia. *Genes Dev.*, 32, 763-780.

Lock, J. G., Hammond, L. A., Houghton, F., Gleeson, P. A., Stow, J. L. (2005) E-Cadherin transport from the trans-Golgi network in tubulovesicular carriers is selectively regulated by golgin-97. *Traffic*, 6, 1142-1156.

Ma, S., Meng, Z., Chen, R., Guan, K. (2018) The Hippo pathway: biology and pathophysiology. *Annu. Rev. Biochem.*, 88:7.2-7.28.

Madhivanan, K., Aguilar, R. C. (2014) Ciliopathies: the trafficking connection. *Traffic*, 15 (10), 1031-1056.

Marthiens, V., Kazanis, I., Moss, L., Long, K., ffrench-Constant, C. (2010) Adhesion molecules in the stem cell niche – more than just staying in shape? *J. Cell. Sci.*, 123, 1613-1622.

Martinez-Martinez, M.A., De Juan Romero, C., Fernandez, V., Cardenas, A., Gotz, M. and Borrell, V. (2016) A restricted period for formation of outer subventricular zone defined by Cdh1 and Trnp1 levels. *Nat Commun*, 7, 11812.

O'Neill, A. C., Kyrousi, C., Einsiedler, M., Burtscher, I., Drukker, M., Markie, D. M., Kirk, E. P., Gotz, M., Robertson, S. P., Cappello, S. (2018) Mob2 insufficiency disrupts neuronal migration in the developing cortex. *Front. Cell. Neuro.*, 12, art 57.

Palade, G. E. (1952) A study of fixation for electron microscopy. *J. Exp. Med.*, 95 (3), 285-298.

Palmer, T.D., Willhoite, A. R., Gage, F. G. (2000) Vascular niche for adult hippocampal neurogenesis. *J. Comp. Neurol.* 425, 479-494

Paridaen, J.T., Wilsch-Brauninger, M. and Huttner, W.B. (2013) Asymmetric inheritance of centrosome-associated primary cilium membrane directs ciliogenesis after cell division. *Cell*, 155, 333-344.

Park, S. M., Lim, J. S., Ramakrishna, S., Kim, S. H., Kim, W. K., Lee, J., Kang, H., Reiter, J. F., Kim, D. S., Kim, H., Lee, J. H. Brain somatic mutations in MTOR disrupt neuronal ciliogenesis, leading to focal cortical dyslamination (2018) *Neuron*, 99, 83-97.

Perez-Riverol, Y., Csordas, A., Bai, J., Bernal-Llinares, M., Hewapathirana, S. Kundu, D. J., Inuganti, A., Griss, J., Mayer, G., Eisenacher, M., Pérez, E., Uszkoreit, J., Pfeuffer, J., Sachsenberg, T., Yilmaz, S., Tiwary, S., Cox, J., Audain, E., Walzer, M., Jarnuczak, A. F., Ternent, T., Brazma, A., Vizcaíno, J. A. (2019) The PRIDE database and related tools and resources in 2019: improving support for quantification data. *Nucleic Acids Res*, 47 (D1), D442-D450

Pouillet P, Carpentier S, Barillot E. (2007) myProMS, a web server for management and validation of mass spectrometry-based proteomic data. *Proteomics*, 7 (15), 2553–2556.

Reillo, I., de Juan Romero, C., Garcia-Cabezas, M.A. and Borrell, V. (2011) A role for intermediate radial glia in the tangential expansion of the mammalian cerebral cortex. *Cereb Cortex*, 21, 1674-1694.

Richards, M. W., O'Regan, L., Roth, D., Montgomery, J. M., Straube, A. Fry, M., Bayliss, R. (2015) Microtubule association of EML proteins and the EML4-ALK variant 3 oncoprotein require an N-terminal trimerization domain. *Biochem. J.* 437 (3), 529-536.

Shaheen, R., Sebai, M. A., Patel, N., Ewida, N., Kurdi, W., Altweijri, I., Sogaty, S., Almardawi, E., Seidahmed, M. Z., Alnemri, A., et al. (2017) The genetic landscape of familial congenital hydrocephalus. *Ann. Neurol.* 81, 890-897.

Sheen, V. L., Ganesh, V. S., Topcu, M., Sebire, G., Bodell, A., Hill, R. S., Grant, E., Shugart, Y. Y., Imitola, J., Khoury, S. J., Guerrini, R., Walsh, C. A. (2004). Mutations in ARFGEF2 implicate vesicle trafficking in neural progenitor proliferation and migration in the human cerebral cortex. *Nat. Genet.*, 36 (1), 64-76.

Schiavo, G., Greensmith, L., Hafezparast, M., Fisher, E. M. (2013) Cytoplasmic dynein heavy chain: the servant of many masters. *Trends Neurosci.*, 36 (11), 641-651.

Shi, Y., Kirwan, P., Smith, J., Robinson, H. P., Livesey, F. J. (2012) Human cerebral cortex development from pluripotent stem cells to functional excitatory synapses. *Nat. Neurosci.*, 15 (3), 477-486.

Sun, T., Wang, X. J, Xie, S. S., Zhang, D. L., Wang, X. P, Li, B. A., Ma, W., Xin, H. (2011) A comparison of proliferative capacity and passaging potential between neural stem and progenitor cells in adherent and neurosphere cultures. *Int. J. Devl. Neuroscience*, 29, 723-731.

Taverna, E., Mora-Bermudez, F., Strzyz, P. J., Florio, M., Icha, J., Haffner, C., Norden, C., Wilsch-Bräuninger, Huttner, W. B. (2016) Non-canonical features of the Golgi apparatus in bipolar epithelial neural stem cells. *Sci Rep*, 6, 21206.

Uchiyama, K., Jokitalo, E., Kano, F., Murata, M., Zhang, X., Canas, B., Newman, R., Rabouille, C., Pappin, D., Freemont, P., Kondo, H. (2002) VCIP135, a novel factor for p97/p47-mediated membrane fusion is required for Golgi and ER assembly in vivo. *J. Cell Biol.*, 159 (5), 855-866.

Uzquiano, A., Gladwyn-Ng, I., Nguyen, L., Reiner, O., Gotz, M., Matsuzaki, F., Francis, F. (2018) Cortical progenitor biology, cell cycling versus neurogenesis. *J. Neurochem.* 146, 500-525.

Valot B, Langella O, Nano E, Zivy M. (2011) MassChroQ: A versatile tool for mass spectrometry quantification. *Proteomics*, 11, 3572-3577.

Wang, B. Wylie, F. G., Teasdale, R. D., Stow, J. L. (2005) Polarized trafficking of E-cadherin is regulated by Rac1 and Cdc42 in Madin-Darby canine kidney cells. *Am J. Physiol. Cell Physiol*, 288, 1411-1419.

Wang, L., Hou, S., Han, Y.G. (2016) Hedgehog signaling promotes basal progenitor expansion and the growth and folding of the neocortex. *Nat. Neuro*, 19, 888-896.

Wheway, G., Nazlamova, L., Hancock, J. T. (2018) Signaling through the primary cilium. *Front. Cell Dev. Biol.*, 8, art 8.

Wiegering, A., R  ther, U., Gerhardt, C. (2018) The ciliary protein Rpgrip1l in development and disease. *Dev. Biol.* 442, 60-68.

Zhang, X., Zhang, H., Wang, Y. (2014) Phosphorylation regulates VCIP135 function in Golgi membrane fusion during cell cycle. *J. Cell Sci.* 127, 172-181.

Yabut, O. R., Pleasure, S. J. (2018) Sonic Hedgehog signaling rises to the surface: emerging roles in neocortical development. *Brain Plast.*, 3 (2), 119-128.

Zahnleiter, D., Hauer, N., Kessler, K., Uebe, S., Sugano, Y., Neuhauss, S. C. F., Giessl, A., Ekici, A. B., Blessing, H., Sticht, H., D  rr, H., Reis, A., Thiel, C. T. (2015) MAP4-dependent regulation of microtubule formation affects centrosome, cilia and golgi architecture as a central mechanism in growth regulation. *Hum Mutat.*, 36 (1), 87-97.

Zhang, X., Wang, Y. (2015) Cell cycle regulation of VCIP135 deubiquitinase activity and function in p97/947-mediated Golgi assembly. *Mol Biol Cell.*, 26 (12), 2242-2251.

### Figure legends

**Figure 1. Primary cilia are disrupted in the *HeCo* ventricular zone.** A) *En face* confocal imaging of the WT and *HeCo* ventricular surface using anti- $\gamma$ -tubulin (green) and anti-Arl13b (red) immunostainings. B) Quantification of  $\gamma$ -tubulin+ puncta per ROI in WT (n=7 from 4 litters) and *HeCo* (n=6 from 5 litters). Each point represents an embryo. C) Quantification of Arl13b+ puncta per ROI in WT (n=7 from 4 litters) and *HeCo* (n=6 from 5 litters). Each point represents

an embryo. D) Quantifications of Arl13b+ primary cilia length in WT (n=5 from 3 litters) and *HeCo* (n=5 from 4 litters). Each point represents an embryo. E) Schematic representation of primary cilium formation in aRGs. After mitosis, the centrosome becomes the basal body and is trafficked towards the apical surface in order to dock a primary cilium. The mother centriole associates with *de novo* synthesized membrane or ciliary remnants, which are often carried in vesicle-like structures and that will then become the primary cilium. Once this complex reaches the apical plasma membrane, the basal body is docked and the primary cilium is assembled. Trafficking of proteins from the Golgi apparatus is required for primary cilium assembly and growth. F) Representative images of electron microscopy acquisitions of the apical surface of WT and *HeCo* embryonic brains. Red arrow: the basal body is not properly assembled in *HeCo* aRGs. Instead densely packed microtubules are observed. Blue asterisk: apically oriented primary cilium within a vesicle. Red asterisk: basally oriented primary cilium within a vesicle. G) Quantifications of primary cilium length in WT (n=4 embryos from 3 litters) and *HeCo* (n=5 embryos from 3 litters) VZ. Each point represents an embryo. H) Percentage of primary cilia found within vesicles in WT and *HeCo* VZ. Each point represents an embryo (n=5 per condition, from 3 litters). I) Percentage of basally oriented primary cilia in WT and *HeCo* VZ. Each point represents an embryo (n=5 per condition, from 3 litters). Scale bar: 10  $\mu$ m (B), 0.5  $\mu$ m (F), mean  $\pm$  SEM and unpaired t-test (B, C, D, G), median  $\pm$  minimum-maximum range and chi square (H, I) \*\*\*\*p<0.0001, \*\*p<0.001, \*p<0.05.

**Figure 2. Apical domain size is increased at the *HeCo* ventricular surface but there are no obvious changes in mTOR activity. Related to Figure S1 and S2.** A) *En face* confocal imaging of the WT and *HeCo* ventricular surface, detecting F-actin (white),  $\gamma$ -tubulin (green) and Arl13b (red). Images for  $\gamma$ -tubulin and Arl13b immunodetections are the same as in Figure 1 A. B) F-actin immunostainings, segmentation (middle panel, Tissue Analyzer) and color-coded image using area as parameter (right panel, CellProfiler) C) Quantification of apical domain area and number in WT (n=6 from 4 litters) and *HeCo* (n=7 from 5 litters). D) Quantification of apical endfeet area and number in WT (n=7 from 4 litters) and *HeCo* (n=6 from 5 litters). E) Representative Western blot of WT and *HeCo* cortex lysates (E13.5) immunodetected for phosphorylated (left) and non-phosphorylated (right) proteins from the mTOR pathway (mTOR, S6R, 4EPB1). F) Quantifications from Western blots, with band intensities normalized to GAPDH. The ratio of the phosphorylated form to the total protein is shown. pmTOR/mTOR WT n=15 embryos from 2 litters, *HeCo* n=13 embryos from 2 litters. pS6R/S6R WT and *HeCo*

n=16 from 2 litters, p4EPB1/4EPB1 WT and *HeCo* n=15 embryos from 2 litters. Each point represents an embryo. Scale bar 10  $\mu$ m, mean  $\pm$  SEM and unpaired t-test, \*\*\*p<0.001, \*\*p<0.01, \*p<0.05.

**Figure 3. EML1 interacts with RPGRIP1L, in which mutations were identified in a heterotopia patient. Related to Figure S3.** A) Representative Western blots showing immunoprecipitation with anti-Flag when co-transfecting Flag/Flag-EML1 with c-myc-RPGRIP1L (n=3 experiments per condition). B) Pedigree of the family (P700), with one healthy boy, one affected boy and one miscarriage. C) Sanger sequence chromatograms for the parents and affected child of a portion of the *RPGRIP1L* gene. Compound heterozygous mutations were identified in patient 700-5 (red arrows), one inherited from the mother and one from the father. Nucleotides: red, T; black, G; green, A; blue, C. D) Representative T1 weighted section of brain MRI of P700-5 and control, showing a unilateral, extensive, subcortical heterotopia spanning from the frontal lobe (D1), to the parieto-temporal region (D2). In the occipital lobe, the cortical malformation is characterized by right sided nodular subependymal heterotopia (D3, green arrow). Note that the overlying cortex is thinner and appears dysplastic (D1, D2, D3). P700-5 presents corpus callosum agenesis (D4, red arrow) and cerebellar dysplasia (D5, blue arrow). E) Schematic representation of the *RPGRIP1L* gene (above) and protein domains (below). Blue arrows indicate the position of compound heterozygous mutations found in P700-5. F) Representative Western blot of immunoprecipitation with anti-Flag when co-transfecting Flag-EML1 with mutant c-myc-RPGRIP1L (n=3 experiments per condition). G) Quantification of immunoprecipitation experiments comparing the amount of WT and mutant RPGRIP1L bound to Eml1. The bound protein was normalized to total levels of the protein. Mean  $\pm$  SEM.

**Figure 4. Primary cilium formation is perturbed in *EML1* and *RPGRIP1L* patient fibroblasts and iPSC-derived cortical progenitors from *EML1* patients. Related to Figure S4 and S5.** A) Representative images of immunocytochemistry for  $\gamma$ -tubulin (green) and Arl13b (red) detecting primary cilia in control (control 1 and 2) and patient fibroblasts (P3489, P135, P700) 48h and 96h after serum starvation (SS). B) Percentage of fibroblasts presenting a primary cilium at 48h SS. 3-4 experiments per condition. C) Quantifications of primary cilium length in fibroblasts at 48h SS. n= 80-122 primary cilia from 3-4 experiments. D) Percentage of fibroblasts presenting a primary cilium at 96h SS. 3-4 experiments per condition. E) Quantifications of primary cilium length in fibroblasts at 96h SS. n= 64-141 primary cilia from

3-4 experiments. F) Representative electron microscopy images of human cortical progenitors derived from control and *EML1* mutation patient iPSCs. Red arrow: primary cilium, yellow arrow: basal body, blue arrow: ciliary pockets. Scale bar 10  $\mu\text{m}$  (A) and 0.5  $\mu\text{m}$  (F), median  $\pm$  minimum-maximum range and chi square (B, D), mean  $\pm$  SEM and one-way ANOVA followed by unpaired t-test (C, E), \*\*\*\* $p < 0.0001$ , \*\*\* $p < 0.001$ , \*\* $p < 0.01$ , \* $p < 0.05$ .

Figure 5. Mass spectrometry analyses reveal new EML1-interacting partners, among them the Golgi protein Vcip135. Related to Figure S5 and S6. A) Schematic of the proteomics workflow. Strep-YFP/Strep-YFP-EML1 purified with Strep-Tactin beads was used for pull down experiments using embryonic cortex lysates. Binding partners were obtained by quantitative label-free mass spectrometry analyses performed from four replicates. A  $\geq 1.5$  fold-change and  $\geq 3$  peptides/protein were used as criteria to obtain a list of EML1 interacting partners (240). Protein ratios were computed as the geometrical mean of related peptides. To estimate ratio significance, a two-tailed *t* test was performed and *p*-values were adjusted with a Benjamini–Hochberg FDR procedure with a control threshold set to 0.05. Further filtering was performed (nucleic acid-associated proteins) refining the list of EML1 protein partners (113). B) Diagram indicating number of common proteins identified in full length and N-ter (Bizzotto et al., 2017) EML1 MS screens. C) Diagram representing expression of EML1-interacting partners in the E14.5 murine cortical wall (GenePaint). D) Gene Ontology analyses performed with the publicly available software DAVID for the 113 protein list. Only those categories with an enrichment score  $>1$  are represented. E) Representative Western blot of immunoprecipitation with anti-Flag when co-transfecting Strep-YFP with Flag-VCIP135, Strep-YFP-EML1 with Flag-VCIP135, GFP-EML1 with Flag-VCIP135 and GFP-EML1-T243A with Flag-VCIP135 (n=2-3 experiments per condition). F) Quantification of immunoprecipitation experiments comparing the amount of EML1 bound to VCIP135 in WT and mutant conditions. The bound protein was normalized to total levels of the protein. G) Representative Western blot of immunoprecipitation with Strep/GFP when co-transfecting Strep-YFP with Flag-VCIP135, Strep-YFP-EML1 with Flag-VCIP135, GFP-EML1 with Flag-VCIP135 and GFP-EML1-T243A with Flag-VCIP135 (2-3 experiments per condition). H) Quantification of immunoprecipitation experiments comparing the amount of VCIP135 bound to EML1 in WT and mutant conditions. The bound protein was normalized to total levels of the protein. Mean  $\pm$  SEM.



Figure 6. The Golgi apparatus is severely disrupted in *Em1* mutant aRGs in brain slices. A) WT and *HeCo* aRGs (E13.5) electroporated with pCAG-IRES-Tomato (cell morphology) and pCAG-Galt-EGFP (Golgi apparatus). B) Schema representing the parameters quantified and the Golgi phenotype observed in aRGs. C) Quantification of number of Golgi elements. Each point represents an embryo. D) Quantification of Golgi extension. Each point represents an embryo. E) Quantification of the percentage of cells containing perinuclear Golgi elements. Each point represents an embryo. F) Quantification of the distance between the basal-most Golgi element to the aRG soma. Each point represents an embryo. D and F are normalized by the apical process length to avoid bias due to interkinetic nuclear migration. WT n=5 embryos from 3 litters (3-6 cells analyzed per embryo), *HeCo* n=4 embryos from 2 litters (2-11 cells analyzed per embryo). G) Representative images of electron microscopy acquisitions of the Golgi apparatus in WT and *HeCo* aRGs at E13.5. Red arrow: Golgi apparatus presenting anastomosis. H) Quantifications of cisternae width. Each point represents an embryo. I) Quantification of the number of vesicles surrounding each Golgi apparatus. Each point represents an embryo. J) Quantification of the percentage of Golgi apparatus presenting anastomosis. Each point represents an embryo. n= 3 embryos per condition from 3 litters (4-12 cells analyzed per embryo). Scale bar 10  $\mu$ m (A) and 0.5  $\mu$ m (G), mean  $\pm$  SEM and unpaired t-test (C, D, F, H, I), median  $\pm$  minimum-maximum range and Fisher's exact test (E, J), \*\*\*\*p<0.0001, \*\*\*p<0.001, \*\*p<0.01.

Figure 7. Golgi trafficking is perturbed in *Em1* mutant progenitors *in vitro*, and this organelle is also disrupted in hiPSC-derived cortical progenitors. Related to Figure S7. A) Pax6 (green) immunostainings in primary cultures of mouse neuronal progenitors from WT and *HeCo* mice (E13.5). B) Neuronal progenitor cells were transfected with VSVG-EGFP and incubated at 39°C. Then they were incubated at 32°C and fixed 5 min or 30 min later. Immunostaining with GM130 (red) was performed. C) Percentage of cells containing GFP+ puncta outside the Golgi at 5 min. D) Percentage of cells containing GFP+ puncta outside the Golgi at 30 min E) Percentage of cells containing >2 GFP+ puncta/cell outside the Golgi at 30 min. F) Number of GFP+ puncta/cell outside the Golgi at 30 min. n=13-19 cells per condition, from cultures from at least 3 embryos from 2 litters. G) Representative images of electron microscopy acquisitions of the Golgi apparatus in iPSC-derived patient cortical progenitors. Red asterisk: vacuolized Golgi apparatus. H) Quantification of the percentage of Golgi apparatuses containing vacuolized Golgi. 20-28 cells analyzed for condition. Scale bar 10  $\mu$ m (A, B) and 0.5  $\mu$ m (G)

median  $\pm$  minimum-maximum range, Fisher's exact test (C, D, E, H, I), Mann-Whitney test (F).  
\*\*\*\* $p < 0.0001$ , \*\* $p < 0.01$ , \* $p < 0.05$ .

## **Materials and methods**

### **Animals**

Research was conducted according to national and international guidelines (EC directive 2010/63/UE, French MESR 00984.02) with protocols followed and approved by the local ethical committee (Charles Darwin, Paris, France). *HeCo* mutant mice arose spontaneously in a colony of NOR-CD1 outbred stock, and selective inbreeding including crossing of living relatives and backcrossing were used to increase the occurrence of the phenotype in offspring as described in Croquelois et al., 2009. WT and *HeCo* mice derived from regularly crossed colonies were used for all the experiments described. The mode of inheritance of the phenotype is autosomal recessive. Normal, full-length transcripts of *Eml1* are absent in *HeCo* brains due to the insertion of an early retrotransposon (ETn) in the last intron of the gene, and are replaced by trace levels of shortened and chimeric *Eml1*-ETn transcripts (Kielar et al, 2014). Timed-pregnant Swiss mice obtained from Janvier Labs (<https://www.janvier-labs.com/>) were used to prepare embryonic cortex lysates for mass spectrometry experiments as well as for *in utero* electroporation experiments. For staging of embryos, the day of vaginal plug was considered E0.5. Mice were housed with a standard 12 h light/dark schedule (lights on at 07:00 a.m.).

### **Human cell culture**

Research on human cells was approved by the French Ministry of Health (L.1243.3, DC-2015-2559). The CIMH has ethical agreement for patient recruitment with respect to neurodevelopmental disorders and healthy controls. Patients involved were provided with detailed information about the study and gave written informed consent before being included in the study. All experiments with human material are in accordance with the declaration of Helsinki. The genetic analysis performed was subject to informed consent procedures and approved by the Institutional Review Boards at Necker Enfants Malades Hospital and Paris Descartes University.

### ***En face* immunohistochemistry and imaging**

*En face* immunohistochemistry (IHC) was performed as described in Bizzotto et al., 2017. F-actin immunodetection was performed to delineate cell boundaries (Marthiens et al., 2010),

combined with centrosome and primary cilium markers ( $\gamma$ -tubulin and Arl13b, respectively), as a means of further identifying apical endfeet. Briefly, mouse embryonic brains were fixed in 4% w/v paraformaldehyde (PFA) (Sigma-Aldrich, France). Cortical explants were dissected and incubated 15 min at RT in PBST 1% (PBS 1X containing 1% Triton X-100 v/v and 0.02% sodium azide). Explants were then incubated 2 hours (h) at room temperature (RT) in blocking solution (PBS 1X, 0.3% Triton X-100 v/v, 0.02% sodium azide, 3% w/v Bovine Serum Albumin). Primary antibodies mouse anti- $\gamma$ -tubulin (GTU-88, T6557, Sigma-Aldrich, 1:500) and rabbit anti-Arl13b (17711-1-AP, Proteintech, 1:500) were applied O/N at RT. After extensive washing in blocking solution, explants were incubated O/N at RT with secondary antibodies anti-mouse Alexa 488 and anti-rabbit Alexa 568 (1:1000, ThermoFisher) together with Hoechst (1:1000, ThermoFisher). Washes were performed in blocking solution and PBST 1%, and then the explants were incubated with Alexa Fluor 633 Phalloidin (1:100, Life Technologies) in PBST 1% O/N at RT. Extensive washing was performed in PBST 1% and PBS 1X before mounting the explants with Fluoromount G (Invitrogen) with the ventricular surface (VS) up to obtain an *en face* view of the ventricular side of the cortex. Fluorescently stained sections were imaged with a confocal TCS Leica SP5-II microscope. Images were acquired with a 0.17  $\mu$ m z-stack depth. At least two randomly-chosen ROIs (100 x 100  $\mu$ m) were analyzed per embryo, and the analyzed images had a total depth of 1  $\mu$ m. Images were analyzed using the Image J plugin Tissue Analyzer (Aigouy et al., 2010) and the publicly available software Cell Profiler (Lamprecht et al., 2007), a method previously described in Foerster et al., 2017.

## **Electron microscopy**

### *Mouse embryos*

Mouse embryos were transcardially perfused with a solution containing 4 % PFA (Electron Microscopy Science), 2.5% glutaraldehyde in sodium phosphate buffer (PB) 0.1 M, pH 7.4. 3 h after perfusion, brains were dissected and post-fixed in the same solution O/N at 4°C. The samples were washed extensively with PB 0.1M, and afterwards 3x 10 min washes with Palade buffer (Palade, 1952) were performed. The samples were incubated in 2% osmium tetroxide in Palade buffer for 40 min at RT, and then rinsed in Palade buffer for 3 min, followed by another 3 min wash in distilled water. They were dehydrated in a series of ethanol baths and flat-embedded in epoxy resin (EPON 812, Polysciences). After polymerization, blocks containing the dorsal telencephalon were cut at 70 nm thickness using an ultramicrotome (Ultracut E Leica). Sections were cut with a diamond knife and picked up on formvar-coated

200 mesh nickel one slot grids. Digital images were obtained with a CCD camera (Gatan Orius). Images were analyzed using Image J.

#### *Human neuronal progenitor cells*

Cells were fixed for 1 h in PB 0.1M buffer containing 4 % PFA and 2.5 % glutaraldehyde at 4°C. Following fixation, cells were postfixed in 2% osmium tetroxide diluted in 0.2M Palade buffer (Palade, 1952). After osmication, cells were dehydrated in a series of ethanol baths and flat-embedded in epoxy resin (EPON 812, Polysciences). After resin polymerization, small pieces were dissected from flat-embedded cultures, mounted in plastic stubs and sectioned. Ultrathin sections (70 nm) were stained with uranyl acetate and lead citrate. Sections were examined in a Philips CM100 electron microscope. Digital images were obtained with a CCD camera (Gatan Orius). Images were analyzed using ImageJ.

#### **Ferret *in situ* hybridization**

To generate the ferret *Eml1* probe, cDNA was reverse-transcribed from P0 ferret brain total RNA, and a fragment amplified using primers fEml1F, CTTTCTATGAACTCTTC, and fEml1R, AAGGATACATACAAACAG, was ligated into pGEM-T-Easy vector (Promega). *In situ* hybridization on ferret brain sections was performed as described previously in Reillo et al., 2011.

#### **Exome sequencing of heterotopia patients: analyses of *RPGRIP1L* mutations**

Prior to exome analysis, for each patient, DNA was analyzed by CGH-microarray using the NimbleGen chip 720,000-probes (720 K) array (Roche-NimbleGen, Madison, WI) to exclude potential pathogenic CNVs.

Whole exome sequencing of peripheral blood DNA from the proband and both parents was performed using the Agilent SureSelect Human All Exon Kits v5, and sequences were generated on a HiSeq2500 machine (Illumina). Sequences were aligned to hg19 by using BWA v.0.6.1, and single nucleotide variants (SNVs) and indels were called by using GATK v.1.3. Annotation of variants was performed with GATK Unified Genotyper. All calls with read coverage of  $\leq 2$  or a Phred-scaled SNP quality score of  $\leq 20$  were removed from consideration. The annotation process was based on the latest release of the Ensembl database. Variants were annotated and analysed using the Polyweb software interface designed by the Bioinformatics platform of University Paris Descartes and Imagine Institute.

Filters used for variant screening were as follows: (i) all variants previously observed (in dbSNP138 and/or in in-house projects) were excluded; (ii) only variants leading to abnormal protein sequence (splicing, non-synonymous, frameshift, stop) were retained; (iii) we considered the PolyPhen-2 and SIFT prediction status as informative but not restrictive. Because the patient was a sporadic case from unrelated parents, the following models of inheritance in the variant screening were considered: autosomal recessive (in particular compound heterozygous but without excluding homozygous variants), X-linked and *de novo* SNVs.

A compound heterozygous mutation in *RPGRIP1L* was identified in a patient with subcortical heterotopia (P700; a c.3562G>A nucleotide mutation in exon 22 was transmitted from the mother and c.3706C>T nucleotide mutation in exon 24 was transmitted from the father, Table S1). Genomic DNA amplifications were performed for *RPGRIP1L* using standard procedures (RPGRIP1L-ex22-F : 5'CAGTAGTGTACATTGCATTC 3' ; RPGRIP1L-ex22-R : 5' TCTCTCTGTTCTTTCCACTTC 3' ; RPGRIP1L-ex24-F : 5' CTTAGAAAGTGGATTAGTGTTTC 3' ; RPGRIP1L-ex24-R : 5' GCCTCCCAGGTATCTGGG 3'), and PCR products were analyzed by direct sequencing using an 3500xL Genetic Analyzer (Applied Biosystems, Foster City, CA).

### **Clinical phenotype of the patient (P700)**

P700-5 is a child of non-consanguineous Caucasian parents and was born at term with normal neonatal parameters. The patient was brought to medical attention at the age of 4, for developmental delay, secondary generalized focal seizures and left hemianopsia. During infancy, epilepsy became drug-resistant, with at least one seizure type consisting of left hemibody tonic seizure, with expression of fear, followed by left clonic movement for 30 seconds. Seizure frequency is up to 2 per day, in spite of multiple anti-epileptic drug combinations.

At last evaluation at 15 years of age, P700-5 presents moderate intellectual disability. He attended a specialized school, was able to read and write fluently, although showed difficulties in memorization. P700-5 is right handed. On examination, he demonstrated left hemiplegia, is able to walk but is extremely fatigable, and so uses a wheelchair in everyday life. He shows impaired oculo-manual coordination with oculo-cephalic apraxia associated with left hemianopsia.

On MRI performed at the age of 7 years, 7 months, P700-5 showed right subcortical heterotopia spanning the whole right hemisphere, surrounded by fronto-parieto temporal polymicrogyria, associated with almost complete corpus callosum agenesis and cerebellar dysplasia affecting the superior cerebellar vermis (Table S2).

### **Embryonic cortex lysate**

For mass spectrometry experiments E13.5 timed-pregnant Swiss mice (Janvier Labs, France) were sacrificed by cervical dislocation. Embryos were dissected and both brain hemispheres collected in ice cold L-15 medium. Explants were immediately frozen in liquid nitrogen and ground into a powder. Hemispheres coming from different embryos were pooled. The powder was re-suspended in 10 µl/mg lysis buffer (Tris HCl 50 mM, NaCl 150 mM, EDTA 1 mM pH 8) supplemented with NP-40 1% and protease inhibitors 1x (Complete Protease Inhibitor Cocktail Tablets EDTA-Free, Roche). The lysate was homogenized by rotation during 45 min at 4 °C, then centrifuged for 30 min at 15000 rcf and 4 °C. The supernatant was collected and stored at -80°C.

For Western blot experiments designed to study the mTOR signaling pathway the protocol was mildly modified. Once the cortex was dissected and fast-frozen in liquid nitrogen, lysis of each embryonic cortex (from both hemispheres) was performed individually, by re-suspending the tissue continuously with lysis buffer for a period of 2 h at 4°C. Then the lysate was centrifuged (30 min, 15000 rcf, 4 °C), the supernatant collected and protein concentration measured using the BCA Protein Assay Kit (Thermo Fisher) and the ELISA microplate reader BertholdTech Mithras.

### **Freestyle 293F cell culture, protein purification and pull down for mass spectrometry**

293F cells were cultured in FreeStyle 293 Expression Medium (ThermoFisher), under constant agitation, at 37 °C and 8 % CO<sub>2</sub>. For transfection, 1 x 10<sup>6</sup> cells were cultured in a 125 ml Erlenmeyer. 45 µg of Polyethylenimine (PEI, Polysciences) were mixed with 750 µl of OPTI-MEM (ThermoFisher) and 22.5 µg of DNA with 750 µl of OPTI-MEM, for a 1:2 ratio of DNA: PEI. The DNA was mixed with the PEI solution and after a period of 10 min at RT the mix was applied to the cells. 72 h later the cells were recovered, washed with 1 x PBS and lysed with 750 µl of lysis buffer (Tris HCl 50 mM, NaCl 150 mM, EDTA 1 mM pH 8) supplemented with NP-40 1% and protease inhibitors 1X (Complete Protease Inhibitor Cocktail Tablets EDTA-Free,

Roche). After 30 min of rotation at 4°C, the samples were centrifuged for 15 min, 14000 rcf, at 4°C. The supernatant was kept and protein content was measured with the BCA Protein Assay Kit (ThermoFisher) and the ELISA microplate reader BertholdTech Mithras, in order to ensure similar protein concentrations across the different conditions.

For protein purification, Strep-Tactin beads Superflow Plus (30002, Qiagen) were used. 40 µl of beads previously washed with lysis buffer were used for each purified protein sample. They were incubated with 2 mg of protein lysate (in a 100 µl volume) for 1 h at 4 °C under rotation. The samples were then centrifuged (3 min, 200 rcf, 4°C), and the supernatant was kept as the 'unbound' fraction. The beads were washed (3x) with a more stringent lysis buffer containing 500 mM NaCl, in order to eliminate possible proteins binding to the beads in a non-specific fashion. For control experiments to check correct protein purification, elution was performed with NuPAGE LDS Buffer (ThermoFisher). For pull down samples to analyze by mass spectrometry, the Strep-Tactin beads already bound to the protein of interest (Strep-YFP or Strep-YFP-EML1) were incubated with 15 µg of cortex lysate (described above) O/N, at 4°C, under rotation. Then the samples were centrifuged (3 min, 200 rcf, 4°C), and the 'unbound cortex' recovered. The beads containing the purified protein of interest and its interacting partners were extensively washed with lysis buffer (150 mM NaCl). They were stored at 4°C for mass spectrometry analyses.

### **Mass spectrometry**

Strep-Tactin beads containing the purified protein of interest and its interacting partners were washed twice with 100 µL of 25 mM NH<sub>4</sub>HCO<sub>3</sub> and an on-bead digestion with 0.2 µg of trypsin/LysC (Promega) was performed for 1 h in 100 µL of 25 mM NH<sub>4</sub>HCO<sub>3</sub>. Samples were then loaded onto homemade C18 StageTips for desalting. Peptides were eluted using 40/60 MeCN/H<sub>2</sub>O + 0.1 % formic acid and vacuum concentrated to dryness. Samples were chromatographically separated using an RSLCnano system (Ultimate 3000, Thermo Scientific) coupled online to an Orbitrap Fusion Tribrid mass spectrometer (Thermo Scientific). Peptides were trapped on a C18 column (75 µm inner diameter × 2 cm; nanoViper Acclaim PepMap™ 100, Thermo Scientific) with buffer A (2/98 MeCN/H<sub>2</sub>O in 0.1% formic acid) at a flow rate of 4.0 µL/min over 4 min. Separation was performed on a 50 cm x 75 µm C18 column (nanoViper Acclaim PepMap™ RSLC, 2 µm, 100Å, Thermo Scientific) regulated to a temperature of 45 °C with a linear gradient of 5 % to 25 % buffer B (100% MeCN in 0.1% formic acid) at a flow rate of 300 nL/min over 100 min. Full-scan MS was acquired in the Orbitrap analyzer with a

resolution set to 120,000 and ions from each full scan were HCD fragmented and analyzed in the linear ion trap.

For identification, the data were searched against the mouse SwissProt database using Sequest HF through proteome discoverer version 2.1. Enzyme specificity was set to trypsin and a maximum of two-missed cleavage sites were allowed. Oxidized methionine, N-terminal acetylation, and carbamidomethyl cysteine were set as variable modifications. Maximum allowed mass deviation was set to 10 ppm for monoisotopic precursor ions and 0.6 Da for MS/MS peaks.

The resulting files were further processed using myProMS (Pouillet et al., 2007). FDR calculation used Percolator and was set to 1% at the peptide level for the whole study. The label free quantification was performed by peptide Extracted Ion Chromatograms (XICs) computed with MassChroQ version 1.2 (Valot et al., 2011).

For protein quantification, XICs from proteotypic and non-proteotypic peptides shared between compared conditions (TopN matching) with no missed cleavages were used. Global MAD normalization was applied on the total signal to correct the XICs for each biological replicate. Protein ratios were computed as the geometrical mean of related peptides. To estimate ratio significance, a two-tailed *t* test was performed and *p*-values were adjusted with a Benjamini–Hochberg FDR procedure with a control threshold set to 0.05.

The mass spectrometry proteomics data have been deposited to the ProteomeXchange Consortium via the PRIDE (Perez-Riverol et al., 2019) partner repository with the dataset identifier PXD012714.

Additionally, to check for the specificity of the list of proteins obtained, we used the CRAPome (Contaminant Repository for Affinity Purification, [www.crapome.org](http://www.crapome.org)), a depository that contains multiple negative controls from mass spectrometry experiments allowing to query the specificity of the proteins obtained in MS results (Mellacheruvu et al., 2013). Only 3,3 % of the proteins were recognized as frequently found in the CRAPome data base, which ensures the specificity of the protein list.

### **Human fibroblast cultures**

Skin biopsies were obtained with consent to isolate dermal fibroblasts using standard practices. Human fibroblasts were cultured in Dulbecco Modified Eagle Medium (DMEM) + GlutaMax (31966-021, Thermo Fisher) supplemented with 10% fetal bovine serum (FBS) and 50 µg/ml of primocin (Invivogen). Before splitting, the cells were washed with Hanks-Balanced



Salt Solution (HBSS) followed by incubation for 3-5 minutes at 37°C with a 0.25% (w/v) Trypsin, 0.53 mM EDTA, PBS 1x solution. Then  $3 \times 10^4$  cells were plated on 14 mm glass coverslips previously coated with Poly-L-Lysine 1x (PLL, Sigma Aldrich) O/N at 37°C, followed by extensive washing with sterile water. For serum starvation experiments, the cells were split, plated ( $3 \times 10^4$  in previously coated 14 mm coverslips) and cultured for 24h in complete medium. After 24h, the cells were cultured in the same medium without FBS.

### **Generation of hiPSC-derived cortical progenitors**

Differentiation of hiPSC-derived cortical progenitors was performed as described with slight adaptations (Shi et al., 2012, Iefremova et al., 2017). In brief, iPSCs were cultured in PluriPro medium (Cell Guidance Systems). Once the cell culture reached 98% confluence, neural induction was initiated by changing the culture medium to neural induction media containing DMEM/F12 (N2 supplement, 1:50; B27 supplement, 1:50), cAMP (300 ng/ml, Sigma-Aldrich), LDN-193189 (0.5  $\mu$ M, Miltenyi), A83-01 (0.21  $\mu$ g, Miltenyi) and XAV939 (2 $\mu$ M, Enzo). Cells were maintained in this medium for 8–11 days, collected by dissociation with TrypL Express (Invitrogen) and replated in neural differentiation media containing DMEM/F12 (N2 supplement, 1:50; B27 supplement, 1:50) and cAMP (300 ng/ml, Sigma Aldrich) on Geltrex-coated (GT, Life Technologies) plastic dishes. Cortical progenitors were split in a 1:2 ratio when cultures reach 100% confluence using TrypL Express (Invitrogen). EM analyses were performed between passage one – three. See also Figure S4.

### **Retina Epithelial Pigmented cell (hTERT RPE-1) cell culture**

RPE1 cells were cultured in DMEM:F12 medium (30-2006, ThermoFisher) complemented with 10 % FBS at 37 °C and 5 % CO<sub>2</sub>. Before splitting the cells were washed with Hanks-Balanced Salt Solution (HBSS) followed by incubation for 3-5 minutes at 37 °C with a 0.25 % (w/v) Trypsin, 0.53 mM EDTA, 1 x PBS solution.  $6 \times 10^4$  cells were plated in previously coated 14 mm glass coverslips (PLL, 10 min RT, followed by extensive washing with sterile water). 24 h later, cells were transfected with a ratio of 1:4 DNA and lipofectamine 2000 (Invitrogen). 2  $\mu$ l of lipofectamine were combined with 50  $\mu$ l of OPTI-MEM Media (ThermoFisher). In parallel 0.5  $\mu$ g of DNA were combined with 50  $\mu$ l of OPTI-MEM. The latter solution was mixed with the former and after 20 min at RT, the mix was applied to the cells. 24 h after transfection the cells were fixed and immunostained (see below).

### **Mouse neuronal progenitor cell culture**

The neuronal progenitor cell culture was adapted from Sun et al., 2011. Briefly, 6-well cell culture plates were coated with Poly-D-lysine (PDL, P6407, Sigma Aldrich) 2  $\mu\text{g}/\text{cm}^2$  in sterile 1 x PBS, O/N, at 37 °C and 5 %  $\text{CO}_2$ . The following day, the PDL was removed, and the plates were coated with 1  $\mu\text{g}/\text{cm}^2$  fibronectin (F1141, Sigma Aldrich) in sterile 1 x PBS. E13.5 timed-pregnant mice were sacrificed by cervical dislocation and the uterus was placed in ice cold basal medium (DMEM/F12 Hams, 21041, Thermo Fisher, 1 % Pen-Strep (Gibco), 2.9 mg/ml glucose and 1.2 mg/ml sodium bicarbonate). The embryos were extracted from the uterus one by one and the cortex from both hemispheres was dissected and kept at 4 °C in basal medium. The medium was removed and substituted by pre-warmed sterile complete medium (basal medium complemented with 1 x B27 without vitamin A (12589-010, Gibco), 20 ng/ml of EGF (E9644, Sigma Aldrich) and 20 ng/ml of FGF (F0291, Sigma Aldrich). The tissue was dissociated and each sample was centrifuged (3 min, 100 rcf). The medium was removed and substituted by fresh pre-warmed complete medium followed by re-suspension of the cells. 1 x 10<sup>5</sup> cells were plated in coated 6-well culture plates. The cells were split once before performing transfection experiments. Half of the culture medium was changed by fresh complete medium every 2 days. For splitting, cells were washed with pre-warmed Versene (Gibco), followed by a 3 min incubation with pre-warmed StemPro Accutase (Gibco) at 37°C. Cells were plated (6-8 x 10<sup>5</sup>) on coated 14 mm glass coverslips for transfection.

For transfections (VSVts405-G-EGFP), a ratio of 1:2:2 DNA with Lipofectamine 3000 and Lipofectamine 3000 Reagent was used. 1  $\mu\text{l}$  of lipofectamine was mixed with 25  $\mu\text{l}$  of OPTI-MEM, and 0.5  $\mu\text{g}$  of DNA were mixed with 2  $\mu\text{l}$  of lipofectamine reagent in 50  $\mu\text{l}$  of OPTI-MEM. The latter solution was mixed with the former and after 5 min at RT the mix was applied to the cells.

For the VSVG experiments, cells were incubated at 39.5 °C and 5%  $\text{CO}_2$ . 24 h later the cells were incubated at 32 °C to allow the release of the VSVG protein. The cells were fixed 5 and 30 min afterwards, and immunostained (see below).

### **Neuro2A cell culture, transfection and co-immunoprecipitation (co-IP)**

Cells were cultured in 10 % FBS-supplemented DMEM (ThermoFisher) at 37 °C and 5 %  $\text{CO}_2$ . Cells were dissociated with 0.025 % trypsin–EDTA (25300-054, Gibco) diluted in DMEM and plated into 100 mm Petri dishes (1 x 10<sup>6</sup>/dish). After 24 h in culture, cells reaching 70-80 % confluence were transfected using a ratio of 1:3 DNA and PEI, respectively (10  $\mu\text{g}$  of DNA and

30 µg of PEI, Polysciences). The following constructs were used for co-immunoprecipitation experiments: pMAX-Strep-YFP-EML1, CMV-3xFlag-Eml1, CMV-3xFlag-EML1 T243A, pEGFP-C3-EML1, pEGFP-C3-EML1 T243A, pCS2-c-myc-RPGRIP1L, pCS2-c-myc-RPGRIP1L R1236C, pCS2-c-myc-RPGRIP1L V1188M, pC3-YFP-EML4, CMV-3xFlag-VCIP135 (Delous et al., 2007, Kielar et al., 2014, Richards et al., 2015, Zhang and Wang, 2015), and the corresponding control vectors. Site directed mutagenesis to obtain the c-myc-RPGRIP1L mutant constructs was performed with the QuikChange Lightning Kit (Agilent Technologies). To test the shmiRNA efficiency, the pCAGMIR30-shRNA scrambled and pCAGMIR30-shRNA Vcip135 constructs were transfected in Neuro2A cells.

For co-IPs, after 48 h, cells were recovered and washed twice with 1 X PBS and lysed by rotation for 20 min at 4 °C in 150 µl of RIPA buffer (50 mM Tris-HCl, pH 8, 100 mM NaCl, 1 mM EDTA, 0.1% SDS, 1% Nonidet P-40, 0.5 % sodium deoxycholate and protease inhibitor mix from Roche). The samples were centrifuged at 14000 rcf for 15 min at 4°C. Protein G sepharose beads (Sigma Aldrich) were diluted 1/10 in TNE buffer (50 mM Tris-HCl pH 7.4, 100 mM NaCl, 5 mM EDTA) and 60 µl of diluted beads were used for each IP experiment. The beads were extensively washed with 1 x RIPA buffer, followed by centrifugation (12000 rcf, 4°C, 30 s). A pre-clearing step was performed by incubating the cell lysates with the already-washed beads in a rotating wheel at 4 °C for 1 h 30 min. The samples were then centrifuged (12000 rcf, 4°C, 30 s) and the supernatant collected. The latter was incubated with the following primary antibodies (1 µg): mouse anti-GFP (G6539, Sigma-Aldrich), rabbit anti-GFP (A6455, Invitrogen), rabbit anti-Flag (F7425, Sigma-Aldrich), mouse anti-Flag (F1804, Sigma Aldrich), mouse anti-c-myc (Cell Signaling Technology) and mouse anti-Strep (GT661, Invitrogen) (O/N, 4°, rotating wheel).

Afterwards, these samples were incubated with 100 µl of diluted washed Protein G Sepharose beads (5 h, 4 °C, rotating wheel). The unbound fraction was recovered after centrifugation (12000 rcf, 4 °C, 30 s). 5x washes of the beads in 1 x RIPA buffer were performed before elution with NuPAGE LDS Buffer (Thermo Fisher), 10 min at 70°C. The bound fraction was recovered after centrifugation (12000 rcf, RT, 2 min).

### **Western blot**

Samples were denatured with 2x NuPAGE LDS Buffer (ThermoFisher) for 10 min at 70 °C. Denaturing electrophoresis was performed on a 4-12 % Bis-Tris Gel with MOPS SDS running buffer for 2 h at 110V. Proteins were transferred onto nitrocellulose membranes for 2 h at

110V and 4 °C in a Tris-Glycine transfer buffer (Tris 25 mM, Glycine 192 mM, ethanol 10 %). After protein transfer, the membranes were stained with Ponceau S to check the transfer quality. The membranes were extensively washed with distilled water, followed by a 30 min incubation in TBST 1x (100 mM Tris pH 7.5, 150 mM NaCl, 10 % ethanol, 0.05% Tween) supplemented with 5 % milk. Incubation with the secondary antibody (see below) was performed to identify non-specific binding sites. Briefly, the antibody was incubated in the dark for 2h, and afterwards extensive washes with TBST 1x were performed, prior to imaging (see below). The primary antibodies were then incubated O/N at 4 °C with agitation or for a period of 2 h at RT. The following primary antibodies were used: rabbit anti-mTOR (Proteintech, 1:500-1:1000), rabbit anti-pmTOR (Cell Signaling Technology, 1:1000), rabbit anti-S6R (Cell Signaling Technology, 1:1000), rabbit anti-pS6R (Cell Signaling Technology, 1:1000), rabbit anti-4EBP1 (Cell Signaling Technology, 1:1000), rabbit anti-p4EBP1 (Cell Signaling Technology, 1:1000), mouse anti-GFP (G6539, Sigma-Aldrich), rabbit anti-GFP (A6455, Invitrogen), rabbit anti-Flag (F7425, Sigma-Aldrich, 1:300), mouse anti-Flag (F1804, Sigma Aldrich, 1:500), mouse anti-c-myc (Cell Signaling Technology, 1:400), mouse anti-Strep (GT661, Invitrogen, 1:1000), chicken anti-GAPDH (AB2302, Millipore, 1:10000). The membranes were extensively washed with TBST, followed by incubation with the secondary antibody: Dylight anti-mouse 800, anti-rabbit 800 and anti-chicken 680 (ThermoFisher, 1:10000). After extensive washes in TBST, the membranes were scanned using an Odyssey (Licor) infrared scanner. Images were analyzed using ImageJ. For co-immunoprecipitation experiments, the bound fraction was normalized to the total (bound and unbound).

### **Immunocytochemistry**

Cells were washed in 1 x PBS prior to fixation with 4 % w/v PFA in 0.1 M phosphate buffer, pH 7.4, for 15 min at RT. The cells were extensively washed in 1 x PBS followed by a 15 min wash in PBST 0.2 % (Triton X-100 0.2 % in 1 x PBS). Incubation with blocking solution (3 % BSA, 0.2 % Triton X-100 in 1 x PBS) was performed for 1 h at RT and the following primary antibodies were applied for 2 h at RT or O/N at 4°C: mouse anti-GFP (G6539, Sigma-Aldrich, 1:500), rabbit anti-Flag (F7425, Sigma-Aldrich, 1:500), mouse anti- $\gamma$ -tubulin (GTU-88, T6557, Sigma-Aldrich, 1:500), rabbit anti-Arl13b (17711-1-AP, Proteintech, 1:500), sheep anti-TGN46 (AHP500GT, BioRad, 1:500), mouse anti-GM130 (610822, BD Transduction Laboratories, 1:300). The cells were extensively washed with PBST 0.2% and the following secondary antibodies were incubated combined with Hoechst (1:1000, ThermoFisher) for 45 min at RT in the dark: anti-

mouse Alexa 488, anti-mouse Alexa 568, anti-rabbit Alexa 568, anti-goat Alexa 568 (1:1000, ThermoFisher). The cells were extensively washed in PBST 0.2% and the coverslips mounted with Fluoromount G (Southern Biotechnology).

Images were acquired with a TCS Leica SP5-II confocal microscope, and quantifications performed with ImageJ.

For detection of the neural and/or cortical progenitor markers Sox2, Pax6, FoxG1 and OTX2 cells were fixed for 10 min in 4% w/v PFA (Sigma-Aldrich), washed three times with PBS and transferred to blocking solution containing 10% FCS in PBS and 0.1% Triton X-100 for 1 h, incubated with the primary antibodies for 16 h at 4 °C, washed three times with PBS, incubated for 1 h with secondary antibodies, counterstained with DAPI (BioLegend) and mounted with Mowiol 4-88. Antibodies and concentrations were as follows: Sox2 (MAB2018, R&D Systems, 1:500), Pax6 (153011, Synaptic Systems, 1:300), Otx2 (M199, TaKaRa, 1:400), FoxG1 (M227, TaKaRa, 1:400), anti-rabbit Alexa 488 (1:1000, ThermoFisher) and anti-mouse Alexa 555 (1:1000, ThermoFisher). Images were acquired with a Celldiscoverer 7 microscope (Zeiss).

#### **Shmir design and RT-qPCR**

pCAGMIR30-shRNA (Addgene) scrambled and pCAGMIR30-shRNA Vcip135 were designed with the siRNA Wizard tool (Invivogen), sequences are respectively: 5' TTGTGCCTCAGGACCTTATTA 3' and 5' TCCTAATTTCCGTGTGACAGT 3'. Total RNA samples were extracted from transfected Neuro2A cells (RNeasy protect mini kit, Qiagen). First-strand cDNA was synthesized using oligo (dT) and the Superscript III Reverse Transcriptase kit (Invitrogen). Gene-specific primers were designed by KiCqStart SYBR green primers (Sigma Aldrich, primer set 1). The cyclophilin B (*Ppib*, peptidylpropyl isomerase B) and prosaposin (*Psap*) genes were used for normalization (geometric mean). Real-time qPCRs were performed using the SYBR green method, following MIQE guidelines (Bustin et al., 2009). Standard curves were generated from assays made with serial dilutions of cDNA to calculate PCR efficiencies ( $90\% < \text{efficiency} < 105\%$ , with  $r^2 > = 0.998$ ). Threshold cycles (Ct) were transformed into quantity values using the formula  $(1 + \text{efficiency})^{-\text{Ct}}$ . Differential expression analyses were performed with Student *t*-tests.

#### ***In utero* electroporation**

Timed-pregnant mice (E13) were anesthetized with isoflurane (4 % during induction and 2–2.5 % during surgery) and embryos exposed within the intact uterine wall after sectioning the

abdomen. Embryos were constantly hydrated with NaCl 0.9 % (B. Braun). A solution containing DNA (1 µg/µl per plasmid) and 20 % w/v fast green in sterile endo-free water was injected in the lateral ventricles of the embryos. Different combinations of plasmids were used of the following vectors: pCAG-IRES-Tomato, pEGFP-C3-EML1, pCAG-Galt-EGFP (Kimura and Murakami, 2014), pCAGMIR30-shRNA scrambled and pCAGMIR30-shRNA Vcip135. Forceps electrodes (System CUY650P5 NepaGene Co) were placed around the embryo head at a 45° angle and plasmids electroporated by discharging a 4,000-µF capacitor charged to 35 V (five electric pulses of 50 ms with 500 ms intervals) with a CUY21 NepaGene electroporator. The embryos were then placed back in the abdominal cavity until a later developmental time point for subsequent analyses.

### **BrdU injections and immunohistochemistry**

For cycling progenitor analyses at E12.5, pregnant females were injected with 5-bromo-2'-deoxyuridine (BrdU, 99 % Bioultra, Sigma-Aldrich, 50 µg per gram body weight in NaCl 0.9%) and sacrificed after 30 min. Embryonic brains were fixed by immersion O/N at 4 °C in 4 % w/v PFA in 0.1 M phosphate buffer, pH 7.4, followed by extensive washes in 1 x PBS. Brains were cut in 70 µm thick coronal sections using a vibrating blade microtome (Leica VT1000 S). In order to perform immunohistochemistry combining the primary antibodies mouse anti-Ki67 (BD 556003, 1:200) and rat anti-BrdU (BioRad, clone Bu20a, 1:1000), antigen retrieval was performed by incubating the sections in sodium citrate 10 mM pH 6 at 95 °C for 20 min and allowing them to cool before blocking. Blocking was performed for 1 h at RT with blocking solution (1X PBS with 10 % Goat Serum and 0.5 % Triton X-100) before incubation O/N at 4 °C with the primary antibody (Ki67). After extensive washes, sections were incubated with the secondary antibody anti-rabbit Alexa 488 (Life Technologies, 1:1000) for 2 h at RT. This was followed by a 10 min incubation in Hoechst (ThermoFisher, 1:1000) and then sections were fixed with 8 % PFA w/v for 15 min at RT (Palmer et al., 2000). Extensive washes with PBST 0.1% (1X PBS and 0.1% Triton X-100) were performed, followed by incubation in 2N hydrochloric acid for 30 min at 37 °C. After extensive washes, the sections were incubated with the primary antibody (BrdU), secondary antibody Alexa 568 (Life Technologies, 1:1000), Hoechst, and then mounted with Fluoromount G (Invitrogen).

Brain sections (50 µm thick) from *in utero* electroporation experiments related to Vcip135 were exclusively incubated with Hoechst and extensively washed before mounting. IHC with a primary antibody mouse anti-GFP (G6539, Sigma-Aldrich, 1:500) and a secondary antibody

Alexa-488 (ThermoFisher) was performed in brain sections (70  $\mu\text{m}$ ) electroporated with EGFP-EML1 and pCAG-IRES-Tomato.

### **Immunohistochemistry and immunocytochemistry images analyses**

For Ki67+BrdU+ cell distribution analyses, regions of interest (ROI) were selected from both hemispheres, spanning the whole cortical wall and with a width of 100  $\mu\text{m}$ . Two ROIs were quantified per animal. The E12.5 cortical wall was divided in 5-equally sized bins, bin 1 and 5 corresponding to the most apical (apical ventricular zone) and basal (cortical plate) regions of the developing cortex, respectively (Figure S1 A). For *in utero* electroporation experiments, the E14 cortex was subdivided in 6-equally sized bins, bin 1 and 6 corresponding to the most apical (apical ventricular zone) and basal (cortical plate) regions of the developing cortex, respectively (Figure S7 A). Cells that were positive in each bin for the selected markers were quantified, and the percentage relative to the total number of positive cells across the cortical wall was compared between the two conditions in each different bin.

For *in utero* electroporation experiments addressing Golgi apparatus localization in aRGs, individual electroporated Tomato+ cells were selected and analyzed. Similar parameters to the ones described in Taverna et al., 2016 were quantified.

For patient fibroblast primary cilium and Golgi apparatus analyses ImageJ was used. Axonome length was measured manually using Arl13b immunodetections. Golgi analyses were performed with the plugin 3D Object Counter.

Images for all experiments were acquired with a TCS Leica SP5-II confocal microscope. A stack projection 10  $\mu\text{m}$  thick was used for the IHC analyses. A stack projection 3-5  $\mu\text{m}$  thick was used for ICC analyses. Stacks were performed using Image J.

### **Statistical analyses**

Statistical analyses were performed using GraphPad Prism and BiostaTGV (<https://biostatgv.sentiweb.fr/>). The specific test used in each experiment is specified in the figure legend. Data were collected and processed randomly. No data points were excluded.

Figure 1

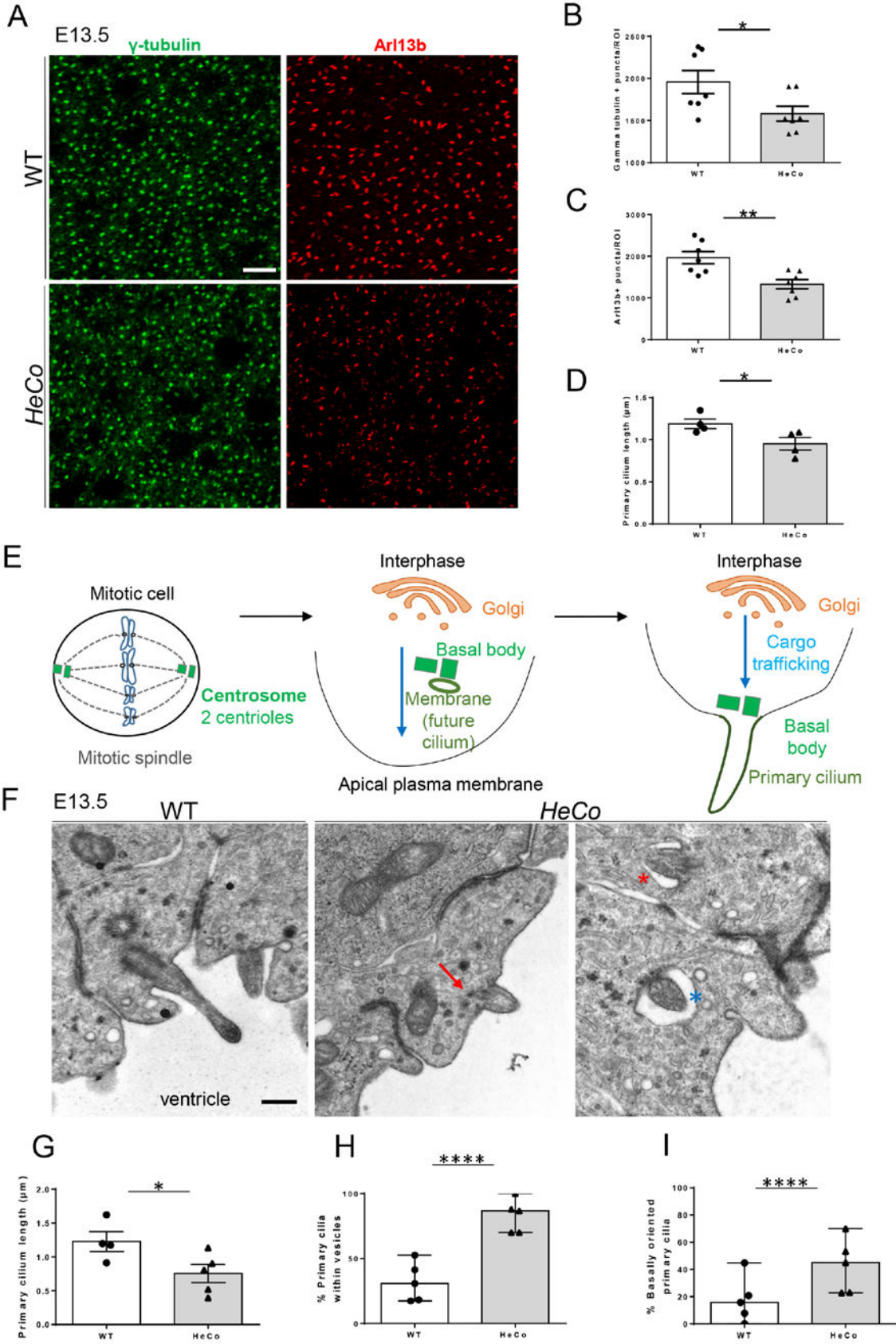
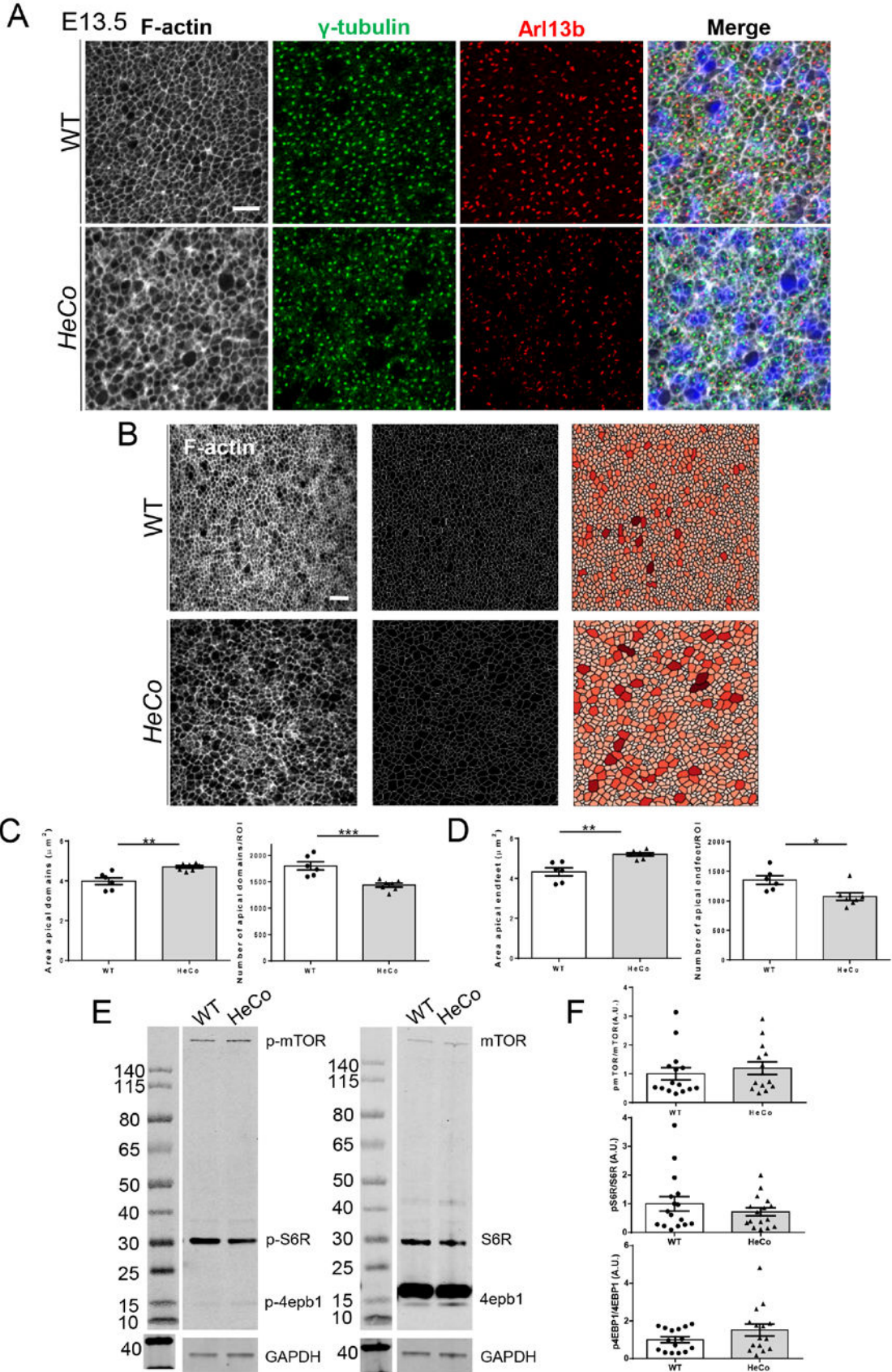
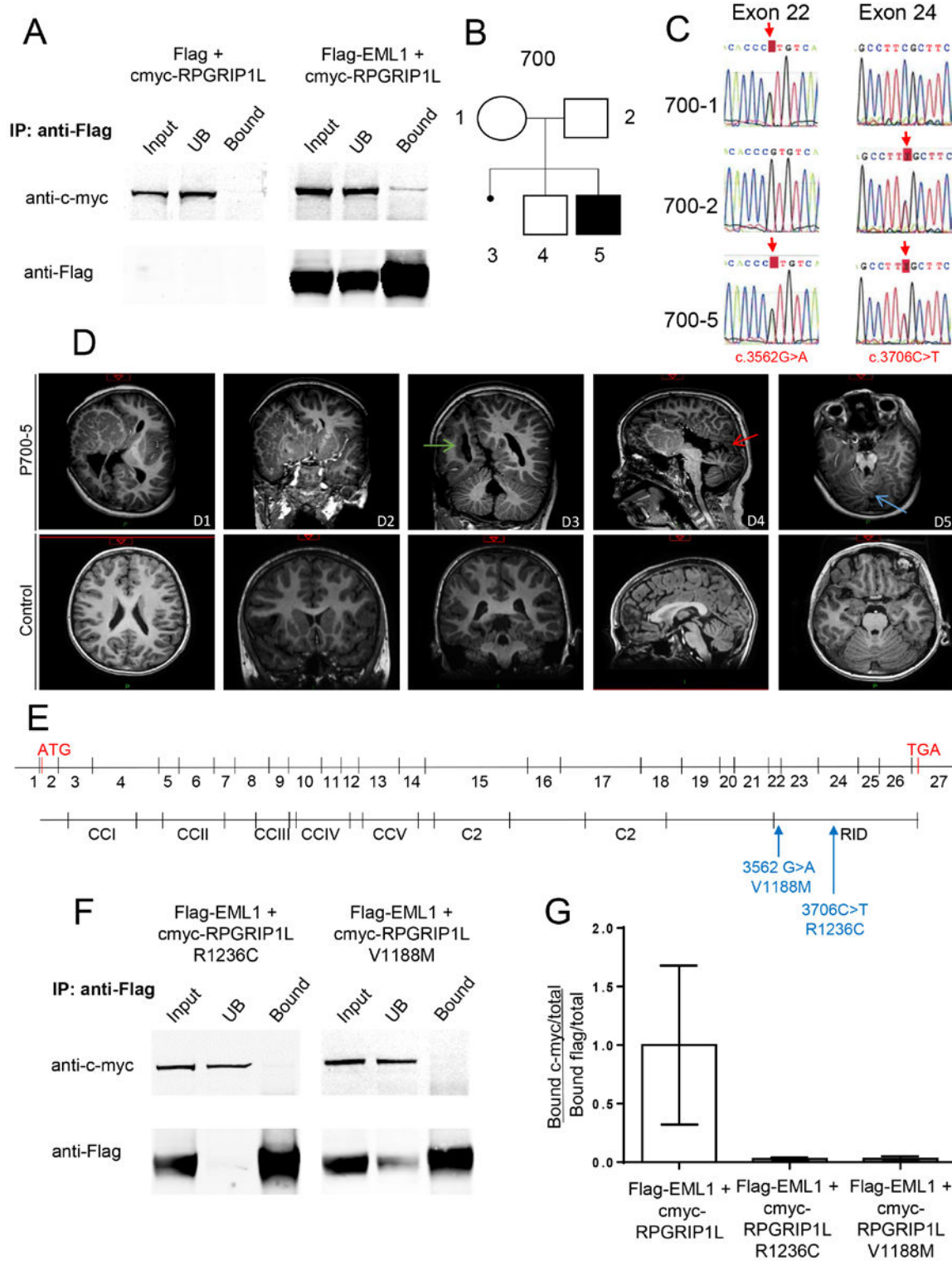




Figure 2



**Figure 3**



**Figure 4**

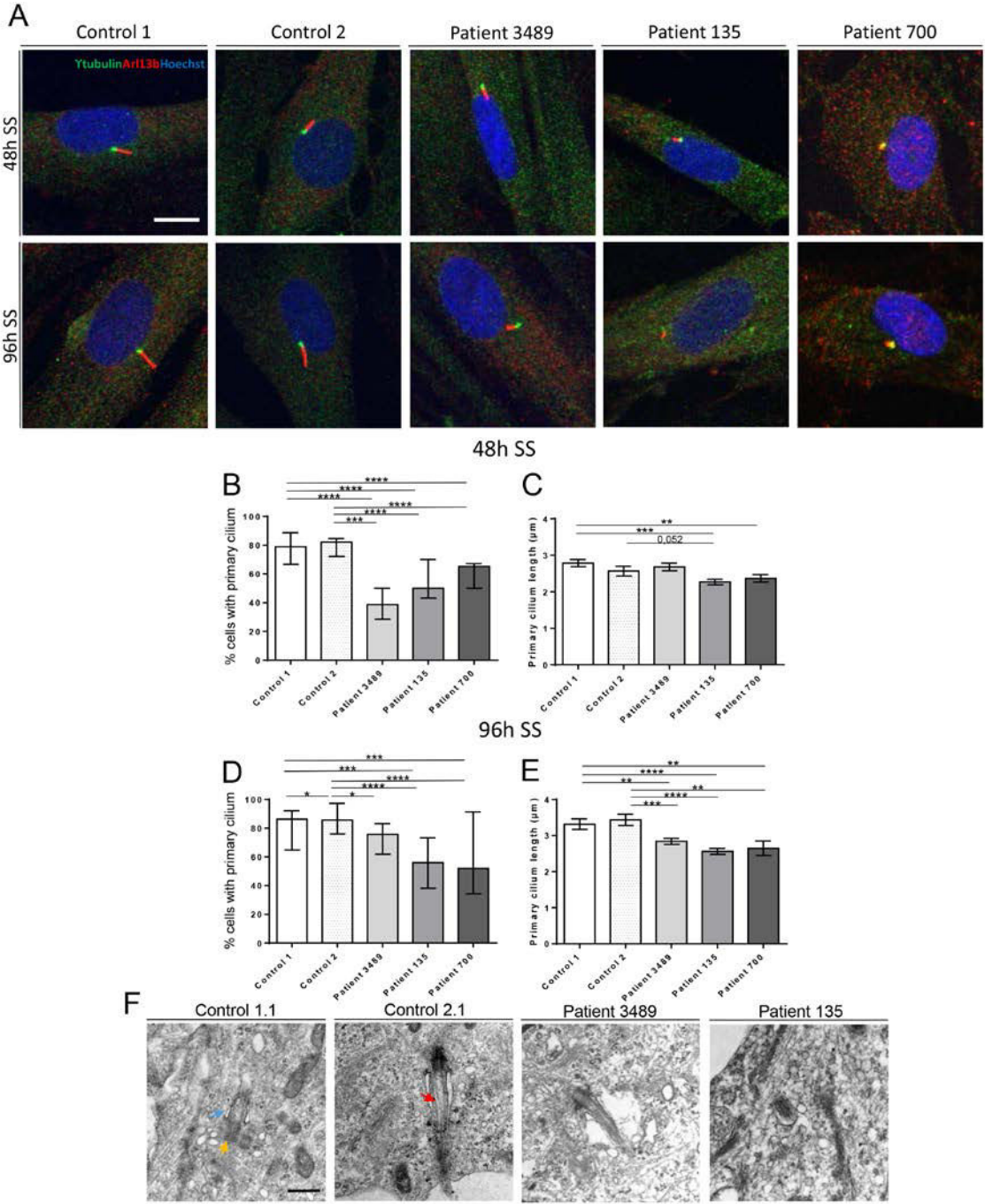
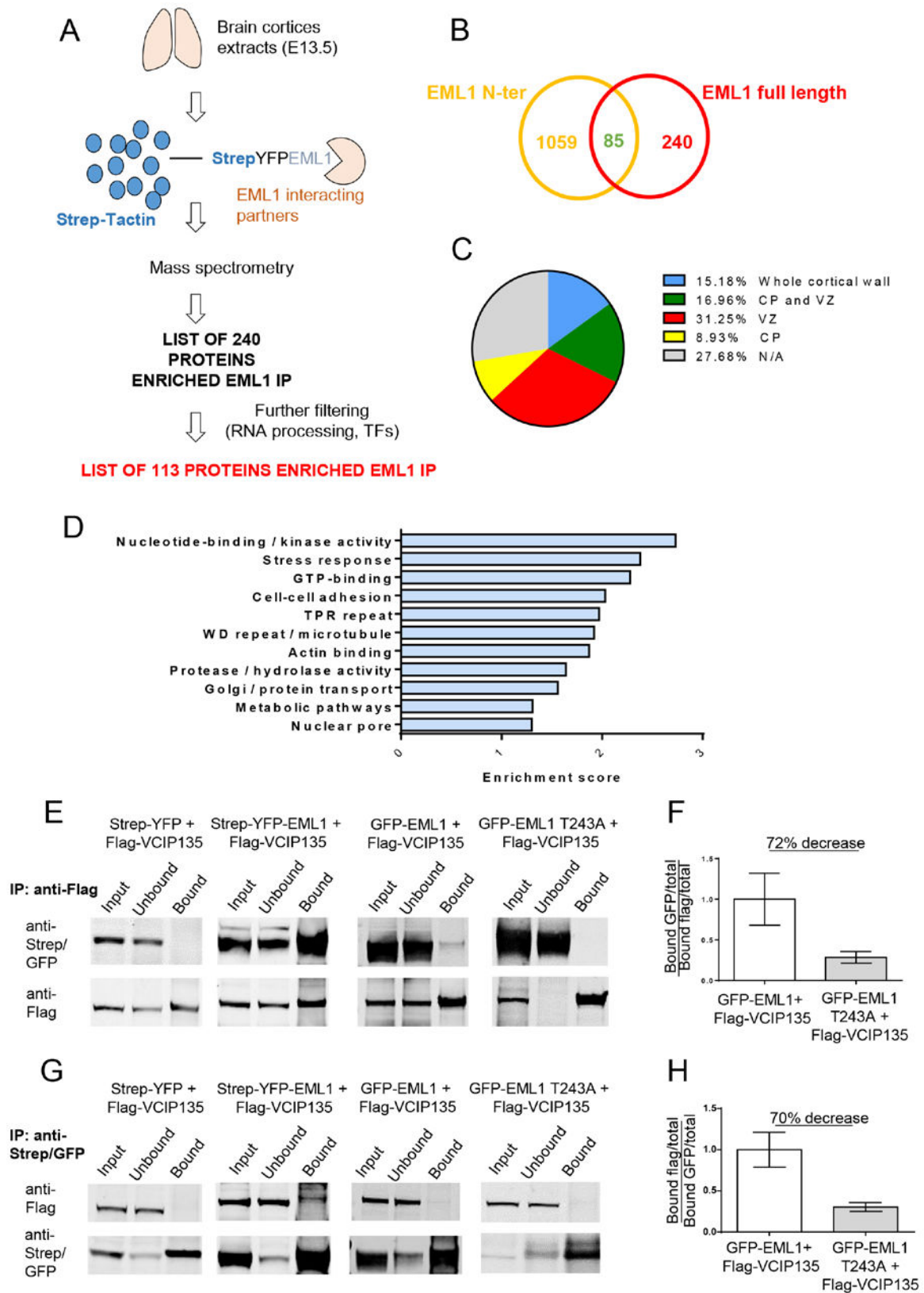


Figure 5



**Figure 6**

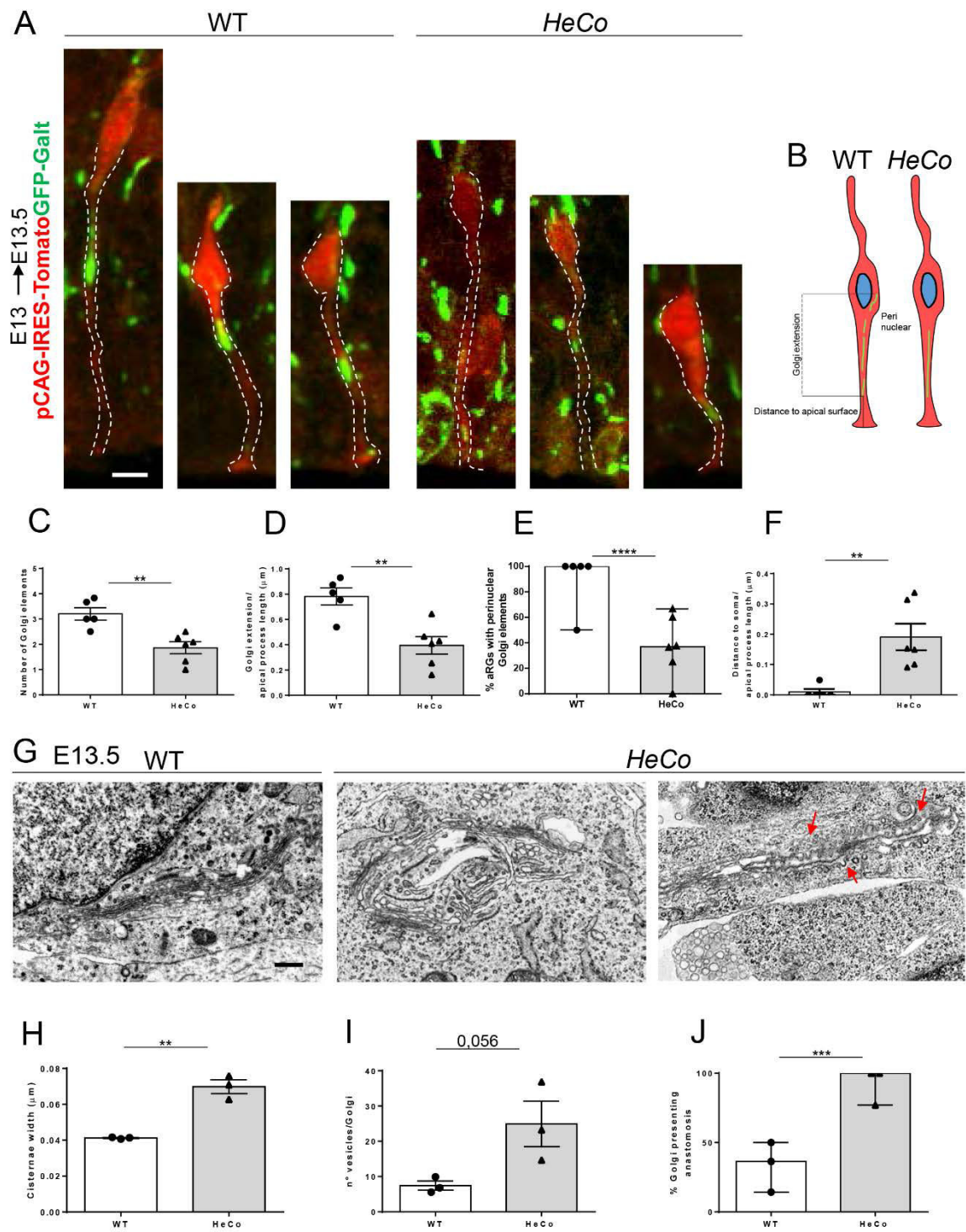
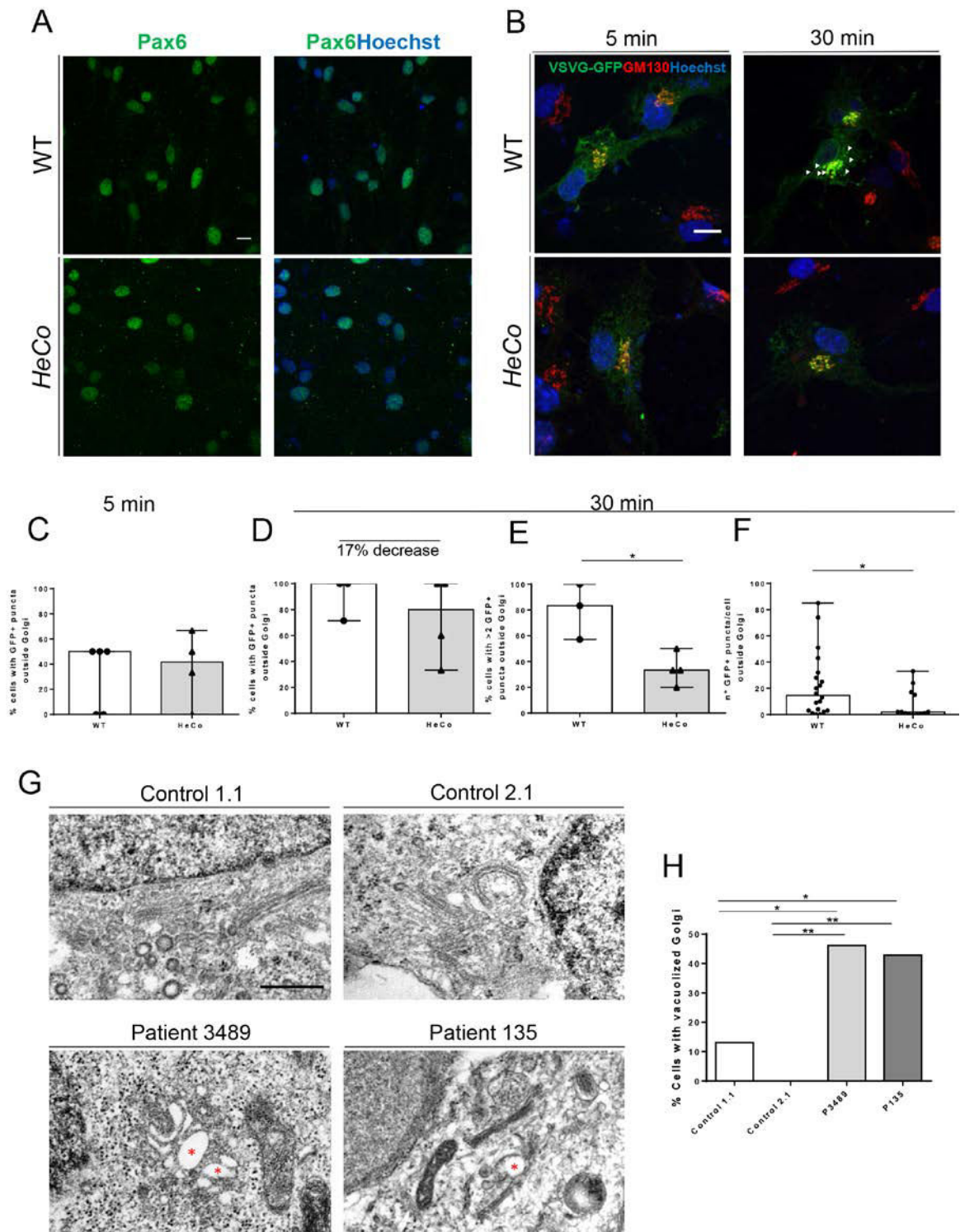
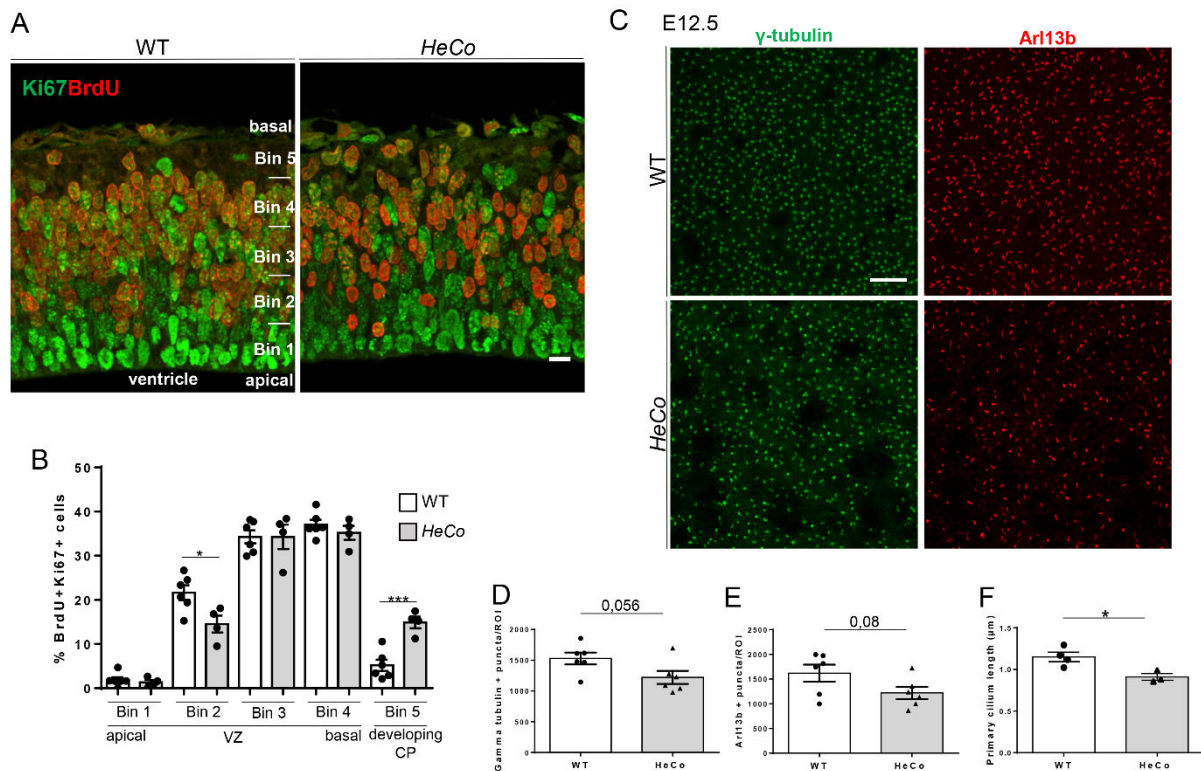
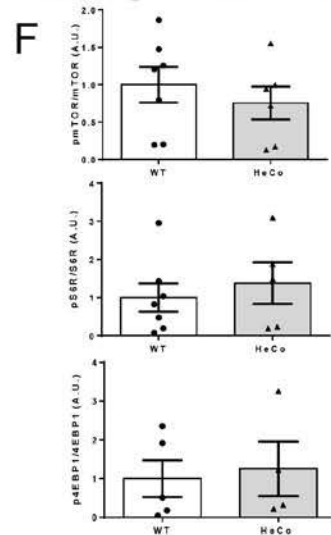
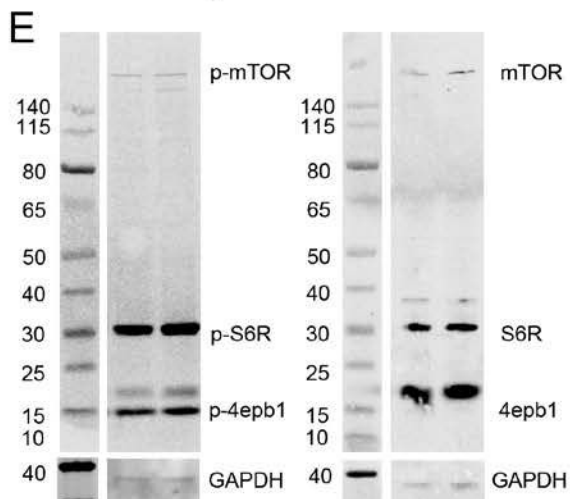
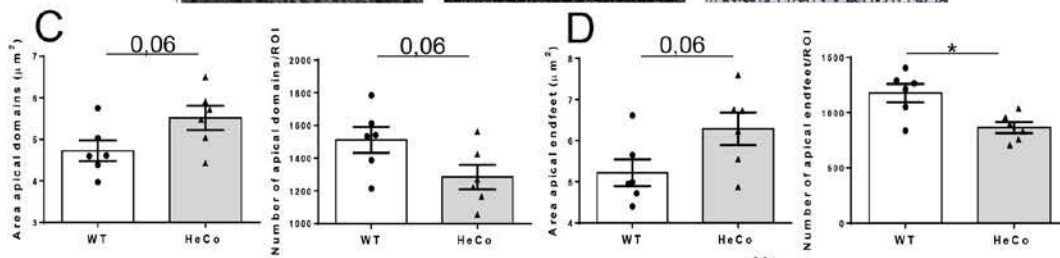
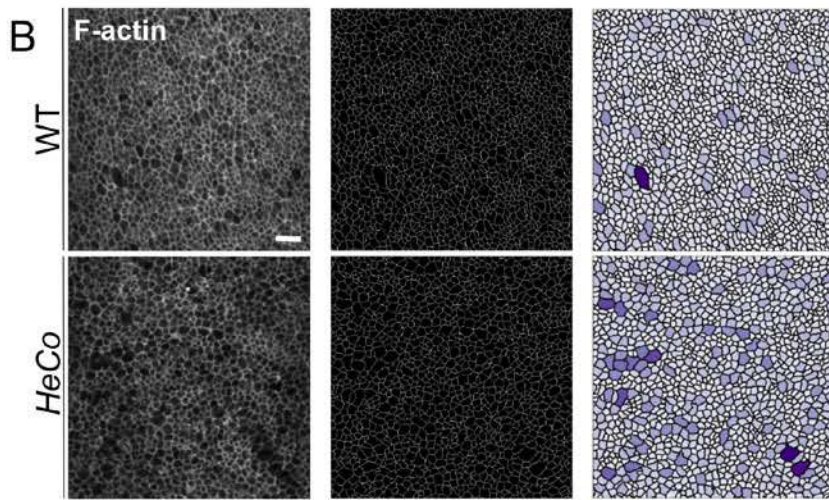
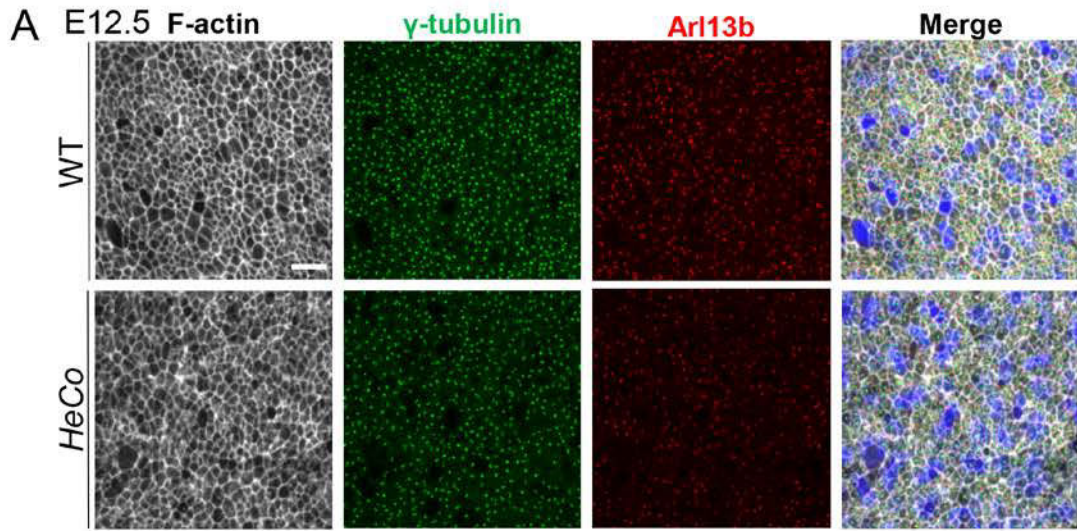


Figure 7





**Figure S1. Ectopic progenitors in *HeCo* mice at E12.5 but no major changes in  $\gamma$ -tubulin+ and Arl13b+ puncta numbers. Related to Figure 2.** A) Representative images of WT and *HeCo* cortices at E12.5, immunostained for Ki67 (green) and BrdU (red) after a 30 min BrdU-pulse. An example of the binning procedure is shown in the WT image. B) Quantification of percentage of Ki67+BrdU+ cells present in each of the five bins in WT (n=5 from 3 litters) and *HeCo* (n=4 from 2 litters) cortices. Bins 1-4 span across the ventricular zone (VZ). Bin 5 spans across the developing cortical plate (CP). C) *En face* confocal imaging of the WT and *HeCo* ventricular surface showing  $\gamma$ -tubulin (green) and Arl13b (red) immunostainings. D) Quantification of  $\gamma$ -tubulin+ puncta per ROI in WT and *HeCo*. Each point represents an embryo (n=6 from 3 litters for both conditions). E) Quantification of Arl13b+ puncta per ROI in WT and *HeCo*. Each point represents an embryo (n=6 from 3 litters for both conditions). F) Quantification of primary cilia length in WT (n=4 from 2 litters) and *HeCo* (n=3 from 3 litters). Each point represents an embryo. Scale bar 10  $\mu$ m, mean  $\pm$  SEM, one-way ANOVA followed by unpaired t-test (B), unpaired t-test (D, E, F), \*\*p<0.01, \*p<0.05.





**Figure S2. Apical domains do not show major differences in the *HeCo* VS at E12.5 and there are no changes in mTOR activity. Related to Figure 2.** A) *En face* confocal imaging of the WT and *HeCo* ventricular surface with immunodetections for F-actin (white),  $\gamma$ -tubulin (green) and Arl13b (red). B) F-actin immunostainings, segmentation (middle panel, Tissue Analyzer) and color-coded image using area as parameter (right panel, CellProfiler) C) Quantification of apical domain area and number in WT and *HeCo*. Each point represents an embryo (n=6 from 3 litters for both conditions). D) Quantification of apical endfeet area and number in WT and *HeCo*. Each point represents an embryo (n=6 from 3 litters for both conditions). E) Representative Western blot of WT and *HeCo* cortex lysates (E13.5) for phosphorylated (left) and non-phosphorylated (right) proteins involved in the mTOR pathway (mTOR, S6R, 4EPB1). F) Quantifications from Western blots, with band intensities normalized to GAPDH. The ratio of the phosphorylated form to the total protein is shown. pmTOR/mTOR WT n=7 embryos from 2 litters, *HeCo* n=6 embryos from 2 litters. pS6R/S6R WT n=7 embryos from 2 litters, *HeCo* n=5 embryos from 2 litters, p4EPB1/4EPB1 WT n=5 embryos from 2 litters, and *HeCo* n=4 embryos from 2 litters. Each point represents an embryo. Scale bar 10  $\mu$ m, mean  $\pm$  SEM, unpaired t-test, \*p<0.05.

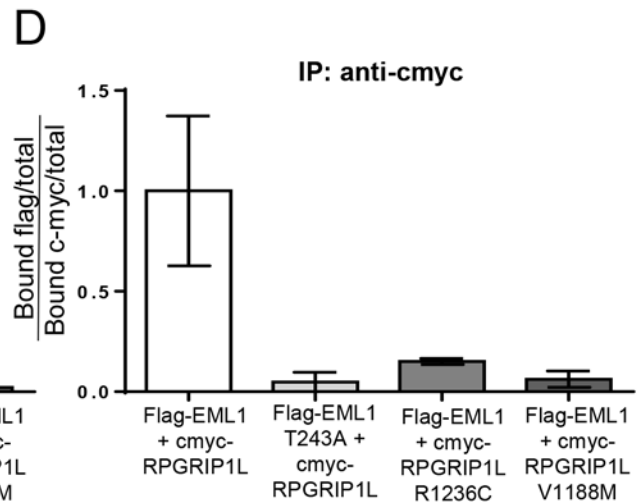
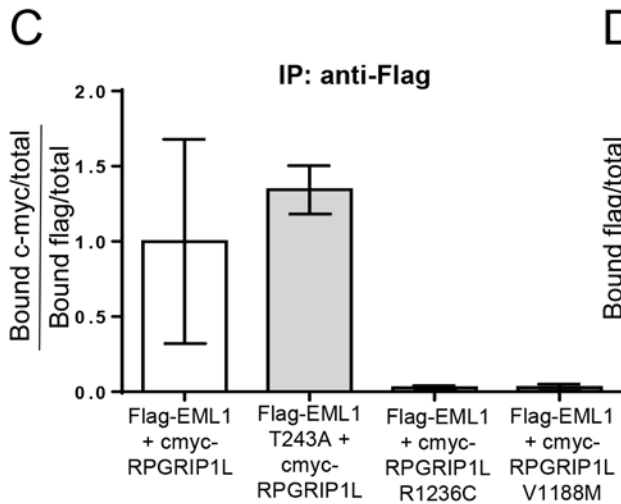
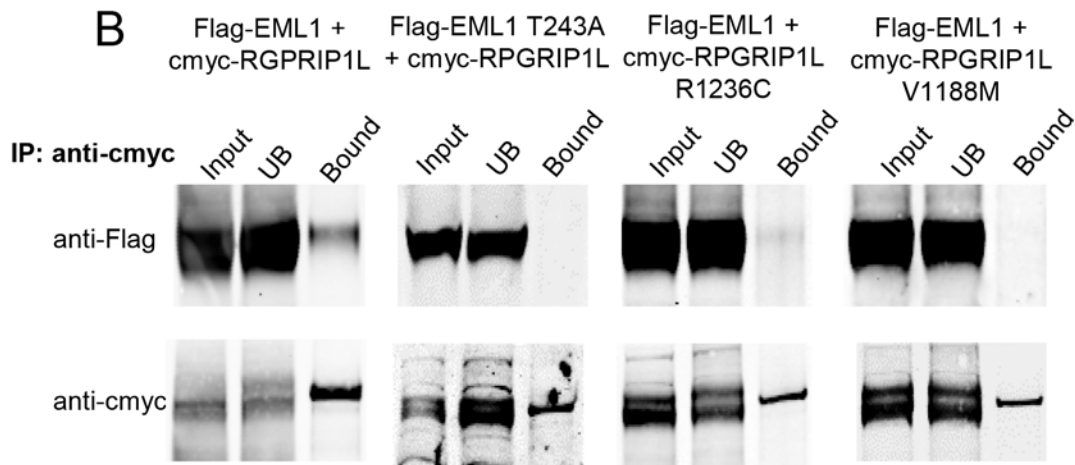
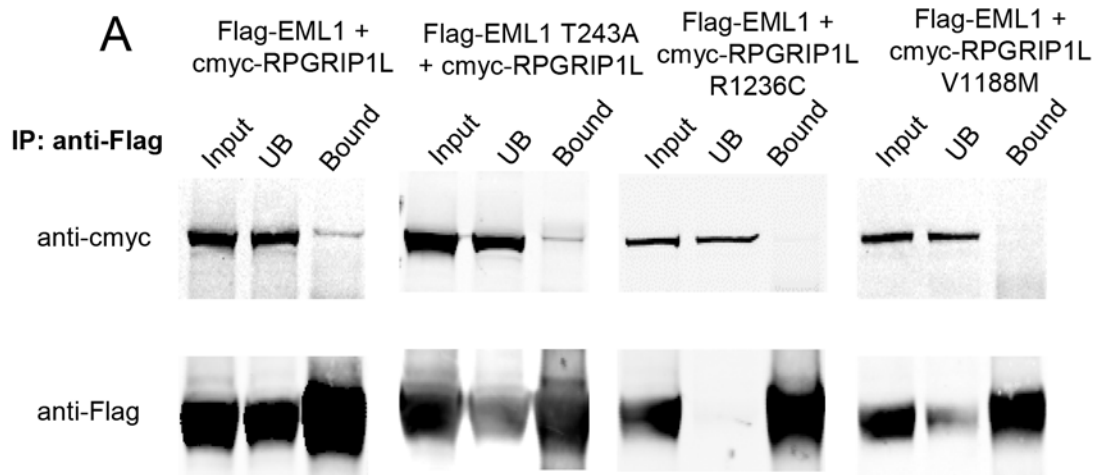
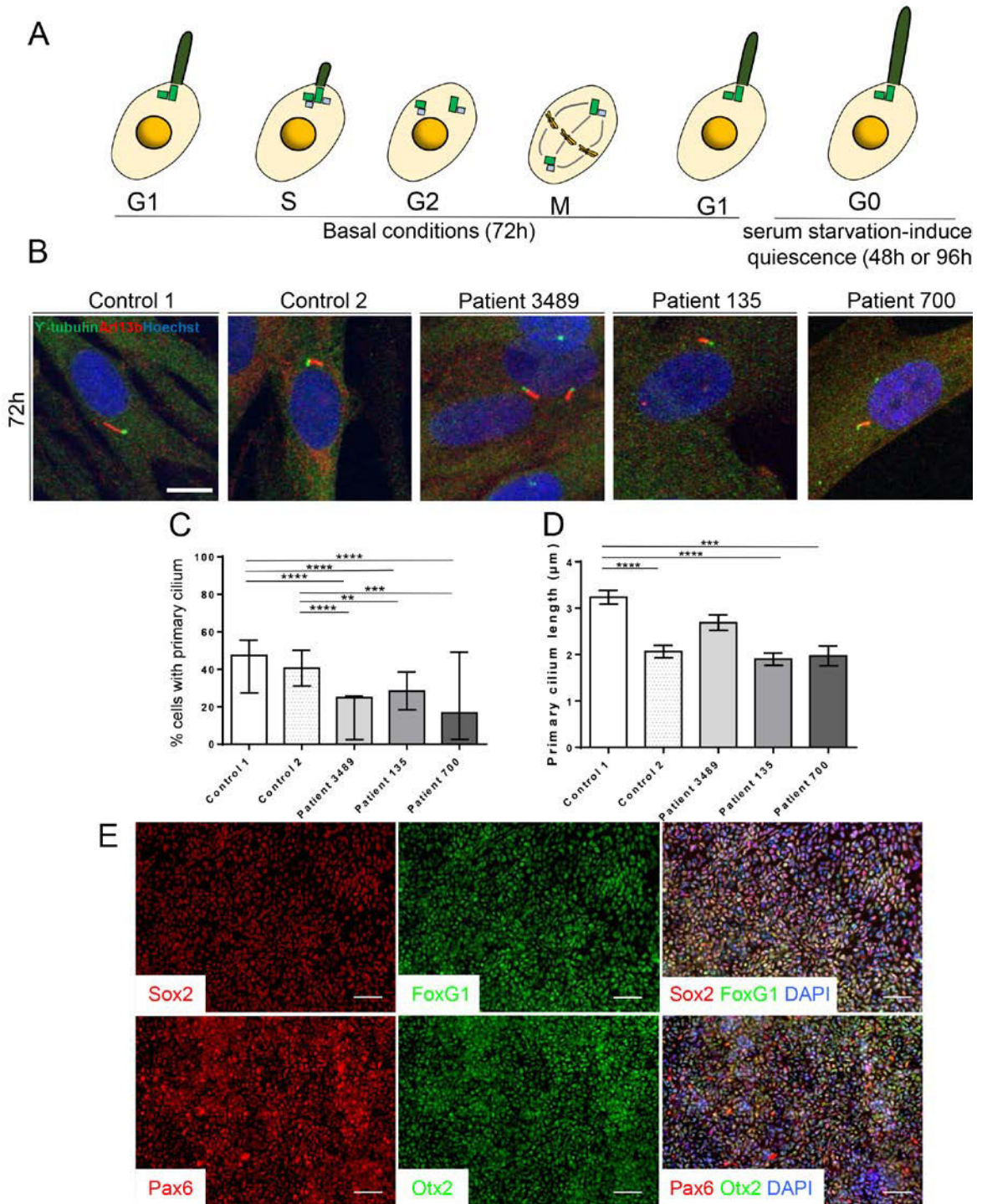
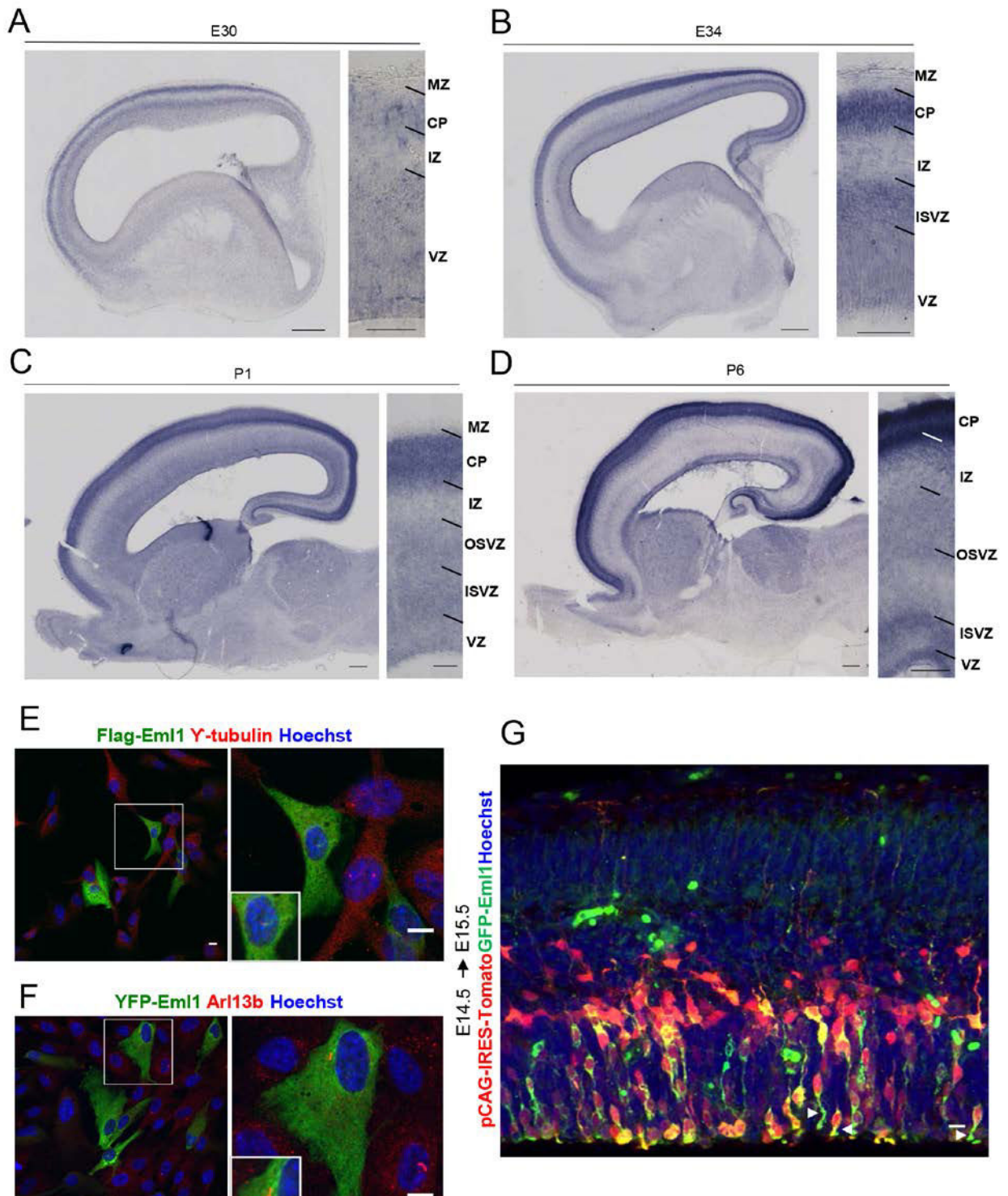


Figure S3. Patient mutations in *EML1* and *RPGRIP1L* alter their interaction. Related to Figure 3. A) Representative Western blot of immunoprecipitation with anti-Flag when co-transfecting Flag-EML1 with c-myc-RPGRIP1L, Flag-EML1-T243A with c-myc-RPGRIP1L, Flag-EML1 with c-myc-RPGRIP1L-R1236C, Flag-EML1 with RPGRIP1L-V1188M (n=3 experiments per condition). B) Representative Western blot of immunoprecipitation with anti-c-myc, same conditions as in a) (n=3 experiments per condition). C) Quantification of immunoprecipitation experiments comparing the amount of RPGRIP1L bound to EML1 in WT and mutant conditions. The bound protein was normalized to total levels of the protein. D) Quantification of immunoprecipitation experiments comparing the amount of EML1 bound to RPGRIP1L in WT and mutant conditions. The bound protein was normalized to total levels of the protein. Mean  $\pm$  SEM.

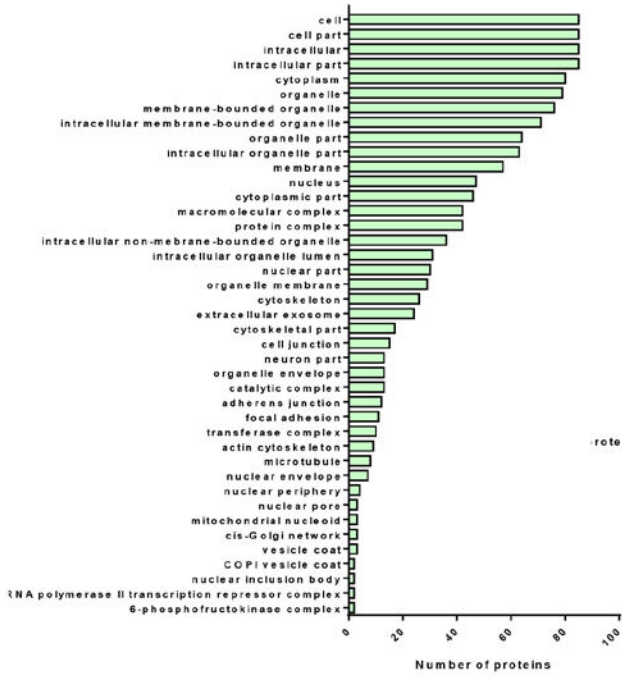


**Figure S4. Primary cilium length in patient fibroblasts under basal conditions. hiPSC-derived cortical progenitor 2D culture model. Related to Figure 4.** A) Schematic representation of experimental approach. Fibroblasts were cultured and analyzed either at basal conditions, 48 or 96h after serum starvation (SS). B) Representative images of immunocytochemistry for  $\gamma$ -tubulin (green) and Arl13b (red) in control (control 1 and 2) and patient fibroblasts (P3489, P135, P700) in basal conditions (72h) C) Percentage of fibroblasts presenting a primary cilium in basal conditions. 2-4 experiments per condition. D) Quantifications of primary cilium length in control and patient fibroblasts in basal conditions. n= 24-109 primary cilia from 2-4 experiments. E) Representative images of hiPSC-derived cortical progenitors stained for the neural stem cell marker Sox2 and the forebrain markers FoxG1, Pax6 and Otx2. Scale bar 10  $\mu$ m (B), 50  $\mu$ m (E), mean  $\pm$  SEM, one-way ANOVA followed by unpaired t-test, \*\*\*\*p<0.0001, \*\*\*p<0.001, \*\*p<0.01.

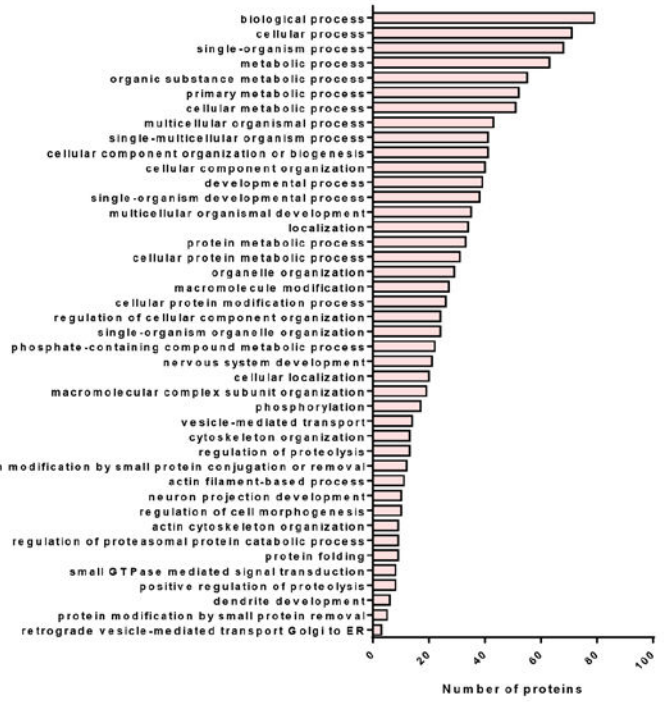


**Figure S5. *Eml1* expression in the ferret developing cortex and recombinant EML1 localization in RPE1 cells and in the mouse neuroepithelium. Related to Figure 4 and 5.** *In situ* hybridization for *Eml1* in ferret sagittal sections at E30 (A), E34 (B), P1 (C) and P6 (D). E) Representative images of RPE1 cells transfected with Flag-Eml1 (green) and immunostained for  $\gamma$ -tubulin (red). F) Representative images of RPE1 cells transfected with YFP-Eml1 (green) and immunostained for Arl13b (red). G) Confocal image of the cortical wall of a E15.5 embryo electroporated with pCAG-IRES-Tomato (aRG morphology) and EGFP-EML1 at E14.5. White arrow heads point to EGFP+ apical processes. VZ: ventricular zone, ISVZ: inner subventricular zone, OSVZ: outer subventricular zone, IZ: intermediate zone, CP: cortical plate, MZ: marginal zone. Scale bar low magnification images: 500  $\mu$ m, scale bar high magnification images: 100  $\mu$ m (B, C, D), 50  $\mu$ m (A), 10  $\mu$ m (E, F, G).

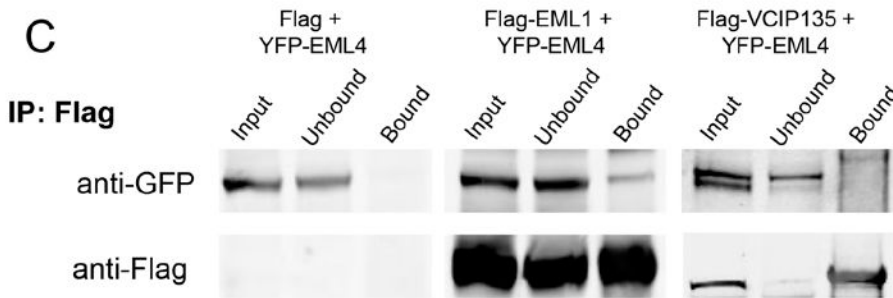
### A Cellular component



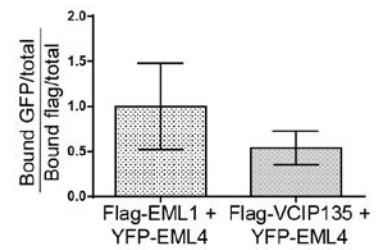
### B Biological process



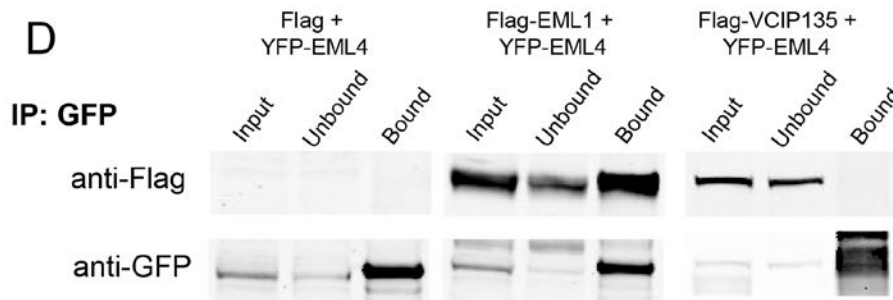
### C



### E



### D



### F

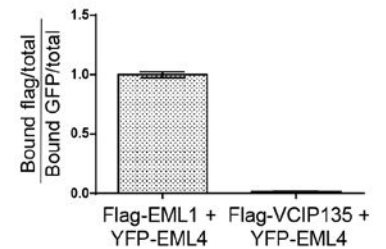
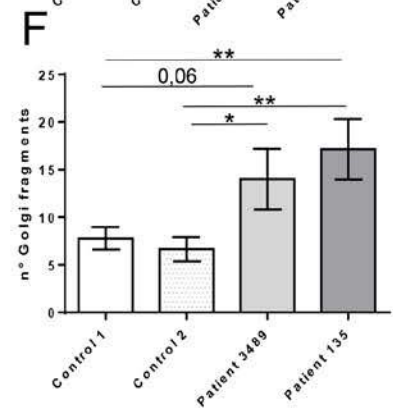
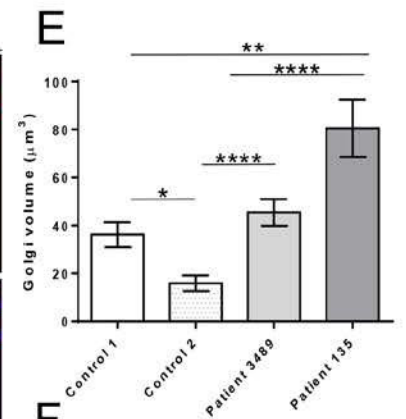
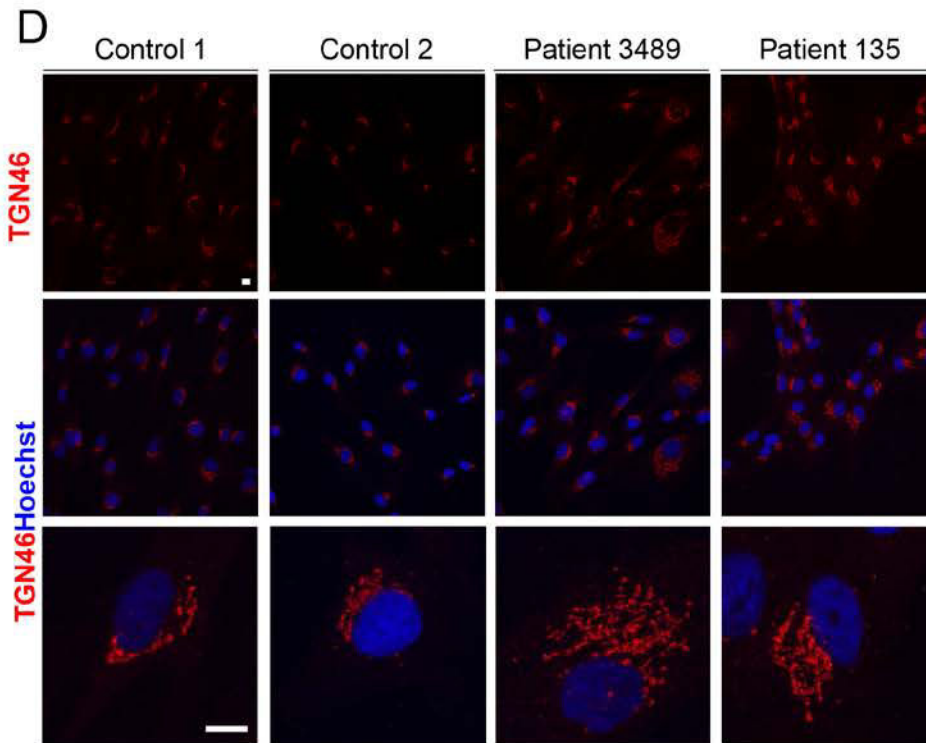
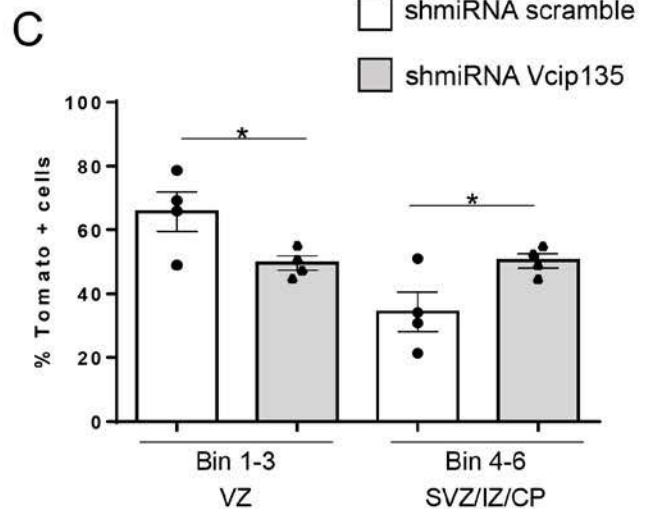
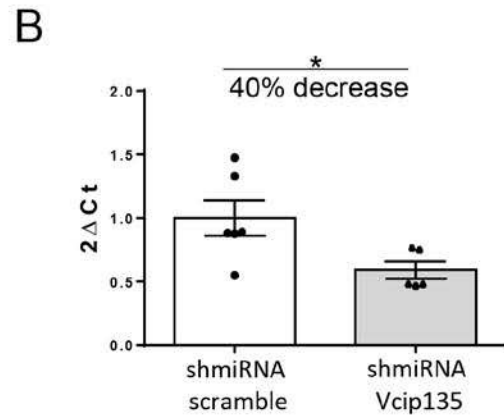
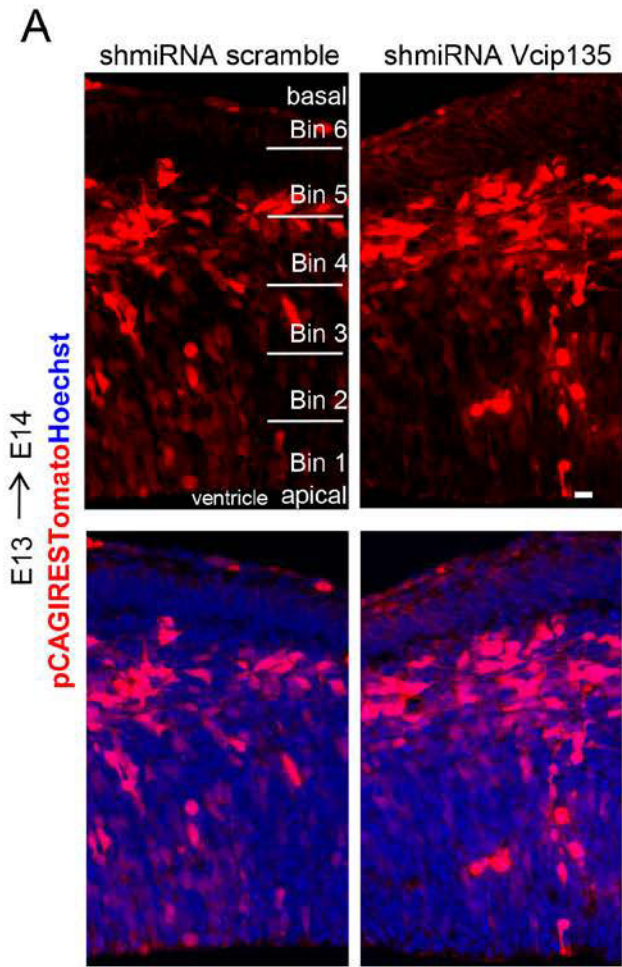




Figure S6. Mass spectrometry analyses and validation of EML1-interacting partners: EML4 and VCIP135. Related to Figure 5. A) Gene Ontology analyses (STRING) for cellular component. B) Gene Ontology analyses (STRING) for biological process. C) Representative Western blot of immunoprecipitation with Flag when co-transfecting Flag with YFP-EML4, Flag-EML1 with YFP-EML4 and Flag-VCIP135 with YFP-EML4 (at least 2 experiments per condition). D) Representative Western blot of immunoprecipitation with GFP when co-transfecting Flag with YFP-EML4, Flag-EML1 with YFP-EML4 and Flag-VCIP135 with YFP-EML4 (at least 2 experiments per condition). E-F) Quantification of immunoprecipitation experiments comparing the amount of EML1 or VCIP135 bound to EML4. The bound protein was normalized to total levels of the protein (F-H). Mean  $\pm$  SEM.



**Figure S7. Knockdown of Vcip135 in the mouse neuroepithelium leads to an altered distribution of electroporated cells. EML1 patient fibroblast show abnormal Golgi apparatus. Related to Figure 5 and 7.** A) Representative images of brains electroporated with a shmiRNA scramble or shmiRNA Vcip135 construct combined with pCAG-IRES-Tomato. B) RT-qPCR results after transfection of constructs in Neuro2A cells.  $2\Delta Ct$  values normalized to shmiRNA scramble condition. Each point represents one experiment. C) Quantification of percentage of Tomato+ cells present in each of the six bins in shmiRNA scramble (n=4 from 2 litters) and shmiRNA Vcip135 (n=4 from 2 litters) cortices. Bins 1-3 span across the VZ. Bins 4-6 span across the developing SVZ, IZ and CP. Each point represents an embryo. D) Representative images of TGN46 (red) immunostainings in control and patient fibroblasts. E) Quantifications of Golgi volume. F) Quantification of the number of fragments per Golgi. n= 20-23 cells per condition from 2 different experiments. Scale bar 10  $\mu$ m, mean  $\pm$  SEM, unpaired t-test (B) and one-way ANOVA followed by unpaired t-test (C, E, F), \*\*\*\*p<0.0001, \*\*p<0.01, \*p<0.05.

**Table S1. Exome sequencing of P700 family. Related to Figure 3.**

Gene	<i>RPGRIP1L</i>	<i>PBDC1</i>	<i>NYX</i>	<i>ZDBF2</i>
Genomic position	16_53639522_G_A	X_75392978_C_T	X_41333757_A_C	2_207174436dup
Mode of transmission	AR Compound	X-linked	X-linked	<i>De novo</i>
Dbsnp	rs151332923 rs142317242	rs868964354	rs745741032	rs777866286
Reference	NM_015272.2 NM_015272.2	NM_016500.3	NM_022567.2	NM_020923.2
cDNA	c.3706C>T c.3562G>A	c.5C>T	c.1051A>C	c.5184dup
Protein	p.Arg1236Cys p.Val1188Met	p.Ala2Val	p.Met351Leu	p.Arg1729Thrfs*7
Polyphen	Benign Benign	Benign	Benign	
SIFT	Deleterious Tolerated	Tolerated	Tolerated	
Inherited from	Father Mother	Mother	Mother	

**Table S2. Clinical history of P700. Related to Figure 3.**

Clinical features	P700
Sex	Male
Birth (gestational week)	39
Birth weight	3950 g
Birth Head circumference	37 cm
<b>Age at investigation</b>	<b>15 y</b>
<i>Growth parameters</i>	
Head circumference (cm)	51 cm (>3DS)
Height (cm)	168.5 (M)
Weight (kg)	79 kg (+2,5DS)
Developmental delay	Severe ID
Feeding problems	absent
Neurological signs	Left hemiplegia
Seizures	Focal (right frontal and temporal)
Response to AED	refractory
Age of seizure onset	15 months
Ophthalmological signs – ocular fundus	Normal fundus
Small/ tilted optic discs	-
Myopia	-
Amblyopia	Left hemianopsia
Other	Oculomotor apraxia
Hemolytic anemia	-

**Table S3. Mass spectrometry protein list of embryonic cortical EML1 interactors. Related to Figure 5.** A  $\geq 1.5$  fold-change and  $\geq 3$  peptides/protein were used as criteria to obtain a list of EML1 interacting partners (240). Protein ratios were computed as the geometrical mean of related peptides. To estimate ratio significance, a two-tailed *t test* was performed and *p*-values were adjusted with a Benjamini–Hochberg FDR procedure with a control threshold set to 0.05. Further filtering was performed (nucleic acid-associated proteins) refining the list of EML1 protein partners (113) (list provided below).

**Table S4. Gene Ontology analyses of the 113-protein list of EML1 potential interactors with the DAVID tool. Related to Figure 5.** (Gene Ontology analyses not provided for simplicity, available upon request).

**Table S5. List of Golgi and primary cilium related proteins in EML1 N-ter and full length screens. Related to Figure 5.** See tables below.

**Table S6. Gene Ontology analyses of the 113-protein list of EML1 potential interactors with STRING. Related to Figure 5.** (Gene Ontology analyses not provided for simplicity, available upon request).

**List of EML1 candidate protein interacting partners (113)**

Gene & Synonyms	Description
Pfkm,Pfk-m,Pfka	ATP-dependent 6-phosphofructokinase, muscle type
Atad3,Atad3a,Kiaa1273	ATPase family AAA domain-containing protein 3
Nckap1,Hem2,Kiaa0587,Nap1	Nck-associated protein 1
Nxf1,Tap	Nuclear RNA export factor 1
Coro2b	Coronin-2B
Pfkp,Pfkc	ATP-dependent 6-phosphofructokinase, platelet type
Tubb2b	Tubulin beta-2B chain
Zc2hc1a,Fam164a	Zinc finger C2HC domain-containing protein 1A
Map7d1,Kiaa1187,Mtap7d1	MAP7 domain-containing protein 1
Irs4	Insulin receptor substrate 4
Map4k4,Nik	Mitogen-activated protein kinase kinase kinase kinase 4
Tmco1	Transmembrane and coiled-coil domain-containing protein 1
Hyou1,Grp170	Hypoxia up-regulated protein 1
Llgl1,Llglh	Lethal(2) giant larvae protein homolog 1
Rala,Ral,Ral-a	Ras-related protein Ral-A
Map4,Mtap4	Microtubule-associated protein 4
Usp15,Kiaa0529	Ubiquitin carboxyl-terminal hydrolase 15
Map6,Mtap6	Microtubule-associated protein 6
Usp7,Hausp	Ubiquitin carboxyl-terminal hydrolase 7
Kti12	Protein KTI12 homolog
Scyl1	N-terminal kinase-like protein
Dnajc7,Ttc2	DnaJ homolog subfamily C member 7
Anapc7,Apc7	Anaphase-promoting complex subunit 7
Cd33,Siglec3	Myeloid cell surface antigen CD33
Hdac2,Yy1bp	Histone deacetylase 2
Tmem33,Db83	Transmembrane protein 33
Picalm,Calm,Fit1	Phosphatidylinositol-binding clathrin assembly protein
Letm1	LETM1 and EF-hand domain-containing protein 1, mitochondrial

Tpi1,Tpi	Triosephosphate isomerase
Vprbp,Dcaf1,Kiaa0800	Protein VPRBP
Nup50,Npap60	Nuclear pore complex protein Nup50
Senp1,Supr2	Sentrin-specific protease 1
Arcn1,Copd	Coatomer subunit delta
Aipl1	Aryl-hydrocarbon-interacting protein-like 1
C2cd2l,Tmem24	C2 domain-containing protein 2-like
Ube4a {ECO:0000312 MGI:MGI:2154580},Ufd2b {ECO:0000312 MGI:MGI:2154580}	Ubiquitin conjugation factor E4 A
Kif22	Kinesin-like protein KIF22
Slc25a17,Pmp34,Pmp35	Peroxisomal membrane protein PMP34
Enc1,Enc-1	Ectoderm-neural cortex protein 1
Hspa4l,Apg1,Hsp4l,Osp94	Heat shock 70 kDa protein 4L
Rab6a,Rab6,MNCb-1660	Ras-related protein Rab-6A
G6pdx,G6pd,G6pd-1	Glucose-6-phosphate 1-dehydrogenase X
Ctnna2,Catna2	Catenin alpha-2
Ophn1	Oligophrenin-1
Anp32b,Pal31	Acidic leucine-rich nuclear phosphoprotein 32 family member B
Etv3,Mets,Pe1	ETS translocation variant 3
Lima1,D15Erd366e,Eplin	LIM domain and actin-binding protein 1
Rheb	GTP-binding protein Rheb
Hn1	Hematological and neurological expressed 1 protein
Arf4	ADP-ribosylation factor 4
Naa40,Nat11	N-alpha-acetyltransferase 40
Fam171a2	Protein FAM171A2
Gnpat,Dhapat	Dihydroxyacetone phosphate acyltransferase
Tox4	TOX high mobility group box family member 4
Eml4	Echinoderm microtubule-associated protein-like 4
Eml1	Echinoderm microtubule-associated protein-like 1
Epb41I5,Epb4.1I5,Kiaa1548	Band 4.1-like protein 5
Ckap4	Cytoskeleton-associated protein 4
Lrrc59	Leucine-rich repeat-containing protein 59
Hspa1l,Hsc70t	Heat shock 70 kDa protein 1-like
Rac1	Ras-related C3 botulinum toxin substrate 1
Pnpla6,Nte	Neuropathy target esterase
Acp1	Low molecular weight phosphotyrosine protein phosphatase
Dgke	Diacylglycerol kinase epsilon
Cep170,Kiaa0470	Centrosomal protein of 170 kDa
Nr2e1,Tll,Tlx	Nuclear receptor subfamily 2 group E member 1
Gnl3,Ns	Guanine nucleotide-binding protein-like 3
Senp3,Smt3ip,Smt3ip1	Sentrin-specific protease 3
Myo19,Myohd1	Unconventional myosin-XIX

Stub1,Chip	STIP1 homology and U box-containing protein 1
Armcx3	Armadillo repeat-containing X-linked protein 3
Csnk1e	Casein kinase I isoform epsilon
Clpx	ATP-dependent Clp protease ATP-binding subunit clpX-like, mitochondrial
Aip	AH receptor-interacting protein
Csnk1d,Hckid	Casein kinase I isoform delta
Anp32a,Anp32,Lanp	Acidic leucine-rich nuclear phosphoprotein 32 family member A
Csnk1g3	Casein kinase I isoform gamma-3
Sbf1,Kiaa3020,Mttr5	Myotubularin-related protein 5
Cbr4	Carbonyl reductase family member 4
Sbk1,Sbk	Serine/threonine-protein kinase SBK1
Sox5,Sox-5	Transcription factor SOX-5
Usmg5,Dapit	Up-regulated during skeletal muscle growth protein 5
Hagh,Glo2	Hydroxyacylglutathione hydrolase, mitochondrial
Abhd12	Monoacylglycerol lipase ABHD12
Ufm1	Ubiquitin-fold modifier 1
Txn1,Trp32,Txn1	Thioredoxin-like protein 1
Mepce,Bccin3,Bipl1,D5Wsu46e	7SK snRNA methylphosphate capping enzyme
Pdcl,PhLP1	Phosducin-like protein
Usp9x,Faf1,Fam	Probable ubiquitin carboxyl-terminal hydrolase FAF-X
Pik3r1	Phosphatidylinositol 3-kinase regulatory subunit alpha
Myrip	Rab effector MyRIP
Csnk1a1	Casein kinase I isoform alpha
Limk2	LIM domain kinase 2
Clcn7,Clc7	H(+)/Cl(-) exchange transporter 7
Glipr2,Gapr1	Golgi-associated plant pathogenesis-related protein 1
Cdk4,Crk3	Cyclin-dependent kinase 4
Sccpdh	Saccharopine dehydrogenase-like oxidoreductase
Nepro	Protein nepro
Kif21a,Kiaa1708	Kinesin-like protein KIF21A
Rnf138,Trif	E3 ubiquitin-protein ligase RNF138
Gna12,Gna-12	Guanine nucleotide-binding protein subunit alpha-12
Zadh2	Zinc-binding alcohol dehydrogenase domain-containing protein 2
Cap1,Cap	Adenylyl cyclase-associated protein 1
Dcaf7,Han11,Wdr68	DDB1- and CUL4-associated factor 7
Nup98	Nuclear pore complex protein Nup98-Nup96
Hbb-b2	Hemoglobin subunit beta-2
Ccdc136	Coiled-coil domain-containing protein 136
Vcpi1,Vcip135	Deubiquitinating protein VCIP135

Dlg3,Dlgh3	Disks large homolog 3
Gmpr2	GMP reductase 2
Iqcf5	IQ domain-containing protein F5
Snap23,Sndt	Synaptosomal-associated protein 23
Rnd2,Arhn,Rho7,Rhon	Rho-related GTP-binding protein RhoN

**List of Golgi and primary cilium related proteins in EML1 N-ter and full length screens (proteins in blue: common to EML1 N-ter and full length screens).**

**Proteins related to the primary cilium**

EML1 full length screen	
Protein	Reference
Coro2b	Castro-Sanchez et al 2017
Map4	Zanhleiter et al 2015
Hdac2	Kobayashi et al 2017
Aipl1	Hidalgo de Quintana et al 2015
Enc1,Enc-1	Qian et al 2013
Rab6a,Rab6,MNCb-1660	Ward et al 2009
Arf4	Mazelova et al 2009, Ward et al 1011, Wang et al 2012, Wang et al 2017, Folling et al 2014
Rac1	Madhivanan et al 2012
Cep170,Kiaa0470	Kodani et al 2013
Stub1,Chip	Porpora et al 2018
Csnk1d,Hckid	Greer et al 2014
Pdcl,PhLP1	Pusapati et al 2018
Usp9x,Fafl,Fam	Das et al 2017, Reijnders et al 2016
Limk2	Kim et al 2015
Nup98	Endicott et al 2015
Dlg3,Dlgh3	Gegg et al 2014

EML1 N-ter screen	
Protein	Reference
Macf1	May Simera et al 2016
Par3	Sfakianos et al 2007
Staufen2	Kusek et al 2012
Csnk1d	Greer et al 2014
Pip5k1a	Xu et al 2018
Apc2	Morgan et al 2002
Cep78	Nikopoulos et al 2016



Ftm,Rpgr1p1l	Delous et al 2007, Besse et al 2011, Laclef et al 2016, Andreu Cervera et al 2019
Plk1	Kim et al 2016, Zhang et al 2017
Nde1	Gabriel et al 2016
Akap5,Akap150	Choi et al 2011
ANK3	Kizhatil et al 2009
Map9	Jensen et al 2016
Neurl4	Loukil et al 2017
Numb	Ramamurthy et al 2014
Sin1, Mapkap1	Yuan et al 2015
Tsg101	Leitch et al 2014
Usp8	Troilo et al 2014, Kasahara et al 2018
<a href="#">Cep170</a>	Kodani et al 2013
Clasp2	Dillon et al 2017
Kif2a	Miyamoto et al 2015, Ding et al 2019, Broix et al 2018, Miyamoto et al 2015
Vangl2	May Simera et al 2010
Kifc1	Lee et al 2018, Zhu et al 2014
Gsk3b	Thoma et al 2007, Zhang et al 2015
Hdac6	Deakin and Turner 2014, Haggarty et al 2003
Kif27	Wilson et al 2009
Kif7	Du toit 2014
Ndel1	Inaba et al 2016

## Proteins related to the Golgi apparatus

EML1 full length screen	
Protein	Reference
Rala,Ral,Ral-a	Luo et al 1998, Spiczka and Yeaman 2008, Teodoro et al 2013, Personnic et al 2014
Map4,Mtap4	Zanhleiter et al 2015
<a href="#">Map6,Mtap6</a>	Gory Faure et al 2014
Scyl1	Burman et al 2008, Burman et al 2010, Hamlin et al 2014, Witkos et al 2019
Picalm,Calm,Fit1	Tebar et al 1999,Sahlender et al 2013, Funaki et al 2013
Senp1,Supr2	Zhou et al 2018
Arcn1,Copd	Izumi et al 2016
<a href="#">Kif22</a>	Girisha et al 2016
Rab6a,Rab6,MNcb-1660	Young et al 2005, Jiang and Storrie 2005, Del Nery et al 2006, Rosing et al 2007
Rheb	Hao et al 2018, Buerger et al 2006, Hanker et al 2010, Yadav et al 2013
Arf4	Balch et al 1992, Deretic et al 2005, Mazelova et al 2009, Propoff et al 2011, Wang et al 2012, Wang et al 2017, Folling et al 2014
Ckap4	Schweizer et al 1994,
Rac1	Jou et al 2000, Deretic et al 2004, Wang et al 2005, Meseke et al 2013
<a href="#">Cep170,Kiaa0470</a>	Kolobova et al 2017

Stub1,Chip	Kumar et al 2007
Csnk1d,Hckid	Greer et al 2014
Usp9x,Fafl,Fam	Murray et al 2004, Mouchantaf et al 2006, Xu et al 2010
Myrip	Rojo Pullido et al 2011
Limk2	Acevedo et al 2006
Glipr2,Gapr1	Eberle et al 2002,
Cdk4,Crk3	Fernandez et al 2011
Vcpip1,Vcip135	Uchiyama et al 2006, Zhang and Wang 2015
Snap23,Sndt	Wong et al 1999, Valdez et al 1999, Bertuccio et al 2018

Eml1 N-ter screen	
Protein	Reference
Macf1	Lin et al 2005
Fmnl2	Kage et al 2017
Par3	Odell et al 2012, Matsui et al 2015, Sun et al 2017
Staufen2	Cao et al 2016
Csnk1d,Hckid	Greer et al 2014
Tpx2	Wei et al 2015
Pip5k1a	Anitei et al 2017
Trim3	Labonte et al 2013
Apc2	Jarrett et al 2001
Dab2ip	Keyel et al 2006
Dystonin	Ryan et al 2012, Poliakova et al 2014
Agap1	Jacques et al 2002
Alg2	Janik et al 2003
Ap1m1	Ohno et al 1996
Camsap3	Wang et al 2017
Plk1	Litvak et al 2004, Preisinger et al 2005, Sengupta et al 2010, Truschel et al 2012, Tang et al 2012
Cope	Hara Kuge et al 1994, Faulstich et al 1996
Nde1	Lam et al 2010, Monda et al 2018
Numbl	Zhou et al 2007
Vps4a	Bishop et al 2000
Map6	Gory Faure et al 2014
Birc6	Bartke et al 2004
Clip3	Deng et al 2012
Dlg1	Philippe et al 2013
Jakmip1	Vidal et al 2012
Numb	Zhou et al 2007
Tbce	Schaefer et al 2007, Bellouze et al 2014
Tsg101	Wie et al 1998
Usp8	MacDonald et al 2014, Kawaguchi et al 2018
Dync1h1	Jaarsma and Hoogenraad, 2015

Cep170	Kolobova et al 2017
Clasp2	Dillon et al 2017, Efimov et al 2007, Miller et al 2009
Clasp1	Efimov et al 2007, Miller et al 2009
Vangl2	Merte et al 2010 Yang et al 2013 Ma et al 2018
Ap3d1	Nishimura et al 2003
Kif21b	Labonte et al 2013
Kifc1	She et al 2017, Lee et al 2018
Magi1	Xu et al 2010
Gsk3b	Adachi et al 2010
Mink1	Hu et al 2004
Hdac6	Dubois et al 2017
Kif7	Dafinger et al 2011
Mapk3	Wortzel et al 2015
Ndel1	Lam et al 2010
Ppp2ca	Schmitz et al 2010
Ppp2cb	Schmitz et al 2010
Copa	Todd et al 2013, Watkin et al 2015
Glypican-1	Award et al 2015
Kif22	Girisha et al 2016

### Proteins related to the primary cilium and the Golgi apparatus

EML1 full length screen		
	Primary Cilium	Golgi Apparatus
Protein	Reference	Reference
Map4,Mtap4	Zanhleiter et al 2015	Zanhleiter et al 2015
Rab6a,Rab6,MNcb-1660	Ward et al 2009	Young et al 2005, Jiang and Storrie 2005, Del Nery et al 2006, Rosing et al 2007
Arf4	Mazelova et al 2009, Ward et al 1011, Wang et al 2012, Wang et al 2017, Folling et al 2014	Balch et al 1992, Deretic et al 2005, Mazelova et al 2009, Propoff et al 2011, Wang et al 2012, Wang et al 2017, Folling et al 2014
Rac1	Madhivanan et al 2012	Jou et al 2000, Deretic et al 2004, Wang et al 2005, Meseke et al 2013
Cep170,Kiaa0470	Kodani et al 2013	Kolobova et al 2017
Stub1,Chip	Porpora et al 2018	Kumar et al 2007
Csnk1d,Hckid	Greer et al 2014	Greer et al 2014
Usp9x,Fafl,Fam	Das et al 2017, Reijnders et al 2016 (patients),	Murray et al 2004, Mouchantaf et al 2006, Xu et al 2010
Limk2	Kim et al 2015	Acevedo et al 2006

EML1 N-ter screen		
	Primary Cilium	Golgi Apparatus
Protein	Reference	Reference
Macf1	May Simera et al 2016	Lin et al 2005
Par3	Sfakianos et al 2007	Odell et al 2012, Matsui et al 2015, Sun et al 2017
Staufen2	Kusek et al 2012	Cao et al 2016
Csnk1d,Hckid	Greer et al 2014	Greer et al 2014
Pip5k1a	Xu et al 2018	Anitei et al 2017
Apc2	Morgan et al 2002	Jarrett et al 2001
Plk1	Kim et al 2016, Zhang et al 2017	Litvak et al 2004, Preisinger et al 2005, Sengupta et al 2010, Truschel et al 2012, Tang et al 2012
Nde1	Gabriel et al 2016	Lam et al 2010, Monda et al 2018
Numb	Ramamurthy et al 2014	Zhou et al 2007
Tsg191	Leitch et al 2014	Wie et al 1998
Usp8	Troilo et al 2014, Kasahara et al 2018	MacDonald et al 2014, Kawaguchi et al 2018
Cep170	Kodani et al 2013	Kolobova et al 2017
Clasp2	Dillon et al 2017	Dillon et al 2017, Efimov et al 2007, Miller et al 2009
Vangl2	May Simera et al 2010	Merte et al 2010 Yang et al 2013 Ma et al 2018
Kifc1	Lee et al 2018, Zhu et al 2014	She et al 2017, Lee et al 2018
Gsk3b	Thoma et al 2007, Zhang et al 2015	Adachi et al 2010
Hdac6	Deakin and Turner 2014, Haggarty et al 2003	Dubois et al 2017
Kif7	Du toit 2014	Dafinger et al 2011
Ndel1	Inaba et al 2016	Lam et al 2010

### 2.3 Extra supplementary results related to Uzquiano et al.

As discussed at the end of the discussion section of the manuscript and in the introduction, the primary cilium is a key structure mediating and integrating several signaling pathways. Foerster and colleagues (2017) associated the absence of primary cilia to hyperactivation of mTOR signaling. As described in the manuscript, we

searched for potential alterations in this pathway given the disruption of primary cilia in Eml1-mutant conditions. We did not find any difference at E12.5 and E13.5, most likely indicating that this pathway is not a key player contributing to aRG delamination at early stages of corticogenesis. However, by performing co-immunoprecipitation studies we confirmed an interaction with the mTORC1 signaling

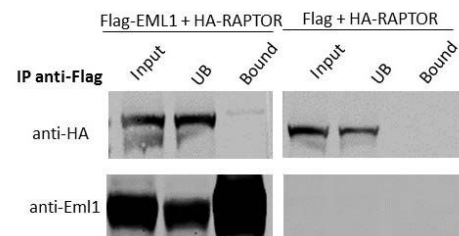


**Figure 48. EML1 interacts with RAPTOR. Representative Western blot of co-immunoprecipitation experiment.** Protocol performed as described in Uzquiano et al. 3 experiments were performed using anti-Flag for immunoprecipitation and 3 further using anti-HA (data not shown).

component Raptor (Figure 48). This result is further addressed in section 4.1 of the discussion. Shh signaling is the main pathway described to be mediated through the primary cilium (Whewey et al., 2018). Briefly, when Shh is not stimulating the cell, the transmembrane receptor Patched1 (Ptch1) is found in the primary cilium, preventing Smoothed (Smo) to enter this cell compartment (Corbit et al., 2005, Rohatgi et al., 2007). The Gli (Gli2 and Gli3) TF full length forms are sequestered at the tip of the cilium by the ciliary protein SuFu (Cooper et al., 2005, Humke et al., 2010) and are being constantly processed in the cytoplasm. Phosphorylation by specific kinases (PKA-GSK3 $\beta$ -CK1) followed by proteosomal processing, results in the production of the Gli short-length repressor form, which translocates to the nucleus to inhibit transcription of target genes. When Shh stimulates the cell, it binds to Ptch1 excluding it from the primary cilium and allowing the entrance of Smo (Corbit et al., 2005, Rohatgi et al., 2007). Smo suppresses SuFu and Gli full length factors are released and undergo proteolytic processing becoming the Gli activator forms. The latter are transported to the nucleus where they activate the transcription of downstream target genes (e.g. Ptch1, Gli1) (Whewey et al., 2018). Thus, several proteins involved in the Shh pathway localize to the primary cilium. This organelle is crucial for the formation of both activator and repressor forms of Gli TFs. It is thus pivotal to balance the activity of the pathway and the transcription of downstream targets.

The role of the Shh pathway was described in section 3.2.7 of the introduction. Mutant mice for SuFu, Gli TFs or Shh itself impair aRG dynamics and alter corticogenesis (reviewed by Yabut and Pleasure, 2018). Additionally, mouse mutants for ciliary proteins can show alterations in the ratio of GliA and GliR forms, or in the responses to Shh signaling. In the context of the developing telencephalon, *Rpgrip1l* mutant mice show an increased Gli3A:Gli3R ratio in the telencephalon (Besse et al., 2011). Similarly, an increase in Gli3A was also observed in the forebrain of *Ift88* mouse mutants at early stages of corticogenesis (E12.5) (Willaredt et al., 2008). Wilson and colleagues (2012) also reported a similar result in the Nestin-Cre conditional knockout of *Kif3A* mouse mutants, although recently Foerster and colleagues (2017) did not find the same results. Of note, in the first paper the experiments were performed at E12.5 and Foerster and colleagues performed the experiments at E14.5, which may explain the different result. Equally, at this later time point they did not observe changes in the Gli3A:Gli3R ratio in the *Ift88* Nestin-Cre conditional knockout mice.

Although these Gli changes may be stage-specific, these results indicate that Shh signaling is likely to be affected upon cilia loss or disruption. We thus decided to assess this pathway in the dorsal telencephalon of *HeCo* mice. I generated cortex lysates from WT and *HeCo* embryos at E12.5 and E13.5 and analyzed Gli activator (full length) and repressor (short length) forms at these stages by Western blot. I decided to assess Gli3 and Gli2, although the latter is not greatly expressed in the neocortex (Yabut and Pleasure, 2018).

I first examined Gli3A and Gli3R levels (Figure 49 A, C). Although no significant changes were observed, there was a tendency towards a decreased Gli3A:Gli3R ratio in the *HeCo* mouse (Figure 49, A, C, E, G). This tendency was stronger at E13.5 than E12.5 (Figure 49, C, G), the stage at which the severe primary phenotype was reported in the *HeCo* mouse. I could only detect the repressor form of Gli2 and no changes were observed between WT and *HeCo* mice neither at E12.5 nor E13.5 (Figure 49, B, D, F, H). It is intriguing that although they are not significant, the changes in the Gli3A:Gli3R ratio do not go in the same direction as the results previously obtained in other mouse mutants in which primary cilia are absent. This probably highlights the differences between these models and the phenotype observed in the *Eml1*-mutant condition, in which although highly disrupted primary cilia are still detected.

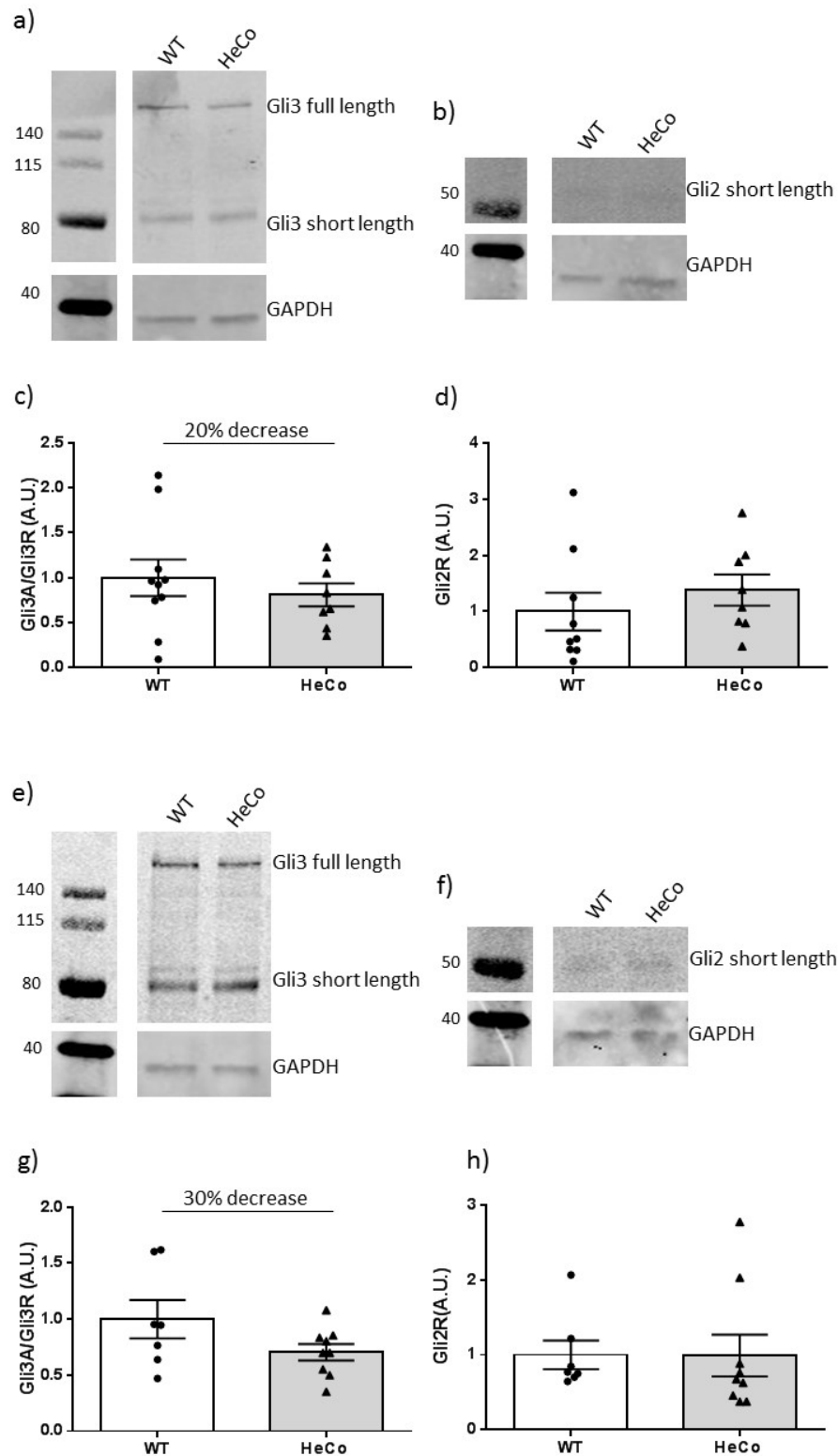


Figure 49. Mild alterations in the Gli3A:Gli3R ratio in the *HeCo* dorsal telencephalon. A, B) Representative Western blot of WT and *HeCo* cortex lysates (E12.5) immunodetected for Gli3 (A) and Gli2 (B). C, D) Quantifications from Western blots, with band intensities normalized to GAPDH. C) WT n=10 embryos from 2 litters, *HeCo* n=8 embryos from 2 litters. D) WT n=9 embryos from 2 litters, *HeCo* n=7 embryos from 2 litters. E, F) Representative Western blot of WT and *HeCo* cortex lysates (E13.5) immunodetected for Gli3 (E) and Gli2 (F). G, H) Quantifications from Western blots, with band intensities normalized to GAPDH. G) WT n=7 embryos from 2 litters, *HeCo* n=9 embryos from 2 litters H) WT n=7 embryos from 2 litters, *HeCo* n=9 embryos from 2 litters. Mean  $\pm$  SEM.

We proceeded to analyze the Hippo pathway, involved in control of cell growth, shape and proliferation (Ma et al., 2018). Briefly, the Hippo pathway depends on a core of kinases modulating its activity. The main mechanism includes the MST1/2 kinases, which phosphorylate the scaffolding proteins SAV1 and MOB1A/B to recruit and phosphorylate LATS1/2. Additionally, MAP4Ks can also phosphorylate LATS1/2. Phosphorylated LATS1/2 in turn phosphorylates and inactivates YAP/TAZ, inhibiting their translocation to the nucleus and thus the transcription of target genes. Instead, they remain in the cytoplasm associated with 14-3-3 and eventually undergo degradation (Meng et al., 2016).

When YAP/TAZ are not targeted for degradation, they translocate to the nucleus and associate to TEAD factors, promoting the transcription of target genes involved in maintenance of proliferation and stemness (Meng et al., 2016).

The relationship of the Hippo pathway with the primary cilium is not greatly studied. However, core components of the pathway interact with proteins found in the ciliary transition zone (Whewey et al., 2018). In addition, primary cilium anomalies have been associated with increased YAP/TAZ activity (Grampa et al., 2016, Seixas et al., 2016). These results combined with the emergence of the importance of the pathway in the etiology of heterotopia phenotypes (Cappello et al., 2013, Liu et al., 2018, O'Neill et al., 2018) prompted us to investigate it in *HeCo* aRGs.

I thus performed IHC for YAP in E13.5 brain slices of WT and *HeCo* mice and analyzed the fluorescence intensity levels in the VZ (Figure 50 A). *HeCo* mice showed an increased YAP signal in the VZ when compared to WT (Figure 50 C).

Additionally, I performed an *in vitro* approach to further validate this result. I prepared cell cultures enriched in Pax6+ progenitors (see manuscript) from E13.5 pregnant females and performed ICC for YAP (Figure 50 B). Then I quantified the nuclear intensity of fluorescence. Indeed, *HeCo* cells had a stronger YAP signal than WT (Figure 50 D). These combined experiments indicate an increase in YAP levels in *HeCo* aRGs, possibly indicating a higher activity.



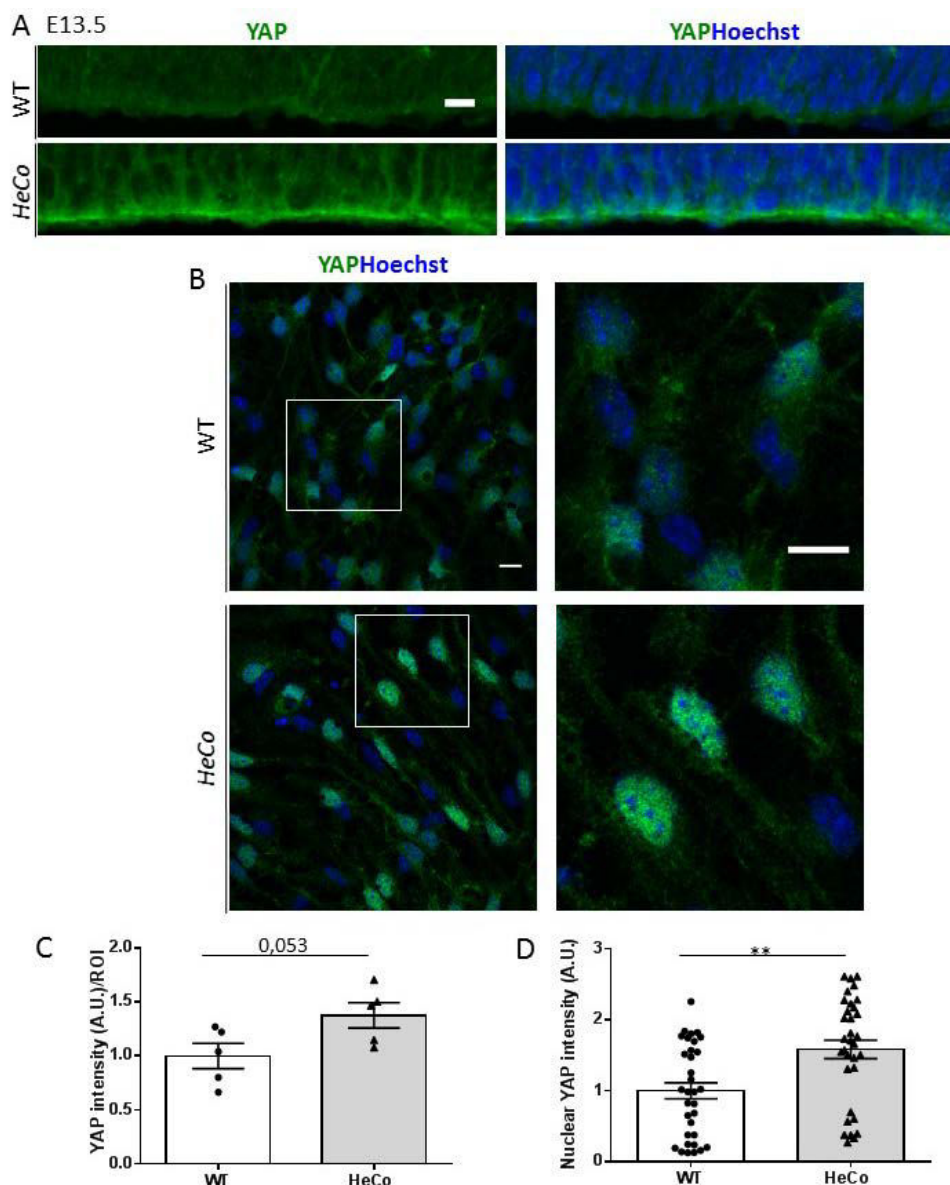


**Figure 50. *HeCo* aRGs show increased YAP levels.** A) Representative images of WT and *HeCo* VZ immunostained for YAP (green). B) Representative image of WT and *HeCo* progenitor cell cultures immunostained for YAP (green). C) Quantifications of YAP intensity of fluorescence normalized by Hoechst. Each point represents an embryo. WT: 5 embryos from 2 litters, *HeCo*: 5 embryos from 3 litters. D) Quantifications of nuclear YAP intensity of fluorescence normalized by Hoechst. Each point represents a cell. Both conditions: 34 cells from 2 embryos from the same litter. ROI: region of interest. Scale bar 10  $\mu$ m, mean  $\pm$  SEM, unpaired t-test, \*\* $p < 0.01$ .

## 2.4 Supplementary methods

### Western blot

Experiments and quantifications were performed as described in the manuscript. The primary antibodies used were the following: mouse anti-Gli2 (AF3635, R&D systems, 1:500), goat anti-Gli3 (AF3690, R&D systems, 1:500). Kind gift from S. Schneider-Maunoury.

### *Immunohistochemistry*

The protocol was adapted from the one described in Uzquiano et al. After fixation, the brains were incubated in a 30% sucrose PBS 1X solution. 20 µm thick coronal sections were obtained using a cryostat. Antigen retrieval was performed by incubating the sections in sodium citrate 10 mM pH 6 at 95 °C for 20 min and allowing them to cool before blocking. After blocking (see Uzquiano et al.), the sections were incubated with the primary antibody YAP (14074T, Cell Signaling Technology, 1:100) O/N at 4°C in a humid chamber. After extensive washes, sections were incubated with the secondary antibody anti-rabbit Alexa 488 (Life Technologies, 1:1000) for 2 hours at RT. This was followed by a 10 min. incubation in Hoechst (Thermo Fisher Scientific, 1:1000). After extensive washes, brain sections were mounted with Fluoromount G (Southern Biotechnology).

Images were acquired with a TCS Leica SP5-II confocal microscope. Two regions of interest (ROI) were analyzed per embryo (150 x 30 µm). Intensity of fluorescence was analyzed using Image J.

### *Immunocytochemistry*

In order to perform immunocytochemistry for YAP (14074T, Cell Signaling Technology, 1:100) a modified protocol was applied to the one described in Uzquiano et al. Antigen retrieval was performed by incubating the fixed cells in sodium citrate 10 mM pH 6 at 95 °C for 10 min and allowing them to cool before blocking. Afterwards the protocol was followed as described in the manuscript.

Images were acquired with a TCS Leica SP5-II confocal microscope. Intensity of fluorescence was analyzed by using Image J.

In both experiments YAP intensity of fluorescence was normalized to Hoechst intensity of fluorescence.

### **3. Introduction to Collins, Uzquiano et al. 'The neuroanatomy of Eml1 knockout mice, a model of subcortical heterotopia.'**

Kielar and colleagues (2014) identified *Eml1* as the mutant gene in the *HeCo* mouse. Gene expression was verified and no full length transcripts were detected. Trace amounts of aberrant transcripts were identified, and indeed a spliceable retrotransposon inserted in an *Eml1* intron is responsible for the mutation. Due to the lack of good antibodies for *Eml1* it was not possible to check if any isoforms were produced. However loss-of-function due to severe disruption of the major scaffolding beta propeller domains is predicted (Richards et al. 2015). Additionally, *HeCo* mice arose on an unusual in-crossed NOR-CD1 background. Although it was possible to transfer the mice to a different genetic background, a new collaboration with the Institute Clinique de la Souris, initiated the generation of an *Eml1* knockout (KO) mouse model using C57BL/6N as background strain. A detailed neuroanatomical characterization was performed in this new rodent model of subcortical heterotopia.

#### **3.1 Summary**

As in the *HeCo* mouse, *Eml1* KO mice showed bilateral subcortical heterotopia in adulthood. Overall, the anomalies detected after an extensive anatomical phenotyping, are more severe than those reported for the *HeCo* mouse (Croquelois et al., 2009). The heterotopia was observed from late embryonic stages (E18.5), whereas in the *HeCo* mouse it is less defined at this developmental time point. The thickness of the KO normotopic cortex was significantly decreased, the animals showed corpus callosum agenesis and some of them presented hydrocephaly. A cluster of ectopic neurons was observed in the CA3 region of the hippocampus. Additionally, we report for the first time a sexual dimorphism, indicating that males seem to be more affected than females.

Finally, related to corticogenesis and neuronal progenitors, analyses at early stages of development (E13.5) also confirmed the presence of ectopically positioned Pax6+ proliferating progenitors outside the VZ in *Eml1* KO embryos. Although not included in the manuscript, we went one step further and analyzed primary cilia in the VZ of *Eml1* KO mice, which phenocopy the results obtained in the *HeCo* mouse (see extra supplementary results). These data suggest a slightly broader role for *Eml1* in brain architecture, than suggested from studies in *HeCo* mice. In addition, we provide a new resource to study the etiology and physiological mechanisms associated with subcortical heterotopia.

### **3.2 Contribution**

At early stages of the project, I contributed to determining the pathological phenotype of adult KO animals. Then I focused on designing, performing and analyzing data from early-mid corticogenesis. I was actively involved in data assembly and writing the manuscript.

## The neuroanatomy of *Em/1* knockout mice, a model of subcortical heterotopia

**Stephan C. Collins**<sup>1-5#</sup>, **Ana Uzquiano**<sup>6-8#</sup>, **Mohammed Selloum**<sup>1, 2, 3, 4, 9</sup>, **Olivia Wendling**<sup>1, 2, 3, 4, 9</sup>, **Marion Gaborit**<sup>1-4</sup>, **Maria Ossipenko**<sup>1-4</sup>, **Marie-Christine Birling**<sup>1, 2, 3, 4, 9</sup>, **Binnaz Yalcin**<sup>1-4\*</sup>, **Fiona Francis**<sup>6-8\*</sup>

<sup>1</sup> Institut de Génétique et de Biologie Moléculaire et Cellulaire, Illkirch, France.

<sup>2</sup> Centre National de la Recherche Scientifique, UMR7104, Illkirch, France.

<sup>3</sup> Institut National de la Santé et de la Recherche Médicale, U964, Illkirch, France.

<sup>4</sup> Université de Strasbourg, Illkirch, France.

<sup>5</sup> Centre des Sciences du Goût et de l'Alimentation, Université de Bourgogne-Franche Comté, Dijon, France.

<sup>6</sup> INSERM UMR S-839, Paris, France

<sup>7</sup> Sorbonne Université, UMR S-839, F-75005 Paris, France

<sup>8</sup> Institut du Fer à Moulin, Paris, France

<sup>9</sup> CELPHEDIA, PHENOMIN, Institut Clinique de la Souris (ICS), 1 rue Laurent Fries, F-67404 Illkirch-Graffenstaden, France

# Contributed equally to this work

\* To whom correspondence should be addressed

## **Abstract**

The cerebral cortex is a highly organized structure, responsible for advanced cognitive functions. Its development relies on a series of steps including neural progenitor cell proliferation, neuronal migration, axonal outgrowth and brain wiring. Disruption of these steps leads to cortical malformations, often associated with intellectual disability and epilepsy. We have generated a new resource to shed further light on subcortical heterotopia, a malformation characterized by abnormal neuronal position. We describe here the generation and characterization of a knockout (KO) mouse model for *Eml1*, a microtubule-associated protein showing mutations in human ribbon-like subcortical heterotopia. As previously reported for a spontaneous mouse mutant showing a mutation in *Em1*, we observe severe cortical heterotopia in the KO. We also observe abnormal progenitor cells in early corticogenesis, likely to be the origin of the defects. *Em1* KO mice on the C57BL/6N genetic background also appear to present a wider phenotype than the original mouse mutant, showing additional brain anomalies, such as corpus callosum abnormalities and hippocampal defects. We compare the anatomy of male and female mice and also study heterozygote animals. This new resource will help unravel roles for *Eml1* in brain development and tissue architecture, as well as the mechanisms leading to severe subcortical heterotopia.

**Keywords:** cortical malformations, heterotopia, mouse model of developmental disorders.

## **Introduction**

Cerebral cortical development relies on highly regulated processes of cell proliferation, neuronal migration, growth of axons and dendrites, as well as synaptogenesis and refined connectivity. Defects in these steps lead to cortical pathology, and severe malformations are associated with abnormal progenitor cells and / or defects in migrating neurons (Bizzotto and Francis, 2015; Stouffer et al. 2015; Romero et al. 2018).

Although human cortical malformations are rare disorders, their combined incidence is of more than 1% in the human population. 14% of epileptic patients are believed to present a neuronal migration disorder. This percentage rises to 40% when considering those patients with intractable epilepsy (Farrell et al. 1992, Meencke and Veigh, 1992, Guerrini et al. 2005). Subcortical heterotopia is a malformation characterized by the presence of masses of neurons

beneath the normal cortex. It can be associated with a delay in somatic development, intellectual disability as well as epilepsy (Bahi-Buisson et al. 2013).

Patients with compound heterozygote or homozygote mutations in *EML1* exhibit giant bilateral ribbon-like heterotopia, presenting large clusters of neurons that are aberrantly positioned within the white matter (Kielar et al. 2014; Shaheen et al. 2017, OMIM #600348). *EML1*-mutation patients can also present hydrocephalus, polymicrogyria and macrocrania (Kielar et al. 2014, Shaheen et al. 2017), and suffer from refractory epilepsy, intellectual disability, and/or psychomotor developmental delay (Kielar et al. 2014, Shaheen et al. 2017).

We previously studied *Heterotopic Cortex (HeCo)* mice, a spontaneously arisen mouse line exhibiting a retrotransposon insertion in the *Eml1* gene (Croquelois et al. 2009; Kielar et al. 2014). These mice show bilateral heterotopia below the cortex in dorso-medial regions, associated with a susceptibility to epilepsy, as well as learning and memory deficits (Croquelois et al. 2009).

*Eml1* is a microtubule-associated protein expressed in proliferative progenitor zones from early stages of corticogenesis (Bizzotto et al. 2017, Kielar et al. 2014). It binds to both microtubules and soluble tubulin (Richards et al., 2015) and contains an N terminal domain with a coiled coil motif, and a C terminal region with a tandem beta propeller structure. Although its function remains relatively unknown, *Eml1* is important for progenitor distribution and function in the developing neocortex (Bizzotto et al. 2017, Kielar et al. 2014). Indeed, heterotopia formation in the *HeCo* mouse was shown to involve abnormal radial glial cell progenitors (RGs) in early-mid corticogenesis (Kielar et al. 2014; Bizzotto et al. 2017), which are the main neuronal progenitor cell in the developing cortex. They are characterized by the presence of an apical and a long basal process, the latter serving as guide for radially migrating neurons (Gotz and Huttner, 2005; Matsuzaki and Shitamukai, 2015; Uzquiano et al. 2018). Because of abnormal RG distribution and basal process morphology in *HeCo* mice, migration is perturbed throughout corticogenesis with upper layer neurons permanently arrested in the neocortical white matter (Kielar et al. 2014). Additionally, RGs were reported to show abnormal spindle orientation and mitotic spindle length, indicating a possible role for *Eml1* in mitosis (Bizzotto et al. 2017, Kielar et al. 2014).

Although other subcortical heterotopia mouse models have arisen (Beattie et al. 2017, Cappello et al. 2012, Jossin et al. 2017, Liu et al. 2018), the *HeCo* mouse line represents a good

disease model, mimicking human subcortical heterotopia, and showing mutations in a gene also mutated in human patients.

*Eml1* gene expression was verified in the *HeCo* mouse mutant and full length transcripts were shown to be absent. The retrotransposon insertion occurs towards the end of the gene and certain chimeric transcripts were identified between *Eml1* and the retrotransposon (Kielar et al. 2014). The absence of reliable antibodies against this protein made it difficult to verify if mutant *Eml1* isoforms were produced, however loss-of-function due to severe disruption of the major scaffolding beta propeller domains is predicted (Richards et al. 2015). *HeCo* mice also arose on an unusual in-crossed NOR-CD1 congenic background. We had the possibility in this project of developing *Eml1* knockout (KO) mice on the C57BL/6N genetic background (B6/N), as well as performing detailed and extensive neuroanatomical analyses. We show here that *Eml1* KO mice resemble *HeCo* mice, faithfully revealing subcortical heterotopia, visible as early as embryonic day (E) 18.5. RG progenitor cells are perturbed at E13.5, similar to *HeCo*. Neuroanatomical measures in adult KO-B6N mice reveal a wider phenotype than observed in *HeCo*, which is not restricted to the neocortex. Males and females are both affected, with especially males showing a consistent heterotopia phenotype. This work hence characterizes a new *Eml1* KO resource, as well as illustrating wide systematic neuroanatomical analyses in neurological mouse mutants.

## **Materials and methods**

### **Mouse line and ethical statement**

All mouse experimental procedures were performed in agreement with the EC directive 2010/63/UE86/609/CEE for the care and use of laboratory animals and every effort was made to minimize the number of animals used and their suffering. The neuroanatomical pipeline was approved by the local animal care, use and ethic committee of the Institute of Genetics and of Molecular and Cellular Biology (IGBMC) under accreditation number 2012-139. Embryonic analyses were approved by the French MESR 00984.02 authorization with protocols followed and approved by local ethical committees (Charles Darwin committee (Paris, France). The light cycle was controlled as 12 h light and 12 h dark (lights on at 7 am) and the temperature was maintained at 23±1 °C.

### **Creation of an *Eml1* mouse KO line**



The *Em1* mutant mouse line was established at the PHENOMIN MCI/ICS (Mouse Clinical Institute -*Institut Clinique de la Souris*-, Illkirch, France; <http://www-mci.u-strasbg.fr>), in the framework of funding from the French Rare Disease Foundation. The *Em1* mutant line was generated and analyzed on the mouse genetic background C57BL/6N (B6N). LoXP sites surrounding exon 8 were first introduced into a genomic DNA targeting construct (**Supp. Fig. 1**). This vector contained a Neo cassette encompassed by two FRT sites upstream of the second loXP site. This targeting construct was introduced by electroporation to allow homologous recombination in B6N embryonic stem cells. After G418 selection, targeted clones were identified by long-range PCR using external primers and further confirmed by Southern blot with an internal Neo probe as well as 5' and 3' external probes. Two positive ES clones were injected into B6N blastocysts. Resulting male chimeras were bred with wild type B6N females in order to obtain germline transmission. Selection cassettes were excised by crossing with a *Rosa Cre Flpase* deleter mouse line (Birling et al. 2012). Standard biochemical and metabolic tests were performed. Briefly, blood collection was performed for hematology and clinical chemistry assessments. Procedures are detailed in the following link (<http://www.mousephenotype.org/impress>).

## Genotyping

The following primers were used for genotyping (**Supp. Fig. 1**):

Position	Primers	Sequence
Ef	7964	CCCTGAGCTTCCTCATAACTTCAGC
Ef2	7965	CAGGTCTGTGGGCTCTGTAACAGG
Er	7966	CACCCACTGAAGAAATGACTGGCAG
Er2	7967	CTTGTTAAAGCGTCTGCAGTCTGTCTG
Lf	7962	GAAAACGTGCTTTGCTGTGTACATAGG
Lr	7963	CGCCACCCTTTTCTACAAGTCATTTTTG
Lxr	4724	CGAAGTTATCTGCAGGTCGACCTTAAG
Mqf	6	GAAGAACGAGATCAGCAGCCTCTGTTCC
Mqr	265	TGCTAAAGCGCATGCTCCAGACTGC

To distinguish the knockout allele, primer pairs Lf-Lr (245 bp, knock-out (KO); 165 bp, WT) and Ef-Er (414 bp, KO; 309 bp WT) were used.

### **Neuroanatomical studies**

Neuroanatomical studies were carried out independently in WT and *Em11*<sup>-/-</sup> male and female mice at 7 weeks of age. We aimed for n=5 per group for male and n=4 per group for female 7 week animals, although for some measures fewer animals were used (comparisons involving only two animals for one of the genotypes are detailed in the Figure legends). Also at postnatal day 13 (P13), we aimed for n=3 per group for male and females in comparisons (see Figure legends for exceptions), as described previously (Collins et al. 2018). Of note, experiments with *Em11*<sup>+/-</sup> mice were performed with n=3-4 for both males and females (see Figure legends for exceptions). In brief, adult mouse brain samples were fixed in 10% buffered formalin for exactly 48 hours. 166 brain parameters, made of area and length measurements, as well as cell level features and 31 co-variates, were taken blind to the genotype across one well-defined sagittal section (**Supp. Fig. 2A, 2B** and Supp. Table 1).

Similarly, neuroanatomical studies were carried out at E18.5 (n=3 per group for a total of six groups including male and female; wild type (WT), heterozygous (het) and homozygous (hom), for exceptions see below). In order to obtain the samples, het-het crosses were established thus allowing analyses of littermates. Mouse embryo head tissue samples were harvested and fixed in Bouin's fixative for exactly 48 hours followed by careful dissection of the brain and incubation in 70% ethanol before paraffin-embedded for sagittal sectioning. Brain sections were cut exactly in the plane of the closest image to the section defined as critical section at Lateral 0.60 mm of the right hemisphere numbered 9 (**Supp. Fig. 2, Supp. Fig. 3**). We failed brain sections that deviated more than 140 µm anterior or posterior to the critical section. When sectioning, great care was taken to avoid dorso-ventral and antero-posterior asymmetry. Sections were co-stained with cresyl violet and luxol blue as described previously (Collins et al. 2018). For E18.5 analyses, 46 brain parameters, concerning area and length measurements, were taken blind to the genotype across one sagittal section, as well as 31 co-variates (**Supp. Fig. 3B**). We have previously shown that our quantitative and ultra-standardized approach allowed us to detect many more features and more subtle phenotypes than previously published data (Mikhaleva et al. 2016).

### **Immunohistochemistry analyses at P13**

Immunohistochemistry analyses were performed in WT (n=3 for male and female), het (n=3 for male and 2 for female) and hom (n=3 for male and female) mice. Brains of P13 mice were

fixed by immersion in ice-cold 4% (w/v) paraformaldehyde (PFA) in PBS during 24 hours, washed in 1 X PBS and embedded in paraffin. The sections from paraffin-embedded tissues were collected on glass slides and were treated with Tris-EDTA Buffer (10mM Tris Base, 1mM EDTA, 0.05% Tween 20, pH 9.0) at 94°C during 40 minutes (min.). The slides were cooled down at room temperature (RT) for 15 min. Blocking was performed during 1 hour at RT (1 X PBS with 5 % normal goat serum, 0.05 % tween 20). The primary antibody Tbr1 (Abcam, ab31940, 1:200) was incubated over-night (O/N) at 4°C. Then the secondary antibody Alexa 555 (Invitrogen, 1:500) was incubated for 1h at RT. The sections were then stained with DAPI (50 mg/ml) diluted in Tris-MWL 4-88 solution (Citifluor, EMS). Images were acquired with a TCS Leica SP5-II confocal microscope.

### **Immunohistochemistry analyses at early embryogenesis**

Mouse embryos were obtained at E13.5 from timed-pregnant females. In order to obtain the samples, het-het crosses were established thus allowing analyses of littermates. For WT, *Em1* het and hom mice n=3-5 were analyzed. Pregnant females were injected with 5-bromo-2'-deoxyuridine (BrdU, 99% Bioultra, Sigma-Aldrich Chimie Sarl, ref B9285, 50 µg per gram body weight) and sacrificed after 30 min. Mouse embryo head tissue samples were fixed by immersion O/N at 4 °C in 4 % w/v PFA in 0.1 M phosphate buffer, pH 7.4. Brains were dissected and extensively washed in 1 X PBS. Brains were cut in 70 µm thick coronal sections using a vibrating blade microtome (Leica VT1000 S), followed by immunohistochemistry. Blocking was performed for 1 h at RT with blocking solution (1X PBS with 10% Goat Serum and 0.5% Triton X-100) before incubation O/N at 4 °C with the following primary antibodies: Pax6 (BioLegend, Poly19013, 1:300) and N-Cadherin (Transduction Laboratories, C70320, 1:2000) (for other primary antibodies see below). After extensive washes, sections were incubated with secondary anti-mouse Alexa 488 or anti-rabbit Alexa 568 (Life Technologies, 1:1000) for 2 hours at RT. This was followed by 10 min. incubation in Hoechst (Thermo Fisher Scientific, 1:1000). After extensive washes, brain sections were mounted with Fluoromount G (Southern Biotechnology). For F-actin immunofluorescence, Alexa Fluor 568 Phalloidin (1:100, Life Technologies) was incubated in PBST 1% at RT after incubation with the secondary antibody. In order to perform immunohistochemistry combining the primary antibodies Ki67 (BD 556003, 1:200) and BrdU (BioRad, clone Bu20a, 1:1000) a modified protocol was applied. Antigen retrieval was performed by incubating the sections in sodium citrate 10 mM pH 6 at

95 °C for 20 min. and allowing them to cool before blocking. After blocking, incubation with the primary antibody (Ki67), secondary antibody and Hoechst, sections were fixed with PFA 8% w/v for 15 min. at RT (Palmer et al. 2000). Extensive washes with PBST-0.1% (1X PBS and 0.1% Triton X-100) were performed, followed by incubation of the sections in 2N hydrochloric acid for 30 min. at 37°C. After extensive washes, the sections were incubated with the primary antibody (BrdU), secondary antibody, Hoechst, and then mounted with Fluoromount G as previously described.

In order to assess Pax6 positive (+) and Ki67+BrdU+ cell distribution, regions of interest (ROI) were selected from both hemispheres, spanning the whole cortical wall and with a width of 100 µm. Two ROIs were quantified per animal. The cortical wall was divided in six equally-sized bins, bin 1 and 6 corresponding to the most apical (apical ventricular zone) and basal (cortical plate) regions of the developing cortex, respectively (**Fig. 4A**, top row, right panel). Cells that were positive for the selected markers were quantified, and the percentage relative to the total number of positive cells was compared between the three genotypes (WT, het and hom), in each different bin. Images were acquired with a TCS Leica SP5-II confocal microscope.

### **Statistical analyses**

For adult and E18.5 analyses, data were analyzed using a two-tailed Student t-test of equal variance to determine whether a brain region was associated with the neuroanatomical defect or not. The level of significance was set at  $p < 0.05$ . Data are represented in a combined graph. Color-coded histograms according to the p-value show the percentage decreased (minus scale) or increased (plus scale) of measured brain regions as compared to the controls (0%). Data are also represented as box plots displaying the median with interquartile range. Box plots additionally indicate the number of animals specifically used for each parameter quantified. We only considered the exact same stereotaxic coordinates thus some animals could not be used to quantify certain specific parameters, explaining sometimes compromised sample size. Equally, due to the lower penetrance of the heterotopia phenotype in females (see below), a lower n number (2) was used when assessing heterotopia-specific characteristics in 7-week adults and E18.5 embryos. Related to heterotopia-specific characteristics, (area and height of HeCo and HoCo), data are represented as mean  $\pm$  SEM.

For E13.5 analyses, data were analyzed using the Kruskal-Wallis test with two factors (bin and genotype), followed by a Chi square test in order to compare between each genotype across the different bins. The level of significance was set at  $p < 0.05$ . The median is represented and the error bars represent the minimum and maximum range. The analyses were performed with StatView and GraphPad Prism.

## Results

### Generation of an *Em1* KO mouse model

A knockout strategy was developed targeting *Em1* exon 8, with a view to drastically impacting the tandem beta propeller (TAPE) organization of the *Em1* protein (**Supp. Fig. 1A, 1B**). The TAPE structure is an important scaffolding domain representing the major part of the protein sequence (Richards et al. 2015). After homologous recombination, mice chimeras were generated incorporating the targeted allele (**Supp. Fig. 1C**) and crossed with a *Flp-Cre* deleter line (Birling et al. 2012). PCR genotyping confirmed the generation of the KO allele. Het mice were crossed to generate homozygotes, and the autosomal recessive nature of the heterotopia phenotype was confirmed (Croquelois et al. 2009).

### Postnatal lethality in a proportion of *Em1* homozygous KO mice

At 3 weeks of age (weaning age) mouse survival was assessed from 175 successfully genotyped mice derived from a het-by-het breeding scheme. We obtained 50% het, 31% WT, and 19% hom, indicating a probable lethality of a proportion of *Em1* homozygous mice. Approximately one third of hom mice (10/34) who survived to weaning, later died between 5-25 weeks of age. Male and female *Em1* KO mice seemed to be equally affected by the lethality, and severe hydrocephalus was noted in certain individuals (see also below). *Em1* het mice were fully viable at 3 weeks, however, a small proportion of het mice (7/77) also died between 5-16 weeks of age. Blood haematology and blood chemistry analyses at 7 weeks of age showed no major differences between WT and KO mice (data not shown).

### Identification of defects in *Em1* KO mice including double cortex, corpus callosum agenesis, abnormal hippocampus and hydrocephalus

We examined the brain anatomy of *Em1* homozygous mice at 7 weeks of age, both in males and females, using a platform for the parasagittal histo-phenotyping of the mouse brain (Collins et al. 2018). Slide scans down to cell level resolution (**Supp. Fig. 2A**) were used to quantify 40 brain parameters across 22 distinct brain structures (**Supp. Table 1** and **Supp. Fig. 2B**) from a single sagittal brain section at Lateral +0.60 mm. This quantification was blind to the genotype. To minimize environmental and genetic variation, mice were analyzed according to their gender, aged exactly 7 weeks, and bred on the same genetic background (B6N).

Severe brain anomalies were found and are summarized in **Fig. 1A**. As previously reported in an *Em1*-spontaneous mouse mutant (Croquelois et al. 2009, Kielar et al. 2014), underneath a homotopic thinner cortex a massive heterotopia surrounded by fiber tracts formed a double cortex (**Fig. 1B**). Considering analyses testing at least 3 mice per genotype, other neuroanatomical defects included cell dispersion in the CA3 region of the hippocampus (**Fig. 1B**), an enlarged area of the hippocampal pyramidal cell layer (+122%,  $P=0.01$  for male compared to +45%,  $P=0.37$  for female *Em1*<sup>-/-</sup> mice; **Fig. 1B**), together with increased area of the dorsal subiculum (+170%,  $P=0.006$  for male compared to +89%,  $P=0.12$  for female *Em1*<sup>-/-</sup> mice; **Fig. 1B**). The commissures were also affected showing corpus callosum agenesis (full penetrance for male with 5/5 affected and only partial penetrance for female with 2/4 affected *Em1*<sup>-/-</sup> mice), a smaller area of the anterior commissure (-27%,  $P=0.015$  for male *Em1*<sup>-/-</sup> mice), and an enlargement of the lateral ventricles (+266%,  $P=0.046$  for male and +136%,  $P=0.12$  for female *Em1*<sup>-/-</sup> mice). Partial penetrance of the phenotypes in females may explain why the significance threshold of 0.05 was never reached despite the large effect size (**Fig. 1A**). It is however important to note that males and females shared a very similar phenotypic profile.

In addition, we also examined the brain anatomy of male *Em1* het mice at 7 weeks of age using the same approach. We were unable to detect any major differences between the brain anatomy of *Em1* het mice when compared to their matched controls (**Fig. 1C**), although a decrease of 8% of the size of the anterior commissure was observed after the analysis of n=2 mice for each genotype.

**The cortical heterotopia is associated with corpus callosum agenesis and hippocampal defects but not with hydrocephalus**

In two *Em1*<sup>-/-</sup> female mice (out of four assessed), we did not see the subcortical heterotopia nor the corpus callosum agenesis and hippocampal-related phenotypes despite the presence of the hydrocephalus. Similarly, in one *Em1*<sup>-/-</sup> male mice (out of five tested), the heterotopia, corpus callosum agenesis and hippocampal-related phenotypes segregated but without the enlarged ventricles. Together, these results suggest that the underlying biological mechanisms leading to heterotopia, corpus callosum agenesis and hippocampal defects might be shared and may be independent of the enlarged ventricle phenotype.

To further characterize the heterotopia phenotype, we quantified seven additional parameters (illustrated in **Supp. Fig. 2C**). We analyzed the normal cortex in WT mice and its corresponding homotopic cortex (HoCo) as well as the heterotopic cortex (HeCo) in *Em1* hom mice that exhibited the heterotopia phenotype. The area and the height of the homotopic cortices were reduced in male *Em1* hom mice (for area: -34.8%,  $P=0.0078$ , for height: -58.9%,  $P=3.19E-05$ ), when compared to the normal total cortex (**Fig. 1D**). Analyzing  $n=2$  female mice with heterotopia revealed similar results (for area: -37.4%; for height: -55.9% compared to wild-types). The combined height of HeCo and HoCo remained the same size in male and female *Em1* hom mice, however their combined area appeared moderately smaller in female *Em1* hom mice (-17.6%, **Fig. 1D**).

### **The hydrocephalus phenotype is visible at postnatal day 13 (P13)**

Next, we assessed neuroanatomical defects in *Em1* hom mice at P13, both in males and females using the same platform as the one used for the parasagittal histo-phenotyping of the adult mouse brain (**Supp. Fig. 2B**). In line with the adult data, similar neuroanatomical defects were also seen at P13 in both male and female KO mice (**Fig. 2A**): a massive heterotopia surrounded by fiber tracts, cell dispersion in the CA3 layer of the hippocampus and an enlarged size of the ventricles (**Fig. 2B**). In analyses of  $n=2$  males, and  $n=3$  females an increased area of the dorsal subiculum was also observed. In one *Em1*<sup>-/-</sup> female mice, the heterotopia, corpus callosum agenesis and hippocampal-related phenotypes did not segregate with enlarged ventricles, further suggesting that these neuroanatomical anomalies are likely to be unrelated. We also analyzed the normal cortex in WT mice and its corresponding homotopic cortex (HoCo) as well as the heterotopic cortex (HeCo) in *Em1*<sup>-/-</sup> mice. In a manner similar to adult mice, there was a tendency towards a reduced area and the height of the homotopic cortices both in male and female *Em1*<sup>-/-</sup> mice when compared to the

normal total cortex (**Fig. 2C**). There was also a tendency towards a decreased area of the combined area of HeCo and HoCo both in male and female mice, however their combined height seemed to be enlarged when compared to matched controls (**Fig. 2C**).

In order to shed further light on the identity of the cells composing the heterotopia, we performed immunostainings for Tbr1 in male and female WT, het and hom (all n=3) mice (**Fig. 2D**). Although Tbr1 is expressed in diverse populations of cortical neurons, it is highly expressed in deep layers of the CxP (Molyneaux et al. 2007), serving as a marker of the latter. We observed that highly-expressing Tbr1<sup>+</sup> neurons are localized in deep layers of the WT and het cortices, as well as in the normotopic cortex of *Em1* KO mice. As previously reported for the *Em1*-spontaneous mouse mutant (Croquelois et al. 2009), Tbr1<sup>+</sup> neurons are mostly absent from the heterotopia. However, we observed some sparse cells positive for Tbr1, suggesting that even if most of the heterotopia is composed of upper-layer neurons, a very small population of deep-layer neurons are also arrested beneath the normotopic cortex.

### **Embryonic origins of the brain anomalies: analysis at E18.5**

The time scale of neuroanatomical defects was further investigated through a similar morphological screen at E18.5. Coherent with the adult brain screen, we assessed 39 brain parameters (listed in **Supp. Table 2** and schematized in **Supp. Fig. 3B**) distributed across 11 distinct brain regions of the developing brain (cortical layers, hippocampus, thalamus, basal ganglia, fiber tracts, cerebellum, pons, ventricle, forebrain and midbrain).

In line with the adult and P13 data, major neuroanatomical defects were identified at E18.5 in both male and female KO mice (summarized in **Fig. 3A**). All the assessed parameters pertaining to the cortical wall (Cxne, neuroepithelial ventricular zone; SubVCx, subventricular zone; ICx, intermediate zone; CxP, deep and superficial cortical plate) appeared decreased in size when compared to matched WT brains. For example, the deep cortical plate (CxP) area was significantly reduced by 79.4% ( $P=0.001$ ) in male *Em1* hom and by 78.9% in females (n=2). Consistently, the superficial CP was also smaller (-64.8%,  $P=0.0009$  for male and -62.0%,  $P=0.0013$  for female *Em1*<sup>-/-</sup> mice). Remarkably, the areas of both the ventricular and subventricular zones (Cxne and SubVCx, respectively) were also smaller in males *Em1*<sup>-/-</sup> mice (Cxne: -50.0%,  $P=0.006$ , SubVCx: -66.4%,  $P=0.0002$ ). A similar tendency was observed in females. Unexpectedly, the lateral ventricles were smaller in size in male *Em1*<sup>-/-</sup> mice (by



88.6%,  $P=0.0016$ ). This trend was mimicked in female *Em1*<sup>-/-</sup> mice ( $n=2$ , smaller by 84.3%). This suggests that the hydrocephalus phenotype seen at 7 weeks of age is likely to originate from postnatal stages onwards, further supporting the hypothesis that independent mechanisms may be responsible for the different phenotypes observed (i.e. cortical anomalies versus hydrocephalus). The height of the cingulate cortex was reduced by 60.6% ( $P=0.0009$ ) in male and by 39.5% ( $P=0.05$ ) in female *Em1* hom mice. In contrast, some parameters were gender specific. For example, the apparent length of the pyramidal layer of the hippocampus was enlarged by 28.1% ( $P=0.0033$ ) in male *Em1*<sup>-/-</sup> mice, indicating that the hippocampal anomalies seen at 7 weeks of age might start in embryonic stages. The size of the anterior commissure appeared smaller in the two female *Em1*<sup>-/-</sup> mice analyzed (-13.7%).

### **Characterization of the cortical heterotopia at E18.5**

The band heterotopia (HeCo) was clearly visible and appeared to be interposed between the ICx and SubVCx zones of the developing cortex (**Fig. 3B**). The position and the general presentation of this subcortical heterotopia was consistent between the mice, however, its size varied more in female than in male *Em1*<sup>-/-</sup> mice. To characterize the E18.5 heterotopia phenotype, we used the quantification of the same seven parameters as in adult and P13 mice which we adapted for embryonic stages (**Supp. Fig. 3C**), and analyzed cortices in *Em1* hom mice. The area and the height of the homotopic cortex was smaller in male *Em1*<sup>-/-</sup> mice (for area: -27.5%,  $P=0.034$ ; for height: -37.8%,  $P=0.0002$ ), when compared to the normal total cortex (**Fig. 3C**). Similar trends were observed for females ( $n=2$ , for area -37.0%; for height, -37.1%). The combined area of HeCo and HoCo was either similar (male mice) or potentially smaller in female *Em1*<sup>-/-</sup> mice when compared to matched WT brains ( $n=2$ , -20.6%). However, the thickness (height) of the combined HeCo and HoCo was moderately larger in male *Em1*<sup>-/-</sup> mice (+16.2%,  $P=0.008$ ), with a similar trend in females ( $n=2$ , +13.0%).

Taken together, these results suggest severe morphological anomalies in both male and female *Em1* hom mice. The origins of these anomalies are observed during embryonic development. The main anomalies were pertaining to the neocortex with the presence of a massive subcortical band heterotopia. Milder to moderate defects were also identified in other brain regions.

### **Absence of cortical heterotopia in *Em1* het mice but brain size defects**

Next, we studied neuroanatomical features in both male and female *Em1* het mice and confirmed the recessive transmission of the heterotopic cortex (Croquelois et al. 2009), since we did not see a single occurrence of heterotopia in the het state. However, we observed some brain size defects in male *Em1* het mice at both P13 and E18.5 stages (for male: **Fig. 2E, Fig. 3D**; for female: **Supp. Fig. 4A, 4B**). These anomalies may be more apparent in male mice due to the possible higher variation of phenotypic traits in females. The average effect size for significant brain parameters in male *Em1* het mice was approximately half the size of the *Em1* hom mice. For example, the deep CxP area was reduced by 39.1% ( $P=0.02$ ) in male *Em1*<sup>+/-</sup> E18.5 mice (compared to a reduction of 79.4% in male *Em1* hom mice), together with a smaller SubVCx of -36.3% ( $P=0.0004$ ), as compared to -66.4% ( $P=0.0002$ ) in male *Em1* hom mice. This may suggest a gene dosage effect of *Em1* on certain aspects of developmental brain anatomy. Taken together, these results suggest a role for *Em1* in the regulation of brain size in a dosage dependent manner.

#### **Ectopic RG progenitors in *Em1* KO mice at early stages of corticogenesis**

Although heterotopia often arises because of aberrant neuronal migration, abnormalities in progenitor cells have also been associated with this cortical malformation (Bizzotto and Francis, 2015). In the spontaneous *Em1* mouse mutant, cycling progenitors were found outside the germinal layers, in basal regions of the cortical wall (Kielar et al. 2014, Bizzotto et al. 2017). These progenitors were often Pax6<sup>+</sup>, a marker of RGs, which are physiologically located in the neuroepithelial ventricular zone (Cxne). RGs are the main progenitor cells in the developing cortex, responsible for the production of other progenitor types and therefore the final neuronal output. Their apical processes extending to the ventricular surface (VS) are characterized by the presence of an adherens junctions-actin belt, which allows cell-cell interactions. Throughout the cell cycle, RG nuclei oscillate between the basal and apical-most region of the VZ, a process known as interkinetic nuclear migration. Basally they undergo S-phase, and mitosis takes place apically (Taverna et al. 2014, Uzquiano et al. 2018).

We assessed the location of cycling and Pax6<sup>+</sup> progenitors at early stages of corticogenesis (E13.5). First, we analyzed the distribution of Ki67<sup>+</sup> (a marker of proliferative cells), BrdU<sup>+</sup> (incorporated during S-phase) cells in E13.5 cortices subjected to a 30 min. BrdU pulse. In order to assess cell distribution, ROIs were divided in six equally-sized bins across the cortical wall (**Fig. 4A**, top row, right panel). No major differences were observed between WT

and het conditions, where Ki67+BrdU+ cells were mainly localized in basal regions of the Cxneas expected (bins 3 and 4, **Fig. 4A and 4C**). Hom mice (n=5) showed a significant increase in the percentage of Ki67+BrdU+ cells present in the SubVCx/ICx/CxP (bins 5 and 6) as well as in the apical-most Cxne (bin 1). Accordingly, there was a significant decrease in the percentage of cells expressing these markers in the most basal regions of the Cxne (**Fig. 4A and 4C**). This data shows the presence of aberrantly positioned cycling neuronal progenitors in *Em1* KO cortices.

In order to assess the identity of aberrantly localized progenitors, we performed the same type of analyses with the RG marker Pax6. Whilst the vast majority of Pax6+ cells was localized in the Cxne in WT and het mice, a significant proportion of Pax6+ cells was shifted towards more basal positions (SubVCx/ICx/CxP, bins 5 and 6) in hom developing cortices (**Fig. 4B, 4D**). Therefore, our immunohistochemistry analyses at early stages of cortical development show the presence of ectopic Pax6+ and cycling progenitors.

Mouse mutants showing ectopically located Pax6+ progenitors can show disruption of the adherens junctions-actin belt delineating the VS (Cappello et al. 2006; Cappello et al. 2012; Gan et al. 2014; Gil-Sanz et al. 2014; Junghans et al. 2005; Kadowaki et al. 2007; Schmid et al. 2014). We performed immunostainings for N-Cadherin and F-actin, both markers for this belt. We confirm that no major changes were observed in *Em1* KO mice when compared to WT mice (**Supp. Fig. 4C**). Similar results were obtained previously for the spontaneous *Em1* mouse mutant (Kielar et al. 2014) suggesting that other primary mechanisms are likely to be responsible for the presence of ectopic Pax6+ progenitors in *Em1* mouse mutants.

## Discussion

A previous study described neuroanatomical defects in a spontaneous mouse mutant of *Em1* (Croquelois et al. 2009), a gene encoding a microtubule-associated protein, as a result of a retrotransposon insertion in the intron lying between exons 22 and 23 (Kielar et al. 2014). In this study, we analyzed the brain morphology of a new KO mouse model of *Em1*, analyzing heterozygotes as well as homozygotes, and males as well as females. Overall, the anomalies we identified appeared more severe than the ones previously reported by spontaneous mutation on the NOR-CD1 genetic background (Croquelois et al. 2009). For example, the thickness of the homotopic cortex was reduced in the KO model in young adult and P13 animals (**Fig. 1D and Fig. 2C**), whereas it did not reach significance in the previously published

spontaneous model (Croquelois et al. 2009). The combined thickness of the homotopic and heterotopic cortices was either unchanged, or only moderately larger in our study (**Fig. 1D**, **Fig. 2C** and **Fig. 3C**), but much larger in the previous report (Croquelois et al. 2009). Another example includes the subcortical band heterotopia that we detected at E18.5, whereas in the published spontaneous model, at a similar embryonic age, an increase of the intermediate zone of the cortex was described but not visibly the heterotopia (Croquelois et al. 2009). It should be noted however, that Croquelois et al mentioned in their study that a proportion of animals were observed with severer phenotypes.

Our results at early stages of corticogenesis (**Fig. 4**) show similar results to those observed in the spontaneous *Em1* mouse mutant (Kielar et al, 2014). In *Em1* KO cortices we also observe the presence of ectopic cycling neuronal progenitors, further supporting that this progenitor displacement may be the original defect leading to the heterotopia phenotype in *Em1*-mutant conditions. The heterotopia develops from this point on, with accumulating neurons in the ICx, at the expense of those in the CxP.

The neuroanatomical anomalies we identified may point to a possible sexual dimorphism. Whilst male and female mice appeared to share similar phenotypes, variability in the female group, which also included apparently unaffected individuals, suggests a more complex pattern of inheritance. Indeed, in two *Em1* hom young adult females, the subcortical band heterotopia was completely absent, and in E18.5 females (n=2 analyzed), the size of the subcortical band heterotopia seemed to be more heterogeneous than in males. Overall, the phenotypes seem severer in males, and indeed, more male homozygotes (7/10) died than females (3/10). The reasons for potential male-female differences remain unclear but may reflect the genetic background used, possibly involving modifier genes, and/or hormones, leading to a less severe phenotype in females. Interestingly as well, at E18.5 and P13, subtle brain size defects may exist only in male heterozygotes. However, few heterozygote defects were detected at 7 weeks of age, which may suggest that these developmental anomalies represent delayed processes that catch up over time.

Our morphological screen of the KO on this genetic background allowed us to associate *Em1* function with spatially distinct brain defects, suggesting a role for the *Em1* gene in the overall architecture of the brain. This is consistent with the wider expression pattern of *Em1* in different types of neuronal progenitors and post mitotic neurons during development (Kielar et al. 2014). Although no defects were reported in the spontaneous model of *Em1* in

structures such as the hippocampus, the striatum, the thalamus and the cerebellum (Kielar et al. 2014), we found perturbations in the KO including corpus callosum agenesis and hydrocephalus, as well as in the organization and/or size of hippocampal regions, at embryonic, postnatal and adult stages. Interestingly, the *BXD29* mouse model for subcortical heterotopia shows ectopic clusters of neurons in CA1 and the dentate gyrus (Ramos et al. 2016). Additionally, other mouse mutants for genes mutated in severe forms of human heterotopia (*Dcx*, *Lis1*, *Tuba1a*) (Barkovich et al. 2012, des Portes et al. 1998, Gleeson et al. 1998) also show a heterotopia-like phenotype in the hippocampus in the form of a ‘double-layer’ in the CA3 region (Corbo et al. 2002; Hirotsune et al. 1998; Kappeler et al. 2007; Keays et al. 2007). It is thus of interest that CA3 cell dispersion was detected in the *Em1* KO model, and future work involving serial sections across the brain will attempt to confirm this phenotype.

Related to the hydrocephalus phenotype here described, a mild ventricular enlargement was previously reported in the *HeCo* mouse (Croquelois et al. 2009). Additionally, 2 out of 3 *EML1*-mutation families present hydrocephalus (Kielar et al. 2014, Shaheen et al. 2017). Further studies of *Em1* hom mice at postnatal stages may help unravel the underlying pathological mechanisms resulting in the hydrocephalus. Additionally, further postnatal studies are required to investigate causes of death of *Em1* hom mice and their relationships with brain morphology.

Rodent models of heterotopia, originally thought to be quite rare, are now becoming available to provide further information on how heterotopia form and disrupt neuronal function (reviewed in Bizzotto and Francis, 2015, Stouffer et al. 2016). This new constitutive KO, finely characterized here, is a valuable tool to contribute further to this domain.

## **Acknowledgements**

We are grateful to the French Fondation Maladies Rares for agreeing to fund this project. We would like to thank the Genetic Engineering and Model Validation Department at the ICS for generating the mouse model; the animal care-takers of the PHENOMIN-ICS animal facility for their technical assistance with mouse care. We would like to thank the Imaging Platform at the Institut du Fer à Moulin, Paris, as well as Dr. Marika-Nosten Bertrand for advice with

statistical analyses. Finally we would like to thank Patrick Reilly, Yann Herault and Tania Sorg from the ICS.

Conflict of Interest statement. None declared.

### **Funding**

AU and FF are associated with the BioPsy Labex project and the Ecole des Neurosciences de Paris Ile-de-France (ENP) network. Our labs are supported by Inserm, Centre national de la recherche scientifique (CNRS), UPMC, French Agence National de la Recherche (ANR-13-BSV4-0008-01; ANR-16-CE16-0011-03), Fondation Bettencourt Schueller, the European Union (EU-HEALTH-2013, DESIRE, No 60253) to FF, the JTC 2015 Neurodevelopmental Disorders, the ANR (for NEURON8-Full- 815-006 STEM-MCD), the Fondation Maladies Rares/Phenomin (project IR4995), and the European Cooperation on Science and Technology (COST Action CA16118) to FF. BY is supported by a French State fund grant (ANR-10-LABX-0030-INRT), managed by the Agence Nationale de la Recherche under the frame program Investissements d'Avenir ANR-10-IDEX-0002-02. AU received an ENP PhD grant, a Company of Biologists travel grant, and is currently funded by the Fondation de France. This study received support from French state funds through the ANR under the frame programme Investissements d'Avenir labelled ANR-10-INBS-07 PHENOMIN.

### **Bibliography**

Bahi-Buisson, N., Souville, I., Fourniol, F. J., Toussaint, A., Moores, C. A., Houdusse, A., Lemaitre, J. Y., Poirier, K., Khalaf-Nazzal, R., Hully, M., Leger, P. L. (2013). New insights into genotype-phenotype correlations for the doublecortin-related lissencephaly spectrum. *Brain* 136 (Pt 1): 223-244.

Barkovich, A.J., Guerrini, R., Kuzniecky, R.I., Jackson, G.D. and Dobyns, W.B. (2012) A developmental and genetic classification for malformations of cortical development: update 2012. *Brain*. 135, 1348–1369.

Beattie, R., M. P. Postiglione, L. E. Burnett, S. Laukoter, C. Streicher, F. M. Pauler, G. Xiao, O. Klezovitch, V. Vasioukhin, T. H. Ghashghaei and S. Hippenmeyer (2017). Mosaic Analysis with Double Markers Reveals Distinct Sequential Functions of Lgl1 in Neural Stem Cells. *Neuron*

94(3): 517-533 e513.

Birling, M.C., Dierich, A., Jacquot, S., Hérault, Y., Pavlovic, G. (2012) Highly-efficient, fluorescent, locus directed cre and FlpO deleter mice on a pure C57BL/6N genetic background. *Genesis*, 50(6):482-9. doi: 10.1002/dvg.20826.

Bizzotto S. and Francis F. (2015) Morphological and functional aspects of progenitors perturbed in cortical malformations. *Front Cell Neurosci.* 9, 30.

Bizzotto, S., Uzquiano, A., Dingli, F., Ershov, D., Houllier, A., Arras, G., Richards, M., Loew, D., Minc, N., Croquelois, A., Houdusse, A., Francis, F. (2017) Eml1 loss impairs apical progenitor spindle length and soma shape in the developing cortex. *Sci. Rep.* 7:17308.

Cappello S., Attardo A., Wu X. et al. (2006) The Rho-GTPase cdc42 regulates neural progenitor fate at the apical surface. *Nat. Neurosci.* 9, 1099–1107.

Cappello S., Bohringer C. R., Bergami M. et al. (2012) A radial glia-specific role of RhoA in double cortex formation. *Neuron*, 73, 911–924.

Collins, S., Wagner, C., Gagliardi, L., Kretz, P. F., Fischer M. C., Kessler, P., Kannan, M., Yalcin, B. (2018) Benefits of using parasagittal over coronal sectioning for neuroanatomical quantification of the adult brain structure in the mouse. *Curr Protoc Mouse Biol.* 8(3):e48. doi: 10.1002/cpmo.48.

Corbo, J.C., Deuel, T.A., Long, J.M., LaPorte, P., Tsai, E., Wynshaw-Boris, A. and Walsh, C.A. (2002) Doublecortin is required in mice for lamination of the hippocampus but not the neocortex. *J. Neurosci.* 22, 7548–7557.

Croquelois, A., Giuliani, F., Savary, C., Kielar, M., Amiot, C., Schenk, F., Welker, E. (2009) Characterization of the HeCo mutant mouse: a new model of subcortical band heterotopia associated with seizures and behavioral deficits. *Cereb Cortex* 19(3):563-575.

desPortes,V., Francis, F., Pinard,J. M. ,Desguerre, I. ,Moutard, M.L., Snoeck, I., Meiners, L.C., Capron, F., Cusmai, R., Ricci, S., et al. (1998) doublecortin is the major gene causing X-linked subcortical laminar heterotopia (SCLH). *Hum. Mol. Genet.* 7, 1063–1070.

Farrell, M. A., DeRosa, M. J., Curran, J. G., Secor, D. L., Cornford, M. E., Comair, Y. G., et al. (1992). Neuropathologic findings in cortical resections (including hemispherectomies) performed for the treatment of intractable childhood epilepsy. *Acta Neuropathol* 83: 246-259.

Gan, Q., Lee, A., Suzuki, R., Yamagami, T., Stokes, A., Nguyen, B. C., Pleasure, D., Wang, J., Chen, H. W. and Zhou, C. J. (2014) Pax6 mediates ss-catenin signaling for self-renewal and neurogenesis by neocortical radial glial stem cells. *Stem Cells*, 32, 45–58.

Gil-Sanz, C., Landeira, B., Ramos, C., Costa, M. R. and Muller, U. (2014) Proliferative defects and formation of a double cortex in mice lacking *Mltt4* and *Cdh2* in the dorsal telencephalon. *J. Neurosci.* 34, 10475–10487.

Gleeson, J.G., Allen, K.M., Fox, J.W., Lamperti, E.D., Berkovic, S., Scheffer, I., Cooper, E.C., Dobyns, W.B., Minnerath, S.R., Ross, M.E., et al. (1998) Doublecortin, a brain-specific gene mutated in human X-linked lissencephaly and double cortex syndrome, encodes a putative signaling protein. *Cell*, 92, 63–72.

Götz, M., Huttner, W. (2005). The cell biology of neurogenesis. *Nat Rev Cell Biol.* 6 (10), 777-7888.

Guerrini, R. (2005). Genetic malformations of the cerebral cortex and epilepsy. *Epilepsia* 46 Suppl 1: 32–37.

Jossin, Y., M. Lee, O. Klezovitch, E. Kon, A. Cossard, W. H. Lien, T. E. Fernandez, J. A. Cooper and V. Vasioukhin (2017). *Llg1* Connects Cell Polarity with Cell-Cell Adhesion in Embryonic Neural Stem Cells. *Dev Cell* 41(5): 481-495 e485.

Junghans, D., Hack, I., Frotscher, M., Taylor, V. and Kemler, R. (2005) Beta-catenin-mediated cell-adhesion is vital for embryonic forebrain development. *Dev. Dyn.* 233, 528–539.

Kadowaki, M., Nakamura, S., Machon, O., Krauss, S., Radice, G. L. and Takeichi, M. (2007) N-cadherin mediates cortical organization in the mouse brain. *Dev. Biol.* 304, 22–33.

Kappeler, C., Dhenain, M., Phan Dinh Tuy, F., Saillour, Y., Marty, S., Fallet-Bianco, C., Souville, I., Souil, E., Pinard, J.M., Meyer, G., et al. (2007) Magnetic resonance imaging and histological studies of corpus callosal and hippocampal abnormalities linked to doublecortin deficiency. *J. Comp. Neurol.* 500, 239–254.



Keays, D.A., Tian, G., Poirier, K., Huang, G.J., Siebold, C., Cleak, J., Oliver, P.L., Fray, M., Harvey, R.J., Molnar, Z., et al. (2007) Mutations in alpha-tubulin cause abnormal neuronal migration in mice and lissencephaly in humans. *Cell*, 128, 45–57.

Kielar M, et al. (2014) Mutations in Eml1 lead to ectopic progenitors and neuronal heterotopia in mouse and human. *Nat Neurosci* 17(7):923-933.

Matsuzaki, F. and Shitamukai, A. (2015) Cell division modes and cleavage planes of neural progenitors during mammalian cortical development. *Cold Spring Harb. Perspect. Biol.* 7, a015719.

Meencke, H. J., and Veith, G. (1992). Migration disturbances in epilepsy. *Epilepsy Res. Suppl.* 9: 31-40.

Mikhaleva, A., Kannan, M., Wagner, C., Yalcin, B. (2016) Histomorphological Phenotyping of the Adult Mouse Brain. *Curr Protoc Mouse Biol.* 6(3):307-332.

Molyneaux, B., Arlotta, P., Menezes, J. R., Macklis, J. D. (2007) Neuronal subtype specification in the cerebral cortex.

Liu, W. A., S. Chen, Z. Li, C. H. Lee, G. Mirzaa, W. B. Dobyns, M. E. Ross, J. Zhang and S. H. Shi (2018). PARD3 dysfunction in conjunction with dynamic HIPPO signaling drives cortical enlargement with massive heterotopia. *Genes Dev* 32(11-12): 763-780.

Palmer, T.D., Willhoite, A. R., Gage, F. G. (2000) Vascular niche for adult hippocampal neurogenesis. *J. Comp. Neurol.* 425, 479-494

Ramos, R. L., Toia, A. R., Pasternack, D. M., Dotzler, J. A. C., Esposito, A. W., Le, M. M., Parker, A. K., Goodman, J. H., Sarkisian, M. R. (2016)

Neuroanatomical characterization of the cellular and axonal architecture of subcortical band heterotopia in the BXD29-Tlr4<sup>lps-2J</sup>/J mouse cortex.

*Neuroscience*, 337, 48-65.

Richards, M. W., O'Regan, L., Roth, D., Montgomery, J. M., Straube, A. Fry, M., Bayliss, R. (2015) Microtubule association of EML proteins and the EML4-ALK variant 3 oncoprotein require an N-terminal trimerization domain. *Biochem. J.* 437 (3), 529-536.

Romero, D. M., Bahi-Buisson, N. and Francis, F. (2018) Genetics and mechanisms leading to human cortical malformations. *Semin. Cell Dev. Biol.* 76, 33–75.

Shaheen, R., Sebai, M. A., Patel, N., Ewida, N., Kurdi, W., Altweijri, I., Sogaty, S., Almardawi, E., Seidahmed, M. Z., Alnemri, A., et al. (2017) The genetic landscape of familial congenital hydrocephalus. *Ann. Neurol.* 81, 890-897.

Schmid M. T., Weinandy F., Wilsch-Brauninger M., Huttner W. B., Cappello S. and Gotz M. (2014) The role of alpha-E-catenin in cerebral cortex development: radial glia specific effect on neuronal migration. *Front Cell Neurosci.* 8, 215.

Stouffer, M. A., Golden, J. A. and Francis, F. (2016) Neuronal migration disorders: focus on the cytoskeleton and epilepsy. *Neurobiol. Dis.* 92, 18–45.

Taverna, E., Gotz, M. and Huttner, W.B. (2014). The cell biology of neurogenesis: toward an understanding of the development and evolution of the neocortex. *Annu Rev Cell Dev Biol*, 30, 465-502.

Uzquiano, A., Gladwyn-Ng, I., Nguyen, L., Reiner, O., Gotz, M., Matsuzaki, F., Francis, F. (2018) Cortical progenitor biology, cell cycling versus neurogenesis. *J. Neurochem.* doi: 10.1111/jnc.14338

## Figure legends

**Figure 1 Juvenile *Em1* KO mouse shows a giant subcortical band heterotopia, abnormal hippocampus, hydrocephalus and corpus callosum agenesis (A)** Schematic representation of affected brain regions in *Em1*<sup>-/-</sup> male (left) and female (right) mice at 7 weeks of age plotted in sagittal planes according to p-values. The top image represents a section at Lateral +0.60 mm. The color map indicates p-value below the threshold of 0.05 whereas grey indicates non measurable parameters. Histograms show the percentage decreased (minus scale) or increased (plus scale) of measured brain regions as compared to the controls (0%). They are combined with box plots displaying the median with interquartile range. Each point represents an animal. Certain data remain preliminary given that n<3 male mice for one or both genotypes were compared for the following areas: fornix, pontine nuclei, transverse fibers of pons and cingulate cortex height, and n<3 females were compared for: total brain area, brain height, temporal cortex area, pons height, cerebellum area, internal granule layer area, medial cerebellar nucleus area, corpus callosum height, caudate-putamen, anterior commissure, stria medullaris arza, substantia nigra area, optic chiasm and cingulate cortex height. **(B)** Nissl-

stained sagittal brain sections from *Em1<sup>-/-</sup>* mouse, showing a giant band of subcortical heterotopic neurons, dispersed neurons in the CA3 layer of the hippocampus and enlarged dorsal subiculum (indicated by black arrows). (C) Schematic representation of brain regions in *Em1<sup>+/-</sup>* male mice at 7 weeks of age plotted in sagittal planes according to p-values. Data concerning the following parameters/regions remain preliminary given the lower n numbers (i.e. n<3): transverse fibers of the pons, anterior commissure, corpus callosum area, lacunosum moleculare layer length and superior colliculus area. (D) Characterization of the heterotopic cortex (HeCo) as well as the homotopic cortex (HoCo) in *Em1<sup>-/-</sup>* male and female mice (n=2 for *Em1<sup>-/-</sup>* female mice). The description of the parameters used is provided in **Supp. Fig. 2C**. Plots are represented as mean  $\pm$ SEM. \* P<0.05, \*\* P<0.005, \*\*\* P<0.005 (Student's *t* test, two-tailed) for the comparison between HoCo and Cx (normal cortex in WT). (E) Details of brain regions assessed in order of appearance in Panel A together with corresponding numbers.

**Figure 2 *Em1* KO mouse shows similar defects at postnatal day 13** (A) Schematic representation of affected brain regions in *Em1<sup>-/-</sup>* male (left) and female (right) mice at P13 plotted in sagittal planes according to p-values. The top image represents a section at Lateral +0.60 mm. The color map indicates p-value below the threshold of 0.05 and grey indicates parameters where the n was too low to perform statistics. Histograms show the percentage decreased (minus scale) or increased (plus scale) of measured brain regions as compared to the controls (0%). They are combined with box plots displaying the median with interquartile range. Each point represents an animal. Certain data remain preliminary given that n<3 male mice for one or both genotypes were compared for the following areas: brain height 2, pons height, dorsal subiculum area, corpus callosum area and cingulate cortex area, and n<3 females were compared for: brain height 1, secondary motor cortex, lateral ventricle area, corpus callosum length, anterior commissure and cingulate cortex height. (B) Nissl-stained sagittal brain sections from *Em1<sup>-/-</sup>* mouse, showing a giant band of subcortical heterotopic neurons, dispersed neurons in the CA3 layer of the hippocampus and enlarged dorsal subiculum. (C) Characterization of the heterotopic cortex (HeCo) as well as the homotopic cortex (HoCo) in *Em1<sup>-/-</sup>* male and female mice. Plots are represented as mean  $\pm$ SEM. \* P<0.05, \*\* P<0.005, \*\*\* P<0.005 (Student's *t* test, two-tailed) for the comparison between HoCo and Cx (normal cortex in WT), and § P<0.05, §§ P<0.005 for the comparison between HoCo+HeCo

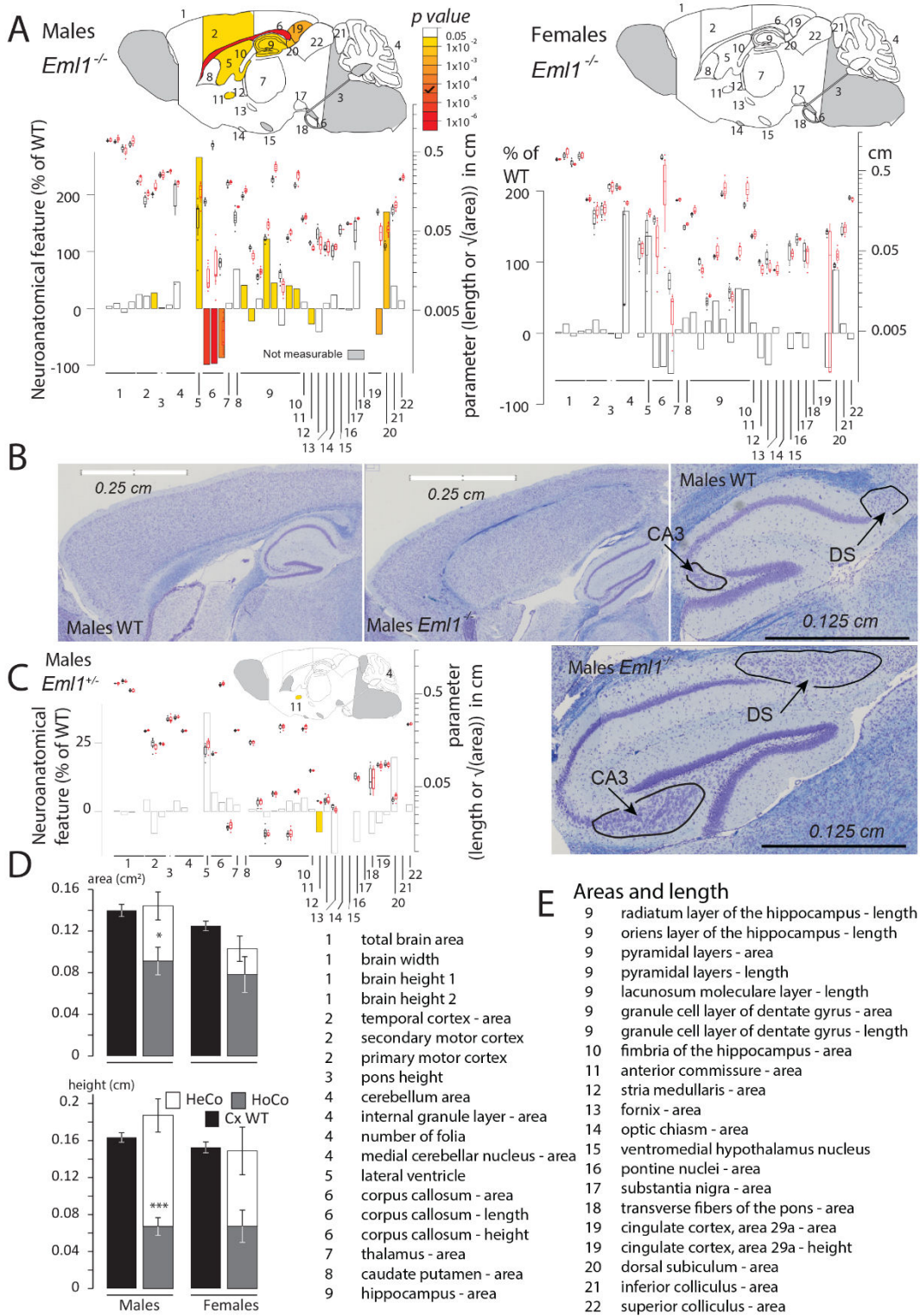
and Cx. **(D)** Immunostainings for Tbr1 at P13 in male and female WT, het and hom mice. Tbr1 (green) and DAPI (blue). White dashed lines delineate the heterotopia (\*). Scale bar: 100  $\mu$ m **(E)** Schematic representation of brain regions in *Em1*<sup>+/-</sup> male mice at P13 plotted in sagittal planes according to p-values. Histograms and box plots illustrate the results as described for A. Data concerning the following parameters/regions remain preliminary given n<3 numbers for one or both genotypes: total brain area, brain width, total brain height 1 & 2, temporal cortex, primary motor cortex length, pons height, thalamus area, caudate putamen area, radiatum layer of the hippocampus length, lacunosum moleculare layer length, dentate gyrus area and length, cingulate cortex area, dorsal subiculum area.

**Figure 3 Late embryonic *Em1* KO mouse exhibits subcortical band heterotopia but not enlarged ventricle size** **(A)** Histograms comparing E18.5 male and female *Em1*<sup>-/-</sup> to matched WT and showing variation (decreased-minus scale or increased-positive scale) in areas and lengths expressed as percentage of WT together with a color map indicating the significance level. They are combined with box plots displaying the median with interquartile range. Each point represents an animal. Certain data remain preliminary given that n<3 male mice for one or both genotypes were compared for the following areas: stria medullaris and optic chiasm area, and n<3 females were compared for: total brain height, subventricular zone, intermediate zone, lower cortical plate, lateral ventricles area, anterior commissure area, stria medullaris, optic chiasm area, inferior and superior colliculus, mesencephalic reticular formation area and pons area (left panel). A schematic representation of a section at Lateral +0.60mm with the colored regions indicating the presence of at least one significant parameter within the brain region (right panel). White coloring indicates a p-value higher than 0.05 and grey shows not enough data to calculate a p-value. **(B)** Representative Nissl-stained sagittal brain sections from E18.5 *Em1*<sup>-/-</sup> mouse (bottom panels), showing a giant band of subcortical heterotopic neurons (black arrow), compared to a WT section (top panels). **(C)** Characterization of the size and the average thickness of the homotopic (HoCo) and the heterotopic (HeCo) cortices in E18.5 *Em1*<sup>-/-</sup> male mice (top panels) and E18.5 *Em1*<sup>-/-</sup> female mice (bottom panels). The description of the parameters used is provided in **Supp. Fig. 3B**. Plots are represented as mean  $\pm$ SEM. \* P<0.05, \*\* P<0.005, \*\*\* P<0.005 (Student's *t* test, two-tailed) for the comparison between HoCo and Cx (normal cortex in WT), and § P<0.05, for the comparison between HoCo+HeCo and Cx. **(D)** Histograms and box plots comparing E18.5 male

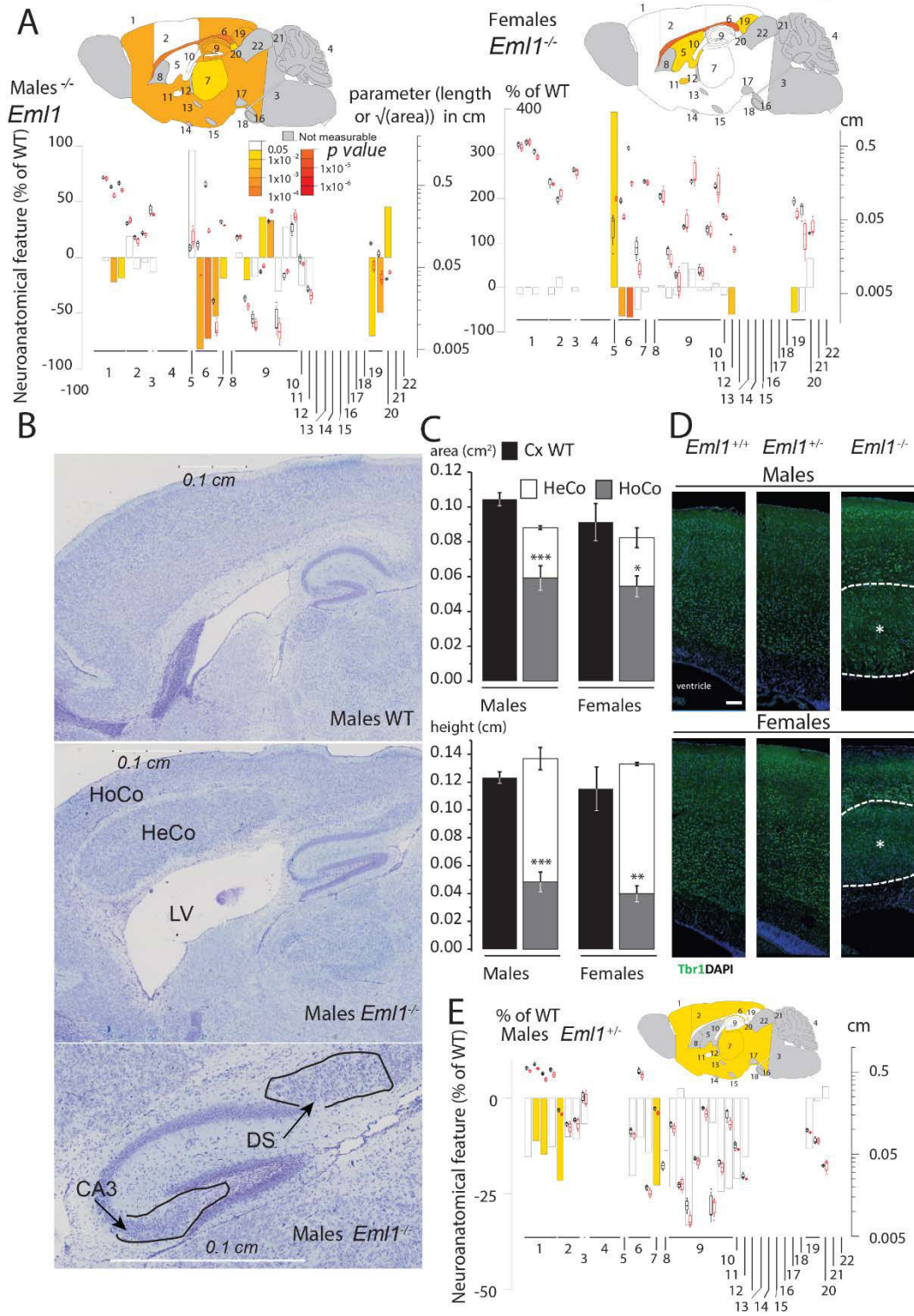
*Em1*<sup>+/-</sup> to matched WT as described for A. A schematic representation of a section at Lateral +0.60mm with the colored regions indicating the presence of at least one significant parameter within the brain region (right panel). White coloring indicates a p-value higher than 0.05 and grey shows not enough data to calculate a p-value. Data concerning the following parameters/regions remain preliminary given the low n numbers (i.e. n<3): lateral ventricles area, fimbria area, fornix area, stria medullaris area, optic chiasm area, total midbrain area, inferior and superior colliculus, mesencephalic reticular formation area, pons area.

**Figure 4 *Em1* KO mice show ectopic progenitors at early stages of corticogenesis.** (A) Representative images of WT (top row), het (middle row) and hom (bottom row) cortices at E13.5, immunostained for Ki67 (green) and BrdU (red) after a 30 min pulse of the latter. The diverse regions of the developing cortical wall are indicated in the first image of the top row (WT). An example of the binning procedure is shown in the last image of the top row (WT). (B) Representative images of WT (top row), het (middle row) and hom (bottom row) cortices at E13.5, immunostained for Pax6 (red) and Hoechst (blue). (C) Quantification of percentage of Ki67+BrdU+ cells present in each of the six bins. (D) Quantification of percentage of Pax6+ cells present in each of the six bins. Bins 1-4 span across the ventricular zone (Cxne or VZ). Bins 5-6 span across the subventricular zone (SVZ or SubVCx), intermediate zone (IZ or ICx) and cortical plate (CP or CxP). Scale bar: 10  $\mu$ m. The median is represented and the error bars represent the minimum and maximum range.

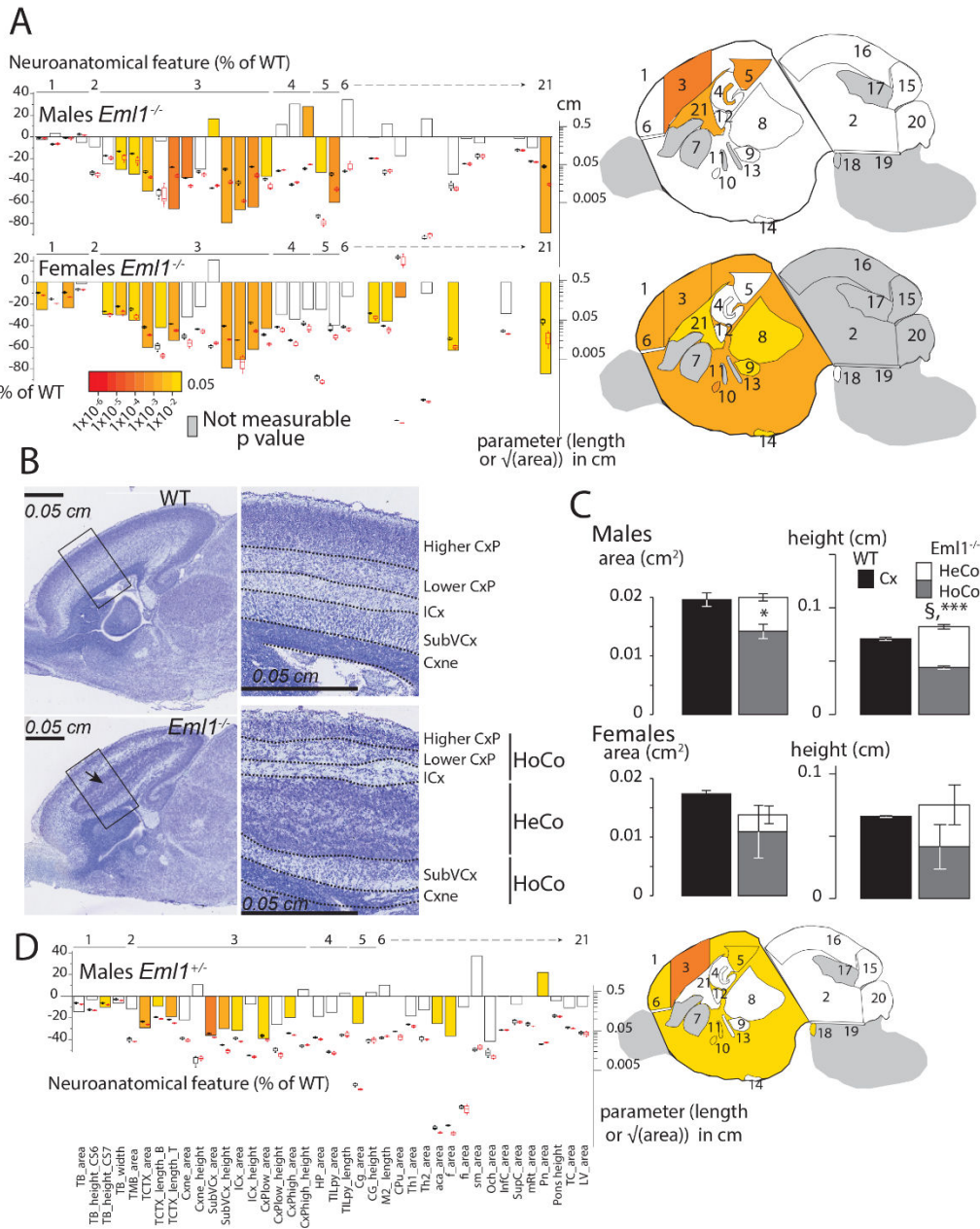
**Fig. 1**



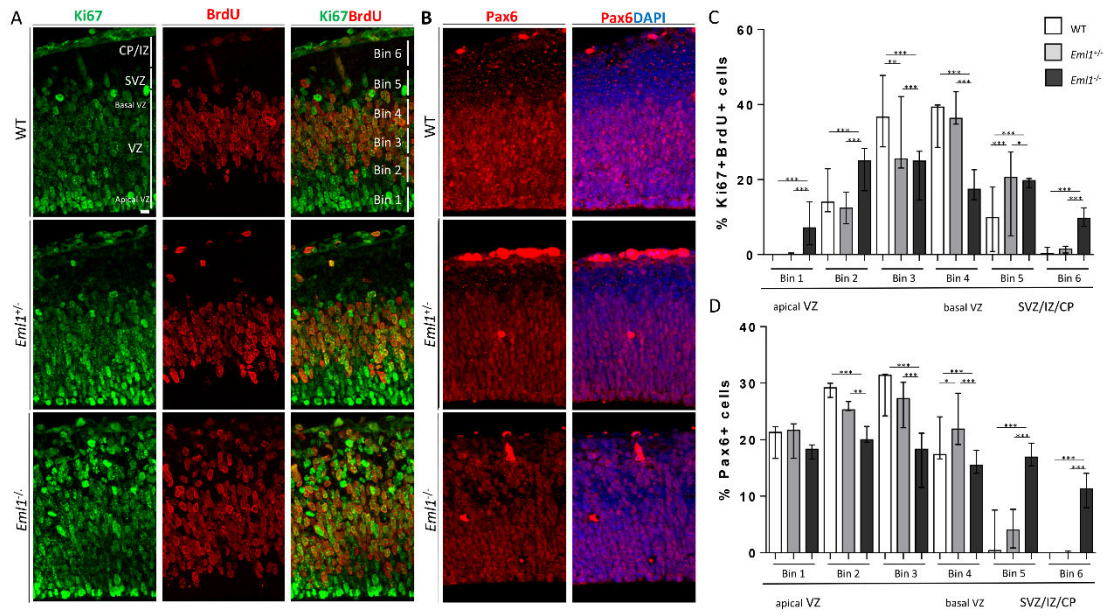
**Fig. 2**



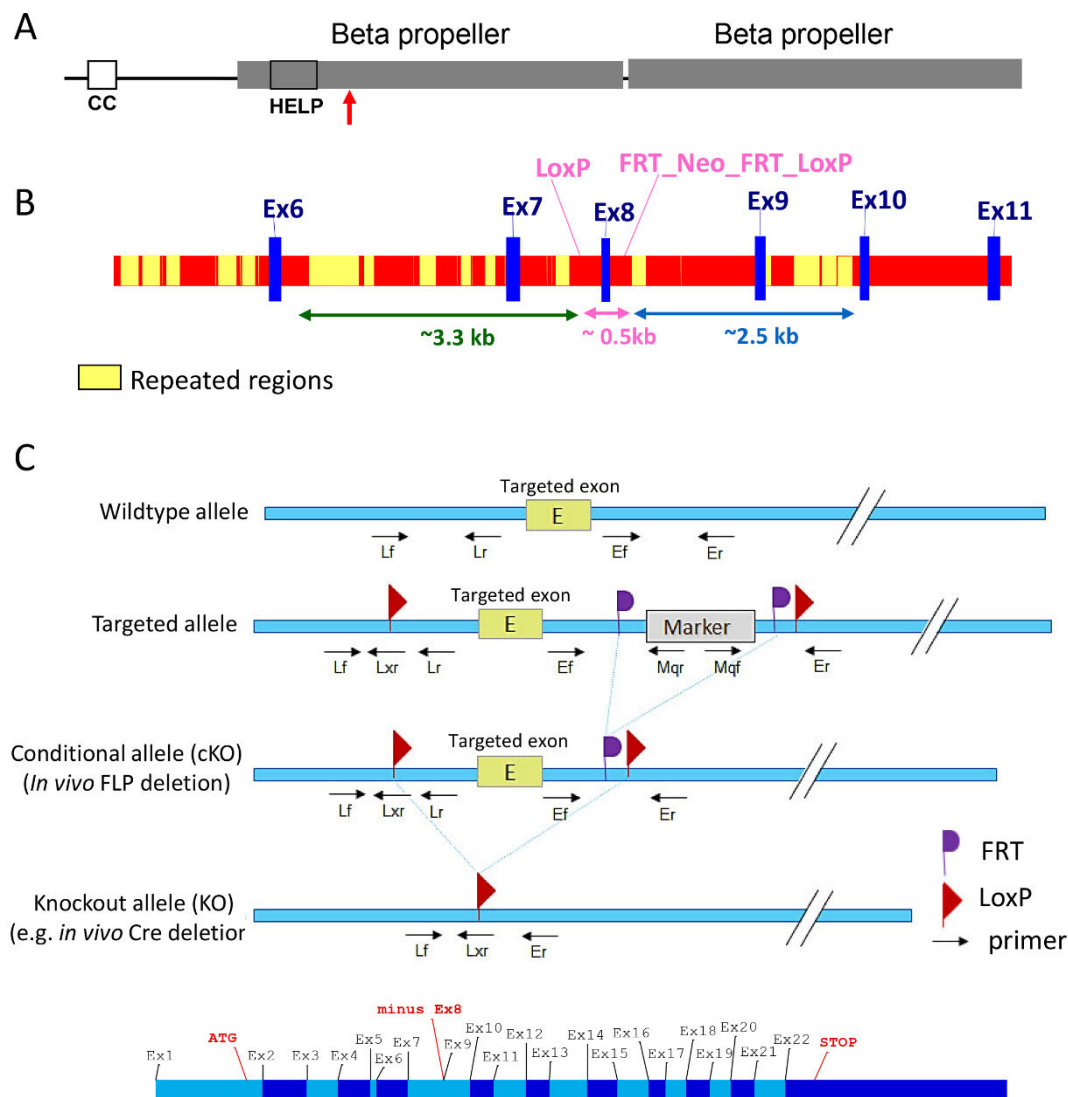
**Fig. 3**







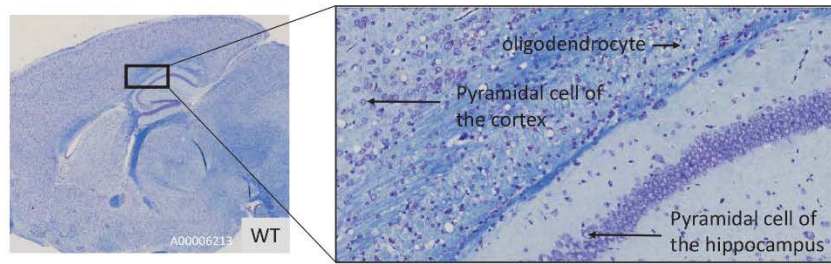
## Supplementary information



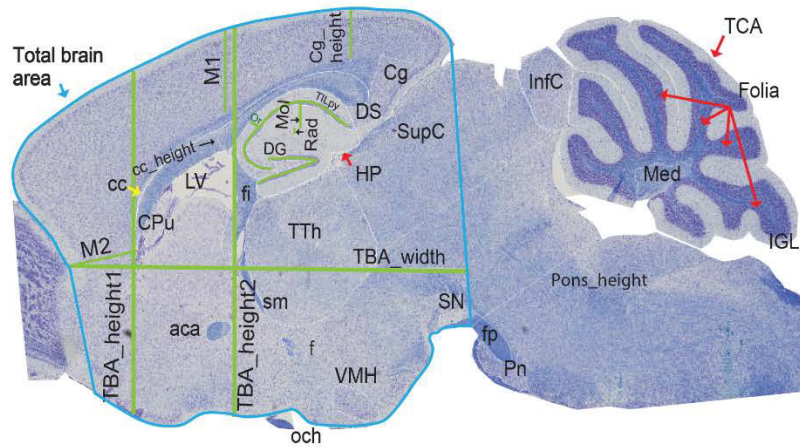
**Supplementary Figure 1 *Em1* KO strategy.** (A) Schematic of *Em1* protein domains, CC, coiled coil motif, HELP, hydrophobic EMAP-Like Protein motif. (B) Gene region showing modifications introduced in the targeting construct surrounding exon 8. (C) Schematic showing primers surrounding targeted exon 8 ('E'), red triangles indicate loxP sites and purple flags indicate FRT sites. Marker indicates Neo cassette. Mice carrying the knockout allele were produced showing a deletion of exon 8 (70 bp), leading to a frameshift and premature stop codon when exon 7 is spliced to exon 9.

Adult screen Lateral +0.60mm (right hemisphere)

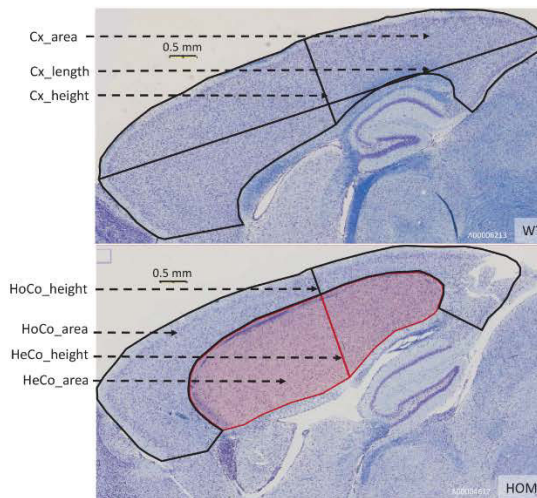
A



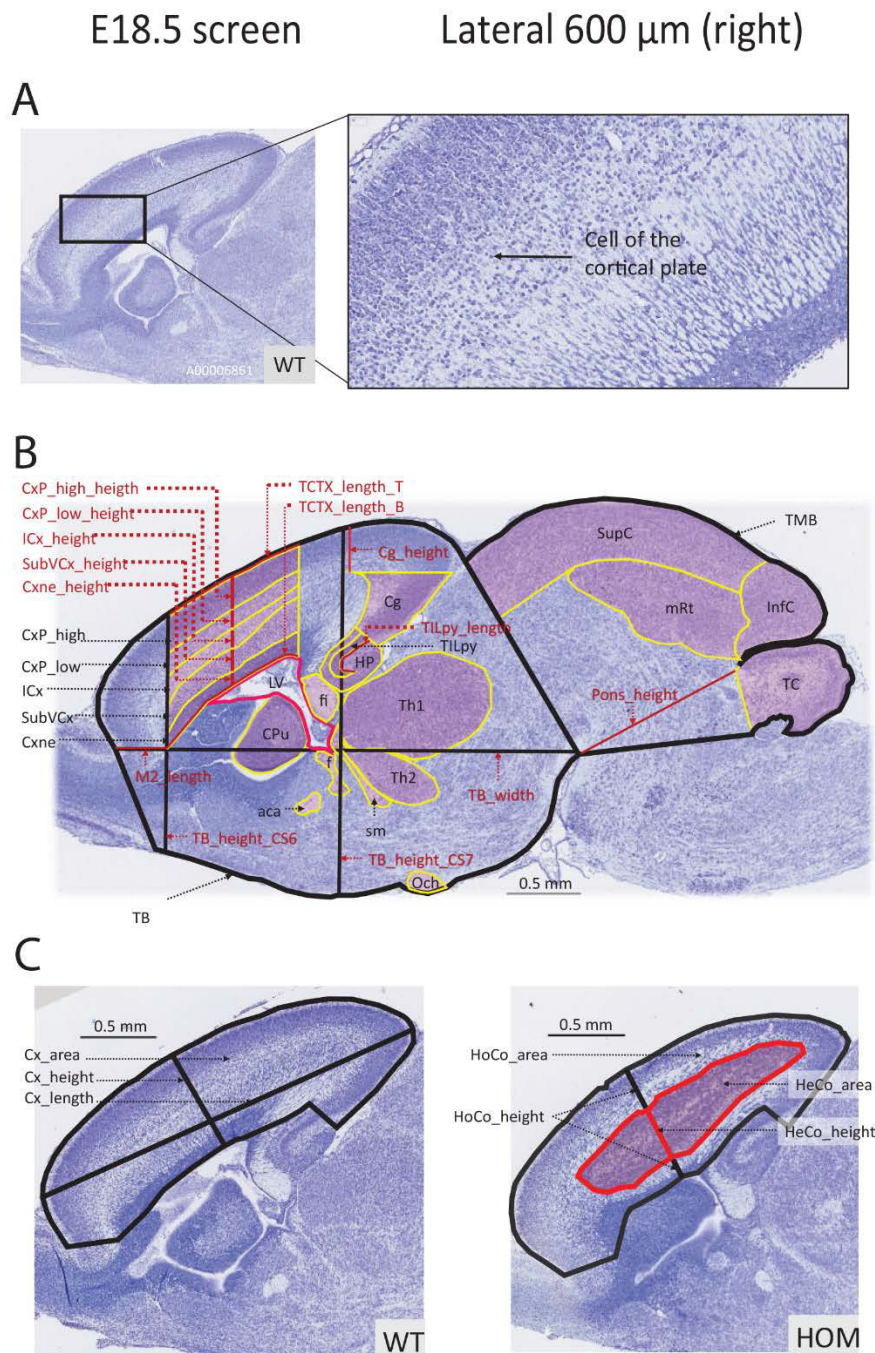
B



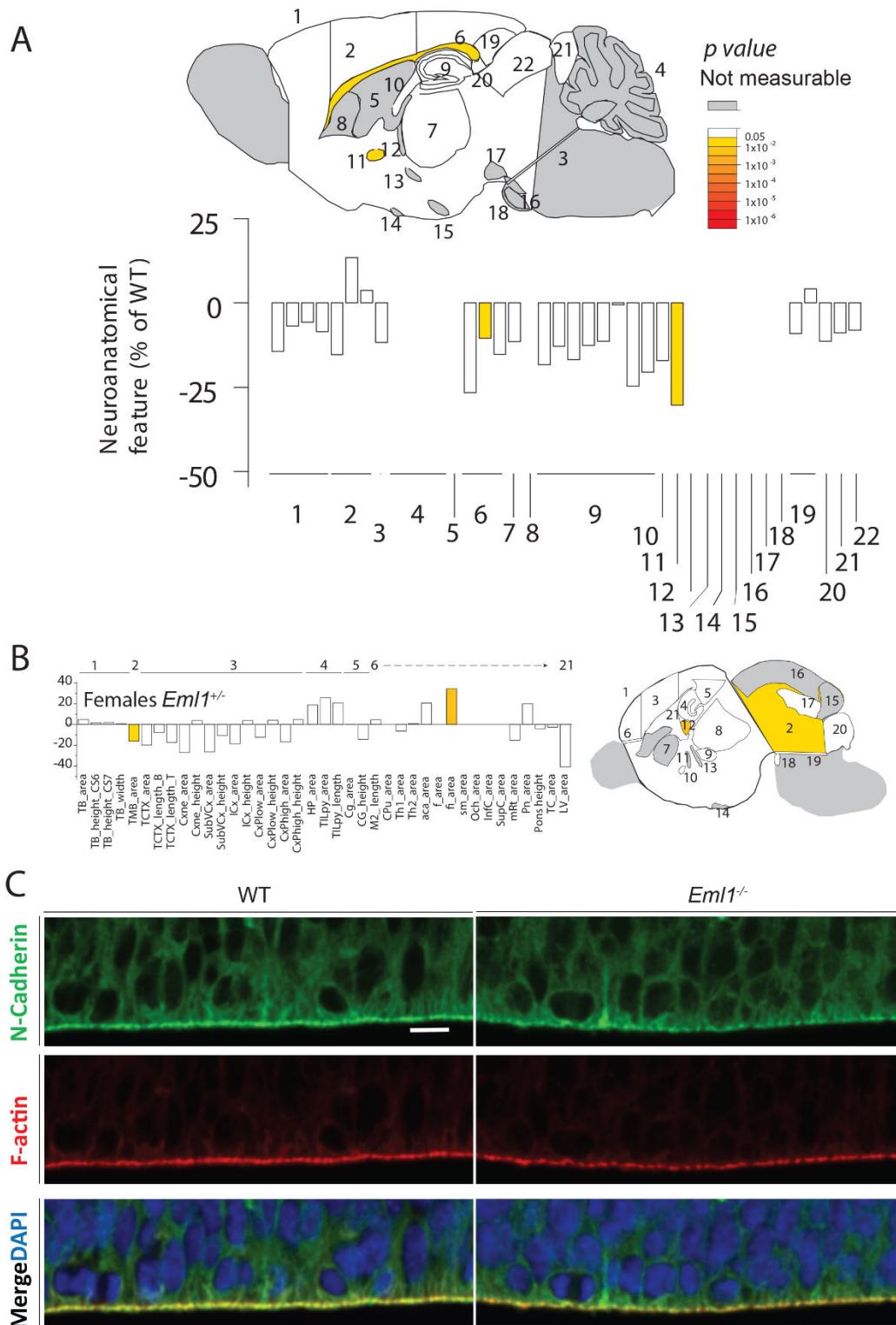
C



**Supplementary Figure 2. Adult screen. Resolution and adult mouse brain atlas.** (A) Zoomed image of a WT animal at 7 weeks of age. (B) Adult mouse brain atlas at Lateral 600  $\mu$ m (right hemisphere). A full description of the acronyms used in this Figure is provided in **Supp. Table 1**. (C) Additional 7 parameters added to the initial screen in order to further characterize the subcortical band heterotopia in *Em1*<sup>-/-</sup> mice.



**Supplementary Figure 3. Embryonic screen (E18.5). Resolution and E18.5 mouse brain atlas.** (A) Zoomed image of a WT animal at E18.5. (B) E18.5 mouse brain atlas of 39 parameters at Lateral 600  $\mu$ m (right hemisphere). Red font indicates length and black font area measurements. (C) Additional 7 parameters added to the initial screen in order to further characterize the subcortical band heterotopia in *Em11*<sup>-/-</sup> mice.



**Supplementary Figure 4. Schematic representation of brain regions in *Eml1*<sup>+/-</sup> female mice at P13 (A) and E18.5 (B). *Eml1* KO mice do not show major disruptions in the adherens junctions - actin belt at E13.5 (C). Representative images of immunohistochemistry performed in WT and hom mice for N-Cadherin (green), F-actin (red) and Hoechst (blue). Scale bar 10  $\mu$ m.**

## Supplementary tables

**Supplementary Table 1 Description of the 166 variables for adult brain sagittal analysis at Lateral 600  $\mu\text{m}$  (right hemisphere).** Column A gives the acronym of the brain parameter, column B its description, and column C the unit of the measurement.

**Supplementary Table 2 List of 39 variables for brain sagittal analysis at E18.5 Lateral 600  $\mu\text{m}$  (right hemisphere).** Column A gives the type of the analysis. Column B is the name of the section of interest (named "critical" section) on which the analysis was done. Column C gives the corresponding brain region analyzed. Column D is the acronym of the assessed parameter (9 refers to the right hemisphere, we keep the left hemisphere for storage). Column E, F and G provide the full description of the parameter, the category of the measurement and its unit, respectively.

**3.3 Extra supplementary results related to Collins, Uzquiano et al.** (not included in the submitted manuscript).

We characterized the ectopic progenitor phenotype in *Eml1* KO mice at E13.5. We then questioned if these mice also present the primary cilia abnormalities previously found in the *HeCo* mouse.

I first performed Arl13b immunohistochemistry on E13.5 brain slices and quantified the number of Arl13b+ puncta at the ventricular surface of WT and *Eml1* KO mice (Figure 51 A). There was a decrease in the number of Arl13b+ puncta at the *Eml1* KO ventricular surface when compared to WT (Figure 51 B), as previously described in the *HeCo* mouse (Bizzotto et al., 2017).

To further analyze the subcellular localization and ultrastructure of these organelles, we performed EM followed by primary cilia assessment in the VZ of WT and *Eml1* KO mice (Figure 51 C). As described for the *HeCo* mouse in Uzquiano et al. (manuscript 2), these organelles were shorter in *Eml1* KO aRGs, and they were often found in vesicle-like compartments and were basally oriented (Figure 51 D, E, F, respectively). Therefore, unrelated to the different genetic backgrounds, primary cilia structure and localization are compromised in *Eml1*-mutant conditions.

### **3.4 Supplementary methods**

#### *Immunohistochemistry*

Experiments were performed as described in Bizzotto et al., 2017. Images were acquired with a TCS Leica SP5-II confocal microscope. Two regions of interest (ROI) were analyzed per embryo (100 x 30  $\mu$ m). The ventricular surface was considered 2  $\mu$ m thick. Quantifications were performed using Image J.

#### *Electron microscopy*

Experiments were performed as described in Uzquiano et al. Images were analyzed using ImageJ.

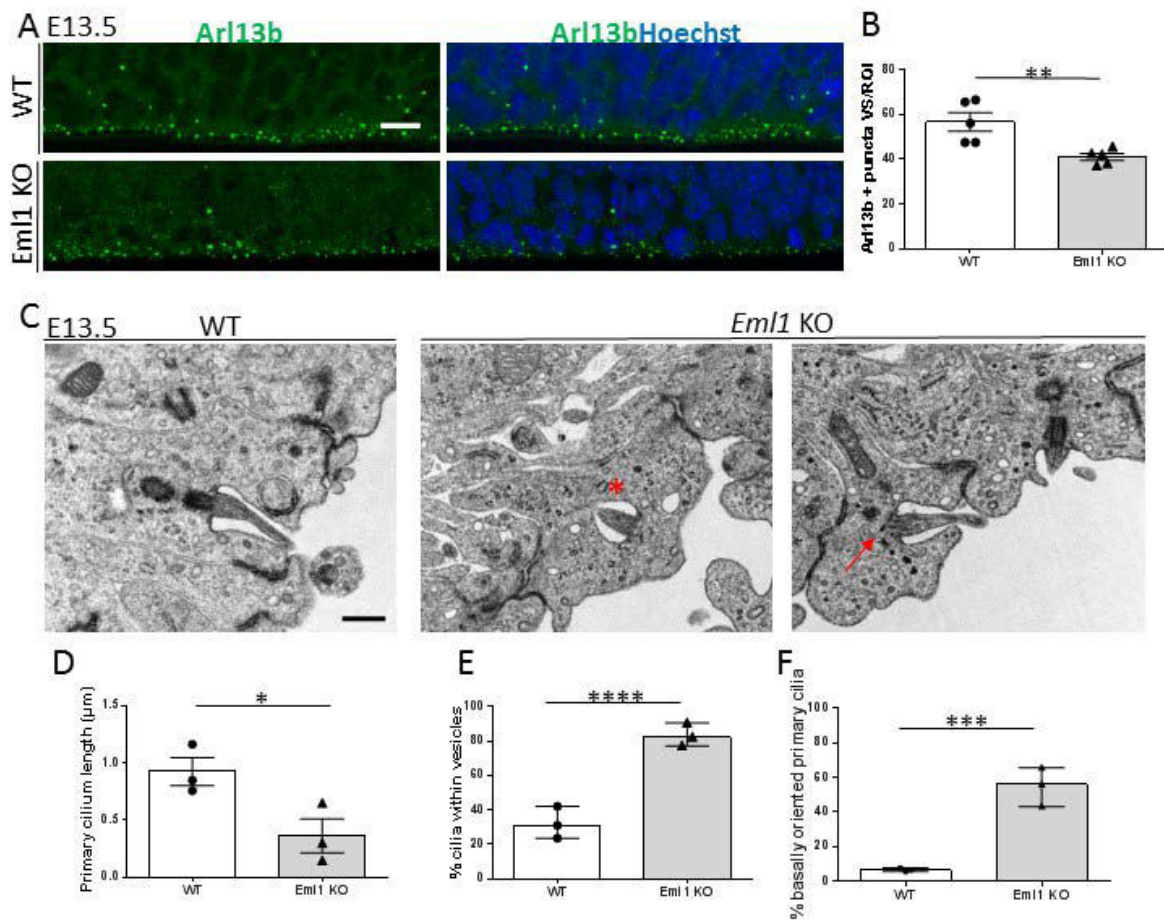


**Figure 51. Primary cilia are severely disrupted in the ventricular zone of *Eml1* KO mice.** A) Representative images of Arl13b (green) immunodetections in the WT and *Eml1* KO ventricular zone. B) Quantifications of Arl13b+ puncta at the ventricular surface (VS) per region of interest (ROI). Each point represents an embryo. WT= 5 embryos from 5 litters, *Eml1* KO: 5 embryos from 5 litters. C) Representative electron microscopy acquisitions. Red asterisk: basally oriented primary cilium in vesicle-like compartment. Red arrow: densely packed microtubules in the region where a properly assembled basal body should be positioned. D) Quantifications of primary cilium length. Each point represents an embryo. Both conditions n= 3 embryos from 3 litters. E) Quantifications of the percentage of primary cilia found within vesicles. Each point represents an embryo. Both conditions n= 3 embryos from 3 litters. F) Quantifications of the percentage of basally-oriented primary cilia. Each point represents an embryo. Both conditions n=3 embryos from 3 litters. Scale bar 10  $\mu\text{m}$  (A), 0.5  $\mu\text{m}$  (F). Mean  $\pm$  SEM, unpaired t-test (B, D), median  $\pm$  maximum and minimum range, Fisher's exact test (E, F), \*p<0.05, \*\*p<0.01, \*\*\*p<0.001, \*\*\*\*p<0.0001.



## **DISCUSSION**

## Discussion

### 1. *Eml1/EML1* mutations lead to subcortical heterotopia in mouse and human

#### 1.1 Cortical phenotype in *Em1*-mutant conditions

My PhD work has focused on the study of the heterotopia gene *Em1/EML1* mutated in mouse and human (Croquelois et al., 2009, Kielar et al., 2014, Shaheen et al., 2017). More precisely, I have focused on characterizing the *HeCo* mouse at early stages of cortical development to elucidate the primary events resulting in the heterotopia phenotype. As described in section 6.4 of the introduction, neuronal migration *per se* does not seem to be affected in this mouse, rather external mechanisms hamper neuronal migration (Kielar et al., 2014). Hence the *HeCo* mouse differs from classical models of human heterotopia thought to arise due to neuronal migration impairment (des Portes et al., 1998, Francis et al., 1999).

Neuronal progenitors presenting an aRG signature were previously found dividing outside the proliferative VZ from early-mid stages of corticogenesis (E13.5) (Kielar et al., 2014). I showed that this phenotype arises at even earlier stages i.e. E12.5. The presence of these mis-localized aRG-like progenitors is likely to be the primary disruption leading to the heterotopia phenotype.

Due to the lack of good antibodies for *Eml1*, the data we have concerning its expression in the developing cortex is based on *in situ* hybridization studies (Bizzotto et al., 2017, Kielar et al., 2014). *Eml1* is expressed in proliferative zones from early stages of corticogenesis. At later stages, it is also expressed in the CP (Bizzotto et al., 2017, Kielar et al., 2014). Public RNA-seq-based studies also allow us to gain more information about *Eml1* expression in the murine developing cortex from mid-stages of corticogenesis. Telley and colleagues (2016) established a single-cell RNA-seq-based approach to specifically investigate gene expression at different stages of neuronal differentiation in the developing cortex. More precisely, mitotic cells dividing in close contact with the ventricle were labelled with 'FlashTag' at E14.5. Tissue microdissection followed by Fluorescence Activated Cell (FACS) sorting and single-cell RNA-seq was performed 6h, 12h, 24h and 48h later. This allows to follow gene expression profiles in apically dividing progenitors, basal progenitors and 'early' and 'late' neurons (Telley et al., 2016). Intriguingly, *Eml1* appeared to be most highly expressed in basal progenitors, followed by a high expression in post-mitotic neurons. At these stages, although showing expression, apical progenitors appeared as the cell type with the lowest levels of *Eml1* mRNA (Figure 52).

This result may be similar to that observed by *in situ* hybridization in the ferret and section 1.4 below).

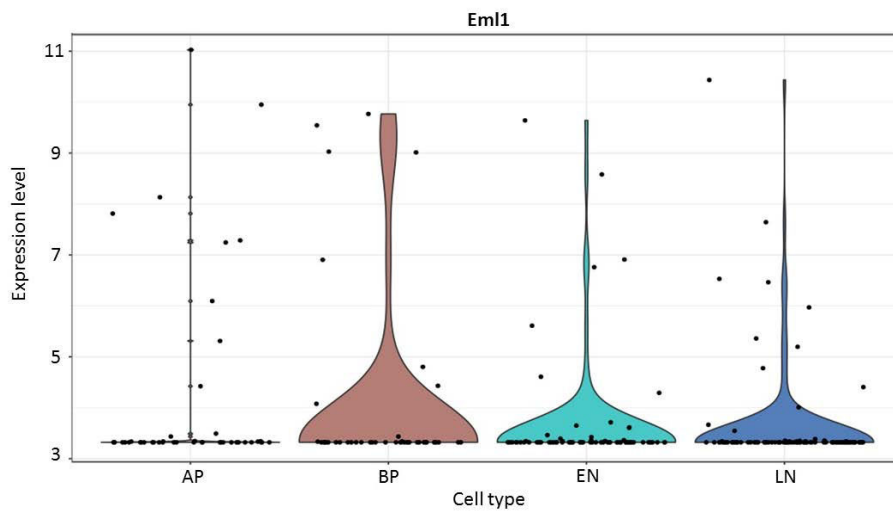


**Figure 52. *Eml1* expression level in cortical cell types.** Data obtained from FlashTag followed by FACS-sorting and single cell RNA-sequencing. AP: apical progenitor, BP: basal progenitor, EN: early neuron, LN: late neuron. <http://genebrowser.unige.ch/science2016/>

To further complement our knowledge about *Eml1* expression in post-mitotic neurons, we used the DeCoN resource (The Developing Cortical Neuron Transcriptome Resource) (Molyneaux et al., 2015), to follow *Eml1* expression from E15 to P1 in three subsets of neurons: subcerebral (ScNP), corticothalamic (CThPN) and callosal (CPN) projection neurons. *Eml1* is constantly expressed at low levels in ScNP, whilst its expression peaks from E16-E18 in CThPN. Concerning CPN, *Eml1* expression increases over these time points, with the highest expression shown at P1 (Figure 53).

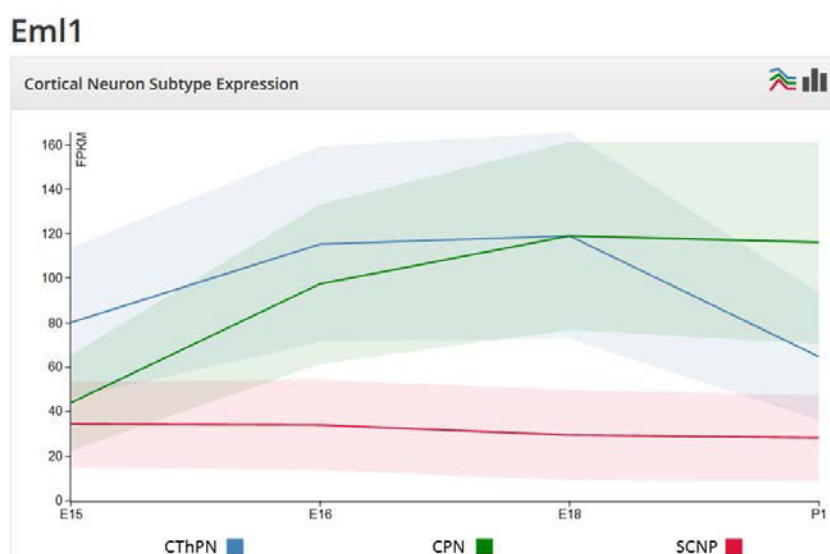


**Figure 53. *Eml1* differential expression in three main cortical neuron subtypes during cortical development from E15.5 to P1.** CThPN: corticothalamic neurons, CPN: callosal neurons, SCNP: subcerebral neurons, FPKM: Fragments per Kilobase of transcript per million. Adapted from <http://decon.fas.harvard.edu/bvramidal/>.

Although these RNA-seq approaches lack information related to earlier stages, they strongly support a role for *Eml1* in different cortical neuron populations as well as progenitors throughout corticogenesis. Additionally, independently of the intrinsic role of *Eml1* in these cells, basal progenitors and newly produced post-mitotic neurons signal to apically dividing progenitors influencing their behavior. We can therefore hypothesize that *Eml1* mutation in these differentiated cell types may influence this cell-cell communication. In section 6.4 of the introduction I described the *HeCo* heterotopic cortex as mainly composed of upper layer neurons (although migration of all neurons appears also to be slowed). The normal high expression of *Eml1* in CPN neurons is thus interesting. Misplaced *Eml1* mutant CPN may function abnormally due to changed intrinsic properties, as well as abnormal position. Although neuronal migration *per se* does not seem to be affected, other neuronal features could be perturbed. Their contribution to the etiology of the heterotopia, agenesis of the corpus callosum, as well as to the epilepsy-like phenotype developed in postnatal stages should further be assessed.

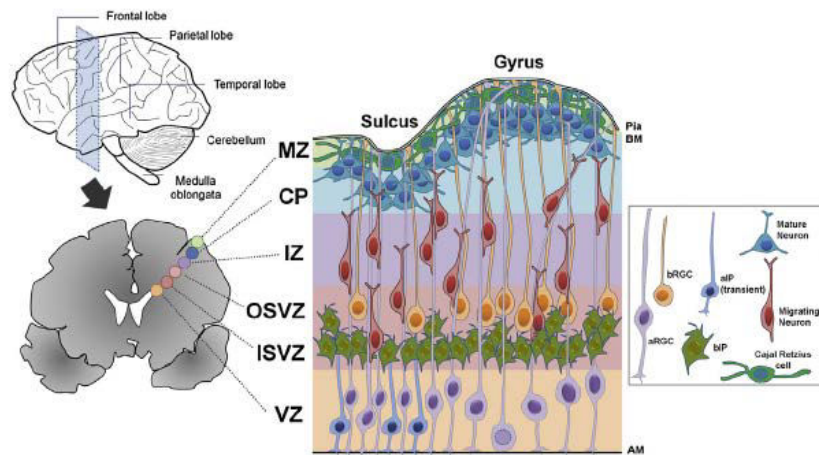
As part of my thesis project I also contributed to the characterization of a new *Eml1* KO mouse, presenting a very similar phenotype to the *HeCo* mouse despite its different genetic background (C57BL/6N). Accordingly, Pax6+ proliferative progenitors were also found outside the normal proliferative VZ, further supporting a role for these ectopic cells in the etiology of the heterotopia. Although we first focused on characterizing the constitutive *Eml1* KO mouse, a conditional mouse is also now available. Related to the above-discussed studies and *Eml1* expression profile throughout corticogenesis, these mice represent an excellent tool to dissect its role in different cortical cell types and thus to assess their contribution to the pathological mechanisms involved in the formation and function of the heterotopia.

## **1.2 Mouse versus human phenotype**

As previously described in sections 6.3 and 6.4 of the introduction, the heterotopia phenotype due to *Eml1/EML1* mutations differs between mouse and human. In the *HeCo* mouse, mis-localized neurons were found beneath the normal cortex and within the white matter (Croquelois et al., 2009, Kielar et al., 2014). *Eml1* KO mice also showed a similar heterotopia phenotype. In human patients, the phenotype is more severe, with huge masses of neurons starting at the level of the ventricles in frontal regions and extending to the subcortical white matter (Kielar et al., 2014). Additionally, the heterotopia was associated with polymicrogyria, corpus callosum agenesis and macrocrania (Kielar et al., 2014).

The mechanisms underlying these differences remain unknown. However as described in the introduction, the folded human neocortex presents a high variety of neuronal progenitors absent in the smooth mouse neocortex (Figure 54). Particularly, bRGs have emerged in the last decade as a key cell type involved in neocortical expansion and gyrification (Fernandez et al., 2016). Recent studies point to this cell type as a target

#### A. Human cortical development



#### B. Mouse cortical development

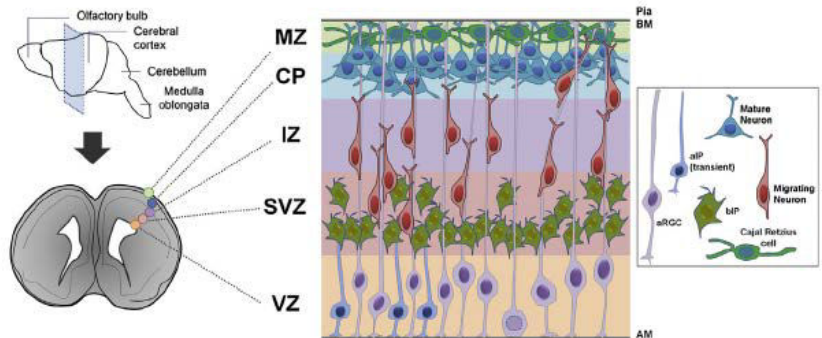


**Figure 54. The folded human neocortex presents a higher diversity of neuronal progenitors absent in the smooth mouse neocortex.** MZ: marginal zone, CP: cortical plate, IZ: intermediate zone, OSVZ: outer subventricular zone, ISVZ: inner subventricular zone, VZ: ventricular zone, BM: basal membrane, AM: apical membrane, aRGC: apical radial glia cell, aIP: apical intermediate progenitor, bIP: basal intermediate progenitor, bRGC: basal radial glia cell. Romero et al., 2018.

in certain cortical malformations, which might help explain the differences observed between rodent models and human patient phenotypes (Bershteyn et al., 2017, Ostrem et al., 2017). Therefore, it is possible that abnormal behavior of bRGs contributes to the phenotype observed in *EML1*-mutant conditions. As described in section 3.4 of the introduction, bRGs are important for neuronal production but also to act as a scaffold for migrating neurons. bRG basal anchoring is likely to be important for the correct gyri and sulci pattern. The basal processes of ectopic progenitors in the *HeCo* mouse sometimes appear to be misoriented (see below). In a human context, bRG basal processes may also be impaired affecting as well the basal membrane. Abnormal aRG basal process anchoring and basal membrane breakages have been previously associated with cortical malformations affecting cortical folding (see section 4.2 of the introduction). *Eml1*-mutant mice do not show a polymicrogyria-like

phenotype and aRGs remaining in the VZ appear to be properly attached to the basal membrane, although a further analysis of basal endfeet is warranted.

In the last years, several studies have identified genes specific to primate/human aRGs (Fiddes et al., 2018, Fietz et al., 2012, Florio et al., 2015, Florio et al., 2018, Johnson et al., 2015, Ju et al., 2016, Li et al., 2014, Liu et al., 2014, Pollen et al., 2015, Suzuki et al., 2018). Human aRGs have also been shown to change their morphology during corticogenesis (Nowakowski et al., 2016). Therefore, we can hypothesize that other features of aRGs are likely to show primate and/or human specific traits. For instance, the VS may be more affected when *EML1* is mutated, which could explain the presence of big masses of neurons at the level of the ventricles.

Finally, some *EML1* SH patients also present hydrocephaly. Related to this, a mild ventricular enlargement was reported in the *HeCo* mouse (Croquelois et al., 2009). *Eml1* KO mice described in section 3 of the results also show a partially penetrant hydrocephaly phenotype. Interestingly, the latter arises at postnatal stages and this trait appears segregated from the heterotopia phenotype. Hence the mechanisms leading to these two phenotypes seem to be independent. Hydrocephaly can arise due to impairment of motile cilia in ependymal cells (Spassky and Meunier, 2017), which derive from aRGs (Spassky et al., 2005). Precursors of multiciliated ependymal cells have one centrosome from which multiple centrioles are produced. Afterwards, centrioles are docked in the apical plasma membrane and nucleate cilia. Once in the plasma membrane, they acquire a rotational polarity, important for the direction of cilia beating (Spassky and Maunier, 2017). Anomalies in any of these steps can result in pathological conditions i.e. hydrocephaly. Given the centrosome-primary cilium phenotype I describe in *Eml1/EML1*-mutant conditions, it would be interesting to further assess the aRG-to-ependymal transition in *Eml1*-mutant conditions, as well as to carefully analyze centriole duplication in prospective ependymal cells, as well as the motile cilia. Abnormalities in any of these processes could contribute to explain the postnatal hydrocephaly phenotype both in mouse and human. Other more common mechanism have been described to be responsible for the development of hydrocephaly i.e. narrowing of the passage between the third and fourth ventricle and thus impaired draining of cerebrospinal fluid. Therefore, other processes may be responsible for the hydrocephaly phenotype observed in *EML1/Eml1* mutant conditions.

### 1.3 Basal radial glia versus ectopic progenitors

*Eml1*-mutant conditions lead to the presence of ectopically dividing Pax6+ progenitors outside the normal proliferative VZ in the mouse developing cortex. Further studies are required to understand the identity of these ectopic cells. In the *HeCo* model, they appear to lack apical processes and their basal processes in some cases are mis-oriented, not reaching the basal membrane, as shown in pVimentin stainings (Kielar et al., 2014). Experiments using Dil to further examine the basal fibers as previously performed in other studies (Florio et al.,

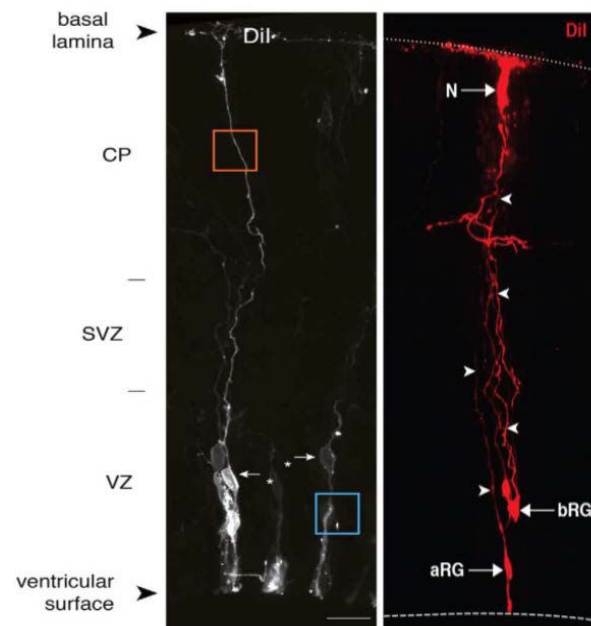


**Figure 55. Analysis of radial glia processes using Dil.** CP: cortical plate, SVZ: subventricular zone, VZ: ventricular zone, aRG: apical radial glia, bRG: basal radial glia. Adapted from Taverna et al., 2016-(left), Florio et al., 2015 (right).

2015, Taverna et al., 2016, Figure 55) would help more fully clarify morphologies. Ectopic progenitors are Pax6+ Sox2+ and BLBP+, markers shared by aRGs and bRGs. Testing for newly identified bRG-specific markers such as HOPX or FAM107A (Pollen et al., 2015) would also complement the characterization of these cells. Other experiments aiming to analyze their mode of division would also help discern between aRG versus bRG identities.

It is intriguing how Pax6+ cells found proliferating outside the VZ can result in different outcomes in the mouse neocortex. Several studies have shown how forced bRG-like production results in the appearance of fold-like structures (Ju et al., 2016, Liu et al., 2017, Stahl et al., 2013, Florio et al., 2015, Wang et al., 2016). In other cases, ectopic Pax6+ progenitors lead to subcortical heterotopia (Kielar et al., 2014, Liu et al., 2018), or eventually undergo cell death resulting in a small brain (Insolera et al., 2014, Marthiens et al., 2013). Other studies have reported the presence of non-apically dividing Pax6+ progenitors (Asami et al., 2011, Konno et al., 2008), although the adult phenotype was not examined. In addition, recent work describes the presence of bRG-like cells upon up- or down-regulation of certain genes in the mouse neuroepithelium (Tavano et al., 2018, Wong et al., 2015) without describing postnatal phenotypes.

The mechanisms responsible for the production of different Pax6+ basally dividing progenitor populations remain largely unexplored. It would be interesting to carefully examine aRG features responsible for bRG-like versus aberrant ectopic progenitor production. Although some mechanisms may converge, production of the latter is likely to involve pathological processes altering 'correct' aRG behavior and thus impacting a 'true' bRG-like cell fate. Ideally, RNA-sequencing analyses could further unravel the differences between bRG-like/ectopic progenitor transcriptional profiles, possibly pointing to distinct intracellular pathways involved in the final cortical phenotype i.e. cortical folding vs heterotopia. In addition, examining the postnatal phenotype of mouse models with basally dividing Pax6+ progenitors may help pinpoint the downstream effectors and cascades leading to a bRG versus ectopic progenitor identity.

In the context of my thesis project, it would also be of great interest to compare not only the transcriptional profile of Pax6+ ectopic progenitors but also the progeny present in *Eml1* mutant mouse models to assess cell developmental trajectories.

#### **1.4 A role for Eml1 in basal radial glia?**

The ectopic progenitor phenotype observed in the mouse neocortex in *Eml1*-mutant conditions does not rule out a role for Eml1 in bRG production, function(s) and/or neocortical expansion. Data obtained from different studies suggest this may actually be the case.

A large-scale transcriptome analysis was performed in the ferret comparing gene expression in different proliferative layers in regions of folds (splenial gyrus) versus fissures (lateral sulcus) (de Juan Romero et al., 2015). Many of the genes showing a differential profile in gyri versus sulci were associated with cortical malformations (de Juan Romero et al., 2015). Interestingly, Eml1 was upregulated in gyri versus sulci regions. In addition, *in situ* hybridization expression data shows Eml1 expression in the expanded SVZ of the ferret neocortex (Kielar et al., 2014, section 2 of the results). At P1 and P6 it is expressed in the bRG-abundant proliferative oSVZ, as well as the iSVZ and VZ (coll. Borrell lab). A similar distribution was also observed in human fetal brain (Borrell lab, unpublished). These data together may suggest an expression in bRGs. Two recent studies assessing mechanisms of bRG production in the mouse neuroepithelium further point towards a role for Eml1 in bRG production. Narayanan and colleagues (2018) described a role for BAF155, a subunit of the BAF chromatin remodeling complex, in bRG-like



cell production in the mouse neocortex. *Emx1*-Cre driven conditional KO for *BAF155* showed an increase of bRG-like progenitors at mid-late stages of corticogenesis (E15.5 and E16.5) (Figure 56). The authors performed RNA-sequencing of the E15.5 cortex to identify genes with altered expression in *BAF155* conditional KO mice. *Eml1* was found amongst the downregulated genes, and the deregulated molecules included as well some of the proteins found in the mass spectrometry screens when searching for *Eml1* interacting partners (e.g. *Kif21b*, *Rnd2*, *Map4*, *Plk1*) (Bizzotto et al., 2017, Narayanan et al., 2018). Analyses at postnatal stages showed no alterations of cortical layering, area or thickness (Narayanan et al., 2018). Concomitantly with bRG-like cell production, the authors found a decrease of IPs (Narayanan et al., 2018), which may help explain the absence of a cortical phenotype at later stages.

Tavano and colleagues (2018) also described a role for the Zinc finger TF *Insm* in bRG-like cell generation. Overexpression of *Insm* by *in utero* electroporation in the mouse neuroepithelium at E13.5 led to aRG delamination resulting in bRG-like cell production (Tavano et al., 2018). In order to elucidate the subcellular mechanisms involved in this process, the authors performed *in utero* electroporation of *Insm* followed by FACS sorting and RNA-seq 24h later. Interestingly, *Eml1* was also downregulated upon *Insm* overexpression. As for the study mentioned previously, some proteins found in our mass spectrometry screens were also downregulated (e.g. *Kif21b*, *Numbl*) (Bizzotto et al., 2017, Tavano et al., 2018). In the human cortex, the highest levels of *INSM1* protein were detected in *HOPX*<sup>+</sup> newborn BPs in the VZ. In agreement, in the mouse cortex some newborn *Insm1*-expressing BPs are still present in the VS (Tavano et al., 2018). bRG-like cells produced upon *Insm* overexpression were shown to delaminate from the VS as previously described in the human brain (Gertz et al., 2014). Additionally, they show correct anchoring of the basal process to the basement membrane. Therefore with the downregulation of *Eml1* (as well as many other genes), *Insm* appears to induce a ‘true’ bRG identity and may be a key player in bRG production, SVZ formation and ultimately neocortical

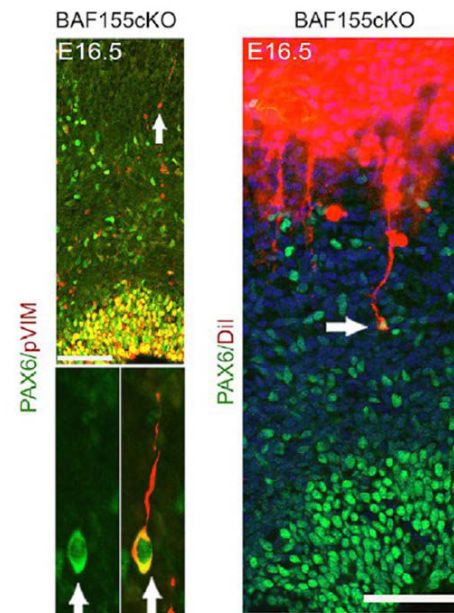


**Figure 56.** *BAF155* cKOs present bRG-like cells at E16.5. bRG-like cells are Pax6<sup>+</sup> and are properly anchored to the basal membrane. From Narayanan et al., 2018.

expansion (Tavano et al., 2018). It would be interesting to assess postnatal stages upon *Insm* overexpression. Although the mechanisms are still unclear, these two studies suggest a role for *Eml1/EML1* in normally inhibiting bRG production, as well as potentially a specific function in the oSVZ of gyrencephalic species.

### **1.5 Recent models to address human specific features of cortical development**

New models to study brain and/or cortical development have emerged with the possibility of reprogramming somatic cells into iPSCs. This has led to the development of 2D and 3D *in vitro* models derived from human cells, recapitulating events of physiological and/or pathological brain development. Rodents are an excellent model to study specific features of development, however they lack the complexity of the primate/human brain (Figure 54). Hence, these new approaches represent an entry point to study specific features of human brain development. 2D cultures are proving to be useful to study disease-specific features. For instance, several studies have used neurons differentiated from patient-derived iPSCs to study psychiatric disorders (reviewed by Quadrato et al., 2016). In collaboration with the lab of Dr. J. Ladewig, Germany, we have also examined iPSC-derived cortical progenitors, derived from patients showing mutations in *EML1*. Similar subcellular abnormalities were identified as those previously found in the *HeCo* neuroepithelium. The convergence of the '2D human' and mouse phenotypes suggests a conserved role of *Eml1/EML1* across species and suggests that at least some cortical progenitor 'pathological' mechanisms overlap, potentially responsible for the subcortical heterotopia phenotype. 2D models are a great tool to study subcellular specific features in a relatively homogenous cell population. Although this can be an advantage, it also represents a drawback since these cells lack to a certain degree an 'endogenous' organization as well as tissue specific interactions, likely to be critical for their behavior (Brown et al., 2018). 3D human organoid/spheroid models hold the potential of recapitulating to a better degree the anatomical organization and cell-cell interactions more closely related to those found *in vivo*. Broadly, two main protocols are used to develop brain organoids (reviewed by Di Lullo and Kriegstein, 2017, Quadrato et al., 2016). The first one relies on intrinsic properties prompting self-patterning and self-organization. Although reproducibility between organoids can be challenging, they have the advantage of producing multiple brain regions and thus great cell diversity (Brown et al., 2018). The second protocol relies on external patterning signals provided to the culture to favor the production of a particular brain region and thus certain cell types. They have the advantage of being more reproducible, and hence modelling

certain pathogenic conditions can be simpler (Brown et al., 2018). However, they do not account for the large cell variety often found in a given brain region. For instance, dorsal cortical organoids lack GABAergic interneurons, even if progress has been made to incorporate this cell type in the model (Bagley et al., 2017, Birey et al., 2017, Xiang et al., 2017).

Dorsal cortical organoids have ventricle-like cavities, surrounded by aRGs which are capable of producing IPs and neurons (Krefft et al., 2018, Figure 57). bRGs have also been shown to be present (Bershteyn et al., 2017, Krefft et al., 2018). Therefore, this system holds the potential to further assess this cell type in

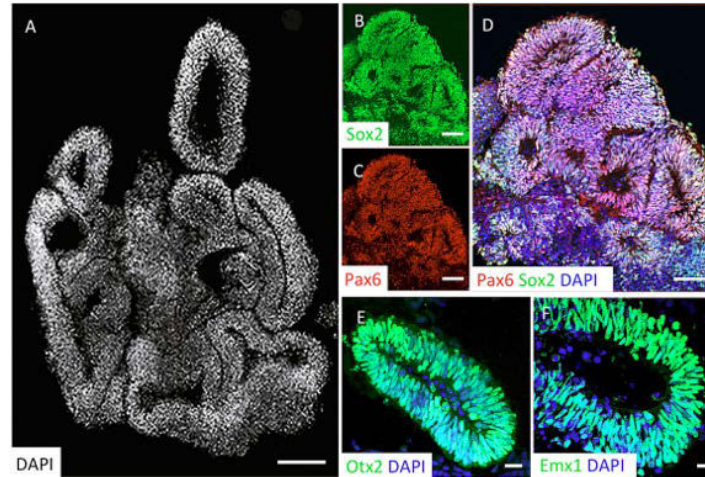


Figure 57. Characterization of dorsal cortical organoids. From Krefft et al., 2018.

physiological and pathological conditions. The cortical malformation most studied with these models has been microcephaly, given the ability of organoids to relatively consistently reproduce events of early cortical development (Gabriel et al., 2016, Lancaster et al., 2013, Qian et al., 2017). Very recently, some studies have addressed the role of heterotopia-related genes in this human 3D *in vitro* context (Klaus et al., 2019, O'Neill et al., 2018a, O'Neill et al., 2018b). It would thus be pertinent to study the role of *EML1* using this approach. Testing both protocols would be interesting as they may reveal different aspects related to the pathology. Dorsal cortical organoids may help unravel progenitor-specific features related to heterotopia formation in a human context. As discussed in section 1.4, *EML1* may have bRG-specific functions which cannot be studied in the mouse. Additionally, this model may unravel human-specific pathological traits related to *EML1* mutations in different progenitors, including aRGs. On the other hand, self-patterning models may help address issues more related to how cell diversity is affected when *EML1* is mutated, as well as to study aspects related to the interaction between different cell types, for instance, projection neurons and GABAergic interneurons.

hiPSC patient-derived 3D organoids may also provide some insight into genotype-phenotype correlations. As described in 6.3 of the introduction, the missense mutation found in family P135 (T243A) is likely to result in protein production. It would be interesting to compare the

phenotype of organoids derived from patients with different mutations and thus examine their possible differential contribution to pathological features.

Additionally, it would be interesting to generate 3D organoids taking advantage of new gene engineering technologies, such as CRISPR/Cas9. These would allow the generation of EML1 knockout organoids with the corresponding isogenic control, potentially revealing contributions of specific genetic backgrounds to the phenotypes in patient cells.

## **2. Eml1 function in apical radial glia cells**

### **2.1 Eml1 may have different roles throughout cell cycle**

Eml1 has a cell cycle dependent localization (see section 6.2 of the introduction). In mitosis, Eml1 co-localizes with the mitotic spindle (Kielar et al., 2014). Additionally, other EMAP proteins have been previously described to co-localize with the spindle and shown to mediate its assembly (Chen et al., 2015, Tegha-Dunghu et al., 2008, reviewed in Fry et al., 2016). In Bizzotto, Uzquiano et al. we focused on analyzing Eml1's role in mitotic aRGs. We observed an increase in (pro)-metaphase spindle length at early-mid stages of corticogenesis. A first mass spectrometry screen searching for Eml1 interacting partners pointed to a network of kinesins and microtubule-binding proteins also previously reported to modulate spindle length (Bizzotto et al., 2017). Concomitantly, we observed an increase in metaphase aRG area, and although the overall volume of these cells did not differ between *HeCo* and WT mice, they had an altered shape; indeed, they were flatter, possibly occupying a larger space in the VS (Bizzotto et al., 2017). Although the increase in spindle length could be responsible for the aRG morphological changes, we cannot rule out that other mechanisms may be upstream of both phenotypes.

aRGs are actively dividing and many proteins involved in mitotic processes also have important functions during interphase. For the central work of my thesis I focused on interphase-related mechanisms which could be responsible for the aRG phenotype. In Uzquiano et al. I describe a role for Eml1 in primary cilium formation. However, Eml1 does not seem to localize to the basal body of the primary cilium. This is also the case for the EMAP protein Eml4 (Dr. A. Fry, personal communication). My data suggests that Eml1 influences Golgi-derived trafficking towards the ciliary compartment, and this has not been shown before for the EMAP family.

Although my results and previously published data (Kielar et al., 2014) show an overall distribution of recombinant Eml1 throughout the cytoplasm of diverse cell types in interphase (Vero cells, RPE1, aRGs in tissue), we cannot completely rule out a localization at the basal

body-primary cilium complex. Indeed, related to this, Eml1 was found in proteome data from the mouse photoreceptor sensory cilium complex in the retina (Liu et al., 2007). Therefore, the use of robust antibodies, as well as modified protocols to detect ciliary proteins (Hua and Ferland, 2017) would be required to fully rule out its presence at the basal body or in the primary cilium e.g. of aRGs. Analyzing recombinant Eml1 expression upon serum starvation and thus ciliogenesis induction in different cell types may provide additional information about its subcellular localization, although until now primary cilia have not shown recombinant Eml1 expression. An alternative experiment would be to isolate aRG primary cilia followed by protein content analyses (Ishikawa and Marshall, 2013) to search for Eml1 in these fractions.

Interestingly, many proteins related to the basal body-primary cilium complex have also been associated with other subcellular functions, namely mitotic spindle formation and orientation, as well as Golgi apparatus-derived protein transport (Hua and Ferland, 2018). Focusing on proteins found in the Eml1 mass spectrometry screens, Cep170 is localized to the basal body during interphase and interacts with FHDC1, which mediates primary cilium assembly (Copeland et al., 2018). During mitosis, it localizes to the mitotic spindle and recruits Kif2b, contributing to correct mitotic spindle assembly (Welburn and Cheeseman, 2012). KifC1 regulates mitotic spindle assembly (Zhu et al., 2005) and more precisely spindle length (Cai et al., 2009). Very recently, a study reported a role for this kinesin in Golgi-primary cilium trafficking (Lee et al., 2018). Knockdown of KifC1 in RPE1 cells led to a decreased number of ciliated cells and impaired delivery of ciliary cargoes (Lee et al., 2018). Another example is Plk1, previously shown to regulate spindle orientation in aRGs (Sakai et al., 2012). Plk1 interacts with the Golgi protein GRASP65 regulating Golgi assembly/disassembly and thus cell cycle progression (Preisinger et al., 2005, Sengupta and Linstedt, 2010). Several studies also show a role for Plk1 in primary cilium disassembly (Lee et al., 2012, Seeger-Nukpezah et al., 2012, Wang et al., 2013).

It is thus likely that Eml1 is involved in diverse microtubule-dependent processes throughout the cell cycle. This may imply that aRG pathological features involve several subcellular processes, which makes it difficult to identify the primary pathological event. I have identified ectopic progenitors and mild primary cilium abnormalities as early as E12.5. Assessing mitotic spindle length and orientation, as well as Golgi apparatus distribution and structure at this early time point may shed light on a primary triggering factor.

## 2.2 An unexpected role for Eml1 in primary cilium formation

As previously discussed, EMAP proteins do not appear to localize to the primary cilium. However, severe primary cilium anomalies exist in *Eml1/EML1*-mutant conditions. In mouse aRGs primary cilia are shorter and often found mis-oriented in vesicle-like compartments. Patient fibroblasts show a decreased number of primary cilia which are also shorter. These combined data strongly suggest that primary cilium formation is impaired.

However, could perturbed primary cilium disassembly account for these results? To further rule out an increased endocytosis of ciliary structures, surface biotinylation experiments could be performed to follow ciliary membrane internalization, as previously performed by Paridaen et al., 2013. Also, shedding of ciliary particles in the ventricle has been previously described in physiological conditions in the chick neuroepithelium (Dubreuil et al., 2007). We searched for the presence of detached particles in E13.5 WT and *HeCo* mouse brains (Figure 58). However,

no differences were observed between the genotypes, most probably excluding abnormalities affecting this process in the *HeCo* mouse. It hence remains improbable that perturbed shedding of ciliary particles contributes to the shorter primary cilia phenotype.

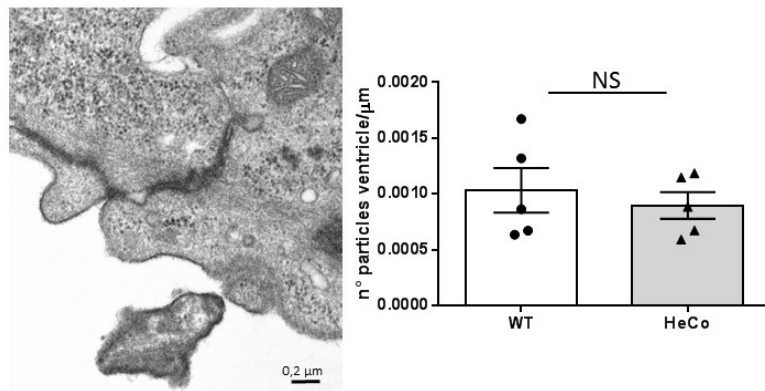


**Figure 58. The number of detached ventricular particles does not differ between WT and *HeCo* mice at E13.5.** Representative image of a detached particle in the ventricle of an E13.5 embryonic brain (left). Quantification of the number of particles per  $\mu\text{m}$  of VS in WT and *HeCo* brains (right). Each point represents an embryo. Both condition  $n=5$  from at least 3 different litters. NS: no significant.

*Eml1* is widespread in the cytoplasm in interphase, decorating microtubules in a vesicular-like pattern (Kielar et al., 2014). Gene ontology (GO) analyses of mass spectrometry data pointed to Golgi apparatus and protein transport as represented categories. We thus focused on Golgi-derived trafficking as a potential upstream mechanism contributing to the primary cilium phenotype.

However, several other subcellular mechanisms could also regulate primary cilium formation, including docking of the basal body at the plasma membrane. Although no obvious defects were observed in  $\gamma$ -tubulin+ centrosome structures when performing immunohistochemistry and immunocytochemistry experiments followed by confocal microscopy in *Eml1*-mutant

conditions, electron microscopy showed an abnormal ultra-structure of the basal body. Further experiments should therefore address specific centrosomal features, for instance mother centriole maturation.

This structure is characterized by the presence of distal and subdistal appendages (DA and SDA) (Figure 59), identified by specific proteins such as Cep83, Cep89, Cep164, Sclt1 and Ofd2, as well as Centriolin, Cep128 and Cep170, respectively (Wang and Dynlacht, 2018). On the other hand, daughter centrioles associate with 'daughter centriole-specific/enriched proteins' (DCPs) such as Cep120, Centrobin and Neurl4. These proteins are likely to exert antagonistic interactions regulating centriole maturation, although this topic still needs further study. Interestingly, correct interaction and

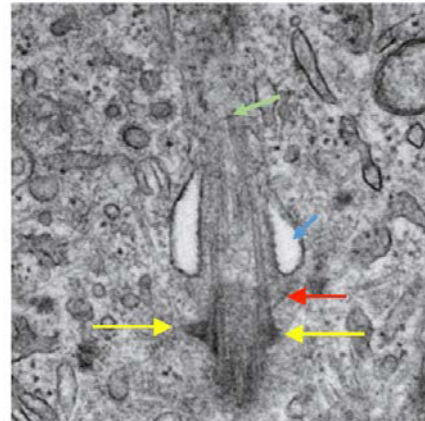


**Figure 59. The mother centriole is characterized by the presence of distal and subdistal appendages.** DA and SDA, respectively. Green arrow: primary cilium, blue arrow: ciliary pocket, red arrow: DA/transition fibers. yellow arrow: SDA.

targeting of these centriole components is important for ciliary-vesicle docking and primary cilium formation (Wang et al., 2018). Further assessment of DAs and SDAs, measurements of centriole length and immunodetections for DA, SDA and DCPs specific proteins could shed light on the centriole anomalies already observed in Eml1-mutant conditions. In addition, the SDA protein Cep170 and the DCP protein Neurl4 were found in the mass spectrometry screens when searching for Eml1-interacting partners. Confirming the interaction of these two proteins with Eml1 might suggest a basal body-related function. These experiments could unravel a potential docking problem, which might co-exist with impaired Golgi-derived trafficking.

As previously discussed, we could not detect recombinant Eml1 in the ciliary axoneme of RPE1 cells, and if this result is confirmed, it seems unlikely that a problem of primary cilium growth *per se* is responsible for the phenotype observed. However, it is worth mentioning that some proteins previously described to localize to the primary cilium axoneme were present in the mass spectrometry screens e.g. Kif7, Par3, Map4 (Ghossoub et al., 2013, He et al., 2014, Liem et al., 2009, Sfakianos et al., 2007). It is however possible that Eml1 interacts with these proteins in other subcellular regions.

### 2.3 EML1 interacts with the ciliary protein RPGRIP1L

Combining mass spectrometry data, biochemistry experiments and exome-sequencing of patients with severe subcortical heterotopia, we identified RPGRIP1L as an EML1 interacting partner, as well as the first heterotopia patient with mutations in this protein (P700).

Mutations in *RPGRIP1L* are mostly associated with classical ciliopathies such as Meckel and Joubert syndromes (Wiegering et al., 2018). Meckel syndrome is a lethal ciliopathy characterized by renal dysplasia, occipital encephalocele, polydactyly and pulmonary hypoplasia. Joubert syndrome is a classical ciliopathy affecting the cerebellum and often including other phenotypes such as polydactyly and cleft lip. Although these pathologies show neurological abnormalities, the cortex is apparently unaffected. It is thus still not clear why P700 with RPGRIP1L mutations presents giant subcortical heterotopia. We hypothesize that the precise compound heterozygous mutations found in the RID domain of the protein, impairing the interaction with EML1, are likely to be responsible for the cortical phenotype. Interestingly, the majority of mutations resulting in Meckel or Joubert syndrome are found in more N-terminal regions of the protein (Figure 60). Of note, one patient was reported presenting Joubert syndrome with a heterozygous mutation in the RID domain of RPGRIP1L. This consists of a deletion resulting in a stop codon towards the 3' of the gene. No mutations were identified in the other allele. It is possible that missense heterotopia mutations in the RID domain impair RPGRIP1L C-terminal structure in a particular way and hence perturb the interaction with specific protein partners (e.g. EML1) leading to a malformed cortex. Testing the interaction of a Joubert syndrome mutant form of RPGRIP1L with EML1 could perhaps confirm that

indeed the compound heterozygous mutations found in the heterotopia patient impair the interaction of RPGRIP1L with EML1 in a specific fashion.

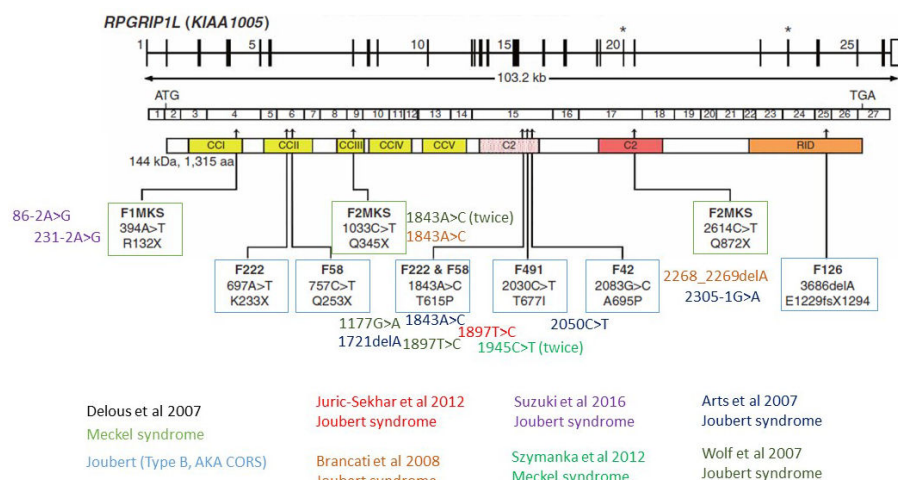


**Figure 60. Schematic representation of *RPGRIP1L* mutations associated with Joubert and Meckel syndromes.** Adapted from Delous et al., 2007.



Rpgrip1l is localized in the primary cilium transition zone and it is important for its assembly (Wiegering et al., 2018). It has also been found to have extra-ciliary locations (Gerhardt et al., 2015, Sang et al., 2011). For instance, it localizes to the spindle pole in mouse embryonic fibroblasts (MEFs) (Gerhardt et al., 2015) and it has also been shown to localize to cell-cell contacts in a mouse kidney cell line (IMCD3) (Sang et al., 2011). Thus its interaction with Eml1 could occur at one or several locations.

Rpgrip1l has been shown to regulate proteosomal activity at the base of the primary cilium (Gerhardt et al., 2015). *Rpgrip1l* KO MEFs and isolated limbs showed decreased Gli3 proteolytic processing as well as an accumulation of proteins targeted for proteosomal degradation at the base of the primary cilium (Gerhardt et al., 2015). Independently of its function regulating proteosomal activity, Rpgrip1l has also been shown to regulate autophagy. *Rpgrip1l* KO MEFs show upregulated mTOR activity and decreased autophagic activity, which was rescued upon inhibition of the former pathway (Struchtrup et al., 2018).

Gerhardt et al. (2015) showed that *Rpgrip1l* KO embryos present longer primary cilia in many organs (i.e. limbs, heart, lung and liver) as well as in MEFs. A study analyzing fibroblasts from Joubert syndrome patients also reported an increase in primary cilium length (Stratigopoulous et al., 2014, Figure 61). However, the ciliary phenotype upon *Rpgrip1l* deficiency is cell type specific: in neuroepithelial cells, primary cilia are either absent or very short (Figure 62), and a similar phenotype is

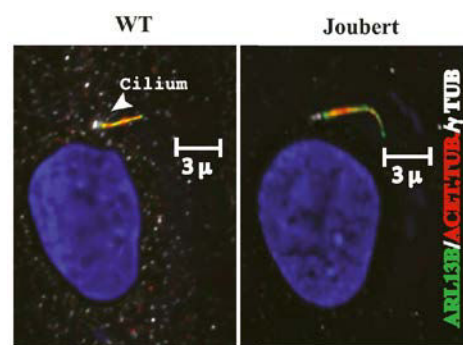


Figure 61. Joubert syndrome patient fibroblasts show longer primary cilia than control lines. From Stratigopoulous et al., 2014.

observed in the node and the heart (Vierkotten et al., 2007, Besse et al., 2011, Gerhardt et al., 2015).

Thus, our experiments in *RPGRIP1L* heterotopia patient fibroblasts show different dynamics than Joubert patient fibroblasts (Stratigopoulous et

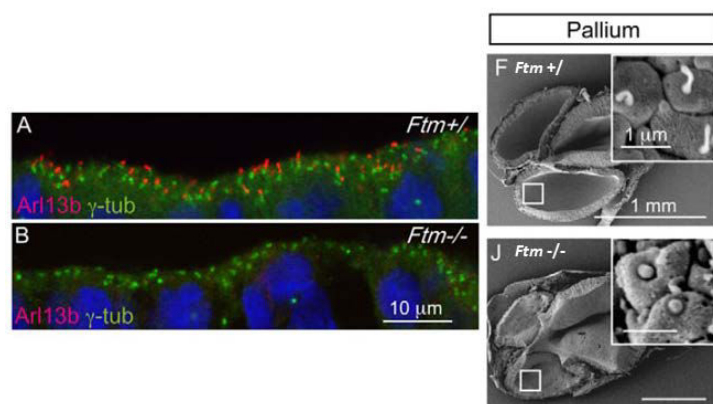


Figure 62. Primary cilia are absent or very short in neuroepithelial cells of *Rpgrip1l* (also called *Ftm*) KO mice. Images of immunohistochemistry and scanning microscopy at E12.5. Adapted from Besse et al., 2011.

al., 2014, section 2 of the results). Instead of being excessively long, primary cilia are decreased in number and length, showing a similar ciliary phenotype to *EML1* patient fibroblasts (section 2 of the results). To further distinguish them from other features previously associated with deficiency of *Rpgrip1l*, it would be pertinent to analyze proteosomal activity (e.g. Gli3 processing) and autophagy activity (Gerhardt et al., 2015, Stratigopoulous et al., 2014). However, these subcellular pathways may not be involved in the heterotopia phenotype given the primary cilium differences between the heterotopia and Joubert syndrome patients.

*Rpgrip1l* KO mice die at birth and recapitulate Meckel and Joubert syndromes phenotypes such as polydactyly, polycystic kidney, laterality and cardiac defects (reviewed by Wiegering et al., 2018). Related to the brain, they show cerebellar hypoplasia, microphthalmia, olfactory bulb agenesis and corpus callosum agenesis (Besse et al., 2011, Laclef et al., 2015, Wiegering et al., 2018). Gli3 processing is hampered in the telencephalon (Besse et al., 2011) and overexpression of the Gli3 repressor form rescues the olfactory bulb and corpus callosum phenotypes (Besse et al., 2011, Laclef et al., 2015). Although it will be highly interesting to carefully examine the cortex and cortical progenitors, it is unlikely that deciphering abnormal processes in these mice will provide further information related to heterotopia formation since in this case *RPGRIP1L* harbors specific compound heterozygous mutations.

Conversely, functional studies (e.g. *in utero* electroporation of *RPGRIP1L*-mutant constructs in the mouse neuroepithelium) could shed light on the mechanisms influencing heterotopia-formation in the *RPGRIP1L* patient. Given the similarities to *EML1* patient fibroblasts in primary cilium dynamics, it would be relevant to assess if similar upstream mechanisms may be responsible for the phenotype. Indeed, assessing Golgi distribution in aRGs after *RPGRIP1L*-mutant constructs electroporation would be interesting as it could point to the Golgi-primary cilium axis as a perturbed subcellular mechanism due to these compound heterozygous mutations.

#### **2.4 The Golgi apparatus in *Eml1*-mutant conditions**

*Eml1* aRG interphase subcellular localization, mass spectrometry analyses and primary cilia abnormalities led us to examine the Golgi apparatus in WT and *Eml1*-mutant conditions. *In utero* electroporation experiments and electron microscopy in the mouse neuroepithelium at early-mid stages of corticogenesis (E13.5) showed an abnormal distribution and disrupted ultra-structure of the Golgi apparatus in *HeCo* aRGs. These results were further confirmed by

experiments in patient fibroblasts and hiPSC-derived cortical progenitors (coll. Dr. J. Ladewig). It is now important to further understand these perturbed processes.

#### **2.4.1 The Golgi apparatus and cortical malformations**

The Golgi apparatus has been little studied in the developing cortex. This organelle has been associated with brain and more precisely cortical malformations in only a few cases.

Early work in the 90s described ultrastructural alterations of the Golgi apparatus in the cerebral cortex of post-mortem samples of patients showing hydrocephaly (Castejon et al., 1994). Few subsequent studies have associated the Golgi apparatus and Golgi trafficking to cortical malformations. As described in section 4.2 of the introduction, mutations in *GPR56* are associated with polymicrogyria (Bae et al., 2014). Disease-associated mutant forms of *GPR56* show reduced trafficking and decreased surface expression, remaining trapped in the trans-Golgi network (Jin et al., 2007). Mutations in the neuronal-specific Golgi protein *RAB39B* were identified in two patients presenting X-linked intellectual disability associated with autism, epilepsy and macrocephaly (Giannandrea et al., 2010). Recently mutations in the ER and Golgi trafficking protein *TRAPPC6B* were linked to six individuals showing microcephaly, epilepsy and autistic traits (Marin-Valencia et al., 2018). Finally, mutations in the dynein heavy chain (*DYNC1H1*) are associated with spinal muscular atrophy, but also with cortical malformations (Poirier et al., 2013, Fiorillo et al., 2014). Related to the latter, studies in patient fibroblasts show Golgi fragmentation (Fiorillo et al., 2014). All these studies examined protein localization and/or Golgi structure in cell lines, patient fibroblasts or dissociated neuronal cultures.

Related to subcortical heterotopia, Sheen et al., 2004 also described a function for the PVH protein *Big2 (ARFGEF2)* in Golgi-derived protein trafficking. Experiments were performed in neurospheres and cell lines, however the authors did not assess the Golgi apparatus or trafficking directly in aRGs in tissue nor *in vitro*.

My work assessed for the first time Golgi apparatus distribution and structure in aRGs in tissue in the context of subcortical heterotopia. This structure was also compromised in hiPSC-derived cortical progenitors (coll. Dr. J. Ladewig); to our knowledge the Golgi had not been previously investigated in these human *in vitro* cell culture model. In addition, we assessed trafficking directly in aRG-like progenitor cultures, showing this subcellular process is impaired in *Eml1*-mutant aRG-like cells. Thus the published and unpublished studies here described point towards the Golgi and Golgi-derived functions as potential targets in cortical

malformations. It is hence important to study the Golgi as well as other membrane bound organelles in the context of neurodevelopmental disorders.

#### 2.4.2 Golgi apparatus-related proteins and Eml1

We confirmed the interaction of Eml1 with the Golgi protein Vcip135, involved in Golgi stack reassembly after mitosis (Uchiyama et al., 2002, Zhang et al., 2014, Zhang and Wang, 2015). It had previously been shown that knockdown of *Vcip135* in HeLa cells leads to Golgi fragmentation (Zhang et al., 2014, Figure 63). Immunodetections for the Golgi apparatus performed in *EML1* patient fibroblasts resemble these results. To our knowledge, no other localization or role has been ascribed to Vcip135, hence this interaction seems to directly link Eml1 to the Golgi apparatus. This data combined with the presence of several Golgi proteins in

the mass spectrometry leads us to hypothesize that Eml1 may form a protein complex in the vicinity of this organelle. Recombinant Eml1 is localized throughout the cytoplasm during interphase masking a possible co-localization. However, fractionation experiments isolating the Golgi apparatus and assessing Eml1 expression could help determine if indeed Eml1 associates with this subcellular compartment.

Knockdown of *Vcip135* in the mouse neuroepithelium led to a shift of electroporated cells towards basal positions, potentially highlighting the importance of Golgi proteins and function in VZ progenitors. To link Vcip135 with the primary cilium, which has not yet been shown, knockdown in RGs in tissue and in neuronal progenitor cultures, followed by primary cilium assessment would potentially provide a further indirect link between this organelle, the function of Vcip135 and the Golgi apparatus.

I already discussed the different functions throughout the cell cycle of Cep170, KifC1 and Plk1, which were found in the mass spectrometry screens searching for Eml1 interacting partners. Other proteins important for the Golgi and primary cilium also appeared in these screens. Thus, Kif7 represents an example of a protein important for both organelles. Kif7 localizes to the primary cilium tip (He et al., 2014) and modulates Shh signaling (Liem et al., 2009, Putoux

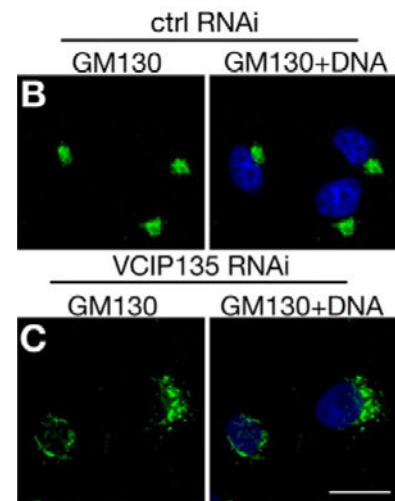


**Figure 63. Knockdown of *Vcip135* leads to Golgi fragmentation in HeLa cells.** Note dispersion of green fluorescence. Adapted from Zhang et al., 2014.

et al., 2011). It is associated with brain malformations including hydroletharus, acrocallosal and Joubert syndromes (Dafinger et al., 2011, Putoux et al., 2011).

Interestingly, knockdown of Kif7 in RPE1 cells results in Golgi fragmentation, as well as a decrease in the percentage of ciliated cells (Dafinger et al., 2011, Figure 64). Kif7 KO mice show 'classical ciliopathies' phenotypes, including polydactyly, neural tube closure defects and corpus callosum agenesis (Endoh-Yamagami et al., 2009, Putoux et al., 2018). As in many ciliary mutants, Gli3 processing is altered in E10.5 embryos and MEFs (Endoh-Yamagami et al., 2009), and overexpression of the Gli3 repressor



**Figure 64. Knockdown of Kif7 in RPE1 cells leads to Golgi fragmentation.** Pink: Golgin-97. Adapted from Dafinger et al., 2011.

form partially rescued the corpus callosum phenotype (Putoux et al., 2019). In this same study the authors report no changes in Satb2 upper layer neurons, although the cortex was not further studied (Putoux et al., 2019). It could hence be of interest to analyze the cortical phenotype and Gli3 processing specifically in cortical extracts. Additionally, it would be interesting to specifically knockdown Kif7 in aRGs followed by primary cilium, Golgi apparatus and cell distribution assessment.

We decided to focus on Golgi-derived trafficking due to its importance for protein delivery to the ciliary base for establishment and maintenance of this structure. Additionally, given the localization of recombinant-Eml1 in apical processes (and not obviously in primary cilia), we thought this aspect of Golgi function would be the most pertinent to examine. Arf4 and KifC1, two proteins described to participate in Golgi-primary cilium trafficking (Lee et al., 2018, Mazelova et al., 2009, Ward et al., 2011, Wang et al., 2017, Follit et al., 2014), were also present in the mass spectrometry screens. Co-immunoprecipitation studies could not confirm the interaction of Eml1 with these proteins, although other approaches are needed to fully rule out a direct interaction. First, pull down experiments with embryonic cortex lysates may provide additional information. Also, a ciliated cell line such as RPE1 may be more appropriate to unravel protein complexes involved in primary cilium formation. In this line, inducing serum starvation and thus primary cilium formation possibly encourages protein trafficking towards the cilium accompanied thus by the formation of complexes involved in this process. Ciliated cell lines classically used to study the primary cilium (RPE1, IMCD3) could hence be further exploited to dissect out these interactions.

### 2.4.3 Golgi apparatus-derived trafficking is impaired in *HeCo* neuronal progenitors

I performed an assay in Pax6+ neuronal progenitors *in vitro* to further assess Golgi-derived protein trafficking towards the plasma membrane. WT and *HeCo* Pax6+ progenitors were transfected with a thermosensitive VSVG-GFP construct. Whilst at 39.5°C this protein remains in the ER-Golgi compartment, it is released towards the plasma membrane upon incubation at 32°C. Therefore fixing the cells at different time points upon incubation at 32°C gave us a proxy of Golgi-derived protein transport in mutant compared to WT. Cargo sorting and/or protein trafficking seemed to be impaired and/or slowed in *HeCo* cells. Analyses at later stages may provide more information about protein trafficking more generally and delivery to the plasma membrane.

This classical experiment provides an overall view of Golgi-derived trafficking and is indeed useful to assess membrane targeted protein trafficking (Lafay, 1974, Boncompain and Perez, 2013). However, non-physiological temperatures are required to perform the experiment, and specific cargos cannot be monitored (Boncompain and Perez, 2013). The RUSH system constitutes a relatively novel approach which could solve these drawbacks (Boncompain et al., 2012,

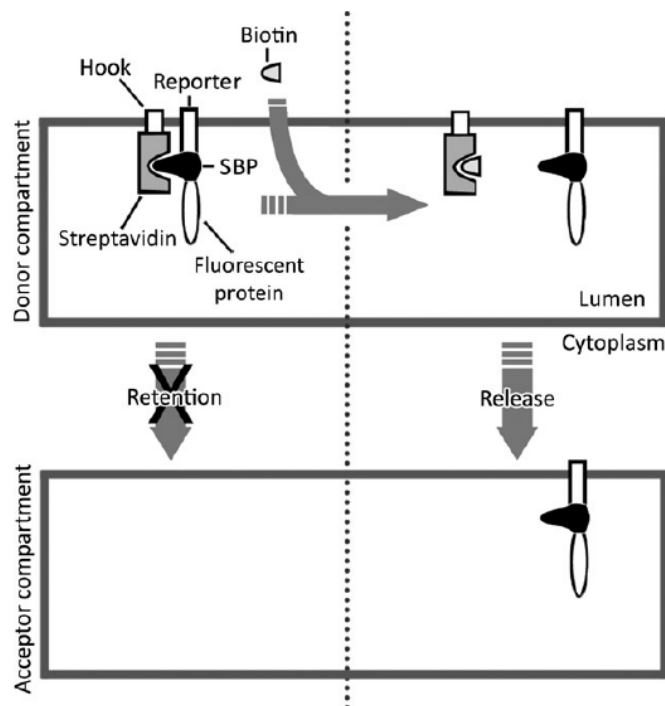


Figure 65. Schematic representation of the RUSH system. From Boncompain and Perez, 2013.

Boncompain and Perez, 2013). This method relies on the retention of the cargo (the reporter) in a donor compartment, for instance, the ER or the Golgi apparatus. Briefly, the donor compartment contains a streptavidin-hook protein that ensures the retention of the reporter, which is fused to a streptavidin-binding peptide. This interaction is released upon addition of biotin to the cell medium. The biotin binds to the streptavidin-hook resulting in the synchronous release of the reporter protein (Figure 65). This approach could allow us to specifically monitor trafficking from the Golgi apparatus (i.e. donor compartment) of a ciliary

specific cargo (i.e. reporter) to its final destination (the acceptor compartment, in this case the primary cilium).

Simpler methods can also be applied to confirm a disrupted delivery of ciliary cargoes. For instance, immunodetections for the Shh signaling component Smoothed, followed by fluorescence intensity and distribution analyses are often performed to address this question (Lee et al., 2018, Monis et al., 2017). The same type of experiment could be performed for the Golgi-primary cilium protein IFT20 (Stoetzel et al., 2015). These experiments could also reveal the differential contribution of the cis and/or trans-Golgi to the pathological aRG phenotype.

Although our electron microscopy analyses showed an increased number of vesicles surrounding the Golgi apparatus in *HeCo* aRGs when compared to WT, further study of vesicles associated with these two Golgi compartments showed no further differences (Figure 66). However, further confirmation by different approaches would be useful to fully assess if either of these Golgi compartments is particularly affected in *Eml1*-mutant conditions.

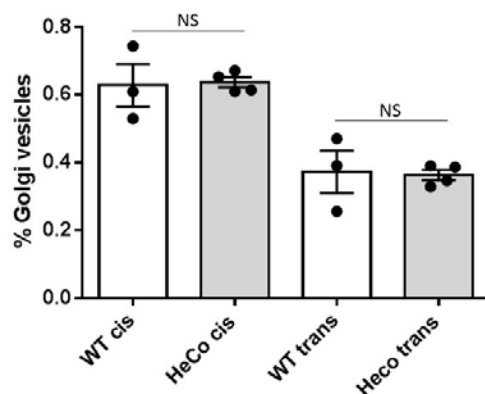


**Figure 66. No differences between cis and trans Golgi vesicles in WT and *HeCo* aRGs at E13.5.** Quantification of the percentage of Golgi vesicles in cis and trans. Each point represents an embryo. WT n=3, *HeCo* n=4, from at least 3 different litters. NS: no significant.

## 2.5 The adherens junction (AJ)-actin belt in *Eml1*-mutant conditions

The Golgi-derived trafficking assay performed in *Eml1* mutants assessed general post-Golgi traffic, and hence not only ciliary-directed movements. It hence remains possible that protein transport to other structures of the apical plasma membrane is perturbed.

The AJ-actin belt mediates aRG cell-cell contact in the VS. Disruption and/or loosening of this belt has been previously associated with progenitor cell delamination in 'physiological' conditions (Camargo-Ortega et al., 2019, Tavano et al., 2018), and also in the context of perturbed corticogenesis (Cappello et al., 2006, Jossin et al., 2017, Junghans et al., 2005, Schmid et al., 2014). Key components of this AJ belt have been previously shown to be trafficked from the Golgi apparatus (Asada et al., 2004, Lock et al., 2005, Sheen et al., 2004, Wang et al., 2005). Related to this, in the context of cortical malformations, the PVH protein Big2 has been shown to have a role in Golgi-derived protein trafficking, regulating the expression of the AJ components E-Cadherin and  $\beta$ -catenin in the plasma membrane (Sheen

et al., 2004). Therefore, it may be possible that delivery of some AJ components are perturbed in *Eml1*-mutant cells, even though VS breakages have not been observed in mouse mutants. Mass spectrometry data also contained cell adhesion-related proteins such as Epb4115 and Llg1. Llg1 interacts with the AJ component N-Cadherin and regulates its correct location in aRG apical endfeet (Jossin et al., 2017). Conditional KO mouse models of Llg1 result in a subcortical heterotopia phenotype (Beattie et al., 2017, Jossin et al., 2017, Zhang et al., 2019). Epb4115 is important for cell-cell contacts and E-Cadherin distribution (Gosens et al., 2007, Hirano et al., 2008). Although it is expressed in the developing cortex and more precisely in the VZ (Gosens et al., 2007) it has not been studied in the context of cortical progenitors or corticogenesis. The function of these proteins makes them appealing potential *Eml1*-interacting partners. Thus it is important to examine their interaction with *Eml1* as well as to assess their expression in an *Eml1*-mutant context.

Related to the AJ belt in *Eml1*-mutant conditions, no major differences were observed when performing immunohistochemistry for other AJ and polarity complex markers in WT and *HeCo* brain slices at E13 and E16 (Kielar et al., 2014). Similarly, no obvious defects were observed in *Eml1* KO mice when immunostaining for N-Cadherin and F-actin.

Despite the previously described results, *en face* imaging for F-actin showed a disorganized pattern of expression in *HeCo* brains when compared to WT at E12.5 and E13.5 (sections 2 of results). Additionally, EM data of the *HeCo* and *Eml1* KO VZ might suggest that AJs are partially disrupted (data not shown). More severe disruptions of these structures has been finely analyzed by EM experiments in

other studies (Imai et al., 2005, Jossin et al., 2017, Figure 67). Deeper analyses of AJ components in *Eml1*-mutant conditions may still unravel a contribution of these structures to the aRG delamination phenotype.

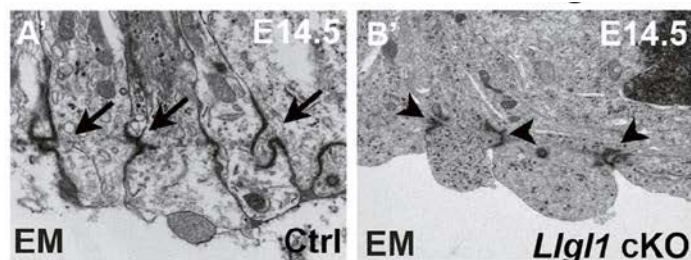


**Figure 67. Adherens junctions are disrupted in Llg1 cKO mouse brain.**  
From Jossin et al., 2017.

Analysis of actin dynamics in *Eml1*-mutant conditions is also a promising route of investigation. Indeed, altered actin dynamics could disrupt the AJ-actin belt, compromising aRG behavior and corticogenesis overall. For instance, this has been observed in  $\alpha$ -E-catenin conditional KO mice which exhibit a double-cortex like phenotype (Schmid et al., 2014). At early stages of



development, the VS of these mice is disrupted, and rosette-like structures form in the developing cortical wall (Schmid et al., 2014). Additionally, the authors reported altered actin dynamics: the F/G actin ratio was decreased in the VS of  $\alpha$ -E-catenin conditional KO mice (Schmid et al., 2014). Additionally, mutations in the actin remodeling protein FLNA often cause PVH (section 5.3 of the introduction), highlighting as well the importance of the actin cytoskeleton in cortical development. Nevertheless, we might expect comparatively more subtle changes in *Em1* mutant conditions, compared to the above-mentioned proteins.

Interestingly, the actin cytoskeleton has been associated with several aspects of ciliary formation and function (Kim et al., 2014, Kohli et al., 2017, Saito et al., 2017, Wu et al., 2018). More precisely, actin depolymerization has been shown to promote ciliogenesis (Kim et al., 2014, Kohli et al., 2017, Figure 68), whilst actin polymerization

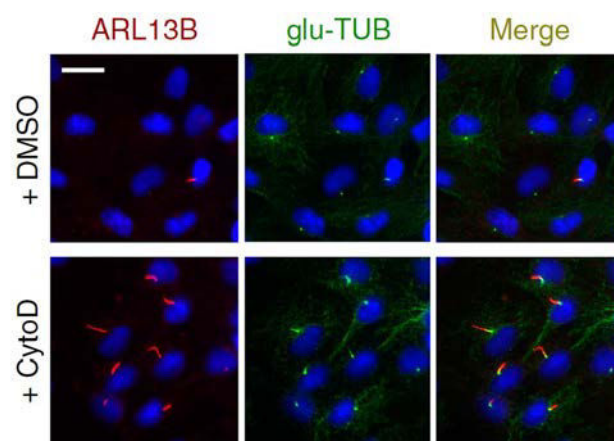


**Figure 68. Actin depolymerization promotes ciliogenesis.** Treatment with the actin depolymerizing drug CytoD induces primary cilium formation. From Kim et al., 2014

contributes to ciliary reabsorption (Saito et al., 2017). It would thus be relevant to study actin dynamics in *Em1*-mutant conditions, as well as to test the interaction of *Eml1* with actin remodeling proteins which were present in the mass spectrometry screens, for instance Rac1 and Limk2.

Limk2 is a RhoGTPase effector, that once activated phosphorylates members of the ADF/cofilin family and inactivates them, preventing thus actin depolymerization (reviewed by Cuberos et al., 2015). Accordingly, Kim et al. (2014) described a role for Limk2 in ciliogenesis repression; knockdown of Limk2 in RPE1 cells increases the percentage of ciliated cells (Kim et al., 2014). Interestingly, this same study correlated YAP activity and ciliogenesis: increased levels of nuclear YAP correlated with decreased ciliogenesis. Knockdown of Limk2 not only promoted ciliogenesis but it also decreased YAP activity (Kim et al., 2014) (Hippo signaling is further discussed in section 4.2). Limk2 has three different isoforms, and recently LIMK2-1 has been described as a hominid-specific isoform with high expression in the fetal human brain (Tastet et al., 2019). However, the role of Limk2 in corticogenesis has not been examined.

Rac1 is involved in actin polymerization (reviewed by Sit and Manser, 2011) and has been more studied in the context of cortical development, more precisely neuronal migration (reviewed by Kawauchi, 2015). Nevertheless, a few studies have assessed its role in neuronal progenitors. Minobe et al. (2009) showed that Rac1 seems to be important for apically-directed nuclei movement during aRG INM. Treatment of brain slices with a Rac1 inhibitor as well as *in utero* electroporation of a Rac1 dominant negative construct led to a decreased speed of nuclear movement towards the VS (Minobe et al., 2009). Additionally, Leone et al. (2010) analyzed Foxg1-Cre Rac1 conditional KO mice and showed impairment of aRG basal anchoring. This was accompanied by disorganization of lower and upper layer neurons, which were found clustered in basal regions of the CP (Leone et al., 2010).

These studies further highlight the importance of actin dynamics in not only aRG behavior and corticogenesis, but also primary cilium formation. It thus seems pertinent to analyze further the role of these proteins in the developing cortex, especially in the case of Limk2, and in the context of my project, investigate their potential relationship with Eml1.

### **3. The ventricular zone in *Eml1*-mutant conditions**

#### **3.1 All radial glial cells do not seem equally affected**

The heterotopia described in *HeCo* and *Eml1* KO mice does not span across the whole cortex, it is localized in dorso-medial regions (Croquelois et al., 2009, Kielar et al., 2014, section 3 of the results). Similarly, in human patients the heterotopia is most obvious in frontal regions (Kielar et al., 2014). It remains unknown why the heterotopia develops in these particular localizations. Neurogenesis occurs in a lateral to medial gradient, therefore one hypothesis has suggested that upper layer neurons in medial regions might be more susceptible to be trapped in the intermediate zone when neuronal migration can no longer occur postnatally (Kielar et al., 2014). However, we cannot rule out a differential susceptibility of specific cortical cells to *Eml1* mutations. Analyzing *Eml1* expression along the dorso-caudal and latero-medial axes of the developing cortex in different organisms could shed light on this issue. Additionally, some key interacting partners or regulators may also have specific gradients of expression, which could impact particular cortical cell populations. Gradients of expression have been discussed previously in relationship with cortical malformations, although few relevant molecules have been identified. However, Bae et al., (2014) showed that a noncoding mutation in a regulatory element of the polymicrogyria gene *GPR56* ablates gene expression in the lateral cortex, thus restricting its expression pattern and causing polymicrogyria in the

vicinity of the perisylvian fissure. The authors also found that RFX TFs are likely to control *GPR56* transcription and their expression pattern correlates with *GPR56* expression in the human cortex (Bae et al., 2014).

To further test the hypothesis of cell heterogeneity across lateral to medial neuroepithelium, it would be interesting to perform FlashTag and single cell RNA-seq experiments to test for differences in aRG populations which may help explain sensitivity to *Em11*-mutations. This type of experiment could profile all cell types found in this germinal zone at early stages of corticogenesis, providing valuable information about potential cell-specific transcriptional variability in WT and mutant conditions. Different developmental trajectories and division characteristics may also help explain the position of the heterotopia.

### **3.2 Space constraints in the *HeCo* ventricular zone**

As described in section 3.1.1 of the introduction, aRGs in the VZ undergo INM. Their nuclei move apico-basally during the different stages of cell cycle, with mitosis occurring at the VS. It is believed that INM occurs in order to create space at the VS so more aRGs can undergo M-phase (Miyata et al., 2014). It has also been proposed that aRGs that become bRGs may leave the VZ to escape this space constraint, moving basally to the oSVZ whilst maintaining aRG traits (Florio and Huttner, 2014).

Work from the Miyata lab has focused on further deciphering INM and VZ dynamics in terms of VZ stiffness, aRG apical domain and/or endfoot size and density as well as apical surface contractility (Nagasaka et al., 2016, Minobe et al., 2009, Nishizawa et al., 2007, Okamoto et al., 2013, Okamoto et al., 2014, Watanabe et al., 2018). To understand the dynamics of the VS throughout corticogenesis, Nishizawa and colleagues (2007) analyzed apical domain and/or endfeet density from early to late corticogenesis. They described a peak in apical endfeet density at E12, which they hypothesize can be due to the change in mode of division of aRGs i.e. from symmetric proliferative to asymmetric in order to produce a daughter cell more differentiated in the neuronal lineage (Nishizawa et al., 2007). My analyses at E12.5 and E13.5 do not show the same results: apical endfeet density does not appear to differ significantly from E12.5 to E13.5 (results section 2 and data not shown). However, technical differences between these studies and different genetic backgrounds may explain the different results. Nishizawa and colleagues considered the whole apical surface to perform their analyses, whilst I only consider dorso-medial regions, where the heterotopia develops in *Em11*-mutant conditions at later stages. It is plausible that apical endfoot density does not undergo drastic

changes between E12.5 and E13.5 in this particular cortical region. Additionally, in their study apical endfeet were exclusively identified based on ZO1 and Hoechst stainings, whilst I considered specifically F-actin domains containing a centrosome ( $\gamma$ -tubulin+ puncta). More recently, Nagasaka et al. (2016) assessed differences in the mechanical properties of mouse versus ferret VZ by using atomic force microscopy. The authors showed that VZ stiffness is greater in the ferret than in the mouse, most probably due to the denser apical surface in terms of endfeet previously reported in ferret (Nagasaka et al., 2016, Okamoto et al., 2014). The authors also examined if apical surface contractility differed between both species. They applied short-pulse laser to the midpoint of a boundary line formed by two apices of neighboring cells (Figure 69). Then they measured the separation speed of both vertices at the end of the laser-targeted side (Nagasaka et al., 2016). They could not find any difference in the velocity of separation of the tracked vertices, implying that contractility of the apical surface is similar in mouse and ferret (Nagasaka et al., 2016). The consequences of different stiffness in the VZ of mouse and ferret still needs to be unraveled. However, it could contribute to differential aRG dynamics, including different patterns of INM which were previously revealed by Okamoto et al. (2014), as well daughter cell production and fate e.g. bRGs.

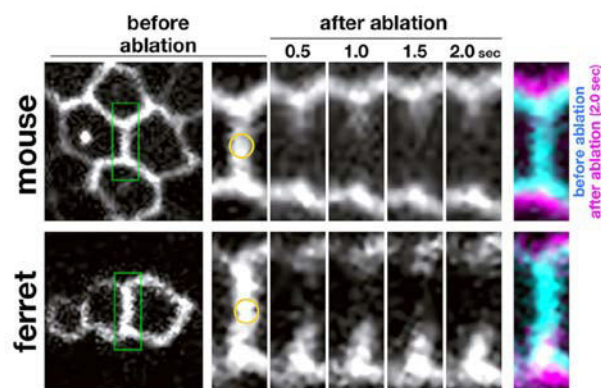


Figure 69. Laser ablation experiments performed on the apical surface of embryonic cerebral walls of mouse and ferret. From Nagasaka et al., 2016.

In line with these two studies, Okamoto et al. (2013) described an ‘overcrowding’ situation in the mouse neuroepithelium: knockdown of the adhesion molecule TAG-1 led to basal process detachment, loss of basal-ward movement during INM and eventually progenitor overcrowding in the VZ (Figure 70). By combining two approaches the authors showed that knockdown of TAG1 generates mechanical stress in the VZ. They first assessed bending and/or curling of fresh telencephalic hemispheres in WT and TAG1-knockdown conditions. The latter bent poorly when compared to the control, indicating that they are stiffer. Then, laser ablation experiments were performed as described above. TAG1-knockdown apical domains were not only bigger than WT, but their vertices also showed a greater separation upon laser pulse application, supporting the hypothesis that pressure is higher in the VZ of knockdown mice

(Okamoto et al., 2013). Progenitor overcrowding and thus mechanical constraints in the VZ led to aRG delamination, resulting in the presence of ectopias throughout the cortical wall composed of lower and upper layer neurons (Okamoto et al., 2013). This study further supports that the VZ responds to mechanical constraints in order to assure correct aRG population dynamics (Miyata et al., 2014).

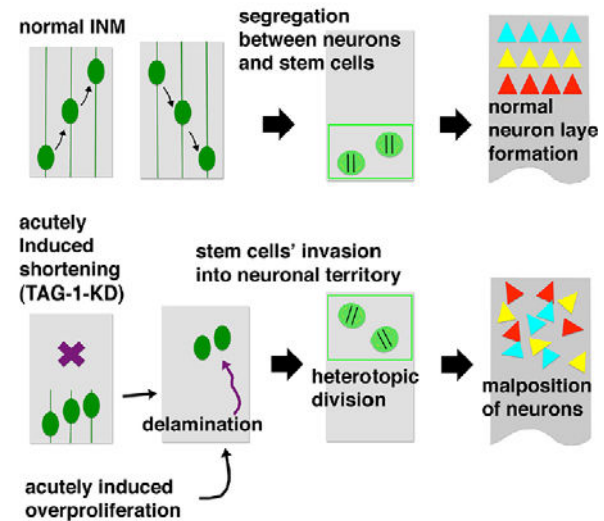


Figure 70. Schematic representation of progenitor overcrowding and delamination upon *TAG-1* knockdown. From Miyata et al., 2014.

Although my work mostly focused on subcellular processes affected when *Em1* is mutated, our results also point towards aRG size and/or shape defects. In Bizzotto et al. (2017), we reported an increased 2D area of metaphase aRGs due to an abnormal cell shape rather than a change in overall volume. Correlation analyses suggested that while metaphase area decreases with increased nuclear density in the WT VS, it does not do this to the same extent in the *HeCo* mouse. Additionally, I analyzed general apical domains, as well as more specifically, centrosome-containing 'endfeet' areas. Ectopic progenitors are found as early as E12.5 in the *HeCo* mouse. At this stage, my results reveal that both apical domains and endfeet showed a tendency towards increased area in the *HeCo* VS when compared to WT. This result became significant when performing these experiments at E13.5. Therefore, at E13.5 mitotic and interphase aRGs appear to have bigger VS areas in *HeCo*. Although the number of endfeet is also reduced within a fixed ROI, the increase in area and abnormal shape could cause higher mechanical forces in the *HeCo* VS; potentially encouraging some cells to escape this tissue constraint and divide in more basal positions as previously described for TAG1-knockdown mice (Okamoto et al., 2013). An increase in mechanical stress in the *HeCo* VZ could be validated by performing laser ablation experiments as previously described in Nagasaka et al., 2016 and Okamoto et al., 2013. These experiments may shed light on mechanical mechanisms in the VZ influencing ectopic progenitor production.

In addition, videomicroscopy experiments at early stages of corticogenesis i.e. E12.5-E13.5 would provide a more detailed characterization of the cellular mechanisms leading to aRG detachment in *Em1*-mutant conditions. Additionally, it remains to be addressed if aRG

delamination occurs after mitosis or is rather an interphase phenomenon. If indeed space constraints are responsible for aRG detachment, it is likely that interphase G2 cells are unable to reach the VS to undergo M-phase and thus delaminate at this stage of the cell cycle to divide in more basal regions. Alternatively and/or concomitantly, aRGs not reaching the VS may divide in basal regions of the VZ, disrupting thus INM. Although videomicroscopy experiments could finely elucidate INM defects, simpler methods can also give us an insight of mitoses across the VZ, for instance, pH3 stainings followed by binning of the VZ and cell distribution analyses.

#### **4. Signaling pathways involved in the ectopic progenitor phenotype**

The cellular and subcellular mechanisms described and discussed throughout my thesis are likely to impact different signaling pathways, or for some, even to be caused by perturbed signaling. Indeed, the primary cilium acts as a platform to mediate Shh, mTOR and Hippo signaling amongst other pathways. Inspired by previous studies assessing cortical phenotypes that share some characteristics with the *HeCo* mouse, I focused on analyzing these three pathways.

##### **4.1 No obvious changes in mTOR activity although Eml1 interacts with Raptor**

The mTOR pathway is well known to regulate cell size amongst other cellular functions (Laplanche and Sabatini, 2012). Recently, Foerster and colleagues (2017) analyzed the VS of mouse mutants in which primary cilia were absent. They showed this resulted in a hyperactivation of the mTOR pathway causing an enlargement of apical domains (Foerster et al., 2017).

The *HeCo* ciliary phenotype accompanied by an increase in apical domain area led me to assess mTOR pathway activity. I investigated possible anomalies in this pathway when the ectopic progenitor phenotype was first observed (E12.5 and E13.5). However, no significant differences were observed between WT and *HeCo* cortex lysates, suggesting that this pathway may not be a key player contributing to the ectopic progenitor phenotype, at least at these early stages of corticogenesis. However, three of the main proteins present in the mTOR signaling cascade appeared in our mass spectrometry data: Rictor, Raptor and Rheb. Furthermore, the interaction between Eml1 and Raptor was confirmed by biochemistry experiments (Extra supplementary results section 2). More meticulous approaches to study the mTOR pathway exclusively in aRGs would be required to fully rule out the implication of this pathway in the ectopic progenitor phenotype. Alternatively, this interaction and hence

this pathway could be important in neurons, given that Eml1 is also expressed in the CP during corticogenesis, during mid- late stages (Kielar et al., 2014). This could explain why no changes were detected in the activity of the pathway at earlier stages of cortical development, when the cortical wall is mainly populated by progenitor cells.

#### 4.2 The Hippo pathway as a convergent signaling cascade in mouse models of subcortical heterotopia

As already mentioned in section 2 of the results, the Hippo pathway (Figure 71) has also been associated with the primary cilium (Whewey et al., 2018), although the relationship remains quite unexplored. The Hippo pathway is known to regulate tissue homeostasis, and hence to influence cell growth, size and shape (Ma et al., 2018).

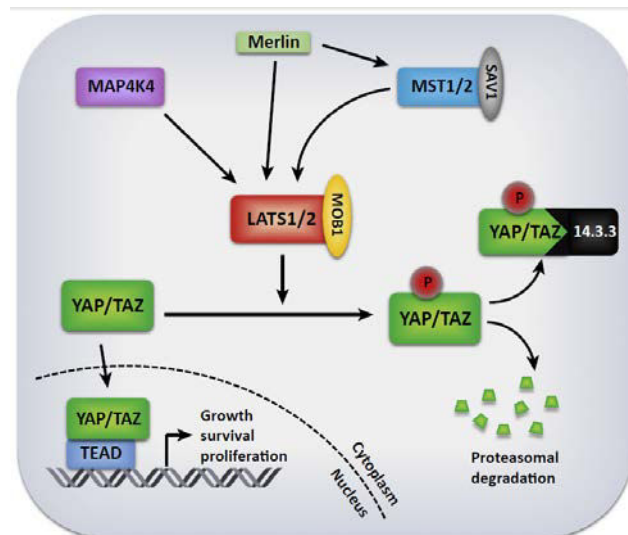


Figure 71. Schematic representation of the Hippo pathway. From Ardestani et al., 2018.

Primary cilia defects were previously

associated with increased Hippo pathway activity (Grampa et al., 2016, Seixas et al., 2016). Mutations in the ciliopathy gene NEK8/NPHP9 lead to renal dysplasia amongst other ciliopathy features (Frank et al., 2013, Grampa et al., 2016). These mutations can lead to decreased primary cilia length, as shown by assessing this organelle in patient fibroblasts (Grampa et al., 2016). In this study, patient fibroblasts also showed an increase of nuclear YAP compared with a control line (Grampa et al., 2016). The authors also showed that knockdown of NEK8 in a kidney cell line (IMCD3)-derived 3D spheroids led to a larger size of these structures, which also showed an increased YAP immunofluorescence (Grampa et al., 2016). Additionally, YAP levels were assessed in Jck mice, carrying a missense mutation in NEK8. These mice exhibited polycystic kidney disease, and Western blot analyses of kidney extracts showed an increase in YAP levels (Grampa et al., 2016). By RT-qPCR the authors also confirmed that YAP target genes were upregulated (Grampa et al., 2016). A different study showed that knocking-out Arl13b in the mouse kidney inhibits ciliogenesis and leads to an increased activation of the Hippo pathway, shown by Western blot experiments of kidney lysates (Seixas et al., 2016). Therefore, these two studies performed in the kidney and/or kidney cells show a relationship

between impaired ciliogenesis and Hippo pathway hyperactivation (Grampa et al., 2016, Seixas et al., 2016).

In the context of cortical development, several studies have also associated the Hippo pathway to cortical malformations (Cappello et al., 2013, Liu et al., 2018, O'Neill et al., 2018a). Mutations in the Hippo pathway protein MOB2 have been reported in one patient presenting PVH (O'Neill et al., 2018a). Mob2 knockdown in the mouse neuroepithelium

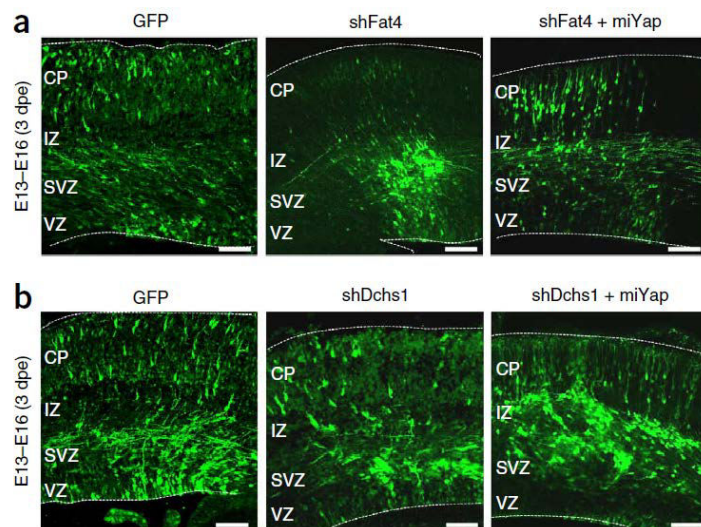


**Figure 72.** Cortical cell distribution abnormalities caused by Fat4/Dchs1 knockdown (a and b, respectively) in the mouse neuroepithelium were rescued by knocking-down concomitantly YAP. From Cappello et al., 2013.

results in neuronal migration defects, although no neuronal progenitor phenotype was described (O'Neill et al., 2018a). Mutations in the cell adhesion proteins FAT4 and DCHS1 lead to PVH in human patients (Cappello et al., 2013). Knockdown of Fat4 and Dchs1 in the mouse neuroepithelium leads to abnormal progenitor proliferation and abnormal cell distribution in the cortical wall (Cappello et al., 2013). This phenotype could be rescued (or partially rescued) by knocking-down YAP, implying that its hyperactivation contributed to the abnormal progenitor phenotype (Cappello et al., 2013, Figure 72). Interestingly, Liu and colleagues (2018) have recently reported changes in the levels of YAP and phospho-YAP in the VZ of Par3 conditional KO mice, a model for subcortical heterotopia which phenocopies *HeCo* and *Eml1* KO mice (Liu et al., 2018, Figure 73). Although the authors did not study the primary cilium, Par3 has been previously found in the cilium axoneme and its knockdown has been described to alter ciliogenesis (Sfakianos et al., 2007).

Given the above-mentioned studies, Hippo signaling is an appealing pathway which could be responsible for the emergence of subcortical heterotopia. Therefore, I decided to assess this pathway in *Eml1*-mutant conditions to shed light on the molecular mechanisms potentially downstream of the Golgi-primary cilium aRG phenotype. Immunohistochemistry experiments in brain slices showed increased YAP levels in the *HeCo* VZ compared to WT. Additionally, YAP immunofluorescence was increased in the nuclei of *HeCo* Pax6+ progenitors *in vitro*.



Therefore, there seems to be a hyperactivation of the Hippo pathway in *HeCo* aRGs, as previously reported in the *Par3* conditional KO mouse (Liu et al., 2018).

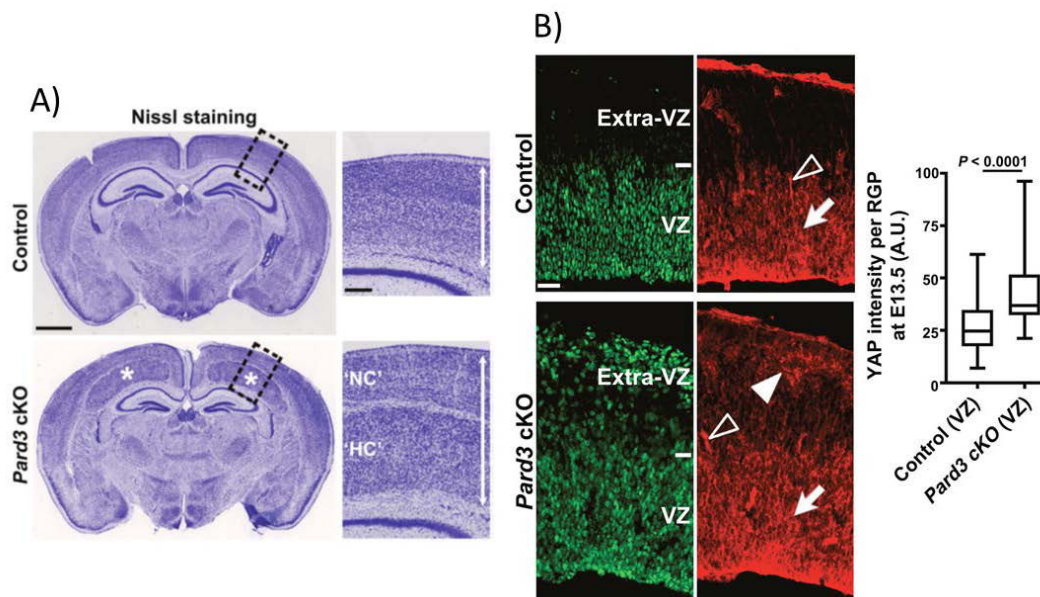


**Figure 73. *Par3* conditional knockout mice are a model of subcortical heterotopia and show increased YAP levels in the ventricular zone at early-mid corticogenesis (E13.5).** A) *Par3* conditional KO mice show subcortical heterotopia phenocopying *HeCo* and *Eml1* KO mice. B) YAP levels are increased in the ventricular zone (VZ) at E13.5. Green: Pax6, red: YAP.

We hypothesize that primary cilium abnormalities may be responsible for the dysregulation of the Hippo pathway. It would be interesting to carefully assess this organelle in *Par3* conditional KO mice. Furthermore, perturbing Golgi function upstream of cilia and then assessing YAP levels could provide a further link between the Golgi-primary cilium axis and the Hippo pathway. We have previously shown and discussed the interaction of *Eml1* with the Golgi protein *Vcip135*. It would be interesting not only to assess primary cilia upon knockdown of *Vcip135*, but also to examine YAP levels.

Alternatively, although the Hippo downstream effectors YAP/TAZ have not been directly correlated with ciliogenesis, other components of the pathways have been shown to influence this process (Endicott et al., 2015, Kim et al., 2014). For instance, MST1/2 localize to the base of the primary cilium and their knockdown in RPE1 cells impairs ciliogenesis (Kim et al., 2014). Therefore, we cannot exclude that dysregulation of YAP in *Eml1*-mutant conditions may be upstream of the primary cilium phenotype.

In addition, other mechanisms important for aRG behavior are well described to regulate the Hippo pathway (reviewed by Ma et al., 2018). Cell density, confluency and shape provide mechanical cues shown to be important for Hippo signaling (Ma et al., 2018). Regulation of

this pathway is often achieved through cell-cell contacts e.g. AJs. As described in section 3.2.2 of the introduction, AJs and polarity proteins are critical for aRG behavior and they mediate features such as cell fate determination and delamination from the VZ. Related to the Hippo pathway, proteins such as E-Cadherin and  $\alpha/\beta$ -catenin can regulate YAP/TAZ translocation to the nucleus and thus activity of the pathway (Kim et al., 2011, Ma et al., 2018). It is thus possible that other ‘pathological’ features of *Em11*-mutant aRGs are responsible for the increased activity of the Hippo pathway.

#### 4.3 The Shh pathway is not severely perturbed in the *HeCo* developing cortex

The Shh pathway has already been discussed in section 3.2.7 of the introduction as well as in section 2 of the results (Figure 74). I assessed downstream effectors of the Shh pathway, the Gli TFs, by performing Western blot experiments with cortex extracts of WT and *HeCo* mice at E12.5 and E13.5, time points at which ectopic progenitors emerge. I analyzed Gli2 and Gli3, although only the repressor form

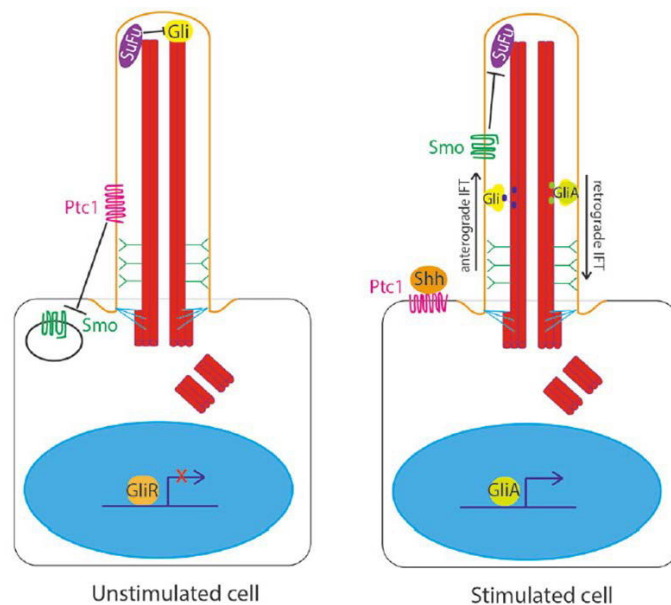


**Figure 74. Schematic representation of the Shh signaling pathway.** From Wheway et al., 2018.

of the former could be examined and no changes were observed between the phenotypes. Analyses of the Gli3A:Gli3R ratio at E12.5 and E13.5 did not show any major change in the *HeCo* mouse when compared to WT conditions. However, there was a tendency towards a decreased in the ratio which was stronger at E13.5 than E12.5. This may suggest that analyses at later stages could unravel stronger abnormalities of the Shh pathway in the *HeCo* cortex. Additionally, it may point to defects in this pathway being a consequence rather than a cause of the aRG pathological phenotype. Other approaches frequently used to assess the pathway could be performed as well to confirm these results e.g. *in situ* hybridization of downstream targets such as *Ptch1* and *Gli1* (Andreu-Cervera et al., 2019, Besse et al., 2011).

As previously mentioned in section 2 of the results, in other mouse mutants for primary cilium proteins the Gli3A:Gli3R ratio changes do not go in the same direction as the results that I

obtained in the *HeCo* mouse. However, in other cell types and more precisely in the context of specific cancers, primary cilium dysfunction results in several outcomes related to Gli TFs and transcription of target genes (reviewed by Nishimura et al., 2018). We can hypothesize that different primary cilium 'pathological' phenotypes in the context of cortical progenitors may also lead to a variety of subcellular outcomes. Additionally, *Eml1* does not seem to localize to the basal body and primary cilium, and the previously mentioned studies assessing Gli TFs during cortical development involve ciliary proteins such as *Kif3a*, *Ift88* or *Rpgrip11* (Besse et al., 2011, Foerster et al., 2017, Wilson et al., 2012). Thus, my results probably highlight the differences between these models and the primary cilium phenotype observed in *Eml1*-mutant conditions.


### **Conclusions**

Cortical development depends on correct neuronal progenitor behavior. When the latter is altered, cortical malformations arise. In my thesis I have studied the role of the subcortical heterotopia gene *Eml1/EML1* mutated in mouse and human. In *Eml1*-mutant conditions (*HeCo* and KO), ectopic aRG-like progenitors were found dividing outside the normal proliferative VZ. Combining mouse and human models as well as a diversity of techniques (electron microscopy, immunodetections followed by confocal imaging, mass spectrometry), I have studied in detail *Eml1/EML1* mutant aRGs, in an attempt to elucidate the mechanisms underlying their delamination from the VZ. The central work of my thesis has unraveled a clear role for *Eml1/EML1* in primary cilium formation. In mutant conditions this organelle is severely disrupted both in mouse and human and my data suggests it is likely to be due to impaired Golgi-to-primary cilium trafficking. Golgi apparatus trafficking defects were indeed revealed in *Eml1*-mutant aRGs. As well as cilia, the abnormal Golgi apparatus phenotype may impact other structures important for aRG behavior such as the AJ-actin belt. Therefore, my work highlights the importance of studying the Golgi apparatus and protein processing in these pathological conditions. I have revealed novel subcellular mechanisms little studied in cortical progenitors which appear to be crucial for their correct behavior and for overall cortical development.

## **ANNEXE I**

## REVIEW

## Cortical progenitor biology: key features mediating proliferation versus differentiation

Ana Uzquiano\*†‡, Ivan Gladwyn-Ng§, Laurent Nguyen§, Orly Reiner¶, Magdalena Götz\*\*††‡‡, Fumio Matsuzaki§§ and Fiona Francis\*†‡ 

\*INSERM, UMR-S 839, Paris, France

†Sorbonne Université, Université Pierre et Marie Curie, Paris, France

‡Institut du Fer à Moulin, Paris, France

§GIGA-Neurosciences, Interdisciplinary Cluster for Applied Genoproteomics (GIGA-R), University of Liège, C.H.U. Sart Tilman, Liège, Belgium

¶Department of Molecular Genetics, Weizmann Institute of Science, Rehovot, Israel

\*\*Physiological Genomics, Biomedical Center, Ludwig Maximilians University Munich, Planegg/Munich, Germany

††Institute for Stem Cell Research, Helmholtz Center Munich, German Research Center for Environmental Health, Neuherberg, Germany

‡‡SYNERGY, Excellence Cluster of Systems Neurology, Biomedical Center, Ludwig-Maximilian University Munich, Planegg/Munich, Germany

§§Laboratory for Cell Asymmetry, Center for Developmental Biology, RIKEN Kobe Institute, Kobe, Hyogo, Japan

Received December 28, 2017; revised manuscript received February 26, 2018; accepted March 8, 2018.

Address correspondence and reprint requests to Fiona Francis, Institut du Fer à Moulin, 17 rue du Fer à Moulin, 75005 Paris, France. E-mail: fiona.francis@inserm.fr

**Abbreviations used:** 3-D, three dimensional; AGS3, activator of G protein signaling 3; AIPS, apical intermediate progenitors; AJ, adherens junction; APs, apical progenitors; aRGs, apical radial glial cells; ARHGAP11B, Rho GTPase-Activating Protein 11B; Arhgef2, Rho guanine nucleotide exchange factor 2; Aspm, abnormal spindle-like microcephaly associated protein homolog; Atf4-6, activating transcription factor 4-6; BAC, bacterial artificial chromosome; BPs, basal progenitors; bRGs, basal radial glia-like cells; Cdc42, cell division control protein 42 homolog; Cdk5rap2, CDK5 regulatory subunit-associated protein 2; Celsr3, cadherin EGF LAG seven-pass G-type receptor 3; Cenpj/CENPJ, centromere protein J; CITK, citron kinase; CP, cortical plate; Crb2, Crumbs2; CR, ciliary remnants; CSF, cerebrospinal fluid; Dlg1, disks large homolog 1; Dynl1, dynein light chain Tctex-type 1; eIF2, eukaryotic initiation factor 2; Elp3, elongator complex protein 3; Eml1, echinoderm microtubule-associated protein-like 1; ER, endoplasmic reticulum; FGF, fibroblast growth factor; Flrt1/3, Fibronectin leucine-rich transmembrane protein 1/3; Fzd3, Frizzled-3; GE, ganglionic eminences; hES, human embryonic stem cells; hiPSCs, induced pluripotent stem cells; hNSC, human neural stem cells; IGF-1, insulin-like growth factor-1; INM, interkinetic nuclear migration; IPs, intermediate progenitors; IRE-1, inositol-requiring enzyme-1; iSVZ, inner

subventricular zone; Jag1, Jagged 1; JAMS, junctional adhesion molecules; Lfc, Rho guanine nucleotide exchange factor 2; LGN, G-protein-signaling modulator 2, called LGN for its Leucine–Glycine–Asparagine repeats; Lis1/LIS1, lissencephaly-1 protein; Llg1, lethal giant larvae homolog 1; MADM, mosaic analysis with double markers; mES, mouse embryonic stem cells; Mib1, Mindbomb1; miRNAs, microRNAs; MST, mitotic somal translocation; mtROS, mitochondrial-reactive oxygen species; Nde1, nuclear distribution protein homolog 1; NES, neuroepithelial cells; NICD, notch intracellular domain; Nt3, neurotrophin-3; NuMA, nuclear-mitotic apparatus protein; oSVZ, outer subventricular zone; Pals1, protein associated with lin seven 1; Par3/6, partitioning defective 3/6 homolog; PDGFD, platelet-derived growth factor D; PDGFRβ, platelet-derived growth factor receptor β; Perk/PERK, PKR-like endoplasmic reticulum kinase; Prdm16, PR domain zinc finger protein 16; RhoA, ras homolog gene family, member A; Sas4, spindle assembly abnormal protein 4; Sip1, Smad-interacting protein 1; SNPs, short neural progenitors; SSA, spindle size asymmetry; SVZ, subventricular zone; TBC1D3, TBC1 domain family member 3; Tctex-1, T-complex testis-specific protein 1 homolog; TF, transcription factor; TMEM14B, transmembrane protein 14B; Trnp1, TMF1-regulated nuclear protein 1; UPR, unfolded protein response; Vangl2, vang-like protein 2; VS, ventricular surface; VZ, ventricular zone; Wdr62, WD repeat-containing protein 62; Wnt7, Wingless 7; Xbp1, X-box-binding protein 1; ZIKV, Zika virus; ZO-1, Zona occludens-1; αPKC, α protein kinase C.

### Abstract

The cerebral cortex is a highly organized structure whose development depends on diverse progenitor cell types, namely apical radial glia, intermediate progenitors, and basal radial glia cells, which are responsible for the production of the correct neuronal output. In recent years, these progenitor cell types have been deeply studied, particularly basal radial glia and their role in cortical expansion and gyrification. We review here a broad series of factors that regulate progenitor behavior and daughter cell fate. We first describe the different neuronal progenitor types, emphasizing the differences between lissencephalic and gyrencephalic species. We then review key factors shown to influence progenitor proliferation versus differentiation, discussing their roles in progenitor dynamics, neuronal production, and potentially brain size and complexity.

Although spindle orientation has been considered a critical factor for mode of division and daughter cell output, we discuss other features that are emerging as crucial for these processes such as organelle and cell cycle dynamics. Additionally, we highlight the importance of adhesion molecules and the polarity complex for correct cortical development. Finally, we briefly discuss studies assessing progenitor multipotency and its possible contribution to the production of specific neuronal populations. This review hence summarizes recent aspects of cortical progenitor cell biology, and pinpoints emerging features critical for their behavior.

**Keywords:** cell division (symmetric, asymmetric), cerebral cortex evolution, cortical neurogenesis, mouse mutant, neurodevelopment, progenitor cell.

*J. Neurochem.* (2018) **146**, 500–525.

The cerebral cortex is the brain region responsible for higher cognitive functions. It is a highly organized structure, and its development depends on diverse progenitor cell types, which give rise to post-mitotic neurons that migrate extensively to find their appropriate positions in the developing cortical wall (for review see Kawauchi, 2015; Stouffer *et al.* 2016). This extremely dynamic yet highly regulated process leads to the formation of the six-layered adult neocortex. Toward understanding its development, invertebrate models such as *Drosophila* have provided valuable insights (Homem and Knoblich, 2012), and rodents (mice and rats) are commonly used model organisms for unraveling the complex mechanisms underlying cortex development and the cell biology of neuronal progenitors. Rodents are, however, lissencephalic species and the neuronal progenitor cell populations within their developing cortices are less diverse as compared to gyrencephalic species, such as the ferret and primates. Recent analyses of primate brains, including human postmortem brains, have allowed an improved discernment of progenitor cell diversity, as well as their contributions to increased cortical complexity, and folding of the brain (Fernandez *et al.* 2016).

The timing and duration of neurogenesis varies, and correlates with brain complexity, *vis-à-vis* the studied model organism. For instance, murine neurogenesis lasts around 2 weeks, whereas it takes 3 months in the developing human brain. This extended period of human neurogenesis relies on increased neuronal progenitor self-renewal, promoting the expansion of the germinal layers, and increasing the number of neurons produced throughout corticogenesis. This in turn will lead to expansion of the neocortex, contributing to the appearance of *gyri* and *sulci*. In addition, the advent of human embryonic stem cells (hES) and

induced pluripotent stem cells (hiPSCs) has introduced novel *in vitro* systems to study diverse aspects of neuronal progenitor dynamics. Human organoids are three-dimensional (3-D) structures derived from hES or hiPSCs, and include cortical-like tissue containing ventricular lumen, germinal zones, and neurons. These *in vitro* models augment our ability to analyze and dissect the characteristics of corticogenesis in human brains, aiding dissection of the pathophysiology underlying brain disorders, as analogous processes in mutant mouse models are more limited (Eiraku *et al.* 2008; Lancaster *et al.* 2013, Lancaster and Knoblich 2014; Clevers 2016; Bershteyn *et al.* 2017; Di Lullo and Kriegstein, 2017; Iefremova *et al.* 2017). Understandably, a holistic appraisal of all steps of cortical development (e.g., proliferation, modes of cell division, cell differentiation, cell migration) is key to unraveling the pathophysiological mechanisms underlying cortical malformations such as microcephaly (small brain), lissencephaly (smooth brain), and heterotopia (abnormally positioned neurons), often associated with intractable epilepsy and intellectual disability (for a recent review of human cortical malformations see Romero *et al.* 2018). Genetic and environmental factors (e.g., viruses such as Zika) can perturb these critical steps. Elucidating the intrinsic and extrinsic mechanisms controlling progenitor cell proliferation versus neuronal differentiation will help shed light on cortical expansion, gyrification, and ultimately neocortical evolution.

In this review, we describe the different types of neuronal progenitor populating the developing cortex. We focus on the critical factors that control progenitor self-renewal and cell differentiation, emphasizing those either promoting a proliferative potential, or leading to cell cycle exit and neuronal commitment. Ultimately, we discuss how the broad variety of progenitors found in gyrencephalic species contributes to

increasing the final neuronal output, resulting in the highly expanded and folded neocortex characteristic of human brains.

### Introduction to cortical progenitor types

The neocortex develops from the anterior-most region of the neural tube, the dorsal telencephalon. This region gives rise to glutamatergic excitatory neurons (principal or pyramidal neurons), which account for around 80% of the neurons of the neocortex (Lodato and Arlotta, 2015). The other 20% of cells of the neocortex are GABAergic interneurons. Murine cortical interneurons are generated in the ganglionic eminences (GE), located in the ventral telencephalon, and migrate long distances to integrate in the developing cortex (for a review of interneuron development see Marin, 2013; Bandler *et al.* 2017; Laclef and Metin, 2018). However, the origin of primate, human interneurons is still a controversial topic. Diverse studies support that in primates, including humans, the germinal zones located in the dorsal telencephalon are an important source of interneuron production (Letinic *et al.* 2002; Rakic and Zecevic, 2003; Jakovcevski *et al.* 2011; Al-Jaberi *et al.* 2015). However, two recent studies showed primate, human interneurons to be mainly produced in the GE, as it occurs in the mouse brain (Hansen *et al.* 2013; Ma *et al.* 2013). In this review, we focus on mechanisms controlling the behavior of progenitors responsible for the generation of projection neurons.

### Apical progenitors (APs): neuroepithelial cells (NEs), apical radial glial cells (aRGs), and short neural progenitors (SNPs)

The walls of the neural tube are populated by neuroepithelial cells (NEs) that possess an apico-basal polarity with attachment of their basal processes to the basement membrane and junctional coupling at the apical side. These NEs undergo the distinctive process of interkinetic nuclear migration (INM) during the cell cycle: their nuclei move apico-basally within the neuroepithelium, entering M-phase at the apical surface (Bertipaglia *et al.* 2017). NEs are characterized by the presence of occludin-positive (+) tight junctions (Aaku-Saraste *et al.* 1996), as well as gap junctions for intercellular connections and the flux of small molecules, thus enabling cellular communication (Elias and Kriegstein, 2008). They have a prominin<sup>+</sup> apical domain that accommodates a primary cilium protruding into the ventricles (Taverna *et al.* 2014), which senses signals from the cerebrospinal fluid (CSF) that will influence NE behavior (Lehtinen and Walsh, 2011; Arbeille *et al.* 2015).

NEs divide in a symmetric proliferative fashion, amplifying their numbers and hence the neural progenitor pool. Upon the onset of neurogenesis from embryonic day (E)10–12 of murine development, NEs transit from a purely proliferative to a neurogenic state (Gotz and Huttner, 2005; Matsuzaki and Shitamukai, 2015), while their tight junctions

are gradually annexed by an adherens junction (AJ) belt that is characterized by the presence of proteins such as N-cadherin and zona occludens (ZO)-1 (Aaku Saraste *et al.* 1996) (AJs will be further discussed in the section ‘Influence of the polarity complex and cell adhesion molecules’). Consequently, NEs become apical radial glial cells (aRGs) that comprise the predominant neuronal progenitor cell type within the developing neocortex (Malatesta *et al.* 2000; Noctor *et al.* 2001; Noctor *et al.* 2004). aRGs are also highly polarized cells, exhibiting basal processes attached to the basement membrane, and apical processes linked by adhesion forming a transition region [termed here the ‘ventricular surface (VS)’] with CSF in the ventricles (Fig. 1a). As for NEs, aRG apical domains are prominin<sup>+</sup> and contain a primary cilium (Taverna *et al.* 2014). Their basal process has been extensively described to be a scaffold for migrating neurons to reach their positions in the cortical plate (CP) (Borrell and Gotz, 2014). aRGs also undergo INM, although the nuclear oscillation is restricted to the ventricular zone (VZ), where their somata reside (Gotz and Huttner, 2005). Because of this highly dynamic cell cycle process, the VZ is often described as a pseudostratified neuroepithelium.

The transition of NEs to aRGs is critical for determining the size of the initial pool of progenitors available to generate neurons, thereby determining the final neuronal output and brain size (Fernandez *et al.* 2016). Several factors involved in this transition, for example, fibroblast growth factors (FGFs), are also key for maintaining aRG identity. Notably, FGF10 triggers expression of aRG markers in NEs (Sahara and O’Leary, 2009) and also supports an aRG fate by inhibiting their transition toward a more committed neuronal progenitor (Kang *et al.* 2009). The Notch signaling pathway has also been described to be important for the transition from NEs to aRGs (Gaiano *et al.* 2000; Hatakeyama *et al.* 2004; Martynoga *et al.* 2012). While they lose tight junctions and develop the AJ belt, aRGs acquire astroglial features (Florio and Huttner, 2014; Gotz *et al.* 2015) and become positive for a set of astroglial markers, such as the astrocyte-specific glutamate transporter and others. They also express key neurogenic transcription factors (TF), such as Pax6 (Gotz *et al.* 1998).

aRGs are more restricted in their proliferative potential than NEs. They mainly undergo asymmetric proliferative divisions in the rodent, self-renewing while producing post-mitotic neurons or neurogenic progenitors (see section ‘Basal progenitors (BPs): intermediate progenitors (IPs) and basal radial glia-like cells (bRG), and their implication in cortical expansion’ and Fig. 1). Direct neurogenesis involves the process by which neurons are produced directly from aRGs. On the other hand, indirect neurogenesis refers to the process by which aRGs produce other intermediary types of progenitor cells that will subsequently produce neurons, thereby increasing the net neuronal output. Neurons that are produced earlier during corticogenesis (e.g., E11.5–

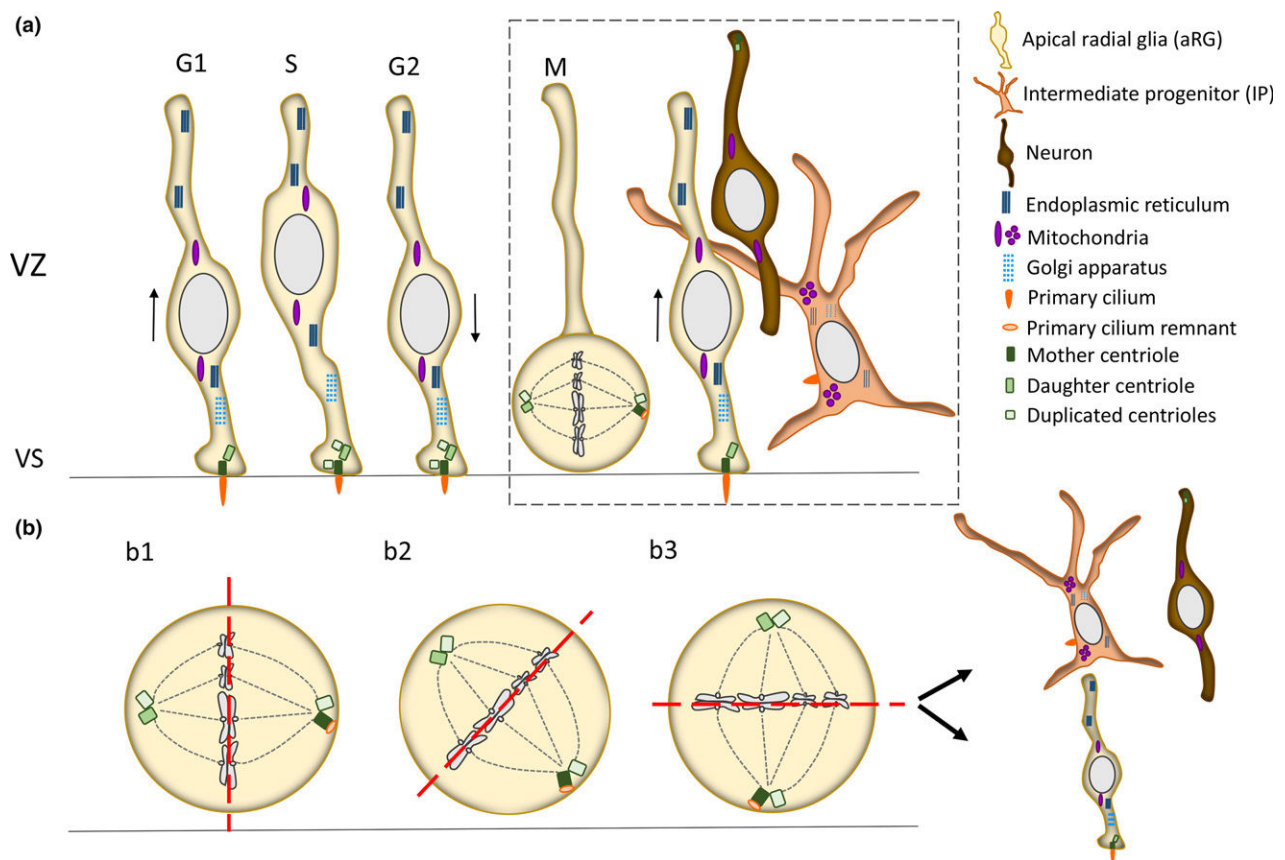


**Fig. 1** Ventricular zone (VZ) dynamics and apical radial glia (aRG) behavior in the developing cortex. **(a)** VZ containing interphase and mitotic aRG, which divide to self-renew and produce intermediate progenitors (IP) or neurons. aRG nuclei move apico-basally through the different stages of the cell cycle, S-phase occurring in the most basal part of the VZ and mitosis at the ventricular surface (VS). Cellular organelles show a diverse distribution in interphase aRGs: the endoplasmic reticulum is localized in the basal and apical processes, whereas the Golgi apparatus is localized exclusively in the latter. Mitochondria present an elongated morphology. The older centriole, within the centrosome, constitutes the basal body docking a primary cilium, which becomes shorter as the cell cycle progresses. The mother and daughter centriole duplicate before M-phase. In IPs the Golgi acquires a more basal position and the mitochondria present a

fragmented morphology. As it delaminates from the VZ, the IP docks a basolateral primary cilium. Newly born neurons migrate far from the VZ, while their mitochondria recover an elongated morphology. **(b)** aRG mitosis. For simplicity, the basal process of mitotic aRGs is not represented. aRGs mainly divide asymmetrically, self-renewing and producing a more committed cell in the neuronal lineage, for example, an IP or a neuron. Spindle orientation has been associated with daughter cell fate. Depending on the insertion of the cleavage furrow (red dashed line), divisions are defined as vertical (b1), oblique (b2), or horizontal (b3). The mother centriole as well as primary cilium remnants associated with it are inherited by the daughter cell acquiring an aRG fate thus remaining in the VZ. In this schema, the other daughter cell represents a multipolar IP or a newly born neuron.

E14.5 in mouse) are destined for the deeper layers of the neocortex. Later in corticogenesis, neurons are produced (e.g., E14.5–E17.5 in mouse) that migrate past the early born neurons to reach their appropriate positions in the upper layers of the CP. aRGs appear to be restricted over time in their potential to produce different neuronal subtypes. Thus, as neurogenesis proceeds, aRGs become more committed to a specific neuronal output (Luskin *et al.* 1988; McConnell and Kaznowski, 1991; Walsh and Cepko, 1993; Frantz and McConnell, 1996; Desai and McConnell 2000; Shen *et al.* 2006; Gao *et al.* 2014; Kaplan *et al.* 2017). This topic will

be further discussed in section ‘Multipotency and potential subpopulations of aRGs’, and certain specific features of human aRGs in section ‘Basal progenitors (BPs): intermediate progenitors (IPs) and basal radial glia-like cells (bRG), and their implication in cortical expansion’.

Another apical progenitor cell type that co-exists with aRGs in the VZ are the short neural progenitors (SNP), also known as apical intermediate progenitors (AIPs). SNPs have an apical process as aRGs, however, their basal process remains constrained within the VZ and hence does not span the entire cortical wall. SNPs located in the dorsal



telencephalon are mainly neurogenic progenitors, producing neurons upon symmetric division (Gal *et al.* 2006; Stancik *et al.* 2010). Nevertheless, SNPs found in the VZ of the GE are capable of self-renewing, as well as producing other types of progenitors (Pilz *et al.* 2013).

### Basal progenitors (BPs): intermediate progenitors (IPs) and basal radial glia-like cells (bRGs), and their implication in cortical expansion

As corticogenesis progresses, aRGs produce basal progenitors (BPs), mainly intermediate progenitors (IPs) in the rodent, which are multipolar transit-amplifying progenitors. IPs are Tbr2+ (Englund *et al.* 2005) and they divide in a basally located germinal zone: the subventricular zone (SVZ). The Notch signaling pathway also plays a role in the transition from aRGs to IPs: activation of Notch signaling inhibits the production of IPs from aRGs (Mizutani *et al.* 2007; Martynoga *et al.* 2012). Another pathway modulating the switch between self-renewal and neurogenic commitment is the Wnt signaling pathway. In early corticogenesis it promotes aRG proliferation (Woohead *et al.* 2006), while in later stages it is crucial for IP and even neuronal production (Hirabayashi *et al.* 2004; Munji *et al.* 2011).

In the mouse, IPs are mainly neurogenic, dividing symmetrically to produce two neurons (Haubensak *et al.* 2004; Miyata *et al.* 2004; Noctor *et al.* 2004). Diverse mechanisms have been described to control this process (Borrell *et al.* 2012; Laguesse *et al.* 2015a, Haushalter *et al.* 2017). While murine IPs mainly undergo terminal divisions to produce neurons, in the primate–human brain they have a higher proliferative potential, being capable of self-renewing several times before their terminal division (Ostrem *et al.* 2017).

The initial pool of aRGs is larger in gyrencephalic species and these cells mostly promote indirect neurogenesis by giving rise to a diversity of basally located progenitors. This results in a higher neuronal production, which will have an effect on cortical size and folding (Fernandez *et al.* 2016).

While the developing murine cortex predominantly comprises aRGs and IPs, another type of progenitor can be found in very small numbers within the SVZ: the basal radial glia-like cells (bRGs), present at less than 1% of the cortical progenitors in mouse (Shitamukai *et al.* 2011; Wang *et al.* 2011). bRGs represent a large proportion of BPs in gyrencephalic species. They are produced from aRGs within a specific time-window early during corticogenesis (LaMonica *et al.* 2013; Gertz *et al.* 2014; Martinez-Martinez *et al.* 2016), and share similar features, as well as a wide range of characteristic markers with aRGs, such as Pax6, nestin, and vimentin (Ostrem *et al.* 2017). bRGs are considered essential for neocortical expansion and gyrification, and thus are mainly studied in human, ferret, and macaque brains (Fernandez *et al.* 2016; Ostrem *et al.* 2017). In these species, bRGs are localized in the most basal region of the SVZ,

which is bisected by axons into an inner SVZ (iSVZ) and an outer SVZ (oSVZ). The oSVZ is the most proliferative germinal zone in the primate and human developing neocortex. bRGs are generally attached to the basement membrane by a basal process, although they lack the apical process characteristic of aRGs (Fietz *et al.* 2010; Hansen *et al.* 2010; Reillo *et al.* 2011; Wang *et al.* 2011). Although this is the classical morphological description of bRGs, it has been shown that they can present different combinations of progenitor markers and diverse shapes, and up to five different morphologies have been described in the primate SVZ (Betizeau *et al.* 2013). Upon cell division and prior to cytokinesis, their soma moves toward the developing CP in a process known as mitotic somal translocation (MST). In the mouse, they mainly divide in an exhaustive symmetric fashion to produce two neurons (Wang *et al.* 2011). However, in the ferret and primate (including human) brains, bRGs are capable of self-renewing while producing IPs and neurons (Hansen *et al.* 2010; Betizeau *et al.* 2013; Gertz *et al.* 2014; Martinez-Martinez, 2016). This phenomenon results in a greater number of progenitor cells, which in turn increases the final number of neurons produced. Activation of the Notch signaling pathway has been reported to be important for human bRG proliferation (Hansen *et al.* 2010).

bRGs have been shown to be produced by aRG horizontal cell divisions (LaMonica *et al.* 2013; Gertz *et al.* 2014; Martinez-Martinez *et al.* 2016), although direct delamination of aRGs has also been suggested (Gertz *et al.* 2014). In the mouse dorsal telencephalon, most aRG divisions are vertical, but in primate–human brains there is a shift toward horizontal divisions, which may be important for bRG production and oSVZ expansion (LaMonica *et al.* 2013). It is worth noting that the murine GE is the telencephalic region with the biggest diversity of progenitor types and a major production of BPs. GE-AP vertical divisions are less abundant, and proliferative SNPs divide mainly in a horizontal/oblique fashion (Pilz *et al.* 2013; Falk *et al.* 2017).

Two molecules were initially described to play a key role in temporally regulated bRG production and oSVZ seeding in the ferret: Cadherin 1 and Trnp1. Down regulation of Cadherin 1 and Trnp1 levels promotes horizontal aRG divisions and delamination from the VZ, resulting in bRG production. On the other hand, up-regulation of these proteins decreases bRG production, stopping the seeding of the oSVZ (Martinez-Martinez *et al.* 2016). Knockdown of Trnp1 in mouse aRGs had been previously correlated with a switch toward horizontal divisions and the production of bRG-like cells resulting in the appearance of folds in the otherwise smooth mouse neocortex. (Stahl *et al.* 2013). Related to this study, other molecules and signaling pathways have been shown to induce bRG production in the mouse developing cortex. For example, activation of Shh signaling in mouse aRGs during early corticogenesis leads to

the expansion of both IP and bRG-like cell populations, resulting as well in the presence of folds in the mouse cortex (Wang *et al.* 2016a). Forced expression of Pax6 in mouse aRGs and their progeny also induces the generation of primate-like bRGs (Wong *et al.* 2015).

In addition to these molecules, other studies have revealed certain genes only present in human aRGs that seem to be crucial for BP production. This is the case for the platelet-derived growth factor D (PDGFD). Although the latter is expressed in murine GE-aRGs it is exclusively expressed in dorsally located aRGs in human. Expression of PDGFD or ectopic expression of its receptor PDGFR $\beta$  in the mouse dorsal neuroepithelium induces production of bRG-like cells (Lui *et al.* 2014). Similarly, Florio and colleagues (2015) found the gene Rho GTPase-Activating Protein 11B (ARHGAP11B) to be preferentially expressed in human aRGs, and when over-expressed in the mouse neuroepithelium, it led to the generation of BPs (both IP- and bRG-like cells) (Florio *et al.* 2015). In line with these studies, Ju and colleagues (2016) revealed a novel function for *TBC1D3*, a great ape-specific gene which has undergone segmental duplications during evolution, in brain development and bRG production. Expression of *TBC1D3* in the mouse VZ led to the production of primate-like bRGs, indicating the potential role of this gene in neocortical evolution (Ju *et al.* 2016). Very recently, Liu and colleagues (2017) identified the primate-specific gene *TMEM14B* as a marker for bRGs. Expression of this gene by *in utero* electroporation in the mouse VZ promoted neuronal progenitor production and expansion of the SVZ. In addition, Nestin-Cre-mediated knock-in mice for *TMEM14B* exhibited cortical folding (Liu *et al.* 2017). Taken together, these studies open the gate to the discovery of more primate and/or human-specific RG genes that could mediate the switch from aRGs toward BP production, particularly bRGs, as well as shed light into the cellular and molecular mechanisms that promote a bRG-like identity (Heide *et al.* 2017). Lastly, it would be of great interest to unravel why in the mouse developing cortex, Pax6+ progenitors located outside the VZ sometimes lead to cortical anomalies (Cappello *et al.* 2012; Insolera *et al.* 2014; Kielar *et al.* 2014), while other times they behave as proper bRG-like cells leading to expansion of the SVZ, increased number of upper layer neurons and/or cortical area, and ultimately the appearance of fold-like structures (Stahl *et al.* 2013; Florio *et al.* 2015; Wong *et al.* 2015; Ju *et al.* 2016; Liu *et al.* 2017).

The VZ contains aRGs, which move apico-basally through different stages of cell cycle by INM, with mitosis occurring at the VS. It is believed that INM occurs in order to create space in the VZ so more aRGs can undergo M-phase at the VS. It has been hypothesized that aRGs that eventually become bRGs may leave the VZ to escape this space constraint, moving basally to the oSVZ while maintaining several aRG traits (Florio and Huttner, 2014).

Although they lack apical anchoring, bRGs maintain their basal processes which are likely to be important for their self-renewal potential. In addition, integrin signaling through basal contact has been shown to be involved in bRG proliferation and amplification. When integrin signaling was blocked in ferret brain organotypic slices, the pool of cycling progenitors both in the VZ and SVZ was decreased, the effect being more prominent in the SVZ (Fietz *et al.* 2010). The basal process of bRGs is important for MST, and the length, frequency and directionality of MST have been proposed to be associated with brain evolution. In human fetal brain, MST appears to be more frequent than in other species, and the distance travelled by the nuclei seems to be greater, following a straighter pattern of movement toward the pial surface (Ostrem *et al.* 2017).

Although we have focused on the importance of generating a large quantity of progenitors to increase neuronal output, bRGs also contribute to the tangential expansion of the neocortex by providing more basal fibers, without corresponding apical attachments, which act as a scaffold for migrating neurons to reach their final position (Florio and Huttner, 2014; Borrell and Gotz, 2014). These cells hence allow a 'fan-like' pattern of neuronal migration, which was recently proposed to contribute to cortical folding (del Toro *et al.* 2017). By using a mouse model in which the adhesion molecules *Flrt1* and *Flrt3* were deleted, the authors observed the appearance of gyri and sulci in the mouse cortex. Strikingly, this effect was not because of progenitor amplification, but rather a change in the pattern of neuronal migration (Del Toro *et al.* 2017). Therefore, although progenitor amplification and increased neuronal output are key for neocortical expansion, emerging studies are uncovering novel mechanisms which seem to be important for the cortical folding process (see also Heide *et al.* 2017).

Finally, it is worth mentioning that these primate-human-specific traits may be one of the main targets of brain diseases and cortical malformations, which may explain why mouse models often fail to recapitulate the patients' phenotype. The use of cerebral organoids will help to unravel human-specific mechanisms of brain development as well as generating novel *in vitro* human models of neurodevelopmental and neurodegenerative diseases (Di Lullo and Kriegstein, 2017). Lately, two different studies used brain organoids to study the mechanisms leading to Miller-Dieker syndrome (Bershteyn *et al.* 2017; Iefremova *et al.* 2017), a severe form of lissencephaly. While defects in aRG divisions could be detected (Bershteyn *et al.* 2017; Iefremova *et al.* 2017), potentially recapitulating what had already been found by using mouse models (Yingling *et al.* 2008), a defect in bRG division was also observed (Bershteyn *et al.* 2017). Hence, it is important to further develop human-like models to study certain diseases, since human-specific traits may be altered.

### Intrinsic versus extrinsic influences on progenitor transitions

Diverse studies have shown the importance of feedback signaling from post-mitotic neurons to maintain the aRG proliferative state. Notch signaling is probably the most studied: differentiating cells express Notch ligands belonging to the Delta-like and Jagged families, which signal toward aRGs triggering the Notch signaling cascade and thus the repression of proneural factors (Agirman *et al.* 2017). The Wnt7-Celsr3-Fzd3 pathway was shown to mediate Jag1 expression in immature neurons (Wang *et al.* 2016b). Immature neurons lacking Celsr3 or Fzd3 do not respond to cortical Wnt7, which results in a down-regulation of Jag1 levels, and a consequent down-regulation of Notch signaling in aRGs (Wang *et al.* 2016b). The TF Smad-interacting protein 1 (Sip1) is highly and exclusively expressed in post-mitotic neurons throughout corticogenesis, and its deletion also impacts aRG behavior triggering a production of upper layer neurons at the expense of deep layer neurons, and eventually a precocious gliogenesis (Seuntjens *et al.* 2009). Related to this work, Parthasarathy and coworkers showed that neurotrophin 3 (Nt3), which is a target of Sip1, modulates the balance between aRG self-renewal and commitment to a more differentiated progenitor cell type (Parthasarathy *et al.* 2014). However, down-regulating Nt3 levels does not rescue the Sip1 mouse mutant phenotype, suggesting that in the latter there are additional mechanisms regulating progenitor fate switch (Parthasarathy *et al.* 2014). Signals derived from other neuronal populations also influence aRGs. Cajal Retzius cells are among the first neurons produced arising from different regions of the telencephalon and distributing superficially around the developing cortex. Changed distributions of these cells were shown to alter aRG proliferation (Griveau *et al.* 2010). Lastly, deletion of a transient tangentially migrating glutamatergic population derived from ventral regions of the cortex also alters aRG proliferation and enhances a precocious switch toward neuronal production (Teissier *et al.* 2010).

Extrinsic factors are also emerging to be crucial not only for aRG but also for bRG proliferation. Transcriptome analyses point toward a role for extracellular matrix components produced in a cell-autonomous manner in controlling bRG proliferation (Fietz *et al.* 2012; Florio and Huttner, 2014; Pollen *et al.* 2015). Additionally, extrinsic factors derived from neurons in different brain regions could affect the proliferation of SVZ progenitors. Particularly, thalamo-cortical axons invading the intermediate zone (IZ) have been proposed to be an important source of mitogens for progenitors located in the SVZ in gyrencephalic species (Dehay and Kennedy, 2007). Recent work by Reillo and colleagues (2017) supports the influence of growing axonal tracts on progenitor dynamics. By combining axonal and cell lineage tracing with immunostainings, the authors correlated progenitors with different axonal tracts, and illustrated the

dynamic interactions occurring throughout development (Reillo *et al.* 2017).

Although extrinsic mechanisms mediate progenitor dynamics, other studies support an intrinsic control of the latter. For instance, Albert and colleagues (2017) have also recently reported that transitions between cell types are moderated by different histone methylation profiles. By isolating diverse progenitor populations in the mouse developing cortex (namely NEs, aRGs, bRGs, and neurons) followed by ChIP-seq, they traced different methylation patterns regulating the expression of TFs known to be involved in progenitor transitions (Albert *et al.* 2017). Thus, this paper proposes additional strategies controlling progenitor cell fate.

### Factors influencing symmetric versus asymmetric division

#### Mitotic spindle and cleavage plane, inheritance of apical and basal processes

Invertebrate models have been used extensively to study the mechanisms controlling symmetric versus asymmetric cell division (for a review see di Pietro *et al.* 2016). Orientation of the cleavage plane may influence daughter cell fate and control the mode of division (Fig. 1). In these models, cell fate determinants are asymmetrically positioned within the cell prior to mitosis. When the mitotic spindle is oriented parallel to the apico-basal gradient of fate determinants, the cleavage furrow gives rise to an uneven repartition of these factors between the daughter cells, leading to an asymmetric cell division. On the contrary, when the mitotic spindle is positioned perpendicular to this gradient, the cleavage furrow will be oriented in the same direction of the gradient, leading to an even distribution of fate determinants: the progeny generated will acquire the same identity.

Initially it was thought that a similar situation occurs in mammalian aRGs. More precisely, symmetric divisions would be achieved by insertion of the cleavage furrow perpendicular to the VS (vertical divisions), while a parallel or oblique insertion of the latter (horizontal or oblique divisions, respectively) would lead to an asymmetric cell division producing two daughter cells with different fate (spindle orientations depicted in Fig. 1b) (Chenn and McConnell, 1995). However, association between orientation of the cleavage plane and daughter cell fate is not as straightforward, and this will be discussed further here.

Inheritance of the apical domain of aRGs was initially thought to be critical for daughter cell fate determination. A previous model proposed that the daughter cell inheriting the apical domain, would retain aRG identity, while the cell deprived of this apical structure would be committed to a different fate, for example, by being more restricted to the neuronal lineage (but see below). Since asymmetric inheritance of the apical structure may lead to differentiative

divisions, a slight tilt in spindle orientation, enough for the cleavage plane to bypass the apical domain, could trigger an asymmetric cell division (Kosodo *et al.* 2004; Marthiens and French-Constant, 2009). Thus, it is important to carefully determine whether the cleavage furrow bypasses or divides the apical domain during aRG mitoses, since it may have an impact on the identity of the newly generated daughter cells. This domain was originally identified by immunohistochemistry (Kosodo *et al.* 2004; Marthiens and French-Constant, 2009). More recently live-imaging techniques provide information concerning the dynamics of its cleavage through the last steps of M-phase (Konno *et al.* 2008; Asami *et al.* 2011; Matsuzaki and Shitamukai, 2015). These reports showed that only in a relatively low proportion of cell divisions during the neurogenic period of corticogenesis, the apical domain was uniquely inherited by one of the daughter cells (Konno *et al.* 2008; Asami *et al.* 2011; Shitamukai *et al.* 2011). Accordingly, these observations suggest that factor(s) other than apical domain inheritance determine cell fate, and this is in agreement with the fact that during mouse neurogenesis there is a majority of vertical divisions (Matsuzaki and Shitamukai, 2015) not all of them being proliferative and symmetric. Thus, although classically the inheritance of the apical epithelial structure, dependent on cleavage furrow insertion, was believed to be key to acquiring proliferating aRG identity, this vision is currently changing, indicating that other features are crucial to determine daughter cell identity and to provide self-renewal potential.

Inheritance of the aRG basal process has also been shown to contribute to cell fate determination. Basal process-dependent integrin signaling appears to be important for maintaining aRG and bRG proliferative potential (Fietz *et al.* 2010). In addition, Tsunekawa and coworkers (2012) described how the mRNA of cyclin D2, responsible for G1 progression, is mainly present in aRG basal processes. This implies that upon aRG cell division, only the daughter cell inheriting the basal process will progress through G1 while retaining proliferative potential (the relationship between cell cycle length, particularly G1, and proliferative potential is further addressed in section 'Cell cycle considerations'). Thus, inheritance of the basal process seems to promote a proliferative state and to maintain aRG self-renewal potential (Konno *et al.* 2008, Fietz *et al.* 2010; Tsunekawa *et al.* 2012). Emphasizing the importance of epithelial structure inheritance, in zebrafish it was described how upon aRG division, aRG-fated daughter cells often lose their apical endfoot, which then regrows allowing maintenance of the whole epithelial structure (i.e., apical and basal processes) (Alexandre *et al.* 2010). In addition, delaminating neurons in the chick spinal cord lose their apical structure while leaving the VZ (Das and Storey, 2014). Therefore, inheritance and maintenance of epithelial features (apical and basal processes) seem to be a key

factor controlling cell fate upon aRG division (Matsuzaki and Shitamukai, 2015).

Related to the distribution of cell fate determinants and retention of epithelial features, mitotic spindle assembly and attachment to the cell cortex is also a tightly controlled process which can influence these processes. Centrosomes, which are localized in the apical process of aRGs during interphase, move a short distance basally before undergoing duplication and forming the spindle poles (Hu *et al.* 2013). The latter nucleate microtubules constituting the spindle, and they are also associated with astral microtubules, which link the mitotic spindle to the cell cortex. Mitotic spindle orientation is likely to be regulated by a complex of proteins involved in its attachment to the cell cortex by astral microtubules. This complex includes the GoLoco domain-containing protein LGN, which associates with the cell cortex through G $\alpha$ i. In addition, LGN binds to nuclear-mitotic apparatus protein (NuMA), which binds to the dynein–dynactin complex. This motor complex exerts forces on the astral microtubules, thus orienting the mitotic spindle (for a review see di Pietro *et al.* 2016).

Several studies have shown the impact of altering the level of these proteins on spindle orientation and aRG progeny after cell division. Interfering with the levels of LGN leads to a randomization of spindle orientation, both in the chick (Morin *et al.* 2007) and in the mouse neuroepithelium (Konno *et al.* 2008). Both studies show that LGN is crucial to maintain vertical cell divisions, and randomization of the mitotic spindle leads to the presence of aberrantly positioned cycling progenitors (Konno *et al.* 2008). Despite the spindle fluctuations, there is no change in neuronal output or in brain size when deleting LGN in the mouse, suggesting that ectopic progenitors still generate neurons (Konno *et al.* 2008). Also, the LGN-interacting protein disks large homolog 1 (Dlg1) controls vertical divisions in the chick neuroepithelium (Saadaoui *et al.* 2014). Dlg1 ensures the proper localization of LGN to the cell cortex and it is necessary for correct spindle orientation (Saadaoui *et al.* 2014). The GoLoco-containing protein activator of G protein signaling 3 (AGS3), which also interacts with NuMA, was initially described to have similar functions to LGN and to be important for spindle orientation, since knockdown of AGS3 in mouse aRGs led to a decrease in oblique spindle orientations (Sanada and Tsai, 2005). However, this function of AGS3 is controversial, since a recent study has shown that despite its interaction with NuMA, AGS3 is not recruited to the cell cortex in mouse aRGs, and it does not control mitotic spindle orientation during cell division (Saadaoui *et al.* 2017). This study is in agreement with previous work showing no brain anomalies in AGS3 knockout mice (Blumer *et al.* 2008).

Several proteins associated with cortical malformations have been shown to have an impact on mitotic spindle

positioning (for a review of cortical progenitors and malformations see Bizzotto and Francis, 2015). Mutations in the dynein regulators Lis1 and nuclear distribution protein homolog 1 (Nde1) lead to spindle orientation defects, resulting in neuronal progenitor depletion, and thus affecting neuronal production (Feng and Walsh, 2004; Yingling *et al.* 2008). Tctex-1 (*Dynlt1*), the light chain component of the dynein motor complex, and the guanine nucleotide exchange factor Lfc also regulate spindle orientation in a convergent fashion (Gauthier-Fisher *et al.* 2009). The interplay between these two proteins regulates the balance between aRG proliferation and neuronal differentiation. More precisely, Tctex-1 inhibits the pro-neurogenic actions of Lfc and enhances aRG vertical divisions (Gauthier-Fisher *et al.* 2009). Many genes involved in centrosome-related functions are associated with microcephaly and have been reported to influence spindle orientation. For instance, knockdown of *Aspm*, the most frequently affected gene in autosomal recessive human primary microcephaly, leads to a decrease in vertical symmetric cell divisions in NEs, promoting asymmetric mitoses, and precocious cell delamination from the neuroepithelium (Fish *et al.* 2006). Citron kinase (CITK), another protein known to be responsible for microcephaly in humans, has been shown to be important for maintenance of vertical divisions in early corticogenesis (Gai *et al.* 2016). CITK possibly converges with *Aspm* function to promote symmetric cell divisions and NE amplification, since CITK over-expression rescues the mitotic spindle defects observed upon *Aspm* knockdown (Gai *et al.* 2016). Loss of *Cdk5rap2* also perturbs spindle orientation of aRGs (Lizarraga *et al.* 2010), although other mitotic spindle defects were also observed in this study. Related to other diseases, mutations in echinoderm microtubule-associated protein-like 1 (*Eml1*), a microtubule-binding protein associated with subcortical band heterotopia, also lead to an increase in oblique divisions, as well as to increased mitotic spindle length (Kielar *et al.* 2014; Bizzotto *et al.* 2017). In addition, silencing of Huntingtin, the protein associated with Huntington's disease, also affects aRG mitotic spindle orientation (Godin *et al.* 2010). Additionally, mutant Huntingtin perturbs these processes by altering the localization of proteins such as NuMA and dynein (Molina-Calavita *et al.* 2014). Although these disease-associated proteins have been associated with spindle orientation defects, it still remains to be elucidated if this is a main and primary phenotype observed upon their deregulation. Other microtubule-associated processes, such as ciliogenesis, centrosome biogenesis, and correct mitotic spindle assembly could also be altered (Lizarraga *et al.* 2010; Insolera *et al.* 2014; Garcez *et al.* 2015; Gabriel *et al.* 2016; Jayaraman *et al.* 2016; Bizzotto *et al.* 2017). Thus, further work is required questioning if abnormal spindle orientation represents the direct cause and/or the consequences of other

primary defects which eventually lead to the cortical anomalies.

Although still controversial, spindle orientation has been suggested to regulate NE and aRG progeny fate, and to ensure that the progenitor pool expands enough to produce the appropriate number of neurons. Spindle orientation changes toward a horizontal/oblique aRG division have been associated with the generation of daughter cells which differentiate prematurely (Fish *et al.* 2006, Gai *et al.* 2016). In addition, as mentioned above, bolstering horizontal and oblique divisions in the mouse neuroepithelium in early- to mid-corticogenesis has been associated with the production of bRGs (Shitamukai *et al.* 2011; Stahl *et al.* 2013; Wong *et al.* 2015), as well as in ferret and human corticogenesis (LaMonica *et al.* 2013; Martinez-Martinez *et al.* 2016). Thus, tilting the mitotic spindle resulting in an horizontal/oblique division can lead to depletion of the aRG pool and a decreased number of neurons (Feng and Walsh, 2004; Fish *et al.* 2006, Yingling *et al.* 2008; Gauthier-Fisher *et al.* 2009; Gai *et al.* 2016), to the presence of aberrantly positioned cycling progenitors (Konno *et al.* 2008; Insolera *et al.* 2014, and reviewed in Bizzotto and Francis, 2015), as well as being related to the production of IPs and bRGs (Fish *et al.* 2006; Shitamukai *et al.* 2011; LaMonica *et al.* 2013; Stahl *et al.* 2013; Wong *et al.* 2015; Gai *et al.* 2016, Martinez-Martinez *et al.* 2016). In addition, recently it has been reported that randomization of the mitotic spindle can also alter the ratios of different AP populations, decreasing aRG numbers while increasing the amount of SNPs (Falk *et al.* 2017). These combined data strongly support the idea that other factors contribute to daughter cell fate determination, and we need to further unravel the mechanisms by which spindle orientations become perturbed and impact cell fate.

### Cellular organelle behavior in progenitors

#### *Role of microtubule-based organelles in cortical progenitor dynamics: centrosome, primary cilium, and midbody*

As discussed in the preceding section, centrosome-related proteins that are associated with cortical malformations, particularly with primary microcephaly, can affect spindle orientation (Feng and Walsh 2004; Fish *et al.* 2006; Gai *et al.* 2016). There are also other processes related to centrosomes that can be abnormal, leading to alterations in progenitors and neuronal production. Conditional deletion in aRGs of Centromere protein J (*Cenpj*) (also known as spindle assembly abnormal protein 4, *Sas4*), a critical protein for centrosome biogenesis, leads to progressive loss of centrosomes, causing mitotic delay and aRG delamination from the VZ. These ectopic proliferating Pax6<sup>+</sup> progenitors eventually undergo p53-mediated apoptosis resulting in a thinning of upper cortical layers and microcephaly (Insolera *et al.* 2014). A more recent study also addressed the role of *Cenpj*

by performing acute knockdown of the protein at mid-corticalogenesis (Garcez *et al.* 2015). The latter interferes with centrosome biogenesis, specifically affecting centriole duplication, which in turn results in a decrease of astral microtubules and spindle orientation defects. In this study, perturbing centriole duplication causes Cenpj-depleted aRGs to remain in M-phase, eventually leading to the appearance of ectopic Tbr2<sup>+</sup> progenitors in the VZ (Garcez *et al.* 2015), a phenotype hence differing from that previously described for the Cenpj conditional knockout mice (Insolera *et al.* 2014). A role for Wdr62 and Aspm was shown interacting and localizing to the mother centriole, and showing gene dose-related centriole duplication defects which correlate with the severity of the reduced cortical thickness and brain size observed in mutant mice (Jayaraman *et al.* 2016). No spindle orientation defects were observed in the Wdr62 mouse model (Jayaraman *et al.* 2016). In different studies, the production of extra-numerary centrosomes and the formation of multipolar mitotic spindles were reported to deplete the aRG pool, which in turns results in a decreased neuronal output and a smaller brain (Marthiens *et al.* 2013). Increased numbers of mitotic spindle poles were also observed upon loss of Cdk5rap2, resulting in a decrease of aRGs and premature neurogenesis (Buchman *et al.* 2010; Lizarraga *et al.* 2010).

Therefore, centrosome-related proteins have a critical role in controlling aRG cell division, progeny fate, and neuronal output. In addition, it was elegantly shown that in mouse aRGs, upon asymmetric division, the daughter cell that inherits the eldest centriole, namely the ‘old mother’ centriole, acquires the self-renewal aRG fate remaining in the VZ, while the cell inheriting the ‘new mother’ centriole is committed to differentiate (Fig. 1b) (Wang *et al.* 2009). Recently, it was discovered that Mindbomb1 (Mib1), known for its role in the Notch signaling pathway, also acts as a fate determinant by associating with centriolar satellites. In asymmetric divisions in the chick spinal cord neuroepithelium, Mib1 is inherited by the daughter cell that differentiates into a neuron (Tozer *et al.* 2017). Inheritance of pericentriolar material components may hence be important for determining cell fate, potentially regulating signaling pathways such as Notch. In an unrelated study, Delaunay and coworkers (2014) showed that the mitotic spindle *per se* could as well determine the asymmetry of a cell division. Spindle size asymmetry (SSA), which appears to be mediated by Wnt signaling through Vangl2, has a role in determining cell fate upon aRG division: cells that become neurons preferentially arise from the daughter cell (often apical) receiving the pole with the larger spindle volume (Delaunay *et al.* 2014).

The centrosome is also a critical organelle during interphase in aRGs since the mother centriole acts as a basal body to dock the primary cilium (Fig. 1a). The primary cilium is an antenna-like structure located in the apical

domain of aRGs, sensing signals from the CSF, and triggering signaling pathways (Shh, Wnt, mTOR) that can control diverse features of these cells, such as proliferation (Itoh, 2010; Lehtinen *et al.* 2011) and apical domain size (Foerster *et al.* 2017). The primary cilium is reabsorbed before mitosis, when the centrosomes constitute the spindle poles. Although reabsorption of the primary cilium prior to M-phase has been classically accepted, Paridaen and colleagues (2013) showed that ciliary membrane remnants (CR) remain attached to the mother centriole throughout mitosis in aRGs in the mouse neuroepithelium (Fig. 1b). The cell inheriting both the old mother centriole and the CR docks a primary cilium apically before its sister cell, thus being exposed to CSF signals first (Piotrowska-Nitsche and Caspary, 2012). This CR-inheriting cell tends to remain an aRG in the VZ, while the other cell acquires a neurogenic fate (Fig. 1b) (Paridaen *et al.* 2013). Tbr2<sup>+</sup> differentiated cells leaving the VZ after cell division dock a primary cilium in the basolateral membrane while delaminating (Fig. 1b) (Wilsch-Bräuninger *et al.* 2012).

Although CR present in M-phase appear to have a role in the production and maintenance of aRGs, disassembly of the primary cilium prior to mitosis has also been reported to be critical for correct progression of the neuronal progenitor cell cycle, and generation of the appropriate number of neurons (Gabriel *et al.* 2016). By using organoids derived from hiPSCs, a role for CENPJ in promoting cilium disassembly was unraveled. This previously unknown function of CENPJ was found critical for cell cycle re-entry and progenitor proliferation: the neuronal progenitors of organoids derived from CENPJ-mutant hiPSCs showed impaired cell cycle re-entry, accompanied by premature neuronal differentiation (Gabriel *et al.* 2016), hence differing from data generated in mouse models. Related to primary cilium disassembly, in the chick neuroepithelium, neurons leaving the VZ upon cell division showed abscission of the primary cilium (Das and Storey, 2014). Shedding and excision of ciliary (and midbody, see below) particles into the ventricle was also previously identified (Dubreuil *et al.* 2007).

Therefore, the centrosome and primary cilium, which are tightly connected throughout the cell cycle, play a key role in controlling aRG proliferation. Disruption of proteins associated with these organelles can result in diverse aRG defects, such as spindle orientation abnormalities (Feng and Walsh, 2004; Fish *et al.* 2006; Gai *et al.* 2016), altered centrosomal biogenesis (Insolera *et al.* 2014; Garcez *et al.* 2015; Jayaraman *et al.* 2016) abnormal mitotic spindle assembly (Lizarraga *et al.* 2010; Marthiens *et al.* 2013), and disruption of primary cilium assembly/disassembly (Paridaen *et al.* 2013; Gabriel *et al.* 2016).

Apical cilium assembly in epithelial cells requires midbody remnants (Bernabé-Rubio *et al.* 2016). When the cleavage furrow grows toward the apical membrane, microtubules of the central spindle are compacted and give rise to

the midbody, which is formed at the bridge between apical cells during cytokinesis. Several midbody proteins are recruited prior to cytokinetic abscission, which are either inherited by one daughter cell or released into the extracellular space, to be engulfed by another cell (Dionne *et al.* 2015; Dwyer *et al.* 2016). As for the primary cilium, shedding and excision of midbody-derived particles has been previously described in the chick neuroepithelium (Dubreuil *et al.* 2007). Disruption of midbody morphology and abscission has been reported in mouse mutants for the microtubule motor protein Kif20b (Janisch *et al.* 2013). Remarkably, in this study, no mitotic defects were observed. However, in early stages of corticogenesis, misalignment of the midbody with the apical membrane and change in its morphology appear to trigger apoptosis, leading to a reduction in the progenitor pool, and a thinner cortex (Janisch *et al.* 2013). The relationship between the midbody and NEs and/or the apical membrane of aRGs, as well as the primary cilium, is still not well understood. However, the retention of this structure, known for its role in mediating the final steps of cell division, could also be important for progenitor proliferation and maintenance, and like CR inheritance, appears to be crucial for aRG fate acquisition (Paridaen *et al.* 2013).

#### *Insights into mitochondria and Golgi apparatus function in APs*

Mitochondria are crucial in post-mitotic neurons to provide energy, and abnormalities in this organelle are associated with neurodegenerative diseases. Additionally, several mitochondria-related diseases show developmental manifestations (Khacho and Slack, 2017). Although the role of mitochondria and the Golgi apparatus in early steps of corticogenesis are not extensively described, and their roles in cortical neuronal progenitors remain largely unknown, recent studies have shed light on their functions during progenitor proliferation and neuronal differentiation. Firstly, mitochondrial morphology has been reported to differ between aRGs, IPs, and neurons (Khacho *et al.* 2016). While mitochondria morphology is elongated both in aRGs and neurons (Fig. 1a), it has a fragmented appearance in IPs (Fig. 1a) (Khacho *et al.* 2016). Loss of mitochondrial function in aRGs leads to defects in proliferation, disruption of cell cycle exit, and inability of cells to differentiate into neurons, resulting in cortical thinning (Khacho *et al.* 2017). Related to this study, the level of mitochondrial reactive oxygen species was shown to be decreased in differentiating neurons as compared to APs progenitors (NEs and aRGs) (Inoue *et al.* 2017). Additionally, the acute loss or gain-of-function of PR domain zinc finger protein 16 (Prdm16), a TF that regulates mitochondrial reactive oxygen species levels, led to defects in aRG proliferation, whereupon differentiating cells showed aberrant morphologies and locations in the cortical wall (Inoue *et al.* 2017).

Taverna and colleagues (2016) described different behaviors of the Golgi apparatus in aRGs and committed IPs. The Golgi localizes in the apical process of aRGs, and is not associated with the centrosome (Fig. 1a). When an aRG commits to an IP fate, the Golgi translocates toward a more basal position, bypassing the nucleus and locating itself in a basally located process (Fig. 1a) (Taverna *et al.* 2016). Another role ascribed to Golgi is in symmetric versus asymmetric divisions, since a pool of the pericentriolar fate determinant Mib1 is stored in this organelle (Tozer *et al.* 2017). When a progenitor undergoes symmetric division, Mib1 is released from the Golgi to ensure its equal repartition among the progeny (Tozer *et al.* 2017). Thus, the location and potential storage function of the Golgi apparatus in progenitors seems to contribute to the mode of aRG division.

#### *Contribution of the Unfolded Protein Response (UPR), within the endoplasmic reticulum (ER), to neurogenesis*

As previously described, aRGs begin to divide asymmetrically at E12 in mice via a temporal progression from direct to indirect neurogenesis to give rise to IPs, a transient albeit crucial population of precursors (reviewed in Tiberi *et al.* 2012).

Although the molecular mechanisms that control this transition from direct to indirect neurogenesis during embryonic development remain to be clarified, accumulating reports have demonstrated the unfolded protein response (UPR) within the endoplasmic reticulum (ER) of aRGs to be a key modulatory factor (reviewed in Laguesse *et al.* 2015b, Dwyer *et al.* 2016). The ER is well-documented to be a specialized and dynamic tubular organelle that is a keystone in many metabolic processes, a reservoir of intracellular calcium, and also critical for proper folding of proteins (reviewed in Hetz, 2012). The latter is essential for synthesis and post-translational modifications of newly synthesized secretory and membrane proteins, as well as their 3-D conformation and eventual export. Upon induction of ER stress within cells, a series of complementary adaptive mechanisms are activated to reduce translation and manage the protein-folding alterations, hence collectively categorized as the UPR (reviewed in Hetz, 2012).

The regulation of UPR signaling during neurogenesis has been demonstrated in various *in vivo* (Shim *et al.* 2004; Zhang *et al.* 2007; Mimura *et al.* 2008; Laguesse *et al.* 2015a,b) and *in vitro* models (Hayashi *et al.* 2007; Firtina *et al.* 2009; Firtina and Duncan, 2011) with the activation of PERK and IRE-1 of the three-armed UPR pathway in murine embryonic stem cells (mES) (Cho *et al.* 2009) and human neural stem cells (hNSC) (Tseng *et al.* 2017). Furthermore, chemical induction of ER stress (by brefeldin A, thapsigargin, or tunicamycin) facilitates neurogenesis and neuronal differentiation at the expense of gliogenesis and glial differentiation, respectively, in P19 cells (Kawada *et al.* 2014), mES (Cho *et al.* 2009), and hNSC (Tseng *et al.*

2017). These findings are corroborated by accumulating *in vivo* reports of spatio-temporal expression of distinct UPR effectors that are associated with the regulation of UPR signaling, which correlates with milestones of murine corticogenesis that suggests physiological functions of UPR in neuronal commitment and cell fate acquisition (Atf4 (Frank *et al.* 2010; Laguesse *et al.* 2015a); Atf5 (Laguesse *et al.* 2015a); Atf6 (Zhang *et al.* 2007); Xbp1 (Hayashi *et al.* 2007; Zhang *et al.* 2007). Of interest is the progressive reduction of Atf4 signaling (the downstream effector of the PERK-mediated UPR pathway) in aRGs as corticogenesis proceeds, which is inversely correlated with the rate of indirect neurogenesis (Frank *et al.* 2010; Laguesse *et al.* 2015a). Together, these reports indicate that a gradual suppression of basal UPR promotes the transition from direct to indirect neurogenesis in aRGs during corticogenesis.

Furthermore, the physiological relevance of the UPR pathway in cell fate acquisition (Hetz and Papa, 2017) is increasingly supported by reports of neurodevelopmental phenotypes in genetic (Laguesse *et al.* 2015a) and infective (Gladwyn-Ng *et al.* 2018) mouse models, whereupon ER stress induction and UPR up-regulation in aRGs during mid-corticogenesis prolonged direct (at the expense of indirect) neurogenesis in embryonic mouse brains and hNSCs, with a subsequent decrease in the production of IPs (Laguesse *et al.* 2015a, Gladwyn-Ng *et al.* 2018). Laguesse and coworkers demonstrated in mice genetically deficient for the Elongator complex, specifically the loss of its Elongator complex protein 3 (Elp3), an impairment of speed of mRNA translation in aRGs, with an elevation in Perk-eIF2-Atf4 signaling throughout corticogenesis (Laguesse *et al.* 2015a). Gladwyn-Ng and colleagues reported a unique tropism of Zika virus (ZIKV) among the flaviviruses for cortical progenitors during fetal embryogenesis, and viral replication within the ER in various murine models of ZIKV infection (Gladwyn-Ng *et al.* 2018). Mice from both studies displayed severe microcephaly that resulted from a diminished rate of indirect neurogenesis that was linked to the triggering of ER stress and UPR up-regulation in aRGs. Crucially, suppressing the pathological up-regulation of Atf4 levels in either Elongator-deficient or ZIKV-infected progenitors rescued the neurogenic balance, as well as the microcephalic phenotype in the latter (Laguesse *et al.* 2015a, Gladwyn-Ng *et al.* 2018). These reports demonstrate a causal link between UPR dysregulation and protracted direct neurogenesis (at the expense of indirect neurogenesis) that is associated with microcephaly, and suggest this may underlie neurodevelopmental disorders.

Altogether, these reports uncovered the progressive and dynamic down-regulation of UPR in cortical progenitors that contributes to a homeostatic signaling network that modulates the neurogenic transition and cell fate acquisition of aRG progeny. While UPR is crucial within aRGs to dissipate the cellular expenses because of proliferation, continued efforts are crucial to elucidate the exact cellular

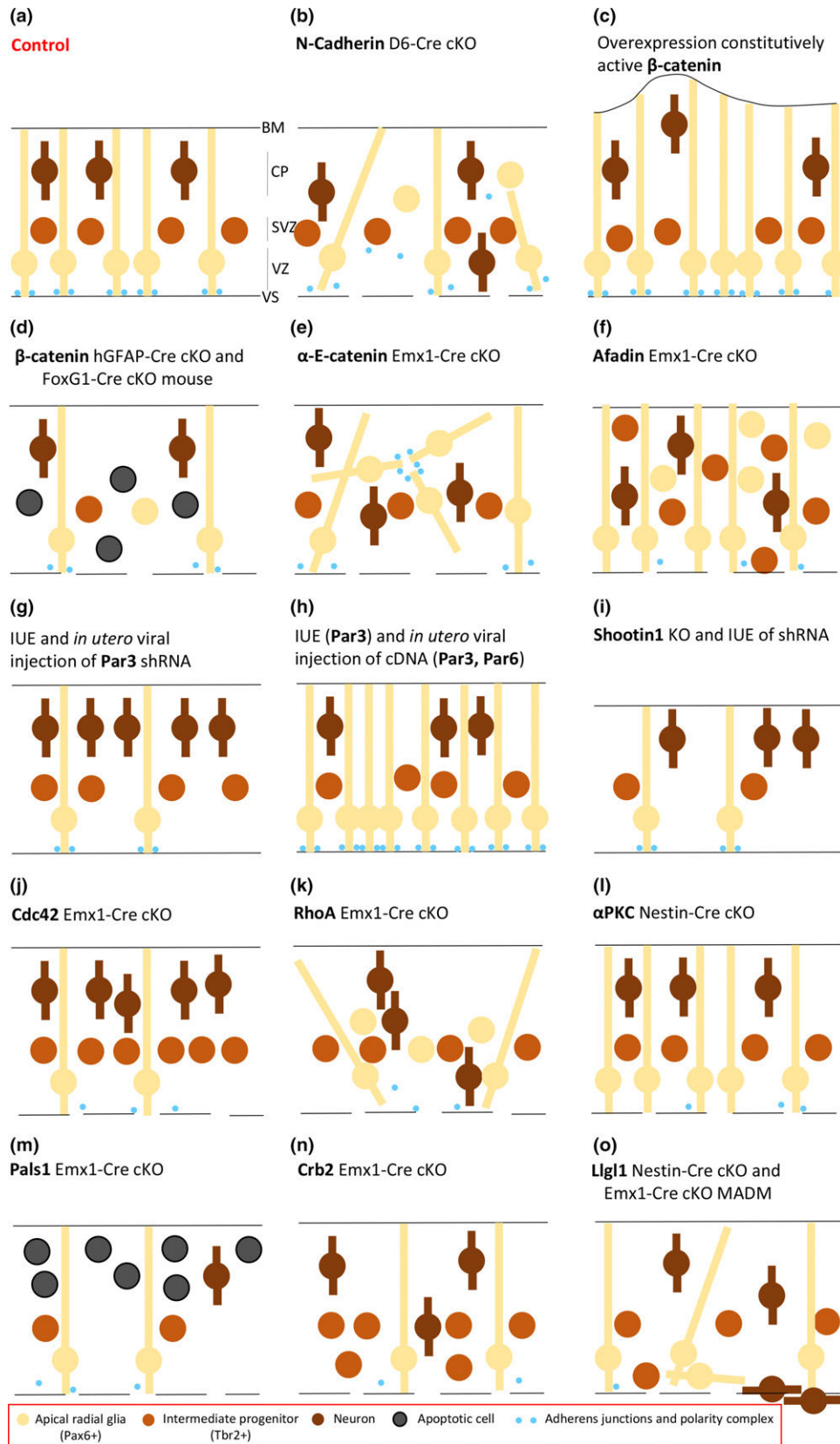
and molecular mechanisms of how UPR signaling may function as a 'developmental rheostat' during corticogenesis.

### Influence of the polarity complex and cell adhesion molecules

AJs are localized in a slightly more basolateral position than the centrosome-containing apical endfoot (Fig. 2a), linked to an F-actin belt, and the combination of the two are responsible for the anchoring of aRGs to each other to form the VS. These intercellular complexes are made up of cadherins and its downstream actors (e.g.,  $\beta$ -catenin), junctional adhesion molecules and nectins (Aaku-Saraste *et al.* 1996; Manabe *et al.* 2002; Junghans *et al.* 2005; Kadowaki *et al.* 2007; Singh and Solecki, 2015). The adhesion molecules making up the AJs are linked to the cytoskeleton and they coordinate different signaling pathways triggered in neighboring cells (Singh and Solecki, 2015). Multiple studies have shown that AJ components are critical for aRG proliferation and proper cortical development (Fig. 2).

Conditional deletion of N-cadherin in the mouse cortex leads to AJ disruption, aberrant aRG morphology and polarity, and consequently, to abnormal corticogenesis. Under these conditions, both mitotic and post-mitotic cells were found to be randomly scattered throughout the cortical wall (Fig. 2) (Kadowaki *et al.* 2007). Expression of a stabilized form of  $\beta$ -catenin in mouse APs promotes their self-renewal and amplification, resulting in an enlarged cortical area and the appearance of fold-like structures (Fig. 2c) (Chenn and Walsh, 2002). On the other hand, ablation of  $\beta$ -catenin causes disruption of the VS and AJs, leading to a decrease in the proliferative potential of aRGs, apoptosis, and aberrant position in the developing cortex of this progenitor cell type (Fig. 2d) (Junghans *et al.* 2005; Gan *et al.* 2014). This results in a severe decrease in cycling progenitors and reduced neurogenesis (Gan *et al.* 2014). Importantly, most of these effects on proliferation and production of the correct number of neurons are seemingly because of Wnt/ $\beta$ -catenin signaling independent of AJ maintenance as shown by a  $\beta$ -catenin mutation only affecting signaling, but sparing AJ function (Draganova *et al.* 2015). Conditional deletion of  $\alpha$ -E-catenin results in the uncoupling of AJs from F-actin, leading to the presence of scattered AJ-like structures throughout the cortical wall. The latter present a rosette-like structure and are positive for N-Cadherin and  $\beta$ -catenin, suggesting that individual aRGs maintain some degree of polarity although randomized (Fig. 2e). In addition, the pattern of actin and RC2 staining suggest defects in the aRG cytoskeleton and radial morphology. These defects in aRGs ultimately lead to the appearance of a 'double cortex'-like structure (Schmid *et al.* 2014). Inactivation in the mouse dorsal telencephalon of the AJ component afadin also results in a 'double cortex'-like phenotype (Gil-Sanz





*et al.* 2014). The absence of afadin disrupts AJs and results in an increase in proliferating progenitors (both aRGs and IPs) found scattered throughout the developing cortex. Although post-mitotic neurons were produced, their laminar distribution was disrupted (Fig. 2f) (Gil-Sanz *et al.* 2014). Additionally, a recent study suggests that aRGs lacking afadin could have impaired primary cilia and spindle orientations (Rakotomamonjy *et al.* 2017). All these studies highlight the essential role of AJs and actin in maintaining aRG morphology, polarity, and localization. In addition, deregulation of these proteins severely impacts aRG proliferative potential, as well as proper neuronal production and position (Fig. 2b–f).

In close vicinity to the AJ belt are localized another set of molecules critical for aRG polarity, the Par polarity complex,  $\alpha$ PKC, cell division control protein 42 homolog (Cdc42), and the Crumbs complex (Singh and Solecki, 2015). When NEs become aRGs and the AJ belt is assembled, the polarity protein Par3 dissociates from the tight junctions characteristic of NEs and associates with the newly formed AJs. This triggers the recruitment of other polarity proteins such as  $\alpha$ PKC and Par6 to the proximity of AJs (Manabe *et al.* 2002). Polarity proteins are not only essential for maintaining aRG morphology, but in some cases they also act as fate determinants upon cell division.

Costa and colleagues (2008) showed that Par3 levels are critical for aRG proliferation: knockdown of Par3 in aRGs promoted premature cell cycle exit and the acquisition of early neuronal fates (Fig. 2g). On the other hand, over-expression of both Par3 and Par6 enhanced aRG self-renewal (Fig. 2h) (Costa *et al.* 2008). Therefore, the Par complex is critical to mediate progenitor self-renewal at the expense of neurogenic differentiation. While in interphase Par3 is localized basolaterally in the apical domain, during mitosis it shows a dynamic distribution in dividing aRGs (Bultje *et al.* 2009). Decreased expression of Par3 in aRGs leads to a switch toward symmetric neurogenic divisions and the subsequent exhaustion of the aRG pool (Fig. 2g). Ectopic expression of Par3 leads to an increase in Notch activity, whereas knockdown of Par3 has the opposite effect (Bultje *et al.* 2009). Bultje and colleagues (2009) suggested that Protein Numb homolog (Numb)/Numb-like protein influences Par3 activation of Notch signaling. Upon Numb/Numb-like knockdown, over-expression of Par3 no longer triggers Notch signaling. In addition, Numb/Numb-like knockdown rescued the aRG pool depletion induced by Par3 knockdown (Bultje *et al.* 2009). Therefore, in mammalian aRGs the interplay between Par3 and Numb/Numb-like may be important for Notch activity, which strongly influences daughter cell fate after division.

**Fig. 2** Schematic representation of the developing cortex in polarity complex and cell adhesion molecule mouse mutants. (a) Wild type developing cortex: Apical radial glia (aRG, yellow cells) have their soma localized in the ventricular zone (VZ). They are attached to each other at the ventricular surface (VS) by their apical processes characterized by the presence of the polarity complex and adherens junctions (AJ) (altogether represented by blue dots). Their basal process is attached to the basement membrane (BM). Intermediate progenitors (IPs, orange cells) are localized in the subventricular zone (SVZ) and lack this polarized morphology. Newly generated neurons (brown cells) are positioned in the developing cortical plate (CP). First and second rows (b–f) depict mouse models for proteins mainly associated with AJs and cell adhesion. Third, fourth, and fifth rows (g–o) depict mouse models for polarity proteins. (b) Conditional deletion of N-cadherin disrupts aRG AJs and the VS. Mitotic cells, particularly Pax6+, were found scattered through the cortical wall and their processes showed an aberrant morphology, not spanning the entire developing cortex. Newborn neurons were also found in abnormal positions (Kadowaki *et al.* 2007). (c) Over-expression of constitutively active  $\beta$ -catenin in the neuroepithelium promotes aRG self-renewal increasing the tangential surface, as well as the final cortical area. This results in the appearance of fold-like structures (Chenn and Walsh, 2002). (d) Conditional deletion of  $\beta$ -catenin disrupts the VS and AJs. aRG decrease their self-renewing potential and they are found in ectopic positions. Mitotic cells (aRGs and IPs) undergo apoptosis, thus there is a decrease in aRG, IP, and neuronal numbers (Junghans *et al.* 2005; Gan *et al.* 2014). (e) Conditional deletion of  $\alpha$ -E-catenin disrupts the VS and AJs. AJ-like structures are scattered in the cortical wall. aRG fibers are disorganized, and neurons are mislocalized forming a 'double-cortex' (Schmid *et al.* 2014). (f) Conditional deletion of afadin

disrupts the VS and AJs. There is an increased proliferation of progenitor cells, accompanied by an increase in aRGs and IPs, localized throughout the entire developing cortex. Neurons are mislocalized, eventually forming a 'double cortex' (Gil-Sanz *et al.* 2014). (g) Par3 knockdown decreases aRG self-renewal potential resulting in a premature production of neurons (Costa *et al.* 2008, Bultje *et al.* 2010). (h) Over-expression of Par3 and Par6 promotes aRG proliferation (Costa *et al.* 2008, Bultje *et al.* 2009). (i) Deletion of shootin1 causes a decrease in mitotic cells (presumably aRGs and IPs), resulting in decreased neuronal numbers (upper layer neurons) and thinning of the cortical plate (Sapir *et al.* 2017). (j) Conditional deletion of Cdc42 leads to gradual loss of AJs and disruption of the VS. There is a decrease in aRG mitoses accompanied by an increase in mitotic IPs and neurons (Cappello *et al.* 2006). (k) Conditional deletion of RhoA results in the presence of aberrantly positioned aRGs and ectopic neurons, accompanied by the disruption of AJs (Cappello *et al.* 2012). (l) Conditional deletion of  $\alpha$ PKC causes AJ and VS anomalies without major effects on corticogenesis (Imai *et al.* 2006). (m) Conditional deletion of Pals1 disrupts the VS and AJs. The aRG pool is depleted followed by a massive death of newly generated neurons (Kim *et al.* 2010). (n) Conditional ablation of Crumbs2 (Crb2) disrupts the VS and AJs. It causes a depletion of the aRG pool and an increase in IPs, found mislocalized in the VZ. Neurons are transiently found in abnormal positions (Dudok *et al.* 2016). (o) Conditional deletion of Ligl1 disrupts the VS and AJs. aRG form rosette-like structures close to the ventricle, where IPs can be found as well. Neurons are found in ectopic positions, both close to the ventricle and forming a 'double cortex' (Beattie *et al.* 2017; Jossin *et al.* 2017).

A recent study has shown that the neuronal polarity protein Shootin1 may have a similar function to Par3 in the mouse neuroepithelium (Sapir *et al.* 2017). Shootin1 is localized at the apical surface and plays a role in daughter cell fate determination upon aRG division. (Sapir *et al.* 2017). Shootin1 increases polyubiquitination of Numb and reduces polyubiquitination of Notch intracellular domain, both of which enhance Notch signaling. In agreement with this, both knockdown by *in utero* electroporation and mice lacking Shootin1 show a decrease in mitotic cells and as a result, Shootin1 knockout mice have a thinner CP (Fig. 2i) (Sapir *et al.* 2017). This study not only uncovers a role for the apically located protein Shootin1 but it also provides insight into potential mechanisms influencing Numb–Notch interplay in the VZ. While Notch signaling appears to be indeed crucial to maintain aRG-proliferative potential, it is important to bear in mind that as well as asymmetric fate determinants there are also other factors as described above (e.g., epithelial structure and oldest-centriole/CR inheritance) which have recently been described to be crucial to determine cell fate and that could also be involved in mediating Notch activation in basal as well as in these mutant conditions.

Other components of the polarity complex have been described to be crucial for aRG morphology and behavior. Conditional deletion of the small Rho-GTPases Cdc42 and RhoA results in the disruption of AJs. In the case of Cdc42, this leads to an immediate increase in basal mitoses accompanied also by an increase in neuronal numbers (Cappello *et al.* 2006) (Fig. 2j), while deletion of RhoA causes also ectopic Pax6+ cells and the formation of a double cortex (Cappello *et al.* 2012) (Fig. 2k). Strikingly, conditional deletion of  $\alpha$ PKC at mid-corticogenesis disrupts apical complexes causing no major effect on corticogenesis (Fig. 2l) (Imai *et al.* 2006). Pals1, another component of the apical domain, was shown to be critical to maintain the pool of cycling aRGs (Kim *et al.* 2010). Deletion of this protein leads to cell cycle exit and premature neuronal production followed by cell death, eventually resulting in the absence of cortical structures (Fig. 2m) (Kim *et al.* 2010). Recently, the role of Crumbs2 (Crb2) was described in apical complex maintenance. Conditional deletion of Crb2 in the mouse telencephalon impaired the maintenance of the apical complex and aRG morphology: upon Crb2 deletion, nestin staining was barely present and appeared disorganized in the developing cortical wall. This was accompanied by a decrease in the aRG pool and an increase in IPs (Fig. 2n) (Dudok *et al.* 2016). The outcome of deregulating aRG apical complex proteins often converges in the disruption of the aRG apical domain, which in most cases results in a decrease of the aRG pool and altered distribution of both cycling progenitors and post-mitotic neurons.

In addition to the above-mentioned studies, the WD40 domain-containing protein lethal giant larvae homolog 1 (Llg1) was described to be crucial for aRG polarity and

proliferation, and ultimately proper cortical development (Beattie *et al.* 2017). Conditional deletion of Llg1 in aRGs results in an increase in proliferating cells that form rosette-like structures in the VZ, accompanied by the disruption of the VS (Fig. 2o). This eventually leads to impaired neuronal positioning and a subcortical band heterotopia-like phenotype (Beattie *et al.* 2017). A similar work proposed that Llg1 acts as a link between AJs and polarity complex proteins (Jossin *et al.* 2017). In this paper, the authors use a model in which Llg1 is specifically deleted in progenitors from E12.5 onward. These mice present AJ abnormalities, disruption of the neuroepithelium, and aberrantly located post-mitotic neurons, situated close to the ventricles (Fig. 2o) (Jossin *et al.* 2017). Interestingly, the authors showed that Llg1 is necessary to stabilize N-cadherin at the AJs. When Llg1 is not phosphorylated by the polarity protein  $\alpha$ PKC, it internalizes N-cadherin from the cell membrane. Upon  $\alpha$ PKC phosphorylation of Llg1, N-cadherin is no longer internalized and accumulates at the basolateral part of the apical domain (Jossin *et al.* 2017). Studies such as this emphasize the importance of the localization of adhesion molecules within the aRG wall.

### Cell cycle considerations

Cell cycle length in progenitors is associated with their neurogenic potential. Early studies already suggested that progenitors located in diverse brain regions had different cell cycle lengths, and that the cell cycle lengthens as development proceeds, while switching toward a more neurogenic state (Borrell and Calegari, 2014). Later studies confirmed this initial discovery (Calegari *et al.* 2005; Lukaszewicz *et al.* 2005; Arai *et al.* 2011), pinpointing G1 as the phase responsible for these changes in cell cycle duration (Calegari and Huttner, 2003; Lange *et al.* 2009; Pilaz *et al.* 2009; Salomoni and Calegari, 2010). In relative terms, aRG-proliferative divisions were found to have a shorter cell cycle length when compared to neurogenic divisions (Calegari *et al.* 2005; Arai *et al.* 2011).

The direct implication of cell cycle length in neural progenitor commitment was shown by pharmacologically inhibiting G1-specific Cdk/Cyclins in mouse embryos. This leads to longer cell cycle, and precocious neurogenesis (Calegari and Huttner, 2003). The same result was obtained by performing RNAi-mediated silencing of Cyclin D1/Cdk4 (Lange *et al.* 2009). Accordingly, Pilaz and colleagues (2016) showed recently that mitotic delay promotes neuronal production from aRGs. In this study, two different approaches were used: first, mitotic progression of aRGs was analyzed in the Magoh heterozygous mouse mutant, described as a model for microcephaly with altered neurogenesis (Silver *et al.* 2010). In this mutant, a proportion of aRGs presented delayed mitotic progression, and these aRGs preferentially produced neurons (Pilaz *et al.* 2016). Secondly, a pharmacological approach was used to induce

mitotic delay, reproducing the phenotype observed in Magoh heterozygous mice (Pilaz *et al.* 2016). Another set of experiments demonstrated that shortening the cell cycle of progenitors indeed bolsters their proliferative capacity. Over-expression of Cdk4 and Cyclin D1, or exclusively cyclins, leads to shorter cell cycle, accompanied by a higher proliferation rate, and an increase in the progenitor pool (Lange *et al.* 2009, Pilaz *et al.* 2009, Nonaka-Kinoshita, *et al.* 2013). Thus, all these studies support the idea that cell cycle length is a parameter regulating progression of neurogenesis and progenitor fate.

Different factors regulate cell cycle duration and hence influence cell fate. Thus, triggering FGF signaling leads to a shorter G1, promoting progenitor proliferation and expansion (Lukaszewicz *et al.* 2002). Similarly, insulin-like growth factor 1 (Igf-1) also reduces G1 length, bolstering progenitor cell cycle re-entry (Hodge *et al.* 2004; Mairet-Coello *et al.* 2009). This highlights the fact that factors known to play a role in determining cell fate may do so by impacting cell cycle parameters. Therefore, cell fate determinants and cell cycle progression are probably highly interlinked (Borrell and Calegari, 2014).

MicroRNAs (miRNAs) have also been shown to be involved in controlling the expression of cell cycle proteins

promoting proliferation vs differentiation, or *vice versa* (for a review on miRNAs and neuronal cell fate see Meza-Sosa *et al.* 2014; see also Ghosh *et al.* 2014; Govindan *et al.* 2017). The miRNA let7b regulates aRG proliferation through targeting, among others, cyclin D1 (Zhao *et al.* 2010). Using *in utero* electroporation, let7b was over-expressed in aRGs in early stages of mouse corticogenesis. Let7b over-expression delayed cell cycle progression, promoting neuronal differentiation. This defect in neurogenesis was rescued by co-expressing a cyclin D1 vector resistant to the miRNA (Zhao *et al.* 2010). miR-15b promotes cell cycle exit and neuronal differentiation by indirectly regulating cyclin D1 (Lv *et al.* 2014). The regulation of Cdk7 by miR-210 also appears to be critical for aRG cell cycle progression: over-expression of miR-210 promotes aRG cell cycle exit and cell differentiation (Abdullah *et al.* 2016). Another example is the higher primate-specific miR-1290, whose over-expression in progenitors slows down the cell cycle and promotes neuronal differentiation (Yelamanchili *et al.* 2014).

Most of the studies mentioned previously were performed in the mouse neuroepithelium, in which G1 clearly appears to be critical in controlling cell cycle duration. However, a recent study performed in ferret, indicates that cell cycle duration of progenitors in this species is mainly mediated by

**Table 1** Factors affecting apical radial glia proliferation

Factor	Model	Progenitor and/or neuronal phenotype	References
Apical domain	Analysis of apical domain components in coronal sections and <i>en face</i> imaging of the mouse neuroepithelium	Maintenance of the apical domain promotes aRG fate	Kosodo <i>et al.</i> (2004), Marthiens and French-Constant, (2009)
Integrins (basal process)	Blockage by antibodies and snake venom (echistatin)	Reduced proliferative potential of aRGs and bRGs	Fietz <i>et al.</i> (2010)
Cyclin D2 mRNA (basal process)	IUE of reporter mRNAs carrying Cyclin D2 3'UTR in the mouse neuroepithelium	Maintenance of the basal process promotes aRG fate	Tsunekawa <i>et al.</i> (2012)
Lfc	IUE of shRNA in the mouse neuroepithelium at early to mid corticogenesis	Increase in the number of cycling aRG and decreased number of newly formed neurons	Gauthier-Fisher <i>et al.</i> (2009)
Eldest centriole inheritance	IUE of tagged and photosensitive centrosomal proteins	Inheritance of the eldest centriole is associated with aRG fate acquisition	Wang <i>et al.</i> (2009)
Ciliary remnants inheritance	IUE of tagged-centrosomal and ciliary proteins	Inheritance of ciliary remnants is associated with aRG fate acquisition	Paridaen <i>et al.</i> (2013)
Par3 and Par6	IUE and <i>in utero</i> viral injection	Increased aRG proliferation and numbers	Costa <i>et al.</i> (2008), Bultje <i>et al.</i> (2009)
miR-15b	miR-15b inhibitor in the mouse neuroepithelium	Enhanced proliferation of aRG at the expense of cell differentiation	Lv <i>et al.</i> (2014)
miR-210	miR-210 sponge in the mouse neuroepithelium	Enhanced aRG proliferation and delayed neuronal production	Abdullah <i>et al.</i> (2016)
bFGF	Exposure of cortical progenitor cultures to bFGF	Increase in proliferative divisions	Lukaszewicz <i>et al.</i> (2002)
Igf-1	Nestin-Igf-1 transgenic mouse	Increased cell-cycle re-entry and proliferation (VZ), and increased neuronal numbers in postnatal stages	Hodge <i>et al.</i> (2004)
let7b miR	IUE in the mouse neuroepithelium	Decreased neuronal progenitor cell cycle re-entry (VZ and SVZ)	Zhao <i>et al.</i> (2010)

**Table 2** Factors affecting basal progenitor production (Intermediate progenitors and basal radial glia)

Factor	Model	Progenitor and/or neuronal phenotype	References
Nt3	IUE in the mouse neuroepithelium	Decrease in IPs concomitant with a decrease in aRGs	Parthasarathy <i>et al.</i> (2014)
Citk	KO mouse	Premature aRG cell cycle exit and increased generation of IPs	Gai <i>et al.</i> (2016)
Cdk5rap2	IUE of shRNA in the mouse neuroepithelium	Increased production of IPs at expenses of aRGs, and premature neuronal differentiation	Buchman <i>et al.</i> (2010)
Cenpj	IUE of shRNA in the mouse neuroepithelium	Increased production of IPs aberrantly positioned in the VZ and decreased neuronal production	Garcez <i>et al.</i> (2015)
Wdr62	Gene-trap mouse	Increase in IPs at the expense of aRGs, decreased cortical thickness (mainly upper layers)	Jayaraman <i>et al.</i> (2016)
Aspm	KO mouse	Increase in IPs at the expense of aRGs, decreased cortical thickness (mainly upper layers)	Jayaraman <i>et al.</i> (2016)
Elongator complex ( <i>Eip3</i> )	FoxG1-Cre cKO mouse	Impaired production of IPs from aRG, decreased neuronal numbers	Laguesse <i>et al.</i> (2015a,b)
Cdc42	Emx1-Cre cKO mouse	Altered aRG cell cycle, increase in IPs and neurons	Cappello <i>et al.</i> (2006)
Crumbs2	Emx1-Cre cKO mouse	Decrease in aRG and increase in IPs, followed by subtle cortical lamination defects	Dudok <i>et al.</i> (2016)
CyclinD1 and CyclinE1	IUE in the mouse neuroepithelium	Increased apical and basal mitoses and enlarged SVZ. Higher neuronal density (mainly upper layers)	Pilaz <i>et al.</i> (2009)
CyclinD1/Cdk4	IUE in the mouse neuroepithelium and cKI mouse	Increased Tbr2 <sup>+</sup> progenitor production and enlarged SVZ. Increased neurogenesis, cortical surface and brain size	Lange <i>et al.</i> (2009), Nonaka-Kinoshita <i>et al.</i> (2013)
miR-15b	IUE in the mouse neuroepithelium	Decreased Pax6 <sup>+</sup> progenitors and increase in the number of IPs	Lv <i>et al.</i> (2014)
Retinoic acid	<i>Rdh10</i> KO mouse	Decreased cycling aRGs, decreased cycling IPs, decreased neuronal numbers	Haushalter <i>et al.</i> (2017)
Robo/Slit	<i>Robo 1/2</i> and <i>Slit 1/2</i> KO mice (null allele)	Decrease in cycling aRGs and increase in IPs. No immediate increase in neuronal production	Borrell <i>et al.</i> (2012)
PDGFR $\beta$	Embryonic ventricular injection of recombinant PDGFD and IUE of constitutively active <i>PDGFR<math>\beta</math></i>	Production of bRG-like progenitors	Lui <i>et al.</i> (2014)
ARHGAP11B	Microinjection of <i>ARHGAP11B</i> in organotypic slice culture and IUE in the mouse neuroepithelium	Increase in BPs (IPs and bRG-like progenitors), increased cortical area and folding	Florio <i>et al.</i> (2015)
TBC1D3	Nestin- <i>TBC1D3</i> transgenic mouse and IUE	Production of bRG-like progenitors and cortical folding	Ju <i>et al.</i> (2016)
Pax6	IUE in the neuroepithelium of Tis21-CreERT2 mice	Increased production of bRG-like cells and increased upper layer neuron production	Wong <i>et al.</i> (2015)
Trnp1	IUE of shRNA in the mouse neuroepithelium	Increase in IPs and generation of bRG-like progenitors. Appearance of folds	Stahl <i>et al.</i> (2013)
TMEM14b	Nestin-Cre cKI mouse	Production of bRG-like progenitors, cortical thickening and gyrfication	Liu <i>et al.</i> (2017)

changes in S-phase, since little variation was observed in G1 when comparing different progenitor types (Turrero-Garcia *et al.* 2016). Additionally, the discovery of a broad diversity of progenitor types in different species (Fietz *et al.* 2010; Hansen *et al.* 2010; Reillo *et al.* 2011; Shitamukai *et al.* 2011; Wang *et al.* 2011; Betizeau *et al.* 2013) led to the study of their cell cycle parameters. In these studies, the proliferative potential was found to be decreased from mother to daughter cell, as neurogenesis proceeds (Borrell and Calegari, 2014). Along with the importance of S-phase length in ferret progenitors (Turrero Garcia *et al.* 2016),

Wong and coworkers (2015) reported a longer S-phase in bRG-like cells, suggesting that regulation of this phase is important for the cell cycle of bRGs, which are characteristic of gyrencephalic species, such as the ferret.

As described above, there are multiple studies supporting a correlation between cell cycle length in progenitors with their neurodifferentiation potential. Nevertheless, a recent study showed that upon cell cycle arrest of undifferentiated aRGs, these cells still turn on a transcriptional program associated with the neuronal output they are meant to produce (Okamoto *et al.* 2016). In this study, single-cell

**Table 3** Factors affecting neuronal production

Factor	Model	Progenitor and/or neuronal phenotype	Reference
Celsr3	KO mouse	Increased number of neurons and decreased number of aRGs	Wang <i>et al.</i> (2016a,b)
Fzd3	KO and Nex-Cre cKO mouse	Increased number of neurons and decreased number of aRGs	Wang <i>et al.</i> (2016a,b)
Sip1	Nestin-Cre and Nex-Cre cKO mouse	Premature generation of upper layers neurons at expense of deep layers	Seuntjens <i>et al.</i> (2009)
Lis1	hGFAP-Cre cKO mouse	Premature reduction in the aRG population, precocious neuronal production, and thinning of the cortex	Yingling <i>et al.</i> (2008)
Nde1	KO mouse	Premature reduction in the aRG population, precocious neuronal production, and thin cortex mainly upper layers	Feng and Walsh (2004)
Tctex-1	IUE of shRNA in the mouse neuroepithelium at early- to mid-corticogenesis	Decrease in the number of cycling aRG and increased number of newly formed neurons	Gauthier-Fisher <i>et al.</i> (2009)
Aspm	IUE of shRNA in the mouse neuroepithelium and KO mouse	Premature aRG cell cycle exit, exhaustion of their pool and production of neurogenic Tis21+ cells Decreased neuronal numbers	Fish <i>et al.</i> (2006), Jayaraman <i>et al.</i> (2016)
Cdk5rap2	Hertwig's anemia mutant mouse	Increased aRG cell cycle exit and apoptosis. Decreased number of neurons and cortical thickness	Lizarraga <i>et al.</i> (2010)
Huntingtin	IUE of shRNA in the mouse neuroepithelium and Nestin-Cre cKO mouse	Decreased cycling progenitors (aRGs and IPs) and premature increase in neuronal production	Godin <i>et al.</i> (2010), Molina-Calavita <i>et al.</i> (2014)
Spindle size asymmetry	3-D spindle shape quantification, knockdown by RNAi of Vangl2 in the mouse neuroepithelium	aRG daughter cells inheriting the larger spindle become neurons. Vangl2 KD increases SSA, results in precocious neurogenesis, and decrease in upper layer neurons	Delaunay <i>et al.</i> (2014)
CENPJ	hiPSC-derived organoids	Delayed aRG cell cycle re-entry and premature neuronal differentiation	Gabriel <i>et al.</i> (2016)
Mib1 inheritance	<i>In ovo</i> electroporation of the chick neuroepithelium of a tagged-Mib1 followed by videomicroscopy	The daughter cells inheriting Mib1 are likely to become neurons	Tozer <i>et al.</i> (2017)
Impairment of mitochondria function	<i>Aif</i> Emx1-Cre cKO mouse	aRG inability to exit cell cycle and failed neuronal differentiation	Khacho <i>et al.</i> (2017)
Pals1	Emx1-Cre cKO mouse	Premature aRG cell cycle exit and precocious deep layer neuron production, followed by apoptosis	Kim <i>et al.</i> (2010)
Par3	IUE and <i>in utero</i> viral injection of shRNA	Decrease in cycling aRG and premature neuronal production	Costa <i>et al.</i> (2008), Bultje <i>et al.</i> (2009)
Shootin1	<i>Shtn1</i> KO and IUE of shRNA in the mouse neuroepithelium	Decrease in mitotic cells, decreased neuronal numbers (mainly upper layer neurons) and thinner CP	Sapir <i>et al.</i> (2017)
Magoh	Mos2 heterozygous mutant mouse	Decreased neuronal progenitor production, enhanced neurogenesis, and increased apoptosis	Silver <i>et al.</i> (2010), Pilaz <i>et al.</i> (2016)
CyclinD1/Cdk4	IUE of shRNA in the mouse neuroepithelium	Generation of IPs is inhibited and neuronal production enhanced	Lange <i>et al.</i> (2009)
miR-210	IUE in the mouse neuroepithelium	aRG cell cycle exit and premature neuronal differentiation	Abdullah <i>et al.</i> (2016)
mir-1290	Lentiviral vector-mediated over expression in SH-SY5Y cells and H9-ESC-derived neural progenitors (H9-NPC)	Decreased proliferation and increased neuronal production	Yelamanchili <i>et al.</i> (2014)

transcriptomics revealed a set of genes whose expression changes over time in undifferentiated aRGs at different developmental stages. In order to address if these transcriptional changes could be altered by defects in cell cycle progression, the authors induced cell cycle arrest of aRGs while maintaining them undifferentiated, and performed the same type of single-cell transcriptomics analysis. Strikingly, the pattern of expression of the genes previously identified was not altered (Okamoto *et al.* 2016), implying that unrelated to cell cycle progression, aRGs at different stages can produce particular neuronal cell types (McConnell and Kaznowski, 1991; Kawaguchi and Matsuzaki, 2016). For several years, it has been debated how and why aRGs produce the appropriate neuronal cell type and if there are aRG subtypes which produce neurons destined for a specific cortical layer. These discussions are resumed in the next section.

### Multipotency and potential subpopulations of aRGs

As described throughout this review, aRGs are the main progenitor cell in the developing cortex, responsible for the production of other progenitors as well as neurons. aRGs arise at approximately E10–12 (mouse) from NEs, and although their numbers decrease throughout corticogenesis, they populate the VZ until the late stages of this process.

Deep layer neurons (layers V–VI) are produced during E11.5–E14.5 in the mouse, while upper layers neurons (layers II–IV) are produced at E14.5–E17.5. The latter migrate past the former to reach their final location. Principal neurons are classified by their axonal target, although this is a highly broad and simplistic categorization. They are classified as intracortical neurons (commissural and associative), projecting to other parts of the cortex, and mainly located in upper layers, and corticofugal neurons (corticothalamic and subcerebral), sending projections outside of the cortex, and mostly found in deep layers (Lodato *et al.* 2015). It is frequently questioned if there are different aRG populations that give rise to specific neuronal subtypes, belonging to different cortical layers, and with different axonal targets.

Pioneer heterochronic transplantation studies in the 1990s suggested that as development proceeds, aRGs become more restricted in their fate potential (McConnell and Kaznowski, 1991; Frantz and McConnell, 1996; Desai and McConnell 2000). When transplanting early aRGs into brains already generating upper cortical neurons, these progenitors were capable of generating this neuronal type. However, the opposite experiment showed that aRGs from later stages of corticogenesis failed to generate early neuronal fates (McConnell and Kaznowski, 1991; Frantz and McConnell, 1996; Desai and McConnell 2000). Other studies confirmed this hypothesis by performing fate-mapping studies: retroviral-mediated labeling of individual aRGs showed that early progenitors could generate neurons belonging to all layers of the cortex (Luskin *et al.* 1988; Walsh and Cepko 1993).

Recent work has made use of novel fate-mapping techniques, taking advantage of Mosaic Analysis with Double Markers (MADM), where aRG behavior and progeny can be followed accurately at the single-cell level, which strongly confirms that aRG multipotency decreases as corticogenesis proceeds (Gao *et al.* 2014; Kaplan *et al.* 2017).

Previous work focused on addressing if subtypes of aRGs could be committed to the production of a specific neuronal fate. This topic is still controversial, and no solid conclusions have yet been established. Franco and colleagues (2012) showed that aRGs expressing the TF Cux2 mainly produce upper layer neurons. A knock-in mouse (Cux2-CreERT2) was used to fate-map Cux2-positive aRGs and their progeny from early stages of neurogenesis. This approach showed that aRGs expressing Cux2 are present in the VZ from as early as E10.5, and while deep layers are generated, they mainly divide, until they produce upper layer-fated neurons at a later time-point. In addition, when forced to differentiate in an early environment, Cux2-positive aRGs still produced upper layer neurons (Franco *et al.* 2012). Following this study, work from a different group failed to obtain the same results, using the same Cux2-CreERT2 line, as well as a Fezf2-CreERT2 bacterial artificial chromosome (BAC) line (Guo *et al.* 2013; Eckler *et al.* 2015). The fact that these studies were performed in mice with different genetic backgrounds provided a potential explanation for different outcomes (Eckler *et al.* 2015; Gil-Sanz *et al.* 2015).

Although we focus on aRG progeny, a large amount of research has been performed to understand the contribution of IP progeny to cortical layers. The neuronal subtype produced by IPs has also been a controversial topic: while some studies support that IPs mainly generate upper layer neurons (Tarabykin *et al.*, 2001; Zimmer *et al.* 2004), other more recent studies indicate that they produce neurons belonging to all cortical layers (Vasistha *et al.* 2015). Recently, Mihalas *et al.* (2016) showed that IPs have the potential to generate neurons of all layers. Early generated IPs mainly produce deep layer neurons, while later neuronal fates are produced from IPs generated throughout corticogenesis, therefore, depending on both early and late produced IPs (Mihalas *et al.* 2016).

Finally, it is worth noting that progenitor cells characteristic of the primate–human brain, namely bRGs located in the oSVZ, are thought to be directly involved in the production of neurons belonging to layers II–III, which are increased in size and complexity in primates (Ostrem *et al.* 2017). These cells are hence likely to lead to neuronal production at later stages (Martinez-Martinez *et al.* 2016).

### Conclusions

Neuronal progenitor cell division, that is, symmetric proliferative, asymmetric, or symmetric neurogenic divisions, as

well as daughter cell fate acquisition are tightly controlled processes and many factors ranging from microtubule-based organelles to cellular metabolism have an impact on the mode of cell division. Thus, they contribute to regulating aRG proliferation, the switch toward a BP identity as well as their neuronal output (see Tables 1–3).

Classically spindle orientation was proposed to be key to determine the type of cell division and the identity of aRG progeny. However, this view may be changing since there is no straightforward relationship between spindle orientation, apical and basal process inheritance, and daughter cell identity. However, the inheritance and/or maintenance of processes seems to be crucial to maintain aRG-proliferative potential. Thus, the presence of the apical domain has been correlated with aRG proliferative identity, even if aRGs often first lose an apical endfoot, which is regenerated to recover the entire epithelial structure. In addition, several studies support that aRG-proliferative potential is defined by the inheritance of the basal process upon cell division: daughter cells lacking this structure are more committed to the neuronal lineage.

Other cellular features critical for correct aRG proliferation, polarity, and position are the AJ and the polarity complex components. Disruption of the latter has been shown extensively to perturb not only aRG dynamics but also other steps of corticogenesis. This emphasizes that aRG morphology, polarity, and close contact at the VS and with the CSF are critical not only for aRG behavior and its progeny but also for subsequent neuronal migration and positioning in the developing cortical wall.

Lately, many studies have unraveled the importance of centrosome-related processes in aRG behavior: centrosome and primary cilium dynamics during the cell cycle appear to have a strong influence on cell division and fate acquisition. The ‘old mother’ centriole, which in interphase acts as a basal body docking the primary cilium, appears to be critical for aRG fate acquisition after cytokinesis. Additionally, this organelle is associated with CR that also appear to be essential for daughter cell fate determination. Recently, the role of other organelles is beginning to be addressed, pinpointing the importance of aRG metabolism for proliferation, accurate timing of neurogenesis, and ultimately correct cortical development. For instance, ER-dependent UPR contributes to the switch to indirect neurogenesis, in order to produce BPs at the correct developmental time-point: impairment of this process prompts direct neurogenesis, inducing premature neuronal production and eventually resulting in decreased neuronal numbers and a small brain. Other aRG features, such as their activity pattern, may also influence the mode of cell division and progeny fate.

Finally, related to BPs, studies in ferret, primates, and postmortem human tissue have broadened our knowledge about progenitor diversity in the developing neocortex. Work further characterizing the SVZ of gyrencephalic species and its

progenitor composition, as well as the discovery of primate-specific genes mediating the switch from aRGs to bRGs has opened a window to better understand neocortical expansion, folding, and evolution. In addition, the use of state-of-the-art approaches such as human-based 3-D organoids will shed light not only on the biology of these progenitor cell types but also on their contribution to cortical malformations.

## Acknowledgments and conflict of interest disclosure

AU and FF are associated with the BioPsy Labex project and the Ecole des Neurosciences de Paris Ile-de-France (ENP) network. Our labs are supported by Inserm, Centre national de la recherche scientifique (CNRS), UPMC, French Agence National de la Recherche (ANR-13-BSV4-0008-01; ANR-16-CE16-0011-03), Fondation Bettencourt Schueller, the European Union (EU-HEALTH-2013, DESIRE, No 60253) to FF, the JTC 2015 Neurodevelopmental Disorders, the ANR (for NEURON8-Full-815-006 STEM-MCD), the Fondation Maladies Rares/Phenomin (project IR4995), and the European Cooperation on Science and Technology (COST Action CA16118) to FF, OR, and LN. AU received an ENP PhD and Company of Biologists travel grants. L.N. is also funded by F.R.S.-F.N.R.S., the Fonds Léon Fredericq, the Fondation Médicale Reine Elisabeth, the Fondation Simone et Pierre Clerdent, the Belgian Science Policy (IAP-VII network P7/20), the ARC (ARC11/16-01), the EU H2020 ZIKAlliance (#734548). O.R. is the incumbent of the Bernstein-Mason Chair of Neurochemistry. No conflicts of interest declared.

## References

- Aaku-Saraste E., Hellwig A. and Huttner W. B. (1996) Loss of occludin and functional tight junctions, but not ZO-1, during neural tube closure—remodeling of the neuroepithelium prior to neurogenesis. *Dev. Biol.* **180**, 664–679.
- Abdullah A. I., Zhang H., Nie Y., Tang W. and Sun T. (2016) CDK7 and miR-210 Co-regulate cell-cycle progression of neural progenitors in the developing neocortex. *Stem Cell Rep.* **7**, 69–79.
- Agirman G., Broix L. and Nguyen L. (2017) Cerebral cortex development: an outside-in perspective. *FEBS Lett.* **591**, 3978–3992.
- Albert M., Kalebic N., Florio M., Lakshmanaperumal N., Haffner C., Brandl H., Henry I. and Huttner W. B. (2017) Epigenome profiling and editing of neocortical progenitor cells during development. *EMBO J.* **36**, 2642–2658.
- Alexandre P., Reugels A. M., Barker D., Blanc E. and Clarke J. D. (2010) Neurons derive from the more apical daughter in asymmetric divisions in the zebrafish neural tube. *Nat. Neurosci.* **13**, 673–679.
- Al-Jaberi N., Lindsay S., Sarma S., Bayatti N. and Clowry G. J. (2015) The early fetal development of human neocortical GABAergic interneurons. *Cereb. Cortex* **25**, 631–645.
- Arai Y., Pulvers J. N., Haffner C., Schilling B., Nusslein I., Calegari F. and Huttner W. B. (2011) Neural stem and progenitor cells shorten S-phase on commitment to neuron production. *Nat. Commun.* **2**, 154.
- Arbeille E., Reynaud F., Sanyas I., Bozon M., Kindbeiter K., Causseret F., Pierani A., Falk J., Moret F. and Castellani V. (2015) Cerebrospinal fluid-derived Semaphorin3B orients neuroepithelial cell divisions in the apicobasal axis. *Nat Commun.* **27**, 6:6366.



- Asami M., Pilz G. A., Ninkovic J., Godinho L., Schroeder T., Huttner W. B. and Gotz M. (2011) The role of Pax6 in regulating the orientation and mode of cell division of progenitors in the mouse cerebral cortex. *Development* **138**, 5067–5078.
- Bandler R. C., Mayer C. and Fishell G. (2017) Cortical interneuron specification: the juncture of genes, time and geometry. *Curr. Opin. Neurobiol.* **42**, 17–24.
- Beattie R., Postiglione M. P., Burnett L. E. *et al.* (2017) Mosaic analysis with double markers reveals distinct sequential functions of Lgl1 in neural stem cells. *Neuron* **94**, 517–533, e513.
- Bernabe-Rubio M., Andres G., Casares-Arias J. *et al.* (2016) Novel role for the midbody in primary ciliogenesis by polarized epithelial cells. *J. Cell Biol.* **214**, 259–273.
- Bershteyn M., Nowakowski T. J., Pollen A. A., Di Lullo E., Nene A., Wynshaw-Boris A. and Kriegstein A. R. (2017) Human iPSC-derived cerebral organoids model cellular features of lissencephaly and reveal prolonged mitosis of outer radial glia. *Cell Stem Cell* **20** (435–449), e434.
- Bertipaglia C., Goncalves J. C. and Vallee R. B. (2017) Nuclear migration in mammalian brain development. *Semin. Cell Dev. Biol.* <https://doi.org/10.1016/j.semcdb.2017.11.033>
- Betizeau M., Cortay V., Patti D. *et al.* (2013) Precursor diversity and complexity of lineage relationships in the outer subventricular zone of the primate. *Neuron* **80**, 442–457.
- Bizzotto S. and Francis F. (2015) Morphological and functional aspects of progenitors perturbed in cortical malformations. *Front Cell Neurosci.* **9**, 30.
- Bizzotto S., Uzquiano A., Dingli F. *et al.* (2017) Eml1 loss impairs apical progenitor spindle length and soma shape in the developing cerebral cortex. *Sci. Rep.* **7**, 17308.
- Blumer J. B., Lord K., Saunders T. L., Pacchioni A., Black C., Lazartigues E., Varner K. J., Gettys T. W. and Lanier S. M. (2008) Activator of G protein signaling 3 null mice: I. Unexpected alterations in metabolic and cardiovascular function. *Endocrinology* **149**, 3842–3849.
- Borrell V., Cardenas A., Ciceri G. *et al.* (2012) Slit/Robo signaling modulates the proliferation of central nervous system progenitors. *Neuron* **76**, 338–352.
- Borrell V. and Calegari F. (2014) Mechanisms of brain evolution: regulation of neural progenitor cell diversity and cell cycle length. *Neurosci. Res.* **86**, 14–24.
- Borrell V. and Gotz M. (2014) Role of radial glial cells in cerebral cortex folding. *Curr. Opin. Neurobiol.* **27**, 39–46.
- Buchman J. J., Tseng H. C., Zhou Y., Frank C. L., Xie Z. and Tsai L. H. (2010) Cdk5rap2 interacts with pericentrin to maintain the neural progenitor pool in the developing neocortex. *Neuron* **66**, 386–402.
- Bultje R. S., Castaneda-Castellanos D. R., Jan L. Y., Jan Y. N., Kriegstein A. R. and Shi S. H. (2009) Mammalian Par3 regulates progenitor cell asymmetric division via notch signaling in the developing neocortex. *Neuron* **63**, 189–202.
- Calegari F. and Huttner W. B. (2003) An inhibition of cyclin-dependent kinases that lengthens, but does not arrest, neuroepithelial cell cycle induces premature neurogenesis. *J. Cell Sci.* **116**, 4947–4955.
- Calegari F., Haubensak W., Haffner C. and Huttner W. B. (2005) Selective lengthening of the cell cycle in the neurogenic subpopulation of neural progenitor cells during mouse brain development. *J. Neurosci.* **25**, 6533–6538.
- Cappello S., Attardo A., Wu X. *et al.* (2006) The Rho-GTPase cdc42 regulates neural progenitor fate at the apical surface. *Nat. Neurosci.* **9**, 1099–1107.
- Cappello S., Bohringer C. R., Bergami M. *et al.* (2012) A radial glia-specific role of RhoA in double cortex formation. *Neuron* **73**, 911–924.
- Chenn A. and McConnell S. K. (1995) Cleavage orientation and the asymmetric inheritance of Notch1 immunoreactivity in mammalian neurogenesis. *Cell* **82**, 631–641.
- Chenn A. and Walsh C. A. (2002) Regulation of cerebral cortical size by control of cell cycle exit in neural precursors. *Science*, **297**, 365–369.
- Cho Y. M., Jang Y. S., Jang Y. M. *et al.* (2009) Induction of unfolded protein response during neuronal induction of rat bone marrow stromal cells and mouse embryonic stem cells. *Exp. Mol. Med.* **41**, 440–452.
- Clevers H. (2016) Modeling development and disease with organoids. *Cell* **165**, 1586–1597.
- Costa M. R., Wen G., Lepier A., Schroeder T. and Gotz M. (2008) Par-complex proteins promote proliferative progenitor divisions in the developing mouse cerebral cortex. *Development* **135**, 11–22.
- Das R. and Storey K. G. (2014) Apical abscission alters cell polarity and dismantles the primary cilium during neurogenesis. *Science* **343**, 200–204.
- Dehay C. and Kennedy H. (2007) Cell-cycle control and cortical development. *Nat. Rev. Neurosci.* **8**, 438–450.
- Del Toro D., Ruff T., Cederfjall E., Villalba A., Seyit-Bremer G., Borrell V. and Klein R. (2017) Regulation of cerebral cortex folding by controlling neuronal migration via FLRT adhesion molecules. *Cell* **169**, 621–635, e616.
- Delaunay D., Cortay V., Patti D., Knoblauch K. and Dehay C. (2014) Mitotic spindle asymmetry: a Wnt/PCP-regulated mechanism generating asymmetrical division in cortical precursors. *Cell Rep.* **6**, 400–414.
- Desai A. R. and McConnell S. K. (2000) Progressive restriction in fate potential by neural progenitors during cerebral cortical development. *Development* **127**, 2863–2872.
- Di Lullo E. and Kriegstein A. R. (2017) The use of brain organoids to investigate neural development and disease. *Nat. Rev. Neurosci.* **18**, 573–584.
- di Pietro F., Echard A. and Morin X. (2016) Regulation of mitotic spindle orientation: an integrated view. *EMBO Rep.* **17**, 1106–1130.
- Dionne L. K., Wang X. J. and Prekeris R. (2015) Midbody: from cellular junk to regulator of cell polarity and cell fate. *Curr. Opin. Cell Biol.* **35**, 51–58.
- Draganova K., Zemke M., Zurkirchen L. *et al.* (2015) Wnt/beta-catenin signaling regulates sequential fate decisions of murine cortical precursor cells. *Stem Cells* **33**, 170–182.
- Dubreuil V., Marzesco A. M., Corbeil D., Huttner W. B. and Wilsch-Brauninger M. (2007) Midbody and primary cilium of neural progenitors release extracellular membrane particles enriched in the stem cell marker prominin-1. *J. Cell Biol.* **176**, 483–495.
- Dudok J. J., Murtaza M., Henrique Alves C., Rashbass P. and Wijnholds J. (2016) Crumbs 2 prevents cortical abnormalities in mouse dorsal telencephalon. *Neurosci. Res.* **108**, 12–23.
- Dwyer N. D., Chen B., Chou S. J., Hippenmeyer S., Nguyen L. and Ghashghaei H. T. (2016) Neural stem cells to cerebral cortex: emerging mechanisms regulating progenitor behavior and productivity. *J. Neurosci.* **36**, 11394–11401.
- Eckler M. J., Nguyen T. D., McKenna W. L., Fastow B. L., Guo C., Rubenstein J. L. R. and Chen B. (2015) Cux2-positive radial glial cells generate diverse subtypes of neocortical projection neurons and macroglia. *Neuron* **86**, 1100–1108.
- Eiraku M., Watanabe K., Matsuo-Takasaki M., Kawada M., Yonemura S., Matsumura M., Wataya T., Nishiyama A., Muguruma K. and Sasai Y. (2008) Self-organized formation of polarized cortical tissues from ESCs and its active manipulation by extrinsic signals. *Cell Stem Cell* **3**, 519–532.

- Elias L. A. and Kriegstein A. R. (2008) Gap junctions: multifaceted regulators of embryonic cortical development. *Trends Neurosci.* **31**, 243–250.
- Englund C., Fink A., Lau C., Pham D., Daza R. A., Bulfone A., Kowalczyk T. and Hevner R. F. (2005) Pax6, Tbr2, and Tbr1 are expressed sequentially by radial glia, intermediate progenitor cells, and postmitotic neurons in developing neocortex. *J. Neurosci.* **25**, 247–251.
- Falk S., Bugeon S., Ninkovic J., Pilz G. A., Postiglione M. P., Cremer H., Knoblich J. A. and Gotz M. (2017) Time-specific effects of spindle positioning on embryonic progenitor pool composition and adult neural stem cell seeding. *Neuron* **93**, 777–791, e773.
- Feng Y. and Walsh C. A. (2004) Mitotic spindle regulation by Nde1 controls cerebral cortical size. *Neuron* **44**, 279–293.
- Fernandez V., Llinares-Benadero C. and Borrell V. (2016) Cerebral cortex expansion and folding: what have we learned? *EMBO J.* **35**, 1021–1044.
- Fietz S. A., Kelava I., Vogt J. *et al.* (2010) OSVZ progenitors of human and ferret neocortex are epithelial-like and expand by integrin signaling. *Nat. Neurosci.* **13**, 690–699.
- Fietz S. A., Lachmann R., Brandl H. *et al.* (2012) Transcriptomes of germinal zones of human and mouse fetal neocortex suggest a role of extracellular matrix in progenitor self-renewal. *Proc. Natl Acad. Sci. USA* **109**, 11836–11841.
- Firtina Z., Danysh B. P., Bai X., Gould D. B., Kobayashi T. and Duncan M. K. (2009) Abnormal expression of collagen IV in lens activates unfolded protein response resulting in cataract. *J. Biol. Chem.* **284**, 35872–35884.
- Firtina Z. and Duncan M. K. (2011) Unfolded Protein Response (UPR) is activated during normal lens development. *Gene Exp Patterns* **11**, 135–143.
- Fish J. L., Kosodo Y., Enard W., Paabo S. and Huttner W. B. (2006) Aspm specifically maintains symmetric proliferative divisions of neuroepithelial cells. *Proc. Natl Acad. Sci. USA* **103**, 10438–10443.
- Florio M. and Huttner W. B. (2014) Neural progenitors, neurogenesis and the evolution of the neocortex. *Development* **141**, 2182–2194.
- Florio M., Albert M., Taverna E. *et al.* (2015) Human specific gene ARHGAP11B promotes basal progenitor amplification and neocortex expansion. *Science* **347**, 1465–1470.
- Foerster P., Daclin M., Asm S., Faucourt M., Boletta A., Genovesio A. and Spassky N. (2017) mTORC1 signaling and primary cilia are required for brain ventricle morphogenesis. *Development* **144**, 201–210.
- Franco S. J., Gil-Sanz C., Martinez-Garay I., Espinosa A., Harkins-Perry S. R., Ramos C. and Muller U. (2012) Fate-restricted neural progenitors in the mammalian cerebral cortex. *Science* **337**, 746–749.
- Frank C. L., Ge X., Xie Z., Zhou Y. and Tsai L. H. (2010) Control of activating transcription factor 4 (ATF4) persistence by multisite phosphorylation impacts cell cycle progression and neurogenesis. *J. Biol. Chem.* **285**, 33324–33337.
- Frantz G. D. and McConnell S. K. (1996) Restriction of late cerebral cortical progenitors to an upper-layer fate. *Neuron* **17**, 55–61.
- Gabriel E., Wason A., Ramani A. *et al.* (2016) CPAP promotes timely cilium disassembly to maintain neural progenitor pool. *EMBO J.* **35**, 803–819.
- Gai M., Bianchi F. T., Vagnoni C. *et al.* (2016) ASPM and CITK regulate spindle orientation by affecting the dynamics of astral microtubules. *EMBO Rep.* **17**, 1396–1409.
- Gaiano N., Nye J. S. and Fishell G. (2000) Radial glial identity is promoted by Notch1 signaling in the murine forebrain. *Neuron* **26**, 395–404.
- Gal J. S., Morozov Y. M., Ayoub A. E., Chatterjee M., Rakic P. and Haydar T. F. (2006) Molecular and morphological heterogeneity of neural precursors in the mouse neocortical proliferative zones. *J. Neurosci.* **26**, 1045–1056.
- Gan Q., Lee A., Suzuki R., Yamagami T., Stokes A., Nguyen B. C., Pleasure D., Wang J., Chen H. W. and Zhou C. J. (2014) Pax6 mediates ss-catenin signaling for self-renewal and neurogenesis by neocortical radial glial stem cells. *Stem Cells* **32**, 45–58.
- Gao P., Postiglione M. P., Krieger T. G. *et al.* (2014) Deterministic progenitor behavior and unitary production of neurons in the neocortex. *Cell* **159**, 775–788.
- Garcez P. P., Diaz-Alonso J., Crespo-Enriquez I., Castro D., Bell D. and Guillemot F. (2015) Cenpj/CPAP regulates progenitor divisions and neuronal migration in the cerebral cortex downstream of Ascl1. *Nat. Commun.* **6**, 6474.
- Gauthier-Fisher A., Lin D. C., Greeve M., Kaplan D. R., Rottapel R. and Miller F. D. (2009) Lfc and Tctex-1 regulate the genesis of neurons from cortical precursor cells. *Nat. Neurosci.* **12**, 735–744.
- Gertz C. C., Lui J. H., LaMonica B. E., Wang X. and Kriegstein A. R. (2014) Diverse behaviors of outer radial glia in developing ferret and human cortex. *J. Neurosci.* **34**, 2559–2570.
- Ghosh T., Aprea J., Nardelli J. *et al.* (2014) MicroRNAs establish robustness and adaptability of a critical gene network to regulate progenitor fate decisions during cortical neurogenesis. *Cell Rep.* **7**, 1779–1788.
- Gil-Sanz C., Landeira B., Ramos C., Costa M. R. and Muller U. (2014) Proliferative defects and formation of a double cortex in mice lacking Mlnt4 and Cdh2 in the dorsal telencephalon. *J. Neurosci.* **34**, 10475–10487.
- Gil-Sanz C., Espinosa A., Fregoso S. P., Bluske K. K., Cunningham C. L., Martinez-Garay I., Zeng H., Franco S. J. and Muller U. (2015) Lineage Tracing Using Cux2-Cre and Cux2-CreERT2 Mice. *Neuron* **86**, 1091–1099.
- Gladwyn-Ng I., Cordon-Barris L., Alfano C. *et al.* (2018). Stress-induced unfolded protein response contributes to Zika virus-associated microcephaly. *Nat. Neurosci.*, **21**, 63–71.
- Godin J. D., Colombo K., Molina-Calavita M. *et al.* (2010) Huntingtin is required for mitotic spindle orientation and mammalian neurogenesis. *Neuron* **67**, 392–406.
- Gotz M., Stoykova A. and Gruss P. (1998) Pax6 controls radial glia differentiation in the cerebral cortex. *Neuron* **21**, 1031–1044.
- Gotz M. and Huttner W. B. (2005) The cell biology of neurogenesis. *Nat. Rev. Cell Biol.* **6**, 777–788.
- Gotz M., Sirko S., Beckers J. and Irmeler M. (2015) Reactive astrocytes as neural stem or progenitor cells: In vivo lineage, In vitro potential, and Genome-wide expression analysis. *Glia* **63**, 1452–1468.
- Govindan S. and Jabaudon D. (2017) Coupling progenitor and neuronal diversity in the developing neocortex. *FEBS Lett.* **591**, 3960–3977.
- Griveau A., Borello U., Causeret F., Tissir F., Boggetto N., Karaz S. and Pierani A. (2010) A novel role for Dbx1-derived Cajal-Retzius cells in early regionalization of the cerebral cortical neuroepithelium. *PLoS Biol.* **8**, e1000440.
- Guo C., Eckler M. J., McKenna W. L., McKinsey G. L., Rubenstein J. L. and Chen B. (2013) Fezf2 expression identifies a multipotent progenitor for neocortical projection neurons, astrocytes, and oligodendrocytes. *Neuron* **80**, 1167–1174.
- Hansen D. V., Lui J. H., Parker P. R. and Kriegstein A. R. (2010) Neurogenic radial glia in the outer subventricular zone of human neocortex. *Nature* **464**, 554–561.
- Hansen D. V., Lui J. H., Flandin P., Yoshikawa K., Rubenstein J. L., Alvarez-Buylla A. and Kriegstein A. R. (2013) Non-epithelial stem cells and cortical interneuron production in the human ganglionic eminences. *Nat. Neurosci.* **16**, 1576–1587.

- Hatakeyama J., Bessho Y., Katoh K., Ookawara S., Fujioka M., Guillemot F. and Kageyama R. (2004) Hes genes regulate size, shape and histogenesis of the nervous system by control of the timing of neural stem cell differentiation. *Development* **131**, 5539–5550.
- Haubensak W., Attardo A., Denk W. and Huttner W. B. (2004) Neurons arise in the basal neuroepithelium of the early mammalian telencephalon: a major site of neurogenesis. *Proc. Natl Acad. Sci. USA* **101**, 3196–3201.
- Hayashi A., Kasahara T., Iwamoto K., Ishiwata M., Kametani M., Kakiuchi C., Furuichi T. and Kato T. (2007) The role of brain-derived neurotrophic factor (BDNF)-induced XBP1 splicing during brain development. *J. Biol. Chem.* **282**, 34525–34534.
- Haushalter C., Asselin L., Fraulob V., Dolle P. and Rhinn M. (2017) Retinoic acid controls early neurogenesis in the developing mouse cerebral cortex. *Dev. Biol.* **430**, 129–141.
- Heide M., Long K. R. and Huttner W. B. (2017) Novel gene function and regulation in neocortex expansion. *Curr. Opin. Cell Biol.* **49**, 22–30.
- Hetz C. (2012) The unfolded protein response: controlling cell fate decisions under ER stress and beyond. *Nat. Rev. Mol. Cell Biol.* **13**, 89–102.
- Hetz C. and Papa F. R. (2017) The unfolded protein response and cell fate control. *Mol. Cell*, **69**, 169–181, in press.
- Hirabayashi Y., Itoh Y., Tabata H., Nakajima K., Akiyama T., Masuyama N. and Gotoh Y. (2004) The Wnt/beta-catenin pathway directs neuronal differentiation of cortical neural precursor cells. *Development* **131**, 2791–2801.
- Hodge R. D., D'Ercole A. J. and O'Kusky J. R. (2004) Insulin-like growth factor-I accelerates the cell cycle by decreasing G1 phase length and increases cell cycle reentry in the embryonic cerebral cortex. *J. Neurosci.* **24**, 10201–10210.
- Homem C. C. and Knoblich J. A. (2012) *Drosophila* neuroblasts: a model for stem cell biology. *Development* **139**, 4297–4310.
- Hu D. J., Baffet A. D., Nayak T., Akhmanova A., Doye V. and Vallee R. B. (2013) Dynein recruitment to nuclear pores activates apical nuclear migration and mitotic entry in brain progenitor cells. *Cell* **154**, 1300–1313.
- Iefremova V., Manikakis G., Krefft O. *et al.* (2017) An organoid-based model of cortical development identifies non-cell-autonomous defects in Wnt signaling contributing to miller-dieker syndrome. *Cell Rep.* **19**, 50–59.
- Imai F., Hirai S., Akimoto K., Koyama H., Miyata T., Ogawa M., Noguchi S., Sasaoka T., Noda T. and Ohno S. (2006) Inactivation of aPKC $\lambda$  results in the loss of adherens junctions in neuroepithelial cells without affecting neurogenesis in mouse neocortex. *Development* **133**, 1735–1744.
- Inoue M., Iwai R., Tabata H. *et al.* (2017) Correction: Prdm16 is crucial for progression of the multipolar phase during neural differentiation of the developing neocortex. *Development* **144**, 1735.
- Insolera R., Bazzi H., Shao W., Anderson K. V. and Shi S. H. (2014) Cortical neurogenesis in the absence of centrioles. *Nat. Neurosci.* **17**, 1528–1535.
- Itoh N. (2010) Hormone-like (endocrine) Fgfs: their evolutionary history and roles in development, metabolism, and disease. *Cell Tissue Res.* **342**, 1–11.
- Jakovcevski I., Mayer N. and Zecevic N. (2011) Multiple origins of human neocortical interneurons are supported by distinct expression of transcription factors. *Cereb. Cortex*, **21**, 1771–1782.
- Janisch K. M., Vock V. M., Fleming M. S. *et al.* (2013) The vertebrate-specific Kinesin-6, Kif20b, is required for normal cytokinesis of polarized cortical stem cells and cerebral cortex size. *Development* **140**, 4672–4682.
- Jayaraman D., Kodani A., Gonzalez D. M. *et al.* (2016) Microcephaly proteins Wdr62 and Aspm define a mother centriole complex regulating centriole biogenesis, apical complex, and cell fate. *Neuron* **92**, 813–828.
- Jossin Y., Lee M., Klezovitch O., Kon E., Cossard A., Lien W. H., Fernandez T. E., Cooper J. A. and Vasioukhin V. (2017) Llg1 connects cell polarity with cell-cell adhesion in embryonic neural stem cells. *Dev. Cell* **41**, 481–495, e485.
- Ju X. C., Hou Q. Q., Sheng A. L., Wu K. Y., Zhou Y., Jin Y., Wen T., Yang Z., Wang X. and Luo Z. G. (2016) The hominoid-specific gene TBC1D3 promotes generation of basal neural progenitors and induces cortical folding in mice. *Elife*, **5**, e18197.
- Junghans D., Hack I., Frotscher M., Taylor V. and Kemler R. (2005) Beta-catenin-mediated cell-adhesion is vital for embryonic forebrain development. *Dev. Dyn.* **233**, 528–539.
- Khacho M., Clark A., Svoboda D. S. *et al.* (2016) Mitochondrial dynamics impacts stem cell identity and fate decisions by regulating a nuclear transcriptional program. *Cell Stem Cell* **19**, 232–247.
- Khacho M., Clark A., Svoboda D. S., MacLaurin J. G., Lagace D. C., Park D. S. and Slack R. S. (2017) Mitochondrial dysfunction underlies cognitive defects as a result of neural stem cell depletion and impaired neurogenesis. *Hum. Mol. Genet.* **26**, 3327–3341.
- Kadowaki M., Nakamura S., Machon O., Krauss S., Radice G. L. and Takeichi M. (2007) N-cadherin mediates cortical organization in the mouse brain. *Dev. Biol.* **304**, 22–33.
- Kang W., Wong L. C., Shi S. H. and Hebert J. M. (2009) The transition from radial glial to intermediate progenitor cell is inhibited by FGF signaling during corticogenesis. *J. Neurosci.* **29**, 14571–14580.
- Kaplan E. S., Ramos-Laguna K. A., Mihalas A. B., Daza R. A. M. and Hevner R. F. (2017) Neocortical Sox9 + radial glia generate glutamatergic neurons for all layers, but lack discernible evidence of early laminar fate restriction. *Neural Dev.* **12**, 14.
- Kawada K., Jekumo T., Saito R., Kaneko M., Mimori S., Nomura Y. and Okuma Y. (2014) Aberrant neuronal differentiation and inhibition of dendrite outgrowth resulting from endoplasmic reticulum stress. *J. Neurosci. Res.* **92**, 1122–1133.
- Kawauchi T. (2015) Cellular insights into cerebral cortical development: focusing on the locomotion mode of neuronal migration. *Front Cell Neurosci.* **9**, 394.
- Kawaguchi A. and Matsuzaki F. (2016) Cell cycle-arrested cells know the right time. *Cell Cycle* **15**, 2683–2684.
- Kielar M., Tuy F. P., Bizzotto S. *et al.* (2014) Mutations in Eml1 lead to ectopic progenitors and neuronal heterotopia in mouse and human. *Nat. Neurosci.* **17**, 923–933.
- Kim S., Lehtinen M. K., Sessa A. *et al.* (2010) The apical complex couples cell fate and cell survival to cerebral cortical development. *Neuron* **66**, 69–84.
- Konno D., Shioi G., Shitamukai A., Mori A., Kiyonari H., Miyata T. and Matsuzaki F. (2008) Neuroepithelial progenitors undergo LGN-dependent planar divisions to maintain self-renewability during mammalian neurogenesis. *Nat. Cell Biol.* **10**, 93–101.
- Kosodo Y., Röper K., Haubensak W., Marzesco A.-M., Corbeil D. and Huttner W. B. (2004) Asymmetric distribution of the apical plasma membrane during neurogenic divisions of mammalian neuroepithelial cells. *EMBO J.* **23**, 2314–2324.
- Laclef C. and Metin C. (2018) Conserved rules in embryonic development of cortical interneurons. *Semin. Cell Dev. Biol.* **76**, 86–100.

- Laguesse S., Creppe C., Nedialkova D. D. *et al.* (2015a) A dynamic unfolded protein response contributes to the control of cortical neurogenesis. *Dev. Cell* **35**, 553–567.
- Laguesse S., Peyre E. and Nguyen L. (2015b) Progenitor genealogy in the developing cerebral cortex. *Cell Tissue Res.* **359**, 17–32.
- LaMonica B. E., Lui J. H., Hansen D. V. and Kriegstein A. R. (2013) Mitotic spindle orientation predicts outer radial glial cell generation in human neocortex. *Nat. Commun.* **4**, 1665.
- Lancaster M. A., Renner M., Martin C. A., Wenzel D., Bicknell L. S., Hurles M. E., Homfray T., Penninger J. M., Jackson A. P. and Knoblich J. A. (2013) Cerebral organoids model human brain development and microcephaly. *Nature* **501**, 373–379.
- Lancaster M. A. and Knoblich J. A. (2014) Organogenesis in a dish: modeling development and disease using organoid technologies. *Science* **345**, 1247125.
- Lange C., Huttner W. B. and Calegari F. (2009) Cdk4/cyclinD1 overexpression in neural stem cells shortens G1, delays neurogenesis, and promotes the generation and expansion of basal progenitors. *Cell Stem Cell* **5**, 320–331.
- Lehtinen M. K. and Walsh C. A. (2011) Neurogenesis at the brain-cerebrospinal fluid interface. *Annu. Rev. Cell Dev. Biol.* **27**, 653–679.
- Lehtinen M. K., Zappaterra M. W., Chen X. *et al.* (2011) The cerebrospinal fluid provides a proliferative niche for neural progenitor cells. *Neuron* **69**, 893–905.
- Letinic K., Zoncu R. and Rakic P. (2002) Origin of GABAergic neurons in the human neocortex. *Nature* **417**, 645–649.
- Liu J., Liu W., Yang L. *et al.* (2017) The primate-specific gene TMEM14B marks outer radial glia cells and promotes cortical expansion and folding. *Cell Stem Cell* **21**(635–649), e638.
- Lizarraga S. B., Margossian S. P., Harris M. H., Campagna D. R., Han A. P., Blevins S., Mudbhary R., Barker J. E., Walsh C. A. and Fleming M. D. (2010) Cdk5rap2 regulates centrosome function and chromosome segregation in neuronal progenitors. *Development* **137**, 1907–1917.
- Lodato S. and Arlotta P. (2015) Generating neuronal diversity in the mammalian cerebral cortex. *Annu. Rev. Cell Dev. Biol.* **31**, 699–720.
- Lodato S., Shetty A. S. and Arlotta P. (2015) Cerebral cortex assembly: generating and reprogramming projection neuron diversity. *Trends Neurosci.* **38**, 117–125.
- Lui J. H., Nowakowski T. T., Pollen A. A., Javaherian A., Kriegstein A. R. and Oldham M. C. (2014) Radial glia require PDGFR- $\beta$  signalling in human but not mouse neocortex. *Nature* **515**, 264–268.
- Lukasiewicz A., Savatier P., Cortay V., Kennedy H. and Dehay C. (2002) Contrasting effects of basic fibroblast growth factor and neurotrophin 3 on cell cycle kinetics of mouse cortical stem cells. *J. Neurosci.* **22**, 6610–6622.
- Lukasiewicz A., Savatier P., Cortay V., Giroud P., Huissoud C., Berland M., Kennedy H. and Dehay C. (2005) G1 phase regulation, area-specific cell cycle control, and cytoarchitectonics in the primate cortex. *Neuron* **47**, 353–364.
- Luskin M. B., Pearlman A. L. and Sanes J. R. (1988) Cell lineage in the cerebral cortex of the mouse studied in vivo and in vitro with a recombinant retrovirus. *Neuron* **1**, 635–647.
- Lv X., Jiang H., Liu Y., Lei X. and Jiao J. (2014) MicroRNA-15b promotes neurogenesis and inhibits neural progenitor proliferation by directly repressing TET3 during early neocortical development. *EMBO Rep.* **15**, 1305–1314.
- Ma T., Wang C., Wang L. *et al.* (2013) Subcortical origins of human and monkey neocortical interneurons. *Nat. Neurosci.* **16**, 1588–1597.
- Mairet-Coello G., Tury A. and DiCicco-Bloom E. (2009) Insulin-like growth factor-1 promotes G(1)/S cell cycle progression through bidirectional regulation of cyclins and cyclin-dependent kinase inhibitors via the phosphatidylinositol 3-kinase/Akt pathway in developing rat cerebral cortex. *J. Neurosci.* **29**, 775–788.
- Malatesta P., Hartfuss E. and Götz M. (2000) Isolation of radial glial cells by fluorescent activated cell sorting reveals a neuronal lineage. *Development* **127**, 5253–5263.
- Manabe N., Hirai S., Imai F., Nakanishi H., Takai Y. and Ohno S. (2002) Association of ASIP/mPAR-3 with adherens junctions of mouse neuroepithelial cells. *Dev. Dyn.* **225**, 61–69.
- Marin O. (2013) Cellular and molecular mechanisms controlling the migration of neocortical interneurons. *Eur. J. Neurosci.* **38**, 2019–2029.
- Marthiens V. and French-Constant C. (2009) Adherens junction domains are split by asymmetric division of embryonic neural stem cells. *EMBO Rep.* **10**, 515–520.
- Marthiens V., Rujano M. A., Penetier C., Tessier S., Paul-Gilloteaux P. and Basto R. (2013) Centrosome amplification causes microcephaly. *Nat. Cell Biol.* **15**, 731–740.
- Martinez-Martinez M. A., De Juan Romero C., Fernandez V., Cardenas A., Gotz M. and Borrell V. (2016) A restricted period for formation of outer subventricular zone defined by Cdh1 and Trnp1 levels. *Nat. Commun.* **7**, 11812.
- Martynoga B., Drechsel D. and Guillemot F. (2012) Molecular control of neurogenesis: a view from the mammalian cerebral cortex. *Cold Spring Harb Perspect Biol.* **4**, a008359.
- Matsuzaki F. and Shitamukai A. (2015) Cell division modes and cleavage planes of neural progenitors during mammalian cortical development. *Cold Spring Harb Perspect Biol.* **7**, a015719.
- McConnell S. K. and Kaznowski C. E. (1991) Cell cycle dependence of laminar determination in developing neocortex. *Science* **254**, 282–285.
- Meza-Sosa K. F., Pedraza-Alva G. and Perez-Martinez L. (2014) microRNAs: key triggers of neuronal cell fate. *Front Cell Neurosci.* **8**, 175.
- Mihalas A. B., Elsen G. E., Bedogni F., Daza R. A. M., Ramos-Laguna K. A., Arnold S. J. and Hevner R. F. (2016) Intermediate progenitor cohorts differentially generate cortical layers and require Tbr2 for timely acquisition of neuronal subtype identity. *Cell Rep.* **16**, 92–105.
- Mimura N., Yuasa S., Soma M., Jin H., Kimura K., Goto S., Koseki H. and Aoe T. (2008) Altered quality control in the endoplasmic reticulum causes cortical dysplasia in knock-in mice expressing a mutant BiP. *Mol. Cell. Biol.* **28**, 293–301.
- Miyata T., Kawaguchi A., Saito K., Kawano M., Muto T. and Ogawa M. (2004) Asymmetric production of surface-dividing and non-surface-dividing cortical progenitor cells. *Development* **131**, 3133–3145.
- Mizutani K., Yoon K., Dang L., Tokunaga A. and Gaiano N. (2007) Differential Notch signalling distinguishes neural stem cells from intermediate progenitors. *Nature* **449**, 351–355.
- Molina-Calavita M., Barnat M., Elias S., Aparicio E., Piel M. and Humbert S. (2014) Mutant huntingtin affects cortical progenitor cell division and development of the mouse neocortex. *J. Neurosci.* **34**, 10034–10040.
- Morin X., Jaouen F. and Durbec P. (2007) Control of planar divisions by the G-protein regulator LGN maintains progenitors in the chick neuroepithelium. *Nat. Neurosci.* **10**, 1440–1448.
- Munji R. N., Choe Y., Li G., Siegenthaler J. A. and Pleasure S. J. (2011) Wnt signaling regulates neuronal differentiation of cortical intermediate progenitors. *J. Neurosci.* **31**, 1676–1687.
- Noctor S. C., Flint A. C., Weissman T. A., Dammerman R. S. and Kriegstein A. R. (2001) Neurons derived from radial glial cells establish radial units in neocortex. *Nature* **409**, 714–720.
- Noctor S. C., Martinez-Cerdeno V., Ivic L. and Kriegstein A. R. (2004) Cortical neurons arise in symmetric and asymmetric

- division zones and migrate through specific phases. *Nat. Neurosci.* **7**, 136–144.
- Nonaka-Kinoshita M., Reillo I., Artegiani B., Martinez-Martinez M. A., Nelson M., Borrell V. and Calegari F. (2013) Regulation of cerebral cortex size and folding by expansion of basal progenitors. *EMBO J.* **32**, 1817–1828.
- Okamoto M., Miyata T., Konno D., Ueda H. R., Kasukawa T., Hashimoto M., Matsuzaki F. and Kawaguchi A. (2016) Cell-cycle-independent transitions in temporal identity of mammalian neural progenitor cells. *Nat. Commun.* **7**, 11349.
- Ostrem B., Di Lullo E. and Kriegstein A. (2017) oRGs and mitotic somal translocation - a role in development and disease. *Curr. Opin. Neurobiol.* **42**, 61–67.
- Paridaen J. T., Wilsch-Brauninger M. and Huttner W. B. (2013) Asymmetric inheritance of centrosome-associated primary cilium membrane directs ciliogenesis after cell division. *Cell* **155**, 333–344.
- Parthasarathy S., Srivatsa S., Nityanandam A. and Tarabykin V. (2014) Ntf3 acts downstream of Sip1 in cortical postmitotic neurons to control progenitor cell fate through feedback signaling. *Development* **141**, 3324–3330.
- Pilaz L. J., Patti D., Marcy G. *et al.* (2009) Forced G1-phase reduction alters mode of division, neuron number, and laminar phenotype in the cerebral cortex. *Proc. Natl Acad. Sci. USA* **106**, 21924–21929.
- Pilaz L. J., McMahon J. J., Miller E. E., Lennox A. L., Suzuki A., Salmon E. and Silver D. L. (2016) Prolonged mitosis of neural progenitors alters cell fate in the developing brain. *Neuron* **89**, 83–99.
- Pilz G. A., Shitamukai A., Reillo I. *et al.* (2013) Amplification of progenitors in the mammalian telencephalon includes a new radial glial cell type. *Nat. Commun.* **4**, 2125.
- Piotrowska-Nitsche K. and Caspary T. (2012) Live imaging of individual cell divisions in mouse neuroepithelium shows asymmetry in cilium formation and sonic hedgehog response. *Cilia* **1**, 6.
- Pollen A. A., Nowakowski T. J., Chen J. *et al.* (2015) Molecular identity of human outer radial glia during cortical development. *Cell* **163**, 55–67.
- Rakic P. and Zecevic N. (2003) Emerging complexity of layer I in human cerebral cortex. *Cereb. Cortex* **13**, 1072–1083.
- Rakotomamonjy J., Brunner M., Juschke C., Zang K., Huang E. J., Reichardt L. F. and Chenn A. (2017) Afadin controls cell polarization and mitotic spindle orientation in developing cortical radial glia. *Neural Dev.* **12**, 7.
- Reillo I., de Juan Romero C., Garcia-Cabezas M. A. and Borrell V. (2011) A role for intermediate radial glia in the tangential expansion of the mammalian cerebral cortex. *Cereb. Cortex* **21**, 1674–1694.
- Reillo I., de Juan Romero C., Cardenas A., Clasca F., Martinez-Martinez M. A. and Borrell V. (2017) A complex code of extrinsic influences on cortical progenitor cells of higher mammals. *Cereb. Cortex* **27**, 4586–4606.
- Romero D. M., Bahi-Buisson N. and Francis F. (2018) Genetics and mechanisms leading to human cortical malformations. *Semin. Cell Dev. Biol.* **76**, 33–75.
- Saadaoui M., Machicoane M., di Pietro F., Etoc F., Echard A. and Morin X. (2014) Dlg1 controls planar spindle orientation in the neuroepithelium through direct interaction with LGN. *J. Cell Biol.* **206**, 707–717.
- Saadaoui M., Konno D., Loulier K., Goiaime R., Jadhav V., Mapelli M., Matsuzaki F. and Morin X. (2017) Loss of the canonical spindle orientation function in the Pins/LGN homolog AGS3. *EMBO Rep.* **18**, 1509–1520.
- Sahara S. and O'Leary D. D. (2009) Fgf10 regulates transition period of cortical stem cell differentiation to radial glia controlling generation of neurons and basal progenitors. *Neuron* **63**, 48–62.
- Salomoni P. and Calegari F. (2010) Cell cycle control of mammalian neural stem cells: putting a speed limit on G1. *Trends Cell Biol.* **20**, 233–243.
- Sanada K. and Tsai L. H. (2005) G protein betagamma subunits and AGS3 control spindle orientation and asymmetric cell fate of cerebral cortical progenitors. *Cell* **122**, 119–131.
- Sapir T., Levy T., Kozer N., Shin I., Zamor V., Haffner-Krausz R., McGlade J. C. and Reiner O. (2017) Notch activation by shootin1 opposing activities on 2 ubiquitin ligases. *Cereb. Cortex*, **13**, 1–14.
- Schmid M. T., Weinandy F., Wilsch-Brauninger M., Huttner W. B., Cappello S. and Gotz M. (2014) The role of alpha-E-catenin in cerebral cortex development: radial glia specific effect on neuronal migration. *Front Cell Neurosci.* **8**, 215.
- Seuntjens E., Nityanandam A., Miquelajauregui A., Debruyne J., Stryjewska A., Goebbels S., Nave K., Huylebroeck D. and Tarabykin V. (2009) Sip1 regulates sequential fate decisions by feedback signaling from postmitotic neurons to progenitors. *Nat. Neurosci.* **12**, 1373–1380.
- Shen Q., Wang Y., Dimos J. T., Fasano C. A., Phoenix T. N., Lemischka I. R., Ivanova N. B., Stifani S., Morrissy E. E. and Temple S. (2006) The timing of cortical neurogenesis is encoded within lineages of individual progenitor cells. *Nat. Neurosci.* **9**, 743–751.
- Shim J., Umemura T., Nothstein E. and Rongo C. (2004) The unfolded protein response regulates glutamate receptor export from the endoplasmic reticulum. *Mol. Biol. Cell* **15**, 4818–4828.
- Shitamukai A., Konno D. and Matsuzaki F. (2011) Oblique radial glial divisions in the developing mouse neocortex induce self-renewing progenitors outside the germinal zone that resemble primate outer subventricular zone progenitors. *J. Neurosci.* **31**, 3683–3695.
- Stahl R., Walcher T., De Juan Romero C. *et al.* (2013) Trmp1 regulates expansion and folding of the mammalian cerebral cortex by control of radial glial fate. *Cell* **153**, 535–549.
- Stancik E. K., Navarro-Quiroga I., Sellke R. and Haydar T. F. (2010) Heterogeneity in ventricular zone neural precursors contributes to neuronal fate diversity in the postnatal neocortex. *J. Neurosci.* **30**, 7028–7036.
- Silver D. L., Watkins-Chow D. E., Schreck K. C., Pierfelice T. J., Larson D. M., Burnetti A. J., Liaw H. J., Myung K., Walsh C. A., Gaiano N., *et al.* (2010) The exon junction complex component Magoh controls brain size by regulating neural stem cell division. *Nat. Neurosci.* **13**, 551–558.
- Singh S. and Solecki D. J. (2015) Polarity transitions during neurogenesis and germinal zone exit in the developing central nervous system. *Front Cell Neurosci.* **9**, 62.
- Stouffer M. A., Golden J. A. and Francis F. (2016) Neuronal migration disorders: focus on the cytoskeleton and epilepsy. *Neurobiol. Dis.* **92**, 18–45.
- Tarabykin V., Stoykova A., Usman N. and Gruss P. (2001) Cortical upper layer neurons derive from the subventricular zone as indicated by Svet1 gene expression. *Development* **128**, 1983–1993.
- Taverna E., Gotz M. and Huttner W. B. (2014) The cell biology of neurogenesis: toward an understanding of the development and evolution of the neocortex. *Annu. Rev. Cell Dev. Biol.* **30**, 465–502.
- Taverna E., Mora-Bermudez F., Strzyz P. J., Florio M., Icha J., Haffner C., Norden C., Wilsch-Bräuninger M. and Huttner W. B. (2016) Non-canonical features of the Golgi apparatus in bipolar epithelial neural stem cells. *Sci. Rep.*, **6**, 21206.
- Teissier A., Griveau A., Vigier L., Piolot T., Borello U. and Pierani A. (2010) A novel transient glutamatergic population migrating from the pallial-subpallial boundary contributes to neocortical development. *J. Neurosci.* **30**, 10563–10574.

- Tiberi L., van den Vanderhaeghen P. and Amele J. (2012) Cortical neurogenesis and morphogens: diversity of cues, sources and functions. *Curr. Opin. Cell Biol.* **24**, 269–276.
- Tozer S., Baek C., Fischer E., Goiaime R. and Morin X. (2017) Differential routing of mindbomb1 via centriolar satellites regulates asymmetric divisions of neural progenitors. *Neuron* **93**(542–551), e544.
- Tsunekawa Y., Britto J. M., Takahashi M., Polleux F., Tan S. S. and Osumi N. (2012) Cyclin D2 in the basal process of neural progenitors is linked to non-equivalent cell fates. *EMBO J.* **31**, 1879–1892.
- Turrero Garcia M., Chang Y., Arai Y. and Huttner W. B. (2016) S-phase duration is the main target of cell cycle regulation in neural progenitors of developing ferret neocortex. *J. Comp. Neurol.* **524**, 456–470.
- Tseng K. Y., Danilova T., Domanskyi A., Saarma M., Lindahl M. and Airavaara M. (2017) MANF is essential for neurite extension and neuronal migration in the developing cortex. *eNeuro*, **4**.
- Vasistha N. A., Garcia-Moreno F., Arora S., Cheung A. F., Arnold S. J., Robertson E. J. and Molnar Z. (2015) Cortical and clonal contribution of Tbr2 expressing progenitors in the developing mouse brain. *Cereb. Cortex* **25**, 3290–3302.
- Walsh C. and Cepko C. L. (1993) Clonal dispersion in proliferative layers of developing cerebral cortex. *Nature* **362**, 632–635.
- Wang X., Tsai J. W., Imai J. H., Lian W. N., Vallee R. B. and Shi S. H. (2009) Asymmetric centrosome inheritance maintains neural progenitors in the neocortex. *Nature* **461**, 947–955.
- Wang X., Tsai J. W., LaMonica B. and Kriegstein A. R. (2011) A new subtype of progenitor cell in the mouse embryonic neocortex. *Nat. Neurosci.* **14**, 555–561.
- Wang L., Hou S. and Han Y. G. (2016a) Hedgehog signaling promotes basal progenitor expansion and the growth and folding of the neocortex. *Nat. Neurosci.* **19**, 888–896.
- Wang W., Jossin Y., Chai G., Lien W. H., Tissir F. and Goffinet A. M. (2016b) Feedback regulation of apical progenitor fate by immature neurons through Wnt7-Celsr3-Fzd3 signalling. *Nat. Commun.* **4**(7), 10936.
- Wilsch-Brauninger M., Peters J., Paridaen J. T. and Huttner W. B. (2012) Basolateral rather than apical primary cilia on neuroepithelial cells committed to delamination. *Development* **139**, 95–105.
- Wong F. K., Fei J. F., Mora-Bermudez F., Taverna E., Haffner C., Fu J., Anastassiadis K., Stewart A. F. and Huttner W. B. (2015) Sustained Pax6 expression generates primate-like basal radial glia in developing mouse neocortex. *PLoS Biol.* **13**, e1002217.
- Woodhead G. J., Mutch C. A., Olson E. C. and Chenn A. (2006) Cell-autonomous beta-catenin signaling regulates cortical precursor proliferation. *J. Neurosci.* **26**, 12620–12630.
- Yelamanchili S. V., Morsey B., Harrison E. B., Rennard D. A., Emanuel K., Thapa I., Bastola D. R. and Fox H. S. (2014) The evolutionary young miR-1290 favors mitotic exit and differentiation of human neural progenitors through altering the cell cycle proteins. *Cell Death Dis.* **5**, e982.
- Yingling J., Youn Y. H., Darling D., Toyo-Oka K., Pramparo T., Hirotsune S. and Wynshaw-Boris A. (2008) Neuroepithelial stem cell proliferation requires LIS1 for precise spindle orientation and symmetric division. *Cell* **132**, 474–486.
- Zhang X., Szabo E., Michalak M. and Opas M. (2007) Endoplasmic reticulum stress during the embryonic development of the central nervous system in the mouse. *Int. J. Dev. Neurosci.* **24**, 455–463.
- Zhao C., Sun G., Li S., Lang M. F., Yang S., Li W. and Shi Y. (2010) MicroRNA let-7b regulates neural stem cell proliferation and differentiation by targeting nuclear receptor TLX signaling. *Proc. Natl Acad. Sci. USA* **107**, 1876–1881.
- Zimmer C., Tiveron M. C., Bodmer R. and Cremer H. (2004) Dynamics of Cux2 expression suggests that an early pool of SVZ precursors is fated to become upper cortical layer neurons. *Cereb. Cortex* **14**, 1408–1420.

## **ANNEXE II**

## SCIENTIFIC COMMENTARIES

### Rotatin' the phenotypes

This scientific commentary refers to 'Heterogeneous clinical phenotypes and cerebral malformations reflected by rotatin cellular dynamics', by Vandervore *et al.* (doi:10.1093/brain/awz045).

The development of the cerebral cortex depends on a series of finely regulated processes including neural progenitor proliferation, neuronal migration, synaptogenesis and the establishment of neuronal networks. Cortical malformations, which have an incidence of more than 1%, are associated with disruption of one or more of these steps. Abnormal progenitor cells are associated with disorders such as microcephaly, whilst altered neuronal migration and/or organization are associated with subcortical or periventricular heterotopia (i.e. abnormally positioned neurons), lissencephaly (characterized by absence of gyri) and polymicrogyria (abundant small gyri) (Uzquiano *et al.*, 2018).

In this issue of *Brain*, Vandervore *et al.* (2019) thoroughly examine the clinical phenotypes that result from autosomal recessive (homozygous or compound heterozygous) mutations in rotatin (*RTTN*), coding for a centrosome-related protein. Performing homozygosity mapping as well as whole genome and exome sequencing, they identify three new families presenting mutations in this gene. *RTTN* mutations lead to a spectrum of malformations, not obviously correlated with mutation position in the gene. These include simplified gyriification, lissencephaly and/or

pachygyria (simplified and thickened gyri), polymicrogyria, subcortical heterotopia and microcephaly, the latter being the most common feature amongst the patients (Fig. 1A). As with other cortical malformation genes, the factors determining malformation type and severity remain unclear.

Vandervore *et al.* obtained fibroblasts from eight patients and analysed the amounts and sequences of mRNA transcripts. Fibroblasts from different patients contained various levels of *RTTN* mRNA/protein, and sometimes even the wild-type version. Of note, the authors revealed a probable correlation between greater amounts of residual wild-type *RTTN* and lower malformation severity. Additionally, deep sequencing analyses uncovered novel intronic mutations, affecting splicing and introducing nonsense mutations, most likely leading to nonsense-mediated RNA decay. These results are highly relevant for diagnostic purposes: they indicate that the lack of exonic mutations in an allele does not rule out *RTTN* as being responsible for cortical malformations.

*RTTN* is a centrosome-related protein (Fig. 1B), although its multi-functional roles still remain largely unexplored. The centrosome has critical functions during the cell cycle: in interphase, the mother centriole acts as a basal body docking a primary cilium in the plasma membrane. Prior to mitosis, the centrosome undergoes duplication: each centriole is replicated and these 'procentrioles' undergo an elongation process to

reach the size of the previously existing ones. The mature centrosomes constitute the spindle poles during mitosis, ensuring proper establishment of the mitotic spindle and thus chromosome segregation. The study by Vandervore *et al.* addresses the role of wild-type and mutant *RTTN* at different stages of the cell cycle, linking mitosis, cell cycle and ciliogenesis defects and highlighting how centrosomal proteins are crucial for multiple cellular processes (Fig. 1C).

Throughout mitosis, wild-type *RTTN* is localized to the spindle poles (Fig. 1B). However, patient fibroblasts showed a diffuse, largely non-centrosomal cytoplasmic location of the protein. Mutant fibroblasts also showed centrosome amplification leading to multipolar spindles and divisions, causing aneuploidy. Increased cell cycle length was observed with time-lapse imaging (Fig. 1C). In addition, flow cytometry experiments showed an increase in DNA fragmentation, implying increased apoptosis.

Most microcephaly genes code for centrosomal proteins (i.e. *PLK4*, *STIL*, *MCPH1*, *ASPM*, *WDR62*, *CEP135*, *CDK5RAP2*, *CENPJ*) (Megraw *et al.*, 2011). Overexpression of master regulators of centrosome duplication (*PLK4* and *STIL*) can lead to centrosome amplification. Comparably, knockdown of *ASPM* and *WDR62* causes a decrease in centriole number (Jayaraman *et al.*, 2016). However, downregulation of *CDK5RAP2* leads to supernumerary centrosomes, similar to data obtained in fibroblasts with *RTTN* mutations. *CDK5RAP2* has been shown to



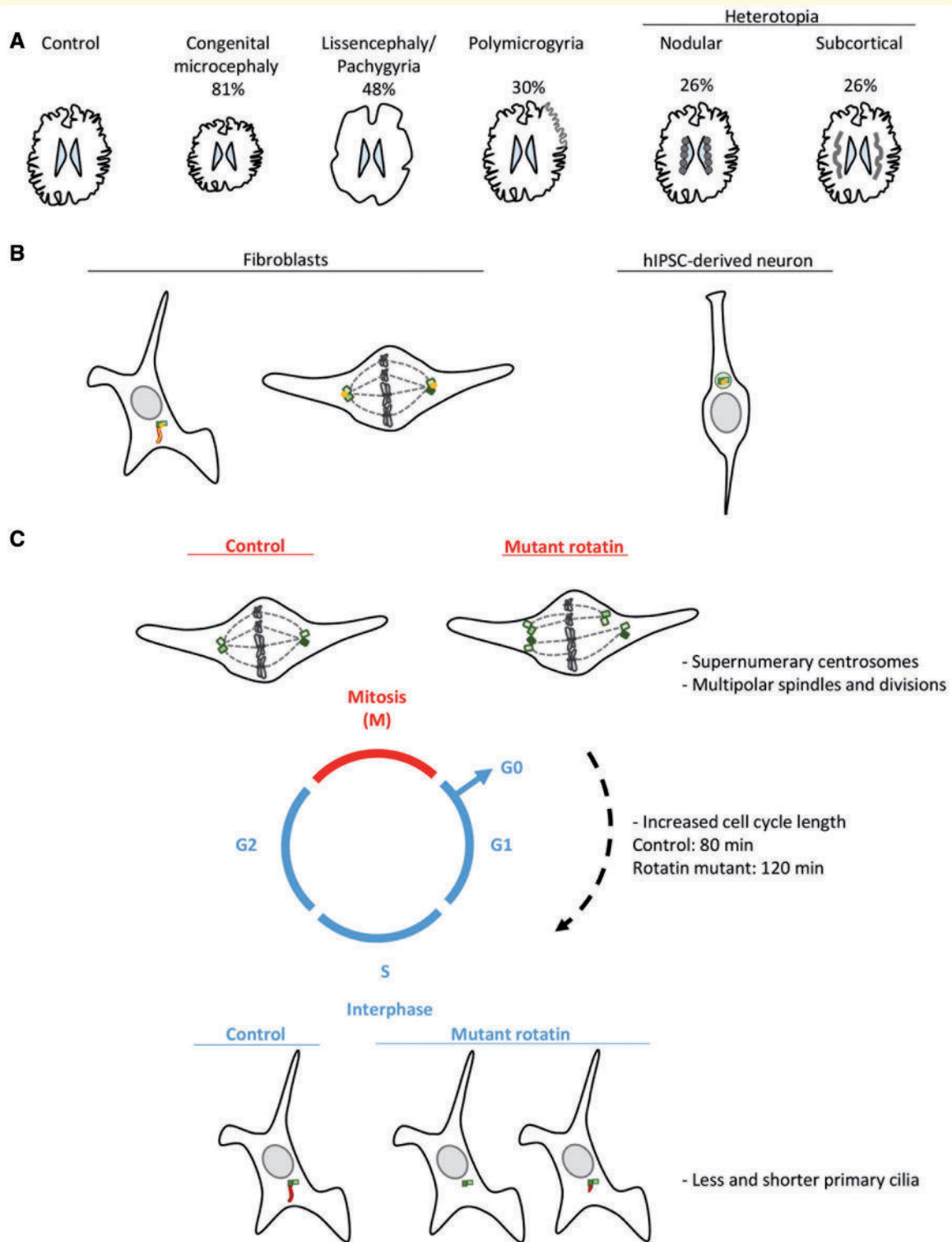


**Figure 1** Mutations in *RTTN* lead to subcellular anomalies during the cell cycle linked to a wide spectrum of cortical malformations. **(A)** Schematic representation of the different cortical malformations observed in *RTTN* patients, including the percentage of affected individuals (total of 23 patients from 13 families). **(B)** Rotatin subcellular localization in fibroblasts and human iPSC-derived neurons. Rotatin (yellow) was shown to co-localize with centrosomes (green) both during interphase and mitosis. During interphase it also co-localized with the primary cilium axoneme (red). In human iPSC-derived neurons it co-localized with the centrosome proximal to the nucleus. **(C)** Summary of subcellular phenotypes observed in patient fibroblasts in different stages of the cell cycle. hiPSC = human induced pluripotent stem cell.

mediate centrosome cohesion amongst other functions (Megraw *et al.*, 2011). Previous work in *Drosophila* suggested a role for the *RTTN* homologue *Ana3* in pericentriolar material recruitment and centrosome cohesion (Stevens *et al.*, 2009). Therefore, whilst overexpression of master regulators of centrosome duplication can cause amplification of this organelle, it is possible that downregulation of ‘cohesion-mediating proteins’ leads to centriole mis-segregation resulting in a similar phenotype. The DNA damage response can also be a cause or consequence of centrosome amplification linked to microcephaly, and anomalies in this process may contribute to the phenotypes observed. Several of the candidate partners of *RTTN* identified from a mass spectrometry screen in HEK293T cells are involved in this process.

Centrosome amplification may be cell-type specific (Marthiens *et al.*, 2012), thus it would be of interest to confirm that *RTTN* defects are present in neural progenitor cells. Searching for mitosis defects in neural progenitor cells in *RTTN*-mutant conditions would help further clarify how such a phenotype contributes to microcephaly. Previous studies in mouse neuroepithelium reported that the presence of supernumerary centrosomes in apical radial glial cells results in apoptosis, depleting the progenitor pool and thus contributing to a small brain size (Uzquiano *et al.*, 2018). Additionally, for cell cycle and apical radial glial daughter cell fate, increased cell cycle length is correlated with neurogenic divisions, which can result in precocious neuronal production and apical radial glial cell depletion (Uzquiano *et al.*, 2018). It is thus important to further explore abnormal *RTTN*-mutant apical radial glial cell dynamics to explain the microcephaly phenotype. Other processes influencing apical radial glial cell behaviour, such as spindle orientation, have also been associated with

microcephaly phenotypes in mouse mutants (Uzquiano *et al.*, 2018). Studying this in *RTTN*-mutant mouse brain or human *in vitro* models would complement characterization of mitosis phenotypes, and help clarify mutant mechanisms.

During interphase, the centrosome docks a primary cilium at the plasma membrane, allowing responses to signalling pathways, many of them known to be crucial for corticogenesis. Primary cilium defects, affecting number and/or length, were identified in patient fibroblasts (Fig. 1C). Nevertheless, fibroblasts of only three of eight patients showed functional anomalies (*GLI1* mRNA levels) when assessing stimulated activity of the SHH pathway. However, given the localization of *RTTN* both at the basal body and the primary cilium axoneme (Fig. 1B), together with the defective phenotypes reported, a wider range of approaches will most likely identify further functional alterations due to aberrant primary cilium-mediated signalling.

The presence of supernumerary centrosomes during mitosis warrants further assessment of the number of primary cilia per cell during interphase and in neurons. If this number is not above normal, this suggests that the mitotic centrosome amplification phenotype is not maintained in surviving daughter cells. Cell cycle-specific protein interactions may contribute to the supernumerary centrosome phenotype. Extra-centrosome clustering may also be stronger during interphase, in neurogenic progenitors and in neurons, overcoming the abnormal function of mutant *RTTN*. Future studies addressing numbers of cortical progenitor and neuronal cilia will help answer these questions.

Although neural interactors were not assessed in this work, *RTTN* centrosome-ciliary protein partners (some previously associated with ciliopathies) were identified. In addition, and as focused on by Vandervore *et al.*, the non-muscle myosin complex

appeared to be a significant interactor, including MYH10 (non-muscle myosin II, isoform NM II-B). This protein has previously been shown to be important for cell, including cerebellar neuron, migration (Ma *et al.*, 2004; Vicente-Manzanares *et al.*, 2009). Based on this function, Vandervore *et al.* were interested in the possible role of *RTTN* in neuronal migration, since defects in the latter could contribute to the cortical malformations observed in *RTTN* patients. In control iPSC-derived neurons (Fig. 1B), they showed *RTTN* and NM II-B to co-localize in the cytoplasm proximal to the nucleus. It would now be of interest to further assess *RTTN* mutant migrating neurons using such a model.

NM II-B has also been shown to mediate cell-cell adhesion and its activity is regulated by proteins including RhoA, deletion of which causes severe defects in the adherens junction belt, which anchors apical radial glial cells to each other (Vicente-Manzanares *et al.*, 2009; Uzquiano *et al.*, 2018). Additionally, mutations in *MYH10* have been reported in a patient with severe microcephaly (Tuzovic *et al.*, 2013). For these reasons, it is important to assess *RTTN* and its interactors in neuronal progenitors further. Also, using conditional knockout mice to target apical radial glial cells versus neurons would help discern the differential contribution of each cell type in the *RTTN* cortical malformation spectrum.

The cortex of gyrencephalic species is characterized by abundant, highly proliferative basal radial glial cells, possibly crucial for the appearance of gyri and sulci, and for the expansion of the neocortex during evolution. Basal radial glial cells perform basally directed somal translocation during mitosis. This process is mediated through a RhoA-ROCK-NM II-dependent mechanism, and interactors of this pathway have been associated with various cortical malformations (Ostrem *et al.*, 2017).

## Glossary

**Apical radial glia:** Main neuronal progenitor cell type responsible for production of the final neuronal output in the developing cortex. They also produce other progenitor cell types such as intermediate progenitors and basal radial glia. They have a polarized morphology with an apical process extending to the ventricles and a basal process reaching the pial surface, which serves as a substrate for migrating neurons.

**Axoneme:** A cytoskeletal structure made up of nine doublets of microtubules ('9 + 0').

**Basal body:** Modified centrioles associated with protein complexes that nucleate primary cilia.

**Centrosome:** The major microtubule organizing centre, composed of two barrel-like structures, the centrioles, which are surrounded by pericentriolar material.

**Centrosome cohesion:** Duplicated centrosomes are held together to form a single functional unit.

**DNA damage response:** Proteins that monitor DNA integrity can activate cell cycle checkpoints and DNA repair pathways in response to DNA damage.

**Flow cytometry:** Cell analysis technique that allows measurements of cells in solution as they pass by a laser. Different fluorescence parameters can be measured at the same time in a cell.

**Gyrencephalic species:** Species such as humans that exhibit folds in the cerebral cortex

**Homozygosity mapping:** A method for mapping recessive traits in consanguineous families, based on the identification of genomic regions linked to the disease.

**HEK293T cells:** Human ciliated embryonic kidney cells.

**iPSCs (induced pluripotent stem cells):** Cells derived from adult cells (often skin or blood) that have been reprogrammed into an embryonic-like pluripotent state. They can propagate and give rise to many cell types in the body.

**Mitotic somal translocation:** During mitosis, the soma translocates prior to cytokinesis.

**Nonsense-mediated RNA decay:** Cellular process by which mRNAs containing a premature stop codon are degraded.

**Primary cilium:** A microtubule-based antenna-like structure inserted in the plasma membrane that serves as a platform for signalling pathways.

**SHH:** Sonic hedgehog, a ligand activating the SHH signalling pathway.

**Whole exome sequencing:** Sequencing of the protein-coding regions of the genome.

**Whole genome sequencing:** Sequencing of all nucleotides in the genomic DNA of an organism.

These data, together with absent neocortical phenotypes in many cortical malformation gene mouse models, could suggest that basal radial glial cells are cellular targets in these disorders. Studying *RTTN* expression and function using gyrencephalic or 'human-like' models seems pertinent, given also the 'lissencephaly' phenotypes observed in some patients.

Vandervore and colleagues thus identify changes in the nature and/or amount of *RTTN* mRNAs as contributing to the variability of malformations, although at the cellular phenotype level there were no obvious further correlations identified. *RTTN* is nevertheless an important centrosomal-primary cilium protein dynamically changing its localization and mediating several subcellular processes, all of them interlinked and highly connected to correct cell division and cell cycle progression. Mutations could variably disrupt these processes in neural cells. Identification of new protein partners showing differential disruptions with mutant *RTTN* may

be important to further identify mechanisms. Concerning microcephaly, new studies addressing *RTTN* function and mutation specifically in neuronal progenitors would shed light on the aetiology of the disorder. Analysis of its role in specific neural populations should further help unravel the diverse mechanisms by which the different cortical phenotypes arise.

Ana Uzquiano<sup>1,2,3</sup> and Fiona Francis<sup>1,2,3</sup>

1 Sorbonne Université, UMR-S 1270,

F-75005, Paris

2 Inserm U 1270, Paris, France

3 Institut du Fer à Moulin, Paris, France

Correspondence to: Fiona Francis  
Institut du Fer à Moulin, 17 rue du Fer à  
Moulin, 75005, Paris, France  
E-mail: fiona.francis@inserm.fr

doi:10.1093/brain/awz048

## Competing interests

The authors report no competing interests.

## References

- Jayaraman D, Kodani A, Gonzalez DM, Mancias JD, Mochida GH, Vagnoni C, et al. Microcephaly proteins Wdr62 and Aspm define a mother centriole complex regulating centriole biogenesis, apical complex, and cell fate. *Neuron* 2016; 92: 813–28.
- Ma X, Kawamoto S, Hara Y, Adelstein RS. A point mutation in the motor domain of nonmuscle myosin II-B impairs migration of distinct groups of neurons. *Mol Biol Cell* 2004; 215: 2568–79.
- Marthiens V, Piel M, Basto R. Never tear us apart—the importance of centrosome clustering. *J Cell Sci* 2012; 125: 3281–92.
- Megraw TL, Sharkley JT, Nowakowski RS. Cdk5rap2 exposes the centrosomal root of microcephaly syndromes. *Trends Cell Biol* 2011; 21: 470–780.
- Ostrem B, Di Lullo E, Kriegstein A. oRGs and mitotic somal translocation—a role in development and disease. *Curr Opin Neurobiol* 2017; 42: 61–7.
- Stevens NR, Dobbelaere J, Wainman A, Gergely F, Raff JW. Ana3 is a conserved protein required for the structural integrity of centrioles and basal bodies. *J Cell Biol* 2009; 187: 355–63.
- Tuzovic L, Yu L, Zeng W, Li X, Lu H, Lu HM, et al. A human de novo mutation in MYH10 phenocopies the loss of function mutation in mice. *Rare Dis* 2013; 1: e26144.

Uzquiano A, Gladwyn-Ng I, Nguyen L, Reiner O, Gotz M, Matsuzaki F, et al. Cortical progenitor biology, cell cycling versus neurogenesis. *J Neurochem* 2018; 146: 500–25.

Vandervore L, Schot R, Kasteleijn E, Oegema R, Stouffs K, Gheldof A, et al. Heterogeneous clinical phenotypes and cerebral malformations reflected by Rotatin cellular dynamics. *Brain* 2019; 142: 868–85.

Vicente-Manzanares M, Ma X, Adelstein RS, Horwitz AR. Non-muscle myosin II takes centre stage in cell adhesion and migration. *Nat Rev Mol Cell Biol* 2009; 10: 778–90.

## Secondary progressive multiple sclerosis and the gut-brain axis

This scientific commentary refers to ‘Gut microbiota-dependent CCR9<sup>+</sup> CD4<sup>+</sup> T cells are altered in secondary progressive multiple sclerosis’, by Kadowaki *et al.* (doi:10.1093/brain/awz012).

The gut microbiota and the brain make strange bedfellows. Although radically different in nature and physically separated, they entertain most intimate functional relations. They regulate each other's functions in health, but in disease each may drive pathology in the other. This is the case in multiple sclerosis, where accumulating evidence indicates that signals from the gut microbiota spark an autoimmune attack on the white matter, while at the same time, the brain triggers changes in intestinal functions. In this issue of *Brain*, Kadowaki and co-workers shed new light on the immune pathogenesis of secondary progressive multiple sclerosis (SPMS) (Kadowaki *et al.*, 2019). They identify a subset of CD4<sup>+</sup> ‘helper’ T cells that are decreased in number and that tend to switch from a regulatory to a pro-inflammatory function in patients. These cells have two structures on their surface that indicate their affinity for the gut-associated lymphoid tissue (GALT), the immune organ that surrounds and directly interacts with the intestinal microbiota. The results of Kadowaki *et al.* suggest that a T cell population that may have been educated by gut microbes is altered in SPMS. This is an intriguing observation in two respects. First, it suggests an immune regulatory effect in SPMS, a disease stage with a disputed immune

pathogenesis, and second, it invokes a gut-homing T cell class as a cellular messenger of deviant signalling in the brain (Fig. 1).

In most patients, multiple sclerosis proceeds in two distinct phases. The disease commonly begins as serial bouts interspersed with remissions [relapsing-remitting multiple sclerosis (RRMS)]. A decade or so later, the disease may assume a progressive course without remissions (SPMS). SPMS and RRMS differ in key ways. First, the brain lesions change their structural patterns: in RRMS, inflammatory infiltrates sit mostly within the demyelinating lesions and the surrounding normal-appearing white matter, while in SPMS the invading cells accumulate preferentially in perivascular and leptomeningeal spaces (Lassmann, 2019). Most importantly, however, immune cell therapies, which substantially mitigate RRMS, are largely inefficient in SPMS. This has been ascribed to a change of pathomechanism, from adaptive to innate immune response or to autonomous neurodegeneration (Weiner, 2008). The discovery by Kadowaki *et al.* of an aberrant immune regulation redirects attention to the possible role of immune mechanisms also in SPMS.

A second key observation of the current work is of a link between immune regulation of SPMS and the GALT. Kadowaki *et al.* report a decrease in the CCR9<sup>+</sup> T cell subpopulation in the blood of patients with SPMS. These lymphocytes make up ~5% of the healthy circulating lymphocyte pool, but in patients with SPMS, this proportion drops to

roughly 3% on average, a subtle but significant change. In addition, in SPMS this reduced population of gut-experienced lymphocytes changes its functional phenotype. In contrast to their counterparts in healthy people, in SPMS most of the remaining CCR9<sup>+</sup> T cells assume an effector signature with increased expression of the transcription factor RORC, and increased production of interferon- $\gamma$  and the pro-inflammatory cytokine IL-17.

T cells are divided into numerous subclasses, dependent on their effector functions and their migratory behaviours. The SPMS-affected immune population is part of the CD4<sup>+</sup> T cell pool, which express on their membrane the chemokine receptor CCR9, along with the cell adhesion molecule,  $\alpha 4\beta 7$ . Both structures indicate a special affinity of migratory T cells for the GALT. CCR9 binds and responds preferentially to the chemokine CCL25 (TACK), which is produced in the gut by intestinal wall epithelial cells. It attracts CCR9<sup>+</sup> immune cells with the complementary receptor from the circulation to the gut (Hernandez-Ruiz and Zlotnik, 2017). Most CCR9<sup>+</sup> T cells also express the integrin  $\alpha 4\beta 7$ , a cell adhesion molecule that binds to the complementary gut-specific addressin MAdCAM, and by so doing captures incoming T cells within the gut milieu (Habtezion *et al.*, 2016). Thus, most blood circulating T cells co-expressing both CCR9 and  $\alpha 4\beta 7$  likely had a ‘gut history’, but it remains unclear how the CCR9<sup>+</sup> T cells later home to the brain. This question also arose a few years ago, when the

## Bibliography

Aaku-Saraste, E., Hellwig, A., and Huttner, W. B. (1996). "Loss of occludin and functional tight junctions, but not ZO-1, during neural tube closure--remodeling of the neuroepithelium prior to neurogenesis." *Dev Biol* 180: 664–679.

Adams, M., Simms, R. J., Abdelhamed, Z., Dawe, H. R., Szymanska, K., Logan, C. V., Wheway, G., Pitt, E., Gull, K., Knowles, M. A., Blair, E., Cross, S. H., Sayer J. A., Johnson, C. A. (2012). "A meckelin-filamin A interaction mediates ciliogenesis." *Hum Mol Genet* 21(6): 1272-1286.

Al-Jaberi, N., Lindsay, S., Sarma, S., Bayatti, N. and Clowry, G.J. (2015). "The early fetal development of human neocortical GABAergic interneurons." *Cereb Cortex*, 25: 631-645.

Alcantara, D., Timms, A. E., Gripp, K., Baker, L., Park, K., Collins, S., Cheng, C., Stewart, F., Mehta, S. G., Saggari, A., Sztriha, L., Zombor, M. et al. (2017). "Mutations of AKT3 are associated with a wide spectrum of developmental disorders including extreme megalencephaly." *Brain* 140(10): 2610-2622.

Alexandre, P., Reugels, A.M., Barker, D., Blanc, E. and Clarke, J.D. (2010). "Neurons derive from the more apical daughter in asymmetric divisions in the zebrafish neural tube." *Nat Neurosci* 13: 673-679.

Al-Jaberi, N., Lindsay, S., Sarma, S., Bayatti, N. and Clowry, G.J. (2015) "The early fetal development of human neocortical GABAergic interneurons." *Cereb Cortex*, 25: 631-645.

Alfano, C., Studer, M. (2013). "Neocortical arealization: evolution, mechanisms, and open questions." *Dev Neurobiol* 73(6): 411-447.

Alkuraya, F. S., Cai, X., Emery, C., Mochida, G. G., Al-Dosari, M. S., Felie, J. M., Hill, R. S., Barry, B. J., Partlow, J. N., Gascon, G. G., Kentab, A., Jan, M., Shaheen, R., Feng, Y., Walsh, C. A. (2011). "Human mutations in NDE1 cause extreme microcephaly with lissencephaly." *Am J Hum Genet* 88(5): 536-547.

Allen, N. J., Lyons, D. A. (2018) "Glia as architects of central nervous system formation and function." *Science* 362(6411): 181-185.

Andreu-Cervera, A., Anselme, I., Karam, A., Laclef, C., Catala, M., Schneider-Maunoury, S. (2019). "The ciliopathy gene *ftm/rpgr1p1l* controls mouse forebrain patterning via region-specific modulation of hedgehog/gli signaling." *J Neurosci* pii: 2199-18

Anton-Bolanos, N., A., Lopez-Bendito, G. (2018). "Developmental interactions between thalamus and cortex: a true love reciprocal story." *Curr Opin Neurobiol* 52: 33-41.

Arai, Y., Pierani, A. (2014). "Development and evolution of cortical fields." *Neurosci Res* 86: 66-76.

Arai, Y., Pulvers, J. N., Haffner, C., Schilling, B., Nusslein, I., Calegari, F., Huttner, W. B. (2011). "Neural stem and progenitor cells shorten S-phase on commitment to neuron production." *Nat Commun* 2: 154.

Arbeille, E., Reynaud, F., Sanyas, I., Bozon, M., Kindbeiter, K., Causeret, F., Pierani, A., Falk, J., Moret, F., Castellani, V. (2015). "Cerebrospinal fluid-derived Semaphorin3B orients neuroepithelial cell divisions in the apicobasal axis." *Nat Commun* 6: 6366.

Ardestani, A., Lupse, B., Maedler, K. (2018). "Hippo signaling: key emerging pathway in cellular and whole-body metabolism." *Trends Endocrinol Metab* 29(7): 492-509.

Armentano, M., Chou, S.-J., Tomassy, G. S., Leingärtner, A., O'Leary, D. D. M., and Studer, M. (2007). "COUP-TFI regulates the balance of cortical patterning between frontal/motor and sensory areas". *Nat Neurosci* 10: 1277–1286.

Asada, M., Irie, K., Yamada, A., Takai, Y. (2004). "Afadin and  $\alpha$ -actinin-binding protein ADIP directly binds  $\beta'$ -COP, a subunit of the coatomer complex." *Biochem and Biophys Res Comm*, 321, 350–354.

Asami, M., Pilz, G. A., Ninkovic, J., Godinho, L., Schroeder, T., Huttner W. B., Gotz, M. (2011). "The role of Pax6 in regulating the orientation and mode of cell division of progenitors in the mouse cerebral cortex." *Development* 138(23): 5067-5078.

Assimacopoulos, S., Grove, E. A., Ragsdale, C. W. (2003). "Identification of a Pax6- dependent epidermal growth factor family signaling source at the lateral edge of the embryonic cerebral cortex." *J Neurosci* 23: 6399–6403.

Assimacopoulos, S., Kao, T., Issa, N. P., Grove, E. A. (2012). "Fibroblast growth factor 8 organizes the neocortical area map and regulates sensory map topography." *J Neurosci* 32(21): 7191-7201.

Bae, B.-I., Tietjen, I., Atabay, K. D., Evrony, G. D., Johnson, M. B., Asare, E., et al. (2014). "Evolutionarily dynamic alternative splicing of GPR56 regulates regional cerebral cortical patterning." *Science* 343: 764–768.

Bagley, J. A., Reumann, D., Bian, S., Lévi-Strauss, J., Knoblich, J. A. (2017). "Fused cerebral organoids model interactions between brain regions." *Nat Methods* 14(7): 743-751.

Bahi-Buisson, N., Poirier, K., Boddaert, N., Fallet-Bianco, C., Specchio, N., Bertini, E., et al. (2010). "GPR56-related bilateral frontoparietal polymicrogyria: further evidence for an overlap with the cobblestone complex." *Brain* 133 : 3194–3209.

Bahi-Buisson, N., Poirier, K., Boddaert, N., Saillour, Y., Castelnau, L., Philip, N., et al. (2008). "Refinement of cortical dysgeneses spectrum associated with TUBA1A mutations." *J Med Genet* 45: 647–653.

Bahi-Buisson, N., Souville, I., Fourniol, F. J., Toussaint, A., Moores, C. A., Houdusse, A., Lemaitre, J. Y., Poirier, K., Khalaf-Nazzal, R., Hully, M., Leger, P. L. (2013). "New insights into genotype-phenotype correlations for the doublecortin-related lissencephaly spectrum." *Brain* 136 (Pt 1): 223-244.

Bakircioglu, M., Carvalho, O. P., Khurshid, M., Cox, J., J., Tuysuz, B., Barak, T., Yilmaz, S., Caglayan, O., Dincer, A., Nicholas, A. K., et al. (2011). "The Essential Role of Centrosomal NDE1 in Human Cerebral Cortex Neurogenesis." *The American Journal of Human Genetics* 88(5): 523-535.

Beattie, R., Postiglione, M., P., Burnett, L. E., Laukoter, S., Streicher, C., Pauler, F. M., Xiao, G., Klezovitch, O., Vasioukhin, V., Ghashghaei, T. H., Hippenmeyer, S. (2017). "Mosaic Analysis with Double Markers Reveals Distinct Sequential Functions of Lgl1 in Neural Stem Cells." *Neuron* 94(3): 517-533 e513.

Bechstedt, S., Albert, J. T., Kreil, D. P., Müller-Reichert, T., Göpfert, M. C., Howard, J. (2010). "A doublecortin containing microtubule-associated protein is implicated in mechanotransduction in *Drosophila* sensory cilia." *Nat Commun* 12, 1:11.

Bernabe-Rubio, M., Alonso, M. A. (2017). "Routes and machinery of primary cilium biogenesis." *Cell Mol Life Sci* 74(22): 4077-4095.

Bernabe-Rubio, M., Andres, G., Casares-Arias, J., Fernandez-Barrera, J., Rangel, L., Reglero-Real, N., Gershlick, D. C., Fernandez, J. J., Millan, J., Correas, I., Miguez, D. G., Alonso, M. A. (2016). "Novel role for the midbody in primary ciliogenesis by polarized epithelial cells." *J Cell Biol* 214(3): 259-273.

Bernier, R., Golzio, C., Xiong, B., Stessman, H. A., Coe, B. P., Penn, O., Witherspoon, K., Gerdt, J., Baker, C., Vulto-van Silfhout, A. T. et al. (2014). "Disruption CHD8 mutations define a subtype of autism early in development." *Cell* 158(2): 263-276.

Bershteyn, M., Nowakowski, T. J., Pollen, A. A., Di Lullo, E., Nene, A., Wynshaw-Boris, A., Kriegstein, A. R. (2017). "Human iPSC-Derived Cerebral Organoids Model Cellular Features of

Lissencephaly and Reveal Prolonged Mitosis of Outer Radial Glia." *Cell Stem Cell* 20(4): 435-449 e434.

Bertipaglia, C., Gonçalves, J. C., Vallee, R. B. (2018). "Nuclear migration in mammalian brain development." *Semin Cell Dev Biol* 82: 57-66.

Besse, L., Neti, M., Anselme, I., Gerhardt, C., Rütger, U., Laclef, C., Schneider-Maunoury, S. (2011). Primary cilia control telencephalic patterning and morphogenesis via Gli3 proteolytic processing." *Development*, 138(10): 2079-2088.

Betizeau, M., Cortay, V., Patti, D., Pfister, S., Gautier, E., Bellemin-Menard, A., Afanassieff, M., Huissoud, C., Douglas, R. J., Kennedy, H., Dehay, C. (2013). "Precursor diversity and complexity of lineage relationships in the outer subventricular zone of the primate." *Neuron* 80(2): 442-457.

Bielle, F., Griveau, A., Narboux-Nême, N., Vigneau, S., Sigrist, M., Arber, S., et al. (2005). "Multiple origins of Cajal-Retzius cells at the borders of the developing pallium." *Nat Neurosci* 8: 1002–1012.

Bilgüvar, K., Oztürk, A. K., Louvi, A., Kwan, K. Y., Choi, M., Tatli, B. Yalnizoglu, D., Tüysüz, B., Caglayan, A. O., Gökben, S., Kaymakçalan, H., Barak, T., et al. (2010). "Whole-exome sequencing identifies recessive WDR62 mutations in severe brain malformations." *Nature* 467(7312): 207-210.

Binder, J. R. (2015). "The Wernicke area: modern evidence and a reinterpretation." *Neurology* 85(24): 2170-2175.

Birey, F., Andersen, J., Makinson, C. D., Islam, S., Wei, W., Huber, N., Fan, H. C., Metzler, K. R. C., Panagiotakos, G., Thom, N., O'Rourke, N. A., et al. (2017). "Assembly of functionally integrated human forebrain spheroids." *Nature* 545(7652): 54-59.

Bishop, K. M., Goudreau, G., and O'Leary, D. D. (2000). "Regulation of area identity in the mammalian neocortex by Emx2 and Pax6." *Science* 288: 344–349

Bishop, K. M., Rubenstein, J. L. R., and O'Leary, D. D. M. (2002). "Distinct actions of Emx1, Emx2, and Pax6 in regulating the specification of areas in the developing neocortex." *J Neurosci* 22: 7627–7638.

Bisschoff, I. J., Zeschngk, C., Horn, D., Wellek, B. Rier, A., Wessels, M., Willems, P., Jensen, P., Busche, A., Bekkebraten, K., et al. (2013). "Novel mutations including deletions of the entire OFD1 gene in 30 families with type 1 orofacioidigital syndrome: a study of extensive clinical variability." *Hum Mutat* 34(1): 237-247.



Bizzotto, S., Francis, F. (2015). "Morphological and functional aspects of progenitors perturbed in cortical malformations." *Front Cell Neurosci* 9: 30.

Bizzotto, S., Uzquiano, A., Dingli, F., Ershov, D., Houllier, A., Arras, G., Richards, M., Loew, D., Minc, N., Croquelois, A. et al. (2017). "Eml1 loss impairs apical progenitor spindle length and soma shape in the developing cerebral cortex." *Sci Rep* 7: 17308.

Bogen, J. E., Bogen, G. M. (1976). "Wernicke's region--Where is it?" *Ann N Y Acad Sci* 280: 834–843.

Boncompain, G., Divoux, S., Gareil, N., de Forges, H., Lescure, A., Latreche, L., Mercanti, V., Jollivet, F., Raposo, G., Perez, F. (2012). "Synchronization of secretory protein traffic in populations of cells." *Nat Methods* 9(5): 493-498.

Boncompain, G., Perez, F. (2013). "Fluorescence-based analysis of trafficking in mammalian cells." *Methods Cell Biol* 118: 179-1994.

Bond, J., Roberts, E., Springell, K., Lizarraga, S. B., Scott, S., Higgins, J., Hampshire, D. J., Morrison, E. E., Leal, G. F., et al. (2005). "A centrosomal mechanism involving CDK5RAP2 and CENPJ controls brain size." *Nat Genet* 37(4): 353-355.

Borrell, V., Calegari, F. (2014). "Mechanisms of brain evolution: regulation of neural progenitor cell diversity and cell cycle length." *Neurosci Res* 86: 14-24.

Borrell, V., Gotz, M. (2014). "Role of radial glial cells in cerebral cortex folding." *Curr Opin Neurobiol* 27: 39-46.

Borrell, V., Cardenas, A., Ciceri, G., Galceran, J., Flames, N., Pla, R., Nobrega-Pereira, S., Garcia-Frigola, C., Peregrin, S., Zhao, Z. et al. (2012). "Slit/Robo signaling modulates the proliferation of central nervous system progenitors." *Neuron* 76: 338-352.

Brisch, E., Daggett, M. A., and Suprenant, K. A. (1996). "Cell cycle-dependent phosphorylation of the 77 kDa echinoderm microtubule-associated protein (EMAP) in vivo and association with the p34cdc2 kinase." *J Cell Sci* 109 (Pt 12): 2885–2893.

Broix, L., Asselin, L., Silva, C. G., Ivanova, E. L., Tilly, P., Gilet, J. G., Lebrun, N., Jagline, H., Muraca, G., Saillour, Y., et al. (2018). "Ciliogenesis and cell cycle alterations contribute to KIF2A-related malformations of cortical development." *Hum Mol Genet* 27(2): 224-238.

Broix, L., Jagline, H., Ivanova, E., Schmucker, S., Drouot, N., Clayton-Smith, J., Pagnamenta, A. T., Metcalfe, K. A., Isidor, B., Louvier, U. W. et al. (2016). "Mutations in the HECT domain of NEDD4L lead to AKT-mTOR pathway deregulation and cause periventricular nodular heterotopia." *Nat Genet* 48(11): 1349-1358.

Brown, J., Quadrato, G., Arlotta, P. (2018). "3D cell culture models of human brain development and disease." *Curr Top Dev Biol* 129: 99-122.

Buchman, J. J., Tseng, H. C., Zhou, Y., Frank, C. L., Xie, Z., Tsai, L. H. (2010). "Cdk5rap2 interacts with pericentrin to maintain the neural progenitor pool in the developing neocortex." *Neuron* 66(3): 386-402.

Buchsbaum, I. Y., Cappello, S. (2019). "Neuronal migration in the CNS during development and disease: insights from in vivo and in vitro models." *Development* 146(1).

Bulchand, S., Grove, E. A., Porter, F. D., and Tole, S. (2001). "LIM-homeodomain gene *Lhx2* regulates the formation of the cortical hem." *Mech Dev* 100: 165–175.

Bultje, R. S., Castaneda-Castellanos, D. R., Jan, L. Y., Jan, Y. N., Kriegstein A. R., Shi, S. H. (2009). "Mammalian Par3 regulates progenitor cell asymmetric division via notch signaling in the developing neocortex." *Neuron* 63(2): 189-202.

Buysse, K., Riemersma, M., Powell, G., van Reeuwijk, J., Chitayat, D., Roscioli, T., et al. (2013). "Missense mutations in  $\beta$ -1,3-N-acetylglucosaminyltransferase 1 (B3GNT1) cause Walker-Warburg syndrome." *Hum Mol Genet* 22: 1746–1754.

Cadwell, C. R., Scala, F., Fahey, P., Kobak, D., Sinz, H., Johnson, P., Li, S., Cotton, R. J., Sandberg, R., Berens, P., Jiang, X., Tolias, A. S. (2019). "Cell type composition and circuit organization of neocortical radial clones." *BioRxiv*, 526681.

Cai, S., Weaver, L. N., Ems-McClung, S. C., Walczak, C. E. (2009). "Kinesin-14 family proteins HSET/XCTK2 control spindle length by cross-linking and sliding microtubules." *Mol Biol Cell* 20(5): 1348-1359.

Calegari, F., Haubensak, W., Haffner, C., Huttner, W. B. (2005). "Selective lengthening of the cell cycle in the neurogenic subpopulation of neural progenitor cells during mouse brain development." *J Neurosci* 25(28): 6533-6538.

Calegari, F., Huttner, W. B. (2003). "An inhibition of cyclin-dependent kinases that lengthens, but does not arrest, neuroepithelial cell cycle induces premature neurogenesis." *J Cell Sci* 116(Pt 24): 4947-4955.

Camargo-Ortega, G., Falk, S., Johansson, P. A., Peyre, E., Broix, L., Sahu, S. K., Hirst, W., Schichthaerle, T., de Juan Romero, C., Draganova, K., et al. (2019). "The centrosome protein AKNA regulates neurogenesis via microtubule organization." *Nature*, doi: 10.1038/s41586-019-0962-4.

Campi, K. L., Collins, C. E., Todd, W. D., Kaas, J., and Krubitzer, L. (2011). "Comparison of area 17 cellular composition in laboratory and wild-caught rats including diurnal and nocturnal species." *Brain Behav Evol* 77: 116–130.

Campi, K. L., and Krubitzer, L. (2010). "Comparative studies of diurnal and nocturnal rodents: differences in lifestyle result in alterations in cortical field size and number." *J Comp Neurol* 518: 4491–4512.

Cappello, S., Attardo, A., Wu, X., Iwasato, T., Itohara, S., Wilsch-Brauninger, M., Eilken, H. M., Rieger, M. A., Schroeder, T. T., Huttner, W. B., Brakebusch, C., Gotz, M. (2006). "The Rho-GTPase cdc42 regulates neural progenitor fate at the apical surface." *Nat Neurosci* 9(9): 1099-1107.

Cappello, S., Bohringer, C. R., Bergami, M., Conzelmann, K. K., Ghanem, A., Tomassy, G. S., Arlotta, P., Mainardi, M., Allegra, M., Caleo, M., van Hengel, J., Brakebusch, C., Gotz, M. (2012). "A radial glia-specific role of RhoA in double cortex formation." *Neuron* 73(5): 911-924.

Cappello, S., Gray, M. J., Badouel, C., Lange, S., Einsiedler, M., Srour, M., Chitayat, D., Hamdan, F. F., Jenkins, Z. A., Morgan, T. et al. (2013). "Mutations in genes encoding the cadherin receptor-ligand pair DCHS1 and FAT4 disrupt cerebral cortical development." *Nat Genet* 45(11): 1300-1308.

Carabalona, A., Beguin, S., Pallesi-Pocachard, E., Buhler, E., Pellegrino, C., Arnaud, K., Hubert, P., Oualha, M., Siffroi, J. P., Khantane, S., et al. (2012). "A glial origin for periventricular nodular heterotopia caused by impaired expression of Filamin-A." *Hum Mol Genet* 21(5): 1004-1017.

Castejon, O. J., Diaz, M., Valero, C. (1994). "Ultrastructural alterations of Golgi apparatus in the nerve cells of cerebral cortex in human hydrocephalus. A qualitative study using cortical biopsies." *Scanning Microsc* 8(1): 89-96.

Cavallin, M., Bery, A., Maillard, C., Salomon, L. J., Bole, C., Reilly, M. L., Nitschké, P., Boddaert, N., Bahi-Buisson. (2018). "Recurrent RTTN mutation leading to severe microcephaly, polymicrogyria and growth restriction." *Eur J Med Genet* 61(2): 755-758.

Cavallin, M., Bijlsma, E., K., El Morjani, A., Moutton, S., Peeters, E. A., Maillard, C., Pedespan, J. M., Guerrot, A. M., Drouin-Garaud, V., Coubes, C. et al. (2017). "Recurrent KIF2A mutations are responsible for classic lissencephaly." *Neurogenetics* 18(2): 73-79.

Chenn, A., McConnell, S.K. (1995). "Cleavage orientation and the asymmetric inheritance of Notch1 immunoreactivity in mammalian neurogenesis." *Cell* 82: 631–641.

Chenn, A., Walsh, C. A. (2002). "Regulation of cerebral cortical size by control of cell cycle exit in neural precursors." *Science* 297: 365–369.

Chou, S. J., Babot, Z., Leingärtner, A., Studer, M., Nakagawa, Y., and O’Leary, D. D. M. (2013). "Geniculocortical input drives genetic distinctions between primary and higher-order visual areas." *Science* 340: 1239–1242.

Colonna, M., Butovsky, O. (2017). "Microglia Function in the Central Nervous System During Health and Neurodegeneration." *Annu Rev Immunol* 35: 441-468.

Costa, M. R., Wen, G., Lepier, A., Schroeder, T., Gotz, M. (2008). "Par-complex proteins promote proliferative progenitor divisions in the developing mouse cerebral cortex." *Development* 135(1): 11-22.

Croquelois, A., Giuliani, F., Savary, C., Kielar, M., Amiot, C., Schenk, F., Welker, E. (2009). "Characterization of the HeCo mutant mouse: a new model of subcortical band heterotopia associated with seizures and behavioral deficits." *Cereb Cortex* 19(3): 563-575.

Colas, J. F., Schoenwolf, G. C. (2001). "Towards a cellular and molecular understanding of neurulation." *Dev Dyn* 221: 117–145.

Cooper, A. F., Yu, K. P., Brueckner, M., Brailey, L. L., Johnson, L., McGrath, J. M., Bale, A. E. (2005). "Cardiac and CNS defects in a mouse with targeted disruption of suppressor of fused." *Development* 132(19): 4407-4417.

Copeland, S. J., McRae, A., Guarguaglini, G., Trinkle-Mulcahy, L., Copeland, J. W. (2018). "Actin-dependent regulation of cilia length by the inverted formin FHDC1." *Mol Biol Cell* 29(13): 1611-1627.

Corbit, K. C., Aanstard, P., Singla, V., Norman, A. R., Stainier, D. Y., Reiter, J. F. (2005). "Vertebrate Smoothed functions at the primary cilium." *Nature* 437(7061): 1018-1021.

Corbo, J. C., Deuel, T. A., Long, J. M., LaPorte, P., Tsai, E., Wynshaw-Boris, A., et al. (2002). "Doublecortin is required in mice for lamination of the hippocampus but not the neocortex." *J Neurosci* 22: 7548–7557.

Cotney, J., Muhle, R. A., Sanders, S. J., Liu, L., Willsey, A. J., Niu, W., Liu, W., Klei, L., Lei, J., Yin, J., et al. (2015). "The autism-associated chromatin modifier CHD8 regulates other autism risk genes during human neurodevelopment." *Nat Commun* 10(6): 6404.

Crossley, P. H., Martin, G. R. (1995). "The mouse *Fgf8* gene encodes a family of polypeptides and is expressed in regions that direct outgrowth and patterning in the developing embryo." *Development* 121, 439–451.

Cuberos, H., Vallée, B., Vourc'h, P., Tastet, J., Andres, C. R., Bénédicti, H. (2015). "Roles of LIM kinases in central nervous system function and dysfunction." *FEBS Lett* 589(24 Pt B): 3795-3806.

Cushion, T. D., Paciorkowski, A. R., Pilz, D. T., Mullins, J. G., Seltzer, L. E., Marion, R. W., Tuttle, E., Ghoneim, D., Christian, S. L., Chung, S. K., Rees, M. I., Dobyns, W. B. (2014). "De novo mutations in the beta-tubulin gene TUBB2A cause simplified gyral patterning and infantile-onset epilepsy." *Am J Hum Genet* 94(4): 634-641.

Dafinger, C., Liebau, M. C., Elsayed, S. M., Hellenbroich, Y., Boltshauser, E., Korenke, G. C., Fabretti, F., Janecke, A. R., Ebermann, I., Nürnberg, G., et al. (2011). "Mutations in KIF7 link Joubert syndrome with Sonic Hedgehog signaling and microtubule dynamics." *J Clin Invest* 121(7): 2662-2667.

Darnell, D., Gilbert, S. F. (2017). "Neuroembryology." *Wiley Interdiscip Rev Dev Biol* 6 (1).

Davish, H., Esmaeeli-Nieh, S., Monajemi, G. B., Mohseni, M., Ghasemi-Firouzabadi, S., Abedini, S. S., Bahman, I., Jamali, P., Azimi, S., Mojahedi, F., et al. (2010). "A clinical and molecular genetic study of 112 Iranian families with primary microcephaly." *J Med Genet* 47(12): 823-828.

D'Arcangelo, G., Miao, G. G., Chen, S. C., Soares, H. D., Morgan, J. I. Curran, T. (1995). "A protein related to extracellular matrix proteins deleted in the mouse mutant reeler." *Nature* 374: 719–723.

de Juan Romero, C., Bruder, C., Tomasello, U., Sanz-Anquela, J. M., Borrell, V. (2015). "Discrete domains of gene expression in germinal layers distinguish the development of gyrencephaly." *EMBO J* 34(14): 1859-1874.

De Keersmaecker, K., Graux, C., Odero, M. D., Mentens, N., Somers, R., Maertens, J., et al. (2005). "Fusion of EML1 to ABL1 in T-cell acute lymphoblastic leukemia with cryptic t(9;14)(q34;q32)." *Blood* 105: 4849–4852.

Del Giudice, E., Macca, M., Imperati, F., D'Amico, A., Parent, P., Pasquier, L., Layet, V., Lyonnet, S., Stamboul-Darmency, V., Thauvin-Robinet, C., Franco, B. (2014). "CNS involvement of OFD1 syndrome: a clinical, molecular, and neuroimaging study." *Orphanet J Rare Dis* 9:74.

Del Toro, D., Ruff, T., Cederfjall, E., Villalba, A., Seyit-Bremer, G., Borrell, V., Klein, R. (2017). "Regulation of Cerebral Cortex Folding by Controlling Neuronal Migration via FLRT Adhesion Molecules." *Cell* 169(4): 621-635 e616.

des Portes, V., Carrié, A., Billuart, P., Kieffer, V., Bienvenu, T., Vinet, M. C., et al. (1998a). "Inherited microdeletion in Xp21.3-22.1 involved in non-specific mental retardation." *Clin Genet* 53 : 136-141.

des Portes, V., Francis, F., Pinard, J. M., Desguerre, I., Moutard, M. L., Snoeck, I., et al. (1998b). "Doublecortin is the major gene causing X-linked subcortical laminar heterotopia (SCLH)." *Hum Mol Genet* 7: 1063-1070.

deAzevedo, L. C., Fallet, C., Moura,-Neto, V., Dumas-Duport, C., Hedin-Pereira, C. Lent, R. (2003). "Cortical radial glial cells in humans fetuses: depth-correlated transformation into astrocytes." *J Neurobiol* 55(3): 288-298.

Delaunay, D., Cortay, V., Patti, D., Knoblauch, K., Dehay, C. (2014). "Mitotic spindle asymmetry: a Wnt/PCP-regulated mechanism generating asymmetrical division in cortical precursors." *Cell Rep* 6(2): 400-414.

Desai, A. R., McConnell, S. K. (2000). "Progressive restriction in fate potential by neural progenitors during cerebral cortical development." *Development* 127: 2863-2872.

Di Donato, N., Timms, A. E., Aldinger, K. A., Mirzaa, G. M., Bennett, J. T., Collins, S., Olds, C., Mei, D., Chiari, S., Carvill, G., et al., (2018). "Analysis of 17 genes detects mutations in 81% of 811 patients with lissencephaly." *Genet Med* 20(11): 1354-1364.

Di Lullo, E., Kriegstein, A.R. (2017). "The use of brain organoids to investigate neural development and disease." *Nat Rev Neurosci* 18: 573-584.

di Pietro, F., Echard, A., Morin, X. (2016). "Regulation of mitotic spindle orientation: an integrated view." *EMBO Rep* 17(8): 1106-1130.

Ding, W., Wu, A., Sun, L., Pan, N. C., Wang, X. (2019). "Cenpj regulates cilia disassembly and neurogenesis in the developing mouse cortex." *J Neurosci* pii: 1849-18.

Dubreuil, V., Marzesco, A. M., Corbeil, D., Huttner, W. B., Wilsch-Brauninger, M. (2007). "Midbody and primary cilium of neural progenitors release extracellular membrane particles enriched in the stem cell marker prominin-1." *J Cell Biol* 176(4): 483-495.

Dudok, J. J., Murtaza, M., Henrique Alves, C., Rashbass, P., Wijnholds, J. (2016). "Crumbs 2 prevents cortical abnormalities in mouse dorsal telencephalon." *Neurosci Res* 108: 12-23.

Dulabon, L., Olson, E. C., Taglienti, M. G., Eisenhuth, S., McGrath, B., Walsh, C. A., Kreidberg, J. A., Anton, E. S. (2000). "Reelin binds  $\alpha 3\beta 1$  integrin and inhibits neuronal migration." *Neuron* 27: 33-44.

Durak, O., Gao, F., Kaeser-Woo, Y. J., Rueda, R., Martorell, A. J., Nott, A., Liu, C. Y., Watson, L. A., Tsai, L. H. (2016). "Chd8 mediates cortical neurogenesis via transcriptional regulation of cell cycle and Wnt signaling." *Nat Neurosci* 19(11): 1477-1488.

Eckler, M. J., Nguyen, T. D., McKenna, W. L., Fastow, B. L., Guo, C., Rubenstein, J. L. R., Chen, B. (2015). "Cux2-positive radial glial cells generate diverse subtypes of neocortical projection neurons and macroglia." *Neuron* 86(4): 1100-1108.

Eichenmüller, B., Everley, P., Palange, J., Lepley, D., and Suprenant, K. A. (2002). "The human EMAP-like protein-70 (ELP70) is a microtubule destabilizer that localizes to the mitotic apparatus." *J Biol Chem* 277: 1301–1309.

Elias, L. A., Kriegstein, A. R. (2008). "Gap junctions: multifaceted regulators of embryonic cortical development." *Trends Neurosci* 31(5): 243-250.

Endicott, S. J., Basu, B., Khokha, M., Brueckner, M. (2015). "The NIMA-like kinase Nek2 is a key switch balancing cilia biogenesis and resorption in the development of left-right asymmetry." *Development* 42(23): 4068-4079.

Endoh-Yamagami, S., Evangelista, M., Wilson, D., Wen, X., Theunissen, J. W., Phamluong, K., Davis, M., Scales, S. J., Solloway, M. J., de Sauvage, F. J., Peterson, A. S. (2009). "The mammalian Cos2 homolog Kif7 plays an essential role in modulating Hh signal transduction during development." *Curr Biol* 19(15): 1320-1326.

Englund, C., Fink, A., Lau, C., Pham, D., Daza, R. A., Bulfone, A., Kowalczyk, T. and Hevner, R. F. (2005). "Pax6, Tbr2, and Tbr1 are expressed sequentially by radial glia, intermediate progenitor cells, and postmitotic neurons in developing neocortex." *J Neurosci* 25, 247-251.

Falk, S., Bugeon, S., Ninkovic, J., Pilz, G. A., Postiglione, M. P., Cremer, H., Knoblich, J. A., Gotz, M. (2017). "Time-Specific Effects of Spindle Positioning on Embryonic Progenitor Pool Composition and Adult Neural Stem Cell Seeding." *Neuron* 93(4): 777-791 e773.

Fallet-Bianco, C., Loeuillet, L., Poirier, K., Loget, P., Chapon, F., Pasquier, L., et al. (2008). "Neuropathological phenotype of a distinct form of lissencephaly associated with mutations in TUBA1A." *Brain* 131: 2304-2320.

Farrell, M. A., DeRosa, M. J., Curran, J. G., Secor, D. L., Cornford, M. E., Comair, Y. G., et al. (1992). "Neuropathologic findings in cortical resections (including hemispherectomies) performed for the treatment of intractable childhood epilepsy." *Acta Neuropathol* 83: 246-259.

Feng, Y., Walsh, C. A. (2004). "Mitotic spindle regulation by Nde1 controls cerebral cortical size." *Neuron* 44(2): 279-293.

Ferland, R. J., Batiz, L. F., Neal, J., Lian, G., Bundock, E., Lu, J., Hsiao, Y. C., Diamond, R., Mei, D., Banham, A. H. et al. (2009). "Disruption of neural progenitors along the ventricular and subventricular zones in periventricular heterotopia." *Hum Mol Genet* 18(3): 497-516.

Fernandez, V., Llinares-Benadero, C., Borrell, V. (2016). "Cerebral cortex expansion and folding: what have we learned?" *EMBO J* 35(10): 1021-1044.

Fiddes, I. T., Lodewijk, G. A., Mooring, M., Bosworth, C. M., Ewing, A. D., Mantalas, G. L., Novak, A. M., van den Bout, A., Bishara, A., Rosenkrantz, J. L. et al. (2018). "Human-Specific NOTCH2NL Genes Affect Notch Signaling and Cortical Neurogenesis." *Cell* 173(6): 1356-1369 e1322.

Fietz, S. A., Kelava, I., Vogt, J., Wilsch-Brauninger, M., Stenzel, D., Fish, J. L., Corbeil, D., Riehn, A., Distler, W., Nitsch, R., Huttner, W. B. (2010). "OSVZ progenitors of human and ferret neocortex are epithelial-like and expand by integrin signaling." *Nat Neurosci* 13(6): 690-699.

Fiorillo, C., Moro, F., Yi, J., Weil, S., Brisca, G., Astrea, G., Severino, M., Romano, A., Battini, R., Rossi, A., Minetti, C., Bruno, C., Santorelli, F. M., Vallee, R. (2014). "Novel dynein DYNC1H1 neck and motor domain mutations link distal spinal muscular atrophy and abnormal cortical development." *Human Mutat* 35(3): 298-302.

Fish, J. L., Kosodo, Y., Enard, W., Paabo, S., Huttner, W. B. (2006). "Aspm specifically maintains symmetric proliferative divisions of neuroepithelial cells." *Proc Natl Acad Sci U S A* 103(27): 10438-10443.

Florio, M., Albert, M., Taverna, E., Namba, T., Brandl, H., Lewitus, E., Haffner, C., Sykes, A., Wong, F., K., Peters, J., et al. (2015). "Human-specific gene ARHGAP11B promotes basal progenitor amplification and neocortex expansion." *Science* 347(6229): 1465-1470.

Florio, M., Heide, M., Pinson, A., Brandl, H., Albert, M., Winkler, S., Wimberger, P., Huttner, W. B., Hiller, M. (2018). "Evolution and cell-type specificity of human-specific genes preferentially expressed in progenitors of fetal neocortex." *Elife* 7.

Florio, M., Huttner, W. B. (2014). "Neural progenitors, neurogenesis and the evolution of the neocortex." *Development* 141(11): 2182-2194.

Foerster, P., Daclin, M., Asm, S., Faucourt, M., Boletta, A., Genovesio A., Spassky, N. (2017). "mTORC1 signaling and primary cilia are required for brain ventricle morphogenesis." *Development* 144(2): 201-210.



Follit, J. A., San Agustin, J. T., Jonassen, J. A., Huang, T., Rivera-Perez, J. A., Tremblay, K. D., Pazour, G. J. (2014). "Arf4 is required for Mammalian development but dispensable for ciliary assembly." *PLoS Genet* 10(2): e1004170.

Follit, J. A., San Agustin, J. T., Xu, F., Jonassen, J. A., Samtani, R., Lo, C. W., Pazour, G. J. (2008). "The Golgin GMAP210/TRIP11 anchors IFT20 to the Golgi complex." *PLoS Genet* 4(12): e1000315.

Follit, J. A., Tuft, R. A., Fogarty, K. E., Pazour, G. J. (2006). "The intraflagellar transport protein IFT20 is associated with the Golgi complex and is required for cilia assembly." *Mol Biol Cell* 17(9): 3791-3792.

Francis, F., Koulakoff, A., Boucher, D., Chafey, P., Schaar, B., Vinet, M. C., et al. (1999). "Doublecortin is a developmentally regulated, microtubule-associated protein expressed in migrating and differentiating neurons." *Neuron* 23: 247-256.

Franco, S.J., Gil-Sanz, C., Martinez-Garay, I., Espinosa, A., Harkins-Perry, S.R., Ramos, C. and Muller, U. (2012). "Fate-restricted neural progenitors in the mammalian cerebral cortex." *Science* 337: 746-749.

Frank, V., Habbig, S., Bartram, M. P., Eisenberger, T., Veenstra-Knol, H. E., Decker, C., Boorsma, R. A., Göbel, H., Nürnberg, G., et al. (2013). "Mutations in NEK8 mink multiple organ dysplasia with altered Hippo signalling and increased c-MYC expression." *Hum Mol Genet* 22(11): 2177-2185.

Frantz, G. D., S. K., McConnell (1996). "Restriction of late cerebral cortical progenitors to an upper-layer fate." *Neuron* 17 : 55–61.

Friocourt, G., Marcorelles, P., Saugier-veber, P., Quille, M.-L., Marret, S., and Laquerrière, A. (2011). "Role of cytoskeletal abnormalities in the neuropathology and pathophysiology of type I lissencephaly." *Acta Neuropathol* 121: 149–170.

Furuta, Y., Piston, D. W., and Hogan, B. L. (1997). "Bone morphogenetic proteins (BMPs) as regulators of dorsal forebrain development." *Development* 124: 2203–2212.

Fry, A. M., O'Regan, L., Montgomery, J., Adib, R., Bayliss, R. (2016). "EML proteins in microtubule regulation and human disease." *Biochem Soc Trans* 44(5): 1281-1288.

Gabriel, E., Wason, A., Ramani, A., Gooi, L. M., Keller, P., Pozniakovsky, A., Poser, I., Noack, F., Telugu, N. S., Calegari, F., et al. (2016). "CPAP promotes timely cilium disassembly to maintain neural progenitor pool." *EMBO J* 35(8): 803-819.

Gai, M., Bianchi, F. T., Vagnoni, C., Verni, F., Bonaccorsi, S., Pasquero, S., Berto, G. E., Sgro, F., Chiotto, A. M., Annaratone, L., et al. (2016). "ASPM and CITK regulate spindle orientation by affecting the dynamics of astral microtubules." *EMBO Rep* 17(10): 1396-1409.

Gan, Q., Lee, A., Suzuki, R., Yamagami, T., Stokes, A., Nguyen, B.C., Pleasure, D., Wang, J., Chen, H.W. and Zhou, C.J. (2014). "Pax6 mediates beta-catenin signaling for self-renewal and neurogenesis by neocortical radial glial stem cells." *Stem Cells* 32: 45-58.

Gaiano, N., Nye, J. S., Fishell, G. (2000). "Radial glial identity is promoted by Notch1 signaling in the murine forebrain." *Neuron* 26: 395-404.

Gao, P., Postiglione, M. P., Krieger, T. G., Hernandez, L., Wang, C., Han, Z., Streicher, C., Papisheva, E., Insolera, R., Chugh, K., et al. (2014). "Deterministic progenitor behavior and unitary production of neurons in the neocortex." *Cell* 159(4): 775-788.

Garcez, P. P., Diaz-Alonso, J., Crespo-Enriquez, I., Castro, D., Bell, D., Guillemot, F. (2015). "Cenpj/CPAP regulates progenitor divisions and neuronal migration in the cerebral cortex downstream of Ascl1." *Nat Commun* 6: 6474.

Garcia-Gonzalo, F. R., Corbit, K. C., Simerol-Piquer, M. S., Ramaswami, G., Otto, E. A., Noriega, T. R., Seol, A. D., Robinson, J. F., Bennett, C. L., Josifova, D. J. et al. (2011). "A transition zone complex regulates mammalian ciliogenesis and ciliary membrane composition." *Nat Genet* 43(8): 776-784.

Garcia-Marin, V., Garcia-Lopez, P., Freire, M. (2007). "Cajal's contributions to glia research." *Trends Neurosci* 30(9): 479-487.

Gauthier-Fisher, A., Lin, D. C., Greeve, M., Kaplan, D. R., Rottapel, R., Miller, F. D. (2009). "Lfc and Tctex-1 regulate the genesis of neurons from cortical precursor cells." *Nat Neurosci* 12(6): 735-744.

Gerhardt, C., Lier, J. M., Burmühl, S., Struchtrup, A., Deutschmann, K., Vetter, M., Leu, T., Reeg, S., Grune, T., Rütger, U. (2015). "The transition zone protein Rpgrip1l regulates proteosomal activity at the primary cilium." *J Cell Biol* 210(1): 115-133.

Gertz, C. C., Lui, J. H., LaMonica, B. E., Wang, X., Kriegstein, A. R. (2014). "Diverse behaviors of outer radial glia in developing ferret and human cortex." *J Neurosci* 34(7): 2559-2570.

Ghossoub, R., Hu, A., Failler, M., Rouyez, M. C., Spitzbarth, B., Mostowy, S., Wolfrum, U., Sauner, S., Cossart, P., Jamesnelson, W., Benmerah, A. (2013). "Septins 2, 7 and 9 and MAP4 colocalize along the axoneme in the primary cilium and control ciliary length." *J Cell Sci* 126: 2583-2594.

Giannandrea, M., Bianchi, V., Mignogna, M. L., Sirri, A., Carrabino, S., D'Elia, E., Vecellio, M., Russo, S., Cogliati, F., Larizza, L., et al. (2010). "Mutations in the small GTPase gene RAB39B are responsible for X-linked mental retardation associated with autism, epilepsy, and macrocephaly." *Am J Hum Genet* 86(2): 185-195.

Gil-Sanz, C., Espinosa, A., Fregoso, S. P., Bluske, K. K., Cunningham, C. L., Martinez-Garay, I., Zeng, H., Franco, S. J., Muller, U. (2015). "Lineage Tracing Using Cux2-Cre and Cux2-CreERT2 Mice." *Neuron* 86(4): 1091-1099.

Gil-Sanz, C., Landeira, B., Ramos, C., Costa, M. R., Muller, U. (2014). "Proliferative defects and formation of a double cortex in mice lacking *Mid1* and *Cdh2* in the dorsal telencephalon." *J Neurosci* 34(32): 10475-10487.

Gladwyng-Ng, I., Cordon-Barris, L., Alfano, C., Creppe, C., Couderc, T., Morelli, G., Thelen, N., America, N., Bessières, B., Encha-Razavi, F., et al. (2018). "Stress-induced unfolded protein response contributes to Zika virus-associated microcephaly." *Nat Neurosci* 21(1): 63-71.

Grandone, A., Torella, A., Santoro, C., Giugliano, T., Del Vecchio Blanco, F., Mutarelli, M., Cirillo, M., Cirillo, G., Piluso, G., Festa, A., et al. (2016). "Expanding the phenotype of *RITN* variations: a new family with primary microcephaly, severe growth failure, brain malformations and dermatitis." *Clin Genet* 90(5): 445-450.

Gotz, M., Huttner, W.B. (2005). "The cell biology of neurogenesis". *Nat Rev Mol Cell Biol*, 6, 777-788.

Gotz, M., Stoykova, A., Gruss P. (1998). "Pax6 controls radial glia differentiation in the cerebral cortex." *Neuron* 21: 1031–1044.

Gotz, M., Sirko, S., Beckers, J., Irmeler, M. (2015). "Reactive astrocytes as neural stem or progenitor cells: In vivo lineage, in vitro potential, and genome-wide expression analysis." *Glia* 63(8): 1452-1468.

Gleeson, J. G., Allen, K. M., Fox, J. W., Lamperti, E. D., Berkovic, S., Scheffer, I., et al. (1998). "Doublecortin, a brain-specific gene mutated in human X-linked lissencephaly and double cortex syndrome, encodes a putative signaling protein." *Cell* 92: 63–72.

Grampa, V., Delous, M., Zaidan, M., Ody, G., Thomas, S., Elkhartoufi, N., Filhol, E., Niel, O., Silbermann, F., Lebreton, C., et al. (2016). "Novel *NEK8* mutations cause severe syndromic renal cystic dysplasia through YAP dysregulation." *PLoS Genet* 12(3): e1005894.

Graus-Porta, D., Blaess, S., Senften, M., Littlewood-Evans, A., Damsky, C., Huang, Z., et al. (2001). "Beta1-class integrins regulate the development of laminae and folia in the cerebral and cerebellar cortex." *Neuron* 31: 367–379.

Greig, L. C., Woodworth, M. B., Greppi, C., Macklis, J. D. (2016). "Ctip1 Controls Acquisition of Sensory Area Identity and Establishment of Sensory Input Fields in the Developing Neocortex." *Neuron* 90(2): 261-277.

Griveau, A., Borello, U., Causeret, F., Tissir, F., Boggetto, N., Karaz, S., Pierani, A. (2010). "A novel role for Dbx1-derived Cajal-Retzius cells in early regionalization of the cerebral cortical neuroepithelium." *PLoS Biol* 8(7): e1000440.

Grove, E. A., Tole, S., Limon, J., Yip, L., and Ragsdale, C. W. (1998). "The hem of the embryonic cerebral cortex is defined by the expression of multiple Wnt genes and is compromised in Gli3-deficient mice." *Development* 125: 2315–2325.

Guerrini, R. (2005). "Genetic malformations of the cerebral cortex and epilepsy." *Epilepsia* 46 Suppl 1: 32–37.

Guerrini, R., Marini, C. (2006). "Genetic malformations of cortical development." *Exp Brain Res* 173(2): 322-333.

Guo, C., Eckler, M. J., McKenna, W. L., McKinsey, G. L., Rubenstein, J. L., Chen, B. (2013). "Fezf2 expression identifies a multipotent progenitor for neocortical projection neurons, astrocytes, and oligodendrocytes." *Neuron* 80(5): 1167-1174.

Guo, J., Higginbotham, H., Li, J., Nichols, J., Hirt, J., Ghukasyan, V., Anton, E. S. (2015). "Developmental disruptions underlying brain abnormalities in ciliopathies." *Nat Commun* 6: 7857.

Habbig, S., Liebau, M. C. (2015). "Ciliopathies - from rare inherited cystic kidney diseases to basic cellular function." *Mol Cell Pediatr* 2(1): 8.

Hamill, D. R., Howell, B., Cassimeris, L., and Suprenant, K. A. (1998). "Purification of a WD repeat protein, EMAP, that promotes microtubule dynamics through an inhibition of rescue." *J Biol Chem* 273: 9285-9291.

Han, Y., Keschull, K. M., Campbell, R. A. A., Cowan, D., Imhof, F., Zador, A. M., Mrsic-Flogel, T. D. (2018). "The logic of single-cell projections from visual cortex." *Nature* 556(7699), 51-56.

Handoko, M., Emrick, L. T., Rosenfeld, J. A., Wang, X., Tran, A. A., Turner, A., Belmont, J. W. Undiagnosed Diseases Network, Lee, B. H., Bacino, C.A., Chao, H. T (2018). "Recurrent mosaic MTOR c.5930C>T (p.Thr1977Ile) variant causing megalencephaly, asymmetric polymicrogyria,

and cutaneous pigmentary mosaicism: Case report and review of the literature." *Am J Med Genet A* 179(3): 475-479.

Hansen, D. V., Lui, J. H., Parker, P. R., Kriegstein, A. R. (2010). "Neurogenic radial glia in the outer subventricular zone of human neocortex." *Nature* 464(7288): 554-561.

Hansen, D.V., Lui, J.H., Flandin, P., Yoshikawa, K., Rubenstein, J.L., Alvarez-Buylla, A. and Kriegstein, A.R. (2013). "Non-epithelial stem cells and cortical interneuron production in the human ganglionic eminences." *Nat Neurosci* 16: 1576-1587.

Hatakeyama, J., Bessho, Y., Katoh, K., Ookawara, S., Fujioka, M., Guillemot, F., Kageyama, R. (2004). "Hes genes regulate size, shape and histogenesis of the nervous system by control of the timing of neural stem cell differentiation." *Development* 131(22): 5539-5550.

Haydar, T. F., Kuan, C. Y., Flavell, R. A., Rakic, P. (1999). "The role of cell death in regulating the size and shape of the mammalian forebrain." *Cereb Cortex* 9: 621-626.

He, M., Subramanian, R., Bangs, F., Omelchenko, T., Leim, K. F., Kapoor, T. M., Anderson, K. V. (2014). "The kinesin-4 protein Kif7 regulates mammalian Hedgehog signalling by organizing the primary cilium tip compartment." *Nat Cell Biol* 16(7): 663-672.

Hebert, J. M., Fishell, G. (2008). "The genetics of early telencephalon patterning: some assembly required." *Nat Rev Neurosci* 9(9): 678-685.

Heide, M., Long, K. R., Huttner, W. B. (2017). "Novel gene function and regulation in neocortex expansion." *Curr Opin Cell Biol* 49: 22-30.

Heinzen, E. L., O'Neill, A. C., Zhu, X., Allen, A. S., Bahlo, M., Chelly, J., Chen, M. H., Dobyns, W. B., Freytag, S., Guerrini, R. et al., (2018). "De novo and inherited private variants in MAP1B in periventricular nodular heterotopia." *PLoS Genet* 14(5): e1007281.

Hevner, R. F. (2019). "Intermediate progenitors and Tbr2 in cortical development." *J Anat* doi: 10.1111/joa.12939.

Higginbotham, H., Guo, J., Yokota, Y., Umberger, N. L., Su, C. Y., Li, J., Verma, N., Hirt, J., Ghukasyan, V., Caspary, T., Anton, E. S. (2013). "Arl13b-regulated cilia activities are essential for polarized radial glial scaffold formation." *Nat Neurosci* 16(8): 1000-1007.

Hoch, R. V., Rubenstein, J. L., Pleasure, S. (2009). "Genes and signaling events that establish regional patterning of the mammalian forebrain." *Semin Cell Dev Biol* 20(4): 278-86

Hoffmeister, H., K. Babinger, S. Gurster, A. Cedzich, C. Meese, K. Schadendorf, L. Osten, U. de Vries, A. Rasclé and R. Witzgall (2011). "Polycystin-2 takes different routes to the somatic and ciliary plasma membrane." *J Cell Biol* 192(4): 631-645.

Hong, S. E., Shugart, Y. Y., Huang, D. T., Shahwan, S. A., Grant, P. E., Hourihane, J. O., Martin, N. D., Walsh, C. A. (2000). "Autosomal recessive lissencephaly with cerebellar hypoplasia is associated with human RELN mutations." *Nat Genet* 26: 93–96.

Houtman, S. H., Rutteman, M., De Zeeuw, C. I., and French, P. J. (2007). "Echinoderm microtubule-associated protein like protein 4, a member of the echinoderm microtubule-associated protein family, stabilizes microtubules." *Neuroscience* 144: 1373-1382.

Hu, D.J., Baffet, A.D., Nayak, T., Akhmanova, A., Doye, V. and Vallee, R.B. (2013). "Dynein recruitment to nuclear pores activates apical nuclear migration and mitotic entry in brain progenitor cells." *Cell* 154: 1300-1313.

Hua, K., Ferland, R. J. (2017). "Fixation methods can differentially affect ciliary protein immunolabeling." *Cilia* 6:5, doi: 10.1186/s13630-017-0045-9.

Hua, K., Ferland, R. J. (2018). "Primary Cilia Reconsidered in the Context of Ciliopathies: Extraciliary and Ciliary Functions of Cilia Proteins Converge on a Polarity theme?" *Bioessays* 40(8): e1700132.

Hueston, J. L., Herren, G. P., Cueva, J. G., Buechner, M., Lundquist, E. A., Goodman, M. B., et al. (2008). "The *C. elegans* EMAP-like protein, ELP-1 is required for touch sensation and associates with microtubules and adhesion complexes." *BMC Dev Biol* 8: 110.

Humke, E. W., Dorn, K. V., Milenkovic, L., Scott, M. P., Rohatgi, R. (2010). "The output of Hedgehog signaling is controlled by the dynamic association between suppressor of fused and the Gli proteins." *Genes Dev* 24(7): 670-682.

Hussain, M. S., Baig, S. M., Neumann, S., Nürnberg, G., Faroog, M., Ahmad, I., Alef, T., Hennies, H. C., Technau, M., Altmüller, J., Frommolt, P., et al. (2012). "A truncating mutation of CEP135 causes primary microcephaly and disturbed centrosomal function." *Am J Hum Genet* 90(5): 871-878.

Iefremova, V., Manikakis, G., Krefft, O., Jabali, A., Weynans, K., Wilkens, R., Marsoner, F., Brandl, B., Muller, F. J., Koch, P., Ladewig, J. (2017). "An Organoid-Based Model of Cortical Development Identifies Non-Cell-Autonomous Defects in Wnt Signaling Contributing to Miller-Dieker Syndrome." *Cell Rep* 19(1): 50-59.

Imai, F., Hirai, S., Akimoto, K., Koyama, H., Miyata, T., Ogawa, M., Noguchi, S., Sasaoka, T., Noda, T., Ohno, S. (2006). "Inactivation of aPKC $\lambda$  results in the loss of adherens junctions in neuroepithelial cells without affecting neurogenesis in mouse neocortex." *Development* 133(9): 1735-1744.

Inoue, M., Iwai, R., Tabata, H., Konno, D., Komabayashi-Suzuki, M., Watanabe, C., Iwanari, H., Mochizuki, Y., Hamakubo, T., Matsuzaki, F., Nagata, K. I., Mizutani, K. I. (2017). "Prdm16 is crucial for progression of the multipolar phase during neural differentiation of the developing neocortex." *Development* 144(9): 1735.

Insolera, R., Bazzi, H., Shao, W., Anderson, K. V., Shi, S. H. (2014). "Cortical neurogenesis in the absence of centrioles." *Nat Neurosci* 17(11): 1528-1535.

Ishikawa, H., Marshall, W. F. (2017). "Intraflagellar transport and ciliary dynamics." *Cold Spring Harb. Perspect Biol.* 9(3). pii: a021998.

Jackson, A. P., McHale, D. P., Campbell, D. A., Jafri, H., Rashid, Y., Mannan, J., Karbani, G., Corry, P., Levene, M. I., Mueller, R. F., Markham, A. F., Lench, N. J., Woods, C. G. (1998). "Primary autosomal recessive microcephaly (MCPH1) maps to chromosome 8p22-pter." *Am J Hum Genet* 63(2): 541-546.

Jaglin, X. H., and Chelly, J. (2009). "Tubulin-related cortical dysgeneses: microtubule dysfunction underlying neuronal migration defects." *Trends Genet* 25: 555-566.

Jaglin, X. H., Poirier, K., Saillour, Y., Buhler, E., Tian, G., Bahi-Buisson, N., Fallet-Bianco, C., Phan-Dinh-Tuy, F., Kong, X. P., Bomont, P., et al. (2009). "Mutations in the beta-tubulin gene TUBB2B result in asymmetrical polymicrogyria." *Nat Genet* 41(6): 746-752.

Jakovcevski, I., Mayer, N., Zecevic, N. (2011). "Multiple origins of human neocortical interneurons are supported by distinct expression of transcription factors." *Cereb Cortex*, 21: 1771-1782.

Janisch, K. M., Vock, V. M., Fleming, M. S., Shrestha, A., Grimsley-Myers, C. M., Rasoul, B. A., Neale, S. A., Cupp, T. D., Kinchen, J. M., Liem, K. F., Dwyer, N. D. (2013). "The vertebrate-specific Kinesin-6, Kif20b, is required for normal cytokinesis of polarized cortical stem cells and cerebral cortex size." *Development* 140(23): 4672-4682.

Jayaraman, D., Kodani, A., Gonzalez, D. M., Mancias, J. D., Mochida, G. H., Vagnoni, C., Johnson, J., Krogan, N., Harper, J. W., Reiter, J. F. et al. (2016). "Microcephaly Proteins Wdr62 and Aspm Define a Mother Centriole Complex Regulating Centriole Biogenesis, Apical Complex, and Cell Fate." *Neuron* 92(4): 813-828.

Jin, Z., Tietjen, I., Bu, L., Liu-Yesucevitz, L., Gaur, S. K., Walsh, C. A., Piao, X. (2007). "Disease-associated mutations affect GPR56 protein trafficking and cell surface expression." *Hum Mol Genet* 16(16): 1972-1985.

Johnson, M. B., Wang, P. P., Atabay, K. D., Murphy, E. A., Doan, R. N., Hecht, J. L., Walsh, C. A. (2015) "Single-cell analysis reveals transcriptional heterogeneity of neural progenitors in human cortex." *Nat Neurosci* 18(5): 637-646.

Johnson, M. B., Sun, X., Kodani, A., Borges-Monroy, R., Girskis, K. M., Ryu, S. C., Wang, P. P., Patel, K., Gonzalez, D. M., Woo, Y. M. et al. (2018). "Aspm knockout ferret reveals an evolutionary mechanism governing cerebral cortical size." *Nature* 556(7701): 370-375.

Joshi, P. S., Molyneaux, B. J., Feng, L., Xie, X., Macklis, J. D., Gan, L. (2008). "Bhlhb5 regulates the postmitotic acquisition of area identities in layers II-V of the developing neocortex." *Neuron* 60(2): 258-272.

Jossin, Y., Lee, M., Klezovitch, O., Kon, E., Cossard, A., Lien, W. H., Fernandez, T. E., Cooper, J. A., Vasioukhin, V. (2017). "Lgl1 Connects Cell Polarity with Cell-Cell Adhesion in Embryonic Neural Stem Cells." *Dev Cell* 41(5): 481-495 e485.

Joukov, V., De Nicolo, A. (2018). "Aurora-PLK1 cascades as key signaling modules in the regulation of mitosis." *Sci. Signal* 11(543): pii: eaar4195.

Ju, X. C., Hou, Q. Q., Sheng, A.L., Wu, K. Y., Zhou, Y., Jin, Y., Wen, T., Yang, Z., Wang, X., Luo, Z. G. (2016). "The hominoid-specific gene TBC1D3 promotes generation of basal neural progenitors and induces cortical folding in mice." *eLife* 5.

Junghans, D., Hack, I., Frotscher, M., Taylor, V. and Kemler, R. (2005). "Beta-catenin-mediated cell-adhesion is vital for embryonic forebrain development." *Dev Dyn* 233: 528-539.

Kadowaki, M., Nakamura, S., Machon, O., Krauss, S., Radice, G.L. and Takeichi, M. (2007). "N-cadherin mediates cortical organization in the mouse brain." *Dev Biol* 304: 22-33.

Kalebic, N., Gilardi, C., Albert, M., Namba, T., Long, K. R., Kostic, M., Langen, B., Huttner, W. B. (2018). "Human-specific ARHGAP11B induces hallmarks of neocortical expansion in developing ferret neocortex." *Elife* 7.

Kang, W., Wong, L. C., Shi, S. H., Hebert, J. M. (2009). "The transition from radial glial to intermediate progenitor cell is inhibited by FGF signaling during corticogenesis." *J Neurosci* 29(46): 14571-14580.

Kaplan, E. S., Ramos-Laguna, K. A., Mihalas, A. B., Daza, R. A. M., Hevner, R. F. (2017). "Neocortical Sox9+ radial glia generate glutamatergic neurons for all layers, but lack discernible evidence of early laminar fate restriction." *Neural Dev* 12(1): 14.



Kappeler, C., Saillour, Y., Baudoin, J. P., Tuy, F. P., Alvarez, C., Houbron, C., Gaspar, P., Hamard, G., Chelly, J., Metin, C., Francis, F. (2006). "Branching and nucleokinesis defects in migrating interneurons derived from doublecortin knockout mice." *Hum Mol Genet* 15(9): 1387-1400.

Kawaguchi, A., Matsuzaki, F. (2016). "Cell cycle-arrested cells know the right time." *Cell Cycle* 15(20): 2683-2684.

Kawauchi, T. (2015). "Cellular insights into cerebral cortical development: focusing on the locomotion mode of neuronal migration." *Front Cell Neurosci* 9: 394.

Keays, D. A., Tian, G., Poirier, K., Huang, G.-J., Siebold, C., Cleak, J., et al. (2007). "Mutations in alpha-tubulin cause abnormal neuronal migration in mice and lissencephaly in humans." *Cell* 128: 45-57.

Khacho, M., A. Clark, Svoboda, D. S., Azzi, J., MacLaurin, J. G., Meghaizel, C., Sesaki, H., Lagace, D. C., Germain, M., Harper, M. E., Park, D. S., Slack, R. S. (2016). "Mitochondrial Dynamics Impacts Stem Cell Identity and Fate Decisions by Regulating a Nuclear Transcriptional Program." *Cell Stem Cell* 19(2): 232-247.

Khacho, M., Clark, A., Svoboda, D. S., MacLaurin, J. G., Lagace, D. C., Park, D. S., Slack, R. S. (2017). "Mitochondrial dysfunction underlies cognitive defects as a result of neural stem cell depletion and impaired neurogenesis." *Hum Mol Genet* 26(17): 3327-3341.

Kheradmand Kia, S., Verbeek, E., Engelen, E., Schot, R., Poot, R. A., de Coo, I. F., Lequin, M. H., Poulton, C. J., Pourfarzad, F., Grosveld, F. G. et al. (2012). "RTTN mutations link primary cilia function to organization of the human cerebral cortex." *Am J Hum Genet* 91(3): 533-540.

Kielar, M., Tuy, F. P., Bizzotto, S., Lebrand, C., de Juan Romero, C., Poirier, K., Oegema, R., Mancini, G. M., Bahi-Buisson, N., Olaso, R., et al. (2014). "Mutations in Eml1 lead to ectopic progenitors and neuronal heterotopia in mouse and human." *Nat Neurosci* 17(7): 923-933.

Kim, J., Jo, H., Hong, H., Kim, M. H., Kim, J. M., Lee, J. K., Heo, W. D., Kim, J. (2014). "Actin remodeling factors control ciliogenesis by regulating YAP/TAZ activity and vesicle trafficking." *Nat Commun* 6: 6781.

Kim, N. G., Koh, E., Chen, X., Gumbiner, B. M. (2011). "E-cadherin mediates contact inhibition of proliferation through Hippo signaling-pathway components." *Proc Natl Acad Sci USA* 108(29): 11930-11935.

Kim, S., Lee, J., Choi, H., Ringstad, N., Dynlacht, B. D. (2015). "Nek2 activation of Kif24 ensures cilium disassembly during the cell cycle." *Nat Commun* 6: 8087.

Kim, S., Lehtinen, M. K., Sessa, A., Zappaterra, M. W., Cho, S. H., Gonzalez, D., Boggan, B., Austin, C. A., Wijnholds, J., Gambello, M. J., et al. (2010). "The apical complex couples cell fate and cell survival to cerebral cortical development." *Neuron* 66(1): 69-84.

Kim, S., Zaghloul, N. A., Bubenshchikova, E., Oh, E. C., Rankin, S., Katsanis, N., Obara, T., Tsiokas, L. (2011). "Nde1-mediated inhibition of ciliogenesis affects cell cycle re-entry." *Nat Cell Biol* 13(4): 351-360.

Kingsbury, M. A., Rehen, S.K., Contos, J.J., Higgins, C.M., Chun, J. (2003). "Non-proliferative effects of lysophosphatidic acid enhance cortical growth and folding." *Nat Neurosci* 6: 1292-1299.

Kinzel, D., Boldt, K., Davis, E. E., Burtscher, I., Trumbach, D., Diplas, B., Attie-Bitach, T., Wurst, W., Katsanis, N., Ueffing, M., Lickert, H. (2010). "Pitchfork regulates primary cilia disassembly and left-right asymmetry." *Dev Cell* 19(1): 66-77.

Klaus, J., Kanton, S., Kyrousi, C., Ayo-Martin, A. C., Di Giaimo, R., Riesenberger, S., O'Neill, Camp, G. J., Tocco, C., Santel, M., et al. (2019). "Altered neuronal migratory trajectories in human cerebral organoids derived from individuals with neuronal heterotopia." *Nat Med* doi: 10.1038/s41591-019-0371-0.

Kohli, P., Höhne, M., Jüngst, C., Bertsch, S., Ebert, L. K., Schauss, A. C., Benzing, T., Rinschen, M. M., Schermer, B. (2017). "The ciliary membrane-associated proteome reveals actin-binding proteins as key components of cilia." *EMBO Rep* 18(9): 12521-1535.

Komada, M., Iguchi, T., Takeda, T., Ishibashi, M., Sato, M. (2013). "Smoothed controls cyclin D2 expression and regulates the generation of intermediate progenitors in the developing cortex." *Neurosci Lett* 547: 87-91.

Komada, M., Saitsu, H., Kinboshi, M., Miura, T., Shiota, K., Ishibashi, M. (2008). "Hedgehog signaling is involved in development of the neocortex." *Development* 135(16): 2717-2727.

Konno, D., Shioi, G., Shitamukai, A., Mori, A., Kiyonari, H., Miyata, T., Matsuzaki, F. (2008). "Neuroepithelial progenitors undergo LGN-dependent planar divisions to maintain self-renewability during mammalian neurogenesis." *Nat Cell Biol* 10(1): 93-101.

Kosodo, Y., Röper, K., Haubensak, W., Marzesco, A. M., Corbeil, D., and Huttner, W. B. (2004). "Asymmetric distribution of the apical plasma membrane during neurogenic divisions of mammalian neuroepithelial cells." *EMBO J.* 23: 2314-2324.

Kreffft, O., Jabali, A., Iefremova, V., Koch, P., Ladewig, J. (2018). "Generation of standardized and reproducible forebrain-type cerebral organoids from human induced pluripotent stem cells." *J Vis Exp* 131.

Kriegstein, A., Noctor, S., Martinez-Cerdeno, V. (2006). "Patterns of neural stem and progenitor cell may underlie evolutionary cortical expansion." *Nat Rev Neurosci* 7(11), 883-890.

Kroenke, C. D., Bayly, P. V. (2018). "How Forces Fold the Cerebral Cortex." *J Neurosci* 38(4): 767-775.

Kumar, A., Girimaji, S. C., Duwari, M. R., Blanton, S. H. (2009). "Mutations in STIL, encoding a pericentriolar and centrosomal protein, cause primary microcephaly." *Am J Hum Genet* 84(2): 286-290.

Kumar, A., Markandaya, M., Girimaji, S. C. (2002). "Primary microcephaly: microcephalin and ASPM determine the size of the human brain." *J Biosci* 27(7): 629-632.

Laclef, C., Anselme, I., Besse, L., Catala, M., Palmure, A., Baas, D., Paschaki, M., Pedraza, M., Métin, C., Durand, B., Schneider-Maunoury, S. (2015). "The role of primary cilia in corpus callosum formation is mediated by production of the Gli3 repressor." *Hum Mol Genet* 24(17) 4997-5014.

Laclef, C., Metin, C. (2018). "Conserved rules in embryonic development of cortical interneurons." *Semin Cell Dev Biol* 76: 86-100.

Lafay, F. (1974). "Envelope proteins of vesicular stomatitis virus: effect of temperature-sensitive mutations in complementation groups III and V." *J Virol* 14(5): 1220-1228.

Laguesse, S., Creppe, C., Nedialkova, D. D., Prevot, P. P., Borgs, L., Huysseune, S., Franco, B., Duysens, G., Krusy, N., Lee, G., et al. (2015). "A Dynamic Unfolded Protein Response Contributes to the Control of Cortical Neurogenesis." *Dev Cell* 35(5): 553-567.

Laguesse, S., Peyre, E., Nguyen, L. (2015). "Progenitor genealogy in the developing cerebral cortex." *Cell Tissue Res* 359(1): 17-32.

LaMonica, B. E., Lui, J. H., Hansen, D. V., Kriegstein, A. R. (2013). "Mitotic spindle orientation predicts outer radial glial cell generation in human neocortex." *Nat Commun* 4: 1665.

Lancaster, M. A., Renner, M., Martin, C. A., Wenzel, D., Bicknell, L. S., Hurles, M. E., Homfray, T., Penninger, J. M., Jackson, A. P., Knoblich, K. A. (2013). "Cerebral organoids model human brain development and microcephaly." *Nature* 501(7467): 373-379.

Lange, C., Huttner, W.B., Calegari, F. (2009). "Cdk4/cyclinD1 overexpression in neural stem cells shortens G1, delays neurogenesis, and promotes the generation and expansion of basal progenitors." *Cell Stem Cell* 5, 320-331.

Lange, M., Kasper, B., Bohring, A., Rutsch, F., Kluger, G., Hoffjan, S., Spranger, S., Behnecke, A., Ferbert, A., Hahn, A., Oehl-Jaschkowitz, B., et al. (2015). "47 patients with FLNA associated periventricular nodular heterotopia." *Orphanet J Rare Dis* 10: 134.

Laplane, M., Sabatini, D. M. (2012). "mTOR signaling in growth control and disease." *Cell* 149(2): 274-293.

Lehtreck, K. F. (2015). "IFT-Cargo interactions and protein transport in cilia." *Trends Biochem Sci* 40(12): 765-778.

Lee, K. H., Johmura, Y., Yu, L. R., Park, J. E., Gao, Y., Bang, J. K., Zhou, M., Veenstra, T. D., Yeon Kim, B., Lee, K. S. (2012). "Identification of a novel Wnt5a-CK1E-Dvl2-Plk1-mediated primary cilia disassembly pathway." *EMBO J* 31(14): 3104-3117.

Lee, S. H., Joo, K., Jung, E. J., Hong, H., Seo, J., Kim J. (2018). "Export of membrane proteins from the Golgi complex to the primary cilium requires the kinesin motor, KIFC1." *FASEB J* 32(2): 957-968.

Lee, K. S., Schottler, F., Collins, J. L., Lanzino, G., Couture, D., Rao, A., et al. (1997). "A genetic animal model of human neocortical heterotopia associated with seizures." *J Neurosci* 17: 6236–6242.

Lehtinen, M. K., Walsh, C. A. (2011). "Neurogenesis at the brain-cerebrospinal fluid interface." *Annu Rev Cell Dev Biol* 27: 653-679.

Leone, D. P., Srinivasan, K., Brakebusch, C., McConnell, S. K. (2010). "The rho GTPase Rac1 is required for proliferation and survival of progenitors in the developing forebrain." *Dev Neurobiol* 70(9): 659-678.

Letinic, K., Zoncu, R. and Rakic, P. (2002). "Origin of GABAergic neurons in the human neocortex." *Nature*, 417: 645-649.

Lewitus, E., Kelava, I., Kalinka, A. T., Tomancak, P., Huttner, W. B. (2014). "An adaptive threshold in mammalian neocortical evolution." *PLoS Biol* 12: e1002000.

Li, Q., Barres, B. A. (2017). "Microglia and macrophages in brain homeostasis and disease." *Nat Rev Immunol* 18(4): 225-242.

Li, A., Saito, M., Chuang, J. Z., Tseng, Y. Y., Dedesma, C., Tomizawa, K., Kaitsuka, T., Sung, C. H. (2011). "Ciliary transition zone activation of phosphorylated Tctex-1 controls ciliary resorption, S-phase entry and fate of neural progenitors." *Nat Cell Biol* 13(4): 402-411.

Lian, G., Wong, T., Lu, J., Hu, J., Zhang, J., Sheen, V. (2019). "Cytoskeletal Associated Filamin A and RhoA Affect Neural Progenitor Specification During Mitosis." *Cereb Cortex* 29(3): 1280-1290.

Liem, K. F., He, M., Ocbina, P. J., Anderson, K. V. (2009). «Mouse Kif7/Costal2 is a cilia-associated protein that regulates Sonic hedgehog signaling." *Proc Natl Acad USA* 106(32): 13377-13382.

Lien, W. H., Klezovitch, O., Fernandez, T. E., Delrow, J., Vasioukhin, V. (2006). "alpha E-catenin controls cerebral cortical size by regulating the hedgehog signaling pathway." *Science* 311: 1609-1612.

Lim, L., Mi D., Llorca, A., Marin, O. (2018). "Development and Functional Diversification of Cortical Interneurons." *Neuron* 100(2): 294-313.

Liu, W. A., Chen, S., Li, Z., Lee, C. H., Mirzaa, G., Dobyys, W. B., Ross, M. E, Zhang, J., Shi, S. H. (2018). "PARD3 dysfunction in conjunction with dynamic HIPPO signaling drives cortical enlargement with massive heterotopia." *Genes Dev* 32(11-12): 763-780.

Liu, J., Liu, W., Yang, L., Wu, Q., Zhang, H., Fang, A., Li, L., Xu, X., Sun, L., Zhang, J., Tang, F., Wang, X. (2017). "The Primate-Specific Gene TMEM14B Marks Outer Radial Glia Cells and Promotes Cortical Expansion and Folding." *Cell Stem Cell* 21(5): 635-649 e638.

Liu, A., Tan, G., Levenkova, N., Li, T., Pugh, E. N., Rux, J. J., Speicher, D. W., Pierce, E. A. (2007). "The proteome of the mouse photoreceptor sensory cilium complex." *Mol Cell Proteomics* 6(8): 1299-1317.

Lizarraga, S. B., Margossian, S. P., Harris, M. H., Campagna, D. R., Han, A. P., Blevins, S., Mudbhary, R., Barker, J. E., Walsh, C. A. and Fleming, M. D. (2010). "Cdk5rap2 regulates centrosome function and chromosome segregation in neuronal progenitors." *Development* 137: 1907-1917.

Llinares-Benadero, C., Borrell, V. (2019). "Deconstructing cortical folding: genetic, cellular and mechanical determinants." *Nat Rev Neurosci* 20(3): 161-176.

Llorca, A., Ciceri, G., Beattie, R., Wong, K., Diana, G., Serafeimidou, E., Fernandez-Otero, M., Stricher, C., Arnold, S. J., Meyer, M., Hippenmeyer, S., et al. (2018). "Heterogeneous progenitor cell behaviors underlie assembly of neocortical cytoarchitecture." *BioRxv*, 494088.

Lock, J. G., Hammond, L. A., Houghton, F., Gleeson, P. A., Stow, J. L. (2005). "E-Cadherin transport from the trans-Golgi network in tubulovesicular carriers in selectively regulated by golgin-97." *Traffic* 6: 1142-1156.

Lodato, S., Arlotta, P. (2015). "Generating neuronal diversity in the mammalian cerebral cortex." *Annu Rev Cell Dev Biol* 31: 699-720.

Lodato, S., Shetty, A. S., Arlotta, P. (2015). "Cerebral cortex assembly: generating and reprogramming projection neuron diversity." *Trends Neurosci* 38(2): 117-125.

Loncarek, J., Bettencourt-Dias, M. (2018). "Building the right centriole for each cell type." *J Cell Biol* 217(3): 823-835.

Lopez-Bendito, G., Cautinat, A., Sanchez, J. A., Bielle, F., Flames, N., Garratt, A. N., Talmage, D. A., Role, L. W., Charnay, P., Marin, O., Garel, S. (2006). "Tangential neuronal migration controls axon guidance: a role for neuregulin-1 in thalamocortical axon navigation." *Cell* 125(1): 127-142.

Lu, L., Madugula, V. (2018). "Mechanisms of ciliary targeting: entering importins and Rabs." *Cell Mol Life Sci* 75(4): 597-606.

Lukaszewicz, A., Savatier, P., Cortay, V., Giroud, P., Huissoud, C., Berland, M., Kennedy, H., Dehay, C. (2005). "G1 phase regulation, area-specific cell cycle control, and cytoarchitectonics in the primate cortex." *Neuron* 47(3): 353-364.

Luskin, M. B., Pearlman, A. L., and Sanes, J. R. (1988). "Cell lineage in the cerebral cortex of the mouse studied in vivo and in vitro with a recombinant retrovirus." *Neuron* 1: 635-647.

Ma, S., Meng, Z., Chen, R., Guan, K. L. (2018). "The Hippo pathway: biology and pathophysiology." *Annu Rev Biochem*, doi: 10.1146/annurev-biochem-013118-111829.

Ma, T., Wang, C., Wang, L., Zhou, X., Tian, M., Zhang, Q., Zhang, Y., Li, J., Liu, Z., Cai, Y. et al. (2013). "Subcortical origins of human and monkey neocortical interneurons." *Nat Neurosci*, 16: 1588-1597.

Madhivanan, K., Aguilar, R. C. (2014). "Ciliopathies: the trafficking connection." *Traffic* 15(10): 1031-1056.

Malatesta, P., Hartfuss, E., and Götz, M. (2000). "Isolation of radial glial cells by fluorescent activated cell sorting reveals a neuronal lineage." *Development*, 127: 5253–5263.

Mallamaci, A., Muzio, L., Chan, C.H., Parnavelas, J., Boncinelli, E. (2000). "Area identity shifts in the early cerebral cortex of *Emx2*<sup>-/-</sup> mutant mice." *Nat Neurosci*. 3: 679–686.

Manabe, N., Hirai, S., Imai, F., Nakanishi, H., Takai, Y., Ohno, S. (2002). "Association of ASIP/mPAR-3 with adherens junctions of mouse neuroepithelial cells." *Dev Dyn* 225(1): 61-69.

Mancinelli, S., Lodato, S. (2018). "Decoding neuronal diversity in the developing cerebral cortex: from single cells to functional networks." *Curr Opin Neurobiol* 53: 146-155.

Marin, O. (2013). "Cellular and molecular mechanisms controlling the migration of neocortical interneurons." *Eur J Neurosci* 38(1): 2019-2029.

Marin-Valencia, I., Novarino, G., Johansen, A., Rosti, B., Issa, M. Y., Musaev, D., Bhat, G., Scott, E., Silhavy, J. L., Stanley, V., Rosti, R. O., Gleeson, J. W., Imam, F. B., Zaki, M. S., Gleeson, J. G. (2018). "A homozygous founder mutation in TRAPPC6B associates with a neurodevelopmental disorder characterized by microcephaly, epilepsy and autistic features." *J Med Genet* 55(1): 48-54.

Marthiens, V., ffrench-Constant, C. (2009). "Adherens junction domains are split by asymmetric division of embryonic neural stem cells." *EMBO Rep* 10(5): 515-520.

Marthiens, V., Rujano, M. A., Pannetier, C., Tessier, S., Paul-Gilloteaux, P., Basto, R. (2013). "Centrosome amplification causes microcephaly." *Nat Cell Biol* 15(7): 731-740.

Martin, C. A., Ahmad, I., Klingseisen, A., Hussain, M. S., Bicknell, L. S., Leitch, A., Nürnberg, G., Toliat, M. R., Murray, J. E., Hunt, D., et al. (2014). "Mutations in PLK4, encoding a master regulator of centriole biogenesis, cause microcephaly, growth failure and retinopathy." *Nat Genet* 46(12): 1283-1292.

Martinez-Cerdeno, V., Cunningham, C. L., Camacho, J., Antczak, J. L., Prakash, A. N., Cziep, M. E., Walker, A. I., Noctor, S. C. (2012). "Comparative analysis of the subventricular zone in rat, ferret and macaque: evidence for an outer subventricular zone in rodents." *PLoS One* 7(1): e30178.

Martinez-Martinez, M. A., De Juan Romero, C., Fernandez, V., Cardenas, A., Gotz, M., Borrell, V. (2016). "A restricted period for formation of outer subventricular zone defined by Cdh1 and Trnp1 levels." *Nat Commun* 7: 11812.

Martínez-Martínez M. A., Ciceri, G., Espinós, A., Fernández, V., Marín, O., Borrell, V. (2019). "Extensive branching of radially migrating neurons in the mammalian cerebral cortex." *J Comp Neurol* doi: 10.1002/cne.24597

Martynoga, B., Drechsel, D., Guillemot, F. (2012). "Molecular control of neurogenesis: a view from the mammalian cerebral cortex." *Cold Spring Harb Perspect Biol* 4(10).

Matsuzaki, F., Shitamukai, A. (2015). "Cell Division Modes and Cleavage Planes of Neural Progenitors during Mammalian Cortical Development." *Cold Spring Harb Perspect Biol* 7(9): a015719.

Mazelova, J., Astuto-Gribble, L., Inoue, H., Tam, B. M., Schonteich, E., Prekeris, R., Moritz, O. L., Randazzo, P. A., Deretic, D. (2009). "Ciliary targeting motif VxPx directs assembly of a trafficking module through Arf4." *EMBO J* 28(3): 183-192.

McConnell, S. K., Kaznowski, C. E. (1991). "Cell cycle dependence of laminar determination in developing neocortex." *Science* 254: 282–285.

Meencke, H. J., Veith, G. (1992). "Migration disturbances in epilepsy." *Epilepsy Res. Suppl.* 9: 31-40.

Megraw, T. L., Sharkey, J. T., Nowakowski, R. S. (2011). "Cdk5rap2 exposes the centrosomal root of microcephaly syndromes." *Trends Cell Biol* 21(8): 470-480.

Meng, Z., Moroishi, T., Guan, K. L. (2016). "Mechanisms of Hippo pathway regulation." *Genes Dev* 30(1): 1-17.

Mihalas, A. B., Elsen, G. E., Bedogni, F., Daza, R. A. M, Ramos-Laguna, K. A., Arnold, S. J., Hevner, R. F. (2016). "Intermediate Progenitor Cohorts Differentially Generate Cortical Layers and Require Tbr2 for Timely Acquisition of Neuronal Subtype Identity." *Cell Rep* 16(1): 92-105.

Mihalas, A. B, Hevner, R. F. (2018). "Clonal analysis reveals laminar fate multipotency and daughter cell apoptosis of mouse cortical intermediate progenitors." *Development* 145(17): pii: dev164335.

Minobe, S., Sakakibara, A., Ohdachi, T., Kandara, R., Kimura, M., Nakatani, S., Tadokoro, R., Ochiai, W., Nishizawa, Y., Mizoguchi, A., Kawauchi, T., Miyata, T. (2009). "Rac is involved in the interkinetic nuclear migration of cortical progenitor cells." *Neurosci Res* 63(4): 294-301.

Mirzaa, G. M., Conti, V., Timms, A. E., Smyser, C. D., Ahmed, S., Carter, M., Barnett, S., Hufnagel, R. B., Goldstein, A., Narumi-Kishimoto, et al. (2015). "Characterisation of mutations of the phosphoinositide-3-kinase regulatory subunit, PIK3R2, in perisylvian polymicrogyria: a next-generation sequencing study." *Lancet Neurol* 14(12): 1182-1195.

Miyamoto, T., Hosoba, K., Ochiai, H., Royba, E., Izumi, H., Sakuma, T., Yamamoto, T., Dynlacht, B. D., Matsuura, S. (2015). "The Microtubule-Depolymerizing Activity of a Mitotic Kinesin Protein KIF2A Drives Primary Cilia Disassembly Coupled with Cell Proliferation." *Cell Rep.* pii: S2211-1247(15)00004-2.



Miyata, T., Okamoto, M., Shinoda, T., Kawaguchi, A. (2014). "Interkinetic nuclear migration generates and opposes ventricular-zone crowding: insight into tissue mechanics." *Front Cell Neurosci* 8 : 473.

Mizutani, K., Yoon, K., Dang, L., Tokunaga, A., Gaiano, N. (2007). "Differential Notch signalling distinguishes neural stem cells from intermediate progenitors." *Nature* 449(7160): 351-355.

Molyneaux, B. J., Arlotta, P., Menezes, J. R., Macklis, J. D. (2007). "Neuronal subtype specification in the cerebral cortex." *Nat Rev Neurosci* 8(6): 427-437.

Molyneaux, B. J., Goff, L. A., Brettler, A. C., Chen, H. H., Hrvatin, S., Rinn, J. L., Arlotta, P. (2015). "DeCoN: genome-wide analysis of in vivo transcriptional dynamics during pyramidal neuron fate selection in neocortex." *Neuron* 85(2): 275-288.

Monis, W. J., Faundez, V., Pazour, G. J. (2017). "BLOC-1 is required for selective membrane protein trafficking from endosomes to primary cilia." *J Cell Biol* 216(7): 2131-2150.

Monuki, E. S., Porter, F. D., Walsh, C. A. (2001). "Patterning of the dorsal telencephalon and cerebral cortex by a roof plate-Lhx2 pathway." *Neuron* 32: 591–604.

Mora-Bermudez, F., Huttner, W. B. (2015). "Novel insights into mammalian embryonic neural stem cell division: focus on microtubules." *Mol Biol Cell* 26(24): 4302-4306.

Morin, X., Jaouen, F., Durbec, P. (2007). "Control of planar divisions by the G-protein regulator LGN maintains progenitors in the chick neuroepithelium." *Nature Neuroscience* 10(11): 1440-1448.

Morris- Rosendahl, D. J., Najm, J., Lachmeijer, A. M., Sztriha, L., Martins, M., Kuechler, A., Haug, V., Zeschnigk, C., Martin, P., Santos, M., et al. (2008). "Refining the phenotype of  $\alpha$ -1a Tubulin (TUBA1A) mutation in patients with classical lissencephaly." *Clin. Genet.* 74: 425–433.

Munji, R. N., Choe, Y., Li, G., Siegenthaler, J. A., Pleasure, S. J. (2011). "Wnt signaling regulates neuronal differentiation of cortical intermediate progenitors." *J Neurosci* 31(5): 1676-1687.

Nagasaka, A., Shonida, T., Kawaue, T., Suzuki, M., Nagayama, K., Matsumoto, T., Ueno, N., Kawaguchi, A., Miyata, T. (2016). "Differences in the mechanical properties of the developing cerebral cortical proliferative zone between mice and ferrets at both the tissue and single-cell levels." *Front Cell Dev Biol* 4: 139.

Narayanan, R., Pham, L., Kerimoglu, C., Watanabe, T., Castro Hernandez, R., Sokpor, G., Ulmke, P. A., Kiszka, K. A., Tonchev, A. B., Rosenbusch, J., et al. (2018). "Chromatin Remodeling BAF155 Subunit Regulates the Genesis of Basal Progenitors in Developing Cortex." *iScience* 4: 109-126.

Negishi, Y., Miya, F., Hattori, A., Johmura, Y., Nakagawa, M., Ando, N., Hori, I., Togawa, T., Aoyama, K., Ohashi, K., et al. (2017). "A combination of genetic and biochemical analyses for the diagnosis of PI3K-AKT-mTOR pathway-associated megalencephaly." *BMC Med Genet* 18(1): 4.

Nicholas, A. K., Khurshid, M., Désir, J., Carvalho, O. P., Cox, J. J., Thornton, G., Kausar, R., Ansar, M., Ahmad, W., Verloes, A. (2010). "WDR62 is associated with the spindle pole and is mutated in human microcephaly." *Nat Genet* 42(11): 1010-1014.

Nikolopoulou, E., Galea, G. L., Rolo, A., Greene, N. D., Copp, A. J. (2017). "Neural tube closure: cellular, molecular and biomechanical mechanisms." *Development* 144(4): 552-566.

Nishimura, Y., Kasahara, K., Shiromizu, T., Watanabe, M., Inagaki, M. (2018). "Primary cilia as signaling hubs in health and disease." *Adv Sci (Weinh)* 6(1): 1801138.

Nishizawa, Y., Imafuku, H., Saito, K., Kanda, R., Kimura, M., Minobe, S., Miyazaki, F., Kawakatsu, S., Masaoka, M., Ogaka, M., Miyata, T. (2007). "Survey of the morphogenetic dynamics of the ventricular surface of the developing mouse cortex." *Dev Dyn* 236(11): 3061-3070.

Noctor, S.C., Flint A.C., Weissman T.A., Dammerman R.S., Kriegstein A.R. (2001). "Neurons derived from radial glial cells establish radial units in neocortex." *Nature*, 409: 714-720.

Noctor, S. C., Martinez-Cerdeno, V., Ivic, L., Kriegstein, A. R. (2004). "Cortical neurons arise in symmetric and asymmetric division zones and migrate through specific phases." *Nat Neurosci* 7(2): 136-144.

Nonaka-Kinoshita, M., Reillo, I., Artegiani, B., Martinez-Martinez, M. A., Nelson, M., Borrell, V., Calegari, F. (2013). "Regulation of cerebral cortex size and folding by expansion of basal progenitors." *EMBO J* 32(13): 1817-1828.

Nowakowski, T. J., Pollen, A. A., Sandoval-Espinosa, C., Kriegstein, A. R. (2016). "Transformation of the Radial Glia Scaffold Demarcates Two Stages of Human Cerebral Cortex Development." *Neuron* 91(6): 1219-1227.

O'Leary, M. A., Bloch, J. I., Flynn, J. J., Gaudin, T. J., Giallombardo, A., Giannini, N. P., Goldberg, S. L., Kraatz, B. P., Luo, Z.-X., Meng, J. et al. (2013). "The placental mammal ancestor and the post-K-Pg radiation of placentals." *Science* 339: 662-667.

O'Leary, D. D., Chou, S. J., Sahara, S. (2007). "Area patterning of the mammalian cortex." *Neuron* 56(2): 252-269.

O'Neill, A. C., Kyrousi, C., Einsiedler, M., Burtscher, I., Drukker, M., Markie, D. M., Kirk, E. P., Gotz, M., Robertson, S. P., Cappello, S. (2018a). "Mob2 Insufficiency Disrupts Neuronal Migration in the Developing Cortex." *Front Cell Neurosci* 12: 57.

O'Neill, A. C., Kyrousi, C., Klaus, J., Leventer, R. J., Kirk, E. P., Fry, A., Pilz, D. T., Morgan, T., Jenkins, Z. A., Drukker, M., et al. (2018b). "A Primate-Specific Isoform of PLEKHG6 Regulates Neurogenesis and Neuronal Migration." *Cell Rep* 25(10): 2729-2741 e2726.

O'Roak, B. J., Vives, L., Egertson, J. D., Stanaway, I. B., Phelps, I. G., Carvill, G., Kumar, A., Lee, C., Ankenman, K., Munsion, J., et al. (2012). "Multiplex targeted sequencing identifies recurrently mutated genes in autism spectrum disorder." *Science* 338(6114): 1619-1622.

Oberst, O., Fievre, S., Baumann, N., Concetti, C., Jabaudon, D. (2018). "Apical progenitors remain multipotent throughout cortical neurogenesis." *BioRxiv*, 47889.

Ohkubo, Y., Chiang, C., and Rubenstein, J. L. R. (2002). "Coordinate regulation and synergistic actions of BMP4, SHH and FGF8 in the rostral prosencephalon regulate morphogenesis of the telencephalic and optic vesicles". *Neuroscience* 111, 1–17.

Ohta, Y., Suzuki, N., Nakamura, S., Hartwig, J. H. Stossel, T. P. (1999). "The small GTPase RalA targets filamin to induce filopodia." *Proc. Natl. Acad. U S A* 96(5), 2122-2128.

Okamoto, M., Miyata, T., Konno, D, Ueda, H. R., Kasukawa, T., Hashimoto, M., Matsuzaki, F., Kawaguchi, A. (2016). "Cell-cycle-independent transitions in temporal identity of mammalian neural progenitor cells." *Nat Commun* 7: 11349.

Okamoto, M., Namba, T., Shinoda, T., Kondo, T., Watanabe, T., Inoue, Y., et al. (2013). "TAG-1-assisted progenitor elongation streamlines nuclear migration to optimize subapical crowding." *Nat Neurosci* 16: 1556-1566.

Okamoto, M., Shinoda, T., Kawaue, T., Nagasaka, A., Miyata, T. (2014). "Ferret-mouse differences in interkinetic nuclear migration and cellular densification in the neocortical ventricular zone." *Neurosci Res* 86: 88-95.

Ostrem, B., Di Lullo, E., Kriegstein, A. R. (2017). "oRGs and mitotic somal translocation - a role in development and disease." *Curr Opin Neurobiol* 42: 61-67.

Paridaen, J. T., Huttner, W. B. (2014). "Neurogenesis during development of the vertebrate central nervous system." *EMBO Rep* 15(4): 254-364.

Paridaen, J. T., Wilsch-Brauninger, M., Huttner, W. B. (2013). "Asymmetric inheritance of centrosome-associated primary cilium membrane directs ciliogenesis after cell division." *Cell* 155(2): 333-344.

Park, R., Moon, U. Y., Park, J. Y., Hughes, L. J., Johnson, R. L., Cho, S. H., Kim, S. (2016). "Yap is required for ependymal integrity and is suppressed in LPA-induced hydrocephalus." *Nat Commun* 7: 10329.

Parrini, E., Conti, V., Dobyns, W. B., Guerrini, R. (2016). "Genetic Basis of Brain Malformations." *Mol Syndromol* 7(4): 220-233.

Pilaz, L. J., McMahon, J. J., Miller, E. E., Lennox, A. L., Suzuki, A., Salmon, E., Silver, D. L. (2016). "Prolonged Mitosis of Neural Progenitors Alters Cell Fate in the Developing Brain." *Neuron* 89(1): 83-99.

Pilaz, L. J., Patti, D., Marcy, G., Ollier, E., Pfister, S., Douglas, R. J., Betizeau, M., Gautier, E., Cortay, V., Doerflinger, N., Kennedy, H., Dehay, C. (2009). "Forced G1-phase reduction alters mode of division, neuron number, and laminar phenotype in the cerebral cortex." *Proc Natl Acad Sci U S A* 106(51): 21924-21929.

Pilz, G. A., Shitamukai, A., Reillo, I., Pacary, E., Schwausch, J., Stahl, R., Ninkovic, J., Snippert, H. J., Clevers, H., Godinho, L., Guillemot, F., Borrell, V., Matsuzaki, F., Gotz, M. (2013). "Amplification of progenitors in the mammalian telencephalon includes a new radial glial cell type." *Nat Commun* 4: 2125.

Pilz, D. T., Kuc, J., Matsumoto, N., Bodurtha, J., Bernadi, B., Tassinari, C. A., et al. (1999). "Subcortical band heterotopia in rare affected males can be caused by missense mutations in DCX (XLIS) or LIS1." *Hum Mol Genet* 8: 1757-1760.

Pilz, D. T., Matsumoto, N., Minnerath, S., Mills, P., Gleeson, J. G., Allen, K. M., et al. (1998). "LIS1 and XLIS (DCX) mutations cause most classical lissencephaly, but different patterns of malformation." *Hum Mol Genet* 7: 2029-2037.

Piotrowska-Nitsche, K., Caspary, T. (2012). "Live imaging of individual cell divisions in mouse neuroepithelium shows asymmetry in cilium formation and sonic hedgehog response." *Cilia* 1:6.

Plotnikova, O. V., Nikonova, A. S., Loskutov, Y. V., Kozyulina, P. Y., Pugacheva, E. N., Golemis, E. A. (2012). "Calmodulin activation of Aurora-A kinase (AURKA) is required during ciliary disassembly and in mitosis." *Mol Biol Cell* 23(14): 2658-2670.

Poirier, K., Keays, D. A., Francis, F., Saillour, Y., Bahi, N., Manouvrier, S., et al. (2007). "Large spectrum of lissencephaly and pachygyria phenotypes resulting from de novo missense mutations in tubulin alpha 1A (TUBA1A)." *Hum Mutat* 28: 1055-1064.

Poirier, K., N. Lebrun, L. Broix, G. Tian, Y. Saillour, C. Boscheron, E. Parrini, S. Valence, B. S. Pierre, M. Oger, et al. (2013). "Mutations in TUBG1, DYNC1H1, KIF5C and KIF2A cause malformations of cortical development and microcephaly." *Nat Genet* 45(6): 639-647.

Pollen, A.A., Nowakowski, T.J., Chen, J., Retallack, H., Sandoval-Espinosa, C., Nicholas, C.R., Shuga, J., Liu, S.J., Oldham, M.C., Diaz, A. et al. (2015) "Molecular identity of human outer radial glia during cortical development." *Cell* 163(1): 55-67.

Pollmann, M., R. Parwaresch, S. Adam-Klages, M. L. Kruse, F. Buck and H. J. Heidebrecht (2006). "Human EML4, a novel member of the EMAP family, is essential for microtubule formation." *Exp Cell Res* 312(17): 3241-3251.

Pouchelon, G., Gambino, F., Bellone, C., Telley, L., Vitali, I., Lüscher, C., et al. (2014). "Modality-specific thalamocortical inputs instruct the identity of postsynaptic L4 neurons." *Nature* 511: 471-474.

Preisinger, C. Körner, R., Winder, M., Lehmann, W. D., Kopajtich, R., Barr, F. A. (2005). "Plk1 docking to GRASP65 phosphorylated by Cdk1 suggests a mechanism for Golgi checkpoint signalling." *EMBO J* 24(4): 753-765.

Putoux, A., Baas, D., Paschaki, M., Morlé, L., Maire, C., Attié-Bitach, T., Thomas, S., Durand, B. (2018). "Altered GLI3 and FGF signaling underlies acrocallosal syndrome phenotypes in Kif7 depleted mice." *Hum Mol Genet* doi: 10.1093/hmg/ddy392.

Putoux, A., Thomas, S., Coene, K. L., Davis, E. E., Alanay, Y., Ogur, G., Uz, E., Buzas, D., Gomes, C., Patrier, S., et al. (2011). "KIF7 mutations cause fetal hydroletharus and acrocallosal syndromes." *Nat Genet* 43(6): 601-606.

Qian, X., Nguyen, H. N., Jacob, F., Song, H., Ming, G. L. (2017). "Using brain organoids to understand Zika virus-induced microcephaly." *Development* 144(6): 952-957.

Quadrato, G., Brown, J., Arlotta, P. (2016). "The promises and challenges of human brain organoids as models of neuropsychiatric disease." *Nat Med*, 22(11): 1220-1228.

Radmanesh, F., Caglayan, A. O., Silhavy, J. L., Yilmaz, C., Cantagrel, V., Omar, T., et al. (2013). "Mutations in LAMB1 cause cobblestone brain malformation without muscular or ocular abnormalities." *Am J Hum Genet* 92: 468-474.

Rakic, P. (1995). "Radial versus tangential migration of neuronal clones in the developing cerebral cortex." *Proc Natl Acad Sci U.S.A.* 92: 11323-11327.

Rakic, P. (2002). "Evolving concepts of radial and areal specification." *Prog Brain Res* 136: 265-280.

Rakic, P. (2009). "Evolution of the neocortex: a perspective from developmental biology." *Nat Rev Neurosci* 10: 724-735.

Rakic, S., Zecevic, N. (2003). "Emerging complexity of layer I in human cerebral cortex." *Cereb Cortex*, 13: 1072-1083.

Rallu, M., Machold, R. Gaiano, N., Corbin, J. G., McMahon, A. P., Fishell, G. (2002). "Dorsoventral patterning is established in the telencephalon of mutants lacking both Gli3 and Hedgehog signaling." *Development* 129(21) : 4963-74.

Ramón y Cajal, S. (1909). "Histologie du systeme nerveux de l'homme et des vertebres", Maloine.

Ramos, R. L., Bai, J., LoTurco, J. J. (2006). "Heterotopia formation in rat but not mouse neocortex after RNA interference knockdown of DCX." *Cereb Cortex* 16: 1323-1331.

Reillo, I., de Juan Romero, C., Garcia-Cabezas, M. A., Borrell, V. (2011). "A role for intermediate radial glia in the tangential expansion of the mammalian cerebral cortex." *Cereb Cortex* 21(7): 1674-1694.

Reiner, O., Carrozzo, R., Shen, Y., Wehnert, M., Faustinella, F., Dobyns, W. B., et al. (1993). "Isolation of a Miller-Dieker lissencephaly gene containing G protein beta-subunit-like repeats." *Nature* 364: 717-721.

Reiner, O., Sapir, T. (2013). "LIS1 functions in normal development and disease." *Curr Opin Neurobiol* 23(6): 951-956.

Reiter, J. F., Blacque, O. E., Leroux, M. R. (2012). "The base of the cilium: roles for transition fibres and the transition zone in ciliary formation, maintenance and compartmentalization." *EMBO Rep* 13(7): 608-618.

Reiter, J. F., Leroux, M. R. (2017). "Genes and molecular pathways underpinning ciliopathies." *Nat Rev Mol Cell Biol* 18(9): 533-547.

Rice, D. S., Curran, T. (2001). "Role of the Reelin signaling pathway in central nervous system development." *Annu Rev Neurosci* 24: 1005-1039

Richards, M. W., Law, E. W. P., Rennalls, L. P., Busacca, S., O'Regan, L., Fry, A. M., et al. (2014). "Crystal structure of EML1 reveals the basis for Hsp90 dependence of oncogenic EML4-ALK by disruption of an atypical  $\beta$ -propeller domain." *Proc. Natl. Acad. Sci. U.S.A.* 111: 5195-5200.

Richards, M. W., O'Regan, L., Roth, D., Montgomery, J. M., Straube, A., Fry, A. M., et al. (2015). "Microtubule association of EML proteins and the EML4-ALK variant 3 oncoprotein require an N-terminal trimerization domain." *Biochem J* 467: 529-536.

Rohatgi, R., Milenkovic, L., Scott, M. P. (2007). "Patched1 regulates hedgehog signaling at the primary cilium." *Science* 317(5836): 372-376.

Romero, D. M., Bahi-Buisson, N., Francis, F. (2018). "Genetics and mechanisms leading to human cortical malformations." *Semin Cell Dev Biol* 76: 33-75.

Roscioli, T., Kamsteeg, E. J., Buysse, K., Maystadt, I., van Reeuwijk, J., van den Elzen, C., et al. (2012). "Mutations in ISPD cause Walker-Warburg syndrome and defective glycosylation of  $\alpha$ -dystroglycan." *Nat Genet* 44: 581-585.

Rosen, G. D., Azoulay, N. G., Griffin, E. G., Newbury, A., Koganti, L., Fujisaki, N., et al. (2013). "Bilateral subcortical heterotopia with partial callosal agenesis in a mouse mutant." *Cereb Cortex* 23: 859-872.

Saadaoui, M., Machicoane, M., di Pietro, F., Etoc, F., Echard, A., Morin, X. (2014). "Dlg1 controls planar spindle orientation in the neuroepithelium through direct interaction with LGN." *J Cell Biol* 206(6): 707-717.

Sahara, S., O'Leary, D. D. (2009). "Fgf10 regulates transition period of cortical stem cell differentiation to radial glia controlling generation of neurons and basal progenitors." *Neuron* 63(1): 48-62.

Saito, M., Otsu, W., Hsu, K. S., Chuang, J. Z., Yanagisawa, T., Shieh, V., Kaitsuka, T., Wei, F. Y., Tomizawa, K., Sung, C. H. (2017). "Tctex-1 controls ciliary resorption by regulating branched actin polymerization and endocytosis." *EMBO Rep* 18(8): 1460-1472.

Sakai, D., Dixon, J., Dixon, M. J., Trainor, P. A. (2012). "Mammalian neurogenesis requires Treacle-Plk1 for precise control of spindle orientation, mitotic progression, and maintenance of neural progenitor cells." *PLoS Genet* 8(3): e1002566.

Salomoni, P., Calegari, F. (2010). "Cell cycle control of mammalian neural stem cells: putting a speed limit on G1." *Trends Cell Biol* 20(5): 233-243.

Sanchez, I., Dynlacht, B. D. (2016). "Cilium assembly and disassembly." *Nat Cell Biol* 18(7): 711-717.

Sang, L., Miller, J. J., Corbit, K. C., Giles, R. H., Brauer, M. J., Otto, E. A., Baye, L. M., Wen, X., Scales, S. J., Kwong, M., et al. (2011). "Mapping the NPHP-JBTS-MKS protein network reveals ciliopathy disease genes and pathways." *Cell* 145(4): 513-528.

Sapir, T., Levy, T., Kozler, N., Shin, I., Zamor, V., Haffner-Krausz, R., McGlade, J. C., Reiner, O. (2018). "Notch activation by Shootin1 opposing activities on 2 Ubiquitin Ligases." *Cereb Cortex* 28(9): 3115-3128.

Sarkisian, M. R., Bartley, C. M., Chi, H., Nakamura, F., Hashimoto-Torii, K., Torii, M., Flavell, R. A., Rakic, P. (2006). "MEKK4 signaling regulates filamin expression and neuronal migration." *Neuron* 52(5): 789-801.

Sasaki, T., Rodig, S. J., Chirieac, L. R., and Jänne, P. A. (2010). "The biology and treatment of EML4-ALK non-small cell lung cancer." *Eur J Cancer* 46: 1773–1780.

Schmid, M. T., Weinandy, F., Wilsch-Brauninger, M., Huttner, W. B., Cappello, S., Gotz, M. (2014). "The role of alpha-E-catenin in cerebral cortex development: radial glia specific effect on neuronal migration." *Front Cell Neurosci* 8: 215.

Seeger-Nukpezah, T., Liebau, M. C., Höpker, K., Lamkemeyer, T., Benzing, T., Golemis, E. A., Schermer, B. (2012). "The centrosomal kinase Plk1 localizes to the transition zone of primary cilia and induces phosphorylation of nephrocystin-1." *PLoS One* 7(6): e38838.

Seixas, C., Choi, S. Y., Polgar, N., Umberger, N. L., East, M. P., Zuo, X., Moreiras, H., Ghossoub, R., Benmerah, A., Kahn, R. A., et al. (2016). "Arl13b and the exocyst interact synergistically in ciliogenesis." *Mol Biol Cell* 27(2): 308-320.

Sengupta, D., Linstedt, A. D. (2010). "Mitotic inhibition of GRASP65 organelle tethering involves Polo-like kinase 1 (PLK1) phosphorylation proximate to an internal PDZ ligand." *J Biol Chem* 285(51): 39994-40003.

Sfakianos, J., Togawa, A., Maday, S., Hull, M., Pypaert, M., Cantley, L., Toomre, D., Mellman, I. (2007). "Par3 functions in the biogenesis of the primary cilium in polarized epithelial cells." *J Cell Biol* 179(6): 1133-1140.

Shamseldin, H., Alazami, A. M., Manning, M., Hashem, A., Caluseiu, O., Tabarki, B., Esplin, E., Schelley, S., Innes, A. M., Parboosingh, J. S., et al. (2015). "RTTN mutations cause primary microcephaly and primordial dwarfism in humans." *Am J Hum Genet* 97(6): 862-868.

Sheen, V. L., Ganesh, V. S., Topcu, M., Sebire, G., Bodell, A., Hill, R. S., Grant, P. E., Shugart, Y. Y., Imitola, J. Khoury, S., J., Guerrini, R., Walsh, C. A. (2004). "Mutations in ARFGEF2 implicate vesicle trafficking in neural progenitor proliferation and migration in the human cerebral cortex." *Nat Genet* 36(1): 69-76.

Shen, J., Eyaid, W., Mochida, G. H., Al-Moayyad, F., Bodell, A., Woods, C. G., Walsh, C. A. (2005). "ASPM mutations identified in patients with primary microcephaly and seizures." *J Med Genet* 42(9): 725-729.



Shen, Q., Wang, Y., Dimos, J. T., Fasano, C. A., Phoenix, T. N., Lemischka, I. R., Ivanova, N. B., Stifani, S., Morrisey, E. E., Temple, S. (2006). "The timing of cortical neurogenesis is encoded within lineages of individual progenitor cells." *Nat Neurosci* 9(6): 743-751.

Shimamura, K., Rubenstein, J. L. (1997). "Inductive interactions direct early regionalization of the mouse forebrain." *Development* 124(14): 2709-18.

Shitamukai, A., Konno, D., Matsuzaki, F. (2011). "Oblique radial glial divisions in the developing mouse neocortex induce self-renewing progenitors outside the germinal zone that resemble primate outer subventricular zone progenitors." *J Neurosci* 31(10): 3683-3695.

Sidman, R. L., Rakic, P. (1973). "Neuronal migration, with special reference to developing human brain: a review." *Brain Res.* 62(1): 1-35.

Siegenthaler, J. A., Ashique, A. M., Zarbali, K., Patterson, K. P., Hecht, J. H., Kane, M. A., Folias, A. E., Choe, Y., May, S. R., Kume, T., et al. (2009). "Retinoic acid from the meninges regulates cortical neuron generation." *Cell* 139: 597-609.

Singh, S., Solecki, D. J. (2015). "Polarity transitions during neurogenesis and germinal zone exit in the developing central nervous system." *Front Cell Neurosci* 9: 62.

Sit, S. T., Manser, E. (2011). "Rho GTPases and their role in organizing the actin cytoskeleton." *J Cell Sci* 124(Pt 5): 679-683.

Spassky, N., Merkle, F. T., Flames, N., Tramontin, A. D., Garcia-Verdugo, J. M., Alvarez-Buylla, A. (2005). "Adult ependymal cells are postmitotic and are derived from radial glial cells during embryogenesis." *J Neurosci* 25(1): 10-8.

Spassky, N., Meunier, A. (2017). "The development and functions of multiciliated epithelia." *Nat Rev Mol Cell Biol* 18(7): 423-436.

Stahl, R., Walcher, T., De Juan Romero, C., Pilz, G. A., Cappello, S., Irmeler, M., Sanz-Aquila, J. M., Beckers, J., Blum, R., Borrell, V., Gotz, M. (2013). "Trnp1 regulates expansion and folding of the mammalian cerebral cortex by control of radial glial fate." *Cell* 153(3): 535-549.

Stancik, E.K., Navarro-Quiroga, I., Sellke, R. and Haydar, T.F. (2010). "Heterogeneity in ventricular zone neural precursors contributes to neuronal fate diversity in the postnatal neocortex." *J Neurosci* 30: 7028-7036.

Stoetzel, C., Bär, S., De Craene, J. O., Scheidecker, S., Etard, C., Chicher, J., Reck, J. R., Perrault, I., Geoffroy, V., Chennen, K., et al. (2016). "A mutation in VPS15 (PIK3R4) causes a ciliopathy and affects IFT20 release from the cis-Golgi." *Nat Commun* 7: 13586.

Stouffer, M. A., Golden, J. A., Francis, F. (2016). "Neuronal migration disorders: Focus on the cytoskeleton and epilepsy." *Neurobiol Dis* 92(Pt A): 18-45.

Stratigopoulos, G., Martin Carli J. G., O'Day, D. R., Wang, L., Leduc, C. A., Lanzano, P., Chung, W. K., Rosenbaum, M., Egli, D., Doherty, D. A., Leibel, R. L. (2014). "Hypomorphism for RPGRIP1L, a ciliary gene vicinal to the FTO locus, causes increased adiposity in mice." *Cell Metab* 19(5): 767-779.

Struchtrup, A., Wiegering, A., Stork, B., Rütger, U., Gerhardt, C. (2018). "The ciliary protein RPGRIP1L governs autophagy independently of its proteasome-regulating function at the ciliary base in mouse embryonic fibroblasts." *Autophagy* 14(4): 567-583.

Subramanian, L., Remedios, R., Shetty, A., Tole, S. (2009). "Signals from the edges: the cortical hem and antihem in telencephalic development." *Semin Cell Dev Biol* 20(6): 712-718.

Sugathan, A., Biagioli, M., Golzio, C., Erdin, S., Blumenthal, I., Manavalan, P., Ragavendran, A., Brand, H., Lucente, D., Miles, J., et al. (2014). "CHD8 regulates neurodevelopmental pathways associated with autism spectrum disorder in neural progenitors." *Proc Natl Acad Sci USA* 111(42): E4468-77.

Suprenant, K. A., Dean, K., McKee, J., and Hake, S. (1993). "EMAP, an echinoderm microtubule-associated protein found in microtubule-ribosome complexes." *J Cell Sci* 104: 445-450.

Suzuki, I. K., Gacquer, D., van Heurck, R., Kumar, D., Wojno, M., Bilheu, A., Herpoel, A., Lambert, N., Cheron, J., Polleux, F., Detours, V., Vanderhaeghen, P. (2018). "Human-Specific NOTCH2NL Genes Expand Cortical Neurogenesis through Delta/Notch Regulation." *Cell* 173(6): 1370-1384 e1316.

Takao, D., Wang, L., Boss, A., Verhey, K. J. (2017). "Protein Interaction Analysis Provides a Map of the Spatial and Temporal Organization of the Ciliary Gating Zone." *Curr Biol* 27(15): 2296-2306 e2293.

Tarabykin, V., Stoykova, A., Usman, N., Gruss, P. (2001). "Cortical upper layer neurons derive from the subventricular zone as indicated by Svet1 gene expression." *Development* 128: 1983-1993.

Tasic, B., Menon, V., Nguyen, T. N., Kim, T. K., Jarsky, T., Yao, Z., Levi, B., Gray, L. T., Sorensen, S. A., Dolbeare, T., et al. (2016). "Adult mouse cortical cell taxonomy revealed by single cell transcriptomics." *Nat Neurosci* 19(2): 335-346.

Tasic, B., Yao, Z., Graybuck, L. T., Smith, K. A., Nguten, T. N., Bertagnolli, D., Goldy, J., Garren, E., Economo, M. N., Viswanathan, et al. (2018). "Shared and distinct transcriptomic cell types across neocortical areas." *Nature* 563(7729): 72-78.

Tastet, J., Cuberos, H., Vallée, B., Toutain, A., Raynaud, M., Marouillat, S., Thépault, R. A., Laumonnier, F., Bonnet-Brilhault, F., Vourc'h, P., et al. (2019). "LIMK2-1 is a hominidae-specific isoform of LIMK2 expressed in central nervous system and associated with intellectual disability." *Neuroscience* 399: 199-210.

Tavano, S., Taverna, E., Kalebic, N., Haffner, C., Namba, T., Dahl, A., Wilsch-Brauninger, M., Paridaen, J., Huttner, W. B. (2018). "Insm1 Induces Neural Progenitor Delamination in Developing Neocortex via Downregulation of the Adherens Junction Belt-Specific Protein Plekha7." *Neuron* 97(6): 1299-1314 e1298.

Taverna, E., Gotz, M., Huttner, W.B. (2014). "The cell biology of neurogenesis: toward an understanding of the development and evolution of the neocortex." *Annu Rev Cell Dev Biol*, 30: 465-502.

Taverna, E., Mora-Bermudez, F., Strzyz, P. J., Florio, M., Icha, J., Haffner, C., Norden, C., Wilsch-Brauninger, M., Huttner, W. B. (2016). "Non-canonical features of the Golgi apparatus in bipolar epithelial neural stem cells." *Sci Rep* 6: 21206.

Tegha-Dunghu, J., Neumann, B., Reber, S., Krause, R., Erfle, H., Walter, T., et al. (2008). "EML3 is a nuclear microtubule-binding protein required for the correct alignment of chromosomes in metaphase." *J Cell Sci* 121: 1718–1726.

Telley, L., Govindan, S., Prados, J., Stevant, I., Nef, S., Dermitzakis, E., Dayer, A., Jabaudon, D. (2016). "Sequential transcriptional waves direct the differentiation of newborn neurons in the mouse neocortex." *Science* 351(6280): 1443-1446.

Toriello, H. V., Franco, B., Bruel, A. L., Thauvin-Robinet, C. (2002). "Oral-Facial-Digital Syndrome type I." *GeneReviews*.

Tozer, S., Baek, C., Fischer, E., Gojame, R., Morin, X. (2017). "Differential Routing of Mindbomb1 via Centriolar Satellites Regulates Asymmetric Divisions of Neural Progenitors." *Neuron* 93(3): 542-551 e544.

Turrero Garcia, M., Chang, Y., Arai, Y., Huttner, W. B. (2016). "S-phase duration is the main target of cell cycle regulation in neural progenitors of developing ferret neocortex." *J Comp Neurol* 524(3): 456-470.

Uchiyama, K., Jokitalo, E., Kano, F., Murata, M., Zhang, X., Canas, B., Newman, R., Rabouille, C., Pappin, D., Freemont, P., Kondo, H. (2002). "VCIP135, a novel factor for p97/p47-mediated membrane fusion is required for Golgi and ER assembly in vivo." *J Cell Biol* 159(5): 855-866.

Ulloa, F., Marti, E. (2010). "Wnt won the war: antagonistic role of Wnt over Shh controls dorso-ventral patterning of the vertebrate neural tube." *Dev Dyn* 239(1): 69-76.

Uzquiano, A., Francis, F. (2019). "Rotatin' the phenotypes." *Brain*, in press.

Uzquiano, A., Gladwyng-Ng, I., Nguyen, L., Reiner, O., Götz, M., Matsuzaki, F., Francis, F. (2018). "Cortical progenitor biology: key features mediating proliferation versus differentiation." *J Neurochem* 146(5): 500-525.

van Reeuwijk, J., Janssen, M., van den Elzen, C., Beltran-Valero de Bernabé, D., Sabatelli, P., Merlini, L., et al. (2005). "POMT2 mutations cause alpha-dystroglycan hypoglycosylation and Walker-Warburg syndrome." *J. Med. Genet.* 42, 907–912.

Vaid, S., Camp, J. G., Hersemann, L., Eugster Oegema, C., Heninger, A. K., Winkler, S., Brandl, H., Sarov, M., Treutlein, B., Huttner, W. B., Namba, T. (2018). "A novel population of Hopx-dependent basal radial glial cells in the developing mouse neocortex." *Development* 145(20).

Vasistha, N. A., Garcia-Moreno, F., Arora, S., Cheung, A. F., Arnold, S. J., Robertson, E. J., Molnar, Z. (2015). "Cortical and Clonal Contribution of Tbr2 Expressing Progenitors in the Developing Mouse Brain." *Cereb Cortex* 25(10): 3290-3302.

Verloes, A., Di Donato, N., Masliah-Planchon, J., Jongmans, M., Abdul-Raman, O. A., Albrecht, B., Allanson, J., Brunner, H., Bertola, D., Chassaing, N., et al. (2015). "Baraitser-Winter cerebrofrontofacial syndrome: delineation of the spectrum in 42 cases." *Eur J Hum Genet* 23(3): 292-301.

Vieira, C., Pombero, A., Garcia-Lopez, R., Gimeno, L., Echevarria, D., Martinez, S. (2010). "Molecular mechanisms controlling brain development: an overview of neuroepithelial secondary organizers." *Int J Dev Biol* 54(1): 7-20.

Vue, T. Y., Lee, M., Tan, Y. E., Werkhoven, Z., Wang, L., and Nakagawa, Y. (2013). "Thalamic control of neocortical area formation in mice." *J Neurosci* 33: 8442-8453.

Vyas, A., Saha, B., Lai, E., and Tole, S. (2003). "Paleocortex is specified in mice in which dorsal telencephalic patterning is severely disrupted." *J Comp Neuro.* 466: 545-553.

Walsh, C., Cepko, C.L. (1993). "Clonal dispersion in proliferative layers of developing cerebral cortex." *Nature* 362: 632-635.

Wambach, J. A., Wegner, D. J., Yang, P., Shinawi, M., Baldrige, D., Betleja, E., Shimony, J. S., Spencer, D., Hackett, B. P., Andrews, M. V., et al. (2018). "Functional characterization of biallelic RTTN variants identified in an infant with microcephaly, simplified gyral pattern, pontocerebellar hypoplasia, and seizures." *Pediatr Res* 84(3): 435-441.

Wang, G., Chen, Q., Zhang, X., Zhang, B., Zhuo, X., Liu, J., Jiang, Q., Zhang, C. (2013). "PCM1 recruits Plk1 to the pericentriolar matrix to promote primary cilia disassembly before mitotic entry." *J Cell Sci* 126: 1355-1365.

Wang, L., Dynlacht, B. D. (2018). "The regulation of cilium assembly and disassembly in development and disease." *Development* 145(18).

Wang, L., Failler, M., Fu, W., Dynlacht, B. D. (2018). "A distal centriolar protein network controls organelle maturation and asymmetry." *Nat Commun* 9(1): 3938.

Wang, J., Fresquez, T., Kandachar, V., Deretic, D. (2017). "The Arf GEF GBF1 and Arf4 synergize with the sensory receptor cargo, rhodopsin, to regulate ciliary membrane trafficking." *Journal of Cell Science* 130(23): 3975-3987.

Wang, L., Hou, S., Han, Y. G. (2016). "Hedgehog signaling promotes basal progenitor expansion and the growth and folding of the neocortex." *Nat Neurosci* 19(7): 888-896.

Wang, X., Tsai, J. W., Imai, J. H., Lian, W. N., Vallee, R. B., Shi, S. H. (2009). "Asymmetric centrosome inheritance maintains neural progenitors in the neocortex." *Nature* 461(7266): 947-955.

Wang, X., Tsai, J. W., LaMonica, B., Kriegstein, A. R. (2011). "A new subtype of progenitor cell in the mouse embryonic neocortex." *Nat Neurosci* 14(5): 555-561.

Wang, B., Wylie, F. G., Teasdale, R. D., Stow, J. L. (2005). "Polarized trafficking of E-cadherin is regulated by Rac1 and Cdc42 in Madin-Darby canine kidney cells." *Am J Physiol Cell Physiol* 288: 1411-1419.

Ward, H. H., Brown-Glaberman, U., Wang, J., Morita, Y., Alper, S. L., Bedrick, E. J., Gattone, V. H., Deretic, D., Wandinger-Ness, A. (2011). "A conserved signal and GTPase complex are required for the ciliary transport of polycystin-1." *Mol Biol Cell* 22(18): 3289-3305.

Watanabe, Y., Kawae, T., Miyata, T. (2018). "Differentiating cells mechanically limit the interkinetic nuclear migration of progenitor cells to secure apical cytotogenesis." *Development* 145(14).

Welburn, J. P., Cheeseman, I. M. (2012). "The microtubule-binding protein Cep170 promotes the targeting of the kinesin-13 depolymerase Kif2b to the mitotic spindle." *Mol Biol Cell* 23(24): 4786-4795.

Wheway, G., Nazlamova, L., Hancock, J. T. (2018). "Signaling through the Primary Cilium." *Front Cell Dev Biol* 6: 8.

Wiegering, A., Rütger, U., Gerhardt, C. (2018). "The ciliary protein Rpgrip1l in development and disease." *Dev Biol* 442(1): 60-68.

Willaredt, M. A., Hasenpusch-Theil, K., Gardner, H. A., Kitanovic, I., Hirschfeld-Warneken, V. C., Gojak, C. P., Gorgas, K., Bradford, C. L., Spatz, J., Wölf, S., Theil, T., Tucker, K. L. (2008). "A crucial role for primary cilia in cortical morphogenesis." *J Neurosci* 28(48): 12887-12900.

Willaredt, M. A., Tasouri, E., and K. L. Tucker (2013). "Primary cilia and forebrain development." *Mechanisms of Development* 130(6-8): 373-380.

Wilson, S. L., Wilson, J. P., Wang, C., Wang, B., McConnell, S. K. (2012). "Primary cilia and Gli3 activity regulate cerebral cortical size." *Dev Neurobiol* 72(9): 1196-1212.

Wong, F. K., Fei, J. F., Mora-Bermudez, F., Taverna, E., Haffner, C., Fu, J., Anastassiadis, K., Stewart, A. F., Huttner, W. B. (2015). "Sustained Pax6 Expression Generates Primate-like Basal Radial Glia in Developing Mouse Neocortex." *PLoS Biol* 13(8): e1002217.

Wu, C. T., Chen, H. Y., Tang, T. K. (2018). "Myosin-Va is required for preciliary vesicle transportation to the mother centriole during ciliogenesis." *Nat Cell Biol* 20(2): 175-185.

Xiang, Y., Tanaka, Y., Patterson, B., Kang, Y. J., Govindaiah, G., Roselaar, N., Cakir, B., Kim, K. Y., Lombroso, A. P., Hwang, S. M., et al. (2017). "Fusion of regionally specified hPSC-derived organoids models human brain development and interneuron migration." *Cell Stem Cell* 21(3): 383-398.

Xuan, S., Baptista, C. A., Balas, G., Tao, W., Soares, V. C., Lai, E. (1995). "Winged helix transcription factor BF-1 is essential for the development of the cerebral hemispheres." *Neuron* 14(6): 1141-52.

Yabut, O. R., Pleasure, S. J. (2018). "Sonic Hedgehog signaling rises to the surface: emerging roles in neocortical development." *Brain Plast* 3(2): 119-128.

Yang, J., Gao, J., Adamian, M., Wen, X. H., Pawlyk, B., Zhang, L., Sanderson, M. J., Zuo, J., Makino, C. L., Li, T. (2005). "The ciliary rootlet maintains long-term stability of sensory cilia." *Mol Cell Biol* 25(10): 4129-4137.

Yeung, K. S., Tso, W. W. Y., Ip, J. J. K., Mak, C. C. Y., Leung, G. K. C., Tsang, M. H. Y., Ying, D., Pei, S. L. C., Lee, S. L., Yang, W., Chung, B. H. (2017). "Identification of mutations in the PI3K-AKT-mTOR signalling pathway in patients with macrocephaly and developmental delay and/or autism." *Mol Autism* 8: 66.

Yingling, J., Youn, Y. H., Darling, D., Toyo-Oka, K., Pramparo, T., Hirotsune, S., Wynshaw-Boris, A. (2008). "Neuroepithelial stem cell proliferation requires LIS1 for precise spindle orientation and symmetric division." *Cell* 132(3): 474-486.

Yoon, K. J., Koo, B. K., Im, S. K., Jeong, H. W., Ghim, J., Kwon, M. C., Moon, J. S., Miyata, T., Kong, Y. Y. (2008). "Mind bomb 1-expressing intermediate progenitors generate notch signaling to maintain radial glial cells." *Neuron* 58(4): 519-531.

Yoshida, M., Assimacopoulos, S., Jones, K. R., and Grove, E. A. (2006). "Massive loss of Cajal-Retzius cells does not disrupt neocortical layer order." *Development* 133: 537-545.

Yu, T. W., Mochida, G. H., Tischfield, D. J., Sgaier, S. K., Flores-Sarnat, L., Sergi, C. M., Topçu, M., McDonald, M. T., Barry, B. J., Felie, J. M., et al. (2010). "Mutations in WDR62, encoding a centrosome-associated protein, cause microcephaly with simplified gyri and abnormal cortical architecture." *Nat Genet* 42(11): 1015-1020.

Zembrzycki, A., Griesel, G., Stoykova, A., and Mansouri, A. (2007). "Genetic interplay between the transcription factors Sp8 and Emx2 in the patterning of the forebrain." *Neural Dev* 2: 8.

Zhang, X., Wang, Y. (2015). "Cell cycle regulation of VCIP135 deubiquitinase activity and function in p97/947-mediated Golgi assembly." *Mol Biol Cell* 26(12): 2242-2251.

Zhang, T., Zhang, S., Song, X., Zhao, X., Hou, C., Li, Z., Gao, J. (2019). "Loss of Lgl1 Disrupts the Radial Glial Fiber-guided Cortical Neuronal Migration and Causes Subcortical Band Heterotopia in Mice." *Neuroscience* 400: 132-145.

Zhang, X., Zhang, H., Wang, Y. (2014). "Phosphorylation regulates VCIP135 function in Golgi membrane fusion during cell cycle." *J Cell Sci* 127, 172-181.

Zhu, C., Zhao, J., Bibikova, M., Levenson, J. D., Bossy-Wetzell, E., Fan, J. B., Abraham, R. T., Jiang, W. (2005). "Functional analysis of human microtubule-based motor proteins, the kinesins and dyneins, in mitosis/cytokinesis using RNA interference." *Mol Biol Cell* 16(7): 3187-3199.

Ziesel, A., Munoz-Manchado, A. B., Codeluppi, S., Lönnerberg, P., La Manno, G., Juréus, A., Marques, S., Munguba, H., Betsholtz, C., Rolny, C., et al. (2015). "Brain structure. Cell types in the mouse cortex and hippocampus revealed by single-cell RNA-seq." *Science* 347(6226): 1138-1142.

Zimmer, C., Tiveron, M. C., Bodmer, R., Cremer, H. (2004). "Dynamics of Cux2 expression suggests that an early pool of SVZ precursors is fated to become upper cortical layer neurons." *Cereb Cortex* 14(12): 1408-1420.





## Abstract

Cerebral cortical development is a finely regulated process, depending on diverse progenitor cells. Abnormal behavior of the latter can give rise to cortical malformations. Mutations in *Eml1/EML1* were identified in the *HeCo* mouse, as well as in three families presenting severe subcortical heterotopia (SH). SH is characterized by the presence of mislocalized neurons in the white matter. At early stages of corticogenesis, abnormally positioned apical radial glia progenitors (aRG) were found cycling outside the proliferative ventricular zone (VZ) in the *HeCo* cortical wall. I focused my research on characterizing aRG in the VZ to assess why some cells leave this region and thus to further understand SH mechanisms.

Combining confocal and electron microscopy (EM), I first uncovered abnormalities of centrosomes and primary cilia in *Eml1*-mutant aRGs: primary cilia are shorter, and often remain basally oriented within vesicles. We then reported similar abnormalities in human SH patient fibroblasts and derived cortical progenitors.

Searching for *Eml1*-interacting partners using mass spectrometry (MS), combined with exome sequencing of SH patient DNAs, allowed us to identify a ciliary *Eml1*-interacting partner, *RPGRIP1L*, showing mutations in a SH patient.

Gene ontology analyses of MS data pointed to Golgi apparatus and protein transport as enriched categories. Performing *in utero* electroporation and EM, I also identified Golgi apparatus alterations in *HeCo* aRGs. An *in vitro* assay in *HeCo* aRGs cultures showed that Golgi-derived trafficking is impaired. Golgi anomalies were also then revealed in human patient fibroblast and cortical progenitors. Finally, I also confirmed the interaction of *EML1* with the Golgi partner *VCIP135*, further supporting a Golgi-related function for *EML1*.

Altogether, these data indicate that the Golgi-to-primary cilium axis is perturbed in *Eml1/EML1* mutant conditions, pointing to new intracellular pathways involved in severe neurodevelopmental disorders.

## Résumé

Le cortex cérébral se développe à partir des zones de prolifération des cellules progénitrices dont le comportement anormal peut donner lieu à des malformations corticales. Des mutations dans *Eml1/EML1* ont été identifiées chez la souris *HeCo*, ainsi que dans trois familles présentant une hétérotopie sous-corticale (SH). La SH se caractérise par une position aberrante des neurones dans la substance blanche. Chez la souris *HeCo*, des anomalies de position des progéniteurs de la glie radiale apicale (aRG) ont été observées aux stades précoces de la corticogenèse. Je me suis concentré sur la caractérisation de l'aRG dans la zone ventriculaire (VZ) afin d'identifier pourquoi certaines cellules quittent cette région et ainsi mieux comprendre les mécanismes qui sous-tendent l'hétérotopie.

En combinant la microscopie confocale et électronique (EM), j'ai découvert des anomalies des centrosomes et des cils primaires dans les aRG mutants pour *Eml1* : les cils primaires sont plus courts et souvent mal orientés dans des vésicules. Nous avons ensuite observé des anomalies similaires dans des fibroblastes et des cellules progénitrices corticales de patients SH.

La recherche de partenaires interagissant avec *Eml1* à l'aide de la spectrométrie de masse (MS), combinée au séquençage d'exome des ADN de patients SH, nous a permis d'identifier : 1) un partenaire ciliaire interagissant avec *Eml1*, *RPGRIP1L* ; 2) des mutations du gène *RPGRIP1L* chez un patient SH.

L'analyse ontologique des gènes sur les données de MS a mis en évidence l'appareil de Golgi et le transport des protéines comme catégories enrichies. Après électroporation *in utero* et l'EM, j'ai identifié des altérations de l'appareil de Golgi dans les aRG *HeCo*. Un test *in vitro* sur des cultures des aRG *HeCo* a confirmé les anomalies de transport dérivé du Golgi. Enfin, les anomalies de Golgi ont également été identifiées dans des fibroblastes et des progéniteurs corticaux de patients SH. J'ai également confirmé l'interaction d'*EML1* avec la protéine de l'appareil de Golgi *VCIP135*. L'ensemble de ces données montre que l'axe appareil de Golgi-cil primaire est perturbé quand *Eml1/EML1* est muté et conduit à l'identification de nouvelles voies dans un trouble grave du neurodéveloppement.